ROSACEAE FRUIT DEVELOPMENT AND QUALITY

EDITED BY: Jia-Long Yao, Yuepeng Han, Chunying Kang and Zhongchi Liu

PUBLISHED IN: Frontiers in Plant Science

frontiers Research Topics

frontiers

ISSN 1664-8714
ISBN 978-2-88974-477-0
DOI 10.3389/978-2-88974-477-0

About Frontiers

Frontiers is more than just an open-access publisher of scholarly articles: it is a pioneering approach to the world of academia, radically improving the way scholarly research is managed. The grand vision of Frontiers is a world where all people have an equal opportunity to seek, share and generate knowledge. Frontiers provides immediate and permanent online open access to all its publications, but this alone is not enough to realize our grand goals.

Frontiers Journal Series

The Frontiers Journal Series is a multi-tier and interdisciplinary set of open-access, online journals, promising a paradigm shift from the current review, selection and dissemination processes in academic publishing. All Frontiers journals are driven by researchers for researchers; therefore, they constitute a service to the scholarly community. At the same time, the Frontiers Journal Series operates on a revolutionary invention, the tiered publishing system, initially addressing specific communities of scholars, and gradually climbing up to broader public understanding, thus serving the interests of the lay society, too.

Dedication to Quality

Each Frontiers article is a landmark of the highest quality, thanks to genuinely collaborative interactions between authors and review editors, who include some of the world's best academicians. Research must be certified by peers before entering a stream of knowledge that may eventually reach the public - and shape society; therefore, Frontiers only applies the most rigorous and unbiased reviews.
Frontiers revolutionizes research publishing by freely delivering the most outstanding research, evaluated with no bias from both the academic and social point of view. By applying the most advanced information technologies, Frontiers is catapulting scholarly publishing into a new generation.

What are Frontiers Research Topics?

Frontiers Research Topics are very popular trademarks of the Frontiers Journals Series: they are collections of at least ten articles, all centered on a particular subject. With their unique mix of varied contributions from Original Research to Review Articles, Frontiers Research Topics unify the most influential researchers, the latest key findings and historical advances in a hot research area! Find out more on how to host your own Frontiers Research Topic or contribute to one as an author by contacting the Frontiers Editorial Office: frontiersin.org/about/contact

ROSACEAE FRUIT DEVELOPMENT AND QUALITY

Topic Editors:
Jia-Long Yao, The New Zealand Institute for Plant and Food Research Ltd, New Zealand
Yuepeng Han, Wuhan Botanical Garden, Chinese Academy of Sciences (CAS), China
Chunying Kang, Huazhong Agricultural University, China
Zhongchi Liu, University of Maryland, College Park, United States

Citation: Yao, J.-L., Han, Y., Kang, C., Liu, Z., eds. (2022). Rosaceae Fruit Development and Quality. Lausanne: Frontiers Media SA.
doi: 10.3389/978-2-88974-477-0

Table of Contents

04 ***Editorial: Rosaceae Fruit Development and Quality***
Chunying Kang, Jia-Long Yao, Zhongchi Liu and Yuepeng Han

06 ***Analysis of Metabolites and Gene Expression Changes Relative to Apricot (Prunus armeniaca L.) Fruit Quality During Development and Ripening***
Beatriz Ester García-Gómez, David Ruiz, Juan Alfonso Salazar, Manolo Rubio, Pedro José Martínez-García and Pedro Martínez-Gómez

30 ***Endogenous Auxin Content Contributes to Larger Size of Apple Fruit***
Haidong Bu, Wenquan Yu, Hui Yuan, Pengtao Yue, Yun Wei and Aide Wang

41 ***The Physiological and Molecular Mechanism of Abscisic Acid in Regulation of Fleshy Fruit Ripening***
Qian Bai, Yun Huang and Yuanyue Shen

50 ***Multi-Locus Genome-Wide Association Studies Reveal Fruit Quality Hotspots in Peach Genome***
Cassia da Silva Linge, Lichun Cai, Wanfang Fu, John Clark, Margaret Worthington, Zena Rawandoozi, David H. Byrne and Ksenija Gasic

68 ***An Atlas of Genomic Resources for Studying Rosaceae Fruits and Ornamentals***
Muzi Li, Yuwei Xiao, Steve Mount and Zhongchi Liu

81 ***The MADS-Box Transcription Factor EjAGL65 Controls Loquat Flesh Lignification via Direct Transcriptional Inhibition of EjMYB8***
Hang Ge, Yan-na Shi, Meng-xue Zhang, Xian Li, Xue-ren Yin and Kun-song Chen

91 ***Potential Association of Reactive Oxygen Species With Male Sterility in Peach***
Yaming Cai, Zhishen Ma, Collins Otieno Ogutu, Lei Zhao, Liao Liao, Beibei Zheng, Ruoxi Zhang, Lu Wang and Yuepeng Han

103 ***Genomic Characterization of the Fruity Aroma Gene, FaFAD1, Reveals a Gene Dosage Effect on γ-Decalactone Production in Strawberry (Fragaria × ananassa)***
Youngjae Oh, Christopher R. Barbey, Saket Chandra, Jinhe Bai, Zhen Fan, Anne Plotto, Jeremy Pillet, Kevin M. Folta, Vance M. Whitaker and Seonghee Lee

117 ***Autophagy Is Required for Strawberry Fruit Ripening***
José F. Sánchez-Sevilla, Miguel A. Botella, Victoriano Valpuesta and Victoria Sanchez-Vera

131 ***The Roles of Floral Organ Genes in Regulating Rosaceae Fruit Development***
Jia-Long Yao, Chunying Kang, Chao Gu and Andrew Peter Gleave

frontiers in Plant Science

EDITORIAL
published: 20 January 2022
doi: 10.3389/fpls.2021.837300

Editorial: Rosaceae Fruit Development and Quality

Chunying Kang[1,2]*, *Jia-Long Yao*[3], *Zhongchi Liu*[4] *and Yuepeng Han*[5]

[1] Key Laboratory of Horticultural Plant Biology (Ministry of Education), Huazhong Agricultural University, Wuhan, China, [2] Hubei Hongshan Laboratory, Wuhan, China, [3] The New Zealand Institute for Plant and Food Research Ltd, Auckland, New Zealand, [4] Department of Cell Biology and Molecular Genetics, University of Maryland, College Park, MD, United States, [5] Key Laboratory of Plant Germplasm Enhancement and Specialty Agriculture, Wuhan Botanical Garden, The Innovative Academy of Seed Design, Chinese Academy of Sciences, Wuhan, China

Keywords: Rosaceae, fruit development, fruit ripening, metabolites, post-harvest, database

Editorial on the Research Topic

Rosaceae Fruit Development and Quality

Rosaceae is a large angiosperm family consisting of ∼3,000 species, which contains many economically important fruit crops, such as apple, pear, peach, strawberry, apricot, and cherry. These crops are grown worldwide and provide humans with diverse foods and essential nutrition. There exist a series of fundamental biological questions to address in fruit crops, for instance, the regulation of ripening, aroma and flavor, etc. With the advances of high throughput sequencing and other genomics technologies, it becomes possible to investigate the basic regulatory mechanisms underlying fruit specific biological processes. This Research Topic showcases exciting findings in Rosaceae fruits ranging from male sterility, fleshy fruit development, fruit ripening, metabolite biosynthesis, to post-harvest quality regulation.

Male sterility is a valuable agronomic trait utilized for hybrid crops. In peach, male sterility also frequently occurs. To better understand the underlying reasons, the cytological and physiological changes during microspore development were carefully investigated in the male sterile variety "Jinxiang," a popular yellow flesh peach cultivar in China (Cai et al.). The study found that an increase in reactive oxygen species (ROS) levels along with a decrease in antioxidant levels may cause abnormal development of microspores and tapetum, resulting in male sterility in peach.

In flower development, the four whorls of floral organs were specified by the coordination of ABCE class genes. Many studies showed that these floral identity genes also play important roles in fruit development. Yao et al. summarized recent advances on this aspect, with an emphasis on findings in apple, pear and strawberry.

Fruit ripening can be grouped into two types, climacteric and non-climacteric. The former type is mainly controlled by the hormone ethylene and has been extensively studied. However, the mechanism of non-climacteric ripening is not well-known. Fruit ripening in strawberry undergoes a typical non-climacteric ripening process. Bai et al. summarized the central roles of the ABA-controlled ripening mainly using strawberry as a model. The interactions of ABA with ethylene, IAA, polyamines, and sugars were discussed. In addition, this review also discussed the involvement of ABA in the ripening of climacteric fruit. Besides hormones, autophagy also takes part in fruit ripening. Autophagy is a catabolic and recycling pathway that maintains cellular homeostasis under normal growth and stress conditions. Sánchez-Sevilla et al. discovered autophagy-related structures and expression of autophagy-related genes (*ATG*) in the fruit flesh cells of strawberry. Furthermore, fruit ripening was delayed by blocking autophagy either biochemically or genetically.

Fruit size, flavor, and aroma are important characteristics of fruit quality. In apple, a bud sport mutant with larger fruit was previously identified. Bu et al. found that the content of free auxin

OPEN ACCESS

Edited and reviewed by:
Meng Li,
Nanjing Agricultural University, China

***Correspondence:**
Chunying Kang
ckang@mail.hzau.edu.cn

Specialty section:
This article was submitted to Plant Development and EvoDevo, a section of the journal Frontiers in Plant Science

Received: *16 December 2021*
Accepted: *29 December 2021*
Published: *20 January 2022*

Citation:
Kang C, Yao J-L, Liu Z and Han Y (2022) Editorial: Rosaceae Fruit Development and Quality. Front. Plant Sci. 12:837300. doi: 10.3389/fpls.2021.837300

was increased and expression levels of several auxin pathway genes were altered in the fruit of the bud sport mutant, suggesting that auxin plays an important role in increasing fruit size. Strawberry fruit is rich in volatile compounds. One of these compounds, γ-decalactone (γ-D), has the greatest contribution to the characteristic fruity aroma in strawberry. Previous study revealed that γ-D biosynthesis is controlled by a single gene *FaFAD1*, but the exact mutations occurring in different strawberry varieties remained unknown. Oh et al. uncovered the genomic variations of *FaFAD1,* determined a positive effect of *FaFAD1* allele dosage on the γ-D content by employing the bacterial artificial chromosome (BAC) library in cultivated octoploid strawberry, and developed genetic markers for breeding strawberry cultivars with high volatile contents.

To identify important loci regulating different physiological and fruit quality traits in peach, a multi-locus genome wide association study (GWAS) was performed using 620 individuals (da Silva Linge et al.). Dozens of quantitative trait nucleotides (QTNs) were identified and validated, which would support the development of DNA tools for peach breeding. García-Gómez et al. characterized the fruit quality traits and measured the contents of main metabolites, and then generated and analyzed transcriptomes of fruit flesh at three developmental stages during ripening of two apricot varieties, which differ in fruit color, soluble solid content, and firmness. With the combination of these data, *Carotenoid Cleavage Dioxygenase 4* (CCD4) and *Sucrose Synthase* (SS) were identified as the candidate genes of the light yellow/white fruit color and high soluble solid content during the ripening process.

Optimal postharvest treatments are critical for maintaining fruit quality. Loquat (*Eriobotrya japonica*) fruit flesh accumulates lignins when the fruit suffers chilling injury during postharvest storage. Ge et al. revealed a new regulatory step during this process. They found that the MADS-box protein EjAGL65 could bind to and inhibit the activity of the promoter of *EjMYB8*, encoding a positive regulator of lignin biosynthesis. Under excessive postharvest chilling, expression of *EjAGL65* is reduced and *EjMYB8* becomes active, which leads to accumulation of unwanted lignins.

Availabilities of high-quality reference genomes and transcriptome data are valuable resources for both basic and applied researches. Li et al. summarized the progresses on the latest genome assemblies and annotations of major Rosaceae crop species and provides a list of websites hosting these data. This review is a useful guide to researchers working in the fields of Rosaceae fruits.

AUTHOR CONTRIBUTIONS

CK prepared the first draft of this editorial. J-LY, ZL, and YH revised the editorial. All authors approved the editorial for publication.

FUNDING

This work was supported by the National Key Research and Development Program of China (2018YFD1000102, 2019YFD1000800), National Natural Science Foundation of China (31822044), and PFR Growing Futures Fund.

Conflict of Interest: Author J-LY was employed by company the New Zealand Institute for Plant and Food Research Ltd.

The remaining authors declare that the research was conducted in the absence of any commercial or financial relationships that could be construed as a potential conflict of interest.

Publisher's Note: All claims expressed in this article are solely those of the authors and do not necessarily represent those of their affiliated organizations, or those of the publisher, the editors and the reviewers. Any product that may be evaluated in this article, or claim that may be made by its manufacturer, is not guaranteed or endorsed by the publisher.

frontiers in Plant Science

ORIGINAL RESEARCH
published: 19 August 2020
doi: 10.3389/fpls.2020.01269

Analysis of Metabolites and Gene Expression Changes Relative to Apricot (*Prunus armeniaca* L.) Fruit Quality During Development and Ripening

*Beatriz Ester García-Gómez, David Ruiz, Juan Alfonso Salazar, Manolo Rubio, Pedro José Martínez-García and Pedro Martínez-Gómez**

Departamento de Mejora Vegetal, CEBAS-CSIC, Murcia, Spain

OPEN ACCESS

Edited by:
Jia-Long Yao, The New Zealand Institute for Plant and Food Research Ltd, New Zealand

Reviewed by:
Ke Cao, Zhengzhou Fruit Research Institute (CAAS), China
Carlos H. Crisosto, University of California, Davis, United States

***Correspondence:**
Pedro Martínez-Gómez
pmartinez@cebas.csic.es

Specialty section:
This article was submitted to Plant Development and EvoDevo, a section of the journal Frontiers in Plant Science

Received: *13 May 2020*
Accepted: *04 August 2020*
Published: *19 August 2020*

Citation:
García-Gómez BE, Ruiz D, Salazar JA, Rubio M, Martínez-García PJ and Martínez-Gómez P (2020) Analysis of Metabolites and Gene Expression Changes Relative to Apricot (Prunus armeniaca L.) Fruit Quality During Development and Ripening. Front. Plant Sci. 11:1269. doi: 10.3389/fpls.2020.01269

Apricot (*Prunus armeniaca* L.) is a valuable worldwide agronomical crop, with a delicious fruit highlighted as a functional food with both nutritional and bioactive properties, remarkably beneficial to human health. Apricot fruit ripening is a coordinated developmental process which requires change in the expression of hundreds to thousands of genes to modify many biochemical and physiological processes arising from quality characteristics in ripe fruit. In addition, enhancing fruit and nutraceutical quality is one of the central objectives to be improved in the new varieties developed by breeding programs. In this study we analyzed the contents of main metabolites linked to the nutraceutical value of apricot fruits, together with the most important pomological characteristics and biochemical contents of fruit during the ripening process in two contrasted apricot genotypes. Additionally, the gene expression changes were analyzed using RNA-Seq and real time qPCR. Results showed that genes with differential expression in the biosynthetic pathways, such as phenylpropanoids, flavonoids, starch and sucrose and carotenoid metabolism, could be possible candidates as molecular markers of fruit quality characteristics for fruit color and soluble solid content. The gene involves in carotenoid metabolism *carotenoid cleavage dioxygenase 4*, and the gene *sucrose synthase* in starch and sucrose metabolism were identified as candidate genes in the ripening process for white skin ground color and flesh color and high soluble sugar content. The application of these candidate genes on marker-assisted selection in apricot breeding programs may contribute to the early selection of high-quality fruit genotypes with suitable nutraceutical values.

Keywords: apricot, RNA-Seq, qPCR, fruit quality, ripening, reference genomes, functional analysis, candidate genes

INTRODUCTION

Apricot (*Prunus armeniaca* L.) is an ancient domesticated crop that has co-evolved with human civilization. This stone fruit species have been used for its edible fruits, also being highlighted as a functional food with both nutritional and bioactive properties, including anti-oxidant and anti-inflammatory activity (Sochor et al., 2010; Erdogan-Orhan and Kartal, 2011; Minaiyan et al., 2014). Today, apricots are commercially produced in 65 countries around the world. During the 2016/2017 season, the worldwide production of apricots increased reaching 4.25 million tons (http://www.fao.org/faostat/en/#home), Spain being the first top fresh apricot exporter worldwide, exporting 56 thousand tons (http://www.fepex.es/inicio.aspx). Apricot is a member of the *Prunus* genus inside the highly diverse Rosaceae family and seems phylogenetically closer to *P. armeniaca* than *P. persica* (Mowrey and Werner, 1990; Zhang et al., 2012; García-Gómez et al., 2018).

Apricot fruit ripening is a coordinated developmental process which requires change in the expression of hundreds to thousands of genes to modify many biochemical and physiological processes. Apricot fruit displays a high variability, giving rise to a great diversity in fruit size, shape, color, taste, aroma, firmness, and ripening date; most of these pomological characteristics are of interest for improving quality traits in apricot breeding programs. Fruit ripening leads to the breakdown of complex carbohydrates into sugars, reduces fruit firmness, color changes, decrease titratable acidity as well as an increase in flavor and aroma (Infante et al., 2008; Klee and Giovannoni, 2011). Understanding these mechanisms will enable implementing agronomical strategies that are more adaptable to climatic conditions and optimizing the selection of new apricot varieties with high quality and nutraceutical values. From the point of view of the consumers, these characteristics contribute to increase the attractiveness and acceptance of new apricot cultivars enriched in phenylpropanoids, carotenoids, and other nutraceutical compounds highly beneficial for human health (Machlin, 1995; Van den Berg et al., 2000; Bazzano et al., 2002).

The development and application of High-Throughput Sequencing (HTS) technologies and the existence of new methods of data analysis, which enable finding associations between genomic, transcriptomic and phenomics, have become the new tools applied by breeders to develop new improved varieties. The remarkable advances in computational theory and bioinformatics algorithms have greatly accelerated the implementation of this technology, significantly expanding the scope of studied species. As a result, during the last few years, up to 450 plant genomes were sequenced (October 2019, http://www.ncbi.nlm.nih.gov). From these genomes, 93 are assembled and annotated in the Kyoto Encyclopedia of Genes and Genomes (KEGG), KEGG Orthology (KO), ENZYME, Pathway and InterPro database (Phytozome version 12.1.6, http://phytozome.jgi.doe.gov), including the most important crops with high commercial value as maize, potato, rice, or wheat (Jiao and Schneeberger, 2017).

Another point of attention about the application of HTS technologies to plant breeding programs remains to address the dynamic and adaptive aspect of gene expression over time, and location undergoes in different scenarios because of the environment effect, developmental stage, tissue/organ location, and genotype. Quantitative and qualitative changes in gene expression are studied by transcriptomic disciplines, mRNA sequencing (RNA-Seq) being the best method for measuring and comparing gene expression levels. Although RNA-Seq has become a widely applied analytical technique, there is no consensus on which pipeline is the most appropriate for the analysis of RNA-Seq experiments. The final determination as to which is the best depends on the strategy adopted during the experimental design according to the initial hypothesis or the objectives (Conesa et al., 2016). If the studied organism genome or transcriptome is available, it will be used to identify the transcripts by mapping. On the other hand, the analysis of transcriptomes of non-model organisms whose genomic or transcriptomic sequences are not publicly available can be addressed using the genomes or transcriptomes of phylogenetically related organisms or by performing a *de novo* assembly and gene annotation (Surget-Groba and Montoya-Burgos, 2010). The application of quality controls during each of the phases of the analysis guarantees both the reproducibility and the reliability of the results obtained (MacManes, 2014).

To date, the dynamic changes in gene expression during fruit ripening process have been studied by whole transcriptome sequencing using HTS technologies in many related apricot species from *Prunus* genus including *P. persica* (Zhang et al., 2010; Wang et al., 2013; Pan et al., 2015; Sanhueza et al., 2015; Zhou et al., 2015; Pan et al., 2016; Wu et al., 2017; Ye et al., 2019), *P. salicina* (Kim et al., 2015b; Fang et al., 2016), *P. armeniaca* (Jo et al., 2015; Zhang et al., 2017b; Zhang et al., 2019), *P. mume* (Du et al., 2013; Xu et al., 2014), and *P. avium* (Alkio et al., 2014; Wei et al., 2015)

The objective of this study was the analysis of gene expression changes of fruits in two contrasted apricot genotypes during development and ripening process by using RNA-Seq and qPCR to identify candidate genes responsible for the fruit differences found between the two assayed genotypes in relation to the pomological characteristics and biochemical and metabolite contents.

MATERIALS AND METHODS

Plant Material and Experimental Design

Plant material consisted on two apricot genotypes 'GC 2-11' and 'GC 3-7', both selections obtained from the cross between the North American cultivar 'Goldrich' (G) and the Spanish cultivar 'Currot' (C) (García-Gómez et al., 2018). These apricot releases showed contrasted fruit quality characteristics. 'GC 2-11' is self-compatible, early blooming, and has an intermediate-sized oblong fruit with yellow skin, red blush, and yellow flesh color. It has high soluble solid content and a low ethylene production rate. 'GC 3-7' is also self-compatible, early blooming, and has an intermediate-sized oblong fruit with orange skin, intense red blush, and light orange flesh color. It has a low-medium total soluble solid content and a medium ethylene production rate.

The sampling was carried out the epicarp (including the pericarp and the mesocarp) due to the importance of considering all the edible fruit for assessing the supplementation of health promoter compounds in the diet. Besides, in the case of apricots, it is imperative to emphasize that peel and pulp are consumed together as an edible portion in contrast with other fruits such as peaches. These apricot selections were cultivated in the same experimental orchard of CEBAS-CSIC at Cieza (Murcia, South-East Spain, 241 m above sea level, lat. 38°16′N, long. 1°16′W) according to standard apricot orchard management. Ten fruits of each genotype were collected at three different ripening stages before stone hardening from both genotypes for RNA-Seq (during the first year of study) and qPCR analysis (during the second year) based on their skin ground color and firmness: green fruit (Stage A), during color change (Stage B), and at physiological ripening (Stage C) (**Figure 1**).

Evaluation of Pomological Characteristics and Biochemical Contents

Pomology characteristics were analyzed including physical characterization (fruit weight, stone weight, skin ground color, flesh color, blush color, and firmness), biochemical compounds (total soluble solids, titratable acidity, and metabolite content), total chlorophyll and carotenoid content, CO_2 and ethylene release. First, ten fruits were collected at three different ripening stages (green fruit, during color change, and at physiological ripening) of both genotypes ('GC 2-11' and 'GC 3-7') in 2016 for the evaluation of fruit quality characteristics. Fruit and stone weight was measured using a Blauscal digital balance (model AH-600), with an accuracy of 0.01 g. Skin ground color, blush color, and flesh color were determined with a Minolta Chroma Meter (CR-300; Minolta, Ramsey, NJ, USA) tri-stimulus color analyzer calibrated to a white porcelain reference plate using a CIELAB scale with color space coordinates L*, a*, and b*. The measure used to assess color was the Hue angle [H° = arctangent (b*/a*)], determined around the equatorial fruit (Brown and Walker, 1990). We take into account that values above 90 are closer to white, between 80 and 90 to yellow, 75 and 80 to light orange, 70 and 75 to orange, and below 70 the color tends to be more reddish. Firmness was quantified using a Lloyd press (model LR10K; Fareham, Hants, UK) by a compression test in Newton (N). Total soluble solid content (TSS) was measured as percentage using a hand-held refractometer (ATAGO Co. LTD., Tokyo, Japan). Finally, the titratable acidity (TA) was expressed as the predominant organic acid, malic acid (g/100 ml). TA was evaluated by titrating 2 g of sample diluted in 30 ml of distilled water with 0.1 mol l-1 NaOH to pH 8.1 by an automatic titration system. On the other hand, total chlorophyll (*a* and *b*) and carotenoid contents were determined by the method of Nagata and Yashita (1992) from a pool of ten fruit pericarps at three ripening stages (green fruit, during color change, and at physiological ripening) of both genotypes ('GC 2-11' and 'GC 3-7') in 2017. Three biological replicates for each ripening stage and genotype were analyzed. The dry residue from the lyophilized powder was dissolved in acetone:hexane (2:3) in a 1:10 w/v relation, centrifuged at 3,000 g for 10 min in a refrigerated centrifuge at 4°C and spectrophotometrically determined at 663, 645, 505, and 453 nm. Respiration rate and ethylene release were measured for each sample by placing two or three whole fruits in a sealed glass jar at 20°C per triplicate.

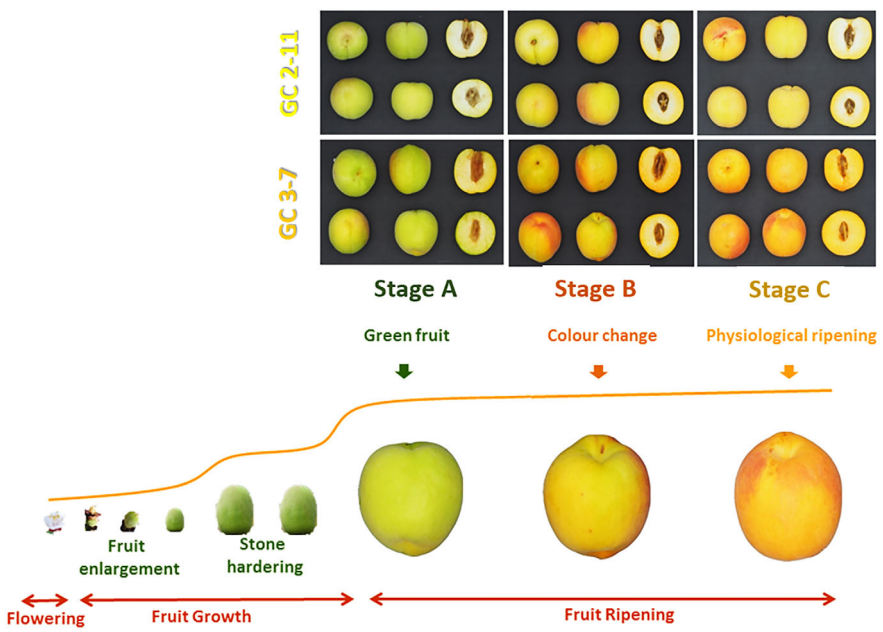

FIGURE 1 | Fruit pictures from *P. armeniaca* fruit genotypes 'GC 2-11' and 'GC 3-7' analyzed in three different ripening stages including green fruit (Stage A), during color change (Stage B), and at physiological ripening (Stage C). Pictures were taken in a cold chamber illuminated with white leds. The photographic camera was an Olympus Pen Mini E-PM2 with 14–42 mm focus lens.

Ethylene concentrations in the glass jar were sampled and monitored with a Perkin Elmer Autosystem gas chromatograph equipped with a thermal conductivity detector (TCD) and a flame ionization detector (FID). Respiration rate was determined by measure CO_2 sampled and monitored by using a gas analyzer (Horiba Via 510, Irving, USA). Samples of 1 ml of headspace gas were taken from each glass jar with a calibrated syringe.

Evaluation of Metabolite Contents

Metabolite content was determined by nuclear magnetic resonance spectroscopy (^{1}H-NMR) from a pool of ten fruits (pericarp portion) at three ripening stages (green fruit, during color change, and at physiological ripening) of both genotypes ('GC 2-11' and 'GC 3-7') in 2016. Portions from this pool (10 g) were frozen in liquid nitrogen, lyophilized, and powdered. The dry residue was dissolved in 0.75 ml of CD_3OD and 0.75 ml of D_2O phosphate buffer containing sodium 3-trimethylsilyl-[2,2,3,3-D4]-propionate (TSP) (0.1% w/w) as internal standard (150 mM), vortex 1 min, centrifuged at 17,000 *g* 5 min and preserve the supernatant at room temperature. The ^{1}H-NMR spectra of aqueous apricot extracts were recorded at 27°C on an AVANCE III HD 500 MHz, CryoProbe Prodigy BBO (Capitani et al., 2012). Carbohydrates (sucrose, glucose, xylose, fructose, and *myo*-inositol), organic acids (fumarate, malate, succinate, citrate, and formate) and precursors of phenylpropanoids (chlorogenate, epicatechin, and methyl nicotinate) were measured. Three biological replicates for each ripening stage and genotype were analyzed.

Phenotype Data Analysis

Statistical analysis was performed in R version 3.5.1. Levene Test was applied for homoscedasticity, Shapiro–Wilk for normal distribution and Kruskal–Wallis Sum Rank Test as an alternative non-parametric ANOVA test. The statistical significance threshold was set at p-value < 0.05. Principal Component Analysis (PCA) was also performed over the phenological and metabolite content data to reduce the dimensionality retaining, thus identifying related groups, trend, or outliers. PCA graph was computed and visualized in R with the package ggbiplot (Wickham, 2016). A correlation matrix by the Spearman method was executed to resolve the correlation relationships between the quality traits analyzed.

RNA Isolation and High-Throughput Sequencing

A pool of ten fruits (pericarp) at three ripening stages (green fruit, during color change, and at physiological ripening) and genotype ('GC 2-11' and 'GC 3-7') were collected during the first year of study, frozen in liquid nitrogen and stored at −80°C. Total RNA was extracted using a modified PowerPlant RNA Isolation Kit® (Qiagen, Hilden, Germany) treated with DNAse On-Spin Column DNase I Kit (Qiagen, Hilden, Germany). Finally, RNA was concentrated and purified with UltraClean Plant RNA Isolation Kit (Qiagen, Hilden, Germany). The purity and quantity of total RNA samples were assessed using a NanoDrop® One Spectrophotometer (Thermo Scientific, Wilmington, USA) and normalized at the same concentration (0.5 μg, 50 ng/μl). Integrity was established by capillary electrophoresis in 2100 Bioanalyzer System (Agilent, Santa Clara, U.S.A.) (Schroeder et al., 2006). Three biological replicates were assayed for each comparison of genotype and stage. RNA samples were sent to Sistemas Genómicos (Valencia, Spain) for library preparation and RNA sequencing. RNA-Seq libraries are prepared from total RNA using poly(A) enrichment of the mRNA. mRNA enriched libraries were sequenced using the HiSeq™2000 Sequencing System platform (Illumina, San Diego, CA, USA), with two technical replicates each sample. The datasets generated for this study can be found in the NCBI SRA repository as a Bioproject entitled 'Prunus armeniaca fruit ripening process', with the accession number PRJNA562811 (https://www.ncbi.nlm.nih.gov/bioproject/562811). The quality control of raw sequencing libraries obtained was analyzed with FastQC version 0.11.7 (Andrews, 2010) (https://www.bioinformatics.babraham.ac.uk/projects/fastqc/). Trimmomatic version 0.38 (Bolger et al., 2014) (http://www.usadellab.org/cms/?page=trimmomatic) was used for trimming adapter and filter low-quality sequences (Phred score < 30) of FASTQ files.

Transcriptome Analysis and Mapping

Reference mei (*P. mume*_V1) (Zhang et al., 2012), peach (*P. persica*_ V2) (Verde et al., 2017), and apricot (*P. armeniaca*_V1) (Jiang et al., 2019) genomes and transcriptomes were simultaneously used as reference sequences for read analysis and mapping our candidates genes. However, for functional candidate gene analysis, studies were focused on mei and apricot reference genomes. Indeed, a synteny between reference genomes was plotted by dot-plot graph executed in D-Genies webpage (Cabanettes and Klopp, 2018) (http://dgenies.toulouse.inra.fr/) to certify the validity of this step. For the backward step, the annotation of *P. armeniaca* was download from GDR (rosaceae.org), having blast information of the whole list of genes (mrna) of the species. The file was parsed, and the already identified IDs of *P. mume* and *P. persica* in the first step were used as identifier to get the list of genes from *P. armeniaca* associated with them. In the case of genes not identified, their sequences were mapped using gmap (Wu and Watanabe, 2005) to the reference genome of apricot and physical position (coordinates), and candidates genes were extracted by a custom python script. If no IDs were identified, at least physical position of these candidates genes are known. Doing this second step avoid to re-do the whole analysis, taking advances of the new resources and allowing also to validate the obtained results, as can been observed. High-quality sequencing libraries were mapped to the references genomes and transcriptomes of *P. persica* and *P. mume* with Tophat version 2.1.1 (Kim et al., 2013) (https://ccb.jhu.edu/software/tophat/index.shtml) and HISAT version 2.1.0 (Kim et al., 2015a) (https://ccb.jhu.edu/software/hisat2/index.shtml). Each genome was indexed with Bowtie version 2.3.4.1 (Langmead and Salzberg, 2012) (https://sourceforge.net/projects/bowtie-bio/). Finally, gene quantification and count matrix construction were performed with featureCounts (Liao et al., 2014) (http://bioinf.wehi.edu.au/featureCounts/). The results obtained were normalized to

Transcript Per Million (TPM) (Li et al., 2010). In addition, representation of nucleotide abundance and other statistical data on mapped and unmapped reads in Sequence Alignment Map and Binary Alignment Map (SAM and BAM files) were analyzed by using SAMStat version 1.5.1 (Lassmann et al., 2010) (http://samstat.sourceforge.net). The index used to determine the quality of alignment and assembly was the Mapping Quality Score (MAPQ) (Li et al., 2008), which quantify the probability of a misplaced read. The optimum MAPQ value is considered to be greater than or equal to 30. SAMtools version 1.8 (Li et al., 2009) (http://samtools.sourceforge.net/) is the tool used to transform, index and sort the files generated by the mappers according to the needs of the protocol.

Differentially Expressed Genes Analysis

Several statistical packages developed in R version 3.5.1 were employed for Differentially Expressed Genes Analysis (DEGs). For DEG analysis were applied five different statistical packages setting on default parameters: edgeR version 3.24.0 (Robinson et al., 2010), baySeq version 2.16.0 (Hardcastle and Kelly, 2010), EBSeq version 1.22.0 (Leng et al., 2015), NOISeq version 2.26.0 (Tarazona et al., 2015) and DESeq2 version 1.22.1 (Love et al., 2014). In most of the analysis Trimmed Mean of M-values (TMM) (Robinson and Oshlack, 2010) were applied, except for EBSeq, where median normalization was applied. As biological replicates, we grouped the samples from each genotype (three replicates each 'GC 2-11' and 'GC 3-7') and ripening stage (two replicates each stage A, stage B and stage C). The DEG analysis was filtered by 0.1 false discovery rate (FDR) (Benjamini and Hochberg, 1995) and the DEGs obtained in each method were merged in a consensus result (Costa-Silva et al., 2017). The consensus result was represented as Venn diagrams done with the web application Venn Diagram (http://bioinformatics.psb.ugent.be/webtools/Venn/).

Gene Annotation, Enrichment Analysis, and Pathway Visualization

Gene Annotation was performed with BiomaRt version 2.38.0 in R (Durinck et al., 2009), which provides easy access to public databases repositories as Ensembl, KEGG, KO, Uniprot, Pfam, Panther, Interpro and Gene Ontology (GO). We also added the best hits found in biomaRt for Arabidopsis (*Arabidopsis thaliana* L.) and peach, by Basic Local Alignment Search Tool (BLAST) (https://blast.ncbi.nlm.nih.gov/Blast.cgi). Enrichment Analysis was plotted with Web Gene Ontology Annotation Plot (WEGO) (http://wego.genomics.org.cn/) web-based tool (Ye et al., 2018) was used for visualizing, comparing, and plotting GO annotation results in a bar chart. Singular Enrichment Analysis (SEA) in AgriGO version 2.0 (Tian et al., 2017) was used to plot GO hierarchical graph containing all statistically significant terms. Broader representation of GO terms was performed on GO Consortium web-based platform (Ashburner et al., 2000; Consortium, 2004). DEGs were plotted on their KEGG biosynthetic pathways with GAGE version 2.32.0 (Luo et al., 2009), and visualized with Pathview version 1.22.0 (Luo and Brouwer, 2013), both R packages.

Weighted Gene Co-expression Network Analysis

For clustering DEGs, we perform Weighted Gene Co-expression Network Analysis (WGCNA) with the R package WGCNA version 1.66 (Zhang and Horvath, 2005; Langfelder and Horvath, 2008). WGCNA is useful for describing the correlation patterns among gene expression across RNA-Seq experiments. The eigengene modules (ME) are obtained using automatic network construction function blockwise. The clustered gene trees were created following the average method (Wilks, 2011). Cluster analysis by gene expression is typically the first step in data analysis, reducing the complexity and dimensionality of the data, predict functions or identify shared regulatory mechanism based on specific features. So, the genes within a ME have similar expression pattern than the genes in different modules, revealing the natural data structures and gaining some initial insights regarding data distribution (Jiang et al., 2004).

Complementary Gene Expression Analysis by quantitative real-time PCR

RNA-Seq experiment was validated by using RT-qPCR in a complementary experiment. New plant material collected during the second year from a pool of ten fruit pericarps, with three replicates for each ripening stage and genotype. Total RNA was extracted following the same protocol detailed above (RNA isolation and High-Throughput Sequencing). Specific primers were designed with Primer3 software based on apricot sequencing libraries (**Supplementary Data Sheet 1**) or from bibliography references as *carotenoid cleavage dioxygenase 4* (*CCD4*), *sorbitol dehydrogenase* (*SDH*), *alcohol acyltransferase* (*AAT*), *sucrose synthase* (*SS*) and *β-galactosidase* (*BGAL*) (Adami et al., 2013; Pirona et al., 2013). The cDNA was synthesized with SuperScript III Reverse Transcriptase (Thermo Fisher Scientific). RT-qPCR experiments were conducted in One Step Plus real-time PCR system (Applied Biosystems). For all RT-qPCR reactions, a 10 µl mix was made including 5 µl Power SYBR® Green PCR Master Mix (Applied Biosystems), 0.5 µl of each primer (5 µM) and 2 µl of cDNA (2.5 ng/µl). The genes from peach *18S rRNA* (*S18*) (Rasori et al., 2002); and plum *cyclophilin 1* (*CYP1*) *ribosomal protein L12* (*RPL12*) and *ubiquitin* (UBI) (Niu et al., 2014) were analyzed as candidate reference genes by RefFinder web-based tool (Xie et al., 2012) (no longer available). Analysis was run with default settings. Amplification conditions were 10 min at 95°C, followed by 40 cycles of 15 seconds (s) at 95°C, 1 min at 60°C, and for melt curve 15 s at 95°C, 1 min at 60°C and increasing 0.3°C till 0.15 s at 95°C. Normalized Relative Quantification (NRQ) for the genes of interest was calculated using the modified $2^{-\Delta\Delta Ct}$ method (Pfaffl, 2001; Vandesompele et al., 2002). Correlations between TPM and NRQ, and TPM and metabolite content were calculated using the Pearson correlation coefficient (Udvardi et al., 2008). Three biological replicates and two technical replicates were assayed.

RESULTS

Evolution of Pomological Characteristics and Biochemical and Metabolite Contents of Apricot Fruit During the Ripening Process

The results obtained from the evaluation of pomological characteristics and biochemical and metabolite contents in fruits for both apricot genotypes at the three ripening stages were analyzed to identify significant statistical differences between genotypes and stages (**Tables 1** and **2**).

Evaluation of pomological traits evidenced the fruit color of 'GC 2-11' (yellow skin, red blush, and yellow flesh color) and 'GC 3-7' (orange skin, intense red blush and light orange flesh color) with a bigger fruit and stone. Values of firmness, however, were similar at the end of the ripening process (**Table 1**). In addition, biochemical evaluation showed a higher soluble solid content and a low ethylene production rate in 'GC 2-11' with a higher content of carotenoids in 'GC 3-7'. Values of acidity and chlorophyll contents, however, were similar at the end of the ripening process (**Table 1**).

On the other hand, evolution of metabolite contents showed the clear increase of sucrose, glucose, xylose, fructose and myo-inositol associated with the decrease of fumarate, malate, succinate, and citrate in both genotypes during the ripening process mainly between the stages B and C. When genotypes are compared, a higher content of chlorogenate is shown in all the assayed stages in 'GC 3-7' in comparison with 'GC 2-11' (**Table 2**).

Levene Test showed no homoscedasticity and Shapiro–Wilk Test showed no normal distribution of the pomological, biochemical and metabolite data, hence we applied the non-parametric Kruskal–Wallis Rank Sum Test with a threshold of p-value < 0.05 for significant statistical differences. Skin ground color, blush color and flesh color, stone weight, fruit weight, titratable acidity, and ethylene release showed statistical differences between genotypes and ripening stages (**Supplementary Table 1**). Glucose, fructose, malate, citrate,

TABLE 1 | Evaluation of fruit pomological characteristics and biochemical contents in the two apricot genotypes assayed 'GC 2-11' and 'GC 3-7' at three ripening stages including green fruit (Stage A), during color change (Stage B), and at physiological ripening (Stage C).

Stage	Stage A		Stage B		Stage C	
Genotype	'GC 2-11'	'GC 3-7'	'GC 2-11'	'GC 3-7'	'GC 2-11'	'GC 3-7'
Fruit weight (g)	52.12 ± 2.18	61.37 ± 2.29	54.98 ± 3.85	69.59 ± 3.91	59.26 ± 3.30	83.85 ± 4.46
Stone weight (g)	4.22 ± 0.22	5.04 ± 0.31	3.57 ± 0.06	4.56 ± 0.22	3.35 ± 0.11	4.21 ± 0.08
Skin ground color (H°)	111.52 ± 1.84	111.21 ± 1.69	102.72 ± 2.49	89.79 ± 6.56	95.20 ± 2.88	77.07 ± 2.93
Blush color (H°)	97.9 ± 3.59	90.8 ± 16.4	81.26 ± 13.3	64.42 ± 7.21	74.10 ± 9.00	63.88 ± 5.60
Flesh color (H°)	105.33 ± 2.84	105.96 ± 3.63	94.18 ± 18.4	86.13 ± 14.50	87.40 ± 3.21	76.69 ± 1.63
Firmness (N)	232.99 ± 36.21	288.11 ± 24.40	76.70 ± 11.05	114.80 ± 19.63	39.07 ± 8.56	40.10 ± 24.94
Total soluble solids (%)	12.3 ± 0.2	6.8 ± 0.2	14.8 ± 0.2	11.9 ± 0.4	14.1 ± 0.3	12.8 ± 0.8
Titratable acidity (malic acid g/100 ml)	2.11 ± 0.01	2.06 ± 0.04	1.98 ± 0.01	2.04 ± 0.10	1.78 ± 0.02	1.89 ± 0.05
CO2 (µl/kg h)	13.46 ± 1.49	9.12 ± 1.37	10.58 ± 5.84	11.42 ± 3.22	7.08 ± 2.44	15.08 ± 5.05
Ethylene (mg/kg h)	–	–	1.15 ± 1.07	1.44 ± 0.91	0.15 ± 0.10	37.86 ± 19.90
Chlorophyll a (mg/g FW)	5.34 ± 1.36	19.33 ± 0.70	1.95 ± 0.01	2.81 ± 0.28	0.29 ± 0.24	0.38 ± 0.21
Chlorophyll b (mg/g FW)	0.21 ± 0.34	1.5 ± 0.06	0.17 ± 0.20	0.11 ± 0.33	0.59 ± 0.42	0.10 ± 0.46
Carotenoids (mg/g FW)	6.22 ± 0.23	33.02 ± 5.81	59.47 ± 0.98	37.79 ± 2.17	15.88 ± 0.98	57.61 ± 1.29

Three biological replicates were assayed.

TABLE 2 | Evaluation of metabolite contents recorded in ^{1}H-NMR spectra in the two apricot genotypes assayed 'GC 2_11' and 'GC 3_7' 7'at three ripening stages including green fruit (Stage A), during color change (Stage B), and at physiological ripening (Stage C).

Stage	Stage A		Stage B		Stage C	
Genotype	'GC 2-11'	'GC 3-7'	'GC 2-11'	'GC 3-7'	'GC 2-11'	'GC 3-7'
Sucrose	19.370 ± 2.790	2.638 ± 0.098	36.494 ± 1.499	31.387 ± 5.782	40.128 ± 1.379	46.965 ± 10.990
Glucose	3.017 ± 0.407	15.588 ± 0.914	3.530 ± 0.083	15.951 ± 2.776	5.639 ± 0.123	11.128 ± 2.346
Xylose	0.185 ± 0.044	0.210 ± 0.017	0.251 ± 0.011	0.250 ± 0.027	0.309 ± 0.014	0.225 ± 0.053
Fructose	0.317 ± 0.042	3.440 ± 0.463	0.510 ± 0.214	1.346 ± 0.647	0.527 ± 0.033	1.521 ± 0.737
Myo-Inositol	0.292 ± 0.040	0.384 ± 0.023	0.364 ± 0.013	0.461 ± 0.081	0.402 ± 0.020	0.404 ± 0.101
Fumarate	0.006 ± 0.001	0.004 ± 0.000	0.008 ± 0.000	0.009 ± 0.001	0.011 ± 0.000	0.014 ± 0.003
Malate	3.754 ± 0.852	4.761 ± 0.373	3.086 ± 0.469	4.387 ± 0.301	3.023 ± 0.069	3.544 ± 0.611
Succinate	0.019 ± 0.002	0.008 ± 0.005	0.009 ± 0.001	0.026 ± 0.003	0.009 ± 0.011	0.016 ± 0.004
Citrate	5.309 ± 2.299	11.106 ± 0.141	2.854 ± 0.155	13.641 ± 2.061	3.456 ± 0.338	6.943 ± 2.425
Formate	0.0001 ± 0.001	0.006 ± 0.001	0.005 ± 0.000	0.001 ± 0.001	0.005 ± 0.001	0.001 ± 0.001
Chlorogenate	0.049 ± 0.003	0.128 ± 0.022	0.045 ± 0.006	0.199 ± 0.032	0.056 ± 0.004	0.077 ± 0.027
Epicatechin	0.009 ± 0.007	0.014 ± 0.0001	0.009 ± 0.001	0.018 ± 0.001	0.014 ± 0.004	0.016 ± 0.006
Methyl nicotinate	0.012 ± 0.006	0.023 ± 0.009	0.013 ± 0.004	0.019 ± 0.007	0.011 ± 0.006	0.016 ± 0.004

Metabolites identified were expressed in mg/g fresh fruit weight (FW). Three biological replicates were assayed.

formate, chlorogenate, and methyl nicotinate show statistical differences only between genotypes. Sucrose, xylose, fumarate, chlorophyll *a*, soluble solids, carotenoid content, and firmness showed statistical differences only between ripening stages. CO_2 releases, *myo*-inositol, succinate, epicatechin, chlorophyll *b* show no statistical differences between genotypes or ripening stages (**Supplementary Table 2**). In addition, Spearman correlation matrix (**Supplementary Figure 1** and **Supplementary Data Sheet 2**) showed a positive correlation between skin ground color, flesh color, blush color, chlorophyll content and firmness, and between sucrose and soluble solid content, while a negative correlation between sucrose and soluble solids with skin ground color, flesh color, blush color, firmness and chlorophyll content. Glucose also showed a positive correlation with phenylpropanoids (chlorogenate, epicatechin, and methyl nicotinate). Fumarate displayed a negative correlation with firmness, skin ground color, blush color, flesh color, while a positive correlation with soluble solids was also observed.

On the other hand, PCA representation of phenological traits and metabolite content (**Figure 2**) showed the relationship between variables after logarithmic transformation of the data. The main principal components obtained explained the variance of 42.6% for Principal Component 1 (PC1) and 33.9% for PC2. Samples by genotype cluster together. Genotype 'GC 2-11' showed a positive correlation, while 'GC 3-7' displays a negative correlation with PC2. Stage A in both genotypes has a negative correlation while stage C has a positive correlation with PC1. Variables as skin ground color, blush color, flesh color, soluble solids and ethylene release were highly explained by PC1, while fructose, citrate, and malate were mainly explained by PC2. Therefore, PC1 mostly explained variance associated with fruit color and ripening stage represented by ethylene

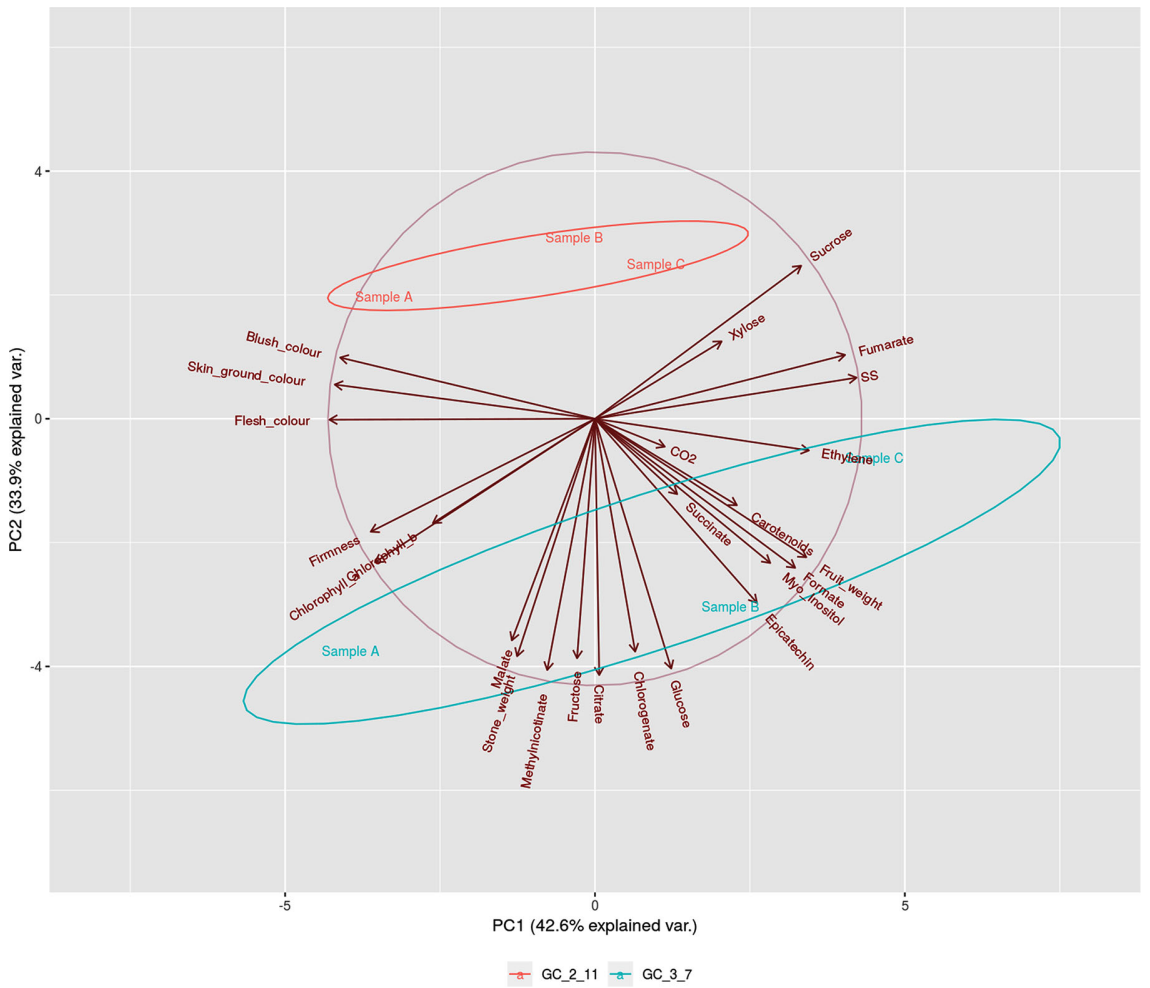

FIGURE 2 | PCA biplot of phenological traits (fruit weight, stone weight, skin ground color, blush color, flesh color and firmness), biochemical (Total soluble solids, Titratable acidity, CO2, Ethylene, Chlorophyll *a*, Chlorophyll *b*, and Carotenoids) and metabolite (Sucrose Glucose, Xylose, Fructose, Myo-Inositol, Fumarate, Malate, Succinate, Citrate, Formate, Chlorogenate, Epicatechinand Methyl nicotinate) contents during ripening process [green fruit (Sample A), during color change (Samble B), and physiological ripening (Sample C)] in the two genotypes of *P. armeniaca* 'GC 2-11' and 'GC 3-7'. Ellipses round samples which belongs to the same group with a 0.68 of probability (default settings for continuous variables). Three biological replicates were assayed to evaluate each phenological, biochemical and metabolite parameter.

release and soluble solid content, while PC2 explained variance associated with acid taste represented by the content of citrate, malate, and fructose.

Sequenced Libraries Quality Control

Sequenced raw read libraries analyzed with FastQC (**Supplementary File 1**) showed poor quality sequencing in 3′ and 5′ ends, with several repeated *k*-mers in forward reads as well as a deficient Phred quality score along the entire length of the reverse reads, with a high degree of repeatability and presence of *k*-mers. An acceptable number of duplication sequences, *k*-mer occurrence or GC percentage are organism-specific, and these values must be homogeneous in all samples which belong to the same experiment (Conesa et al., 2016). The high repeatability of the genomes in plants makes tough filter the sequences without losing valuable information, so it was decided to trim the reads with low-quality or presence of very repetitive sequences, suspected of being residual Illumina adapters. After removing these fragments, the quality of the sequenced libraries was analyzed again with FastQC (**Supplementary File 2**).

Mapping of Whole Transcriptomes

Optimized sequencing libraries were then aligned and assembled with HISAT and TopHat to the reference genomes and transcriptomes of *P. persica* and *P. mume* (**Supplementary Figure 3**, **Supplementary Tables 3** and **4**). The percentage of total pairs of reads mapped to the genomic sequences is higher than to the transcriptomes. When we attend to the differences between species, the assembly and alignment of total pairs of reads to *P. mume* are higher compared to *P. persica*, arising 88.36% mapped pairs of reads to *P. mume* genome performed with HISAT as the best result. Initially, alignment and assembly of total pairs of reads with HISAT lead to a higher percentage of mapped pairs of reads, but also a higher percentage of mapped pairs of reads aligned discordant or in multiple locations. TopHat was more conservative in this sense, avoiding pairs of reads that align discordantly or in multiple sites, so the pairs of reads mapped once with TopHat were higher than those obtained with HISAT.

A comparison between the different MAPQ values on mapping strategies addressed showed 84.62% of mapped reads with a MAPQ ≥ 30, employing *P. mume* genome as reference sequence performed with HISAT as the best result. In opposition, we only get 67.70% of mapped reads using *P. persica* transcriptome as reference sequence with TopHat as the worst result (**Supplementary Figure 4**, **Supplementary Tables 5** and **6**). The best results were the alignment and assembly to the *P. mume* genome using TopHat (82.15%), HISAT to the *P. mume* transcriptome (79.48%), and TopHat to the *P. mume* transcriptome (77.99%). HISAT was selected as the most efficient mapper in terms of percentage of reads aligned with high MAPQ values. Considering the sequence used as the reference sequence, the mapped reads to *P. mume* were higher than *P. persica*. Thus *P. mume* genome is chosen as the reference sequence, which best fits our data.

The assemblies obtained were evaluated for accuracy with SAMStat to determine the quality of the alignments. An average of 51.7 million pairs of reads was generated from the six samples sequenced. The assembly to *P. mume* genome performed with HISAT was filtered by mapping quality score (MAPQ ≥ 30), removing unmapped or multi-mapped reads with SAMtools.

Differentially Expressed Genes Analysis

Count matrix of mapped reads to *P. mume* genome was performed with featureCounts, getting the number of assigned or unassigned reads to features (annotated genes). Unassigned features were likely to align to non-coding genomic regions or unannotated genes (**Supplementary Table 7**). This was the proposed strategy to group the samples that presented greater similarity. So, Euclidian distance matrix of gene expression was calculated after the normalization of each library (**Supplementary Table 8**), and the results were plotted in a heatmap, complemented with a multidimensional scaling plot (MDS) and a correlation matrix chart (**Supplementary Figure 5**). The higher correlation was obtained among the samples that belong to the same genotype, being 'GC 2-11' the genotype, which shows less distance between its samples. Inside each sample, the higher distance was found between stage A and stage C.

DEG analysis was performed grouping the samples as biological replicates by genotype or ripening stage (**Supplementary Table 9A**). In the analysis without replicates (**Supplementary Table 9B**), these were simulated on the assumption that read counts follow a multinomial distribution as NOISeq does. Since version 1.20, DESeq2 did not perform statistical analysis without replicates, DEGs were obtained by logarithmic transformation of the count matrix and selection of genes with fold change values over a range of ±1.5.

After DEG analysis with five different statistical packages, the results obtained were merged in a consensus result with common genes. Consensus results were plotted in a Venn diagram, where only the comparison between genotypes was of interest because of the number of genes differentially expressed for downstream analysis, arising from 443 DEGs (**Figure 3** and **Supplementary Data Sheet 3**). As consequence of the backward step from this set of 443 DEGs, 310 of the total were identified with an *P. amerniaca* IDs (**Figure 3** and **Supplementary Data Sheet 3**, column C). In addition, for the rest of 133 IDs with an unknown IDs from *P. armeniaca*, the backward mapping allowed the identification of 85 of them (**Figure 3** and **Supplementary Data Sheet 3**, column C). Only a total of 48 genes remained without a specific ID from the reference apricot genome but with a physical position on the genome (**Supplementary Data Sheet 4**).

Gene Annotation, Enrichment Analysis, and Pathway Visualization

To elucidate the fundamental processes altered in ripe apricot fruit, we searched for functional enrichment categories in the set of DEGs obtained identifying homologous genes between mei, peach, and Arabidopsis (**Supplementary Data Sheets 5** and **6**). Enrichment analysis (**Figures 4** and **5**) was performed over up- and down-regulated DEGs obtained in contrast to grouping samples by genotype. The keynote GO terms were annotated in Molecular Function and Biological Process (**Supplementary Table 10**). Plotting up-regulated and down-regulated DEGs in a

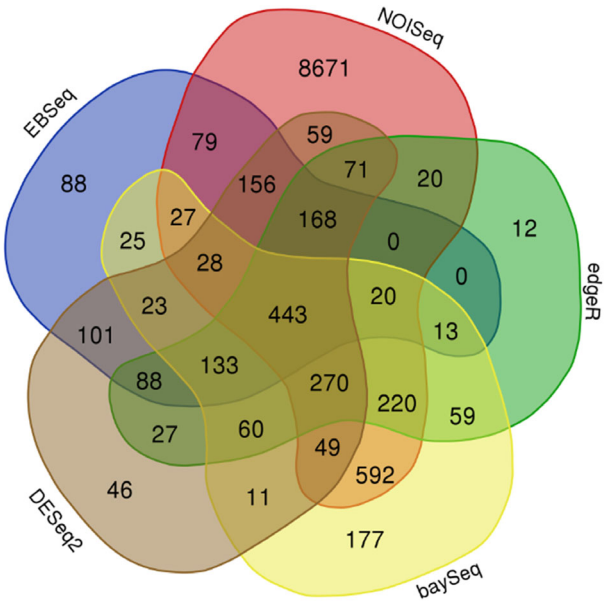

FIGURE 3 | Venn diagram which represents the consensus result obtained from Differentially Expressed Genes Analysis (DEGs) performed on *P. mume*, grouping the samples by genotype and using different statistical packages including NOISeq, edgeR, baySeq, DESeq2, and EBSeq. Three biological replicates and two technical replicates were assayed for each comparison of genotype and stage.

bar chart for Molecular Function GO annotation, DEGs up-regulated are mainly involved in ligase activity, isomerase activity, lyase activity, sulfur compound binding, carbohydrate binding, lipid binding, amide binding, pattern binding, receptor regulatory activity, and peroxidase activity; while DEGs down-regulated are implied in metal cluster binding and enzyme regulator activity. GO terms annotated in Biological Process are up-regulated for glycosylation, catabolic process, secretion by cell, maintenance of location in cell, cellular homeostasis, macromolecule organization, cellular localization, maintenance of location, regulation of biological quality, response to biotic stimulus, response to stress, response to external stimulus, and response to other organisms. On the other side, down-regulated DEGs were annotated in pigment metabolic process and cellular component organization. DEG genes annotated are implicated in catalytic activity (72.2%), followed by binding (25.0%), transcription regulator activity (6.8%), and transporter activity (2.3%). Most of these genes belong to the metabolic process (74.7%). When we analyzed the organic metabolic process affected, significant annotations were macromolecule metabolic process (36.8%), carbohydrate metabolic process (26.3%), organic acid metabolic process (15.8%), and organic cyclic compound metabolic process. Singular enrichment analysis (SEA) for Biological Process indicates protein phosphorylation and drug transmembrane transport as main GO terms, for Molecular Function highlights catalytic and transport activity (**Supplementary Figure 6**).

DEGs annotated in KEGG biosynthetic pathways were mainly located in glycolysis/gluconeogenesis (pmum00010), pentose and glucuronate interconversions (pmum00040) starch and sucrose metabolism (pmum00500), terpenoid biosynthesis (pmum00130), carotenoid biosynthesis (pmum00906), phenylalanine metabolism (pmum00360), phenylpropanoid biosynthesis (pmum00940), flavonoid biosynthesis (pmum00941), and cyanoamino acid metabolism (pmum00460) (**Supplementary File 3**). The most affected pathways are phenylpropanoid and flavonoid biosynthesis (**Figure 6**), followed by starch and sucrose, and phenylalanine metabolism (**Supplementary Figure 7**).

Weighted Gene Co-Expression Network Analysis

We got seven ME after WGCNA including blue, brown, turquoise, red, black, green and yellow (**Figure 7**). A total of 443 genes were clustered in these seven ME. When we analyze each ME, 80 genes belong to ME blue, 49 genes to ME brown, 226 genes to ME turquoise, 17 genes to ME red, 17 genes to ME black, 25 genes to ME green, and 29 genes to ME yellow (**Supplementary Data Sheet 7**). Additionally, we analyzed the principal KEGG pathways involved in fruit ripening for each ME (**Supplementary Data Sheet 8**) and other genes of interest not annotated on KEGG pathways but described in other databases. For significant correlation in ME with quality characteristics, we set a threshold over 0.5 for correlation coefficient and under 0.5 for *p*-value statistical significance.

ME blue was positively correlated with xylose and negatively correlated with fruit weight, stone weight, CO_2 release, glucose, fructose, citrate, formate, chlorogenate, epicatechin, and methyl nicotinate. Cluster in this ME we find the genes of starch and sucrose metabolism *LOC103322685* (*PARG04316m02*; EC:2.4.1.14), *LOC103333663* (*PARG19611m01*; EC:3.1.3.12), *LOC103338042* (unknown PARG ID; EC:3.1.3.12) and *LOC103343477* (*PARG01655m01*; EC:3.2.1.21), phenylpropanoid biosynthesis pathway *LOC103332355* (unknown PARG ID; EC:4.3.1.24), *LOC103335298* (*PARG29723m01*; EC:1.1.1.324), *LOC103338042* (unknown PARG ID; EC:3.2.1.21), *LOC103339178* (unknown PARG ID; EC:1.14.14.91) and *LOC103343477* (*PARG01655m01*; EC:3.2.1.21), phenylalanine metabolism *LOC103332355* (unknown PARG ID; EC:4.3.1.24) and *LOC103339178* (unknown PARG ID; EC:1.14.14.91), *LOC103338042* (EC:3.2.1.21; unknown PARG ID) and *LOC103343477* (EC:3.2.1.21; *PARG01655m01*) and flavonoid biosynthesis *LOC103339178* (EC:1.14.14.91; unknown PARG ID). Other genes of interest are *LOC103329206* (*PARG00063m07*) predicted as a pheophytinase, and *LOC103328016* (*PARG00063m07*) as ABC transporter pleiotropic drug resistance (PDR).

ME brown showed a positive correlation with blush color while a negative correlation with fruit weight, stone weight, glucose, fructose, *myo*-inositol, malate, citrate, formate, chlorogenate, epicatechin, and methyl nicotinate. Cluster in this ME we find genes of starch and sucrose metabolism *LOC103326244* (*PARG10672m01*; EC:3.2.1.21) and *LOC103327693* (*PARG15761m01*; EC:3.2.1.26), phenylalanine metabolism

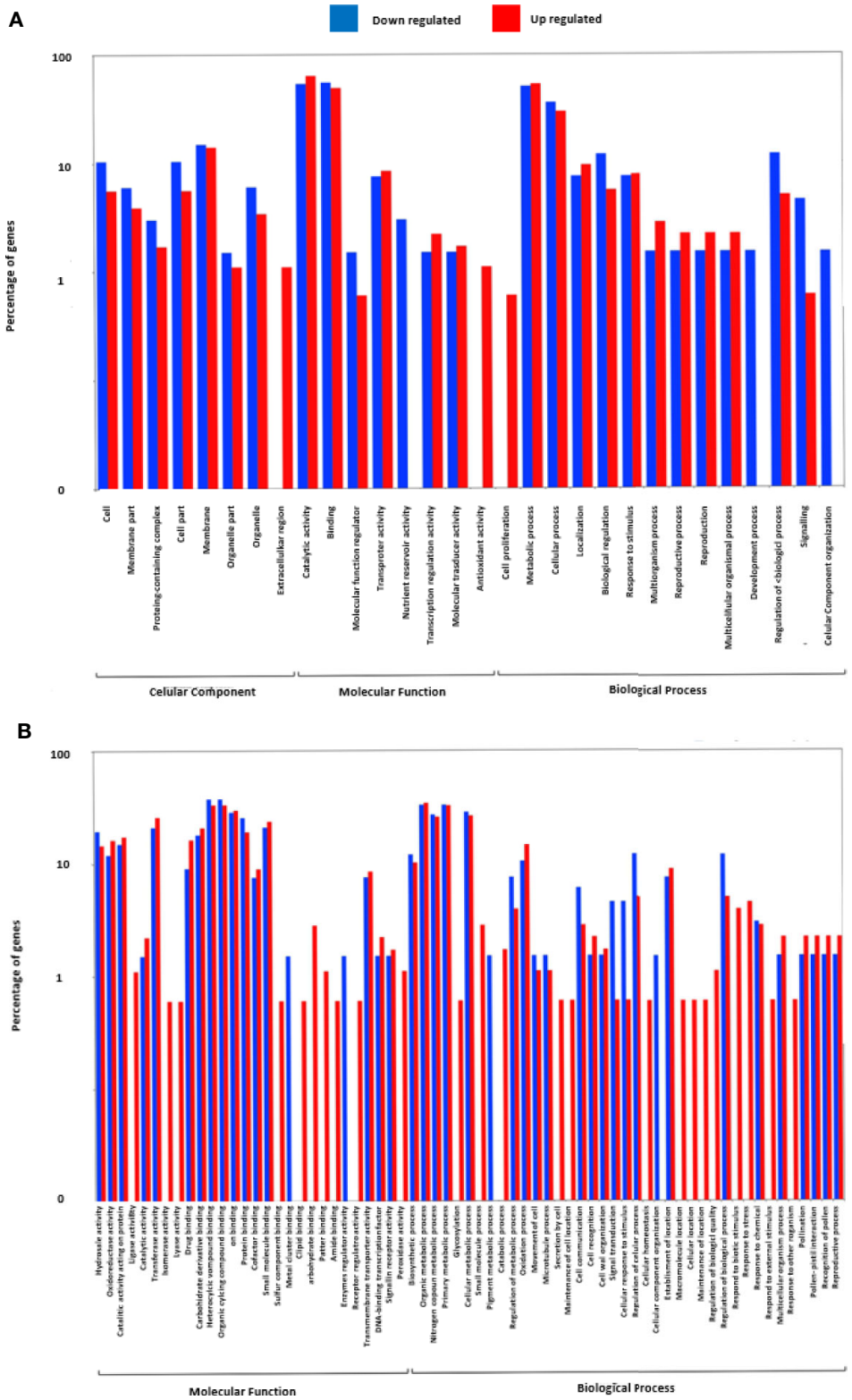

FIGURE 4 | Gene Ontology term enrichment of DEGs found in contrast grouping by genotype. **(A)** Up- and down-regulated DEGs annotated with GO terms. **(B)** Up- and down-regulated DEGs annotated in Molecular Function. Three biological replicates and two technical replicates were assayed for each comparison of genotype and stage.

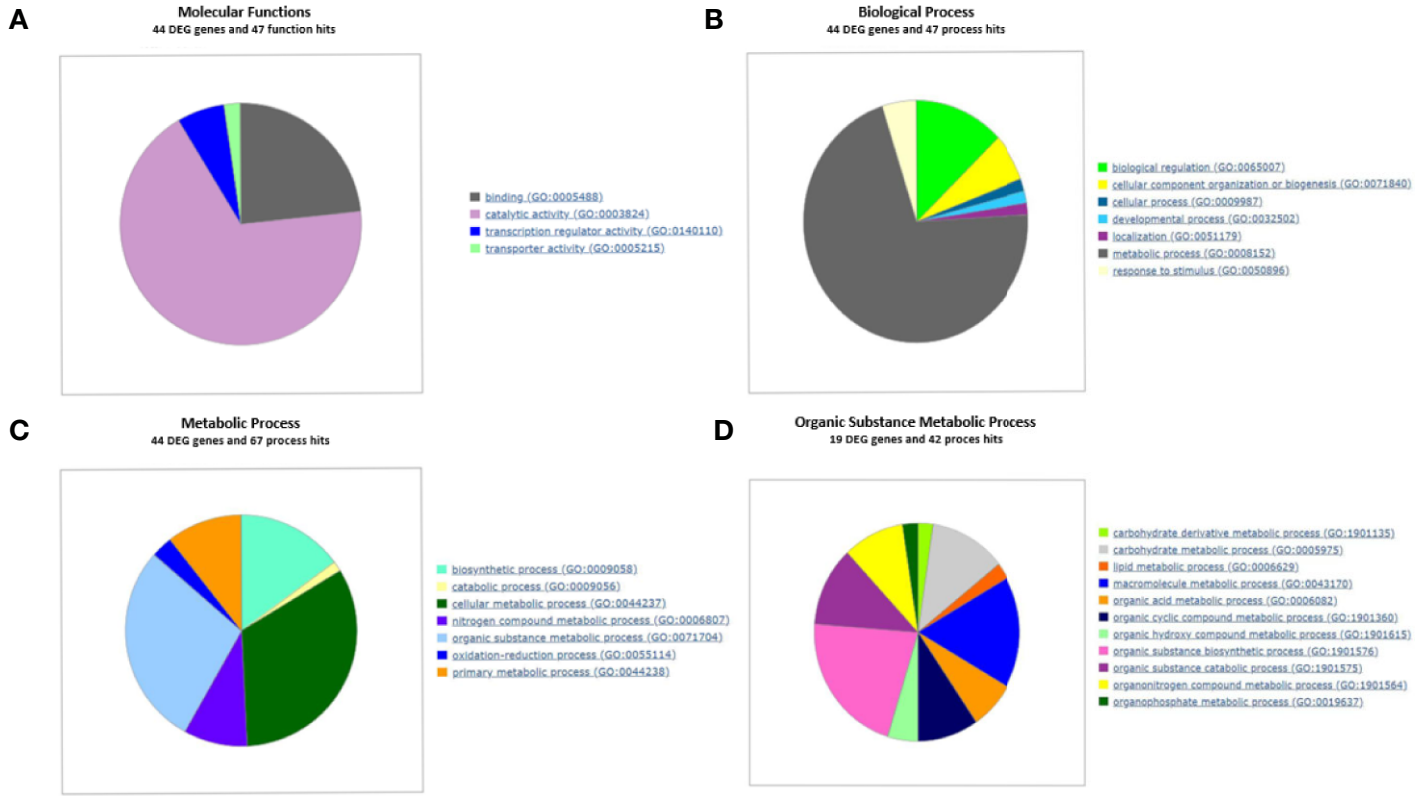

FIGURE 5 | Gene Ontology term enrichment of DEGs found in contrast grouping by genotype for different ontology levels. **(A)** DEGs genes annotated with GO Slim into Molecular Function term. **(B)** DEGs annotated with GO Slim into Biological Process term. **(C)** DEGs annotated with GO Slim into Metabolic Process term. **(D)** DEGs annotated with GO Slim into Organic substance metabolic process. GO enrichment analysis plot with WEGO and GO Consortium webserver. Three biological replicates and two technical replicates were assayed for each comparison of genotype and stage.

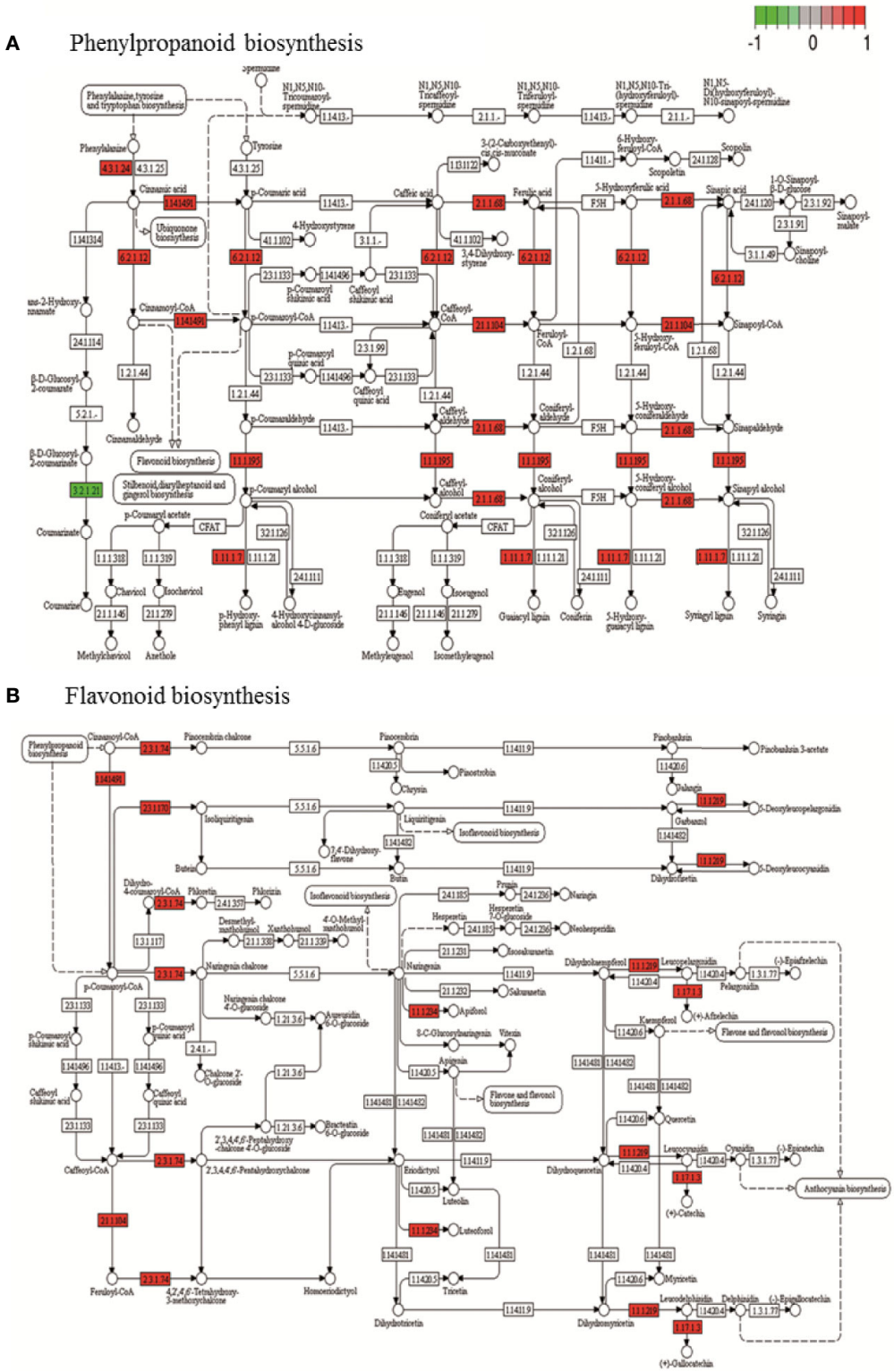

FIGURE 6 | KEGG of phenylpropanoids **(A)** and flavonoid **(B)** biosynthesis pathway with the representation of DEG obtained during genotype contrast in *P. mume* where several genes involved are up-regulated (red) or down-regulated (green) in 'GC 3-7' with respect to 'GC 2-11' genotype. Gene involved in each pathway is represented in small boxes by its Enzyme Commission numbers (E.C.) code. Three biological replicates and two technical replicates were assayed for each comparison of genotype and stage.

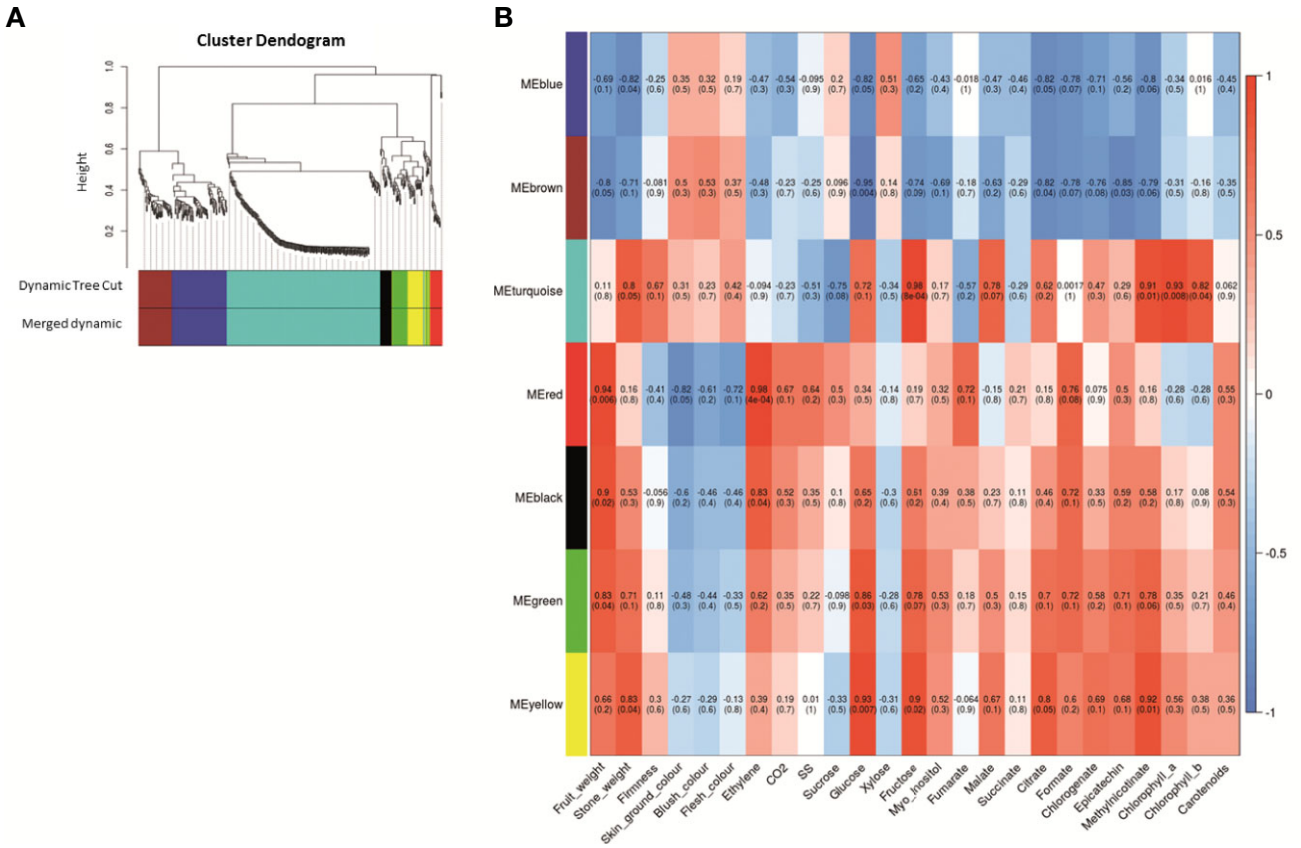

FIGURE 7 | Weighted correlation network analysis during apricot fruit ripening obtained with WGCNA R package. **(A)** Gene dendrogram and module colors obtained by average linkage hierarchical clustering where every leaf represents a DEG. The color row underneath the dendrogram shows the seven eigengene modules (ME) assignments determined by the Dynamic Tree Cut (threshold set for cut the dendrogram and obtain ME clustering). **(B)** Heatmap representation of the eigengene module-quality trait relationship for *P. mume* genotype contrast obtained when analyzing DEG expression and quantitative quality traits. Inside each module the Pearson correlation value is indicated and between parenthesis the *p*-value significance of its correlation. Three biological replicates and two technical replicates were assayed for each comparison of genotype and stage.

LOC103328252 (EC:6.2.1.12; *PARG15135m02*) and *LOC103340770* (EC:2.1.1.104; *PARG27724m01*), phenylpropanoid biosynthesis *LOC103326244* (*PARG10672m01*; EC:3.2.1.21), *LOC103328252* (*PARG15135m02*; EC:6.2.1.12) and *LOC103340770* (EC:2.1.1.104; *PARG27724m01*), and flavonoid biosynthesis *LOC103340770* (EC:2.1.1.104; *PARG27724m01*). Another gene of interest is *LOC103326648* (*PARG22281m01*), predicted as a transcription factor (TF) with MYB/SANT domain, and *LOC103331940* (*PARG18142m01*) predicted as MADS-box protein SOC1.

ME turquoise showed a positive correlation with stone weight, firmness, fructose, glucose, malate, citrate, chlorophylls content, and methyl nicotinate, while a negative correlation with sucrose, soluble solid content, and fumarate. We found several genes related phenylalanine metabolism *LOC103342143* (*PARG02182m01*; EC:4.3.1.24), carotenoid biosynthesis *LOC103328471* (*PARG01425m02*; EC:5.3.99.8), phenylpropanoid biosynthesis *LOC103327307* (*PARG00008m01*; EC:1.11.1.7), *LOC103342143* (*PARG02182m01*; EC:4.3.1.24) and *LOC103343871* (*PARG24274m01*; EC:2.1.1.68), flavonoid biosynthesis *LOC103324315* (*PARG03336m04*; EC:2.3.1.74) and *LOC103341429* (*PARG06615m01*; EC:1.17.1.3), glycolysis and gluconeogenesis *LOC103332280* (*PARG18437m02*; EC:5.1.3.15), and circadian rhythm *LOC103324315* (*PARG03336m04*; EC:2.3.1.74). Other genes of interest were *LOC103323450* (unknown PARG ID) predicted as anthocyanidin 3-O-glucosyltransferase 7-like, *LOC103341429* (*PARG06615m01*) as a leucoanthocyanidin reductase-like, *LOC103322538* (*PARG05244m01*) as probable pectinesterase/pectinesterase inhibitor 35, and *LOC103342143* (*PARG02182m01*) as a phenylalanine ammonia-lyase 1. In addition, other identified genes included the TFs *LOC103327289* (*PARG28632m01*) predicted as MYB108, *LOC103330396* (*PARG12740m01*), *LOC103337200* (*PARG23210m01*) as a probable WRKY TF 45, *LOC107880999* (*PARG12882m01*), *LOC103332564* (*PARG18828m01*), *LOC103323278* (*PARG04365m02*), *LOC103323316* (*PARG04392m03*), and *LOC103323318* (*PARG04392m01*) predicted as ABC transporter-like.

ME red displayed a significant positive correlation with fruit weight, ethylene and CO_2 release, soluble solid content,

fumarate, formate, epicatechin, and carotenoid content, while a negative correlation with skin ground color, flesh color and blush color. We found the gene from starch and sucrose metabolism and phenylpropanoid biosynthesis *LOC103330627* (*PAR G01659m01*; EC:3.2.1.21), and phenylalanine biosynthesis *LOC103329641* (*PARG13381m01;* EC:4.2.1.20). A TF is identified, *LOC103342585* (*PARG26597m01)* as L10-interacting MYB domain-containing protein-like. ME black displayed a positive correlation with stone weight, fruit weight, ethylene and CO_2 release, glucose, fructose, formate, epicatechin, methyl nicotinate, and carotenoids content. The only gene of interest found in this cluster is *LOC103333822* (*PARG04832m02*) as sugar transporter ERD6-like 7.

ME green, however, had a positive correlation with stone weight, fruit weight, ethylene release, glucose, fructose, *myo*-inositol, citrate, formate, chlorogenate, epicatechin, and methyl nicotinate. We find the gene of flavonoid biosynthesis *LOC103320869* (PARG07267m01; EC:1.1.1.219 and 1.1.1.234). Other genes of interest are *LOC103334507* (*PARG20234m01*) predicted as 1-aminocyclopropane-1-carboxylate oxidase homolog 11-like, and *LOC103323820* (*PARG03840m02*) predicted as glutathione transferase GST 23-like.

Finally, ME yellow displayed a positive correlation with stone weight, fruit weight, glucose, fructose, *myo*-inositol, malate, citrate, formate, chlorogenate, epicatechin, methyl nicotinate, and chlorophyll *a* content. In yellow ME, we found a gene involved in phenylpropanoid biosynthesis *LOC103335288* (*PARG29722m01*; EC:1.1.1.324). Other genes of interest are *LOC103324123* (*PARG03642m01*) described as 1-amino cyclopropane-1-carboxylate oxidase homolog 1-like, *LOC103330065* (*PARG13187m01*) as 2-hydroxyflavanone C-glucosyltransferase, *LOC103333172* (*PARG19510m01*) as multidrug resistance protein from MATE family, and *LOC103324364 (PARG00058m01)* predicted as pheophorbide A oxygenase.

Gene Expression Analysis by Quantitative Real-Time PCR

RNA-Seq was validated by analyzing fifteen genes highly expressed through RT-qPCR. According to the analysis run in RefFinder, we obtain a comprehensive gene stability values of 1.141 for *S18*, 1.565 for *CYP1*, 2.28 for *RPL12*, 4.229 for *ACT*, and 4.729 for *UBI*. The lower value of comprehensive gene stability, most stable is the expression of a gene between samples. Then, we use as reference genes *S18*, *RPL12* and *CYP1*, the most stable genes analyzed. These genes were described with *P. persica* and *P. mume* annotation, and most of them are implied in the ripening process (**Supplementary Data Sheet 1**). The samples taken in the course of advanced color change (Stage B) were discarded because of the difficulty to establish effective criteria at sampling and the high variability found in the results obtained. All the genes analyzed have a Pearson correlation coefficient over 0.7 in TPM-NRQ comparison (**Figure 8**), are genome-wide distributed, and most of them are related to quality traits at fruit ripening process. Performing RT-qPCR on a new set of samples gives us the greatest confidence in the results obtained by validating the HTS technology and the underlying biological response.

Candidate Genes Related to Pomological Characteristics and Biochemical and Metabolite Contents in Apricot Fruits

Taking into account the analysis previously accomplished and integrating the results obtained, we proposed a variety of candidate genes for monitoring fruit ripening process linked to quality traits in ripe fruit such as fruit color and soluble solid accumulation.

The most important correlation with significant statistical *p*-value obtained in WGCNA for starch and sucrose metabolism found in ME blue, brown, turquoise and yellow (**Figures 6** and **7**, **Supplementary Data Sheets 5** and **7**). In addition, we found a positive correlation with sucrose, while fructose and sucrose have a negative correlation and *vice-versa* for all the ME cited above. In ME blue, with high negative correlation with glucose, we find a *sucrose-phosphate synthase* (*LOC103322685; PARG04316m02)* which leads to the transformation of D-fructose-6P and UDP-glucose into sucrose-6'P, and two *β-glucosidases* (*LOC103338042* (unknown PARG ID) and *LOC103343477* (*PARG01655m01*). In ME brown, with high negative correlation with glucose, cluster a *β-glucosidase* [*LOC103326244* (*PARG10672m01*)] implied in starch and sucrose metabolism leading to D-glucose, and a *β-fructofuranosidase* [*LOC103327693* (*PARG15761m01*)] which catalyze the dephosphorylation from sucrose into D-glucose and D-fructose. ME turquoise displayed the highest positive correlation with fructose content and lower significant *p*-value due to the presence in this cluster of the gene *glucose-6-phosphate 1-epimerase*, which transforms D-glucose-6P between its two stereoisomers α and β and may lead to β-D-fructose-6P through the *glucose-6-phosphate isomerase*. Sucrose is transported and accumulated into the vacuole by membrane transporter as early-response to dehydration gene (*ERD6*) (Zhang et al., 2019), cluster in ME black. Besides, *SPS1* is up-regulated at the beginning of ripening in 'GC 2-11', while *SS* is up-regulated in 'GC 3-7' at the end of the ripening process (**Figure 8**). When we compared the sucrose content during fruit quality evaluation (**Supplementary Table 2**) and the gene expression of two suspicious genes responsible for sucrose biosynthesis *sucrose synthase* [*SS*, *LOC103340632* (*PARG27579m02*)] and *sucrose-phosphate synthase 1* [*SPS1, LOC103341128* (unknown PARG ID)], Pearson correlation coefficient shows higher positive correlation between sucrose content and *SS* gene expression (Pearson coef.: 0.7) than *SPS1* (Pearson coef.: −0.2) (**Figure 9**), *SS* being a candidate gene for the biosynthesis of sucrose during fruit ripening in apricot.

Several genes related to phenylalanine, phenylpropanoids, and flavonoid biosynthesis, the precursors of anthocyanin compounds, were identified in ME blue, brown, green, yellow, and turquoise (**Figures 6** and **7** and **Supplementary Data Sheets 5** and **7**). In the phenylpropanoid biosynthesis pathway we find two *phenylalanine ammonia lyases* (*PAL, LOC103332355* (unknown PARG ID) and *LOC103342143* (PARG02182m01) which catalyzes the transformation from phenylalanine to

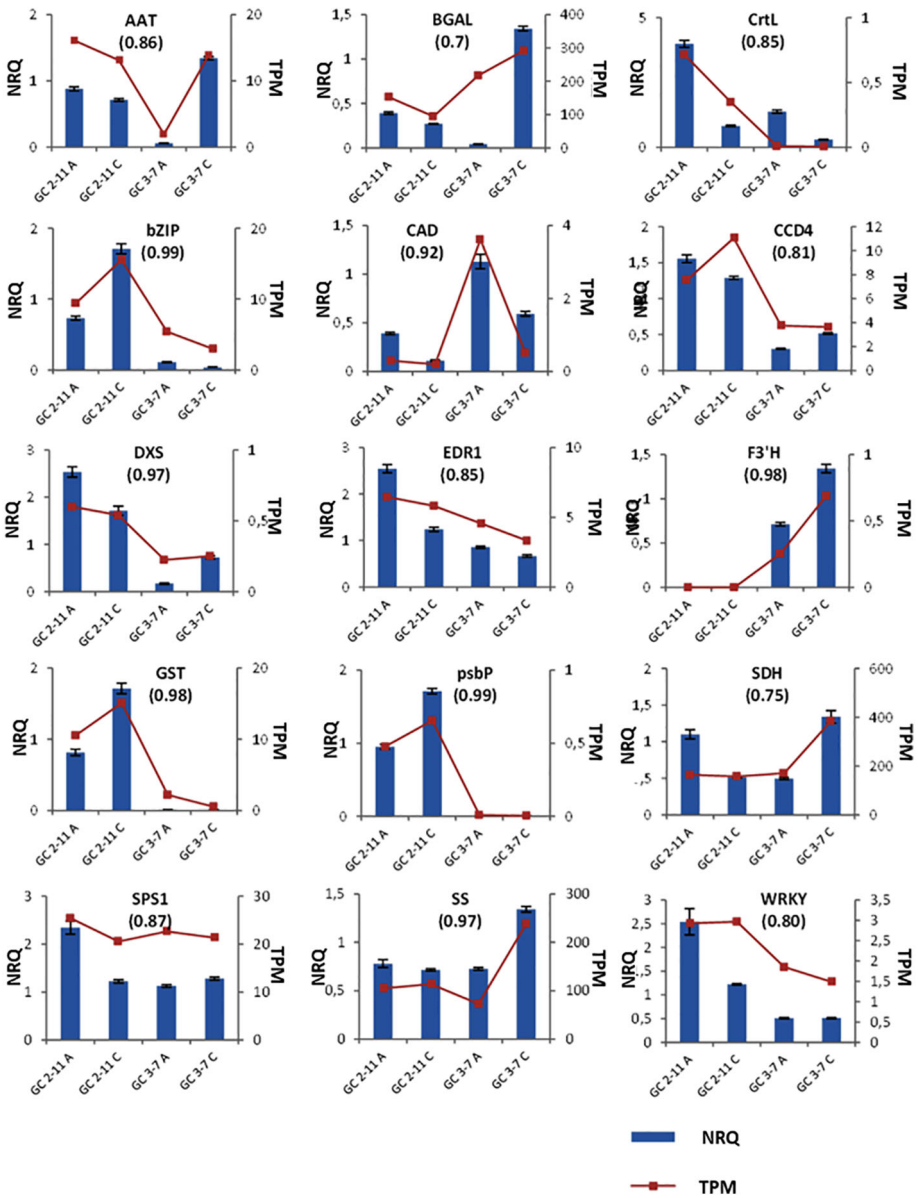

FIGURE 8 | Plots for the NRQ (Normalized Relative Quantification) of 15 genes analyzed by RT-qPCR and each TPM (Transcript Per Million) value obtained in RNA-Seq experiment. In brackets, Pearson correlation coefficient obtained from contrast between TPM and NRQ. From upper left to down right: *Methanol O-anthraniloyl transferase-like* (*AAT*), *β-galactosidase* (*BGAL*), *lycopene β-cyclase* (*CrtL*), *common plant regulatory factor 1-like* (*bZIP*), *cinnamyl-alcohol dehydrogenase* (*CAD*), *carotenoids cleavage dioxygenase 4* (*CCD4*), *1-deoxy-D-xylulose-5-phosphate synthase* (*DXS*), *ethylene transduction gene* (*EDR1*), *flavonoid 3'-hydroxylase 1-like* (*F3'H*), *glutathione transferase GST 23-like* (*GST*), *psbP domain-containing protein 6* (*psbP*), *sorbitol dehydrogenase* (*SDH*), *sucrose-phosphate synthase 1* (*SPS1*), *sucrose synthase* (*SS*) and *probable serine/threonine-protein kinase PBL16* (*WRKY*). Three biological replicates and two technical replicates were assayed. Standard deviations are indicated with vertical bars.

cinnamic acid, a *trans-cinnamate 4-monooxygenase* [*C4H, LOC103339178* (unknown PARG ID)] transforming cinnamic acid to *p*-coumaric acid, a *4-coumarate-CoA ligase 1-like* [*4CL, LOC103328252* (*PARG15135m02*)] catalyzing cinnamic acid or *p*-coumaric acid to cinnamoyl-CoA or *p*-coumaryl-CoA, and in the end of the pathway identified a probable *caffeoyl-CoA O-methyltransferase* [*LOC103340770, PARG27724m01*)] transforming caffeoyl-CoA to feruloyl-CoA. Following with flavonoid biosynthesis pathway, we find the gene for *chalcone/stilbene synthase* [*CHS, LOC103324315* (*PARG03336m04*)] catalyzing the reaction from *p*-coumaroyl-CoA to naringenin chalcone. The last gene implicated on anthocyanin synthesis identified is a bifunctional *dihydroflavonol 4-reductase/flavanone 4-reductase* [*DFR, LOC103320869* (*PARG07267m01*)], which synthesizes leucocyanidin. Other genes of interest not annotated on KEGG pathways are a *leucoanthocyanidin*

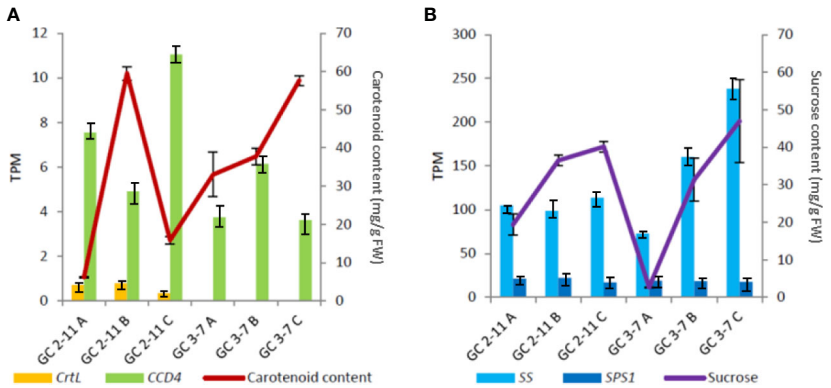

FIGURE 9 | Cross-linked graph of relation between metabolite contents and gene expression obtained in RNA-Seq. **(A)** Relation of carotenoid content with the expression of *capsanthin/capsorubin synthase* or *lycopene β-cyclase* [*CrtL, LOC103328471* (*PARG02182m01*)] and *carotenoid cleavage dioxygenase 4* (*CCD4*). **(B)** Relation of sucrose content with the expression of *sucrose synthase* [*SS, LOC103340632* (*PARG27579m02*)] and *sucrose-phosphate synthase 1* [(*SPS1, LOC103341128* (unknown PARG ID)]. Standard deviations are indicated with vertical bars.

reductase-like [*ANS*, *LOC103341429* (*PARG06615m01*)], leading leucoanthocyanidin, then *anthocyanidin 3-O-glucosyltransferase* [*UFGT*, *LOC103323450* (unknown PARG ID)] convert cyanidin into cyanidin 3-glucoside. *Flavonoid 3'-hydroxylase 1-like* [*F3'H, LOC103337305* (*PARG23256m01*)], a cytochrome P450 responsible for anthocyanin biosynthesis, is up-regulated in 'GC 3-7' (**Figure 8**). Besides, a *glutathione transferase GST 23-like* [*GST*, *LOC103323820* (*PARG03840m02*)], related to the antioxidant system ascorbate-glutathione and degradation of hydrogen peroxide during ripening (Fuentealba et al., 2017) and responsible for organic acid and secondary metabolism compounds translocation into the vacuole (Shiratake and Martinoia, 2007) was differentially expressed in contrast by genotypes in *P. mume* and up-regulated in 'GC 2-11'.

After the analysis of the blush color, this trait showed highest negative (reddish color for lower Hue° values) correlation with ME red (**Figure 7**, **Supplementary Data Sheets 5** and **7**), where we found the gene *LOC103342585* (*PARG26597m01*) as L10-interacting MYB domain-containing protein-like.

ABC and MATE transporters find in ME turquoise, blue, and yellow (**Figure 7** and **Supplementary Data Sheet 5**), were responsible for the transit of many substances like organic acids or secondary metabolism. ATP binding cassette ABC transporters were described as responsible for citrate and malate accumulation. ABC transporters of Multidrug Resistance-associated Protein (MRP) together with glutathione transferases, found one gene in ME green, are described as anthocyanin transporters by the deposition of large amounts of phenolic compounds in vacuoles, being implicated in fruit pigmentation. On the other hand, ABC transporters of Pleiotropic Drug Resistance (PDR) subfamily are responsible for terpenoid transport. Most of these ABC transporters were found up-regulated in 'GC 3-7' (**Supplementary Data Sheet 3**), which display higher levels of citrate, orange flesh and skin ground color, and reddish blush (**Supplementary Tables 1** and **2**). Multidrug and toxin efflux transporters (MATE) family are suggested as responsible for flavonoid and other phenolic compounds transport (Shiratake and Martinoia, 2007), up-regulated in 'GC 3-7' (**Supplementary Data Sheet 3**).

For carotenoids biosynthesis pathway we only identified a *capsanthin/capsorubin synthase* or *lycopene β-cyclase* [*CrtL*, *LOC103328471* (*PARG02182m01*)] in ME turquoise (**Figure 7**, **Supplementary File 3**, **Supplementary Data Sheets 5** and **7**), related to the secondary metabolism of carotenoids by lycopene cyclization, yielding *β*-carotene, which does not correlate with carotenoid content. This gene is up-regulated at the beginning of the ripening process in 'GC 2-11', the light yellow flesh and skin ground color genotype, which is the opposite of what we expect when we take into account that this gene leads the synthesis of *β*-carotene, responsible for the orange color in fruits and the precursor of vitamin A. Going further, we analyze the expression of *carotenoid cleavage dioxygenase 4* (*CCD4*), which has been reported as a carotenoid degradative enzyme responsible for white flesh phenotype in peach. White flesh in peach was described as a monogenic trait controlling *Y* locus ligated to *CCD4* gene expression (Adami et al., 2013); it is up-regulated in 'GC 2-11' (**Figure 8**). It was described in yellow/white peach that carotenoid accumulation in skin ground color and flesh color depends on the expression profile of *lycopene β-cyclase* (*PpLCYB*) and *carotenoid cleavage dioxygenase 4* (*PpCCD4*) (Cao et al., 2017). When we calculated the Pearson correlation coefficient between carotenoid content obtained at fruit quality evaluation (**Supplementary Table 1**) and the gene expression of *CCD4* and *CrtL*, we obtain a negative correlation for *CCD4* (Pearson coef.: −0.71) while a lower correlation with *CrtL* (Pearson coef.: −0.19) taking in account the low expression level for the *CrtL* gene which shows differential expression levels between white fleshed apricot fruits of about 0.5 TPM and yellow flesh of 0 TPM (**Figure 9A**). The coordinate expression of both genes during ripening process caused an increase in the synthesis of carotenoids in both genotypes during color change, followed by a decrease in carotenoid content only

in the light yellow genotype 'GC 2-11', where *CCD4* is up-regulated, the expression of *CCD4* being the major determinant for carotenoid content by degrading β-carotene into apocarotenoid compounds.

As a carotenoid precursor biosynthesis enzyme, we identified *1-deoxy-D-xylulose-5-phosphate synthase* (*DXS*), which catalyzes the fusion of pyruvate and glyceraldehyde-3-phosphate in the 2-C-methyl-D-erythritol 4-phosphate pathway (MEP pathway), yielding 1-deoxy-D-xylulose 5-phosphate (DXP), precursor compound in carotenoid biosynthesis (Brandi et al., 2011). It is found up-regulated in 'GC 2-11'.

Skin ground color and flesh color were negatively correlated with ME green and yellow (**Figure 7**, **Supplementary Data Sheets 5** and **7**), which are also positively correlated with ethylene burst, which is described as the regulator of some genes involved in carotenoid biosynthesis pathways (Marty et al., 2005) (**Supplementary File 3**). Some apricot varieties, as climacteric fruits, release ethylene in the final ripening stages. It has been described that the loss of firmness as a result of the degradation of galactosyl-containing polymers by β-galactosidase, up-regulated in 'GC 3-7' (**Figure 8**), stimulates ethylene release (Kovacs and Nemeth-Szerdahelyi, 2002). We find the genes responsible for ethylene biosynthesis *LOC103334507* (*PARG20234m01*) and *LOC103324123* (*PARG03642m01*), both predicted as *1-aminocyclopropane-1-carboxylate oxidase homolog like* (*ACO*). However, no correlation was found between ethylene release and *ACO* expression even though it was described in apricot that *ACO* was strongly up-regulated during ripening before ethylene production (Mbéguié-A-Mbéguié et al., 1999). The other candidate gene involved in ethylene perception assayed was *Ethylene transduction gene* (*EDR1*), responsible for ethylene response transduction gene at fruit ripening in peach (Wang et al., 2017), and it is up-regulated in 'GC 2-11', which did not produce ethylene. No candidate genes were proposed for ethylene signaling.

Related with loss firmness at ripening process, we found a *pectin methylesterase inhibitor* gene [*PMEI, LOC103322538* (*PARG05244m01*)], cluster in ME turquoise (**Figure 7**, **Supplementary Data Sheets 5** and **7**) and up-regulated in 'GC 2-11' (**Supplementary Data Sheet 3**), with a slow loss of firmness if we compared to 'GC 3-7' (**Supplementary Table 1**). The modification of pectins during ripening resulted in tissue softening and an overall loss of firmness. The inhibition of this enzymatic activity may avoid or retard softening in ripe fruit (Femenia et al., 1998). Another gene assayed was *β-galactosidase* [*BGAL*, *LOC103340681* (*PARG27772m02*)] which induced loss of firmness during ripening by the degradation of galactosyl-containing polymers (Kovacs and Nemeth-Szerdahelyi, 2002) and found up-regulated in 'GC 3-7' at the end of the ripening process. Besides, we analyze the expression of *cinnamyl-alcohol dehydrogenase* [*CAD, LOC103335323* (*PARG29726m01*)], involved in lignin biosynthesis, which may be related to firmness during fruit development (Gabotti et al., 2015; Zhang et al., 2017b). It is up-regulated in 'GC 3-7' at the beginning of the ripening process.

For chlorophyll degradation and color green loss from green to ripe fruit (**Supplementary Table 2**), we found differential expression in genes related with chlorophyll dephytylation in ME blue *LOC103329206* (*PARG00063m07*) as a pheophytinase, and ME yellow *LOC103324364* (*PARG00058m01*) as a pheophorbide A oxygenase (Guyer et al., 2014) (**Figure 7** and **Supplementary Data Sheet 5**). Another gene related with photosynthesis was *psbP domain-containing protein 6* [*psbP*, *LOC103326460* (*PARG10392m01*)]; as part of the photosystem II, *PsbP* increases the affinity of the water oxidation site for chloride ions and provides the conditions required for high-affinity binding of calcium ions (Kochhar et al., 1996). It is differentially expressed in contrast by genotypes in *P. mume*.

Finally, we get some TF as a MADS-box TF found in ME brown (**Figure 7** and **Supplementary Data Sheet 5**), with a major expression in fruit tissues related to fruit development (Xu et al., 2014; Wells et al., 2015). A *common plant regulatory factor 1-like* [*bZIP, LOC103332281* (*PARG18436m04*)], which was a homologous gene of *CPRF1_PETCR* in *Petroselinum crispum* and bind to *chalcone/stilbene synthase* (*CHS*) gene promoter, a key enzyme during anthocyanin biosynthesis, was up-regulated in 'GC 2-11' at the end of the ripening process. Furthermore, a *probable serine/threonine-protein kinase PBL16* (*WRKY*), a plant specific TF that controls environment response to a biotic stimulus, was up-regulated at the beginning of ripening in 'GC 2-11'.

DISCUSSION

Pomological Characteristics and Biochemical and Metabolite Contents in Apricot Fruits

The biosynthesis of carotenoids was responsible for the orange color in the skin ground color and flesh color in both genotypes. In adition, anthocyanins were responsible for the reddish blush color, arise the acquisition of definitive color of the ripe fruit. The content of phenylpropanoids (chlorogenate, epicatechin, and methyl nicotinate), precursors of anthocyanin biosynthesis, showed a slight decrease during the ripening process in 'GC 3-7' while no significant changes in 'GC 2-11'. The principal differences found between genotypes and stages were related to skin ground color, flesh color, and blush color. In genotype 'GC 2-11' the carotenoid content increased during the ripening process reaching the maximum amount during color change, followed by an abrupt decrease at physiological ripening. On the other hand, carotenoid content in genotype 'GC 3-7' undergoes a gradual but constant increase throughout the ripening process, reaching higher levels than 'GC 2-11' at the end of the ripening process. If we pay attention to the skin ground color and flesh color changes, it is correlated with the carotenoid content, while the biosynthesis of phenylpropanoid may be correlated with blush color intensity. Chlorophyll content decreased in both genotypes until it is completely degraded, finishing the ripening process with the total loss of green hue and the acquisition of final light yellow/orange fruit color.

Metabolite evolution of apricot fruits during the ripening process agrees with recent results in peach (Lillo-Carmona et al.,

2020). Total soluble solids measured as a percentage is an approximation to the strength of the solution as the percentage of sucrose in fruit juice, but it was affected by the presence of other solutes, while results of carbohydrate content obtained at ^{1}H-NMR is an accurate and more reliable result. Sucrose and glucose were the major soluble sugars in apricot ripe fruit, reaching the peak of maximum concentration at ripe fruit, higher in genotype 'GC 3-7' than in 'GC 2-11'. At the beginning of the ripening process, glucose content was higher than sucrose, but sucrose content enhanced significantly at the end of ripening, surpassing the amount of glucose in both genotypes. These results represented the pattern of sugar accumulation during the development and ripening of the fruit undergoes from being glucose-predominant to sucrose-predominant at the end of the fruit ripening process.

During the development of apricot fruit, there was a continuous accumulation of organic acids, and their final concentration was determined by the balance between the biosynthesis of organic acids, its degradation, and the vacuolar storage. Malate and citrate were the most abundant organic acids in apricot fruit, and titratable acidity decreases as a result of its degradation during ripening. At green fruit, malate is the predominant compound, whereas the ratio was changing with the rapid increase of citrate at ripening stage when the malate declined at physiological ripening. However, citrate also decreased at the ripening stage; the ratio between citrate and other organic acids increases, becoming the major organic acid at ripe fruit. The significant decrease in citric acid and the small reduction of malic acid contributed to acidity loss. When we compared the amount in organic acids in both genotypes, 'GC 3-7' had higher levels of organic acids than 'GC 2-11', which resumed in higher titratable acidity.

Finally, there was a pronounced release of ethylene and firmness decline. In climacteric fruit, ethylene is the principal ripening trigger, partially responsible for fruit softening rate and carotenoid biosynthesis (Hayama et al., 2006; Kita et al., 2007). In this sense, apricot fruit was described as differentially sensitive to ethylene (Mbeguie-A-Mbeguie et al., 2002). 'GC 3-7' release much more ethylene than 'GC 2-11', which may be related with the faster softening occurred during ripening and the orange fruit color in 'GC 3-7' in contrast with slowly softening and light yellow fruit color in 'GC 2-11'.

Mapping of Whole Transcriptomes

The alignment and assembly of RNA-Seq reads in the non-model organism *P. armeniaca* to the genomes and transcriptomes of *P. persica* and P. *mume* show very different results depending on the protocol applied. A significantly higher percentage of aligned reads with MAPQ ≥ 30 were obtained when we map HISAT to the genome sequence of *P. mume* in comparison with *P. persica*. Although up to now *P. persica* has been used as a model species in the study of the genus *Prunus* sp., this taxon belongs to the subgenus *Amygdalus*, different from the subgenus *Prunus* to which apricot belongs (Potter, 2012). In our case the use of the genome of *P. mume* as a reference sequence owing its closer phylogenetic proximity, because these species belong to the same subgenus *Prunus* and *Armeniaca* section (Potter, 2012), seems an ideal strategy as has been confirmed by the posterior analysis using the reference genome of this species for our backward step. These mapping results were also contrasted with the reference genome of *P. armeniaca*, allowing us the identification of the physical position (coordinates) of candidates genes.

Differentially Expressed Genes and Enrichment in Relation to Pomological Characteristics and Biochemical and Metabolite Contents

There was no agreement on which protocol for DEG identification is the most appropriate, so the consensus among five DEG identification methods guarantees a list of DEGs with more accuracy, sensitivity, and robustness in gene expression estimation reliable results (Costa-Silva et al., 2017). DEGs without replicates will not be considered because they are only useful for exploring the data but will not provide the kind of proper statistical inference on differences between samples or estimate the biological variability of each gene (Love et al., 2014; Conesa et al., 2016; Love et al., 2016).

The DEG identification method was the crucial decision for the differential expression analysis in RNA-Seq data and will be the key to understand the phenotype–genotype variation through the biological interpretation of the data. The confidence in the quantitative analysis depends on this point more than on depth read or read length.

It is essential to include at least three replicates to capture the biological variability between samples. Accordingly, after the exploration of concordance between the samples, we decided to group the samples by genotypes. It means that as DEG analysis result, we obtained those genes differentially expressed in apricot fruit during ripening process among the two genotypes 'GC 2-11' and 'GC 3-7'.

The annotation of DEGs using GO terms as ontologies to represent biological knowledge offered a detailed source for functional transcriptomic studies based on a dynamic, structured, and controlled vocabulary. GO terms provide a classification that covers several domains by developing a comprehensive and computational model of biological systems, ranging from molecular to organism level (Consortium, 2004). Gene Set Enrichment Analysis of DEGs and pathway identification defines even more precisely the exact physiological process affected, describing a comprehensive knowledge representation.

During the development and ripening the main biological processes affected were catalytic activity, binding, and transporter activity, which means degradation, modification, or translocation of molecules; most of these processes are related to secondary metabolism. Transcription regulator activity also appears represented as the importance of gene expression regulation during the ripening process. Main GO terms up-regulated annotated in Biological Process are glycosylation and catabolic process, while down-regulated is pigment metabolic process. This

is strongly correlated with carbohydrate metabolism and pigment content biosynthesis in each of the genotypes under study.

KEGG enrichment analysis of DEGs identifies affected pathways, phenylpropanoid biosynthesis being the most altered pathway. Phenylpropanoid pathway synthesizes the precursor compounds of anthocyanins, which are linked to reddish blush color (Ye et al., 2019) in the genotype 'GC 3-7'. Other precursors of anthocyanin compounds are flavonoids, phenylpropanoid biosynthesis, and phenylalanine metabolism, also up-regulated in 'GC 3-7'. Finally, we can describe the pathways related with soluble solid content, starch and sucrose metabolism and glycolysis/glucogenesis, responsible for the biosynthesis of sucrose from glucose and fructose, increasing soluble solid content as responsible to the sweet taste in the ripe fruit apricot. Some genes of starch and sucrose metabolism pathway were up-regulated in 'GC 3-7', which could be correlated with the higher sucrose and soluble solid content in this genotype.

Candidate Genes Related to Pomological Characteristics and Biochemical and Metabolite Contents in Apricot Fruits

A large-scale transcriptomic studies of apricot and related species ripening process showed a significant up- and down-regulated transcript levels of genes related to stress conditions, cell wall metabolism, transcription factors (MADS-box, AUX/IAA, bZIP, bHLH, and MYB), heat shock proteins (HSPs), ethylene biosynthesis, starch and sucrose metabolism, organic acids metabolism, phenylpropanoid and carotenoid biosynthesis (Trainotti et al., 2003; Grimplet et al., 2005; Trainotti et al., 2006; Trainotti et al., 2007; Manganaris et al., 2009; Manganaris et al., 2010; Manganaris et al., 2011).

The principal enzymes involved in starch and sucrose metabolism are sucrose synthase (SS), sucrose phosphate synthase (SPS), and sorbitol dehydrogenase (SDH). These are under tight regulatory control, increasing its expression at the end of the ripening process, which is consistent with the correlation analysis between enzyme activity and sugar accumulation (Xi et al., 2016; Zhang et al., 2019). The drastic increase of SS and sucrose during the ripening process is responsible for the rapid increase of soluble solid content in fruits (Meixia et al., 2006). In addition, a high positive correlation between sucrose content and *SS* expression during fruit ripening has been shown for the genotype 'GC3-7'. However, this correlation was not observed for the for the genotype 'GC2-1' when sucrose content was increased from stage A to stage C (**Figure 9B**). Another significant increase in glucose and fructose was found due to the increase in the activity of sorbitol oxygenase (SO) and sorbitol dehydrogenase (SDH), where sorbitol was converted to glucose and fructose *via* these two enzymes, which suggest that the accumulation of these sugars mainly comes from sorbitol catalysis. Though there were no significant differences between epicarp and mesocarp, as the sweetest sugar, fructose ratio is significantly higher in the flesh than in the skin, which is consistent with the fact that sweet taste is stronger in the flesh than in the skin (Xi et al., 2016; Zhang et al., 2019). Thus, *SDH* [*LOC103333266* (*PARG19420m03*)], described as a possible key factor during climacteric ripening in Japanese plum (Fernandez i Marti et al., 2018), and *SS* [*LOC103340632* (*PARG27579m02*)] described as the main enzyme responsible for sugar accumulation in apricot fruit (Xi et al., 2016), were both proposed as candidate genes responsible for the increase of sugar content during fruit ripening in apricot.

The red blush present in the skin of apricot was due to the presence of anthocyanins. The major anthocyanin compounds found in apricot fruit are cyanidin-3-O-rutinoside, cyanidin-3-O-glucoside, and peonidin-3-O-rutinoside (Bureau et al., 2009). The early anthocyanin biosynthesis genes (EBGs) are *chalcone synthase* (*CHS*), *chalcone isomerase* (*CHI*), *flavanone 3-hydroxylase* (*F3H*), *flavonoid 3′-hydroxylase* (*F3′H*), *flavonoid 3′5 ′-hydroxylase* (*F3′5 ′H*), and *dihydroflavonol 4-reductase* (*DFR*), which lead to the production of flavonols. The late anthocyanin biosynthesis genes (LBGs) are *anthocyanidin reductase* (*ANR*), *leucoanthocyanidin reductase* (*LAR*), *anthocyanidin synthase/leucoanthocyanidin dioxygenase* (*ANS/LDOX*), and *UDP flavonoid 3-O-glucosyltransferase* (*UFGT*). The TF MYB10 has been implicated in the regulation of the last three enzymes of the metabolic pathway DFR, ANS and UFGT, which were the key to explain contrasting patterns of anthocyanin accumulation in peach and Japanese plum (Ravaglia et al., 2013; Gonzalez et al., 2016). While EBGs are regulated by R2R3-MYB TFs without co-regulators, LBGs need MBW complex (Tanaka et al., 2008; Petroni and Tonelli, 2011; Xu et al., 2015). The expression of flavonoid biosynthesis genes correlated with anthocyanin accumulation and red coloration, but there was some variability in the specific step involved. In most species, only LBGs correlated well with anthocyanin synthesis, such as tomato (Povero et al., 2011) and pepper (Borovsky et al., 2004).

However, in other species the transcript levels not only of LGBs, but also of some EBGs were higher in red compared to non-red fruits, such Chinese bayberry (Niu et al., 2010), apple (Takos et al., 2006a; Takos et al., 2006b), pear (Feng et al., 2010), grape (Boss et al., 1996), cherry (Wei et al., 2015), peach (Ravaglia et al., 2013), Japanese plum (Gonzalez et al., 2016), mei (Zhang et al., 2017a), and apricot (Lin-Wang et al., 2010; Kayesh et al., 2013). In apple, peach, Japanese plum, and sweet cherry, the transcript level of MYB10 was up-regulated during fruit red coloration development (Takos et al., 2006a; Lin-Wang et al., 2011; Cheng et al., 2015; Wei et al., 2015; Gonzalez et al., 2016). Besides, it was described in apricot that anthocyanin biosynthesis is regulated by a *MYB10* TF inducing the expression of *DFR*. Almost the whole precursor pathways for anthocyanin biosynthesis are identified from phenylalanine to cyanidin 3-O-glucoside, the last steps to synthesize cyanidin-3-O-rutinoside, and peonidin-3-O-rutinoside are not yet elucidated, although it is known that the enzymes involved must be of the type UDP-rhamnose as anthocyanidin-3-glucoside rhamnosyl transferase. Similar to this function, we identified some genes with UDP-glucuronosyl/UDP-glucosyltransferase activity like *7-deoxyloganetin glucosy ltransferase-like isoform X1* [*LOC103319666* (*PARG08586m01*)] and *7-deoxyloganetin glucosyltransferase-like* [*LOC103323807* (unknown PARG ID)] as possible candidates. Taking all

together, the genes found as *MYB* [*LOC103342585* (*PARG 26597m01*)], *CHS* [*LOC103324315* (*PARG03336m04*)], *ANS* (*LOC103341429*), *UFGT* (*LOC103323450*, unknown PARG ID), *DFR* [*LOC103320869* (*PARG07267m01*)], *7-deoxyloganetin glucosyltransferase-like isoform X1* [*LOC103319666* (*PARG 08586m01*)] and *7-deoxyloganetin glucosyltransferase-like* [*LOC103323807* (unknown PARG ID)] may be the most probable candidate genes responsible for anthocyanin biosynthesis in apricot. Another interesting gene was the TF *bZIP* [*LOC103332281* (*PARG18436m04*)], bind to *chalcone/ stilbene synthase* (*CHS*) gene promoter, key enzyme during anthocyanin biosynthesis, and it was up-regulated in 'GC 2-11' at the end of ripening process.

In apricot, the amount of carotenoids in the tissues is not attributed solely to the ability to synthesize carotenoids; the regulatory mechanisms based on degradation and accumulation of carotenoids were postulated as responsible for carotenoid content (Marty et al., 2005). We analyze the *carotenoid cleavage dioxygenase 4* (*CCD4*), responsible for the enzymatic cleavage of β-carotene resulting in the production of volatile norisoprenoids (apocarotenoids) and related to fruit aroma during ripening (Zhang et al., 2019). This gene cosegregated with the *Y* locus, which seems to control white/yellow flesh in peach, and it was suggested as a molecular marker for white peach cultivar selection (Brandi et al., 2011; Adami et al., 2013; Ma et al., 2014). Further investigation on carotenoid profile compounds and the potential role of *CCD4* allelic segregation in different apricot varieties will be needed to validate this result. We also propose the gene *DXS* [*LOC103335117* (*PARG01985m01*)] as carotenoid biosynthesis precursor.

Concerning texture in peach, the expression of genes involved in softening started before the appearance of the ethylene climacteric rise at S3 stage, regarding the occurrence of the ethylene climacteric. Moreover, some cell wall modifying enzymes expressed in S3 could be involved in cell enlargement associated with the vigorous fruit growth that occurred after stone hardening (Trainotti et al., 2003; Trainotti et al., 2006). Pectins, the main compound responsible for firmness in apricot fruit, comprised a highly complex polysaccharide network with a structurally diverse range of glycan chains, glycosidic linkages, and other substituents, such as acetyl and methyl groups. Most studies of pectin depolymerization have focused on a small group of enzymes: pectin methylesterase (PME), β-galactosidase (β-GAL), polygalacturonase (PG), and pectin lyases (PL). PL showed maximum expression just before climacteric stage causing massive degradation of pectins and decreasing its expression before ethylene release (Brummell et al., 2004; Vicente et al., 2007). By contrast, the other pectin-degrading enzymes (PG, PME, and β-GAL) show a typical ripening-pattern expression increasing its expression at the ripening stage during ethylene release. PME mainly catalyzes the de-esterification of high methyl esterified pectin to generate low methyl esterified pectin, which can be further hydrolyzed by PG (Chen et al., 2000; Vicente et al., 2007). So, PL would appear to have the task to carry out an early degradation of pectins, making them more susceptible to the subsequent attack of other degrading enzymes as PME and β-GAL. Other enzymes probably involved were acetyl esterase (AE), rhamnogalacturonan hydrolases, and lyases (RG) and pectin methylesterase inhibitor (PMEI) (Chen et al., 2000; Vicente et al., 2007). PMEIs were found up-regulated in half-ripe and ripe stage during fruit ripening. PMEIs also play a role in plant defense mechanism against pathogens. Their expression do not correlate well with fruit firmness in apricot and may correlate with fruit susceptibility to pathogen attacks (Chen et al., 2000). Expansins (EXPs) also affect pectin depolymerization by non-hydrolytic activity, and one expansin transcript was found increased during apricot ripening, possibly by increasing substrate accessibility to other enzymes (Brummell et al., 2004). Finally, *cinnamyl-alcohol dehydrogenase* (*CAD*), as a precursor for phenylpropanoid compounds in lignin biosynthesis, was described as responsible for cleavage stone by affecting the deposition of lignin in the endocarp of apricot fruit (Zhang et al., 2019). Considering all the above, we proposed as candidate genes for firmness control during ripening process *CAD* [*LOC103335323* (*PARG29726m01*)], *PMEI* [*LOC103322538* (*PARG05244m01*)] and *βGAL* [*LOC103 340681* (*PARG27772m02*)].

CONCLUSIONS

Within the framework of this work, we expanded our knowledge about apricot fruit ripening, providing original information about the dynamic expression of genes involved in the fruit ripening process in two genotypes which differ in fruit color, soluble solid content, and firmness. DEGs in the two assayed apricot genotypes at three fruit ripening stages showed important variation in the biosynthetic pathways of phenylpropanoids, flavonoids, carotenoids biosynthesis and, starch and sucrose metabolism. These genes could be possible candidates as molecular markers for fruit color and soluble solid content. We identified the gene for carotenoid biosynthesis *lycopene β-cyclase* differentially expressed between genotypes but not correlated with orange skin ground color and flesh color or carotenoid content. The gene *carotenoid cleavage dioxygenase 4*, which acts downstream *lycopene β-cyclase* in the carotenoid pathways, degrading β-carotene into apocarotenoids compounds, is highly correlated with carotenoid content and correlated with light-yellow/white flesh. On the other hand, sucrose content is mainly due to the expression of the gene *sucrose synthase* in starch and sucrose metabolism. *Carotenoid cleavage dioxygenase 4* and *sucrose synthase* are identified as candidate genes for light yellow/white fruit color and high soluble solid content at the ripening process. This information may be useful to improve agronomical production through the identification of candidate genes involved in fruit ripening and biochemical and metabolite contents that may be applied in monitoring the ripening process in apricot fruit. The expression of these candidate genes was highly correlated with the fruit quality traits of interest and could be implemented in MAS to increase the efficiency of apricot breeding programs by the early selection of new genotypes with high-quality fruits and high nutraceutical values. In addition, results showed the suitability of

using different reference genomes and transcriptomes related to *Prunus* species (mainly mei and apricot but also peach) as reference sequences in transcriptomic analysis due to its phylogenetic proximity.

DATA AVAILABILITY STATEMENT

The datasets generated for this study can be found in the NCBI SRA repository as a Bioproject entitled 'Prunus armeniaca fruit ripening process', with the accession number PRJNA562811 (https://www.ncbi.nlm.nih.gov/bioproject/562811).

AUTHOR CONTRIBUTIONS

BG-G contributed to laboratory experiments, bioinformatics data analysis, manuscript elaboration, and discussion. DR, MR, and PM-G participated in the design and coordination of the study. DR and JS performed the phenotypic evaluation. PJM-G contributed to bioinformatics data analysis and manuscript elaboration. All authors discussed the results and commented on the manuscript.

FUNDING

This study has been supported by the projects "Apricot breeding" (AGL2017-86627-R) from the Spanish Ministry of Economy and Competitiveness and "Breeding stone fruit species assisted by molecular tools" from the Seneca Foundation of the Region of Murcia (19879/GERM/15). The authors offer grateful thanks to Seneca Foundation of the Region of Murcia for financial support to JS in Murcia inside the Saavedra Fajardo program.

SUPPLEMENTARY MATERIAL

The Supplementary Material for this article can be found online at: https://www.frontiersin.org/articles/10.3389/fpls.2020.01269/full#supplementary-material

REFERENCES

Adami, M., De Franceschi, P., Brandi, F., Liverani, A., Giovannini, D., Rosati, C., et al. (2013). Identifying a Carotenoid Cleavage Dioxygenase (ccd4) Gene Controlling Yellow/White Fruit Flesh Color of Peach. *Plant Mol. Biol. Rep.* 31 (5), 1166–1175. doi: 10.1007/s11105-013-0628-6

Alkio, M., Jonas, U., Declercq, M., Van Nocker, S., and Knoche, M. (2014). Transcriptional dynamics of the developing sweet cherry (*Prunus avium* L.) fruit: sequencing, annotation and expression profiling of exocarp-associated genes. *Hortic. Res.* 1, 11. doi: 10.1038/hortres.2014.11

Andrews, S. (2010). *FastQC: a quality control tool for high throughput sequence data*.

Ashburner, M., Ball, C. A., Blake, J. A., Botstein, D., Butler, H., and Cherry, J. M. (2000). Gene Ontology: tool for the unification of biology. *Nat. Genet.* 25, 25–29. doi: 10.1038/75556

Bazzano, L. A., He, J., Ogden, L. G., Loria, C. M., Vupputuri, S., Myers, L., et al. (2002). Fruit and vegetable intake and risk of cardiovascular disease in US adults: the first National Health and Nutrition Examination Survey Epidemiologic Follow-up Study. *Am. J. Clin. Nutr.* 76 (1), 93–99. doi: 10.1093/ajcn/76.1.93

Benjamini, Y., and Hochberg, Y. (1995). Controlling the false discovery rate: a practical and powerful approach to multiple testing. *J. R. Stat. Soc. Ser. B (Methodological)* 59, 289–300. doi: 10.1111/j.2517-6161.1995.tb02031.x

Bolger, A. M., Lohse, M., and Usadel, B. (2014). Trimmomatic: a flexible trimmer for Illumina sequence data. *Bioinformatics* 30 (15), 2114–2120. doi: 10.1093/bioinformatics/btu170

Borovsky, Y., Oren-Shamir, M., Ovadia, R., De Jong, W., and Paran, I. (2004). The A locus that controls anthocyanin accumulation in pepper encodes a MYB transcription factor homologous to Anthocyanin2 of Petunia. *Theor. Appl. Genet.* 109 (1), 23–29. doi: 10.1007/s00122-004-1625-9

Boss, P. K., Davies, C., and Robinson, S. P. (1996). Analysis of the Expression of Anthocyanin Pathway Genes in Developing Vitis vinifera L. cv Shiraz Grape Berries and the Implications for Pathway Regulation. *Plant Physiol.* 111, 1059–1066. doi: 10.1104/pp.111.4.1059

Brandi, F., Bar, E., Mourgues, F., Horváth, G., Turcsi, E., Giuliano, G., et al. (2011). Study of 'Redhaven' peach and its white-fleshed mutant suggests a key role of CCD4 carotenoid dioxygenase in carotenoid and norisoprenoid volatile metabolism. *BMC Plant Biol.* 11 (1), 24. doi: 10.1186/1471-2229-11-24

Brown, G. S., and Walker, T. D. (1990). Indicators of maturity in apricots using biplot multivariate analysis. *J. Sci. Food Agric.* 53 (3), 321–331. doi: 10.1002/jsfa.2740530305

Brummell, D. A., Dal Cin, V., Crisosto, C. H., and Labavitch, J. M. (2004). Cell wall metabolism during maturation, ripening and senescence of peach fruit. *J. Exp. Bot.* 55 (405), 2029–2039. doi: 10.1093/jxb/erh227

Bureau, S., Renard, C. M. G. C., Reich, M., Ginies, C., and Audergon, J.-M. (2009). Change in anthocyanin concentrations in red apricot fruits during ripening. *LWT - Food Sci. Technol.* 42 (1), 372–377. doi: 10.1016/j.lwt.2008.03.010

Cabanettes, F., and Klopp, C. (2018). D-GENIES: dot plot large genomes in an interactive, efficient and simple way. *PeerJ* 6, e4958. doi: 10.7717/peerj.4958

Cao, S., Liang, M., Shi, L., Shao, J., Song, C., Bian, K., et al. (2017). Accumulation of carotenoids and expression of carotenogenic genes in peach fruit. *Food Chem.* 214, 137–146. doi: 10.1016/j.foodchem.2016.07.085

Capitani, D., Sobolev, A. P., Tomassini, A., Sciubba, F., De Salvador, F. R., Mannina, L., et al. (2012). Peach fruit: metabolic comparative analysis of two varieties with different resistances to insect attacks by NMR spectroscopy. *J. Agric. Food Chem.* 61 (8), 1718–1726. doi: 10.1021/jf303248z

Chen, M. H., Sheng, J., Hind, G., Handa, A. K., and Citovsky, V. (2000). Interaction between the tobacco mosaic virus movement protein and host cell pectin methylesterases is required for viral cell-to-cell movement. *EMBO J.* 19 (5), 913–920. doi: 10.1093/emboj/19.5.913

Cheng, Y., Liu, L., Yuan, C., and Guan, J. (2015). Molecular Characterization of Ethylene-Regulated Anthocyanin Biosynthesis in Plums During Fruit Ripening. *Plant Mol. Biol. Rep.* 34 (4), 777–785. doi: 10.1007/s11105-015-0963-x

Conesa, A., Madrigal, P., Tarazona, S., Gomez-Cabrero, D., Cervera, A., McPherson, A., et al. (2016). A survey of best practices for RNA-seq data analysis. *Genome Biol.* 17 (1), 13. doi: 10.1186/s13059-016-0881-8

Consortium, G. O. (2004). The Gene Ontology (GO) database and informatics resource. *Nucleic Acids Res.* 32 (suppl_1), D258–D261. doi: 10.1093/nar/gkh036

Costa-Silva, J., Domingues, D., and Lopes, F. M. (2017). RNA-Seq differential expression analysis: An extended review and a software tool. *PloS One* 12 (12), 18. doi: 10.1371/journal.pone.0190152

Du, D., Hao, R., Cheng, T., Pan, H., Yang, W., Wang, J., et al. (2013). Genome-wide analysis of the AP2/ERF gene family in *Prunus mume*. *Plant Mol. Biol. Rep.* 31 (3), 741–750. doi: 10.1007/s11105-012-0531-6

Durinck, S., Spellman, P. T., Birney, E., and Huber, W. (2009). Mapping identifiers for the integration of genomic datasets with the R/Bioconductor package biomaRt. *Nat. Protoc.* 4, 1184. doi: 10.1038/nprot.2009.97

Erdogan-Orhan, I., and Kartal, M. (2011). Insights into research on phytochemistry and biological activities of *Prunus armeniaca* L.(apricot). *Food Res. Int.* 44 (5), 1238–1243. doi: 10.1016/j.foodres.2010.11.014

Fang, Z. Z., Zhou, D. R., Ye, X. F., Jiang, C. C., and Pan, S. L. (2016). Identification of Candidate Anthocyanin-Related Genes by Transcriptomic Analysis of 'Furongli' Plum (*Prunus salicina* Lindl.) during Fruit Ripening Using RNA-Seq. *Front. Plant Sci.* 7, 1338. doi: 10.3389/fpls.2016.01338

Femenia, A., Sanchez, E. S., Simal, S., and Rossello, C. (1998). Developmental and ripening-related effects on the cell wall of apricot (*Prunus armeniac*a) fruit. *J. Sci. Food Agric.* 77 (4), 487–493. doi: 10.1002/(sici)1097-0010(199808)77:4<487::aid-jsfa70>3.3.co;2-k

Feng, S., Wang, Y., Yang, S., Xu, Y., and Chen, X. (2010). Anthocyanin biosynthesis in pears is regulated by a R2R3-MYB transcription factor PyMYB10. *Planta* 232 (1), 245–255. doi: 10.1007/s00425-010-1170-5

Fernandez i Marti, A., Saski, C. A., Manganaris, G. A., Gasic, K., and Crisosto, C. H. (2018). Genomic Sequencing of Japanese Plum (*Prunus salicina* Lindl.) Mutants Provides a New Model for Rosaceae Fruit Ripening Studies. *Front. Plant Sci.* 9, 21. doi: 10.3389/fpls.2018.00021

Fuentealba, C., Hernández, I., Olaeta, J., Defilippi, B., Meneses, C., Campos, R., et al. (2017). New insights into the heterogeneous ripening in Hass avocado via LC–MS/MS proteomics. *Postharvest Biol. Technol.* 132, 51–61. doi: 10.1016/j.postharvbio.2017.06.001

Gabotti, D., Negrini, N., Morgutti, S., Nocito, F. F., and Cocucci, M. (2015). Cinnamyl alcohol dehydrogenases in the mesocarp of ripening fruit of *Prunus persica* genotypes with different flesh characteristics: changes in activity and protein and transcript levels. *Physiol. Plant* 154 (3), 329–348. doi: 10.1111/ppl.12319

García-Gómez, B., Razi, M., Salazar, J. A., Prudencio, A. S., Ruiz, D., Dondini, L., et al. (2018). Comparative Analysis of SSR Markers Developed in Exon, Intron, and Intergenic Regions and Distributed in Regions Controlling Fruit Quality Traits in *Prunus* Species: Genetic Diversity and Association Studies. *Plant Mol. Biol. Rep.* 36 (1), 23–35. doi: 10.1007/s11105-017-1058-7

Gonzalez, M., Salazar, E., Cabrera, S., Olea, P., and Carrasco, B. (2016). Analysis of anthocyanin biosynthesis genes expression profiles in contrasting cultivars of Japanese plum (*Prunus salicina* L.) during fruit development. *Gene Expr. Patterns* 21 (1), 54–62. doi: 10.1016/j.gep.2016.06.005

Grimplet, J., Romieu, C., Audergon, J.-M., Marty, I., Albagnac, G., Lambert, P., et al. (2005). Transcriptomic study of apricot fruit (*Prunus armeniaca*) ripening among 13 006 expressed sequence tags. *Physiol. Plant.* 125 (3), 281–292. doi: 10.1111/j.1399-3054.2005.00563.x

Guyer, L., Hofstetter, S. S., Christ, B., Lira, B. S., Rossi, M., and Hörtensteiner, S. (2014). Different mechanisms are responsible for chlorophyll dephytylation during fruit ripening and leaf senescence in tomato. *Plant Physiol.* 166 (1), 44–56. doi: 10.1104/pp.114.239541

Hardcastle, T. J., and Kelly, K. A. (2010). baySeq: empirical Bayesian methods for identifying differential expression in sequence count data. *BMC Bioinf.* 11, 422. doi: 10.1186/1471-2105-11-422

Hayama, H., Shimada, T., Fujii, H., Ito, A., and Kashimura, Y. (2006). Ethylene-regulation of fruit softening and softening-related genes in peach. *J. Exp. Bot.* 57 (15), 4071–4077. doi: 10.1093/jxb/erl178

Infante, R., Martínez-Gómez, P., and Predieri, S. (2008). Quality oriented fruit breeding: Peach [*Prunus persica* (L.) Batsch]. *J. Food Agric. Environ.* 6 (2), 342–356. doi: 10.1234/4.2008.1239

Jiang, D., Tang, C., and Zhang, A. (2004). Cluster analysis for gene expression data: a survey. *IEEE Trans. Knowledge Data Eng.* 16 (11), 1370–1386. doi: 10.1109/TKDE.2004.68

Jiang, F., Zhang, J., Wang, S., Yang, L., Luo, Y., Gao, S., et al. (2019). The apricot *(Prunus armeniaca* L.) genome elucidates Rosaceae evolution and beta-carotenoid synthesis. *Hortic. Res.* 6, 128. doi: 10.1038/s41438-019-0215-6

Jiao, W.-B., and Schneeberger, K. (2017). The impact of third generation genomic technologies on plant genome assembly. *Curr. Opin. Plant Biol.* 36, 64–70. doi: 10.1016/j.pbi.2017.02.002

Jo, Y., Lian, S., Cho, J. K., Choi, H., Chu, H., and Cho, W. K. (2015). De novo transcriptome assembly of two different apricot cultivars. *Genomics Data* 6, 275–276. doi: 10.1016/j.gdata.2015.10.012

Kayesh, E., Shangguan, L., Korir, N. K., Sun, X., Bilkish, N., Zhang, Y., et al. (2013). Fruit skin color and the role of anthocyanin. *Acta Physiol. Plant.* 35 (10), 2879–2890. doi: 10.1007/s11738-013-1332-8

Kim, D., Pertea, G., Trapnell, C., Pimentel, H., Kelley, R., and Salzberg, S. L. (2013). TopHat2: accurate alignment of transcriptomes in the presence of insertions, deletions and gene fusions. *Genome Biol.* 14, R36. doi: 10.1186/gb-2013-14-4-r36

Kim, D., Langmead, B., and Salzberg, S. L. (2015a). HISAT: a fast spliced aligner with low memory requirements. *Nat. Methods* 12 (4), 357–360. doi: 10.1038/nmeth.3317

Kim, H.-Y., Saha, P., Farcuh, M., Li, B., Sadka, A., and Blumwald, E. (2015b). RNA-seq analysis of spatiotemporal gene expression patterns during fruit development revealed reference genes for transcript normalization in plums. *Plant Mol. Biol. Rep.* 33 (6), 1634–1649. doi: 10.1007/s11105-015-0860-3

Kita, M., Kato, M., Ban, Y., Honda, C., Yaegaki, H., Ikoma, Y., et al. (2007). Carotenoid Accumulation in Japanese Apricot (Prunus mume Siebold & Zucc.): Molecular Analysis of Carotenogenic Gene Expression and Ethylene Regulation. *J. Agric. Food Chem.* 55 (9), 3414–3420. doi: 10.1021/jf063552v

Klee, H. J., and Giovannoni, J. J. (2011). "Genetics and Control of Tomato Fruit Ripening and Quality Attributes," in *Annual Review of Genetics*, vol. 45 . Eds. B. L. Bassler, M. Lichten and G. Schupbach (Palo Alto: Annual Reviews), 41–59.

Kochhar, A., Khurana, J. P., and Tyagi, A. K. (1996). Nucleotide sequence of the psbP gene encoding precursor of 23-kDa polypeptide of oxygen-evolving complex in Arabidopsis thaliana and its expression in the wild-type and a constitutively photomorphogenic mutant. *DNA Res.* 3 (5), 277–285. doi: 10.1093/dnares/3.5.277

Kovacs, E., and Nemeth-Szerdahelyi, E. (2002). beta-galactosidase activity and cell wall breakdown in apricots. *J. Food Sci.* 67 (6), 2004–2008. doi: 10.1111/j.1365-2621.2002.tb09492.x

Langfelder, P., and Horvath, S. (2008). WGCNA: an R package for weighted correlation network analysis. *BMC Bioinf.* 9 (1), 559. doi: 10.1186/1471-2105-9-559

Langmead, B., and Salzberg, S. L. (2012). Fast gapped-read alignment with Bowtie 2. *Nat. Methods* 9, 357–359. doi: 10.1038/nmeth.1923

Lassmann, T., Hayashizaki, Y., and Daub, C. O. (2010). SAMStat: monitoring biases in next generation sequencing data. *Bioinformatics* 27 (1), 130–131. doi: 10.1093/bioinformatics/btq614

Leng, N., Li, Y., McIntosh, B. E., Nguyen, B. K., Duffin, B., Tian, S., et al. (2015). EBSeq-HMM: a Bayesian approach for identifying gene-expression changes in ordered RNA-seq experiments. *Bioinformatics* 31 (16), 2614–2622. doi: 10.1093/bioinformatics/btv193

Li, H., Ruan, J., and Durbin, R. (2008). Mapping short DNA sequencing reads and calling variants using mapping quality scores. *Genome Res.* gr, 078212.078108. doi: 10.1101/gr.078212.108

Li, H., Handsaker, B., Wysoker, A., Fennell, T., Ruan, J., Homer, N., et al. (2009). The Sequence Alignment/Map format and SAMtools. *Bioinformatics* 25 (16), 2078–2079. doi: 10.1093/bioinformatics/btp352

Li, B., Ruotti, V., Stewart, R. M., Thomson, J. A., and Dewey, C. N. (2010). RNA-Seq gene expression estimation with read mapping uncertainty. *Bioinformatics* 26 (4), 493–500. doi: 10.1093/bioinformatics/btp692

Liao, Y., Smyth, G. K., and Shi, W. (2014). featureCounts: an efficient general purpose program for assigning sequence reads to genomic features. *Bioinformatics* 30, 923–930. doi: 10.1093/bioinformatics/btt656

Lillo-Carmona, V., Espinoza, A., Rothkegel, K., Rubilar, M., Nilo-Poyanco, M., Pedreschi, R., et al. (2020). Identification of Metabolite and Lipid Profiles in a Segregating Peach Population Associated with Mealiness in *Prunus persica* (L.) Batsch. *Metabolites* 10, 154. doi: 10.3390/metabo10040154

Lin-Wang, K., Bolitho, K., Grafton, K., Kortstee, A., Karunairetnam, S., McGhie, T. K., et al. (2010). An R2R3 MYB transcription factor associated with regulation of the anthocyanin biosynthetic pathway in Rosaceae. *BMC Plant Biol.* 10, 50. doi: 10.1186/1471-2229-10-50

Lin-Wang, K., Micheletti, D., Palmer, J., Volz, R., Lozano, L., Espley, R., et al. (2011). High temperature reduces apple fruit colour via modulation of the anthocyanin regulatory complex. *Plant Cell Environ.* 34, 1176–1190. doi: 10.1111/j.1365-3040.2011.02316.x

Love, M. I., Huber, W., and Anders, S. (2014). Moderated estimation of fold change and dispersion for RNA-seq data with DESeq2. *Genome Biol.* 15, 550. doi: 10.1186/s13059-014-0550-8

Love, M. I., Hogenesch, J. B., and Irizarry, R. A. (2016). Modeling of RNA-seq fragment sequence bias reduces systematic errors in transcript abundance estimation. *Nat. Biotechnol.* 34 (12), 1287–1291. doi: 10.1038/nbt.3682

Luo, W., and Brouwer, C. (2013). Pathview: an R/Bioconductor package for pathway-based data integration and visualization. *Bioinformatics* 29 (14), 1830–1831. doi: 10.1093/bioinformatics/btt285

Luo, W., Friedman, M. S., Shedden, K., Hankenson, K. D., and Woolf, P. J. (2009). GAGE: generally applicable gene set enrichment for pathway analysis. *BMC Bioinf.* 10 (1), 161. doi: 10.1186/1471-2105-10-161

Ma, J., Li, J., Zhao, J., Zhou, H., Ren, F., Wang, L., et al. (2014). Inactivation of a gene encoding carotenoid cleavage dioxygenase (CCD4) leads to carotenoid-based yellow coloration of fruit flesh and leaf midvein in peach. *Plant Mol. Biol. Rep.* 32 (1), 246–257. doi: 10.1007/s11105-013-0650-8

Machlin, L. J. (1995). Critical assessment of the epidemiological data concerning the impact of antioxidant nutrients on cancer and cardiovascular disease. *Crit. Rev. Food Sci. Nutr.* 35 (1-2), 41–49. doi: 10.1080/10408399509527684

MacManes, M. (2014). On the optimal trimming of high-throughput mRNA sequence data. *Front. Genet.* 5, 13. doi: 10.3389/fgene.2014.00013

Manganaris, G. A., Ziliotto, F., Rasori, A., Bonghi, C., Ramina, A., Banfi, R., et al. (2009). "Gene Expression Profile During Apricot Fruit Growth, Using a Peach Microarray," in *I International Symposium on Horticulture in Europe*. Ed. G. R. Dixon (Leuven 1: Int Soc Horticultural Science), 113–117.

Manganaris, G. A., Ziliotto, F., Rasori, A., Bonghi, C., Ramina, A., and Tonutti, P. (2010). "A Comparative Transcriptomic Approach to Elucidate Common and Divergent Mechanisms Involved in Apricot and Peach Fruit Development and Ripening," in *Xiv International Symposium on Apricot Breeding and Culture*. Ed. C. Xiloyannis (Leuven 1: Int Soc Horticultural Science), 577–581.

Manganaris, G. A., Rasori, A., Bassi, D., Geuna, F., Ramina, A., Tonutti, P., et al. (2011). Comparative transcript profiling of apricot (Prunus armeniaca L.) fruit development and on-tree ripening. *Tree Genet. Genomes* 7 (3), 609–616. doi: 10.1007/s11295-010-0360-4

Marty, I., Bureau, S., Sarkissian, G., Gouble, B., Audergon, J. M., and Albagnac, G. (2005). Ethylene regulation of carotenoid accumulation and carotenogenic gene expression in colour-contrasted apricot varieties (Prunus armeniaca). *J. Exp. Bot.* 56 (417), 1877–1886. doi: 10.1093/jxb/eri177

Mbeguie-A-Mbeguie, D., Gouble, B., Gomez, R. M., Audergon, J. M., Albagnac, G., and Fils-Lycaon, B. (2002). Two expansin cDNAs from Prunus armeniaca expressed during fruit ripening are differently regulated by ethylene. *Plant Physiol. Biochem.* 40 (5), 445–452. doi: 10.1016/s0981-9428(02)01391-8

Mbéguié-A-Mbéguié, D., Chahine, H., Gomez, R. M., Gouble, B., Reich, M., Audergon, J. M., et al. (1999). Molecular cloning and expression of a cDNA encoding 1-aminocyclopropane-1-carboxylate (ACC) oxidase from apricot fruit (Prunus armeniaca). *Physiol. Plant.* 105 (2), 294–303. doi: 10.1034/j.1399-3054.1999.105215.x

Meixia, C., Xuesen, C., Zhijuan, C., and Zuoan, S. (2006). Changes of sugar and acid constituents in apricot during fruit development. *Acta Hortic. Sin.* 33 (4), 805.

Minaiyan, M., Ghannadi, A., Asadi, M., Etemad, M., and Mahzouni, P. (2014). Anti-inflammatory effect of Prunus armeniaca L.(Apricot) extracts ameliorates TNBS-induced ulcerative colitis in rats. *Res. Pharm. Sci.* 9 (4), 225.

Mowrey, B. D., and Werner, D. J. (1990). Phylogenetic relationships among species of Prunus as inferred by isozyme markers. *Theor. Appl. Genet.* 80 (1), 129–133. doi: 10.1007/bf00224026

Nagata, .M., and Yashita, I. (1992). Simple method for simultaneous determination of chlorophyll and carotenoids in tomato fruits. *J. Japan. Soc. Food Sci.* 39 (10), 925–928

Niu, S. S., Xu, C. J., Zhang, W. S., Zhang, B., Li, X., Lin-Wang, K., et al. (2010). Coordinated regulation of anthocyanin biosynthesis in Chinese bayberry (Myrica rubra) fruit by a R2R3 MYB transcription factor. *Planta* 231 (4), 887–899. doi: 10.1007/s00425-009-1095-z

Niu, J., Zhu, B., Cai, J., Li, P., Wang, L., Dai, H., et al. (2014). Selection of reference genes for gene expression studies in Siberian Apricot (Prunus sibirica L.) Germplasm using quantitative real-time PCR. *PloS One* 9 (8), e103900. doi: 10.1371/journal.pone.0103900

Pan, L., Zeng, W., Niu, L., Lu, Z., Liu, H., Cui, G., et al. (2015). PpYUC11, a strong candidate gene for the stony hard phenotype in peach (*Prunus persica* L. Batsch), participates in IAA biosynthesis during fruit ripening. *J. Exp. Bot.* 66 (22), 7031–7044. doi: 10.1093/jxb/erv400

Pan, H., Sheng, Y., Gao, Z., Chen, H., Qi, Y., Yi, X., et al. (2016). Transcriptome analysis of peach (*Prunus persica* L. Batsch) during the late stage of fruit ripening. *Genet. Mol. Res.* 15 (4), gmr15049335.

Petroni, K., and Tonelli, C. (2011). Recent advances on the regulation of anthocyanin synthesis in reproductive organs. *Plant Sci.* 181 (3), 219–229. doi: 10.1016/j.plantsci.2011.05.009

Pfaffl, M. W. (2001). A new mathematical model for relative quantification in real-time RT–PCR. *Nucleic Acids Res.* 29 (9), e45–e45. doi: 10.1093/nar/29.9.e45

Pirona, R., Vecchietti, A., Lazzari, B., Caprera, A., Malinverni, R., Consolandi, C., et al. (2013). Expression profiling of genes involved in the formation of aroma in two peach genotypes. *Plant Biol. (Stuttg)* 15 (3), 443–451. doi: 10.1111/j.1438-8677.2012.00666.x

Potter, D. (2012). Basic information on the stone fruit crops. *Genet. Genomics Breed. Stone Fruits* 1, 1–21. doi: 10.1201/b13104-2

Povero, G., Gonzali, S., Bassolino, L., Mazzucato, A., and Perata, P. (2011). Transcriptional analysis in high-anthocyanin tomatoes reveals synergistic effect of Aft and atv genes. *J. Plant Physiol.* 168 (3), 270–279. doi: 10.1016/j.jplph.2010.07.022

Rasori, A., Ruperti, B., Bonghi, C., Tonutti, P., and Ramina, A. (2002). Characterization of two putative ethylene receptor genes expressed during peach fruit development and abscission. *J. Exp. Bot.* 53 (379), 2333–2339. doi: 10.1093/jxb/erf097

Ravaglia, D., Espley, R. V., Henry-Kirk, R. A., Andreotti, C., Ziosi, V., Hellens, R. P., et al. (2013). Transcriptional regulation of flavonoid biosynthesis in nectarine (Prunus persica) by a set of R2R3 MYB transcription factors. *BMC Plant Biol.* 13 (1), 68. doi: 10.1186/1471-2229-13-68

Robinson, M. D., and Oshlack, A. (2010). A scaling normalization method for differential expression analysis of RNA-seq data. *Genome Biol.* 11, R25. doi: 10.1186/gb-2010-11-3-r25

Robinson, M. D., McCarthy, D. J., and Smyth, G. K. (2010). edgeR: a Bioconductor package for differential expression analysis of digital gene expression data. *Bioinformatics* 26, 139–140. doi: 10.1093/bioinformatics/btp616

Sanhueza, D., Vizoso, P., Balic, I., Campos-Vargas, R., and Meneses, C. (2015). Transcriptomic analysis of fruit stored under cold conditions using controlled atmosphere in Prunus persica cv."Red Pearl". *Front. Plant Sci.* 6, 788. doi: 10.3389/fpls.2015.00788

Schroeder, A., Mueller, O., Stocker, S., Salowsky, R., Leiber, M., Gassmann, M., et al. (2006). The RIN: an RNA integrity number for assigning integrity values to RNA measurements. *BMC Mol. Biol.* 7 (1), 3. doi: 10.1186/1471-2199-7-3

Shiratake, K., and Martinoia, E. (2007). Transporters in fruit vacuoles. *Plant Biotechnol.* 24 (1), 127–133. doi: 10.5511/plantbiotechnology.24.127

Sochor, J., Zitka, O., Skutkova, H., Pavlik, D., Babula, P., Krska, B., et al. (2010). Content of phenolic compounds and antioxidant capacity in fruits of apricot genotypes. *Molecules* 15 (9), 6285–6305. doi: 10.3390/molecules15096285

Surget-Groba, Y., and Montoya-Burgos, J. I. (2010). Optimization of de novo transcriptome assembly from next-generation sequencing data. *Genome Res.* 20 (10), 1432–1440. doi: 10.1101/gr.103846.109

Takos, A. M., Robinson, S. P., and Walker, A. R. (2006a). Transcriptional regulation of the flavonoid pathway in the skin of dark-grown 'Cripps' Red' apples in response to sunlight. *J. Hortic. Sci. Biotechnol.* 81, 735–744. doi: 10.1080/14620316.2006.11512131

Takos, A. M., Ubi, B. E., Robinson, S. P., and Walker, A. R. (2006b). Condensed tannin biosynthesis genes are regulated separately from other flavonoid biosynthesis genes in apple fruit skin. *Plant Sci.* 170, 487–499. doi: 10.1016/j.plantsci.2005.10.001

Tanaka, Y., Sasaki, N., and Ohmiya, A. (2008). Biosynthesis of plant pigments: anthocyanins, betalains and carotenoids. *Plant J.* 54 (4), 733–749. doi: 10.1111/j.1365-313X.2008.03447.x

Tarazona, S., Furio-Tari, P., Turra, D., Di Pietro, A., Nueda, M. J., Ferrer, A., et al. (2015). Data quality aware analysis of differential expression in RNA-seq with NOISeq R/Bioc package. *Nucleic Acids Res.* 43 (21), 15. doi: 10.1093/nar/gkv711

Tian, T., Liu, Y., Yan, H., You, Q., Yi, X., Du, Z., et al. (2017). agriGO v2. 0: a GO analysis toolkit for the agricultural community 2017 update. *Nucleic Acids Res.* 45 (W1), W122–W129.

Trainotti, L., Zanin, D., and Casadoro, G. (2003). A cell wall-oriented genomic approach reveals a new and unexpected complexity of the softening in peaches. *J. Exp. Bot.* 54 (389), 1821–1832. doi: 10.1093/jxb/erg198

Trainotti, L., Bonghi, C., Ziliotto, F., Zanin, D., Rasori, A., Casadoro, G., et al. (2006). The use of microarray μPEACH1.0 to investigate transcriptome changes during transition from pre-climacteric to climacteric phase in peach fruit. *Plant Sci.* 170 (3), 606–613. doi: 10.1016/j.plantsci.2005.10.015

Trainotti, L., Tadiello, A., and Casadoro, G. (2007). The involvement of auxin in the ripening of climacteric fruits comes of age: the hormone plays a role of its

own and has an intense interplay with ethylene in ripening peaches. *J. Exp. Bot.* 58 (12), 3299–3308. doi: 10.1093/jxb/erm178

Udvardi, M. K., Czechowski, T., and Scheible, W.-R. (2008). Eleven golden rules of quantitative RT-PCR. *Plant Cell* 20 (7), 1736–1737. doi: 10.1105/tpc.108.061143

Van den Berg, H., Faulks, R., Granado, H. F., Hirschberg, J., Olmedilla, B., Sandmann, G., et al. (2000). The potential for the improvement of carotenoid levels in foods and the likely systemic effects. *J. Sci. Food Agric.* 80 (7), 880–912. doi: 10.1002/(SICI)1097-0010(20000515)80:7<880::AID-JSFA646>3.0.CO;2-1

Vandesompele, J., De Preter, K., Pattyn, F., Poppe, B., Van Roy, N., De Paepe, A., et al. (2002). Accurate normalization of real-time quantitative RT-PCR data by geometric averaging of multiple internal control genes. *Genome Biol.* 3 (7), research0034.0031. doi: 10.1186/gb-2002-3-7-research0034

Verde, I., Jenkins, J., Dondini, L., Micali, S., Pagliarani, G., Vendramin, E., et al. (2017). The Peach v2. 0 release: high-resolution linkage mapping and deep resequencing improve chromosome-scale assembly and contiguity. *BMC Genomics* 18 (1), 225. doi: 10.1186/s12864-017-3606-9

Vicente, A. R., Saladie, M., Rose, J. K. C., and Labavitch, J. M. (2007). The linkage between cell wall metabolism and fruit softening: looking to the future. *J. Sci. Food Agric.* 87 (8), 1435–1448. doi: 10.1002/jsfa.2837

Wang, L., Zhao, S., Gu, C., Zhou, Y., Zhou, H., Ma, J., et al. (2013). Deep RNA-Seq uncovers the peach transcriptome landscape. *Plant Mol. Biol.* 83 (4-5), 365–377. doi: 10.1007/s11103-013-0093-5

Wang, X., Ding, Y., Wang, Y., Pan, L., Niu, L., Lu, Z., et al. (2017). Genes involved in ethylene signal transduction in peach (Prunus persica) and their expression profiles during fruit maturation. *Sci. Hortic.* 224, 306–316. doi: 10.1016/j.scienta.2017.06.035

Wei, H., Chen, X., Zong, X., Shu, H., Gao, D., and Liu, Q. (2015). Comparative transcriptome analysis of genes involved in anthocyanin biosynthesis in the red and yellow fruits of sweet cherry (Prunus avium L.). *PloS One* 10 (3), e0121164. doi: 10.1371/journal.pone.0121164

Wells, C. E., Vendramin, E., Jimenez Tarodo, S., Verde, I., and Bielenberg, D. G. (2015). A genome-wide analysis of MADS-box genes in peach [Prunus persica (L.) Batsch]. Berlin (Germany) *BMC Plant Biol.* 15 (1), 41. doi: 10.1186/s12870-015-0436-2

Wickham, H. (2016). *ggplot2: elegant graphics for data analysis* (Amsterdam, Netherlands: Springer).

Wilks, D. S. (2011). "Cluster analysis," in *International geophysics* (Elsevier), 603–616.

Wu, T. D., and Watanabe, C. K. (2005). GMAP: a genomic mapping and alignment program for mRNA and EST sequences. *Bioinformatics* 21, 1859–1875. doi: 10.1093/bioinformatics/bti310

Wu, B., Gao, L., Gao, J., Xu, Y., Liu, H., Cao, X., et al. (2017). Genome-wide identification, expression patterns, and functional analysis of UDP glycosyltransferase family in peach (Prunus persica L. Batsch). *Front. Plant Sci.* 8, 389. doi: 10.3389/fpls.2017.00389

Xi, W., Zheng, H., Zhang, Q., and Li, W. (2016). Profiling Taste and Aroma Compound Metabolism during Apricot Fruit Development and Ripening. *Int. J. Mol. Sci.* 17 (7), 988. doi: 10.3390/ijms17070998

Xie, F., Xiao, P., Chen, D., Xu, L., and Zhang, B. (2012). miRDeepFinder: a miRNA analysis tool for deep sequencing of plant small RNAs. *Plant Mol. Biol.* 80 (1), 75–84. doi: 10.1007/s11103-012-9885-2

Xu, Z., Zhang, Q., Sun, L., Du, D., Cheng, T., Pan, H., et al. (2014). Genome-wide identification, characterisation and expression analysis of the MADS-box gene family in Prunus mume. *Mol. Genet. Genomics* 289 (5), 903–920. doi: 10.1007/s00438-014-0863-z

Xu, W., Dubos, C., and Lepiniec, L. (2015). Transcriptional control of flavonoid biosynthesis by MYB–bHLH–WDR complexes. *Trends Plant Sci.* 20 (3), 176–185. doi: 10.1016/j.tplants.2014.12.001

Ye, J., Zhang, Y., Cui, H., Liu, J., Wu, Y., Cheng, Y., et al. (2018). WEGO 2.0: a web tool for analyzing and plotting GO annotations 2018 update. *Nucleic Acids Res.* 46 (W1), W71–W75. doi: 10.1093/nar/gky400

Ye, J., Wang, G., Tan, J., Zheng, J., Zhang, X., Xu, F., et al. (2019). Identification of candidate genes involved in anthocyanin accumulation using Illmuina-based RNA-seq in peach skin. *Sci. Hortic.* 250, 184–198. doi: 10.1016/j.scienta.2019.02.047

Zhang, B., and Horvath, S. (2005). A general framework for weighted gene co-expression network analysis. *Stat. Appl. Genet. Mol. Biol.* 4 (1), 17. doi: 10.2202/1544-6115.1128

Zhang, B., Shen, J. Y., Wei, W. W., Xi, W. P., Xu, C. J., Ferguson, I., et al. (2010). Expression of Genes Associated with Aroma Formation Derived from the Fatty Acid Pathway during Peach Fruit Ripening. *J. Agric. Food Chem.* 58 (10), 6157–6165. doi: 10.1021/jf100172e

Zhang, Q., Chen, W., Sun, L., Zhao, F., Huang, B., Yang, W., et al. (2012). The genome of Prunus mume. *Nat. Commun.* 3, 1318. doi: 10.1038/ncomms2290

Zhang, Q., Hao, R. J., Xu, Z. D., Yang, W. R., Wang, J., Cheng, T. R., et al. (2017a). Isolation and functional characterization of a R2R3-MYB regulator of *Prunus mume* anthocyanin biosynthetic pathway. *Plant Cell Tissue Organ Cult.* 131 (3), 417–429. doi: 10.1007/s11240-017-1294-4

Zhang, X., Zhang, L., Zhang, Q., Xu, J., Liu, W., and Dong, W. (2017b). Comparative transcriptome profiling and morphology provide insights into endocarp cleaving of apricot cultivar (*Prunus armeniaca* L.). *BMC Plant Biol.* 17 (1), 72. doi: 10.1186/s12870-017-1023-5

Zhang, Q., Feng, C., Li, W., Qu, Z., Zeng, M., and Xi, W. (2019). Transcriptional regulatory networks controlling taste and aroma quality of apricot (*Prunus armeniaca* L.) fruit during ripening. *BMC Genomics* 20 (1), 45. doi: 10.1186/s12864-019-5424-8

Zhou, H., Lin-Wang, K., Wang, H., Gu, C., Dare, A. P., Espley, R. V., et al. (2015). Molecular genetics of blood-fleshed peach reveals activation of anthocyanin biosynthesis by NAC transcription factors. *Plant J.* 82 (1), 105–121. doi: 10.1111/tpj.12792

Conflict of Interest: The authors declare that the research was conducted in the absence of any commercial or financial relationships that could be construed as a potential conflict of interest.

The reviewer CC declared a past co-authorship with one of the authors PJM-G to the handling Editor.

frontiers in Plant Science

ORIGINAL RESEARCH
published: 03 December 2020
doi: 10.3389/fpls.2020.592540

Endogenous Auxin Content Contributes to Larger Size of Apple Fruit

*Haidong Bu[1,2], Wenquan Yu[2], Hui Yuan[1], Pengtao Yue[1], Yun Wei[1] and Aide Wang[1]**

[1] Key Laboratory of Fruit Postharvest Biology, College of Horticulture, Shenyang Agricultural University, Shenyang, China,
[2] Mudanjiang Branch of Heilongjiang Academy of Agricultural Sciences, Mudanjiang, China

Fruit size is an important economic trait that is controlled by multiple genes. However, the regulatory mechanism for fruit size remains poorly understood. A bud sport variety of "Longfeng" (LF) apple (*Malus domestica*) was identified and named "Grand Longfeng" (GLF). The fruit size of GLF is larger than that of LF, and both varieties are diploid. We found that the cell size in GLF fruit was larger than that of LF. Then, we compared the fruit transcriptomes of the two varieties using RNA-Seq technology. A total of 1166 differentially expressed genes (DEGs) were detected between GLF and LF fruits. The KEGG analysis revealed that the phytohormone pathway was the most enriched, in which most of the DEGs were related to auxin signaling. Moreover, the endogenous auxin levels of GLF fruit were higher than those of LF. The expressions of auxin synthetic genes, including *MdTAR1* and *MdYUCCA6*, were higher in GLF fruit than LF. Collectively, our findings suggest that auxin plays an important role in fruit size development.

Keywords: apple, fruit size, cell size, auxin, *MdTAR1*, *MdYUCCA6*

OPEN ACCESS

Edited by:
Chunying Kang,
Huazhong Agricultural University, China

Reviewed by:
Chizuko Yamamuro,
Fujian Agriculture and Forestry University, China
Anish Malladi,
University of Georgia, United States

***Correspondence:**
Aide Wang
awang@syau.edu.cn

Specialty section:
This article was submitted to Plant Development and EvoDevo, a section of the journal Frontiers in Plant Science

Received: *07 August 2020*
Accepted: *03 November 2020*
Published: *03 December 2020*

Citation:
Bu H, Yu W, Yuan H, Yue P, Wei Y and Wang A (2020) Endogenous Auxin Content Contributes to Larger Size of Apple Fruit. Front. Plant Sci. 11:592540. doi: 10.3389/fpls.2020.592540

INTRODUCTION

The apple (*Malus domestica*) is widely cultivated in temperate regions worldwide (Duan et al., 2017; McClure et al., 2018). Fruit size is an important trait that influences the economic value of apple (Zhang et al., 2005; Malladi and Hirst, 2010). Developing an apple variety with a larger fruit size is one of the most important goals for breeders; however, the mechanisms underlying fruit size regulation are poorly understood.

Fruit size is determined by two factors, cell number and/or cell size (Scorzal et al., 1991; Olmstead et al., 2007; Malladi and Hirst, 2010). Previous research has reported that cell number is the major factor influencing fruit size. For example, ectopic expression of *AINTEGUMENTA* (*ANT*), a *APETALA2* (*AP2*)-like domain transcription factor, increased the organ size of *Arabidopsis* by increasing the cell number (Krizek, 1999). Overexpression of *BIG BROTHER*, an E3 ubiquitin ligase gene, reduced the organ size by restricting cell numbers in *Arabidopsis* (Disch et al., 2006). Besides cell number, cell size is also an important factor that controls fruit size. In tomato, the larger fruit varieties have a larger cell size than small fruit varieties because the cell size is positively correlated with fruit size (Cheniclet et al., 2005). In apple, a bud sport variety of "Gala" was identified, named "Grand Gala," and the fruit of "Grand Gala" is larger than "Gala" due to its larger cell size (Malladi and Hirst, 2010), but the underlying mechanism causing the larger cell size of "Grand Gala" is unclear.

Fruit size is regulated by multiple factors, including phytohormones, and genetic factors. For example, the application of N1-(2-chloro-4-pyridyl)-N3-phenylurea (CPPU), an

artificial-synthesized cytokinin, increased fruit size in kiwifruit (*Actinidia chinensis*) by inducing the cell number (Cruz-Castillo et al., 2002). Gibberellin treatment increased the fruit size of pear (*Pyrus pyrifolia*; Ito et al., 2015) and apple (Martin et al., 1970). Auxin has been reported to affect the fruit size in many tree fruits, for example, exogenous auxin treatment increased fruit size by increasing cell size in apple (Devoghalaere et al., 2012).

Auxin is achieved through the coordination of complex processes, including auxin synthesis, metabolism, transport, and signal transduction (Devoghalaere et al., 2012). Indole acetic acid (IAA) is the predominant form of auxin, and the indole-3-pyruvate (IPA) pathway is the predominant path of IAA biosynthesis in plants, which contains two main enzymes, tryptophan aminotransferase of *Arabidopsis*/tryptophan aminotransferase-related (TAA1/TAR), and flavin monooxygenase (YUCCA; Zhao et al., 2001). Additionally, gretchen hagen 3 (GH3) family protein can conjugate amino acids and IAA to form inactive IAA (Staswick et al., 2002). Aside from its synthesis and conjugation, auxin is transported between cells (Zažímalová et al., 2010). Auxin-resistant 1/like auxin-resistant 1 (AUX1/LAX1) mainly transports auxin from extracellular to intracellular regions (Yang et al., 2006; Vanneste and Friml, 2009), and PIN-formed 1 (PIN1) is responsible for auxin transport in the reverse direction (Wabnik et al., 2010). Auxin synthesis, conjugation, and transport are tightly regulated and lead to auxin homeostasis (Perrot-Rechenmann and Napier, 2005).

Changing the concentration of endogenous auxin can modify its signaling response, causing several gene transcription level changes, such as *auxin/indole acetic acid* (*Aux/IAA*) and *small auxin up RNA* (*SAUR*; Paponov et al., 2008). When the auxin concentration is low, its signal transduction is blocked by Aux/IAA transcription repressors that interact with auxin response factors (ARFs), thereby repressing their transcription activity (Lavy and Estelle, 2016). When the auxin concentration is elevated, Aux/IAA interacts with the auxin receptor, transport inhibitor response 1/auxin signaling F-BOX protein (TIR1/AFB), which is a component of E3 ubiquitin ligase that undergoes ubiquitin-mediated protein degradation. ARFs are subsequently released, and auxin signaling is activated (Devoghalaere et al., 2012; Leyser, 2018).

Previous studies have elucidated the roles of genes that regulate fruit size. For example, *fruit weight 2.2* (*FW2.2*) is a negative regulator of fruit size and regulates cell number during the early stage of fruit development in tomato (*Solanum lycopersicum*; Frary et al., 2000). In apple, the overexpression of *microRNA172* inhibits the transcription of *AP2*, leading to decreased cell size and significantly reduced fruit size (Yao et al., 2015). Furthermore, the silencing of *MdMADS8* or *MdMADS9* resulted in smaller cell size and greatly reduced fruit size in apple (Ireland et al., 2013).

The "Longfeng" (LF) apple variety is widely cultivated in Northeast China (Li, 1994). Recently, a bud sport variety of LF was identified and named "Grand Longfeng" (GLF). GLF has a larger fruit size than LF; however, it is unclear why GLF apple fruit becomes larger. In this study, we found that the cell size of GLF fruit was larger than LF. The transcriptomes of GLF and LF fruits were also compared and the probable explanation for the larger fruit size of GLF is discussed.

MATERIALS AND METHODS

Plant Materials and Treatment

Longfeng and GLF apple fruits were collected from an orchard (E129°32′12″, N44°18′00″) located in Dongsheng Village, Ningan Town, Mudanjiang City, Heilongjiang Province, China. LF and GLF trees were grown on *M. baccata* rootstocks with normal management. The maturation date of both varieties is around 120 days after full bloom (DAFB). For fruit size measurements, the fruits of both varieties were collected every 21 days (d) from 9 to 120 DAFB and 10 fruits were collected at each sampling point. Fruit core diameter, longitudinal diameter, and transversal diameter were measured with a digital Vernier caliper (PD-151; Pro'skit, Taiwan, China). For the 1-naphthylacetic acid (NAA; BBI Life Sciences, Shanghai, China) treatment, 1 μM NAA was sprayed on LF fruit at 30 DAFB. Fruits treated with distilled water were used as controls. Fruits were harvested at the commercial harvest day (120 DAFB). For the 2,3,5-triiodobenzoic acid (TIBA; Shanghai Maokang Biotechnology Co., Ltd., Shanghai, China) treatment, 100 μM TIBA, which is an inhibitor of auxin polarity transport, was injected into the calyx tube of GLF fruit at 30 DAFB. Fruits injected with distilled water were used as controls. Fruits were harvested at the commercial harvest day (120 DAFB). Transverse and longitudinal diameters were also measured. Fruit weights were measured by electronic scales (JY10002; Sunny Hengping Scientific Instrument Co., Ltd., Shanghai, China). Student's *t*-test was used for statistical analysis using SPSS v18.0 (IBM, Chicago, Illinois, United States). At each sampling point, the cortex of 10 fruits was sliced, frozen in liquid nitrogen, and stored at the −70°C for future analysis.

SSR Analysis of GLF and LF Apple Fruit

Genomic DNA was extracted according to previously reported methods (Wang et al., 2013), and 16 pairs of SSR (simple sequence repeat) primers were selected for PCR. Denaturing polyacrylamide gel examining was used for PCR products analysis accord to the method of Li et al. (2020). The primers were listed in **Supplementary Table 1**.

Chromosome Ploidy Identification

Fresh leaves were used for ploidy identification using a flow cytometer (FACSCalibar; Beckton Dickinson Co., Franklin lakes, NJ, United States) following the manufacturer's instructions. About 0.5 cm^2 of leaf disk was dipped in 400 μL extracting buffer [1% beta-mercaptoethanol, 0.05% Triton X-100, 20 μg mL^{-1} RNase A, 15 mM Tris–HCl (pH 8.0), 2 mM Na_2EDTA, 20 mM NaCl, and 80 mM KCl], ground into small particles (Zhang et al., 2011), and filtrated through a 500-μm mesh sieve. The filtrate was stained with 20 μg mL^{-1} propidium iodide (Sigma, Louis, Missouri, United States) and incubated in the dark for 15 min at room temperature. After staining, the nuclei were collected by filtering through a 25-μm nylon mesh. Flow

cytometry was performed using the flow cytometer. Diploid "Hanfu" apple (*M. domestica*, 2n = 2x = 34) was used as a control and internal reference (Ma et al., 2016). All chemicals were purchased from the TransGen Biotech Co., Ltd. (Beijing, China) unless otherwise indicated.

Cytological Analysis

Fruit flesh was fixed in FAA (50% ethanol:formaldehyde:glacial acetic acid = 90:5:5) for 24 h, then used for making paraffin sections as previously described (Yao et al., 2015). Sections were cut by a rotary slicer (Leica RM2255; Leica, Wetzlar, Germany) and stained with 1% toluidine blue for 3–5 min. Six consecutive cells were measured between the pericarp and core using a scale tool under a microscope. The average of 6 consecutive cell lengths from the core to the skin was used as the single-cell length. The thickness of the fruit cortex was measured using the digital Vernier caliper. Cell numbers were calculated as the cortex size divided by the single-cell size. Section images were captured using an Olympus BX50f-3 microscope (Olympus Optical Co., Ltd., Tokyo, Japan). Fruits from three trees (one fruit per tree) of each variety were used as 1 biological replicate; a total of three biological replicates were used at each stage. Student's *t*-test was used for statistical analysis using SPSS v18.0.

RNA-Sequencing

Longfeng and GLF fruits were collected at 72 DAFB and used for RNA-Seq. Fruits were collected from 3 trees (3 fruits per tree), and the fruit flesh from each tree was equally mixed and used as 1 biological replicate. A total of 3 biological replicates were used. Total RNA was extracted according to previously reported methods (Gambino et al., 2008). cDNA library construction, RNA-Seq, and the bioinformatics analysis were performed by Biomarker Technologies Co., Ltd. (Beijing, China). RNA-Seq was performed using an Illumina HiSeq^{TM} 2500 system (Illumina, San Diego, California, United States).

Gene Functional Annotation and Enrichment Analysis

Gene functional annotation was performed based on the NCBI non-redundant (Nr) protein sequences, NCBI nucleotide (Nt) sequences, protein family (Pfam), clusters of orthologous groups of proteins (KOG/COG), Swiss-Prot (a manually annotated and reviewed protein sequence database), KEGG ortholog (KO), and gene ontology (GO) databases. The GO enrichment analysis of the differentially expressed genes (DEGs) was implemented using the GOseq R package based on Wallenius non-central hypergeometric distributions (Young et al., 2010). KOBAS software was used to test the statistical enrichment of DEGs in the KEGG pathways (Mao et al., 2005). KEGG annotation of the genes was performed following previously reported methods (Kanehisa et al., 2004).

Determination of Endogenous IAA Contents

The cortex of the fruit from three trees (three fruits per tree) of each variety was mixed and used as one biological replicate with a total of three biological replicates. Fruit cortex was frozen in liquid nitrogen, ground into a fine powder, and dried under a vacuum (0.08 mbar) at −45°C. Endogenous auxin was measured by gas chromatography–mass spectrometry according to previously described methods with slight modifications (Müller et al., 2002). Ten mg fruit cortex was extracted with MeOH:H_2O (4:1) as a solvent and using [$^{13}C_6$] IAA (CLM-1896-0; Cambridge Isotope Laboratories, Inc., Andover, MA, United States) as an internal standard. The extract was evaporated until dry. After briefly cleaning the resuspended dried extract with 80% MeOH (v/v), the fraction containing the phytohormone was collected and dried by a centrifugal concentrator. The IAA in the extracts was trimethylsilylated with N-methyl-N-trimethylsilyl-trifluoroacetamide (MSTFA) at 80°C for 30 min. Samples were freeze dried using vacuum freeze-drying equipment (XYL-LGJ-10D; Beijing Heng Odd Instrument Co., Ltd., Beijing, China) for 24 h and dissolved in hexane before placement in a GC-QqQ MS (7890a-5975b; Agilent, Santa Clara, CA, United States) with a fused silica glass capillary column DB-5 (30 m × 0.25 mm × 0.10 μm; Agilent, Santa Clara, CA, United States). Injection and interface temperatures were 260°C and 280°C, respectively. The column temperature gradient was maintained at 80°C for 2 min, then increased by 6°C min^{-1} to 250°C, followed by 20°C min^{-1} to 300°C. IAA was confirmed by monitoring the diagnostic ions of both endogenous and deuterated hormones according to previously described methods Müller et al. (2002); [$^{13}C_6$] IAA was used as an internal standard. Student's *t*-test was used for statistical analysis.

DEG Analysis

Gene expression levels were determined by fragments per kilobase of transcript per million fragments (FPKM). Differential expression analysis of the sample groups was performed by DESeq (Anders and Huber, 2010). Significant *p*-values were obtained from the original hypothesis test. The false discovery rate (FDR) was obtained using the Benjamini–Hochberg correction method (Anders and Huber, 2010), which was used as a key indicator for DEG screening. The ratio of expression between two sample groups with the screening criteria, fold change >2, and FDR < 0.01 was used to screen the ratio of expression between the two sample groups.

Quantitative Reverse Transcription-PCR

Longfeng and GLF fruits were collected from three trees (three fruits per tree), and the fruit flesh from each tree was equally mixed and used as one biological replicate. A total of three biological replicates were used. Fruit flesh RNA extraction was performed according to previously described methods (Li et al., 2017). First-strand cDNA was synthesized from 1 μg total RNA using an M-MLV RTase cDNA Synthesis kit (D6130; TaKaRa, Shiga, Japan). Quantitative Reverse Transcription-PCR (qRT-PCR) was performed on a qTOWER3G RT-PCR system (Analytik Jena, Jena, Germany) with a 10-μL total volume containing 5 μL SYBR green master mix (Cat. 04707516001; Roche Diagnostic Ltd, Basel, Switzerland), 0.5 μL cDNA, 0.5 μL reverse and forward primers, and 3.5 μL H_2O. The reaction programs were performed as follows: 10 min at 95°C, 40 cycles

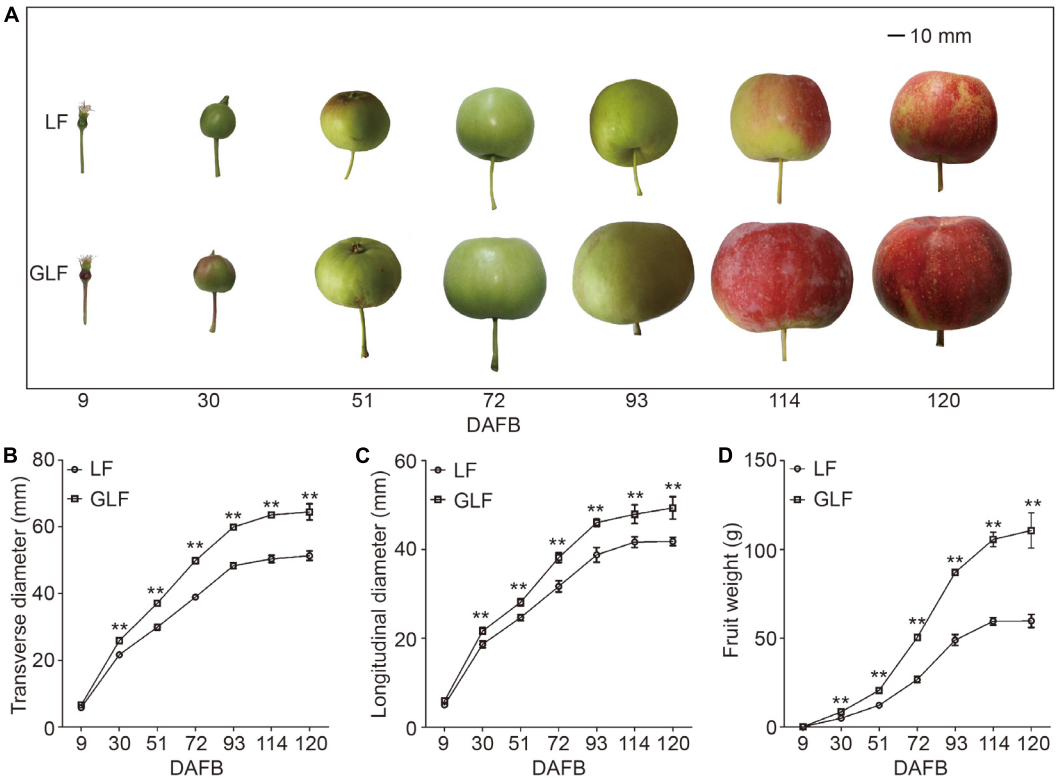

FIGURE 1 | Comparison of LF and GLF fruit growth. LF and GLF fruits were harvested every 21 d from 9 to 120 DAFB (days after full bloom; **A**). Fruit transverse diameter **(B)**, longitudinal diameter **(C)**, and weight **(D)** were measured and compared. **Significant differences ($p < 0.01$, Student's *t*-test). Error bars indicate the standard deviation (SD) of 10 fruits. Bar, 10 mm.

of amplification for 30 s at 95°C, 30 s at 60°C, and 30 s at 72°C, and a final dissociation stage for 6 s at 72°C. Student's *t*-test was used for statistical analysis. Primer3 software[1] was used for designing primers. All primer sequences are listed in **Supplementary Table 1**.

RESULTS

GLF Fruits Were Significantly Larger Than LF Fruits

Grand Longfeng apple is a bud sport variety of LF, which was found in 2003 on a LF tree. GLF showed a fruit size larger than LF (**Figure 1A**). We then used these two varieties to study the molecular basis for the larger fruit size of GLF. We first compared the genetic background of LF and GLF using 16 pairs of SSR primers (**Supplementary Figure 1** and **Supplementary Table 1**) and observed no difference in SSR band patterns between these two varieties (**Supplementary Figure 1**), indicating that GLF and LF have high similarity in genetic background. Next, LF and GLF fruit sizes were measured from 9 to 120 DAFB (days after full bloom; **Figure 1A**). The fruit weight, transverse diameter, and longitudinal diameter of GLF were 1.9, 1.3, and 1.2 × times greater than LF, respectively, at 120 DAFB (**Figures 1B–D**). No significant differences were detected in the core diameter between the two varieties (**Supplementary Figure 2**). Thus, it was concluded that the difference in fruit size between GLF and LF was caused by the thickness of the fruit cortex. Then, we examined the ploidy of the two varieties. Results revealed that both were diploid (**Supplementary Figure 3**).

Next, we compared the cell size and number of the GLF and LF fruit cortexes. The cell size of GLF was significantly larger than that of LF from 30 to 120 DAFB (**Figures 2A,C**). Interestingly, this timespan coincided with the periods when fruit size differences were detected between the two varieties (**Figures 1B–D**). Although the cell number of GLF was greater than LF at the early stage (9 DAFB), no significant differences were detected after 30 DAFB (**Figure 2B**). These results indicated that cell size is a major factor that results in the larger size of GLF fruit.

Comparison of LF and GLF Fruit Transcriptomes

To identify the cause of the fruit size difference between LF and GLF, we compared the transcriptomes of the two varieties using fruit collected at 72 DAFB (cell enlargement period). Three biological replicates were used and a total of six samples were sequenced. A total of 36.42 GB clean data (6.07 GB clean data for

[1]http://frodo.wi.mit.edu/

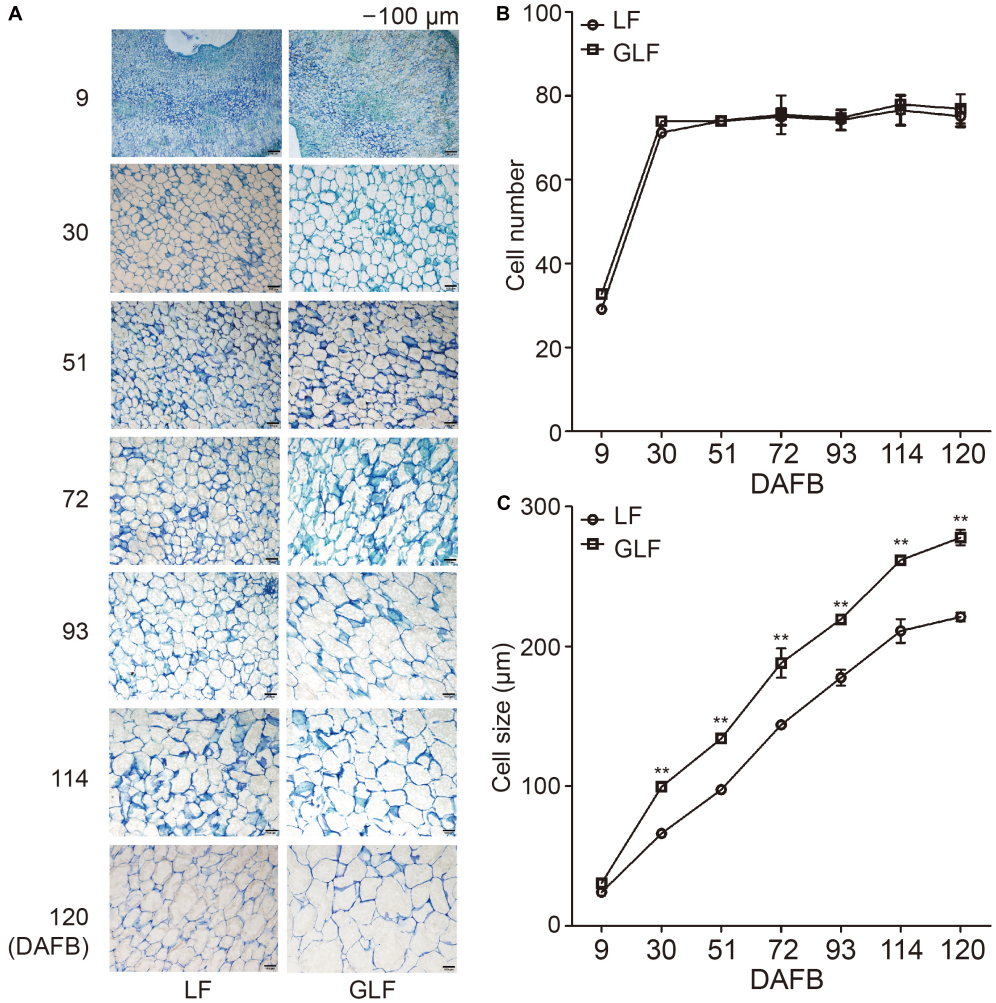

FIGURE 2 | Cell numbers and sizes of LF and GLF fruits. **(A)** Cells of LF and GLF fruits from 9 to 120 DAFB (days after full bloom). Bar, 100 μm. **(B)** Cell numbers of LF and GLF fruits were determined as the ratio between the fruit cortex and single cell size. **(C)** Cell sizes of LF and GLF fruit cortexes were determined as the average diameter of six cells during fruit development. **Significant differences ($p < 0.01$, Student's *t*-test). Error bars indicate the standard deviation (SD) of three biological replicates.

each sample) were obtained. The Q30 percentages of each sample were ≥91.73% (**Table 1**). The clean reads of each sample were mapped to the apple reference genome[2] (Daccord et al., 2017). A total of 1166 DEGs were obtained (**Supplementary Table 2**).

Functional Annotation of DEGs

All DEGs were aligned by conducting BLASTx searches (*E* values ≤ 10^5) against the GO, Swiss-Prot, Nr NCBI, KEGG, and COG/KOG protein databases. A total of 1128 DEGs were annotated (**Supplementary Table 3**). We used the KEGG pathway database to search for functional networks of the biological interactions. A total of 85 KEGG pathways were obtained (**Supplementary Table 4**). Interestingly, plant hormone signal transduction (ko04075) contained the largest number of genes (38 genes; **Supplementary Figure 4**), accounting for 16.52% of the ko04075 pathway (230 genes). Additionally, the *Q*-value (where smaller *Q*-values are the most important in terms of DEGs pathway enrichment significance) of the plant

TABLE 1 | Mapping of RNA-Seq reads obtained from GLF and LF fruits.

Sample	Clean reads (strip)	Clean bases (bp)	GC (%)	Q30 (%)
LF-1	27,537,481	8,221,649,800	47.73	92.67
LF-2	26,912,877	8,043,076,294	47.55	92.37
LF-3	25,693,947	7,665,601,944	47.56	92.38
GLF-1	23,691,600	7,058,675,886	47.49	91.73
GLF-2	24,822,984	7,391,795,358	47.72	92.25
GLF-3	22,064,826	6,589,203,906	47.91	92.55

LF-1, LF-2, and LF-3 represent three biological replicates of LF at 72 DAFB; GLF-1, GLF-2, and GLF-3 represent three biological replicates of GLF at 72 DAFB. Clean reads (strip) represent the total number of paired-end reads in the clean data; clean bases (bp) represent clean data total base numbers.

[2]https://iris.angers.inra.fr/gddh13/

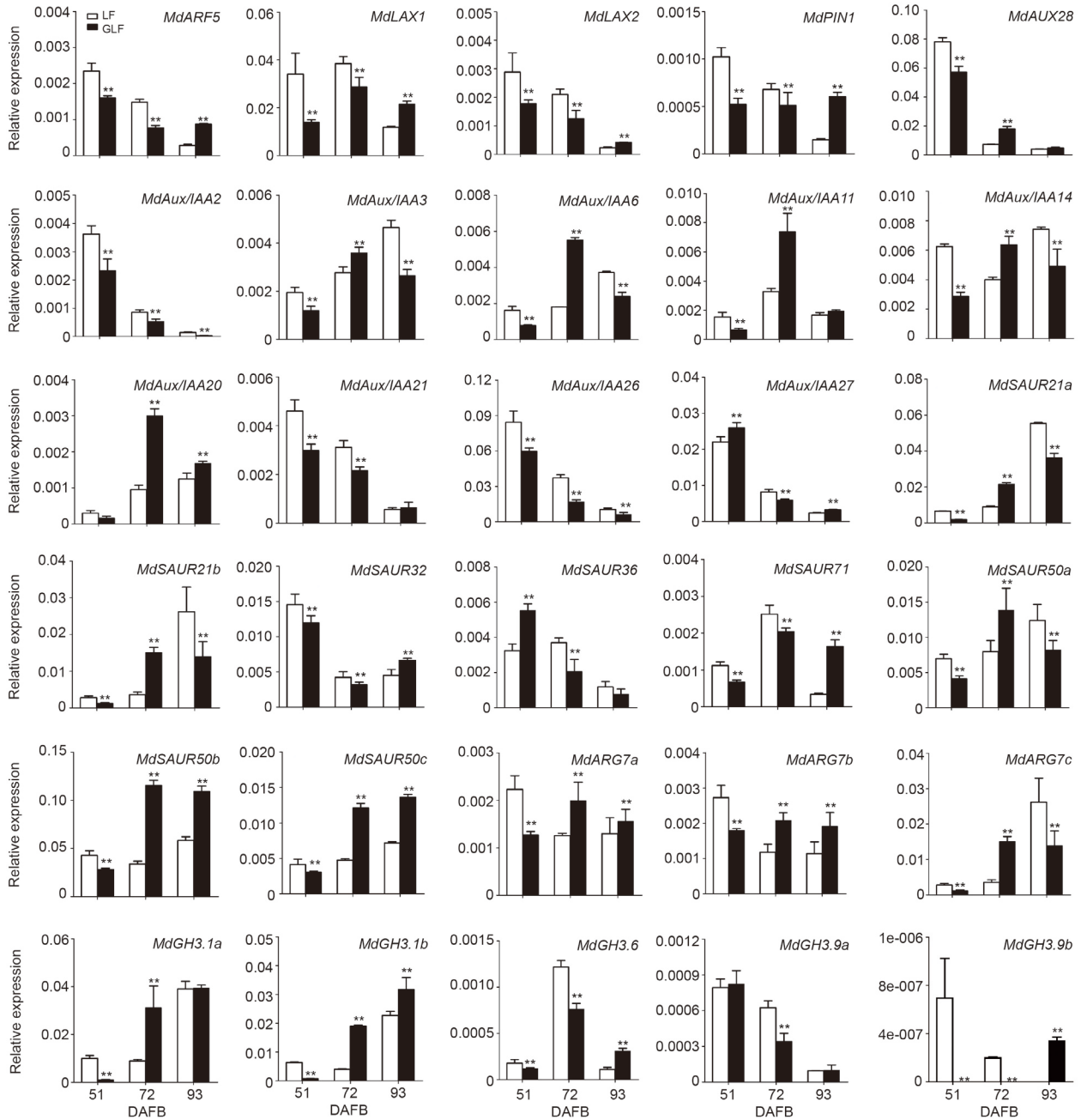

FIGURE 3 | Expression of DEGs in LF and GLF fruits. qRT-PCR was used to measure the expression of DEGs related to auxin signaling in LF and GLF fruits at 51, 72, and 93 DAFB (days after full bloom). **Significant differences ($p < 0.01$, Student's *t*-test). Error bars indicate the standard deviation (SD) of three biological replicates.

hormone signal transduction pathway (Q value = $7.82E^{-09}$) was smaller than all other pathways, indicating that plant hormone signal transduction was the most important pathway (**Supplementary Figure 5** and **Supplementary Table 4**). Among these genes, 30 were associated with the auxin pathway, including six gene families (*AUX1*, *PIN*, *Aux*/*IAA*, *ARF*, *GH3*, and *SAUR*; **Supplementary Table 3**), suggesting that the auxin pathway considerably contributed to the larger fruit size of GLF.

qRT-PCR Verification of the DEGs Between GLF and LF Fruits

To confirm the accuracy of the transcriptome data, 30 of auxin signaling genes were selected for qRT-PCR comparison between GLF and LF fruits. Results revealed a positive correlation with the RNA-Seq data in 72 DAFB samples (**Figure 3** and **Supplementary Table 3**), which confirmed the accuracy of the transcriptome results.

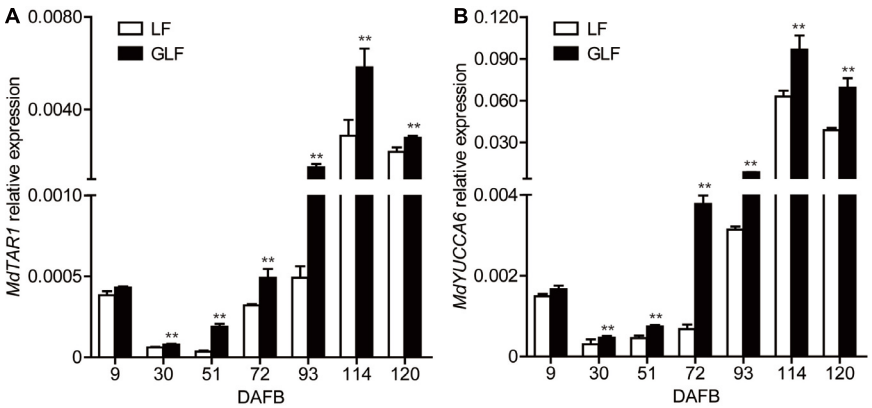

FIGURE 4 | Relative expression of *MdTAR1* and *MdYUCCA6* in LF and GLF fruits. GLF and LF fruit cortexes were collected from 9 to 120 DAFB (days after full bloom). qRT-PCR was used to measure the relative expression of *MdTAR1* **(A)** and *MdYUCCA6* **(B)**. **Significant differences ($p < 0.01$, Student's *t*-test). Error bars indicate the standard deviation (SD) of three biological replicates.

Auxin synthesis, conjugation, and transport are tightly regulated, leading to auxin homeostasis (Perrot-Rechenmann and Napier, 2005). Changing endogenous auxin concentrations can modify the signaling response, causing several gene transcription level changes (Paponov et al., 2008). Combined with the transcriptome results, two genes (*MdTAR1* and *MdYUCCA6*) were found to be responsible for auxin synthesis and upregulated in GLF at 72 DAFB (**Supplementary Table 3**). Thus, we proposed that the upregulation of auxin synthetic genes may lead to increased auxin concentrations. Then, we investigated the transcription levels of *MdTAR1* and *MdYUCCA6* by qRT-PCR. *MdTAR1* and *MdYUCCA6* were expressed at higher levels in GLF than LF at six fruit development stages (30, 51, 72, 93, 114, and 120 DAFB; **Figure 4**), suggesting that the upregulation of these auxin synthetic genes may lead to differential auxin levels, thereby leading to larger fruit sizes in GLF.

Endogenous Auxin Levels Were Higher in GLF Than LF Fruit

Since the expressions of two auxin synthetic genes (*MdTAR1* and *MdYUCCA6*) were higher in GLF fruit than in LF fruit, we speculated that upregulation of auxin synthetic genes may lead to increased auxin in GLF. The endogenous IAA levels of both varieties were measured. Results revealed that the endogenous IAA content in GLF was significantly higher than that in LF at 30, 51, 72, 93, and 114 DAFB (**Figure 5**). To determine whether auxin levels affected fruit size, NAA was used to treat the on-tree fruit of LF at 30 DAFB. Interestingly, the NAA treatment significantly increased the fruit weight, transverse diameter, and longitudinal diameter of LF when harvested at 120 DAFB (**Figures 6A,B**). In addition, LF cell sizes were significantly enlarged after NAA treatment (**Figure 6C**). Next, we used TIBA, an inhibitor of auxin transport polarity, to investigate the effects of the auxin reduction on fruit size. The TIBA treatment significantly decreased the fruit weight, transverse diameter, and longitudinal diameter of GLF when harvested at 120 DAFB (**Figures 6A,B**). GLF cell sizes were

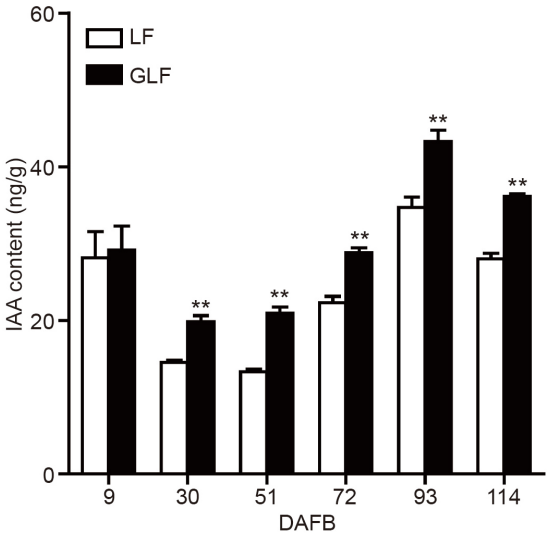

FIGURE 5 | Auxin contents of LF and GLF fruits. The IAA content was measured using fruit cortex of LF and GLF. **Significant differences ($p < 0.01$, Student's *t*-test). Error bars indicate the standard deviation (SD) of three biological replicates.

significantly reduced by the TIBA treatment (**Figure 6C**). These results suggested that the higher levels of endogenous IAA may result in the larger fruit size of GLF.

DISCUSSION

Fruit size is an important trait that influences the economic value of fruit (Malladi and Hirst, 2010). Multiple factors influence fruit size, including ploidy, hormone levels, and genetic controls. For example, the tetraploid "Hanfu" apple has a larger fruit size than the diploid "Hanfu" apple (Xue et al., 2017). In this study, we found that both GLF and LF were diploid

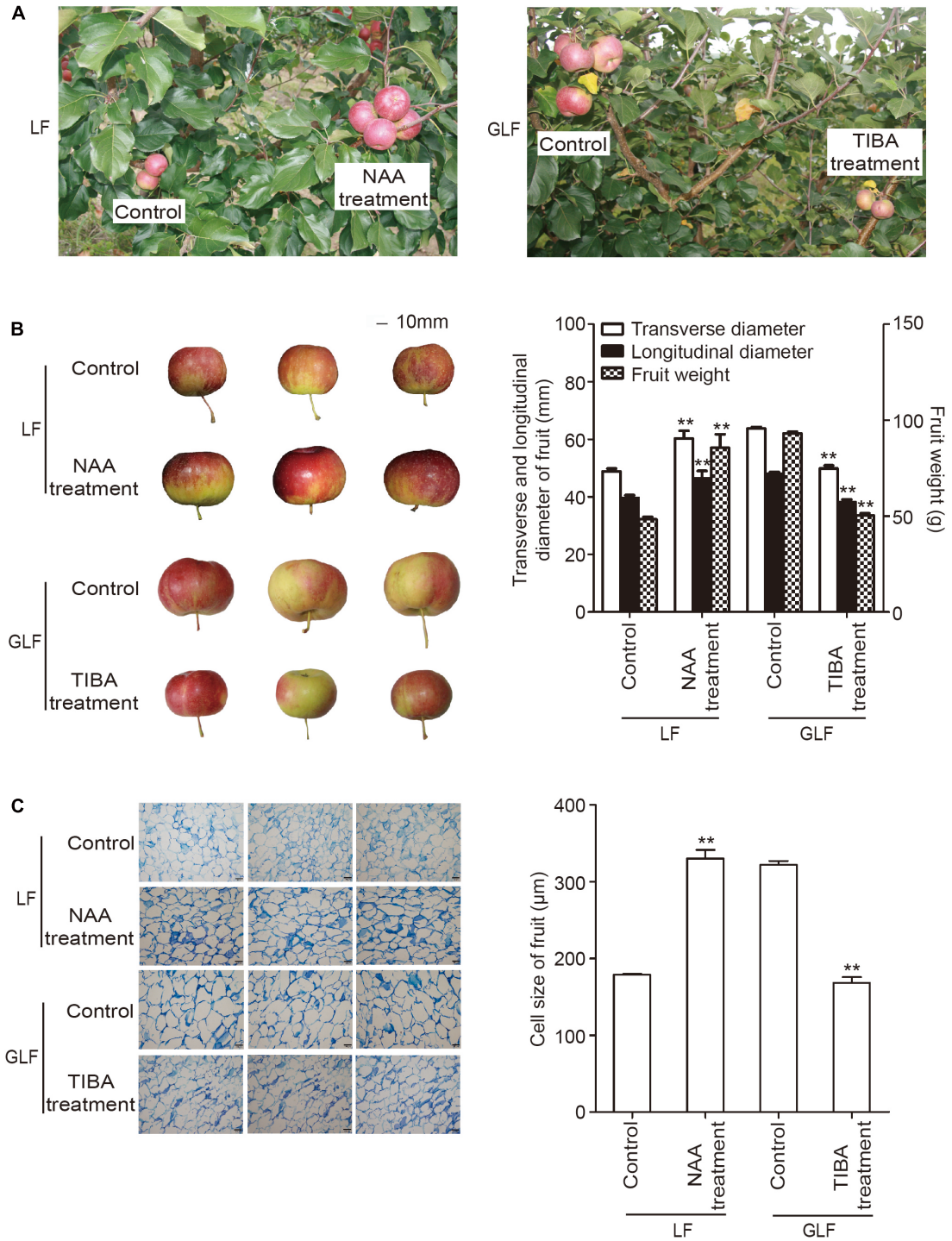

FIGURE 6 | The influence of auxin and TIBA on fruit and cell sizes. On-tree LF and GLF fruits were treated with NAA and TIBA at 30 DAFB (days after full bloom), respectively, and harvested at 120 DAFB **(A)**. Fruit transverse diameter, longitudinal diameter, and weight were measured on harvest fruit. Bar, 10 mm **(B)**. Cell sizes were calculated as the average of six typical cell lengths, which were measured by a scale tool under a microscope at 120 DAFB. Bar, 100 μm **(C)**. **Significant differences ($p < 0.01$, Student's *t*-test). Error bars indicate the standard deviation (SD) of three biological replicates.

(**Supplementary Figure 3**); thus, ploidy could not explain the larger fruit size of GLF. Previous studies have revealed that cell size and number play important roles in affecting the size of different fruit, including tomato (Cheniclet et al., 2005), sweet cherry (Olmstead et al., 2007), and peach (Guo et al., 2018). Here, we found that the large fruit size of GLF correlated with cell size

(**Figure 2C**). This result supports the findings of Malladi and Hirst (2010), in which cell size was a major factor affecting the larger size of "Grand Gala" fruit, a bud sport variety of "Gala" apple. In the early stage of fruit development, it involves both cell division and increase in cell size or cell growth due to addition of additional cellular contents. At later stages, increase in cell size is greatly aided by post-mitotic cell expansion which would also involve greater vacuolation (Warrington et al., 1999; Janssen et al., 2008). In our data, the cell numbers increased greatly from 9 to 30 DAFB and remained the same at later stages (**Figure 2B**), but the cell size was much greater in GLF than in LF throughout fruit development (**Figure 2**). Thus, the cell growth that enhanced during early fruit development of GLF might continue at later stages, leading to larger fruit of GLF. Based upon this, we selected samples of 72 DAFB for RNA-seq.

Previous studies have elucidated the roles of various genes involved in fruit size. For example, *ANT* or *BIG BROTHER* regulated organ size by controlling cell numbers in *Arabidopsis* (Krizek, 1999; Disch et al., 2006). *WEE1* regulated fruit size by controlling cell size in tomato fruit (Gonzalez et al., 2007), and *FW2.2* negatively regulated cell proliferation, which thereby influenced the fruit size (Frary et al., 2000). Silencing of *PaCYP78A9* reduced fruit size through its effect on reducing cell size and cell number in sweet cherry (Qi et al., 2017). In apple, *microRNA172* overexpression inhibits the transcription of *AP2*, conferring significantly reduced fruit size (Yao et al., 2015). Suppression of *MdMADS8* or *MdMADS9* expression significantly reduced cell size, resulting in smaller apple fruits (Ireland et al., 2013). In this study, these genes did not exhibit differential expression between GLF and LF, based on the RNA-Seq data (**Supplementary Table 3**). In addition, fruit size is regulated by phytohormones. For example, the application of CPPU, an artificial-synthesized cytokinin, increased fruit size in kiwifruit (*A. chinensis*) by inducing cell number (Cruz-Castillo et al., 2002). Gibberellin treatment increased the fruit size of pear (*P. pyrifolia*; Ito et al., 2015) and apple (Martin et al., 1970). However, in this study, we did not find DEGs belong to cytokinin or gibberellin synthesis genes (**Supplementary Table 3**). These results suggested the different mechanisms for the formation of larger fruit size of GLF apple.

It was previously reported that auxin increased fruit size by increasing cell size in "Royal Gala" apple (Devoghalaere et al., 2012). In this study, the RNA-Seq analysis revealed 32 DEGs involved in the auxin pathway (**Supplementary Table 3**), among which 2 auxin synthesis genes (*MdTAR1* and *MdYUCCA6*) were upregulated in GLF (**Figure 4**). Induction of *TAR* expression increased the IAA concentrations in grapevine (*Vitis vinifera*; Bottcher et al., 2013); Moreover, when *YUCCA6* was overexpressed in the *Arabidopsis yuc6-1D* mutant, it increased the free IAA levels and displayed typical high-auxin phenotypes (Kim et al., 2011). In this study, the endogenous auxin levels were higher in GLF than LF (**Figure 5**), and the NAA treatment increased the fruit and cell size of LF, while the TIBA treatment decreased the fruit and cell size of LF (**Figure 6**). Thus, we proposed that the upregulation of these auxin synthetic genes may lead to increased endogenous auxin levels in GLF, resulting in larger cell and fruit sizes than LF. In the future, it will be interesting to investigate what underlying factors determine the differential expression of *MdTAR1* or *MdYUCCA6* between GLF and LF fruits, which may help explain the larger fruit size of GLF.

DATA AVAILABILITY STATEMENT

Sequence data from this article can be found in the Genome Database for Rosaceae (https://www.rosaceae.org/) or GenBank/EMBL libraries under the following accession numbers: *MD15G1014400 (MdARF5), MD07G1215900 (MdLAX1), MD12G1162400 (MdLAX2), MD06G1226800 (MdPIN1), MD10G1192900 (MdAUX28), MD08G1111200 (MdAux/IAA2), MD04G1225000 (MdAux/IAA3), MD17G1198100 (MdAux/IAA6), MD10G1176400 (MdAux/IAA11), MD13G1205000 (MdAux/IAA14), MD15G1169100 (MdAux/IAA20), MD09G1208000 (MdAux/IAA21), MD09G1202300 (MdAux/IAA26), MD15G1191800 (MdAux/IAA27), MD10G1059800 (MdSAUR21a), MD10G1059700 (MdSAUR21b), MD16G1124300 (MdSAUR32), MD02G1205700 (MdSAUR36), MD05G1223400 (MdSAUR71), MD05G1052100 (MdSAUR50d), MD10G1059200 (MdSAUR50b), MD10G1059600 (MdSAUR50c), MD15G1222900 (MdARG7a), MD02G1100000 (MdARG7b), MD05G1052400 (MdARG7c), MD05G1092300 (MdGH3.1a), MD05G1092900 (MdGH3.1b), MD11G1230400 (MdGH3.6), MD11G1304200 (MdGH3.9a), MD03G1284700 (MdGH3.9b), MD16G1098400 (MdTAR1)*, and *MD15G1098700 (MdYUCCA6)*. The raw RNA-Seq data were deposited to the NCBI sequence read archive (SRA) database under the accession number, PRJNA551702.

AUTHOR CONTRIBUTIONS

HB and AW conceived this project and designed the work. HB, YW, and PY performed the research. WY and HY analyzed the data. HB and AW wrote the manuscript. All authors contributed critically to the drafts and gave final approval for publication.

FUNDING

This work was supported by the National Natural Science Foundation of China (31722047), the LiaoNing Revitalization Talents Program (XLYC1802019), the Program of Key Laboratory of Biology and Genetic Improvement of Horticultural Crops (Germplasm Resources Utilization), Ministry of Agriculture, China (NYZS202002), and the Heilongjiang Academy of Agricultural Sciences (2020YYYF052).

ACKNOWLEDGMENTS

We thank Dr. Tong Li, Xinyue Li, and Zepeng Yin for assisting with the experiments and commenting on the manuscript, and thank LetPub (www.letpub.com) for its linguistic assistance during the preparation of this manuscript.

SUPPLEMENTARY MATERIAL

The Supplementary Material for this article can be found online at: https://www.frontiersin.org/articles/10.3389/fpls.2020.592540/full#supplementary-material

Supplementary Figure 1 | Simple sequence repeat (SSR) analysis of LF and GLF. Genomic DNA was isolated from LF and GLF fruits, and 16 pairs of SSR primers were selected for PCR. Denaturing polyacrylamide gel examining was used for PCR products analysis, primer names were indicated using the numbers under the figure. L: LF; G: GLF; and M, DNA size marker.

Supplementary Figure 2 | Comparison of core diameter and seed number between LF and GLF fruits. LF and GLF fruits were harvested at 120 DAFB and used for the comparison between core diameter and seed number. Error bars indicate the standard deviation (SD) of 10 fruits.

Supplementary Figure 3 | Ploidy analysis of LF and GLF fruits. Young leaves were used to analyze the ploidy of LF **(B)** and GLF **(C)** fruit by flow cytometry. "Hanfu" apple (*M. domestica*, 2n = 2x = 34) **(A)**, which is diploid, was used as the control and internal reference in **(D,E)**.

Supplementary Figure 4 | KEGG analysis of the DEGs between GLF and LF fruits.

Supplementary Figure 5 | KEGG enrichment analysis of the DEGs between GLF and LF fruits. The top 20 enriched pathways of the DEGs in GLF fruit were compared to LF. The *x*-axis represents the rich factor on a scale from 2 to 5. The color of the circles represents the *Q*-value. The size of the circles represents the gene number (shown on the right).

Supplementary Table 1 | List of primers used in this study.

Supplementary Table 2 | DEGs between GLF and LF fruits.

Supplementary Table 3 | Annotation of DEGs between GLF and LF fruits.

Supplementary Table 4 | KEGG classifications of assembly and enrichment analysis of all DEGs.

REFERENCES

Anders, S., and Huber, W. (2010). Differential expression analysis for sequence count data. *Genome Biol.* 11:R106. doi: 10.1186/gb-2010-11-10-r106

Bottcher, C., Burbidge, C. A., Boss, P. K., and Davies, C. (2013). Interactions between ethylene and auxin are crucial to the control of grape (Vitis vinifera L.) berry ripening. *BMC Plant Biol.* 13, 222–222. doi: 10.1186/1471-2229-13-222

Cheniclet, C., Rong, W. Y., Causse, M., Frangne, N., Bolling, L., Carde, J., et al. (2005). Cell Expansion and Endoreduplication Show a Large Genetic Variability in Pericarp and Contribute Strongly to Tomato Fruit Growth. *Plant Physiol.* 139, 1984–1994. doi: 10.1104/pp.105.068767

Cruz-Castillo, J., Woolley, D., and Lawes, G. (2002). Kiwifruit size and CPPU response are influenced by the time of anthesis. *Sci. Horticult.* 95, 23–30. doi: 10.1016/S0304-4238(01)00384-3

Daccord, N., Celton, J.-M., Linsmith, G., Becker, C., Choisne, N., Schijlen, E., et al. (2017). High-quality de novo assembly of the apple genome and methylome dynamics of early fruit development. *Nat. Genet.* 49:1099. doi: 10.1038/ng.3886

Devoghalaere, F., Doucen, T., Guitton, B., Keeling, J., Payne, W., Ling, T. J., et al. (2012). A genomics approach to understanding the role of auxin in apple (Malus x domestica) fruit size control. *BMC Plant Biol.* 12:7. doi: 10.1186/1471-2229-12-7

Disch, S., Anastasiou, E., Sharma, V. K., Laux, T., Fletcher, J. C., and Lenhard, M. (2006). The E3 ubiquitin ligase BIG BROTHER controls Arabidopsis organ size in a dosage-dependent manner. *Curr. Biol.* 16, 272–279. doi: 10.1016/j.cub.2005.12.026

Duan, N., Bai, Y., Sun, H., Wang, N., Ma, Y., Li, M., et al. (2017). Genome re-sequencing reveals the history of apple and supports a two-stage model for fruit enlargement. *Nat. Commun.* 8:249. doi: 10.1038/s41467-017-00336-7

Frary, A., Nesbitt, T. C., Frary, A., Grandillo, S., Van Der Knaap, E., Cong, B., et al. (2000). fw2. 2: a quantitative trait locus key to the evolution of tomato fruit size. *Science* 289, 85–88. doi: 10.1126/science.289.5476.85

Gambino, G., Perrone, I., and Gribaudo, I. (2008). A rapid and effective method for RNA extraction from different tissues of grapevine and other woody plants. *Phytochem. Analysis* 19, 520–525. doi: 10.1002/pca.1078

Gonzalez, N., Gévaudant, F., Hernould, M., Chevalier, C., and Mouras, A. (2007). The cell cycle−associated protein kinase WEE1 regulates cell size in relation to endoreduplication in developing tomato fruit. *Plant J.* 51, 642–655. doi: 10.1111/j.1365-313X.2007.03167.x

Guo, J., Cao, K., Li, Y., Yao, J.-L., Deng, C., Wang, Q., et al. (2018). Comparative transcriptome and microscopy analyses provide insights into flat shape formation in peach (Prunus persica). *Front. Plant Sci.* 8:2215. doi: 10.3389/fpls.2017.02215

Ireland, H. S., Yao, J. L., Tomes, S., Sutherland, P. W., Nieuwenhuizen, N., Gunaseelan, K., et al. (2013). Apple SEPALLATA1/2−like genes control fruit flesh development and ripening. *Plant J.* 73, 1044–1056. doi: 10.1111/tpj.12094

Ito, A., Sakamoto, D., Itai, A., Nishijima, T., Oyama-Okubo, N., Nakamura, Y., et al. (2015). Effects of GA3+ 4 and GA4+ 7 application either alone or combined with Prohexadione-Ca on fruit development of Japanese pear 'Kosui'. *Horticult. J.* 85, 201–208. doi: 10.2503/hortj.MI-107

Janssen, B. J., Thodey, K., Schaffer, R. J., Alba, R., Balakrishnan, L., Bishop, R., et al. (2008). Global gene expression analysis of apple fruit development from the floral bud to ripe fruit. *BMC Plant Biol.* 8:16. doi: 10.1186/1471-2229-8-16

Kanehisa, M., Goto, S., Kawashima, S., Okuno, Y., and Hattori, M. (2004). The KEGG resource for deciphering the genome. *Nucleic Acids Res.* 32, D277–D280. doi: 10.1093/nar/gkh063

Kim, J. I., Murphy, A. S., Baek, D., Lee, S., Yun, D., Bressan, R. A., et al. (2011). YUCCA6 over-expression demonstrates auxin function in delaying leaf senescence in Arabidopsis thaliana. *J. Exp. Bot.* 62, 3981–3992. doi: 10.1093/jxb/err094

Krizek, B. A. (1999). Ectopic expression of AINTEGUMENTA in Arabidopsis plants results in increased growth of floral organs. *Dev. Genet.* 25, 224–236. doi: 10.1002/(SICI)1520-6408199925

Lavy, M., and Estelle, M. (2016). Mechanisms of auxin signaling. *Development* 143, 3226–3229. doi: 10.1242/dev.131870

Leyser, O. (2018). Auxin signaling. *Plant Physiol.* 176, 465–479. doi: 10.1104/pp.17.00765

Li, S. X. (1994). Fresh and processed new cultivar of apple-Longfeng. *Chin. Forest Products* 3:50.

Li, X., Guo, W., Li, J., Yue, P., Bu, H., Jiang, J., et al. (2020). Histone acetylation at the promoter for the transcription factor PuWRKY31 affects sucrose accumulation in pear fruit. *Plant Physiol.* 182, 2035–2046. doi: 10.1104/pp.20.00002

Li, T., Xu, Y., Zhang, L., Ji, Y., Tan, D., Yuan, H., et al. (2017). The Jasmonate-Activated Transcription Factor MdMYC2 Regulates ETHYLENE RESPONSE FACTOR and Ethylene Biosynthetic Genes to Promote Ethylene Biosynthesis during Apple Fruit Ripening. *Plant Cell* 29:1316. doi: 10.1105/tpc.17.00349

Ma, Y., Xue, H., Zhang, L., Zhang, F., Ou, C., Wang, F., et al. (2016). Involvement of auxin and brassinosteroid in dwarfism of autotetraploid apple (Malus× domestica). *Sci. Rep.* 6:26719. doi: 10.1038/srep26719

Malladi, A., and Hirst, P. M. (2010). Increase in fruit size of a spontaneous mutant of 'Gala'apple (Malus× domestica Borkh.) is facilitated by altered cell production and enhanced cell size. *J. Exp. Bot.* 61, 3003–3013. doi: 10.1093/jxb/erq134

Mao, X., Tao, C. J. G. O., and Wei, L. (2005). Automated genome annotation and pathway identification using the KEGG Orthology (KO) as a controlled vocabulary. *Bioinformatics* 21, 3787–3793. doi: 10.2307/1592215

Martin, G., Brown, D., and Nelson, M. (1970). Apple shape changing possible with cytokinin and gibbereilin sprays. *Calif. Agricult.* 93, 367–373. doi: 10.1111/j.1478-4408.1977.tb03306.x

McClure, K. A., Gardner, K. M., Douglas, G. M., Song, J., Forney, C. F., DeLong, J., et al. (2018). A genome-wide association study of apple quality and scab resistance. *Plant Genom.* 11:170075. doi: 10.3835/plantgenome2017.08.0075

Müller, A., Düchting, P., and Weiler, E. W. (2002). A multiplex GC-MS/MS technique for the sensitive and quantitative single-run analysis of acidic phytohormones and related compounds, and its application to Arabidopsis thaliana. *Planta* 216, 44–56. doi: 10.1007/s00425-002-0866-6

Olmstead, J. W., Iezzoni, A. F., and Whiting, M. D. (2007). Genotypic differences in sweet cherry (Prunus avium L.) fruit size are primarily a function of cell number. *J. Am. Soc. Horticult. Sci.* 132, 697–703. doi: 10.1007/s10658-007-9180-2

Paponov, I. A., Paponov, M., Teale, W., Menges, M., Chakrabortee, S., Murray, J. A., et al. (2008). Comprehensive transcriptome analysis of auxin responses in Arabidopsis. *Mole. Plant* 1, 321–337. doi: 10.1093/mp/ssm021

Perrot−Rechenmann, C., and Napier, R. M. (2005). Auxins. *Vitamins Hormones* 72, 203–233. doi: 10.1016/S0083-6729(04)72006-3

Qi, X., Liu, C., Song, L., Li, Y., and Li, M. (2017). PaCYP78A9, a Cytochrome P450, Regulates Fruit Size in Sweet Cherry (Prunus aviumL.). *Front. Plant Sci.* 8:2076. doi: 10.3389/fpls.2017.02076

Scorzal, R., May, L. G., Purnell, B., and Upchurch, B. (1991). Differences in number and area of mesocarp cells between small-and large-fruited peach cultivars. *J. Am. Soc. Horticult. Sci.* 116, 861–864.

Staswick, P. E., Tiryaki, I., and Rowe, M. (2002). Jasmonate Response Locus JAR1 and Several Related Arabidopsis Genes Encode Enzymes of the Firefly Luciferase Superfamily That Show Activity on Jasmonic, Salicylic, and Indole-3-Acetic Acids in an Assay for Adenylation. *Plant Cell* 14, 1405–1415. doi: 10.1105/tpc.000885

Vanneste, S., and Friml, J. (2009). Auxin: a trigger for change in plant development. *Cell* 136, 1005–1016. doi: 10.1016/j.cell.2009.03.001

Wabnik, K., Kleine-Vehn, J., Balla, J., Sauer, M., Naramoto, S., Reinöhl, V., et al. (2010). Emergence of tissue polarization from synergy of intracellular and extracellular auxin signaling. *Mole. Sys. Biol.* 6:447. doi: 10.1038/msb.2010.103

Wang, Z., Meng, D., Wang, A., Li, T., Jiang, S., and Cong, P. (2013). The Methylation of the PcMYB10 Promoter Is Associated with Green-Skinned Sport in Max Red Bartlett Pear. *Plant Physiol.* 162, 885–96. doi: 10.1104/pp.113.214700

Warrington, I., Fulton, T., Halligan, E., and De Silva, H. (1999). Apple fruit growth and maturity are affected by early season temperatures. *J. Am. Soc. Horticult. Sci.* 124, 468–477.

Xue, H., Zhang, B., Tian, J.-R., Chen, M.-M., Zhang, Y.-Y., Zhang, Z.-H., et al. (2017). Comparison of the morphology, growth and development of diploid and autotetraploid 'Hanfu'apple trees. *Sci. Horticult.* 225, 277–285. doi: 10.1016/j.scienta.2017.06.059

Yang, Y., Hammes, U. Z., Taylor, C. G., Schachtman, D. P., and Nielsen, E. (2006). High-affinity auxin transport by the AUX1 influx carrier protein. *Curr. Biol.* 16, 1123–1127. doi: 10.1016/j.cub.2006.05.043

Yao, J. L., Xu, J., Cornille, A., Tomes, S., Karunairetnam, S., Luo, Z., et al. (2015). A micro RNA allele that emerged prior to apple domestication may underlie fruit size evolution. *Plant J.* 84, 417–427. doi: 10.1111/tpj.13021

Young, M. D., Wakefield, M. J., Smyth, G. K., and Oshlack, A. (2010). Gene ontology analysis for RNA-seq: accounting for selection bias. *Genome Biol.* 11, R14–R14. doi: 10.1186/gb-2010-11-2-r14

Zažímalová, E., Murphy, A. S., Yang, H., Hoyerová, K., and Hošek, P. (2010). Auxin transporters—why so many? *Cold Spring Harbor Perspect. Biol.* 2:a001552. doi: 10.1101/cshperspect.a001552

Zhang, C., Tanabe, K., Tamura, F., Matsumoto, K., and Yoshida, A. (2005). 13C-photosynthate accumulation in Japanese pear fruit during the period of rapid fruit growth is limited by the sink strength of fruit rather than by the transport capacity of the pedicel. *J. Exp. Bot.* 56, 2713–2719. doi: 10.1093/jxb/eri264

Zhang, S. J., Wu, J., Chen, H., Gu, C., Tao, S. T., Wu, J. Y., et al. (2011). Identification of differentially expressed genes in a spontaneous mutant of 'Nanguoli' pear (Pyrus ussuriensis Maxim) with large fruit. *J. Pomol. Horticult. Sci.* 86, 595–602. doi: 10.1080/14620316.2011.11512809

Zhao, Y., Christensen, S. K., Fankhauser, C., Cashman, J. R., Cohen, J. D., Weigel, D., et al. (2001). A role for flavin monooxygenase-like enzymes in auxin biosynthesis. *Science* 291, 306–309. doi: 10.1126/science.291.5502.306

Conflict of Interest: The authors declare that the research was conducted in the absence of any commercial or financial relationships that could be construed as a potential conflict of interest.

frontiers in Plant Science

REVIEW
published: 11 January 2021
doi: 10.3389/fpls.2020.619953

The Physiological and Molecular Mechanism of Abscisic Acid in Regulation of Fleshy Fruit Ripening

Qian Bai[1,2], *Yun Huang*[2]* *and Yuanyue Shen*[2]*

[1]College of Horticulture, China Agricultural University, Beijing, China, [2]College of Plant Science and Technology, Beijing University of Agriculture, Beijing, China

The ripening of fleshy fruits is coupled with the degradation of both chlorophyll and cell walls, as well as changes in the metabolism of phenylpropanoids, flavonoids, starch/sucrose, and carotenoids. These processes are controlled by phytohormones and other factors, including abscisic acid (ABA), ethylene, auxin, polyamines, sugar, and reactive oxygen species. The ripening of climacteric fruits is controlled by ethylene and non-climacteric fruit ripening is regulated mainly by ABA. Also, ABA and ethylene may interact in both types of fruit ripening. ABA concentrations in fleshy fruits are regulated in response to developmental and environmental cues and are controlled by the relative rates of ABA biosynthesis and catabolism, the former mainly *via* 9-cis-epoxycarotenoid dioxygenases (NCEDs) and β-glucosidases and the latter *via* ABA 8'-hydroxylases (CYP707As) and β-glycosyltransferases. In strawberry fruit ripening, ABA is perceived *via* at least two receptors, Pyrabactin resistance (PYR)/PYR-like (PYL) and putative abscisic acid receptor (ABAR), which are linked separately to the conserved signaling pathway ABA-FaPYR1-FaABI1-FaSnRK2 and the novel signaling pathway ABA-FaABAR-FaRIPK1-FaABI4. Downstream signaling components include important transcription factors, such as AREB (ABA responsive element binding protein)/ABF (ABRE binding factors ABA responsive factor), ethylene response factor (ERF), and V-myb Myeloblastosis viral oncogene homolog (MYB), as well as ripening-related genes. Finally, a comprehensive model of ABA linked to ethylene, sugar, polyamines, auxin and reactive oxygen species in the regulation of strawberry fruit ripening is proposed. Next, new integrated mechanisms, including two ABA signaling pathways, ABA and ethylene signaling pathways, and ABA/ethylene to other phytohormones are interesting and important research topics in ripening, especially in non-climacteric fruits.

Keywords: fruit ripening, non-climacteric fruit, abscisic acid, ethylene, signaling transduction, review

OPEN ACCESS

Edited by:
Chunying Kang,
Huazhong Agricultural University, China

Reviewed by:
Aide Wang,
Shenyang Agricultural University, China
Guozheng Qin
Institute of Botany (CAS), China

***Correspondence:**
Yuanyue Shen
sflmn@163.com
Yun Huang
yunhuang@bua.edu.cn

Specialty section:
This article was submitted to Plant Development and EvoDevo, a section of the journal Frontiers in Plant Science

Received: *21 October 2020*
Accepted: *09 December 2020*
Published: *11 January 2021*

Citation:
Bai Q, Huang Y and Shen Y (2021) The Physiological and Molecular Mechanism of Abscisic Acid in Regulation of Fleshy Fruit Ripening. Front. Plant Sci. 11:619953. doi: 10.3389/fpls.2020.619953

INTRODUCTION

Angiosperm fruits can generally be divided into dry or fleshy types. Flowering plants have evolved both conserved and divergent mechanisms for development and maturation of both fleshy and dry fruits (Hershkovitz et al., 2011; Garceau et al., 2017). The molecular mechanisms of dry fruit development and maturation have been revealed through studies of the model plant Arabidopsis (Gazzarrini and Tsai, 2015), while studies of various non-ripening tomato fruit mutants have defined the mechanisms of fleshy fruit ripening (Liu et al., 2015).

Fleshy fruit ripening is mainly divided into two types, climacteric and non-climacteric, based on the presence or absence of a transient peak in respiration rate and ethylene emission. In climacteric fruits, such as tomato and banana, peaks in both respiration and ethylene level occur during ripening; in contrast, no such peaks occur in non-climacteric fruits, such as grape and strawberry, the ripening of which is controlled by abscisic acid (ABA) in an ethylene-independent manner (Kumar et al., 2014; Shen and Rose, 2014). Fruit color break, coinciding with the conversion of chloroplasts into chromoplasts, is a visible sign of ripening in both climacteric and non-climacteric fruits, and is followed by softening and changes in sugars, color, and flavor (Azoulay et al., 2008). During the past decade, studies using strawberry fruit as a model have led to major breakthroughs in understanding the regulation of non-climacteric fruit ripening by ABA and its interaction with other phytohormones. In this review, we focus on the physiological and molecular mechanisms of ABA in regulation of fleshy fruit ripening.

CENTRAL ROLES OF ABA IN REGULATION OF NON-CLIMACTERIC FRUIT RIPENING

Classical studies of ABA effects on fleshy fruit ripening were done on grape (*Vitis vinifera*) berries and uncovered vital roles for ABA in veraison and ripening processes, including coloration, sugar accumulation, acid decline, and flesh softening (Coombe, 1976; Davies et al., 1997). However, a deeper understanding of ABA action in non-climacteric fruit ripening was gained from a breakthrough study in strawberry (Jia et al., 2011). The importance of ABA has recently been confirmed in many non-climacteric fruits, such as sweet cherry (*Prunus avium*; Tijero et al., 2016; Shen et al., 2017), watermelon (*Citrullus lanatus*; Wang et al., 2017b), blueberry (*Semen trigonellae*; Oh et al., 2018), bilberry (*Vaccinium myrtillus*; Karppinen et al., 2018), jujube (*Ziziphus jujuba*; Kou et al., 2019), litchi (*Litchi chinensis*; Hu et al., 2019), orange (*Citrus sinensis*; Romero et al., 2019), and wolfberry (*Lycium ruthenicum*; Li et al., 2019).

ABA Perception and Signaling in Strawberry Fruit Ripening Represent a Model of Non-climacteric Ripening

In developing strawberry fruit, ripening is markedly stimulated by exogenous ABA or DMSO (dimethyl sulfoxide, an accelerator of ABA biosynthesis), whereas fluridone (an inhibitor of ABA biosynthesis) significantly inhibits ripening; furthermore, downregulation of either *FaNCED1* (*9-cis-epoxycarotenoid dioxygenase*, a key gene in ABA biosynthesis) or *FaCHLH/ABAR* (*magnesium chelatase H subunit/putative ABA receptor*) inhibits ripening; importantly, exogenous ABA can rescue coloration of *FaNCED1*-RNAi fruit but not of *FaCHLH/ABAR*-RNAi fruit, confirming that ABA is a key signal molecule in the promotion of strawberry ripening (Jia et al., 2011). Kadomura-Ishikawa et al. (2015) identified FaMYB10 as an important transcription factor mediating signal transduction downstream of ABA perception by the ABAR to stimulate anthocyanin biosynthesis during strawberry fruit ripening. ABA and *FaMYB10* are therefore key regulators for strawberry ripening (Kim et al., 2019). In all, ABA homeostasis in cells involves the regulation of both ABA catabolism and ABA biosynthesis by feedback and feedforward loops, which are tightly linked to the repression of *FveCYP707A4a* expression, key to ABA degradation, and promotion of *FveNCED* expression, key to ABA biosynthesis, in response to the onset of strawberry fruit ripening (Liao et al., 2018). Tightly controlled, synergistic regulation of ABA from biosynthesis to signaling is required to meet the requirements of plant development and fruit ripening.

In addition, the importance of ABA in strawberry ripening was also confirmed by the silencing of genes encoding another ABA receptor, FaPYR1 (Pyrabactin Resistance1; Chai et al., 2011), and its interacting protein FaABI1 (type 2C protein phosphatase1; Jia et al., 2013a). A strawberry FERONIA/FER-like receptor kinase, FaMRLK47, negatively regulates ABA signaling and fruit ripening through its interaction with FaABI1 (Jia et al., 2017a). Importantly, the core ABA signaling pathways, Pyrabactin Resistance 1 (PYR1)/PYR1-like (PYL)/Regulatory Component of ABA Receptor (RCAR) – Type 2C Protein Phosphatase (PP2C)-SNF1-Related Protein Kinase2 (SnRK2) are conserved in plant responses to developmental and environmental cues during stress adaptation, flowering, seed germination, and fruit ripening (Li et al., 2011; Cheng et al., 2019; Gupta et al., 2020).

CHLH/ABAR has multiple functions (Liang et al., 2015). For example, in Arabidopsis, CHLH/ABAR regulates various plant developmental processes in different pathways, such as stomatal movement, seed germination, and seedling growth, through ABA-ABAR-WRKY40-ABI5/ABI4 (Shang et al., 2010). To further explore the mechanisms of FaABAR action in strawberry fruit ripening, Hou et al. (2018) used FaABAR as bait in a yeast two-hybrid assay and isolated a strawberry leucine-rich repeat (LRR) receptor-like kinase, red-initial protein kinase 1 (FaRIPK1) that interacts with FaABAR. FaRIPK1 serves as a co-receptor of FaABAR to synergistically regulate strawberry fruit ripening, namely, FaRIPK1 participates in the onset of ripening while FaABAR is responsible for completion of ripening. Importantly, FaABAR binds to ABA with a K_d (dissociation constant) of 50 μM (Zhang et al., 2017), suggesting that FaABAR is an ABA receptor in strawberry (Jia et al., 2011; Zhang et al., 2017; Hou et al., 2018). Notably, the ABA-ABAR-RIPK1-ABI4 signaling pathway that controls fruit ripening in strawberry (Hou et al., 2018) is distinct from the ABA-ABAR-WRKY40-ABI5/ABI4 pathway in Arabidopsis (Shang et al., 2010).

By contrast, FaPYR1 regulates fruit ripening through the conserved core signaling pathway PYR1-PP2C-SnRK2 (Cheng et al., 2019; Gupta et al., 2020). In addition, among members of FaPYR/PYL and FaPP2C families in strawberry, only FaPYL2/4/9/11 and FaABI1/FaPP2C16 interact with each other, and the interaction of FaPYL2 with FaABI1 might also play a role in strawberry fruit ripening (Hou et al., 2020).

Notably, the SnRK2.6/OST1 protein acts as a linker between ABAR and PYR/PYL/RCAR in Arabidopsis guard cells (Liang et al., 2015). Thus, the relationships between ABAR and PYR/PYL/RCAR in strawberry fruit ripening should be established in the future.

ABA Is a Major Player in the Ripening of Various Non-climacteric Fruits

The relationship between ABA and fruit ripening defined in strawberry facilitates studies of ripening in other non-climacteric fruits, such as grape (Villalobos-González et al., 2016), sweet cherry (Shen et al., 2017), watermelon (Wang et al., 2017b), blueberry (Oh et al., 2018), bilberry (Karppinen et al., 2018), jujube (Kou et al., 2019), litchi (Hu et al., 2019), orange (Romero et al., 2019), and wolfberry (Li et al., 2019).

It is previously reported that ABA is a major phytohormone involved in regulating the onset of grape berry ripening and berry skin secondary metabolism (Villalobos-González et al., 2016). ABA positively regulates sweet cherry development, ripening, and quality through the interaction of PacPP2C1 with six PacSnRK2s, including PacSnRK2.2/2.3/2.6 and PacPP2C1-3 (Tijero et al., 2016; Shen et al., 2017). It is also a major player in watermelon fruit ripening (Wang et al., 2017b). While application of ABA to blueberry fruits has no remarkable effect on fruit growth, it stimulates fruit coloration and softening; however, softening is undesirable during harvest and storage (Oh et al., 2018; Chung et al., 2019). Chinese jujube is a non-climacteric fruit, the ripening of which is regulated by ABA (Kou et al., 2019; Zhang et al., 2019). In addition, ABA plays a key role in ripening-related processes including fruit coloration and softening in both bilberry (Karppinen et al., 2018) and orange fruits (Romero et al., 2019). ABA-mediated anthocyanin biosynthesis during wolfberry fruit maturation and coloration involves the transcription factor complex MYB-bHLH-WD40 (Li et al., 2019). Interestingly, recent reports suggest that the grape U-box E3 ubiquitin ligase VlPUB38 negatively regulates berry ripening in an ABA-dependent manner by degradation of abscisic-aldehyde oxidase (VlAAO), the enzyme catalyzing the last step of ABA biosynthesis (Yu et al., 2020). A synergistic interaction between CrNAC036 and CrMYB68 appears to inhibit CrNCED5-mediated ABA biosynthesis at the transcription level in citrus fruit (Zhu et al., 2020).

De-greening (chlorophyll degradation) and coloration (such as anthocyanin biosynthesis) are major physiological changes during fruit ripening. Application of ABA rapidly initiates chlorophyll breakdown in litchi fruit, and peak ABA concentration is concommitant with the subsequent onset of anthocyanin biosynthesis, demonstrating an important role for ABA during ripening (Hu et al., 2019). ABA response element-binding factors (LcABF1/2/3) play a vital role in litchi fruit ripening: *LcABF1* expression increases in parallel with chlorophyll degradation, while *LcABF3* expression rises at the onset of coloration; moreover, LcABF1/2 mediate expression of ABA-responsive genes related to chlorophyll degradation, while LcABF2/3 mediate expression of genes related to anthocyanin biosynthesisin an ABA-dependent manner (Hu et al., 2019). Collectively, ABA is a major player in regulation of the ripening of various non-climacteric fruits.

Non-climacteric Fruit Ripening Is Regulated by ABA Through Multiple Synergistic Mechanisms

In non-climacteric strawberry fruit, ABA and auxin (IAA) are important regulators, functioning together or independently in response to developmental and environmental cues; auxin is involved in receptacle development and ABA participates in fruit ripening. By contrast, ethylene and gibberellins do not play a prominent role in ripening (Medina-Puche et al., 2016). Contents of both IAA and GA4 (gibberellic acid) are highest in small, green strawberry fruit and gradually decrease throughout fruit development; ABA content increases rapidly, coincident with coloration; methyl jasmonate concentration shows no remarkable variation over time, while salicylic acid content gradually increases; and jasmonic acid and ethylene contents are too low to quantify (Kim et al., 2019). Auxin is produced mainly in achenes, while ABA, ethylene, cytokinins and gibberellins are predominantly biosynthesized in receptacles (Gu et al., 2019). Gibberellin delays ripening to some extent, while cytokinins and ethylene appear to be involved in the later stages of ripening, mostly highlighting possible mechanisms of ABA and auxin interaction in the ripening process (Gu et al., 2019). With the onset of fruit ripening in strawberry, the roles of ABA, ethylene, and polyamines are reinforced while those of GA and IAA are weakened (Wang et al., 2017a). Available data from strawberry suggest that regulation of non-climacteric fruit ripening is rather complex.

Interaction of ABA With Ethylene

Although ethylene is well known as a key regulator in climacteric fruit ripening (Liu et al., 2015), this gaseous molecule also participates in non-climacteric fruit ripening through its interaction with ABA (Li et al., 2020; Tosetti et al., 2020). In postharvest strawberry fruit, ethylene facilitates ABA accumulation in receptacle tissue but does not affect ABA catabolism (Tosetti et al., 2020). Overexpression of *FveERF* (FvH4_5g04470.1), an ethylene response regulator, activates both acyltransferase (AAT) gene transcription and ester accumulation during strawberry fruit ripening (Li et al., 2020). The promoter regions of *ACS1* from both climacteric "Santa Rosa" plum and its non-climacteric mutant "Sweet Miriam" have only minor differences in sequence; however, *ABI5* (*ABA insensitive5*) expression in "Sweet Miriam" fruit is lower than that in "Santa Rosa" fruit during ripening, suggesting a vital role of ABA in ethylene production (Sadka et al., 2019). A cucumber (*Cucumis sativus*) MADS-box (SHATTERPROOF) protein, CsSHP, participates in fruit maturation through ABA-mediated protein complex associated to CsSEPs (SEPALLATA; Cheng et al., 2020). ABA- and ethylene-related genes are differentially modulated during grape berry ripening by a set of transcription factors, including MADS-box, MYB, NAC, AP2/ERF, bHLH, and ZIP (Wong et al., 2016). Thereby,

the interaction of ABA with ethylene plays a vital role in non-climacteric fruit ripening.

Interaction of ABA With IAA

Greater accumulation of IAA and ABA in developing achenes than in the receptacle is important for strawberry fruit maturation and ripening, suggesting a complex ripening mechanism regulated by the two hormones (Araújo et al., 2012; Symons et al., 2012). In fact, auxin plays a dominant role in receptacle growth while ABA plays a vital role in ripening, and other hormones function to different degrees with ABA or ethylene (Estrada-Johnson et al., 2017). Some ripening-related genes are co-regulated by IAA and ABA during strawberry fruit development (Castillejo et al., 2004), such as *FaRGlyase1* (rhamnogalacturonate lyase gene; Molina-Hidalgo et al., 2013), *FaSHP* (a C-type MADS-box gene; Daminato et al., 2013), *FaβGal4* (β-galactosidase gene; Paniagua et al., 2016), and *FaNIP1;1* (plasma membrane aquaporin protein gene; Molina-Hidalgo et al., 2015), which are positively regulated by ABA and negatively regulated by auxins during strawberry fruit ripening. Also, annexins FaAnn5 and FaAnn8 might be involved in the regulation of both ABA and IAA during strawberry fruit growth and ripening through calcium signaling (Chen et al., 2016). The receptor-like kinase and ubiquitin ligase respond to both IAA and ABA and may play an important role in crosstalk between the two hormones (Chen et al., 2016). IAA and ABA are therefore key regulators of strawberry fruit maturation and ripening.

Confirmedly, strong "antagonism" between IAA and ethylene and substantial "synergism" between IAA and ABA occur during grape berry development (Ziliotto et al., 2012). At berry pre-ripening, high auxin levels promote seed tissue development, and transcripts of auxin-response-factor genes accumulate in pericarp tissue; at veraison, auxin action is weakened while ABA action is enforced, suggesting a role for a higher IAA/ABA ratio during growth and a lower ratio during ripening (Gouthu and Deluc, 2015). ABA, auxin and ethylene play important roles in the regulation of non-climacteric fruit maturation and ripening *via* a complex network (Corso et al., 2016).

Interaction of ABA With Polyamines

Blocking ethylene biosynthesis affects the levels of both ABA and putrescine in melon fruit (Concepción Martínez-Madrid et al., 2002). During strawberry fruit ripening, polyamines (PAs), especially spermine, interact with ABA, IAA, and ethylene in a coordinated manner (Guo et al., 2018). Increased transcription of *NCED3*, key to ABA production, at the onset of strawberry fruit ripening facilitates rapid accumulation of ABA, which inhibits transcription of *FaPAO5* (*polyamine oxidase5*), key to PA degradation, leading to accumulation of spermine and spermidine (Mo et al., 2020). Interestingly, the increase in spermine and spermidine contents triggers expression of SAMDC (SAM decar boxylase), SPDS (spermidine synthase), and SPMS (spermine synthase) genes, key to PA biosynthesis, further accelerating spermine and spermidine accumulation and ripening, suggesting that FaPAO5 regulates spermine and spermidine levels in response to ABA signaling during strawberry fruit ripening (Mo et al., 2020). Thus, interactions between ABA and PA play an important role in the regulation of strawberry fruit ripening.

Interaction of ABA With Sugars

Sugars play a central role in fruit ripening and quality because sugar metabolism and accumulation greatly influence taste. Notably, sucrose also serves as a signal, which facilitates strawberry fruit ripening by stimulating ABA production and accumulation (Jia et al., 2011, 2013b). Both ABA and sucrose induce grape berry ripening, with sucrose acting in both ABA-dependent and ABA-independent manners (Jia et al., 2017b). ASR (ABA-, stress-, and ripening-induced protein) regulates strawberry fruit ripening through crosstalk between ABA and sucrose (Jia et al., 2016). Application of sucrose to unripe strawberry fruit promotes ripening by ABA and its derivatives (Siebeneichler et al., 2020). ABA and sucrose accelerate strawberry fruit ripening and induce accumulation of H_2O_2, leading to a transient decrease in glycolysis, demonstrating that the interaction of ABA with sucrose affects ripening by inhibiting glycolysis (Luo et al., 2020a). Moreover, FaGAPC2 (cytosolic glyceraldehyde-3-phosphate dehydrogenase)/FaGAPCp1 (plastid glyceraldehyde-3-phosphate dehydrogenase), key glycolytic enzymes, negatively regulate ABA- and sucrose-mediated ripening in strawberry fruit (Luo et al., 2020b). Therefore, the interaction between ABA and sugar plays a pivotal role in strawberry fruit ripening.

ABA IS ALSO INVOLVED IN THE REGULATION OF CLIMACTERIC FRUIT RIPENING

Although ethylene is an essential regulator of climacteric tomato fruit ripening (Liu et al., 2015), in which, as has been demonstrated over the past decade, ABA also plays a role. Application of ABA accelerates coloration and ethylene biosynthesis in tomato fruit as well as accumulation of phenolic compounds and emission of volatile aromatics (Wu et al., 2018). A tomato gene key to ABA biosynthesis, *SINCED1*, triggers the onset of tomato fruit ripening (Zhang et al., 2009), and suppression of *SINCED1* expression leads to increases in lycopene and β-carotene contents and in shelf life from 15 to 29 days (Sun et al., 2012a,b). Most PYL ABA receptors interact with SlPP2Cs in an ABA-dependent manner; SlPP2C2/SlPP2C3 interact with SlSnRK2s; SlSnRK2.5 interacts with SlABF2/4; and many core components of ABA signaling respond to ABA (Chen et al., 2016). In addition, downregulating the expression of either *SlUGT75C1* (ABA uridine diphosphate glucosyltransferase gene) or *SlPP2C1* (type 2C protein phosphatase gene) alters tomato fruit ripening (Sun et al., 2017; Zhang et al., 2018). The tomato ABA receptor SlPYL9 positively regulates ABA signal transduction and fruit ripening in an ABA-dependent manner (Kai et al., 2019). Overexpression of *LYCOPENE β-CYCLASE* (*LCYb*) leads to an increase in β-carotene and ABA concentrations, as well as a decrease in ethylene emission, which delays softening and increases shelf life,

suggesting that manipulation of β-carotene levels can improve nutritional value and shelf life (Diretto et al., 2020). Similarly, 24 *PYL*, 87 *PP2C*, and 11 *SnRK2* genes have been identified in banana fruit ripening, providing new insights into understanding PYL-PP2C-SnRK2 core signaling (Hu et al., 2017).

The interaction between ABA and ethylene has been studied extensively, contributing to our understanding of the mechanism of ABA involvement in climacteric fruit ripening. ABA may promote ethylene emission and signal transduction by recruiting a set of important genes, including *LeACO1* (*1-amino-cyclopropane-1-carboxylic acid oxidase1*), *LeACS4* (*1-amino-cyclopropane-1-carboxylic acid synthase4*), *GR* (*green-ripe*), and *LeETR6* (*ethylene receptor6*); while ethylene plays an essential role in inducing ABA accumulation at the initiation of ripening, and blocking or removing ethylene leads to low ABA levels (Meyer et al., 2017). Furthermore, a set of transcription factors specific to ethylene production and signaling, including MADS-RIN (MADS-ripening inhibitor), TAGL1 (tomato Agamous-like1), CNR (colorless non-ripening), and NOR (non-ripening), are also ABA responsive, suggesting a crucial function of these transcription factors in ABA-ethylene interactions (Mou et al., 2016). Transient overexpression of *SlAREB1*, a tomato transcription factor gene downstream of ABA signaling, promotes expression of a set of genes including *NOR*, *SlACS2*, *SlACS4*, and *SlACO1*, suggesting that SlAREB1-NOR crosstalk plays a vital role in ABA-mediated ethylene biosynthesis during tomato fruit ripening (Mou et al., 2018).

In addition to tomato, ABA is also involved in ripening of other climacteric fruits. Application of ABA to apple facilitates ethylene emission by AREB/ABF-mediated regulation of *MdACS1/3* and *MdACO1* expression, suggesting a role for ABA in ethylene biosynthesis (Wang et al., 2018). In banana, ABA promotes *MaMADS2* expression and fruit ripening (Yakir et al., 2018). A peach ethylene response transcription factor, PpERF3, positively regulates PpNCED2/3-mediated ABA biosynthesis during fruit ripening (Wang et al., 2019a), while PpERF2 regulates fruit-ripening by inhibiting *PpNCED2/3* expression. PpERF2 binds to the promoters of *PpNCED2*, *PpNCED3*, and *PpPG1* (Wang et al., 2019b).

In all, the ABA-PYL-PP2C-SnRK2 core signaling pathway is also conserved in climacteric fruit. A set of crucial regulators related to the biosynthesis and signaling of both ABA and ethylene, such as NCED, AREB/ABF, ACS, ACO, and ERF, likely play important roles in the interaction of these two hormones, as elucidated by AREB/ABF-mediated *ACS/ACO* expression and ERF-mediated *NCED* expression. MADS-RIN, TAGL1, CNR, and NOR, transcription factors specific to ethylene biosynthesis and signaling, are probably also involved.

AN INTEGRATED, COMPREHENSIVE UNDERSTANDING OF ABA IN FLESHY FRUIT RIPENING

The developmental processes of fleshy fruits include cell division and expansion during fruit growth, followed by chlorophyll degradation, cell wall softening, and changes to phenylpropanoid, flavonoid, starch/sucrose, and carotenoid metabolism during ripening. These processes are controlled by phytohormones, most notably ethylene in climacteric fruit ripening and ABA in non-climacteric fruit ripening, as well as ABA-ethylene interactions in both types of fruit (Forlani et al., 2019; García-Gómez et al., 2020; Jiao et al., 2020).

De-greening through loss of chlorophyll is an obvious indicator of fruit ripening, and ethylene and ABA interact with light during chlorophyll degradation (Zhu et al., 2017). In addition, a decrease in water content occurs at the onset of ripening in both climacteric and non-climacteric fruit in an ethylene-independent manner, suggesting that oxidant-induced cell wall remodeling and consequent wall dehydration may trigger stress signaling that initiates fruit ripening (Frenkel and Hartman, 2012). Fruit ripening and senescence are associated with changes in fruit texture, color, aroma, and flavor, processes in which reactive oxygen species play an important role (Kumar et al., 2016). The interaction of auxin with ethylene is important in ripening of both climacteric and non-climacteric fruits (Paul et al., 2012). The APETALA2/ethylene response factor (AP2/ERF) transcription factor is a crucial response regulator in ethylene signaling, which not only modulates biosynthesis of ABA, ethylene, gibberellin, and cytokinin in a feedback manner but also responds to signaling associated with ABA, IAA, jasmonate, and cytokinin (Wang et al., 2015; Gu et al., 2017). The promotion of grape berry ripening by ABA, ethylene, and brassinosteroids, and ripening inhibition by IAA, jasmonic acid, GAs, cytokinins, and PAs reveal complex interactions among signals (Fortes et al., 2015). Notably, polyamines regulate strawberry fruit ripening by ABA, auxin and ethylene (Guo et al., 2018), while FaPAO5 regulates Spm/Spd levels as a signaling during strawberry fruit ripening by integrating multiple signals including Ca^{2+} and GAs (Mo et al., 2020).

Finally, we propose an integrative model of ABA regulation of fleshy fruit ripening (**Figure 1**). In response to developmental and environmental cues, ABA levels in fleshy fruits are controlled by ABA biosynthesis and catabolism; the former mainly through NCEDs and β-glucosidases and the latter through CYP707As and β-glycosyltransferases. ABA molecules in fleshy fruit are perceived *via* the ABA receptors PYR/PYL and ABAR, which are linked to the conserved signaling pathway ABA-FaPYR1-FaABIl-FaSnRK2 and the novel signaling pathway ABA-FaABAR-FaRIPK1-FaABI4 in strawberry, respectively. In the conserved ABA signaling pathway, ABA levels increase at the onset of fruit ripening; consequently, the accumulated ABA binds to its receptor FaPYR1 to form a FaPYR1-FaABIl complex, releasing the inhibition of protein kinase FaSnRK2 and in turn activating an ABA signaling cascade, which promotes fruit ripening. This pathway constitutes the conserved mechanism of ABA action in plants. In the novel ABA signaling pathway, ABA binding to the receptor FaABAR/FaRIPK1 complex activates the transcription factor FaABI4, which triggers ABA signal transduction, eventually promoting fruit ripening. This signaling pathway is different from the Arabidopsis ABA-ABAR-WRKY40 signaling pathway, thus constituting a novel ABA signaling pathway during strawberry fruit ripening.

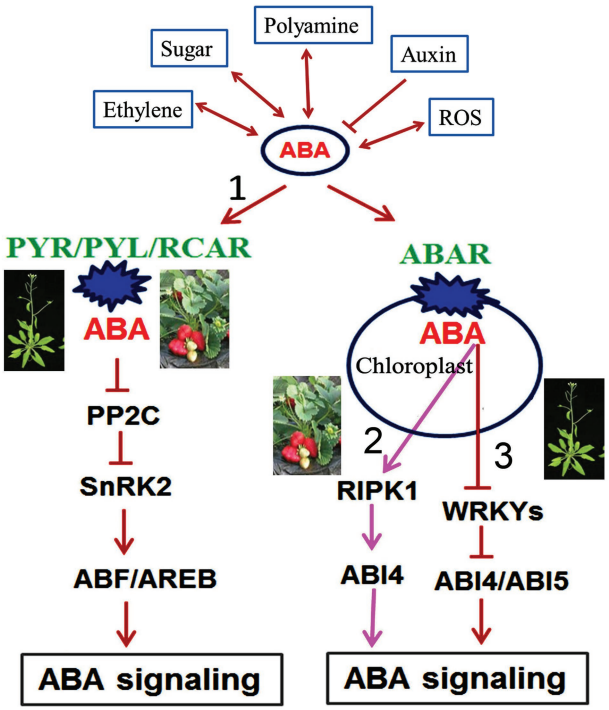

FIGURE 1 | A comprehensive model for ABA in regulating strawberry fruit ripening. The regulation of ABA in strawberry fruit ripening is involved in conserved and novel signaling mechanisms. ABA in fleshy fruits is perceived by its receptors, PYR/PYL/RCAR and ABAR, which initiates signal transduction, including the conserved signaling pathway ABA-PYR/PYL/RCAR-PP2C-SnRK2-ABF/AREB in both Arabidopsis and strawberry (signaling pathway 1) and the novel signaling pathway ABA-FaABAR-FaRIPK1-FaABI4 in strawberry (signaling pathway 2). In strawberry ABA signaling, ABAR/FaRIPK1 serves as a receptor complex, which is distinct from the Arabidopsis ABA-ABAR-WRKY40-ABI4/ABI5 signaling pathway (signaling pathway 3). ABA interacts with several synergistically-regulated molecules such as ethylene, sugar, polyamines, auxin, and reactive oxygen species (ROS) during strawberry fruit ripening. The symbols (→, ⟞, and ↔) represent promotion, inhibition, and cooperation, respectively. ABA, abscisic acid; ABAR, putative abscisic acid receptor; PYR, Pyrabactin resistance; PYL, PYR-like; RCAR, regulatory components of ABA receptors; PP2C, Type 2C protein phosphatase; SnRK2, SNF1-related protein kinases2; ABF, ABRE binding factors ABA responsive factors; AREB, ABA responsive element binding protein; ROS, reactive oxygen species; RIPK1, red-initial protein kinase1; ABI, abscisic acid-insensitive; WRKY, tryptophan-arginine-lysine-tyrosine.

CONCLUSIONS

Fruit ripening is controlled by phytohormones, with ripening of climacteric fruits controlled by ethylene and that of non-climacteric fruits regulated mainly by ABA, as well as by ABA-ethylene interplay in the two types of fruit ripening. ABA participates in the ripening of both non-climacteric and climacteric fruit. The core signaling pathway ABA-PYL-PP2C-SnRK2 is conserved, and a series of crucial regulators including NCED, AREB/ABF, ACS, ACO, and ERF may play important roles in ABA-ethylene interaction, particularly AREB/ABF-mediated *ACS/ACO* expression and ERF-mediated *NCED* expression. ABA levels in fleshy fruit are controlled through a balance between ABA biosynthesis and catabolism involving key enzymes, including NCEDs, β-glucosidases, CYP707As, and β-glycosyltransferases. ABA in fleshy fruits is perceived by at least two ABA receptors, PYR/PYL and ABAR, which are linked separately to the conserved signaling pathway ABA-FaPYR1-FaABIl-FaSnRK2 and the novel signaling pathway ABA-FaABAR-FaRIPK1-FaABI4 in strawberry fruit ripening. This model provides novel insights into the role of ABA in ripening, at least in strawberry, a model plant for non-climacteric-type fruits. Next, new integrated mechanisms, including two ABA signaling pathways, ABA and ethylene signaling pathways, and ABA/ethylene to other phytohormones and regulators, are interesting and important research topics in ripening, especially in non-climacteric fruits.

AUTHOR CONTRIBUTIONS

YS, YH, and QB wrote the review. QB collected references. YS and YH designed the model and revised the review. All authors contributed to the article and approved the submitted version.

FUNDING

This study was supported by the National Natural Science Foundation of China (projects 32030100; 31672125; 32072516), the Beijing Natural Science Foundation (6171001), Scientific Research Project of Beijing Educational Committee (KZ202010020028; KM202110020006), the Construction of Beijing Science and Technology Innovation and Service Capacity in Top Subjects (CEFF_PXM2019_014207_000032), the Opening Project of Beijing Key Laboratory of New Technology in Agricultural Application (kf2020021), and Sichuan Lomon Biotechnology Co., LTD (2018001).

ACKNOWLEDGMENTS

We thank Guo JX very much for suggestions about the role of polyamine in fruit ripening.

REFERENCES

Araújo, W. L., Tohge, T., Osorio, S., Lohse, M., Balbo, I., Krahnert, I., et al. (2012). Antisense inhibition of the 2-oxoglutarate dehydrogenase complex in tomato demonstrates its importance for plant respiration and during leaf senescence and fruit maturation. *Plant Cell* 24, 2328–2351. doi: 10.1105/tpc.112.099002

Azoulay, S. T., Harpaz-Saad, S., Belausov, E., Lovat, N., Krokhin, O., Spicer, V., et al. (2008). Citrus chlorophyllase dynamics at ethylene-induced fruit color-break: a study of chlorophyllase expression, posttranslational processing kinetics, and in situ intracellular localization. *Plant Physiol.* 148, 108–118. doi: 10.1104/pp.108.124933

Castillejo, C., de la Fuente, J. I., Iannetta, P., Botella, M. A., and Valpuesta, V. (2004). Pectin esterase gene family in strawberry fruit: study of FaPE1, a ripening-specific isoform. *J. Exp. Bot.* 55, 909–918. doi: 10.1093/jxb/erh102

Chai, Y. M., Jia, H. F., Li, C. L., Dong, Q. H., and Shen, Y. Y. (2011). FaPYR1 is involved in strawberry fruit ripening. *J. Exp. Bot.* 62, 5079–5089. doi: 10.1093/jxb/err207

Chen, P., Sun, Y. F., Kai, W. B., Liang, B., Zhang, Y. S., Zhai, X. W., et al. (2016). Interactions of ABA signaling core components (SlPYLs, SlPP2Cs, and SlSnRK2s) in tomato (*Solanum lycopersicon*). *J. Plant Physiol.* 205, 67–74. doi: 10.1016/j.jplph.2016.07.016

Cheng, S., Xian, W., Fu, Y., Marin, B., Keller, J., Wu, T., et al. (2019). Genomes of *subaerial zygnematophyceae* provide insights into land plant evolution. *Cell* 179, 1057–1067. doi: 10.1016/j.cell.2019.10.019

Cheng, Z., Zhuo, S., Liu, X., Che, G., Wang, Z., Gu, R., et al. (2020). The MADS-box gene CsSHP participates in fruit maturation and floral organ development in cucumber. *Front. Plant Sci.* 10:1781. doi: 10.3389/fpls.2019.01781

Chung, S. W., Yu, D. J., Oh, H. D., Ahn, J. H., Huh, J. H., and Lee, H. J. (2019). Transcriptional regulation of abscisic acid biosynthesis and signal transduction, and anthocyanin biosynthesis in 'Bluecrop' highbush blueberry fruit during ripening. *PLoS One* 14:e0220015. doi: 10.1371/journal.pone.0220015

Concepción Martínez-Madrid, M., Flores, F., and Romojaro, F. (2002). Behaviour of abscisic acid and polyamines in antisense ACC oxidase melon (*Cucumis melo*) during ripening. *Funct. Plant Biol.* 29, 865–872. doi: 10.1071/PP01164

Coombe, B. (1976). The development of fleshy fruits. *Annu. Rev. Plant Physiol.* 27, 507–528.

Corso, M., Vannozzi, A., Ziliotto, F., Zouine, M., Maza, E., Nicolato, T., et al. (2016). Grapevine rootstocks differentially affect the rate of ripening and modulate auxin-related genes in cabernet sauvignon berries. *Front. Plant Sci.* 7:69. doi: 10.3389/fpls.2016.00069

Daminato, M., Guzzo, F., and Casadoro, G. (2013). A SHATTERPROOF-like gene controls ripening in non-climacteric strawberries, and auxin and abscisic acid antagonistically affect its expression. *J. Exp. Bot.* 64, 3775–3786. doi: 10.1093/jxb/ert214

Davies, C., Boss, P., and Robinson, S. (1997). Treatment of grape berries, a nonclimateric fruit with a synthetic auxin, retards ripening and alters the expression of developmentally regulated genes. *Plant Physiol.* 115, 1155–1161. doi: 10.1104/pp.115.3.1155

Diretto, G., Frusciante, S., Fabbri, C., Schauer, N., Busta, L., Wang, Z., et al. (2020). Manipulation of β-carotene levels in tomato fruits results in increased ABA content and extended shelf life. *Plant Biotechnol. J.* 18, 1185–1199. doi: 10.1111/pbi.13283

Estrada-Johnson, E., Csukasi, F., Pizarro, C. M., Vallarino, J. G., Kiryakova, Y., Vioque, A., et al. (2017). Transcriptomic analysis in strawberry fruits reveals active auxin biosynthesis and signaling in the ripe receptacle. *Front. Plant Sci.* 8:889. doi: 10.3389/fpls.2017.00889

Forlani, S., Masiero, S., and Mizzotti, C. (2019). Fruit ripening: the role of hormones, cell wall modifications, and their relationship with pathogens. *J. Exp. Bot.* 70, 2993–3006. doi: 10.1093/jxb/erz112

Fortes, A. M., Teixeira, R. T., and Agudelo-Romero, P. (2015). Complex interplay of hormonal signals during grape berry ripening. *Molecules* 20, 9326–9343. doi: 10.3390/molecules20059326

Frenkel, C., and Hartman, T. G. (2012). Decrease in fruit moisture content heralds and might launch the onset of ripening processes. *J. Food Sci.* 77, S365–S376. doi: 10.1111/j.1750-3841.2012.02910.x

Garceau, D. C., Batson, M. K., and Pan, I. L. (2017). Variations on a theme in fruit development: the PLE lineage of MADS-box genes in tomato (TAGL1) and other species. *Planta* 246, 313–321. doi: 10.1007/s00425-017-2725-5

García-Gómez, B. E., Ruiz, D., Salazar, J. A., Rubio, M., Martínez-García, P. J., and Martínez-Gómez, P. (2020). Analysis of metabolites and gene expression changes relative to apricot (*Prunus armeniaca* L.) fruit quality during development and ripening. *Front. Plant Sci.* 11:1269. doi: 10.3389/fpls.2020.01269

Gazzarrini, S., and Tsai, A. Y. (2015). Hormone cross-talk during seed germination. *Essays Biochem.* 58, 151–164. doi: 10.1042/bse0580151

Gouthu, S., and Deluc, L. G. (2015). Timing of ripening initiation in grape berries and its relationship to seed content and pericarp auxin levels. *BMC Plant Biol.* 15:46. doi: 10.1186/s12870-015-0440-6

Gu, C., Guo, Z. H., Hao, P. P., Wang, G. M., Jin, Z. M., and Zhang, S. L. (2017). Multiple regulatory roles of AP2/ERF transcription factor in angiosperm. *Bot. Stud.* 58:6. doi: 10.1186/s40529-016-0159-1

Gu, T., Jia, S., Huang, X., Wang, L., Fu, W., Huo, G., et al. (2019). Transcriptome and hormone analyses provide insights into hormonal regulation in strawberry ripening. *Planta* 250, 145–162. doi: 10.1007/s00425-019-03155-w

Guo, J., Wang, S., Yu, X., Dong, R., Li, Y., Mei, X., et al. (2018). Polyamines regulate strawberry fruit ripening by abscisic acid, auxin, and ethylene. *Plant Physiol.* 177, 339–351. doi: 10.1104/pp.18.00245

Gupta, M. K., Lenka, S. K., Gupta, S., and Rawal, R. K. (2020). Agonist, antagonist and signaling modulators of ABA receptor for agronomic and post-harvest management. *Plant Physiol. Biochem.* 148, 10–25. doi: 10.1016/j.plaphy.2019.12.023

Hershkovitz, V., Friedman, H., Goldschmidt, E. E., Feygenberg, O., and Pesis, E. (2011). Effect of seed on ripening control components during avocado fruit development. *J. Plant Physiol.* 168, 2177–2183. doi: 10.1016/j.jplph.2011.07.010

Hou, B., and Chen, X, Shen, Y. (2020). Interactions between strawberry ABA receptor PYR/PYLs and protein phosphatase PP2Cs on basis of Transcriptome and yeast two-hybrid analyses. *J. Plant Growth Regul.* doi: 10.1007/s00344-020-10121-4

Hou, B. Z., Xu, C., and Shen, Y. Y. (2018). A leu-rich repeat receptor-like protein kinase, FaRIPK1, interacts with the ABA receptor, FaABAR, to regulate fruit ripening in strawberry. *J. Exp. Bot.* 69, 1569–1582. doi: 10.1093/jxb/erx488

Hu, B., Lai, B., Wang, D., Li, J., Chen, L., Qin, Y., et al. (2019). Three LcABFs are involved in the regulation of chlorophyll degradation and anthocyanin biosynthesis during fruit ripening in *Litchi chinensis*. *Plant Cell Physiol.* 60, 448–461. doi: 10.1093/pcp/pcy219

Hu, W., Yan, Y., Shi, H., Coombe, J., Miao, H., Tie, W., et al. (2017). The core regulatory network of the abscisic acid pathway in banana: genome-wide identification and expression analyses during development, ripening, and abiotic stress. *BMC Plant Biol.* 17:145. doi: 10.1186/s12870-017-1093-4

Jia, H. F., Chai, Y. M., Li, C. L., Lu, D., Luo, J. J., Qin, L., et al. (2011). Abscisic acid plays an important role in the regulation of strawberry fruit ripening. *Plant Physiol.* 157, 188–199. doi: 10.1104/pp.111.177311

Jia, M., Ding, N., Zhang, Q., Xing, S., Wei, L., Zhao, Y., et al. (2017b). A FERONIA-like receptor kinase regulates strawberry (Fragaria × ananassa) fruit ripening and quality formation. *Front. Plant Sci.* 8:1099. doi: 10.3389/fpls.2017.01099

Jia, H., Jiu, S., Zhang, C., Wang, C., Tariq, P., Liu, Z., et al. (2016). Abscisic acid and sucrose regulate tomato and strawberry fruit ripening through the abscisic acid-stress-ripening transcription factor. *Plant Biotechnol. J.* 14, 2045–2065. doi: 10.1111/pbi.12563

Jia, H. F., Lu, D., Sun, J. H., Li, C. L., Xing, Y., Qin, L., et al. (2013a). Type 2C protein phosphatase ABI1 is a negative regulator of strawberry fruit ripening. *J. Exp. Bot.* 64, 1677–1687. doi: 10.1093/jxb/ert028

Jia, H. F., Wang, Y. H., Sun, M. Z., Li, B. B., Han, Y., Zhan, Y. X., et al. (2013b). Sucrose functions as a signal involved in the regulation of strawberry fruit development and ripening. *New Phytol.* 198, 453–465. doi: 10.1111/nph.12176

Jia, H., Xie, Z., Wang, C., Shangguan, L., Qian, N., Cui, M., et al. (2017a). Abscisic acid, sucrose, and auxin coordinately regulate berry ripening process of the Fujiminori grape. *Funct. Integr. Genomics* 17, 441–457. doi: 10.1007/s10142-017-0546-z

Jiao, B., Meng, Q., and Lv, W. (2020). Roles of stay-green (SGR) homologs during chlorophyll degradation in green plants. *Bot. Stud.* 61:25. doi: 10.1186/s40529-020-00302-5

Kadomura-Ishikawa, Y., Miyawaki, K., Takahashi, A., Masuda, T., and Noji, S. (2015). Light and abscisic acid independently regulated FaMYB10 in *Fragaria* × *ananassa* fruit. *Planta* 241, 953–965. doi: 10.1007/s00425-014-2228-6

Kai, W., Wang, J., Liang, B., Fu, Y., Zheng, Y., Zhang, W., et al. (2019). PYL9 is involved in the regulation of ABA signaling during tomato fruit ripening. *J. Exp. Bot.* 70, 6305–6319. doi: 10.1093/jxb/erz396

Karppinen, K., Tegelberg, P., Häggman, H., and Jaakola, L. (2018). Abscisic acid regulates anthocyanin biosynthesis and gene expression associated with cell wall modification in ripening bilberry (*Vaccinium myrtillus* L.) fruits. *Front. Plant Sci.* 9:1259. doi: 10.3389/fpls.2018.01259

Kim, J., Lee, J. G., Hong, Y., and Lee, E. J. (2019). Analysis of eight phytohormone concentrations, expression levels of ABA biosynthesis genes, and ripening-related transcription factors during fruit development in strawberry. *J. Plant Physiol.* 239, 52–60. doi: 10.1016/j.jplph.2019.05.013

Kou, X., He, Y., Li, Y., Chen, X., Feng, Y., and Xue, Z. (2019). Effect of abscisic acid (ABA) and chitosan/nano-silica/sodium alginate composite film on the color development and quality of postharvest Chinese winter jujube (Zizyphus

jujuba Mill. cv. Dongzao). *Food Chem.* 270, 385–394. doi: 10.1016/j.foodchem.2018.06.151

Kumar, V., Irfan, M., Ghosh, S., Chakraborty, N., Chakraborty, S., and Datta, A. (2016). Fruit ripening mutants reveal cell metabolism and redox state during ripening. *Protoplasma* 253, 581–594. doi: 10.1007/s00709-015-0836-z

Kumar, R., Khurana, A., and Sharma, A. K. (2014). Role of plant hormones and their interplay in development and ripening of fleshy fruits. *J. Exp. Bot.* 65, 4561–4575. doi: 10.1093/jxb/eru277

Li, C. L., Jia, H. F., Chai, Y. M., and Shen, Y. Y. (2011). Abscisic acid perception and signaling transduction in strawberry: a model for non-climacteric fruit ripening. *Plant Signal. Behav.* 6, 1950–1953. doi: 10.4161/psb.6.12.18024

Li, Z., Wang, Z., Wang, K., Liu, Y., Hong, Y., Chen, C., et al. (2020). Co-expression network analysis uncovers key candidate genes related to the regulation of volatile esters accumulation in woodland strawberry. *Planta* 252:55. doi: 10.1007/s00425-020-03462-7

Li, G., Zhao, J., Qin, B., Yin, Y., An, W., Mu, Z., et al. (2019). ABA mediates development-dependent anthocyanin biosynthesis and fruit coloration in Lycium plants. *BMC Plant Biol.* 19:317. doi: 10.1186/s12870-019-1931-7

Liang, S., Lu, K., Wu, Z., Jiang, S. C., Yu, Y. T., Bi, C., et al. (2015). A link between magnesium-chelatase H subunit and sucrose nonfermenting 1 (SNF1)-related protein kinase SnRK2.6/OST1 in Arabidopsis guard cell signalling in response to abscisic acid. *J. Exp. Bot.* 66, 6355–6369. doi: 10.1093/jxb/erv341

Liao, X., Li, M., Liu, B., Yan, M., Yu, X., Zi, H., et al. (2018). Interlinked regulatory loops of ABA catabolism and biosynthesis coordinate fruit growth and ripening in woodland strawberry. *Proc. Natl. Acad. Sci. U. S. A.* 115, E11542–E11550. doi: 10.1073/pnas.1812575115

Liu, M., Pirrello, J., Chervin, C., Roustan, J. P., and Bouzayen, M. (2015). Ethylene control of fruit ripening: revisiting the complex network of transcriptional regulation. *Plant Physiol.* 169, 2380–2390. doi: 10.1104/pp.15.01361

Luo, Y., Ge, C., Ling, Y., Mo, F., Yang, M., Jiang, L., et al. (2020a). ABA and sucrose co-regulate strawberry fruit ripening and show inhibition of glycolysis. *Mol. Gen. Genomics.* 295, 421–438. doi: 10.1007/s00438-019-01629-w

Luo, Y., Ge, C., Yang, M., Long, Y., Li, M., Zhang, Y., et al. (2020b). Cytosolic/plastid glyceraldehyde-3-phosphate dehydrogenase is a negative regulator of strawberry fruit ripening. *Genes (Basel)* 11:580. doi: 10.3390/genes11050580

Medina-Puche, L., Blanco-Portales, R., Molina-Hidalgo, F. J., Cumplido-Laso, G., García-Caparrós, N., Moyano-Cañete, E., et al. (2016). Extensive transcriptomic studies on the roles played by abscisic acid and auxins in the development and ripening of strawberry fruits. *Funct. Integr. Genomics* 16, 671–692. doi: 10.1007/s10142-016-0510-3

Meyer, M. D., Chope, G. A., and Terry, L. A. (2017). Investigation into the role of endogenous abscisic acid during ripening of imported avocado cv. Hass. *J. Sci. Food Agric.* 97, 3656–3664. doi: 10.1002/jsfa.8225

Mo, A., Xu, T., Bai, Q., Shen, Y., Gao, F., and Guo, J. (2020). FaPAO5 regulates Spm/Spd levels as a signaling during strawberry fruit ripening. *Plant Direct.* 4:e00217. doi: 10.1002/pld3.217

Molina-Hidalgo, F. J., Franco, A. R., Villatoro, C., Medina-Puche, L., Mercado, J. A., Hidalgo, M. A., et al. (2013). The strawberry (*Fragaria* × *ananassa*) fruit-specific rhamnogalacturonate lyase 1 (FaRGLyase1) gene encodes an enzyme involved in the degradation of cell-wall middle lamellae. *J. Exp. Bot.* 64, 1471–1483. doi: 10.1093/jxb/ers386

Molina-Hidalgo, F. J., Medina-Puche, L., Gelis, S., Ramos, J., Sabir, F., Soveral, G., et al. (2015). Functional characterization of FaNIP1; 1 gene, a ripening-related and receptacle-specific aquaporin in strawberry fruit. *Plant Sci.* 238, 198–211. doi: 10.1016/j.plantsci.2015.06.013

Mou, W., Li, D., Bu, J., Jiang, Y., Khan, Z. U., Luo, Z., et al. (2016). Comprehensive analysis of ABA effects on ethylene biosynthesis and signaling during tomato fruit ripening. *PLoS One* 11:e0154072. doi: 10.1371/journal.pone.0154072

Mou, W., Li, D., Luo, Z., Li, L., Mao, L., and Ying, T. (2018). SlAREB1 transcriptional activation of NOR is involved in abscisic acid-modulated ethylene biosynthesis during tomato fruit ripening. *Plant Sci.* 276, 239–249. doi: 10.1016/j.plantsci.2018.07.015

Oh, H. D., Yu, D. J., Chung, S. W., Chea, S., and Lee, H. J. (2018). Abscisic acid stimulates anthocyanin accumulation in 'Jersey' highbush blueberry fruits during ripening. *Food Chem.* 244, 403–407. doi: 10.1016/j.foodchem.2017.10.051

Paniagua, C., Blanco-Portales, R., Barcelo-Munoz, M., Garcia-Gago, J. A., Waldron, K. W., Quesada, M. A., et al. (2016). Antisense down-regulation of the strawberry beta-galactosidase gene FabetaGal4 increases cell wall galactose levels and reduces fruit softening. *J. Exp. Bot.* 67, 619–631. doi: 10.1093/jxb/erv462

Paul, V., Pandey, R., and Srivastava, G. C. (2012). The fading distinctions between classical patterns of ripening in climacteric and non-climacteric fruit and the ubiquity of ethylene-An overview. *J. Food Sci. Technol.* 49, 1–21. doi: 10.1007/s13197-011-0293-4

Romero, P., Lafuente, M. T., and Rodrigo, M. J. (2019). A sweet orange mutant impaired in carotenoid biosynthesis and reduced ABA levels results in altered molecular responses along peel ripening. *Sci. Rep.* 9:9813. doi: 10.1038/s41598-019-46365-8

Sadka, A., Qin, Q., Feng, J., Farcuh, M., Shlizerman, L., Zhang, Y., et al. (2019). Ethylene response of plum ACC synthase 1 (ACS1) promoter is mediated through the binding site of abscisic acid insensitive 5 (ABI5). *Plants (Basel).* 8:117. doi: 10.3390/plants8050117

Shang, Y., Yan, L., Liu, Z. Q., Cao, Z., Mei, C., Xin, Q., et al. (2010). The Mg-chelatase H subunit of Arabidopsis antagonizes a group of transcription repressors to relieve ABA-responsive genes of inhibition. *Plant Cell* 22, 1909–1935. doi: 10.1105/tpc.110.073874

Shen, X., Guo, X., Zhao, D., Zhang, Q., Jiang, Y., Wang, Y., et al. (2017). Cloning and expression profiling of the PacSnRK2 and PacPP2C gene families during fruit development, ABA treatment, and dehydration stress in sweet cherry. *Plant Physiol. Biochem.* 119, 275–285. doi: 10.1016/j.plaphy.2017.08.025

Shen, Y. Y., and Rose, J. K. C. (2014). "ABA metabolism and signaling in fleshy fruits" in *Abscisic acid: Metabolism, transport and signaling*. ed. D. P. Zhang (Dordrecht: Springer), 271–286.

Siebeneichler, T. J., Crizel, R. L., Camozatto, G. H., Paim, B. T., da Silva, M. R., Rombaldi, C. V., et al. (2020). The postharvest ripening of strawberry fruits induced by abscisic acid and sucrose differs from their in vivo ripening. *Food Chem.* 317:126407. doi: 10.1016/j.foodchem.2020.126407

Sun, Y., Ji, K., Liang, B., Du, Y., Jiang, L., Wang, J., et al. (2017). Suppressing ABA uridine diphosphate glucosyltransferase (SlUGT75C1) alters fruit ripening and the stress response in tomato. *Plant J.* 91, 574–589. doi: 10.1111/tpj.13588

Sun, L., Sun, Y., Zhang, M., Wang, L., Ren, J., Cui, M., et al. (2012b). Suppression of 9-cis-epoxycarotenoid dioxygenase, which encodes a key enzyme in abscisic acid biosynthesis, alters fruit texture in transgenic tomato. *Plant Physiol.* 158, 283–298. doi: 10.1104/pp.111.186866

Sun, L., Yuan, B., Zhang, M., Wang, L., Cui, M., Wang, Q., et al. (2012a). Fruit-specific RNAi-mediated suppression of SlNCED1 increases both lycopene and β-carotene contents in tomato fruit. *J. Exp. Bot.* 63, 3097–3108. doi: 10.1093/jxb/ers026

Symons, G. M., Chua, Y. J., Ross, J. J., Quittenden, L. J., Davies, N. W., and Reid, J. B. (2012). Hormonal changes during non-climacteric ripening in strawberry. *J. Exp. Bot.* 63, 4741–4750. doi: 10.1093/jxb/ers147

Tijero, V., Teribia, N., Muñoz, P., and Munné-Bosch, S. (2016). Implication of Abscisic acid on ripening and quality in sweet cherries: differential effects during pre- and post-harvest. *Front. Plant Sci.* 7:602. doi: 10.3389/fpls.2016.00602

Tosetti, R., Elmi, F., Pradas, I., Cools, K., and Terry, L. A. (2020). Continuous exposure to ethylene differentially affects senescence in receptacle and achene tissues in strawberry fruit. *Front. Plant Sci.* 11:174. doi: 10.3389/fpls.2020.00174

Villalobos-González, L., Peña-Neira, A., Ibáñez, F., and Pastenes, C. (2016). Long-term effects of abscisic acid (ABA) on the grape berry phenylpropanoid pathway: gene expression and metabolite content. *Plant Physiol. Biochem.* 105, 213–223. doi: 10.1016/j.plaphy.2016.04.012

Wang, Y., Guo, S., Tian, S., Zhang, J., Ren, Y., Sun, H., et al. (2017b). Abscisic acid pathway involved in the regulation of watermelon fruit ripening and quality trait evolution. *PLoS One* 12:e0179944. doi: 10.1371/journal.pone.0179944

Wang, X., Liu, S., Tian, H., Wang, S., and Chen, J. G. (2015). The small ethylene response factor ERF96 is involved in the regulation of the abscisic acid response in Arabidopsis. *Front. Plant Sci.* 6:1064. doi: 10.3389/fpls.2015.01064

Wang, S., Saito, T., Ohkawa, K., Ohara, H., Suktawee, S., Ikeura, H., et al. (2018). Abscisic acid is involved in aromatic ester biosynthesis related with ethylene in green apples. *J. Plant Physiol.* 221, 85–93. doi: 10.1016/j.jplph.2017.12.007

Wang, X., Zeng, W., Ding, Y., Wang, Y., Niu, L., Yao, J. L., et al. (2019a). PpERF3 positively regulates ABA biosynthesis by activating PpNCED2/3 transcription during fruit ripening in peach. *Hortic Res.* 6:19. doi: 10.1038/s41438-018-0094-2

Wang, X., Zeng, W., Ding, Y., Wang, Y., Niu, L., Yao, J. L., et al. (2019b). Peach ethylene response factor PpeERF2 represses the expression of ABA biosynthesis and cell wall degradation genes during fruit ripening. *Plant Sci.* 283, 116–126. doi: 10.1016/j.plantsci.2019.02.009

Wang, Q. H., Zhao, C., Zhang, M., Li, Y. Z., Shen, Y. Y., and Guo, J. X. (2017a). Transcriptome analysis around the onset of strawberry fruit ripening uncovers an important role of oxidative phosphorylation in ripening. *Sci. Rep.* 7:41477. doi: 10.1038/srep41477

Wong, D. C., Lopez Gutierrez, R., Dimopoulos, N., Gambetta, G. A., and Castellarin, S. D. (2016). Combined physiological, transcriptome, and cis-regulatory element analyses indicate that key aspects of ripening, metabolism, and transcriptional program in grapes (*Vitis vinifera* L.) are differentially modulated accordingly to fruit size. *BMC Genomics* 17:416. doi: 10.1186/s12864-016-2660-z

Wu, Q., Tao, X., Ai, X., Luo, Z., Mao, L., Ying, T., et al. (2018). Contribution of abscisic acid to aromatic volatiles in cherry tomato (*Solanum lycopersicum* L.) fruit during postharvest ripening. *Plant Physiol. Biochem.* 130, 205–214. doi: 10.1016/j.plaphy.2018.06.039

Yakir, E., Zhangjun, F., Sela, N., Xu, Y., Singh, V., Dagar, A., et al. (2018). MaMADS2 repression in banana fruits modifies hormone synthesis and signalling pathways prior to climacteric stage. *BMC Plant Biol.* 18:267. doi: 10.1186/s12870-018-1480-5

Yu, Y, Meng, X, Guo, D, Yang, S, Zhang, G, and Liang, Z. (2020). Grapevine U-box E3 ubiquitin ligase VlPUB38 negatively regulates fruit ripening by facilitating abscisic-aldehyde oxidase degradation. *Plant Cell Physiol.* pcaa118. doi: 10.1093/pcp/pcaa118 [Epub ahead of print]

Zhang, S. H., Hou, B. Z., Chai, L., Yang, A. Z., Yu, X. Y., and Shen, Y. Y. (2017). Sigma factor FaSigE positively regulates strawberry fruit ripening by ABA. *Plant Growth Regul.* 83, 417–427. doi: 10.1007/s10725-017-0308-x

Zhang, Z., Kang, C., Zhang, S., and Li, X. (2019). Transcript analyses reveal a comprehensive role of abscisic acid in modulating fruit ripening in Chinese jujube. *BMC Plant Biol.* 19:189. doi: 10.1186/s12870-019-1802-2

Zhang, Y., Li, Q., Jiang, L., Kai, W., Liang, B., Wang, J., et al. (2018). Suppressing type 2C protein phosphatases alters fruit ripening and the stress response in tomato. *Plant Cell Physiol.* 59, 142–154. doi: 10.1093/pcp/pcx169

Zhang, M., Yuan, B., and Leng, P. (2009). The role of ABA in triggering ethylene biosynthesis and ripening of tomato fruit. *J. Exp. Bot.* 60, 1579–1588. doi: 10.1093/jxb/erp026

Zhu, X., Chen, J., Qiu, K., and Kuai, B. (2017). Phytohormone and light regulation of chlorophyll degradation. *Front. Plant Sci.* 8:1911. doi: 10.3389/fpls.2017.01911

Zhu, F., Luo, T., Liu, C., Wang, Y., Zheng, L., Xiao, X., et al. (2020). A NAC transcription factor and its interaction protein hinder abscisic acid biosynthesis by synergistically repressing NCED5 in *Citrus reticulata*. *J. Exp. Bot.* 71, 3613–3625. doi: 10.1093/jxb/eraa118

Ziliotto, F., Corso, M., Rizzini, F. M., Rasori, A., Botton, A., and Bonghi, C. (2012). Grape berry ripening delay induced by a pre-veraison NAA treatment is paralleled by a shift in the expression pattern of auxin- and ethylene-related genes. *BMC Plant Biol.* 12:185. doi: 10.1186/1471-2229-12-185

Conflict of Interest: The authors declare that the research was conducted in the absence of any commercial or financial relationships that could be construed as a potential conflict of interest.

frontiers in Plant Science

ORIGINAL RESEARCH
published: 25 February 2021
doi: 10.3389/fpls.2021.644799

Multi-Locus Genome-Wide Association Studies Reveal Fruit Quality Hotspots in Peach Genome

*Cassia da Silva Linge[1], Lichun Cai[1,2], Wanfang Fu[1], John Clark[3], Margaret Worthington[3], Zena Rawandoozi[4], David H. Byrne[4] and Ksenija Gasic[1]**

[1] Department of Plant and Environmental Sciences, Clemson University, Clemson, SC, United States, [2] Department of Horticulture, Michigan State University, East Lansing, MI, United States, [3] Department of Horticulture, University of Arkansas, Fayetteville, AR, United States, [4] Department of Horticultural Sciences, Texas A&M University, College Station, TX, United States

OPEN ACCESS

Edited by:
Jia-Long Yao, The New Zealand Institute for Plant and Food Research Ltd, New Zealand

Reviewed by:
Satish Kumar, The New Zealand Institute for Plant and Food Research Ltd, New Zealand
Ana M. Casas, Aula Dei Experimental Station (EEAD), Spain

***Correspondence:**
Ksenija Gasic
kgasic@clemson.edu

Specialty section:
This article was submitted to Plant Development and EvoDevo, a section of the journal Frontiers in Plant Science

Received: *21 December 2020*
Accepted: *04 February 2021*
Published: *25 February 2021*

Citation:
da Silva Linge C, Cai L, Fu W, Clark J, Worthington M, Rawandoozi Z, Byrne DH and Gasic K (2021) Multi-Locus Genome-Wide Association Studies Reveal Fruit Quality Hotspots in Peach Genome. Front. Plant Sci. 12:644799. doi: 10.3389/fpls.2021.644799

Peach is one of the most important fruit crops in the world, with the global annual production about 24.6 million tons. The United States is the fourth-largest producer after China, Spain, and Italy. Peach consumption has decreased over the last decade, most likely due to inconsistent quality of the fruit on the market. Thus, marker-assisted selection for fruit quality traits is highly desired in fresh market peach breeding programs and one of the major goals of the RosBREED project. The ability to use DNA information to select for desirable traits would enable peach breeders to efficiently plan crosses and select seedlings with desired quality traits early in the selection process before fruiting. Therefore, we assembled a multi-locus genome wide association study (GWAS) of 620 individuals from three public fresh market peach breeding programs (Arkansas, Texas, and South Carolina). The material was genotyped using 9K SNP array and the traits were phenotyped for three phenological (bloom date, ripening date, and days after bloom) and 11 fruit quality-related traits (blush, fruit diameter, fruit weight, adherence, fruit firmness, redness around pit, fruit texture, pit weight, soluble solid concentration, titratable acidity, and pH) over three seasons (2010, 2011, and 2012). Multi-locus association analyses, carried out using mrMLM 4.0 and FarmCPU R packages, revealed a total of 967 and 180 quantitative trait nucleotides (QTNs), respectively. Among the 88 consistently reliable QTNs detected using multiple multi-locus GWAS methods and/or at least two seasons, 44 were detected for the first time. Fruit quality hotspots were identified on chromosomes 1, 3, 4, 5, 6, and 8. Out of 566 candidate genes detected in the genomic regions harboring the QTN clusters, 435 were functionally annotated. Gene enrichment analyses revealed 68 different gene ontology (GO) terms associated with fruit quality traits. Data reported here advance our understanding of genetic mechanisms underlying important fruit quality traits and further support the development of DNA tools for breeding.

Keywords: FarmCPU, mrMLM 4.0, candidate gene analyses, SNP array, RosBREED, QTN

INTRODUCTION

Peach [*Prunus persica* (L.) Batsch] is a diploid species, with a short juvenile period (2–4 years), relatively simple genome (∼230 Mbp), and one of the best genetically characterized deciduous trees (Verde et al., 2013). Peach is the third most cultivated temperate tree fruit in the world, after apple and pear, with a world production of approximately 24.6 million tons (Food and Agricultural Organization of the United Nations (FAOSTAT), 2018). Despite the high production, peach consumption has declined over the past decades. In the United States, peach per capita consumption decreased to 1.3 kg per year compared to ∼3 kg per year in the 1980s (Minas et al., 2018). Inconsistent and low fruit quality is recognized as the major limiting factor for consumer acceptance and, consequently, the low rates of peach consumption (Cirilli et al., 2016).

Peach breeders have always selected for fruit quality with respect to size, color and firmness, as well as tried to expand harvest season (Laurens et al., 2018). Recently, more emphasis is on other traits such as internal quality and postharvest traits (Elsadr et al., 2019).

Recent advances in next-generation high-throughput sequencing and genotyping techniques, such as development of the 9K peach SNP array by the International Peach SNP Consortium (IPSC) (Verde et al., 2012), allow use of DNA information to develop tools for facilitating breeding efforts (Lambert et al., 2016; da Silva Linge et al., 2018). Understanding the genetic mechanisms that control a specific trait would enable peach breeders to efficiently apply marker-assisted breeding (MAB) through the development of DNA diagnostic tools, and consequently select seedlings with desired quality traits early in the selection process before the characters can be evaluated in the field (Abdelghafar et al., 2020).

The link between the genetic markers and a particular trait could be determined using different approaches. Quantitative trait loci analysis (QTL mapping) and genome-wide association studies (GWAS) are widely used for dissection of complex genetic traits (Meneses and Orellana, 2013). In peach, several linkage maps have been used in QTL discovery of key fruit quality traits such as fruit size, diameter, firmness, acidity, soluble solid concentration, individual sugars, maturity date, pubescence, blush, fruit texture, and phytochemical compounds (Eduardo et al., 2011; Martínez-García et al., 2013; Pirona et al., 2013; Frett et al., 2014; Vendramin et al., 2014; da Silva Linge et al., 2015; Zeballos et al., 2016; Ciacciulli et al., 2018; Nuñez-Lillo et al., 2019; Abdelghafar et al., 2020). These maps were typically developed for mapping particular traits in a specific parental background with limited recombination events and genetic diversity.

Alternatively, GWAS has the advantage of increasing the recombination events and consequently mapping resolution with a significant reduction of the research time (Zhu et al., 2008). However, false positives due to population structure or kinship among genotypes, or false negatives due to removal of rare alleles that are involved in natural variation are some of the weaknesses of GWAS (Brachi et al., 2011). To deal with this problem, GWAS methods utilizing mixed linear models (MLM), which take into account multiple levels of relatedness, have become standard methodology (Yu et al., 2006). Significant marker-trait association based on the single-locus models, such as the general linear model (GLM) and MLM, were reported for several traits such as fruit pubescence, fruit shape, stone adhesion-flesh texture, fruit flesh color, non-melting/melting flesh, fruit weight, titratable acidity, soluble solid concentration, leaf gland type, flower type, bloom date, fruit development period, maturity date, ripening index, and total sugars (Micheletti et al., 2015; Cao et al., 2016, 2019; Elsadr et al., 2019; Font I Forcada et al., 2019). Single-locus models test one locus at a time and fail to match the true genetic model of complex traits that are controlled by numerous loci simultaneously (Xu et al., 2018). Thus, major improvements in GWAS statistical methodology have occurred, and multi-locus GWAS methods considering the information of all loci simultaneously have been developed (Wang et al., 2016).

Recently, six multi-locus GWAS approaches were integrated into an R package, named mrMLM (Zhang et al., 2020). The mrMLM 4.0 R package comprises the mrMLM (Wang et al., 2016), FASTmrMLM (Tamba and Zhang, 2018), FASTmrEMMA (Wen et al., 2017), ISIS EM-BLASSO (Tamba et al., 2017), pLARmEB (Zhang et al., 2017), and pKWmEB (Ren et al., 2018) two-step multi-locus GWAS methods. First, various algorithms are used to select all potentially associated markers. Second, these selected markers are put in one model, in which all the effects are obtained by empirical Bayes, and all the non-zero effects are further identified by likelihood ratio test for true Quantitative Trait Nucleotides (QTNs) (Zhang et al., 2020).

The multi-locus model Fixed and random model Circulating Probability Unification (FarmCPU) uses the associated markers as covariates in a fixed-effect model (FEM) and optimization on the associated covariate markers in a random effect model (REM). FarmCPU adopts REML optimization to replace the criterion that the variance explained by kinship is near zero, which can only be arbitrarily determined. FarmCPU also adopted a binning approach from super to select pseudo QTNs. The whole genome is equally divided into bins, and only one significant marker with the smallest *P*-value from each bin is selected as the candidate pseudo QTN. These candidate pseudo QTNs are determined by a REM. The candidate pseudo QTNs are first ranked by *P*-value. Then, the best combinations between the different bins and the number of candidate pseudo QTNs are determined by REM. Finally, the two types of models (FEM and REM) are performed iteratively until no change occurs in the selection of pseudo QTNs (Huang et al., 2018). Thus, FarmCPU decreases the computer time required, provides reliable results by efficiently removing the confounding between the population structure and Kinship, avoiding model over-fitting, and controlling for false positives (Liu et al., 2016).

The objective of this study was to identify significant marker-trait association for 14 agronomic traits, using the multi-locus GWAS methods in mrMLM 4.0 and FarmCPU in a U.S. peach diversity germplasm panel of 620 individuals, managed by three public fresh market peach breeding programs at University of Arkansas System Division of Agriculture, Texas A&M University and Clemson University.

MATERIALS AND METHODS

Plant Material, DNA Isolation, Quantification, and Genotyping

The material used in this study represents the U.S. peach breeding germplasm assembled under the RosBREED project (Iezzoni et al., 2010, 2020; Peace et al., 2014). A total of 72 cultivars/advanced selections and 548 individuals from three public fresh market peach breeding programs: University of Arkansas System Division of Agriculture (AR), Clemson University (SC), and Texas A&M University (TX), were chosen to effectively represent alleles currently found within North American fresh market peach breeding germplasm (**Supplementary Table 1**).

Peach DNA was extracted from young leaves using the E-Z 96 Tissue DNA Kit (Omega Bio-Tek, Inc., Norcross, GA, United States). DNA was quantitated with the QuantiT PicoGreen Assay (Invitrogen, Carlsbad, CA, United States), using the Victor multi-plate reader (Perkin Elmer Inc., San Jose, CA, United States). The final DNA concentrations were adjusted to a minimum of 50 ng/μL and submitted to the Research Technology Support Facility at Michigan State University (East Lansing, MI, United States).

Samples were genotyped with the IPSC peach 9K SNP array v1 (Verde et al., 2012). The SNP data curation was performed using the workflow for high-resolution genetic marker data described in Vanderzande et al. (2019). After the SNP data curation, a total of 4005 SNPs distributed over the eight peach chromosomes remained and were used in the multi-locus GWAS (**Supplementary Table 2**).

Phenotypic Data

Phenotypic data were recorded over three seasons (2010–2012) at each fresh market peach program. Bloom data (BD; Julian days) were visually assessed in the field and recorded for each tree when 60–80% of the blossoms were open. Ripening date (RD; Julian days) was determined when 20% of fruits were at commercial harvest by visually inspecting the presence of a few soft fruits in the field for maturity two times per week. Days after bloom (DAB; Julian days) was calculated as the number of days between the date of full bloom and ripening date.

Approximately 20 fruits were harvested for phenotyping. A five firm fruit sample was selected for the following traits evaluations: Blush (0–5 scale, 0 = none, and 3 = 40–60%, 5 > 90% red blush on fruit surface) subjective scales were used as described by Frett et al. (2014). Fruit diameter (FDIA; mm) was evaluated with a millimeter caliper, while fruit weight (FW; g) was measured as the average weight of the five selected peaches. Flesh adherence (ADH) was evaluated using 1 - 4 scale where 1 = Freestone; 2 = Semi-freestone; 3 = Semi-clingstone; and 4 = Clingstone. Fruit firmness (FF; N) was measured using an electronic fruit texture analyzer (FTA) fitted with an 8-mm diameter tip (GÜSS Fruit Texture Analyzer; GÜSS Manufacturing (Pty) Ltd., Strand, South Africa). All readings were recorded as kilogram-force (kgf) and then converted to Newton (N) by multiplying the reading by 9.807. Redness around Pit (RP) was measured following the scale 1 = red; 0 = no red. The fruit texture (FT) was evaluated using the scale 1 = melting; 2 = non-melting. Pit weight (PW; g) was measured as the average weight of the five selected pits.

For biochemical traits, a composite sample of one approximately 2 cm wide longitudinal slice from each of the five fruits was used to extract juice with a juicer for the measurement of soluble solid concentration (SSC) using a digital refractometer, pH with a pH meter and titratable acidity (TA) using an automatic titrator (DL 22 Food and Beverage analyzer, Mettler Toledo, Columbus, OH, United States). TA was obtained by the titration of solution of 6 g of the peach juice diluted with 50 mL of distilled water to pH 8.2 with 0.1N NaOH and expressed as milliequivalents of malic acid. The following equation was used to calculate titratable acidity (the milliequivalent factor used corresponded to malic acid, 0.067):

$$Titratable\ acidity\ (\%) = \frac{[NaOH\ titrated\ (ml) \times 0.1N\ (NaOH) \times milliequivalent\ factor \times 100]}{6\ g\ of\ juice}$$

Descriptive Analysis, Genetic Diversity, and Population Structure

The descriptive analysis and the correlations between the traits were performed using the software Past (Hammer et al., 2001). The genetic diversity analysis was performed using the GenAlEx software (Peakall and Smouse, 2012). The broad sense heritability was calculated using the R package Sommer (Covarrubias-Pazaran, 2016) using the h2.fun:

$$h2.fun(object,\ data,\ gTerm,\ eTerm)$$

where: object represents a model fitted with the mmer function; data represents the dataset used to fit the model provided in the object argument; gTerm is a character vector specifying the genetic terms fitted in the model; and eTerm is a character vector specifying the environment term fitted in the model. For the level from the eTerm (environment) the heritability is calculated as:

$$1 - (PEV/(md * V_g))$$

"PEV" is the predicted error variance for the genotype, "md" is the mean value from the diagonal of the relationship (genomic) matrix "G" and where "Vg" refers to the genotype variance. The model included in the h2.fun was:

$$mix\ <-\ mmer(Trait \sim Year,$$
$$random = \sim vs\left(ds\left(Year\right), Selection, Gu = K\right) + vs\left(ds\left(Local\right)\right),$$
$$rcov\ =\ \sim vs\left(ds\left(Year\right), units\right),\ data\ =\ Trait)$$

where "K" refers to the genomic relationship matrix. Population structure, multidimensional scaling (MDS) and Bayesian clustering were performed with fastSTRUCTURE (Raj et al., 2014). The MDS was performed using TASSEL (Bradbury et al., 2007). The MDS results were plotted with the R package "scatterplot3D" (Ligges and Mächler, 2002). The fastSTRUCTURE was run with a "simple prior" option

and remaining default parameters. The number of populations (K), ranging from 1 to 20, and the most probable number of populations was chosen for running the built-in script for multiple choices of K. The admixture proportions of each genotype, estimated by fastSTRUCTURE, were visualized using DISTRUCT plots (Rosenberg, 2004). Accessions were assigned to a specific subpopulation when the estimated membership coefficients (Q) were above 0.80.

Linkage disequilibrium (LD) was measured by correlation coefficients (r^2) for all pairs of SNPs. The LD decay were calculated using PopLDdecay (Zhang et al., 2018a) with the following parameters: -MaxDist 3000 kb -MAF 0.05.

Genome-Wide Association Study

To validate and increase the accuracy of the multi-locus GWAS results, we used mrMLM 4.0 (Zhang et al., 2020) and FarmCPU (Liu et al., 2016). The six multi-locus GWAS methods (mrMLM, FASTmrMLM, FASTmrEMMA, pLARmEB, pKWmEB, and ISIS EM-BLASSO) from mrMLM 4.0 R package were used. The SNP data were converted to character, as described in the user manual, the population structure was the Q matrix obtained from fastSTRUCTURE and the kinship matrix was calculated by mrMLM 4.0. All parameters in GWAS were set at default values. The significantly associated SNPs were determined by the critical threshold of LOD score ≥ 3 as described in previous studies (Tamba et al., 2017). Concerning FarmCPU, the SNP data were converted to numerical using the R package GAPIT (Lipka et al., 2012). Principle component analysis (PCA) was conducted using TASSEL 5.0, and the first three components were incorporated as covariates in the GWAS model. Bonferroni-corrected *P*-value threshold was set at $p < 0.01$.

We considered a QTN reliable when: QTNs repeatedly detected in at least four methods and/or two seasons using the mrMLM 4.0; QTN consistently detected in two seasons using FarmCPU; QTNs detected in at least three methods in mrMLM 4.0 and also identified in the FarmCPU approach. These QTNs were named as "qtn" + trait name abbreviation + scaffold + detected QTL order on chromosome.

Candidate Genes

The candidate gene analysis was performed using two strategies. First, the candidate gene analyses were performed within the haploblock regions in which a QTN was detected with at least three methods in mrMLM 4.0 and with FarmCPU. Haploblock regions encompassing the associated SNPs were determined in PLINK 1.9 (Chang et al., 2015) using the flag "blocks" restricted to 500 kb. From the *Prunus persica* Whole Genome v2.0 Assembly & Annotation v2.1 (Verde et al., 2017) in Genome Database for Rosaceae[1] (Jung et al., 2018), a systematic search was conducted to compile the predicted candidate genes associated with the quality traits. The candidate genes were further analyzed for GO (gene ontology) enrichment using GOseq 1.42.0 R package (Young et al., 2010). The GO terms were considered significantly enriched or depleted at FDR < 0.05. The enriched GO terms were visualized using REVIGO semantic similarities (Supek et al., 2011). Second, we compared the position of the already reported candidate genes responsible for regulating BD, RP (*Cs locus*), Blush, RD, pH, and TA (*D locus*) with the QTL hotspot regions detected in this study.

[1]www.rosaceae.org

RESULTS

Phenotypic Data

Six hundred twenty individuals from the three fresh market public peach breeding programs were evaluated for 14 different fruit quality traits over 3 years (2010–2012) (**Table 1**). The BD, DAB, FDIA, and TA traits were analyzed in two seasons (2011 and 2012), with the BD, DAB, and TA exhibiting the highest mean values in 2011 and FDIA in 2012. The RD, FW, FF, PW, SSC, and pH, as well as the categorical traits Blush, ADH, RP, and FT were evaluated in three seasons (2010–2012). The RD, FW, and pH varied from 111 to 237 Julian days, 30.2 – 351.4 g and 2.8 – 5.1 respectively, with the highest mean values observed in 2010 (197.6 Julian days, 119.4 g and 3.9, respectively). The FF fluctuated from 0.9 N to 106.4N with the highest mean value measured in 2011 (21.1 N). The traits PW and SSC ranged from 2.5 to 12.2 and 7.2 – 26.8, respectively, with the highest mean values in 2012 (6.8 g and 13.2).

Highly significant ($P < 0.01$) correlations were observed between the traits (**Supplementary Table 3**). The highest correlation was observed between the FDIA_2011 and FW_2011 (0.92). As expected, a significant negative correlation was detected between the pH and TA (−0.65 and −0.64 in 2011 and 2012, respectively). The traits DAB and RD revealed a significant positive correlation in the years analyzed (0.82 and 0.87). Concerning the correlation between years, BD showed the highest correlation (0.99), followed by RD (0.92).

The broad sense heritability (H^2) was estimated for all 14 traits (**Supplementary Table 4**). High average values of H^2 (> 0.6) were observed for TA (0.87), RD (0.83), BD (0.77), ADH (0.77), FT (0.76), DAB (0.74), FDIA (0.73), SSC (0.72), Blush (0.71), FW (0.70), PW (0.70), RP (0.69), pH (0.69), and FF (0.68).

Genetic Variability, Population Structure, and Linkage Disequilibrium

The observed mean heterozygosity (Ho) per individual was 0.35, ranging from 0.06 in "St John" to 0.68 in "Elberta." The mean Ho per SNP was 0.36 ranging from 0.07 in SNP_IGA_598267 (scaffold 5) to 0.97 in SNP_IGA_573558 (chromosome 5). The chromosome 6 was the least heterozygous (Ho = 0.281) while the chromosome 1 revealed the highest heterozygosis (Ho = 0.385). The mean expected heterozygosity (He) was 0.370, ranging from 0.08 (SNP_IGA_624226; scaffold 6) to 0.500. The mean average inbreeding coefficient (F = (Ho-He) /Ho) was 0.05, ranging from −0.949 to 0.595.

The population structure was analyzed with Multidimensional scaling (MDS) and fastSTRUCTURE. The MDS revealed two main groups, in which the second group could be divided in two clusters. The first group comprised the individuals from the TX breeding program, while the second group grouped the individuals from the AR and SC breeding programs

TABLE 1 | Descriptive analysis of 14 phenotypic traits observed in 620 individuals from three U.S. public fresh market peach breeding programs (Univ. of Arkansas, Texas A&M and Clemson Univ.) over three seasons (2010–2012).

Trait	Year	Min	Max	Mean	SE	SD
BD	2011/2012	37/36	80/78	65.1/59.31	1.14/0.51	16.19/10.93
RD	2010/2011/2012	158/111/125	230/237/230	197.6/189.1/171.3	1.2/1.1.02	14.9/23.5/22.2
DAB	2011/2012	67/78	196/159	120.8/111.3	1.52/0.82	19.98/17.24
Blush	2010/2011/2012	0/0/0	5/5/5	2.8/3.0/2.7	0.1/0.05/0.04	1.3/1.0.93
FDIA	2011/2012	36.3/42.0	85.2/80.6	55.2/60.8	0.42/0.37	7.47/6.66
FW	2010/2011/2012	49.0/33.4/30.2	214.7/351.4/289.8	119.4/103.1/117.1	2.9/1.9/1.9	34.9/40.7/42.2
ADH	2010/2011/2012	1/1/1	4/4/4	2.2/2.5454	0.1/0.07/0.06	1.4/1.4/1.4
FF	2010/2011/2012	1.4/2.1/0.9	54.6/67.9/106.4	16.2/21.1/17.6	0.9/0.6/0.7	10.5/12.0/14.8
RP	2010/2011/2012	0/0/0	1/1/1	0.8/0.8/0.6	0.04/0.02/0.02	0.4/0.4/0.5
FT	2010/2011/2012	1/1/1	2/2/2	1.1/1.3/1.3	0.02/0.03/0.03	0.3/0.7/0.7
PW	2010/2011/2012	2.6/2.5/2.8	10.7/12.2/11.6	6.0/5.9/6.8	0.1/0.1/0.1	1.8/1.9/1.6
SSC	2010/2011/2012	7.5/7.2/7.6	17.9/22.2/26.8	11.7/13.1/13.2	0.2/0.1/0.1	2.1/2.9/3.3
TA	2011/2012	0.2/0.01	1.7/1.8	0.7/0.6	0.01/0.01	0.3/0.3
pH	2010/2011/2012	3.4/2.9/2.8	5.0/4.8/5.1	3.9/3.8/3.8	0.02/0.02/0.03	0.3/0.3/0.4

BD, bloom date (Julian days); RD, ripening date (Julian days); DAB, days after bloom (Julian days); blush (0–5 scale); FDIA, fruit diameter (mm); FW, fruit weight (g); ADH, adherence (1–4); FF, fruit firmness (N); RP, Redness around pit (0–1 scale); FT, fruit texture (1–2 scale); PW, pit weight (g); SSC, soluble solid concentration (°Brix); TA, titratable acidity (% malic acid); SE, mean standard error; SD, standard deviation.

(**Supplementary Figure 1**). Population structure analysis with fastSTRUCTURE suggested a number of K between 2 and 19. However, the population stratification for $K = 3$ showed clear differences between groups based mainly on the pedigree information of the individuals belonging to each group (**Supplementary Figure 1**). The first group accounted for the individuals related to 'Tropic Beauty', 'TX2293_3', 'TX2B136', 'TXW1293_1', and 'TXW1490_1'. The second group comprised individuals linked to 'A_663', 'A_760', and 'Bolinha', while the third group contained individuals linked either to 'Clayton' and/or 'O'Henry'.

The LD decayed with increase of physical distance between SNPs in all groups (**Supplementary Figure 2**). Considering the total number of individuals, the average of r^2 was 0.16. The physical distance over which LD decayed to half of its maximum value was around 540 kb. Different patterns of LD decays were observed in the three different groups. Group 3 revealed the highest average of r^2 (0.32) and the longest physical distances in which LD decayed to half of its maximum value (1620 kb), while group 2 showed shortest distance (480 kb). In the group 1, the LD decayed of its maximum value of r^2 in approximately 540 kb.

Multi-Locus Genome-Wide Association Study

GWAS using the six multi-locus methods in the R package mrMLM 4.0 revealed a total of 967 QTNs associated with 14 traits (**Supplementary Table 5**). The highest number of associated SNPs was observed on chromosome 4 (99) and the lowest in chromosome 7 (23). Significant QTNs detected in at least four methods in the same season, were detected for almost all traits except TA. In addition, consistently associated QTNs identified in at least two seasons were detected for BD, RD, DAB, ADH, RP, SSC, Blush, FF, FT, TA, and pH. Furthermore, SNPs associated with more than one trait were identified on chromosome 1 (BD and TA; BD and FT; BD and FF; BD and Blush; DAB and Blush; and Blush, FT, and PW; FDIA and FW; FDIA and ADH; RD and SSC; and PW and TA), 2 (RD and PW; RD and pH; FF and FT; and FF and SSC), 3 (RD and DAB; DAB and SSC; Blush and RP; and FDIA and FW, ADH and SSC), 4 (BD and RD; RD and DAB; RD, DAB, FF, RP and FT; RD, DAB, FDIA, ADH, and RP; RD, DAB and Blush; RD, DAB and ADH; RD and FF; RD and ADH, RD, DAB and SSC; RD and SSC; RD, ADH and RP; RD, FF and SSC; RD, DAB, FDIA and RP; DAB and FF; DAB and FF; DAB, FF and RP; DAB, FT and PW, FDIA and FW; FDIA and RP; FDIA and ADH; FW, FF, ADH and RP; FF, ADH and FT; FDIA, FW, FF and RP; FF and FT; ADH and FT; FF, ADH and pH, ADH and PW, ADH and RP; and ADH and FT), 5 (BD and TA; RD and SSC; DAB and Blush, FDIA and FW; FW and SSC; FT, SSC, and TA; FT and PW; SSC and TA; FT and TA; SSC and pH; and TA and pH), 6 (RD and DAB; RD and FW; FDIA, FW, FT and SSC; FDIA and ADH; and FW and PW) and 8 (BD and pH; BD and SSC; BD and RD; BD and FF; RD, FDIA and FF; RD, DAB, PW and SSC; and FT and SSC).

The multi-locus model FarmCPU revealed a total of 180 QTNs (**Supplementary Table 6**). The highest number of QTNs were detected on chromosome 4 (33), while the smallest was observed on chromosome 7 (6). Consistently associated SNPs over at least two seasons were identified for BD, RD, ADH, RP, and SSC. In addition, SNPs associated with more than one trait were detected on chromosomes 1 (DAB and RD), 3 (Blush and RP; FW and RD), 4 (Blush and RD; RD and SSC; FF and SSC), 5 (TA and pH), and 8 (BD and RD; FT and SSC).

To ensure reliable results, further analyses included only QTNs that met the following conditions: QTNs detected in at least four methods in mrMLM and/or detected in at least two seasons using mrMLM (**Table 2** and **Figure 1**); QTNs detected in two seasons using FarmCPU (**Table 3** and **Figure 1**); and QTNs detected in at least three methods in mrMLM 4.0 and also identified in the FarmCPU (**Table 4** and **Figure 1**).

TABLE 2 | Significant associations between SNP markers and quality traits detected in at least three methods of mrMLM 4.0 and/or two seasons.

QTN	Trait	Method[a]	SNP	Chromosome	Position (bp)	LOD	r^2 (%)
qtnBD_1.1	BD	1–4	SNP_IGA_131557	1	45022954	11.7 – 24.2	13.1 – 64.9
qtnBD_1.2	BD	1–4	SNP_IGA_126857	1	46125525	5.5 – 14.8	3.6 – 37.4
qtnBD_1.3	BD	1–4; 6	SNP_IGA_128189	1	45753343	3.7 – 11.1	1.3 – 6.3
qtnBD_1.4	BD	1–4	SNP_IGA_134730	1	43578596	4.9 – 9.4	0.4 – 2.4
qtnBD_1.5	BD	1,2,4,7	SNP_IGA_119391	1	40620294	4.0 – 5.9	1.4 – 8.5
qtnBD_1.6	BD	5; 7	SNP_IGA_84580	1	25541717	3.2 – 5.6	5.6 – 10.9
qtnBD_4.1	BD	2–5	SNP_IGA_440662	4	16306919	4.3 – 10.4	1.5 – 19.9
qtnBD_7.1	BD	1–3;5	SNP_IGA_779594	7	15842240	3.0 – 11.5	0.5 – 11.0
qtnBD_7.2	BD	4;6–7	SNP_IGA_759649	7	10525885	3.1– 4.6	1.1 – 28.7
qtnRD_4.1	RD	1–7	SNP_IGA_415301	4	12523245	3.5 – 12.8	0.8 – 37.2
qtnRD_4.2	RD	1–7	SNP_IGA_410398	4	10696489	4.3 – 43.0	5.7 – 36.3
qtnRD_4.3	RD	1–7	SNP_IGA_411637	4	10981971	5.7 –46.5	11.7 – 54.0
qtnRD_4.4	RD	1–4;6–7	SNP_IGA_386222	4	4045426	5.0 – 11.6	3.4 – 9.0
qtnRD_4.5	RD	1–4	SNP_IGA_417666	4	13091850	6.2 – 12.3	1.5 – 4.9
qtnRD_4.6	RD	1–3;7	SNP_IGA_410336	4	10676008	5.3 – 5.4	2.6 – 10.1
qtnRD_4.7	RD	1;6–7	SNP_IGA_410794	4	10890653	5.0 15.4	19.2 – 29.8
qtnRD_6.1	RD	1–2; 4–6	SNP_IGA_632033	6	8774913	5.1 – 10.1	1.6 – 6.6
qtnDAB_4.1	DAB	1–7	SNP_IGA_410398	4	10696489	5.2 – 38.4	7.9 – 28.4
qtnDAB_4.2	DAB	1–7	SNP_IGA_411637	4	10981971	5.4 – 56.6	16.9 – 56.1
qtnDAB_4.3	DAB	1–3; 5	SNP_IGA_403613	4	9052116	3.6 – 14.1	2.0 – 5.6
qtnDAB_5.1	DAB	1–3; 6	SNP_IGA_602331	5	16550893	5.7 – 10.0	13.0 – 20.3
qtnBlush_1.1	Blush	1–6	SNP_IGA_88046	1	26896332	3.0 – 15.0	3.7 – 24.4
qtnBlush_1.2	Blush	1–2; 7	SNP_IGA_7992	1	2518043	4.0 – 4.8	3.0 – 11.1
qtnBlush_3.1	Blush	1–2; 4–6	SNP_IGA_349831	3	20473077	3.1 – 5.2	1.5 – 8.0
qtnBlush_3.2	Blush	3; 6–7	SNP_IGA_341962	3	18179421	4.7 – 11.3	1.2 – 11.4
qtnBlush_4.1	Blush	2–4; 6	SNP_IGA_397470	4	6624729	3.8 – 5.7	12.1 – 26.1
qtnBlush_5.1	Blush	2–4; 6	SNP_IGA_602331	5	16550893	3.3 – 8.1	1.4 – 6.90
qtnFDIA_7.1	FDIA	1–2; 4; 6	SNP_IGA_726818	7	207697	3.0 – 5.1	4.8 – 7.9
qtnFW_1.1	FW	1–6	SNP_IGA_1129	1	209701	3.5 – 8.6	4.3 – 8.5
qtnFW_1.2	FW	1–2; 4–5	SNP_IGA_89193	1	27244316	4.7 – 10.4	8.5 – 19.4
qtnFW_2.1	FW	1–4; 6	SNP_IGA_275189	2	22195492	3.4 – 7.3	2.2 – 8.9
qtnFW_3.1	FW	1–2; 4; 6	SNP_IGA_298935	3	3989094	6.7 – 8.0	5.8 – 7.7
qtnFW_4.1	FW	1–2; 4; 6	SNP_IGA_404442	4	9321093	3.7 – 4.9	9.8 – 15.7
qtnFW_4.2	FW	1–6	SNP_IGA_439186	4	15742278	6.0 – 10.4	4.2 – 13.4
qtnFW_6.1	FW	1–6	SNP_IGA_652492	6	13508541	3.1 – 5.3	2.6 – 13.8
qtnFW_6.2	FW	1–2; 4–6	SNP_IGA_699516	6	29491714	4.7 – 6.5	5.6 – 7.7
qtnFF_1.1	FF	1–2; 4–5	SNP_IGA_126158	1	46430951	3.3 – 4.1	8.6 –16.4
qtnFF_4.1	FF	2–3; 5–6	SNP_IGA_379393	4	1391180	3.0 – 6.9	2.5 – 16.5
qtnFF_4.2	FF	2–5; 7	SNP_IGA_379856	4	1477791	3.3 – 7.9	1.7 – 4.0
qtnFF_4.3	FF	2–6	SNP_IGA_411161	4	10922075	4.3 – 11.2	2.2 – 9.8
qtnADH_4.1	ADH	1–6	SNP_IGA_450629	4	18235458	8.8 – 20.3	12.9 – 69.2
qtnADH_4.2	ADH	1–7	SNP_IGA_467302	4	19028425	6.3 – 69.0	5.3 – 30.4
qtnADH_4.3	ADH	1–2; 4–6	SNP_IGA_441749	4	16584598	4.1 – 12.4	2.5 –33.1
qtnADH_4.4	ADH	1–7	SNP_IGA_411147	4	10921604	3.8 – 13.0	2.2 – 29.6
qtnADH_4.5	ADH	1; 7	SNP_IGA_410398	4	10696489	4.6 – 7.2	2.8 – 6.5
qtnADH_4.6	ADH	1; 4; 6–7	SNP_IGA_387584	4	4601159	3.1 – 6.9	3.2 – 6.2
qtnADH_4.7	ADH	4; 6–7	SNP_IGA_410165	4	10641209	4.0 – 5.8	1.9 – 3.3
qtnADH_6.1	ADH	1–2; 4; 6	snp_6_13059650	6	13073956	4.1 – 8.5	4.7 – 10.2
qtnRP_3.1	RP	4; 6–7	SNP_IGA_341962	3	18179421	12.0 - 12.1	5.9 – 23.6
qtnRP_3.2	RP	1; 5; 7	SNP_IGA_343288	3	18666687	4.8 – 9.5	23.9 – 55.2
qtnRP_4.1	RP	1–7	SNP_IGA_410398	4	10696489	4.4 – 15.2	6.2 – 19.7
qtnRP_4.2	RP	1–2; 4; 6–7	SNP_IGA_411147	4	10921604	3.5 – 9.9	8.8 - 21.0
qtnRP_4.3	RP	4; 6–7	SNP_IGA_408223	4	10107085	3.3 – 4.2	1.2 – 4.1

(Continued)

TABLE 2 | Continued

QTN	Trait	Method[a]	SNP	Chromosome	Position (bp)	LOD	r^2 (%)
qtnRP_6.1	RP	1–4; 6	SNP_IGA_698951	6	29242212	4.2 – 9.3	6.0 - 8.5
qtnFT_2.1	FT	3–4; 7	SNP_IGA_197236	2	6650921	3.3 – 7.2	2.1 – 4.9
qtnFT_2.2	FT	5–7	SNP_IGA_198691	2	6753400	4.9 – 7.5	5.2 – 16.4
qtnFT_4.1	FT	1–4	SNP_IGA_374610	4	994306	6.4 – 9.4	4.8 – 11.1
qtnFT_5.1	FT	1–3; 5	SNP_IGA_545448	5	850261	5.1 – 30.7	15.3 – 33.8
qtnFT_5.2	FT	1–2; 5–6	SNP_IGA_559057	5	3731800	7.9 –11.2	9.9 –16.7
qtnFT_5.3	FT	4; 6–7	SNP_IGA_553456	5	2477309	3.9 – 7.5	10.1 – 22.7
qtnFT_7.1	FT	1–7	SNP_IGA_769572	7	12248919	3.3 – 10.4	7.6 – 16.0
qtnFT_8.1	FT	1–4; 6	SNP_IGA_821894	8	5071328	3.5 – 6.8	3.4 – 6.4
qtnFT_8.2	FT	1–2; 4–5; 7	SNP_IGA_866041	8	15002010	3.7 – 4.2	0.9 – 4.2
qtnPW_6.1	PW	1–4; 6	SNP_IGA_680747	6	24132839	3.6 – 7.7	2.8 –5.7
qtnPW_6.2	PW	1–4; 6	SNP_IGA_697517	6	28795793	5.2 – 7.6	6.6 – 17.0
qtnPW_6.3	PW	1–2; 4–6	SNP_IGA_684085	6	25090090	3.7 – 9.1	8.4 – 28.6
qtnPW_8.1	PW	2; 4–6	SNP_IGA_879528	8	19234898	3.0 – 4.5	4.5 – 13.2
qtnSSC_1.1	SSC	1–4; 6	SNP_IGA_58626	1	17538855	12.6 – 25.0	1.6 – 17.4
qtnSSC_4.1	SSC	1–4	SNP_IGA_397710	4	6694626	11.8 – 15.0	12.3 – 16.4
qtnSSC_4.2	SSC	1–2; 4–6	SNP_IGA_426994	4	14898353	3.2 – 7.6	2.4 – 11.8
qtnSSC_4.3	SSC	1–2; 4–7	SNP_IGA_411161	4	10922075	4.2 – 13.4	0.8 – 7.5
qtnSSC_5.1	SSC	1–5	SNP_IGA_552247	5	2240224	8.7 – 31.4	5.3 – 24.0
qtnSSC_5.2	SSC	1–2; 4;6	SNP_IGA_544961	5	698215	4.2 – 7.1	3.3 – 8.4
qtnSSC_5.3	SSC	1–7	SNP_IGA_595786	5	13019899	3.2 – 7.4	1.1 – 5.6
qtnSSC_6.1	SSC	1–2; 4;6	SNP_IGA_673205	6	21277895	6.7 – 9.5	4.3 – 12.3
qtnTA_5.1	TA	1–2; 7	SNP_IGA_547830	5	1342919	3.1 – 20.4	1.0–38.7
qtnpH_2.1	pH	1–4; 6	SNP_IGA_288845	2	29376788	4.9 – 11.2	6.9 – 14.6
qtnpH_5.1	pH	1–2; 4–7	SNP_IGA_544428	5	557504	7.1 – 29.51	30.5 – 62.7

BD, bloom date; RD, ripening date; DAB, days after bloom; FF, fruit diameter; FW, fruit weight; FF, fruit firmness; ADH, adherence; RP, redness around pit; FT, fruit texture; PW, pit weight; SSC, soluble solid concentration; TA, titratable acidity.

[a]*Methods: 1 = mrMLM; 2 = FASTmrMLM; 3 = FASTmrEMMA; 4 = pLARmEB; 5 = pKWmEB; 6 = ISIS EM–BLASSO; 7 = detected in at least two seasons.*

QTNs Detected With Four Methods and/or Two Seasons Using mrMLM R Package

The mrMLM revealed nine reliable QTNs distributed on 3 chromosomes significantly associated with BD (**Table 2** and **Figure 1**). The *qtnBD_1.1*, *qtnBD_1.2*, *qtnBD_1.3*, *qtnBD_1.4*, *qtnBD_1.5*, and *qtnBD_1.6*, on chromosome 1, explained 13.1–64.9, 3.6–37.4, 1.3–6.3, 0.4–2.4, 1.4–8.5, and 5.6–10.9% of total phenotypic variation, respectively. The *qtnBD_4.1* located on chromosome 4, demonstrated LOD score of 4.3–10.4 and explained 1.5–19.8% of phenotypic variation. The reliable QTNs identified on chromosome 7 (*qtnBD_7.1* and *qtnBD_7.2*) explained 0.5–11.1 and 1.1–28.7% of total phenotypic variation, respectively. In addition, the *qtnBD_1.5*, *qtnBD_1.6* and *qtnBD_7.2* were detected in two seasons.

Reliable QTNs associated with RD were detected on chromosomes 4 (*qtnRD_4.1*, *qtnRD_4.2*, *qtnRD_4.3*, *qtnRD_4.4*, *qtnRD_4.5*, *qtnRD_4.6* and *qtnRD_4.7*) and 6 (*qtnRD_6.1*). The *qtnRD_4.3* accounted for the highest phenotypic variation (11.7–54.0%) in comparison to the other QTNs identified on chromosome 4 (**Table 2** and **Figure 1**). The *qtnRD_6.1*, on chromosome 6 demonstrated LD scores ranging from 5.1 to 10.1 and explained 1.6–6.6% of phenotypic variation. Almost all QTNs detected on chromosome 4 were detected in at least two seasons, except *qtnRD_4.5*.

Three QTNs on chromosome 4 (*qtnDAB_4.1*, *qtnDAB_4.2* and *qtnDAB_4.3*) were associated with DAB. The greatest phenotypic variation was explained by *qtnDAB_4.2* (16.9–56.1%). The *qtnDAB_5.1* on chromosome 5 explained 13.0 to 20.3% of the phenotypic variance observed (LOD scores 5.7–10.0). The *qtnDAB_4.1* and *qtnDAB_4.2* on chromosome 4 were detected in two seasons.

The reliable QTNs associated with blush were distributed on chromosomes 1 (*qtnBlush_1.1* and *qtnBlush_1.2*), 3 (*qtnBlush_3.1* and *qtnBlush_3.2*), 4 (*qtnBlush_4.1*), and 5 (*qtnBlush_5.1*). The *qtnBlush_3.2* was identified in three seasons, while the *qtnBlush_1.2* was identified in two. The *qtnBlush_4.1* explained the highest phenotypic variation (12.1–26.1%).

The *qtnFDIA_7.1* associated with FDIA was located on chromosome 7, revealed LOD scores ranging from 3.0 to 5.1 and explained 4.8–7.9% of the phenotypic variance observed.

Concerning FW, QTNs were detected on chromosomes 1 (*qtnFW_1.1* and *qtnFW_1.2*), 2 (*qtnFW_2.1*), 3 (*qtnFW*_3.1), 4 (*qtnFW_4.1* and *qtnFW_4.2*), and 6 (*qtnFW_6.1* and *qtnFW_6.2*). The *qtnFW_1.1*, *qtnFW_4.2* and *qtnFW_6.1* were detected with the six methods of the mrMLM R package. The greatest phenotypic variation was explained by *qtnFW_1.2* (8.5–19.4%), followed by *qtnFW_4.1* (9.8–15.7%).

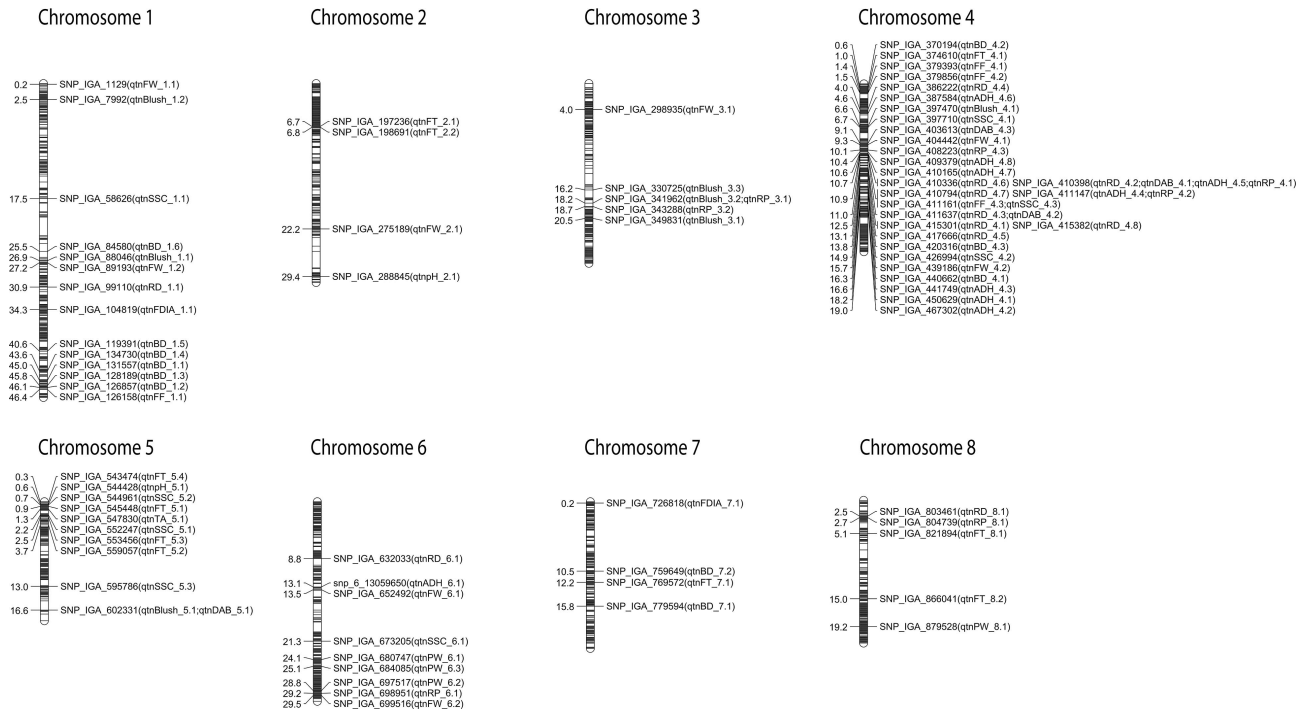

FIGURE 1 | Reliable QTNs detected using different multi-locus GWAS methods and/or at least two seasons. Genetic distance scale in physical position (Mbp) is placed at left margin.

TABLE 3 | Significant associations between SNP markers and fruit quality traits consistently detected in two seasons using FarmCPU.

QTN	Trait/year	SNP	Chromosome	Position (bp)	*P*-value
qtnBD_4.2	BD_2011	SNP_IGA_370194	4	607467	1.37E-07
	BD_2012	SNP_IGA_370194	4	607467	7.74E-07
qtnRD_4.7	RD_2010	SNP_IGA_410794	4	10890653	2.58E-16
	RD_2011	SNP_IGA_410794	4	10890653	3.9E-39
	RD_2012	SNP_IGA_410794	4	10890653	1.47E-55
qtnRD_4.8	RD_2011	SNP_IGA_415382	4	12546297	1.2E-07
	RD_2012	SNP_IGA_415382	4	12546297	7.72E-11
qtnRD_8.1	RD_2011	SNP_IGA_803461	8	2534033	3.24E-13
	RD_2012	SNP_IGA_803461	8	2534033	1.59E-06
qtnADH_4.8	ADH_2010	SNP_IGA_409379	4	10389254	1.01E-06
	ADH_2011	SNP_IGA_409379	4	10389254	9.65E-09
qtnADH_4.5	ADH_2011	SNP_IGA_410398	4	10696489	8.03E-19
	ADH_2012	SNP_IGA_410398	4	10696489	5.49E-09
qtnADH_4.2	ADH_2011	SNP_IGA_467302	4	19028425	8.31E-14
	ADH_2012	SNP_IGA_467302	4	19028425	4.8E-10
qtnRP_3.1	RP_2010	SNP_IGA_341962	3	18179421	6.64E-11
	RP_2011	SNP_IGA_341962	3	18179421	2.93E-16
qtnSSC_5.3	SSC_2011	SNP_IGA_595786	5	13019899	2.87E-08
	SSC_2012	SNP_IGA_595786	5	13019899	1.89E-06
qtnSSC_6.1	SSC_2011	SNP_IGA_673205	6	21277895	1.73E-06
	SSC_2012	SNP_IGA_673205	6	21277895	2.42E-06

BD, bloom date; RD, ripening date; ADH, adherence; RP, red in pit; SSC, soluble solid concentration.

TABLE 4 | Significant associations between SNP markers and quality traits commonly detected using at least three mrMLM 4.0 GWAS methods and FarmCPU.

QTN	Trait	SNP	Chromosome	Position (bp)
qtnBD_1.1	BD	SNP_IGA_131557	1	45022954
qtnBD_1.2	BD	SNP_IGA_126857	1	46125525
qtnBD_1.3	BD	SNP_IGA_128189	1	45753343
qtnBD_4.3	BD	SNP_IGA_420316	4	13813285
qtnRD_1.1	RD	SNP_IGA_99110	1	30864365
qtnRD_4.1	RD	SNP_IGA_415301	4	12523245
qtnRD_4.2	RD	SNP_IGA_410398	4	10696489
qtnRD_4.5	RD	SNP_IGA_417666	4	13091850
qtnDAB_4.2	DAB	SNP_IGA_411637	4	10981971
qtnBlush_3.3	Blush	SNP_IGA_330725	3	16198112
qtnBlush_5.1	Blush	SNP_IGA_602331	5	16550893
qtnFDIA_1.1	FDIA	SNP_IGA_104819	1	34325189
qtnFW_6.1	FW	SNP_IGA_652492	6	13508541
qtnFF_4.1	FF	SNP_IGA_379393	4	1391180
qtnFF_4.3	FF	SNP_IGA_411161	4	10922075
qtnADH_4.1	ADH	SNP_IGA_450629	4	18235458
qtnADH_4.2	ADH	SNP_IGA_467302	4	19028425
qtnADH_4.3	ADH	SNP_IGA_441749	4	16584598
qtnRP_4.2	RP	SNP_IGA_411147	4	10921604
qtnRP_6.1	RP	SNP_IGA_698951	6	29242212
qtnRP_8.1	RP	SNP_IGA_804739	8	2702428
qtnFT_5.1	FT	SNP_IGA_545448	5	850261
qtnFT_5.4	FT	SNP_IGA_543474	5	329318
qtnSSC_1.1	SSC	SNP_IGA_58626	1	17538855
qtnSSC_4.1	SSC	SNP_IGA_397710	4	6694626
qtnSSC_4.2	SSC	SNP_IGA_426994	4	14898353
qtnSSC_4.3	SSC	SNP_IGA_411161	4	10922075
qtnSSC_5.1	SSC	SNP_IGA_552247	5	2240224
qtnSSC_5.3	SSC	SNP_IGA_595786	5	13019899
qtnpH_2.1	pH	SNP_IGA_288845	2	29376788
qtnpH_5.1	pH	SNP_IGA_544428	5	557504

BD, bloom date; RD, ripening date; DAB, days after bloom; FDIA, fruit diameter; FW, fruit weight; FF, fruit firmness; ADH, adherence; RP, redness around pit; FT, fruit texture; SSC, soluble solid concentration.

Quantitative trait nucleotides associated with FF were located on chromosomes 1 (*qtnFF_1.1*) and 4 (*qtnFF_4.1*, *qtnFF_4.2* and *qtnFF_4.3)*. The *qtnFF_4.2* was identified in two seasons and explained 1.7–4.0% of the phenotypic variation with the *qtnFF_1.1* explaining the highest phenotypic variation for FF (8.6–16.4%).

For ADH, seven QTNs on chromosome 4 (*qtnADH_4.1*, *qtnADH_4.2*, *qtnADH_4.3*, *qtnADH_4.4*, *qtnADH_4.5*, *qtnADH_4.6* and *qtnADH_4.7*), and one on chromosome 6 (*qtnADH_6.1)* were identified. The *qtnADH_4.2* was detected in three seasons, while *qtnADH_4.4*, *qtnADH_4.5*, *qtnADH_4.6* and *qtnADH_4.7* were detected in two seasons. The *qtnADH_4.1* was identified with the six methods of mrMLM and explained the highest phenotypic variance (12.9–69.2%).

Quantitative trait nucleotides on chromosome 3 (*qtnRP_3.1* and *qtnRP_3.2*), 4 (*qtnRP_4.1*, *qtnRP_4.2* and *qtnRP_4.3*), and 6 (*qtnRP_6.1*) were significantly associated with RP. The *qtnRP_4.1* was detected in three seasons, while the *qtnRP_3.1*, *qtnRP_3.2, qtnRP_4.2* and *qtnRP_4.3* were detected in two seasons. The highest phenotypic variation (23.9–55.2%) was explained by the *qtnRP_3.2* located on the chromosome 3.

The reliable QTNs associated with FT were distributed on chromosome 2 (*qtnFT_2.1* and *qtnFT_2.2*), 4 (*qtnFT_4.1*), 5 (*qtnFT_5.1*, *qtnFT_5.2* and *qtnFT_5.3*), 7 (*qtnFT_7.1*) and 8 (*qtnFT_8.1* and *qtnFT_8.2*). The *qtnFT_2.1*, *qtnFT_2.2*, *qtnFT_5.3*, *qtnFT_7.1* and *qtnFT_8.2* were detected in two seasons. The *qtnFT_5.1* and *qtnFT_5.3* exhibited the highest phenotypic variation 15.3–33.8 and 10.1–22.7%, respectively.

Quantitative trait nucleotides associated with PW were identified on chromosomes 6 (*qtnPW_6.1*, *qtnPW_6.2* and *qtnPW_6.3*) and 8 (*qtnPW_8.1)*. The *qtnPW_6.2* and *qtnPW_6.3* with LOD scores of 5.2–7.6 and 3.7–9.1 explained 6.6–17.0 and 8.4–28.6% of the phenotypic variation, respectively.

For SSC, 8 reliable QTNs were detected on chromosomes 1 (*qtnSSC_1.1*), 4 (*qtnSSC_4.1*, *qtnSSC_4.2* and *qtnSSC_4.3)*, 5 (*qtnSSC_5.1*, *qtnSSC_5.2* and *qtnSSC_5.3),* and 6 (*qtnSSC_6.1*), with the *qtnSSC_4.3* and *qtnSSC_5.3* detected in two seasons. The *qtnSSC_4.1* and *qtnSSC_5.1* accounted for the highest phenotypic variation (12.3–16.4 and 5.3–24.0%).

The *qtnTA_5.1* on chromosome 5 was associated with TA and detected in two seasons. The LOD score varied from 3.1 to 20.4 and explained 1.0–38.0% of the phenotypic variation.

One reliable QTN associated with pH was identified on chromosome 2 (*qtnpH_2.1*) and chromosome 5 (*qtnpH_5.1*). The *qtnpH_5.1* explained the highest phenotypic variation (30.5–62.7%) and was detected in two seasons.

QTNs Detected in Two Seasons Using FarmCPU

The *qtnBD_4.2* was consistently associated with BD in the two seasons and revealed a *p* values of 1.37E-07 and 7.74E-07, respectively (**Table 3** and **Figure 1**).

The *qtnRD_4.7* located on chromosome 4 (10.9 Mbp) was significantly associated with RD in all three seasons. In addition, the *qtnRD_4.8* and *qtnRD_8.1* were associated with RD in 2011 and 2012 and were located at 12.5 Mbp (chromosome 4) and 2.5 Mbp (chromosome 8), respectively.

A reliable *qtnADH_4.8* on chromosome 4 (10.4 Mb) was consistently associated with ADH in 2010 and 2011, while *qtnADH_4.5* (10.69) and *qtnADH_4.2* (19.02 Mbp) were associated with ADH in 2011 and 2012.

For RP, the *qtnRP_3.1* located at 18.17 Mbp on chromosome 3 was detected in two seasons with *p* values of 6.64E-11 and 2.93E-16, respectively.

Consistent, significant associations with the SSC were detected in two seasons with QTNs on chromosomes 5 (*qtnSSC_5.3*) and 6 (*qtnSSC_6.1*).

QTNs Commonly Detected With Both mrMLM and FarmCPU

A total of 31 QTNs were consistently detected with at least three methods in mrMLM and also with the FarmCPU (**Table 4**). Six QTNs associated with BD, RD, FDIA, and SSC were

identified on chromosome 1 (*qtnBD_1.1*, *qtnBD_1.2*, *qtnBD_1.3*, *qtnRD_1.1*, *qtnFDIA_1.1,* and *qtnSSC_1.1*). Only one QTN (*qtnpH_2.1*) associated with pH, located at 29.4 Mpb on chromosome 2 was detected using both approaches. A QTN associated with blush was detected on chromosome 3 (16.2 Mbp). Most of the QTNs were observed on chromosome 4. A total of twelve QTNs associated with BD (*qtnBD_4.2*), RD (*qtnRD_4.1*, *qtnRD_4.2* and *qtnRD_4.5*), DAB (*qtnDAB_4.2*), FF (*qtnFF_4.1* and *qtnFF_4.3*), ADH (*qtnADH_4.1*, *qtnADH_4.2* and *qtnADH_4.3*), RP (*qtnRP_4.2*) and SSC (*qtnSSC_4.1* and *qtnSSC_4.2*) and a QTN cluster of FF and SSC (*qtnFF_4.3* and *qtnSSC_4.3*) were identified. QTNs for blush (*qtnBlush_5.1*), FT (*qtnFT_5.1* and *qtnFT_5.4*), SSC (*qtnSSC_5.1* and *qtnSSC_5.3*) and pH (*qtnpH_5.1*) were identified on chromosome 5 located at 16.55, 0.85, 0.32, 2.24, 13.01 and 0.55 Mbp, respectively. Two QTNs associated with FW (*qtnFW_6.1*) and RP (*qtnRP_6.1*) were present on chromosome 6. Lastly, the QTN *qtnRP_8.1*, associated with the RP, was present on chromosome 8 (2.7 Mbp).

Candidate Genes

Genomic regions encompassing the QTNs detected using the mrMLM 4.0 methods and FarmCPU revealed a total of twenty-eight haploblocks located at scaffolds 1, 2, 3, 4, 5, 6, and 8 (**Table 5**).

A total of 566 candidate genes (CG) were detected within the haploblock regions for the significantly associated QTNs (**Supplementary Table 7**), from which 93 CG were detected in the regions for BD, 89 for RD, 29 for DAB, 22 for Blush, 39 for FDIA, 24 for FW, 26 for ADH, 31 for FF, 148 for RP, 12 for FT and 90 for SSC. The gene ontology (GO) annotations were retrieved for 435 CG. The GO enrichment analysis revealed 68 GO terms in all three GO aspects, biological process, molecular function, and cellular component. Twenty-six GO terms (78 genes) were described as biological processes, 32 GO terms (108 genes) with the molecular function, and 10 GO terms (36 genes) with the cellular component (**Supplementary Table 8**). The GO term cluster representatives were joined into "superclusters" of terms loosely related to cellulose microfibril organization, THO complex part of transcription export complex and sulfotransferase activity in the biological process, cellular component and molecular function, respectively (**Figure 2**).

Hotspots in Peach Genome

The reliable QTNs revealed fruit quality hotspots in the peach genome (**Figure 1**). On chromosome 1, three reliable QTNs associated with BD, Blush and FW in the interval of 25.5–27.2 Mbp were identified. In addition, at the bottom of the same chromosome (43.6–46.4 Mbp), we also observed QTNs associated with BD and FF. On chromosome 3, a hotspot involving the quality traits Blush and RP was observed in the region located at 18.2–20.2 Mbp. The majority of the reliable QTNs detected were located on chromosome 4 (0.6–19.0 Mbp), especially concentrated in the genomic region located at 9.0–12.5 Mbp with QTNs associated with DAB, FW, RP, ADH, RD, FF, and SSC. A hotspot was also observed on the top of chromosome 5 (0.3–3.7 Mbp) with significant signals associated with FT, pH, SSC, and TA. In the genomic region on chromosome 6 spanning 28.8–29.5 Mbp, QTNs involving PW, RP, and FW were detected. Furthermore, on top of chromosome 8 (2.5–5.1 Mbp), a hotspot with reliable QTNs associated with RD, RP, and FT was observed.

TABLE 5 | Haploblock regions encompassing SNPs markers significantly associated with fruit quality traits in peach.

Trait	Hap	Scaffold	Start (bp)	End (bp)	Associated SNPs
SSC	1_1	1	17400346	17538855	SNP_IGA_58626
RD	1_2	1	30644296	31160594	SNP_IGA_99110
FDIA	1_3	1	34122904	34404100	SNP_IGA_104819
BD	1_4	1	44904968	45237616	SNP_IGA_131557
BD	1_5	1	45753343	45821173	SNP_IGA_128189
BD	1_6	1	46012310	46430951	SNP_IGA_126857
pH	2_1	2	29241773	29376788	SNP_IGA_288845
Blush	3_1	3	16195795	16236799	SNP_IGA_330725
FF	4_1	4	1382161	1413701	SNP_IGA_379393
SSC	4_2	4	6688718	6712809	SNP_IGA_397710
RD	4_3	4	10676008	10760085	SNP_IGA_410398
RP	4_4	4	10760086	10981971	SNP_IGA_411147
FF	4_4	4	10760086	10981971	SNP_IGA_411161
SSC	4_4	4	10760086	10981971	SNP_IGA_411161
DAB	4_4	4	10760086	10981971	SNP_IGA_411637
RD	4_5	4	12429145	12523245	SNP_IGA_415301
RD	4_6	4	13078233	13108512	SNP_IGA_417666
BD	4_7	4	13561808	14018643	SNP_IGA_420316
SSC	4_8	4	14735598	15182577	SNP_IGA_426994
ADH	4_9	4	16511312	16674024	SNP_IGA_441749
ADH	4_10	4	18140428	18235458	SNP_IGA_450629
ADH	4_11	4	18719887	19206580	SNP_IGA_467302
FT	5_1	5	329318	481015	SNP_IGA_543474
pH	5_2	5	521865	821356	SNP_IGA_544428
FT	5_3	5	850261	882334	SNP_IGA_545448
SSC	5_4	5	2086499	2242971	SNP_IGA_552247
SSC	5_5	5	13014155	13019899	SNP_IGA_595786
Blush	5_6	5	16550893	16702088	SNP_IGA_602331
FW	6_1	6	13235506	13565811	SNP_IGA_652492
RP	6_2	6	29231386	29714220	SNP_IGA_698951
RP	8_1	8	2369263	2838462	SNP_IGA_804739

BD, bloom date; RD, ripening date; DAB, days after bloom; FDIA, fruit diameter; FW, fruit weight; FF, fruit firmness; ADH, adherence; RP, red in pit; FT, fruit texture; SSC, soluble solid concentration.

DISCUSSION

We have analyzed peach germplasm containing 620 individuals from three U.S. public fresh market breeding programs [University of Arkansas System Division of Agriculture (AR), Clemson University (SC) and Texas A&M University (TX)] for fourteen traits over three seasons (2010, 2011 and 2012). Phenotypic variation was observed between individuals and seasons, and the mean values for BD, RD, FW, and SSC were lower than those reported in the Spanish and European germplasm (Hernández Mora et al., 2017; Font I Forcada et al., 2019). However, average values for RD and DAB observed in our study were in agreement with the values reported in the

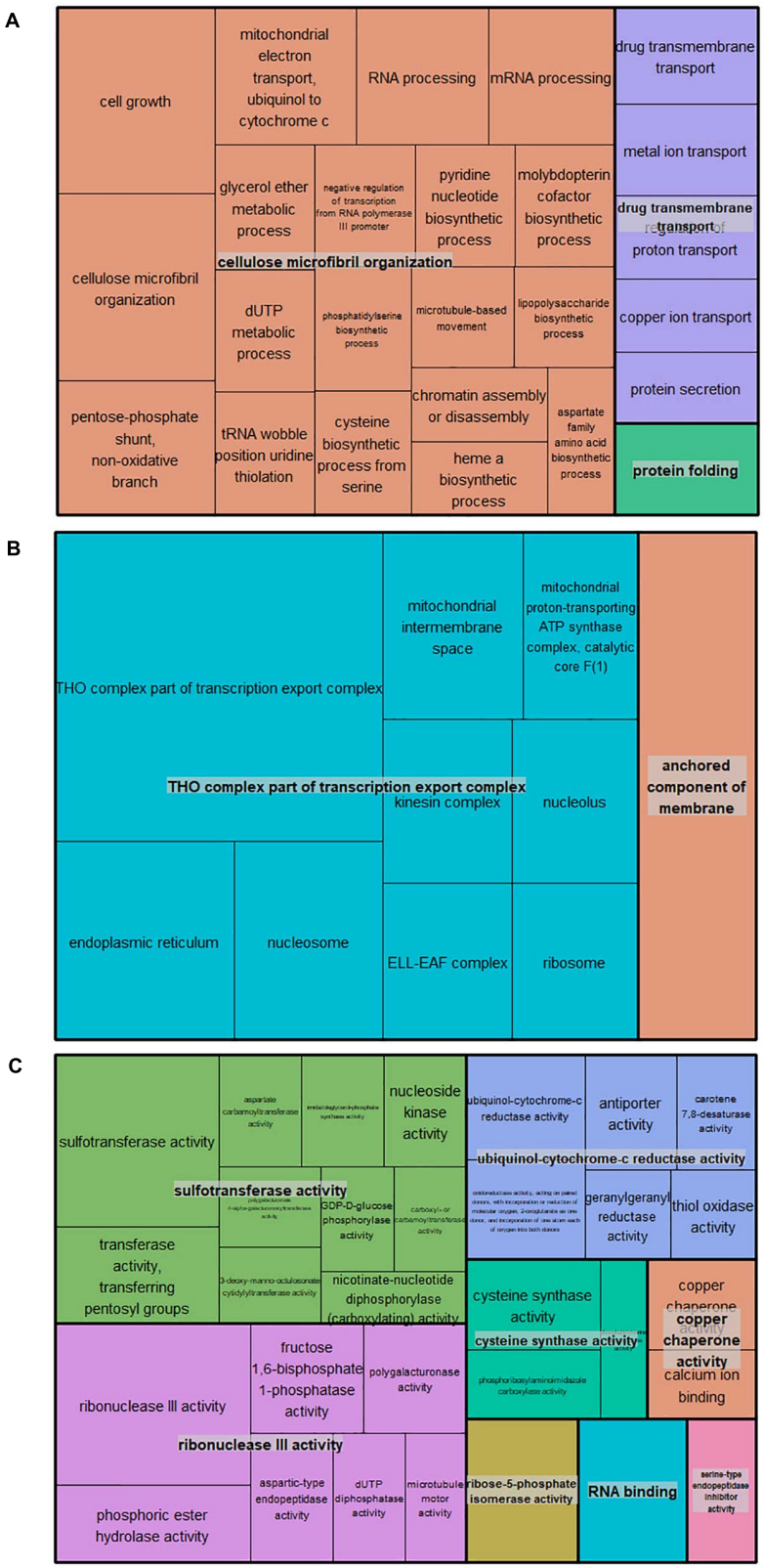

FIGURE 2 | TreeMap of the GO term cluster representatives joined into "superclusters" of biological processes **(A)**, cellular component **(B)**, and molecular functions **(C)** visualized with different colors. Each rectangle is a single cluster representative.

University of Guelph's peach germplasm, comprised of accessions originating from different regions across North America (Elsadr et al., 2019). A high and significant correlation between FW and FDIA (0.92) was previously observed in peach (da Silva Linge et al., 2015; Abdelghafar et al., 2020), as well as the positive correlation between RD and DAB (Elsadr et al., 2019) and the negative correlation between TA and pH (Abidi et al., 2011). In addition, the high estimated broad sense heritability coefficients observed in this study ranging from 0.68 to 0.87, suggesting that the phenotypic variations of all traits are mainly affected by genetic factors, and therefore this dataset can be used for further genetic analyses.

The mean observed heterozygosity (Ho = 0.36) in the U.S. peach germplasm was greater than that observed in the germplasm from four European, one Chinese and one Brazilian peach collections reported in previous studies (Micheletti et al., 2015; Thurow et al., 2019). In addition, the mean inbreeding coefficient of 0.05 indicated a low level of inbreeding. The low mean of the inbreeding coefficient observed in this study could be attributed to the diverse material, including F1 and F2 populations with different genetic backgrounds.

The multidimensional scaling (MDS) clustered material into two groups, a group of individuals from TX fresh market breeding program related to 'Tropic Beauty', 'TX2293_3', 'TX2B136', 'TXW1293_1' and 'TXW1490_1', and the second group, comprised of individuals from the AR and SC fresh market breeding programs. Breeding material from AR and SC clustered in one main group, due to the common founders or pedigree-linkages of some breeding populations. Nevertheless, the second group could further be separated in two clusters in which the first cluster grouped the individuals linked to 'A_663', 'A_760', and 'Bolinha', and the second cluster contained individuals linked to 'Clayton' and/or 'O'Henry'. The population structure indicated by fastSTRUCTURE, between K = 2 and 19, supported MDS clustering, as the K = 3 reflected grouping based on the pedigree background, and number of the breeding programs in the panel.

The population structure influences LD patterns within the genome (Thurow et al., 2019). The LD detected in this study decayed much slower in comparison with the observed by Thurow et al. (2019) and faster than the observed by Micheletti et al. (2015). The difference could be explained by the genetic material analyzed and the methods used for analyzing the LD decay. In addition, a slower decay of LD is expected in selfing materials. The LD decay over distance also determines the number of markers required to cover the genome. Considering the LD decay of our dataset (540 Kb), approximately 421 SNPs covering the total peach genome (227.4 Mb) should be sufficient to perform the GWAS. However, domestication regions containing key genes require more SNPs due to the faster LD decay (Cao et al., 2016).

Multi-Locus GWAS

In order to control the false positive rate in GWAS analysis, conservative correction methods such as false discovery rate (FDR) and Bonferroni correction are frequently adopted in association studies. However, these corrections are often too conservative for detecting many important loci. Thus, multi-locus GWAS methods have been recommended to overcome the problem of stringent correction (Zhang et al., 2020). In this study, we have successfully performed a genome-wide association study using six multi-locus GWAS methods (mrMLM, FASTmrMLM, FASTmrEMMA, pLARmEB, pKWmEB, and ISIS EM-BLASSO) comprised in mrMLM 4.0 and FarmCPU R packages.The mrMLM 4.0 adopts the critical probability value or log of odds (LOD), a less stringent significance threshold while FarmCPU requires Bonferroni correction to detect QTNs. The multi-locus methods detected 967 and 180 QTNs using mrMLM 4.0 and FarmCPU, respectively, allowing the identification of important regions in the peach genome that control fruit quality traits. Furthermore, consistently reliable QTNs (88) for all traits were detected using different multi-locus GWAS methods and/or at least two seasons (**Tables 2–4**). Half of the reliable QTNs (44) detected have already been reported using different progenies, germplasm and approaches. However, to our knowledge, the other 44 reliable QTNs controlling fruit quality traits in peach have not been previously described.

One of the main goals of breeding programs is the development of commercial varieties with predictable bloom time to adapt to various target environments. Therefore, understanding the genetic architecture of phenology-related traits represents a key prerequisite to enable the development of varieties adapted to different climates (Gogorcena et al., 2020). Reliable QTNs associated with bloom date (BD), the *qtnBD_1.1*, *qtnBD_1.2*, *qtnBD_1.3*, *qtnBD_1.4*, *qtnBD_4.1*, *qtnBD_4.3*, *qtnBD_7.1* collocate near or in the same regions previously reported using QTL mapping and pedigree-based analysis (PBA) (Fan et al., 2010; Romeu et al., 2014; Bielenberg et al., 2015; Hernández Mora et al., 2017; Rawandoozi et al., 2020a). The fact that these regions were identified following different approaches (linkage analysis, PBA analysis and GWAS) in diverse genetic material, makes them an interesting source of allelic variation for BD in peach.

QTL mapping and association studies focused on ripening date have been widely reported in peach (Eduardo et al., 2011; Pirona et al., 2013; Fresnedo-Ramírez et al., 2015; Hernández Mora et al., 2017; Elsadr et al., 2019; Font I Forcada et al., 2019; Nuñez-Lillo et al., 2019; Rawandoozi et al., 2020a). The *qtnRD_4.2*, *qtnRD_4.3*, *qtnRD_4.6* and *qtnRD_4.7* overlapped with the major RD QTLs reported in the chromosome 4 located at approximately 10.6 and 11.1 Mbp (Pirona et al., 2013; Elsadr et al., 2019). In addition, the *qtnRD_4.1*, *qtnRD_4.5* and *qtnRD_4.8* were located in the same genetic interval (11.2 - 14.1 Mbp) of the RD QTL reported by Hernández Mora et al. (2017) using the pedigree-based QTL mapping in the European peach germplasm. Beside chromosome 4, we also detected reliable QTNs for RD on chromosome 1 (*qtnRD_1.1*), 6 (*qtnRD_6.1*) and 8 (*qtnRD_8.1*). RD QTLs and associated SNPs on chromosome 1 were previously reported in peach at approximately 12.0 Mbp (Fresnedo-Ramírez et al., 2015), 35 Mbp (Romeu et al., 2014; Font I Forcada et al., 2019), and 40.0–47.0 Mbp (Romeu et al., 2014; Hernández Mora et al., 2017; Font I Forcada et al., 2019; Nuñez-Lillo et al., 2019). The reliable *qtnRD_1.1* detected in this study using mrMLM and FarmCPU was located at 30.9 Mbp.

Moreover, the *qtnRD_6.1* (chr6: 8.8 Mb) and *qtnRD_8.1* (chr8: 2.5 Mbp) were in close proximity of the SNPs associated with RD detected on chromosomes 6 (SNP_IGA_630302; 8.3 Mbp) and 8 (SNP_IGA_806528; 2.9 Mbp) in the Spanish germplasm (Font I Forcada et al., 2019).

QTL clusters for RD and DAB were commonly detected in peach (Fresnedo-Ramírez et al., 2015; Hernández Mora et al., 2017; Elsadr et al., 2019; Rawandoozi et al., 2020a). In this study, two reliable QTNs (*qtnDAB_4.1* and *qtnDAB_4.2*) associated with DAB overlapped with the QTNs associated with RD. The position of the *qtnDAB_4.1* (chr 4: 10.7 Mbp) matched the associated SNPs identified in a panel of 132 peach accessions genotypically characterized via genotyping by sequencing (GBS) approach (Elsadr et al., 2019). In addition, the SNP_IGA_410398 was emphasized as a predictive SNP for RD and DAB in haplotype analysis in a DAB QTL detected using PBA approach (Rawandoozi et al., 2020a). The *qtnDAB_4.2* (10.9 Mbp) was close to QTL for DAB detected using PBA in the European germplasm (Hernández Mora et al., 2017). Thus, our results confirmed the location of RD and DAB associated regions in the peach genome, and due to their importance for breeding, could be useful in selection of various phenology patterns in future studies.

Previous QTL analyses in peach have identified a major QTL for blush on chromosome 3 accounting, in average, for 63.7% of observed phenotypic variation (Frett et al., 2014). The *qtnBlush_3.1, qtnBlush_3.2* and *qtnBlush_3.3* were located within the genetic interval of the major QTL for blush on chromosome 3. QTL regions for blush on chromosome 4 were mapped approximately at 10.5 – 11.5 Mbp (Rawandoozi et al., 2020b); 11.2 – 14.1 Mbp (Hernández Mora et al., 2017); and at 19.8 and 28.6 Mb (Shi et al., 2020). The *qtnBlush_4.1* was detected at 6.6 Mbp and accounted for the highest phenotypic variation observed. Moreover, we identified two QTNs on chromosome 1 (*qtnBlush_1.1:* 26.9 Mbp; *qtnBlush_1.2:* 2.5 Mbp). Analyzing an F1 peach population derived from the cross between "Shahong" and "Hongfurong," Shi et al. (2020) also observed a QTL associated with blush on chromosome 1. However, the genetic interval was approximately at 21.5 Mbp. Although the percentage of the phenotypic variation explained was low, a QTN associated with blush (*qtnBlush_5.1*) on chromosome 5 was also detected.

Understanding the genetic control of fruit diameter and weight is an important goal of breeding programs due to the importance of these traits for the fresh market (Yue et al., 2014). QTL regions associated with fruit diameter and weight have been detected in all chromosomes (da Silva Linge et al., 2015; Fresnedo-Ramírez et al., 2016; Zeballos et al., 2016; Hernández Mora et al., 2017; Cao et al., 2019; Abdelghafar et al., 2020; Shi et al., 2020). In this study, we identified two reliable QTNs associated with FDIA (*qtnFDIA_7.1* and *qtnFDIA_1.1*). The *qtnFDIA_7.1,* on chromosome 7, is in the vicinity to fruit width and fruit depth QTLs (qP-Fwd7.2 and qP-Fd7.2) reported by da Silva Linge et al. (2015) using F_2 progeny resulting from a cross between an ornamental peach PI91459 ("NJ Weeping") × "Bounty." The *qtnFDIA_1.1* (36.9 Mbp) was identified in a different region of chromosome 1 when compared with previous linkage analyses, where QTLs were located approximately at 11 Mbp (da Silva Linge et al., 2015); 27–28 Mbp (Hernández Mora et al., 2017); 41 Mbp (Zeballos et al., 2016) and 43 Mbp (da Silva Linge et al., 2015; Abdelghafar et al., 2020). Concerning position of *qtnFW_1.2* and *qtnFW_6.2* matched the QTL interval identified in European peach germplasm (Hernández Mora et al., 2017). The FW QTN *qtnFW_2.1* and *qtnFW_3.1* could be the FW QTLs mapped in an interspecific cross between peach and a wild relative *Prunus davidiana* (Quilot et al., 2004; Desnoues et al., 2016). On chromosome 4 *qtnFW_4.1* was close to the FW QTL reported by da Silva Linge et al. (2015) and *qtnFW_4.2* was in the same genetic interval of the QTL identified by Shi et al. (2020).

Fruit firmness (FF) represents an essential indicator of fruit quality for peach consumers. For this reason, several authors have investigated the genetic mechanisms controlling this trait in peach (Peace et al., 2005; Eduardo et al., 2011, 2015; Martínez-García et al., 2013; Nuñez-Lillo et al., 2015; Zeballos et al., 2016; Serra et al., 2017; Carrasco-Valenzuela et al., 2019). The *qtnFF_4.1* and *qtnFF_4.2*, reported in this study, were located in chromosome 4 with the position matching the QTL interval associated with firmness loss mapped by Serra et al. (2017). Moreover, the *qtnFF_4.3* was in the same genetic region in which Carrasco-Valenzuela et al. (2019) detected a QTL significantly associated with softening rate and Zeballos et al. (2016) detected a QTL for fruit firmness.

Flesh adherence to the pit (ADH) is another factor determining overall peach fruit quality, with consumers preferring freestone or semi freestone characteristics (Olmstead et al., 2015). Previous studies have shown that ADH is inherited and controlled by the Freestone-Melting (*F-M*) locus on chromosome 4, with genes encoding endopolygalacturonase (endoPG) associated with this trait (Peace et al., 2005; Gu et al., 2016). We detected *qtnADH_4.1* and *qtnADH_4.2* explaining the majority of the phenotypic variation close to the genetic region where the endoPG gene is located. Similar to Shi et al. (2020), we detected significant genetic regions associated to ADH in different regions of chromosome 4 and also in other chromosomes.

The QTNs associated with redness around the pit (RP) (*qtnRP_3.1* and *qtnRP_3.2*) located approximately at 18.2 and 18.7 Mb, on chromosome 3, matched the position of the associated signals to flesh color around the stone detected in the recent GWAS using genome structural variations (SVs) (Guo et al., 2020). In addition, the *Cs* locus associated with red color around the pit was previously mapped in the middle of chromosome 3 (Yamamoto et al., 2001). Interestingly, the SNP_IGA_341962 (*qtnRP_3.1*) was also associated with blush (*qtnBlush_3.2*). Therefore, the QTNs associated with RP identified on chromosome 4 (*qtnRP_4.1*, *qtnRP_4.2* and *qtnRP_4.3*) were close to the associated signals detected by Guo et al. (2020) and in a different region of the associated SNPs reported by Cao et al. (2016), while the QTNs detected on chromosome 6 (*qtnRP_6.1*) and 8 (*qtnRP_8.1*) were located in different regions when compared with previous studies (Cao et al., 2016; Guo et al., 2020).

Concerning pit weight (PW), the *qtnPW_6.1,* identified on chromosome 6, is close to the QTL (qSW6; 24.6 Mb) mapped in the interspecific cross between almond × peach population

(Donoso et al., 2016). Cao et al. (2016) also detected a region significantly associated with PW on chromosome 6; however, the location was approximately at 26.9 Mbp.

Soluble solid concentration is one of the most important quality traits in peach, with consumers expecting an enhanced sugar content or sweetness perception for the low acid types (Cirilli et al., 2016). Therefore, SSC has been a target trait in several studies involving intra- and interspecific progenies and germplasm to access the genetic potential and consequently improve the sugar content in new cultivars. We detected QTNs associated with SSC on chromosome 1, 4, 5, and 6. The *qtnSSC_5.1* on chromosome 5 that explained the majority of the phenotypic variation was in agreement with the QTL interval reported by Hernández Mora et al. (2017) using a PBA analysis in European peach germplasm. In the same chromosome, we also identified *qtnSSC_5.2* (0.7 Mb) and *qtnSSC_5.3* (13.0 Mb) whose positions matched QTLs mapped in previous studies using different germplasm and approaches (Nuñez-Lillo et al., 2019; Abdelghafar et al., 2020; Rawandoozi et al., 2020b). Furthermore, *qtnSSC_4.1* on chromosome 4 (6.6 Mb) was close to the QTL (*qSSC.V-Ch4-2007a*) detected by Zeballos et al. (2016), while *qtnSSC_4.3* was near *MD* locus reported by Eduardo et al. (2011). On the other hand, the *qtnSSC_1.1* (chromosome 1: 17.5 Mb) and *qtnSSC_6.1* (chromosome 6: 21.2 Mbp) were located in a different region in comparison to the QTLs or associated markers previously detected on those chromosomes (Fresnedo-Ramírez et al., 2015; Cao et al., 2016; Hernández Mora et al., 2017; Li et al., 2019; Shi et al., 2020). Concerning the traits pH and TA, the *qtnTA_5.1* and *qtnpH_5.1* collocated with the major locus for low-acid fruit (D-locus) previously reported in peach (Boudehri et al., 2009).

Fruit Quality Hotspots in Peach Genome

Hotspot regions detected on chromosomes 1, 3, 4, 5, 6, and 8 controlled several fruit quality traits. The detection of hotspots in the genome indicates that genes related to certain traits are more densely concentrated in certain genomic regions (Zhang X. et al., 2019). The main hotspot on chromosome 4 (9.0–12.5 Mbp) included reliable QTNs for DAB, FW, RP, ADH, RD, FF, and SSC detected in different seasons and/or approaches and represents a target region for future breeding studies in peach. A QTL hotspot associated with quality traits was previously reported in peach on chromosome 4 (Cantín et al., 2010; Eduardo et al., 2011). However, the study was performed using SSR markers and the QTLs were detected in low-density linkage maps. Using high-density SNP maps, Rawandoozi et al. (2020a) reported QTLs for DAB and RD within the genetic region detected. Likewise, Hernández Mora et al. (2017) detected a hotspot for blush, SSC, RD and DAB in a wider genetic interval located at 11.2–14.1 Mbp in European germplasm. Moreover, Desnoues et al. (2016) identified a QTL hotspot in the same chromosome related to individual sugars and FW, although in a different location. In addition, the hotspot on chromosome 5 (0.3 to 3.7 Mbp) matched with the QTL hotspot for SSC and TA reported by Hernández Mora et al. (2017). Therefore, this study reinforces the importance of breeding programs targeting the improvement of fruit quality traits in peach focusing on the chromosome 4 and also demonstrated the necessity to promote further studies for the hotspot regions in chromosome 1, 3, 5, 6, and 8.

Candidate Genes

Candidate genes (566) were identified within the haploblock regions encompassing the QTNs detected using the mrMLM 4.0 and FarmCPU, and the GO enrichment approach narrowed down the initial CG list (222) and revealed over-representation of certain GO terms (68). RNA binding proteins and serine-type endopeptidase inhibitor-related genes were identified, and previous studies revealed involvement in the regulation of flowering time (Steffen et al., 2019; Zhang F. et al., 2019). In addition, genes functionally annotated as 2-oxoglutarate-dependent dioxygenase, drug transmembrane transport, antiporter activity, pyridine nucleotide biosynthetic process, and chromatin assembly or disassembly were associated with fruit ripening in tomato, apricot, grape, peach, apple, and strawberry (Hanana et al., 2007; Farinati et al., 2017; Decros et al., 2019; Ding et al., 2020; García-Gómez et al., 2020). Furthermore, previous studies have shown that molybdopterin cofactor plays an important role in the metabolic control of avocado fruit growth and final fruit size (Cowan et al., 2001) and ion/H+ exchanger genes (GO: ion transmembrane transport) were critical for providing pH regulation (Pittman, 2012). Lastly, among the CG, *Prupe.4G262200* and *Prupe.4G261900* coding for endopolygalacturonases (GO: polygalacturonase activity) were previously involved in the inheritance of fruit texture and flesh adherence to the stone in peach (Peace et al., 2005; Gu et al., 2016).

Several CGs detected in our study have already been reported for productivity and fruit-related traits in peach. *Prupe.1G531600* (DAM5), *Prupe.1G531700* (DAM6), *Prupe.1G531500*, *Prupe.1G549600*, *Prupe.1G548000*, *Prupe.1G554100* were considered potential CG for bloom date in peach (Rawandoozi et al., 2020a). These genes are located within the hotspot region detected on chromosome 1 associated with BD and FF. Similarly, *Prupe.3G163100* (18.2 Mbp) located in the genetic interval of the hotspot on chromosome 3 was previously associated with blush and RP (redness around the stone) in peach (Frett et al., 2014; Zhang et al., 2018b; Guo et al., 2020). The main hotspot on chromosome 4 (9.0–12.5 Mbp) collocates with: *Prupe.4G186800*, the major locus controlling fruit ripening (Pirona et al., 2013) and CG for fruit flesh softening rate (Carrasco-Valenzuela et al., 2019); *Prupe.4G179900,* CG for RD and DAB (Elsadr et al., 2019); and *Prupe.4G185800* and *Prupe.4G187100* involved in anthocyanin biosynthesis and CGs for blush (Rawandoozi et al., 2020b). In addition, *Prupe_5G008400*, a CG controlling fruit acidity, is located within the hotspot (0.3–3.7 Mbp) on chromosome 5 (Wang et al., 2020).

CONCLUSION

We successfully performed a multi-locus GWAS using mrMLM 4.0 and FarmCPU in 620 individuals from three public fresh market peach breeding programs. A total of 88 reliable QTNs were consistently detected in at least two seasons and/or in

different methods. Hotspots for quality traits were identified on chromosomes 1, 3, 4, 5, 6, and 8. Candidate genes for quality traits were identified in the vicinity of the reliable QTNs detected using mrMLM 4.0 and FarmCPU. Furthermore, we observed that the position of the previously reported candidate genes for fruit-related traits (BD, Blush, DAB, ADH, RP, pH, and TA) matched with the position of the hotspots detected on chromosomes 1, 3, 4, and 5. Therefore, the information reported in this study supports the development of DNA tools for MAS in peach. Moreover, the importance of chromosome 4 hotspot in breeding for improvement of fruit quality is reinforced, and also emphasized the necessity to further study the hotspot regions on chromosomes 1, 3, 5, 6, and 8.

DATA AVAILABILITY STATEMENT

The datasets presented in this study can be found in online repositories. The names of the repository/repositories and accession number(s) can be found below: www.rosaceae.org, tfGDR1048/b.

AUTHOR CONTRIBUTIONS

CS: formal analysis and writing – original draft. LC: SNP data curation and review. WF: candidate genes analysis. MW, JC, and DB: resources and writing – review & editing. ZR: phenotypic analysis and review. KG: conceptualization, funding acquisition, resources, supervision, and writing – review & editing. All authors have read and approved the final manuscript.

FUNDING

This work was funded by USDA's National Institute of Food and Agriculture-Specialty Crop Research Initiative Projects, "RosBREED: Enabling marker-assisted breeding in Rosaceae" (2009-51181-05858) and "RosBREED: Combining disease resistance and horticultural quality in new rosaceous cultivars" (2014-51181-22378).

ACKNOWLEDGMENTS

The authors would like to thank Terrence Frett, Ralph Burrell, and Musser Fruit Research Farm staff at Clemson University; Natalie Anderson, Pamela Hornby, Tim Hartman, and Silvia Carpendo at Texas A&M University; and Paul Sandefur at University of Arkansas and Arkansas System Division of Agriculture Fruit Research Station staff for their help with orchard maintenance and phenotypic data acquisition.

SUPPLEMENTARY MATERIAL

The Supplementary Material for this article can be found online at: https://www.frontiersin.org/articles/10.3389/fpls.2021.644799/full#supplementary-material

REFERENCES

Abdelghafar, A., da Silva Linge, C., Okie, W. R., and Gasic, K. (2020). Mapping Qtls for phytochemical compounds and fruit quality in peach. *Mol.* Breed. 40: 32. doi: 10.1007/s11032-020-01114-y

Abidi, W., Jiménez, S., Moreno, M. Á, and Gogorcena, Y. (2011). Evaluation of antioxidant compounds and total sugar content in a nectarine [*Prunus persica* (L.) Batsch] progeny. *Int. J. Mol. Sci.* 12, 6919–6935. doi: 10.3390/ijms12106919

Bielenberg, D. G., Rauh, B., Fan, S., Gasic, K., Abbott, A. G., Reighard, G. L., et al. (2015). Genotyping by sequencing for SNP-based linkage map construction and QTL analysis of chilling requirement and bloom date in peach [*Prunus persica* (L.) Batsch]. *PLoS One* 10:e0139406. doi: 10.1371/journal.pone.0139406

Boudehri, K., Belka, M. A., Cardinet, G., Capdeville, G., Renaud, C., Tauzin, Y., et al. (2009). Toward the isolation of the d gene controlling the acidity of peach fruit by positional cloning. *Acta Hortic.* 814, 507–510. doi: 10.17660/ActaHortic.2009.814.85

Brachi, B., Morris, G. P., and Borevitz, J. O. (2011). Genome-wide association studies in plants: the missing heritability is in the field. *Genome Biol.* 12:232. doi: 10.1186/gb-2011-12-10-232

Bradbury, P. J., Zhang, Z., Kroon, D. E., Casstevens, T. M., Ramdoss, Y., and Buckler, E. S. (2007). TASSEL: software for association mapping of complex traits in diverse samples. *Bioinformatics* 23, 2633–2635. doi: 10.1093/bioinformatics/btm308

Cantín, C. M., Crisosto, C. H., Ogundiwin, E. A., Gradziel, T., Torrents, J., Moreno, M. A., et al. (2010). Chilling injury susceptibility in an intra-specific peach [*Prunus persica* (L.) Batsch] progeny. *Postharvest Biol. Technol.* 58, 79–87. doi: 10.1016/j.postharvbio.2010.06.002

Cao, K., Li, Y., Deng, C. H., Gardiner, S. E., Zhu, G., Fang, W., et al. (2019). Comparative population genomics identified genomic regions and candidate genes associated with fruit domestication traits in peach. *Plant Biotechnol. J.* 17, 1954–1970. doi: 10.1111/pbi.13112

Cao, K., Zhou, Z., Wang, Q., Guo, J., Zhao, P., Zhu, G., et al. (2016). Genome-wide association study of 12 agronomic traits in peach. *Nat. Commun.* 7:13246. doi: 10.1038/ncomms13246

Carrasco-Valenzuela, T., Muñoz-Espinoza, C., Riveros, A., Pedreschi, R., Arús, P., Campos-Vargas, R., et al. (2019). Expression QTL (eQTLs) analyses aeveal candidate genes associated with fruit flesh softening rate in peach [*Prunus persica* (L.) Batsch]. *Front. Plant Sci.* 10:1581. doi: 10.3389/fpls.2019.01581

Chang, C. C., Chow, C. C., Tellier, L. C., Vattikuti, S., Purcell, S. M., and Lee, J. J. (2015). Second-generation PLINK: rising to the challenge of larger and richer datasets. *GigaScience* 4:7. doi: 10.1186/s13742-015-0047-8

Ciacciulli, A., Cirilli, M., Chiozzotto, R., Attanasio, G., da Silva Linge, C., Pacheco, I., et al. (2018). Linkage and association mapping for the slow softening (SwS) trait in peach (*P. persica* L. Batsch) fruit. *Tree Genet. Genom.* 14, 1–10. doi: 10.1007/s11295-018-1305-6

Cirilli, M., Bassi, D., and Ciacciulli, A. (2016). Sugars in peach fruit: a breeding perspective. *Hortic. Res.* 3:15067. doi: 10.1038/hortres.2015.67

Covarrubias-Pazaran, G. (2016). Genome-assisted prediction of quantitative traits using the r package sommer. *PLoS One* 11:e0156744. doi: 10.1371/journal.pone.0156744

Cowan, A. K., Cripps, R. F., Richings, E. W., and Taylor, N. J. (2001). Fruit size: towards an understanding of the metabolic control of fruit growth using avocado as a model system. *Physiol. Plant.* 111, 127–136. doi: 10.1034/j.1399-3054.2001.1110201.x

da Silva Linge, C., Antanaviciute, L., Abdelghafar, A., Arús, P., Bassi, D., Rossini, L., et al. (2018). High-density multi-population consensus genetic linkage map for peach. *PLoS One* 13:e0207724. doi: 10.1371/journal.pone.0207724

da Silva Linge, C., Bassi, D., Bianco, L., Pacheco, I., Pirona, R., and Rossini, L. (2015). Genetic dissection of fruit weight and size in an F2 peach (*Prunus persica* (L.) Batsch) progeny. *Mol. Breed.* 35:271. doi: 10.1007/s11032-015-0271-z

Decros, G., Beauvoit, B., Colombié, S., Cabasson, C., Bernillon, S., Arrivault, S., et al. (2019). Regulation of pyridine nucleotide metabolism during tomato fruit development through transcript and protein profiling. *Front. Plant Sci.* 10:1201. doi: 10.3389/fpls.2019.01201

Desnoues, E., Baldazzi, V., Génard, M., Mauroux, J.-B., Lambert, P., Confolent, C., et al. (2016). Dynamic QTLs for sugars and enzyme activities provide an overview of genetic control of sugar metabolism during peach fruit development. *J. Exp. Bot.* 67, 3419–3431. doi: 10.1093/jxb/erw169

Ding, Q., Wang, F., Xue, J., Yang, X., Fan, J., Chen, H., et al. (2020). Identification and expression analysis of hormone biosynthetic and metabolism genes in the 2OGD family for identifying genes that may be involved in tomato fruit ripening. *Int. J. Mol. Sci.* 21:5344. doi: 10.3390/ijms21155344

Donoso, J. M., Picañol, R., Serra, O., Howad, W., Alegre, S., Arús, P., et al. (2016). Exploring almond genetic variability useful for peach improvement: mapping major genes and QTLs in two interspecific almond × peach populations. *Mol. Breed.* 36:16. doi: 10.1007/s11032-016-0441-7

Eduardo, I., Pacheco, I., Chietera, G., Bassi, D., Pozzi, C., Vecchietti, A., et al. (2011). QTL analysis of fruit quality traits in two peach intraspecific populations and importance of maturity date pleiotropic effect. *Tree Genet. Genom.* 7, 323–335. doi: 10.1007/s11295-010-0334-6

Eduardo, I., Picañol, R., Rojas, E., Batlle, I., Howad, W., Aranzana, M. J., et al. (2015). Mapping of a major gene for the slow ripening character in peach: co-location with the maturity date gene and development of a candidate gene-based diagnostic marker for its selection. *Euphytica* 205, 627–636. doi: 10.1007/s10681-015-1445-9

Elsadr, H., Sherif, S., Banks, T., Somers, D., and Jayasankar, S. (2019). Refining the genomic region containing a major locus controlling fruit maturity in peach. *Sci. Rep.* 9:7522.

Fan, S., Bielenberg, D. G., Zhebentyayeva, T. N., Reighard, G. L., Okie, W. R., Holland, D., et al. (2010). Mapping quantitative trait loci associated with chilling requirement, heat requirement and bloom date in peach (*Prunus persica*). *N. Phytol.* 185, 917–930. doi: 10.1111/j.1469-8137.2009.03119.x

Farinati, S., Rasori, A., Varotto, S., and Bonghi, C. (2017). Rosaceae fruit development, ripening and post-harvest: an epigenetic perspective. *Front. Plant Sci.* 8:1247. doi: 10.3389/fpls.2017.01247

Font I Forcada, C., Guajardo, V., Chin-Wo, S. R., and Moreno, M. Á (2019). Association mapping analysis for fruit quality traits in *Prunus persica* using SNP markers. *Front. Plant Sci.* 9:2005. doi: 10.3389/fpls.2018.02005

Food and Agricultural Organization of the United Nations (FAOSTAT) (2018). *Food Balance Sheets [Online]*Food and Agricultural Organization of the United Nations (FAOSTAT), 2018. Available online at: http://www.fao.org/faostat/en/#data/FBS (accessed November, 2020).

Fresnedo-Ramírez, J., Bink, M. C. A. M., van de Weg, E., Famula, T. R., Crisosto, C. H., Frett, T. J., et al. (2015). QTL mapping of pomological traits in peach and related species breeding germplasm. *Mol. Breed.* 35:166. doi: 10.1007/s11032-015-0357-7

Fresnedo-Ramírez, J., Frett, T. J., Sandefur, P. J., Salgado-Rojas, A., Clark, J. R., Gasic, K., et al. (2016). QTL mapping and breeding value estimation through pedigree-based analysis of fruit size and weight in four diverse peach breeding programs. *Tree Genet. Genom.* 12, 25. doi: 10.1007/s11295-016-0985-z

Frett, T. J., Reighard, G. L., Okie, W. R., and Gasic, K. (2014). Mapping quantitative trait loci associated with blush in peach [*Prunus persica* (L.) Batsch]. *Tree Genet. Genom.* 10, 367–381. doi: 10.1007/s11295-013-0692-y

García-Gómez, B. E., Ruiz, D., Salazar, J. A., Rubio, M., Martínez-García, P. J., and Martínez-Gómez, P. (2020). Analysis of metabolites and gene expression changes relative to apricot (*Prunus armeniaca* L.) fruit quality during development and ripening. *Front. Plant Sci.* 11:1269. doi: 10.3389/fpls.2020.01269

Gogorcena, Y., Sánchez, G., Moreno-Vázquez, S., Pérez, S., and Ksouri, N. (2020). "Genomic-based breeding for climate-smart peach varieties," in *Genomic Designing of Climate-Smart Fruit Crops*, ed. C. Kole (Cham: Springer International Publishing), 271–331.

Gu, C., Wang, L., Wang, W., Zhou, H., Ma, B., Zheng, H., et al. (2016). Copy number variation of a gene cluster encoding endopolygalacturonase mediates flesh texture and stone adhesion in peach. *J. Exp. Bot.* 67, 1993–2005. doi: 10.1093/jxb/erw021

Guo, J., Cao, K., Deng, C., Li, Y., Zhu, G., Fang, W., et al. (2020). An integrated peach genome structural variation map uncovers genes associated with fruit traits. *Genome Biol.* 21:258. doi: 10.1186/s13059-020-02169-y

Hammer, O., Harper, D., and Ryan, P. (2001). PAST: paleontological statistics software package for education and data analysis. *Palaeontol. Electron.* 4, 1–9.

Hanana, M., Cagnac, O., Yamaguchi, T., Hamdi, S., Ghorbel, A., and Blumwald, E. (2007). A grape berry (*Vitis vinifera* L.) cation/proton antiporter is associated with berry ripening. *Plant Cell Physiol.* 48, 804–811. doi: 10.1093/pcp/pcm048

Hernández Mora, J. R., Micheletti, D., Bink, M., Van de Weg, E., Cantín, C., Nazzicari, N., et al. (2017). Integrated QTL detection for key breeding traits in multiple peach progenies. *BMC Genom.* 18:404. doi: 10.1186/s12864-017-3783-6

Huang, M., Liu, X., Zhou, Y., Summers, R. M., and Zhang, Z. (2018). BLINK: a package for the next level of genome-wide association studies with both individuals and markers in the millions. *GigaScience* 8:giy154. doi: 10.1093/gigascience/giy154

Iezzoni, A., Weebadde, C., Luby, J., Chengyan, Y., van de Weg, E., Fazio, G., et al. (2010). RosBREED: enabling marker-assisted breeding in rosaceae. *Acta Hortic.* 859, 389–394.

Iezzoni, A. F., McFerson, J., Luby, J., Gasic, K., Whitaker, V., Bassil, N., et al. (2020). RosBREED: bridging the chasm between discovery and application to enable DNA-informed breeding in rosaceous crops. *Horticult. Res.* 7:177. doi: 10.1038/s41438-020-00398-7

Jung, S., Lee, T., Cheng, C.-H., Buble, K., Zheng, P., Yu, J., et al. (2018). 15 years of GDR: Nnew data and functionality in the genome database for Rosaceae. *Nucleic Acids Res.* 47, D1137–D1145. doi: 10.1093/nar/gky1000

Lambert, P., Campoy, J. A., Pacheco, I., Mauroux, J.-B., da Silva Linge, C., Micheletti, D., et al. (2016). Identifying SNP markers tightly associated with six major genes in peach [*Prunus persica* (L.) Batsch] using a high-density SNP array with an objective of marker-assisted selection (MAS). *Tree Genet. Genom.* 12:121. doi: 10.1007/s11295-016-1080-1

Laurens, F., Aranzana, M. J., Arus, P., Bassi, D., Bink, M., Bonany, J., et al. (2018). An integrated approach for increasing breeding efficiency in apple and peach in Europe. *Horticult. Res.* 5:11. doi: 10.1038/s41438-018-0016-3

Li, Y., Cao, K., Zhu, G., Fang, W., Chen, C., Wang, X., et al. (2019). Genomic analyses of an extensive collection of wild and cultivated accessions provide new insights into peach breeding history. *Genome Biol.* 20:36. doi: 10.1186/s13059-019-1648-9

Ligges, U., and Mächler, M. (2002). *Scatterplot 3d – an R Package for Visualizing Multivariate Data*. Available online at: http://hdl.handle.net/10419/77160

Lipka, A. E., Tian, F., Wang, Q., Peiffer, J., Li, M., Bradbury, P. J., et al. (2012). GAPIT: genome association and prediction integrated tool. *Bioinformatics* 28, 2397–2399. doi: 10.1093/bioinformatics/bts444

Liu, X., Huang, M., Fan, B., Buckler, E. S., and Zhang, Z. (2016). Iterative usage of fixed and random effect models for powerful and efficient genome-wide association studies. *PLoS Genet.* 12:e1005767. doi: 10.1371/journal.pgen.1005767

Martínez-García, P. J., Parfitt, D. E., Ogundiwin, E. A., Fass, J., Chan, H. M., Ahmad, R., et al. (2013). High density SNP mapping and QTL analysis for fruit quality characteristics in peach (*Prunus persica* L.). *Tree Genet. Genom.* 9, 19–36. doi: 10.1007/s11295-012-0522-7

Meneses, C., and Orellana, A. (2013). Using genomics to improve fruit quality. *Biol. Res.* 46, 347–352.

Micheletti, D., Dettori, M. T., Micali, S., Aramini, V., Pacheco, I., da Silva Linge, C., et al. (2015). Whole-genome analysis of diversity and SNP-major gene association in peach germplasm. *PLoS One* 10:e0136803. doi: 10.1371/journal.pone.0136803

Minas, I. S., Tanou, G., and Molassiotis, A. (2018). Environmental and orchard bases of peach fruit quality. *Sci. Horticult.* 235, 307–322. doi: 10.1016/j.scienta.2018.01.028

Nuñez-Lillo, G., Balladares, C., Pavez, C., Urra, C., Sanhueza, D., Vendramin, E., et al. (2019). High-density genetic map and QTL analysis of soluble solid content, maturity date, and mealiness in peach using genotyping by sequencing. *Sci. Horticult.* 257:108734. doi: 10.1016/j.scienta.2019.108734

Nuñez-Lillo, G., Cifuentes-Esquivel, A., Troggio, M., Micheletti, D., Infante, R., Campos-Vargas, R., et al. (2015). Identification of candidate genes associated

with mealiness and maturity date in peach [*Prunus persica* (L.) Batsch] using QTL analysis and deep sequencing. *Tree Genet. Genomes* 11:86. doi: 10.1007/s11295-015-0911-9

Olmstead, M. A., Gilbert, J., Colquhoun, T., Clark, D. G., and Sims, C. (2015). In pursuit of the perfect peach: Consumer-assisted selection of peach fruit traits. *HortScience* 50, 1202–1212.

Peace, C. P., Crisosto, C. H., and Gradziel, T. M. (2005). Endopolygalacturonase: a candidate gene for freestone and melting fleshin peach. *Mol. Breed.* 16, 21–31. doi: 10.1007/s11032-005-0828-3

Peace, C. P., Luby, J. J., van de Weg, W. E., Bink, M. C. A. M., and Iezzoni, A. F. (2014). A strategy for developing representative germplasm sets for systematic QTL validation, demonstrated for apple, peach, and sweet cherry. *Tree Genet. Genom.* 10, 1679–1694. doi: 10.1007/s11295-014-0788-z

Peakall, R., and Smouse, P. E. (2012). GenAlEx 6.5: genetic analysis in Excel. Population genetic software for teaching and research–an update. *Bioinformatics* 28, 2537–2539. doi: 10.1093/bioinformatics/bts460

Pirona, R., Eduardo, I., Pacheco, I., da Silva Linge, C., Miculan, M., Verde, I., et al. (2013). Fine mapping and identification of a candidate gene for a major locus controlling maturity date in peach. *BMC Plant Biol.* 13:166. doi: 10.1186/1471-2229-13-166

Pittman, J. (2012). Multiple transport pathways for mediating intracellular pH homeostasis: the contribution of H+/ion exchangers. *Front. Plant Sci.* 3:11. doi: 10.3389/fpls.2012.00011

Quilot, B., Wu, B. H., Kervella, J., Génard, M., Foulongne, M., and Moreau, K. (2004). QTL analysis of quality traits in an advanced backcross between Prunus persica cultivars and the wild relative species *P. davidiana*. *Theor. Appl. Genet.* 109, 884–897. doi: 10.1007/s00122-004-1703-z

Raj, A., Stephens, M., and Pritchard, J. K. (2014). fastSTRUCTURE: variational inference of population structure in large SNP data sets. *Genetics* 197, 573–589. doi: 10.1534/genetics.114.164350

Rawandoozi, Z. J., Hartmann, T. P., Carpenedo, S., Gasic, K., da Silva Linge, C., Cai, L., et al. (2020a). Mapping and characterization qtls for phenological traits in seven pedigree-connected peach families. *Res. Square* [preprint]. doi: 10.21203/rs.3.rs-75550/v1

Rawandoozi, Z. J., Hartmann, T. P., Carpenedo, S., Gasic, K., da Silva Linge, C., Cai, L., et al. (2020b). Identification and characterization of QTLs for fruit quality traits in peach through a multi-family approach. *BMC Genom.* 21:522. doi: 10.1186/s12864-020-06927-x

Ren, W.-L., Wen, Y.-J., Dunwell, J. M., and Zhang, Y.-M. (2018). pKWmEB: integration of Kruskal-Wallis test with empirical Bayes under polygenic background control for multi-locus genome-wide association study. *Heredity* 120, 208–218. doi: 10.1038/s41437-017-0007-4

Romeu, J. F., Monforte, A. J., Sánchez, G., Granell, A., García-Brunton, J., Badenes, M. L., et al. (2014). Quantitative trait loci affecting reproductive phenology in peach. *BMC Plant Biol.* 14:52. doi: 10.1186/1471-2229-14-52

Rosenberg, N. A. (2004). distruct: a program for the graphical display of population structure. *Mol. Ecol. Notes* 4, 137–138. doi: 10.1046/j.1471-8286.2003.00566.x

Serra, O., Giné-Bordonaba, J., Eduardo, I., Bonany, J., Echeverria, G., Larrigaudière, C., et al. (2017). Genetic analysis of the slow-melting flesh character in peach. *Tree Genet. Genom.* 13:77. doi: 10.1007/s11295-017-1160-x

Shi, P., Xu, Z., Zhang, S., Wang, X., Ma, X., Zheng, J., et al. (2020). Construction of a high-density SNP-based genetic map and identification of fruit-related QTLs and candidate genes in peach [*Prunus persica* (L.) Batsch]. *BMC Plant Biol.* 20:438. doi: 10.1186/s12870-020-02557-3

Steffen, A., Elgner, M., and Staiger, D. (2019). Regulation of flowering time by the RNA-binding proteins AtGRP7 and AtGRP8. *Plant Cell Physiol.* 60, 2040–2050. doi: 10.1093/pcp/pcz124

Supek, F., Bošnjak, M., Škunca, N., and Šmuc, T. (2011). REVIGO summarizes and visualizes long lists of gene ontology terms. *PLoS One* 6:e21800. doi: 10.1371/journal.pone.0021800

Tamba, C. L., Ni, Y.-L., and Zhang, Y.-M. (2017). Iterative sure independence screening EM-Bayesian LASSO algorithm for multi-locus genome-wide association studies. *PLoS Comput. Biol.* 13:e1005357. doi: 10.1371/journal.pcbi.1005357

Tamba, C. L., and Zhang, Y.-M. (2018). A fast mrMLM algorithm for multi-locus genome-wide association studies. *bioRxiv* [Preprint] doi: 10.1101/341784 bioRxiv:341784

Thurow, L. B., Gasic, K., Bassols Raseira, M. D. C., Bonow, S., and Marques Castro, C. (2019). Genome-wide SNP discovery through genotyping by sequencing, population structure, and linkage disequilibrium in Brazilian peach breeding germplasm. *Tree Genet. Genom.* 16:10. doi: 10.1007/s11295-019-1406-x

Vanderzande, S., Howard, N. P., Cai, L., da Silva Linge, C., Antanaviciute, L., Bink, M. C. A. M., et al. (2019). High-quality, genome-wide SNP genotypic data for pedigreed germplasm of the diploid outbreeding species apple, peach, and sweet cherry through a common workflow. *PLoS One* 14:e0210928. doi: 10.1371/journal.pone.0210928

Vendramin, E., Pea, G., Dondini, L., Pacheco, I., Dettori, M. T., Gazza, L., et al. (2014). A unique mutation in a MYB gene cosegregates with the nectarine phenotype in peach. *PLoS One* 9:e90574. doi: 10.1371/journal.pone.0090574

Verde, I., Abbott, A. G., Scalabrin, S., Jung, S., Shu, S., Marroni, F., et al. (2013). The high-quality draft genome of peach (*prunus persica*) identifies unique patterns of genetic diversity, domestication and genome evolution. *Nat. Genet.* 45, 487–494. doi: 10.1038/ng.2586

Verde, I., Bassil, N., Scalabrin, S., Gilmore, B., Lawley, C. T., Gasic, K., et al. (2012). Development and evaluation of a 9k SNP array for peach by internationally coordinated snp detection and validation in breeding germplasm. *PLoS One* 7:e35668. doi: 10.1371/journal.pone.0035668

Verde, I., Jenkins, J., Dondini, L., Micali, S., Pagliarani, G., Vendramin, E., et al. (2017). The peach v2.0 release: high-resolution linkage mapping and deep resequencing improve chromosome-scale assembly and contiguity. *BMC Genom.* 18:225. doi: 10.1186/s12864-017-3606-9

Wang, L., Jiang, X., Zhao, L., Wang, F., Liu, Y., Zhou, H., et al. (2020). A candidate PpRPH gene of the D locus controlling fruit acidity in peach. *Plant Mol. Biol.* 105, 1–12. doi: 10.1007/s11103-020-01089-6

Wang, S.-B., Feng, J.-Y., Ren, W.-L., Huang, B., Zhou, L., Wen, Y.-J., et al. (2016). Improving power and accuracy of genome-wide association studies via a multi-locus mixed linear model methodology. *Sci. Rep.* 6:19444. doi: 10.1038/srep19444

Wen, Y.-J., Zhang, H., Ni, Y.-L., Huang, B., Zhang, J., Feng, J.-Y., et al. (2017). Methodological implementation of mixed linear models in multi-locus genome-wide association studies. *Brief. Bioinform.* 19, 700–712. doi: 10.1093/bib/bbw145

Xu, Y., Yang, T., Zhou, Y., Yin, S., Li, P., Liu, J., et al. (2018). Genome-wide association mapping of starch pasting properties in maize using single-locus and multi-locus models. *Front. Plant Sci.* 9:1311. doi: 10.3389/fpls.2018.01311

Yamamoto, T., Shimada, T., Imai, T., Yaegaki, H., Haji, T., Matsuta, N., et al. (2001). Characterization of morphological traits based on a genetic linkage map in peach. *Breed. Sci.* 51, 271–278. doi: 10.1270/jsbbs.51.271

Young, M. D., Wakefield, M. J., Smyth, G. K., and Oshlack, A. (2010). Gene ontology analysis for RNA-seq: accounting for selection bias. *Genome Biol.* 11:R14. doi: 10.1186/gb-2010-11-2-r14

Yu, J., Pressoir, G., Briggs, W. H., Vroh Bi, I., Yamasaki, M., Doebley, J. F., et al. (2006). A unified mixed-model method for association mapping that accounts for multiple levels of relatedness. *Nat. Genet.* 38, 203–208. doi: 10.1038/ng1702

Yue, C., Gallardo, K. R., Luby, J. J., Rihn, A. L., McFerson, J. R., McCracken, V., et al. (2014). An evaluation of U.S. peach producers' trait prioritization: evidence from audience surveys. *HortSci. Horts* 49, 1309–1314. doi: 10.21273/HORTSCI.49.10.1309

Zeballos, J. L., Abidi, W., Giménez, R., Monforte, A. J., Moreno, M. Á, and Gogorcena, Y. (2016). Mapping QTLs associated with fruit quality traits in peach [*Prunus persica* (L.) Batsch] using SNP maps. *Tree Genet. Genom.* 12:37. doi: 10.1007/s11295-016-0996-9

Zhang, C., Dong, S.-S., Xu, J.-Y., He, W.-M., and Yang, T.-L. (2018a). PopLDdecay: a fast and effective tool for linkage disequilibrium decay analysis based on variant call format files. *Bioinformatics* 35, 1786–1788. doi: 10.1093/bioinformatics/bty875

Zhang, C., Ma, R., Xu, J., Yan, J., Guo, L., Song, J., et al. (2018b). Genome-wide identification and classification of MYB superfamily genes in peach. *PLoS One* 13:e0199192. doi: 10.1371/journal.pone.0199192

Zhang, F., Liu, X., Zhang, A., Jiang, Z., Chen, L., and Zhang, X. (2019). Genome-wide dynamic network analysis reveals a critical transition state of flower development in Arabidopsis. *BMC Plant Biol.* 19:11. doi: 10.1186/s12870-018-1589-6

Zhang, J., Feng, J. Y., Ni, Y. L., Wen, Y. J., Niu, Y., Tamba, C. L., et al. (2017). pLARmEB: integration of least angle regression with empirical Bayes for multilocus genome-wide association studies. *Heredity* 118, 517–524. doi: 10.1038/hdy.2017.8

Zhang, X., Hina, A., Song, S., Kong, J., Bhat, J. A., and Zhao, T. (2019). Whole-genome mapping identified novel "QTL hotspots regions" for seed storability in soybean (*Glycine max* L.). *BMC Genom.* 20:499. doi: 10.1186/s12864-019-5897-5

Zhang, Y.-W., Tamba, C. L., Wen, Y.-J., Li, P., Ren, W.-L., Ni, Y.-L., et al. (2020). mrMLM v4.0: an R platform for multi-locus genome-wide association studies. *Genom. Proteom. Bioinform.* 18. doi: 10.1016/j.gpb.2020.06.006

Zhu, C., Gore, M., Buckler, E. S., and Yu, J. (2008). Status and prospects of association mapping in plants. *Plant Genome* 1, 5–20. doi: 10.3835/plantgenome2008.02.0089

Conflict of Interest: The authors declare that the research was conducted in the absence of any commercial or financial relationships that could be construed as a potential conflict of interest.

frontiers in Plant Science

REVIEW
published: 01 April 2021
doi: 10.3389/fpls.2021.644881

An Atlas of Genomic Resources for Studying Rosaceae Fruits and Ornamentals

*Muzi Li, Yuwei Xiao, Steve Mount and Zhongchi Liu**

Department of Cell Biology and Molecular Genetics, University of Maryland, College Park, MD, United States

Rosaceae, a large plant family of more than 3,000 species, consists of many economically important fruit and ornamental crops, including peach, apple, strawberry, raspberry, cherry, and rose. These horticultural crops are not only important economic drivers in many regions of the world, but also major sources of human nutrition. Additionally, due to the diversity of fruit types in Rosaceae, this plant family offers excellent opportunities for investigations into fleshy fruit diversity, evolution, and development. With the development of high-throughput sequencing technologies and computational tools, an increasing number of high-quality genomes and transcriptomes of Rosaceae species have become available and will greatly facilitate Rosaceae research and breeding. This review summarizes major genomic resources and genome research progress in Rosaceae, highlights important databases, and suggests areas for further improvement. The availability of these big data resources will greatly accelerate research progress and enhance the agricultural productivity of Rosaceae.

Keywords: Rosaceae fruits, Rosaceae ornamentals, genome assembly, genome annotation, databases, domestication, origin of species

OPEN ACCESS

Edited by:
Raju Datla, Global Institute for Food Security (GIFS), Canada

Reviewed by:
Aikaterini Symeonidi, Technical University of Munich, Germany
Janet Slovin, USDA/ARS Genetic Improvement of Fruits and Vegetables Laboratory, United States

****Correspondence:***
Zhongchi Liu
zliu@umd.edu

Specialty section:
This article was submitted to Plant Development and EvoDevo, a section of the journal Frontiers in Plant Science

Received: *22 December 2020*
Accepted: *22 February 2021*
Published: *01 April 2021*

Citation:
Li M, Xiao Y, Mount S and Liu Z (2021) An Atlas of Genomic Resources for Studying Rosaceae Fruits and Ornamentals. Front. Plant Sci. 12:644881. doi: 10.3389/fpls.2021.644881

INTRODUCTION

Rosaceae is a large angiosperm family consisting of three subfamilies—Rosoideae, Amygdaloideae, and Dryadoideae—and ∼3,000 species (Xiang et al., 2017). The Rosaceae family of plants is diverse in architecture, including herbs, shrubs, and trees, and has a large number of hybrids and ploidy levels. Most importantly, Rosaceae fruits and ornamentals, such as apple, pear, peach, plum, cherry, almond, strawberry, raspberry, flowering cherry, and rose, are of tremendous economic and agronomic value. Rosaceae fruits are also surprisingly diverse in morphology and fruit type, including fleshy pome, drupe, and achenetum as well as dry fruits (Xiang et al., 2017; Liu Z. et al., 2020). Therefore, the Rosaceae family is also an ideal family for investigations of fruit diversity, domestication, and evolution.

Second- and third-generation sequencing technologies have allowed genome sequencing and genome-wide analyses to revolutionize plant research. The increasing number of sequenced plant genomes and higher quality genomes make molecular research, genome editing, and marker-assisted breeding possible in species previously recalcitrant to molecular genetic research. Further, the establishment of various online databases provides easy access and interaction with the genomic data. These databases help organize genomic resources, facilitate data sharing, and enable genome comparison across different species. In this review, we summarize the latest genome assemblies and annotations of major Rosaceae species, giving examples of findings enabled by genome sequencing. In addition, we present databases useful for the study of Rosaceae species.

GENOME SEQUENCING AND ASSEMBLIES OF ROSACEAE SPECIES

Since 2016, there has been a rapid increase in the number of new Rosaceae genomes, from three new genomes in 2016 to 16 new genomes in 2020 (**Figure 1**). This trend will likely accelerate as research groups are moving into pan-genome sequencing. **Figure 2** shows the nuclear phylogeny of Rosaceae and illustrates genera with different fruit types. **Table 1** summarizes the status of genome sequencing in a selective number of economically important Rosaceae lineages. A more comprehensive summary of Rosaceae genomes and transcriptomes is provided in **Supplementary Table 1**, in which a total of 72 Rosaceae genomes or transcriptome assemblies are included. In addition, **Supplementary Table 1** provides specific information on species name, variety name, ploidy level, and genome assembly as well as annotation versions, references, available websites, associated transcriptomes, and accession numbers for accessing these resources. In the following sections, we discuss and highlight some of the important Rosaceae genome studies.

Ornamentals

Two high-quality genomes of Chinese rose (*Rosa chinensis* cv. "Old Blush") were generated from double haploid or homozygous lines (Hibrand Saint-Oyant et al., 2018; Raymond et al., 2018). The genome assembly by Raymond et al. (2018) consists of 82 contigs with an N50-value of 24 Mb, 36,377 protein-coding genes, and 3,971 long non-coding RNAs (lncRNAs), and the genome by Hibrand Saint-Oyant et al. (2018) is composed of 564 contigs (N50: 3.4 Mb), 39,669 predicted protein-coding genes, and 4,812 non-coding genes. The rose genomes show extensive synteny with the genome of diploid strawberry *Fragaria vesca* and provide valuable resources for identifying the molecular basis of key ornamental traits. For example, the "double flower" rose is more attractive due to large numbers of petals. Taking advantage of the sequenced genome, a GWAS study was conducted with 96 cultivated roses, which led to the identification of a transposon insertion in the intron of an *APETALA2(AP2)/TOE* homolog (Hibrand Saint-Oyant et al., 2018). Hence, the mis-regulated *AP2/TOE* appears to have resulted in reduced expression of *AGAMOUS*, leading to the double-flower phenotype.

Another worldwide ornamental tree is the flowering cherry native to Korea, Japan, and China. Due to a long history of cultivation, hybridization, and selection, there is confusion concerning the names and origins of many varieties. For example, the relationship between the King cherry (*Prunus yedoensis* var. *nudiflora*), a Korean cherry tree originating on Jeju Island, and the Yoshino cherry (*Prunus x yedoensis*), a popular hybrid cherry tree enjoyed in Japan and other regions of the world (**Figures 3A,B**), was unknown. A draft genome of King cherry was constructed, and genome-wide variome analysis using the King cherry assembly as a reference revealed that the King and Yoshino cherry trees can be clearly distinguished genetically (Baek et al., 2018).

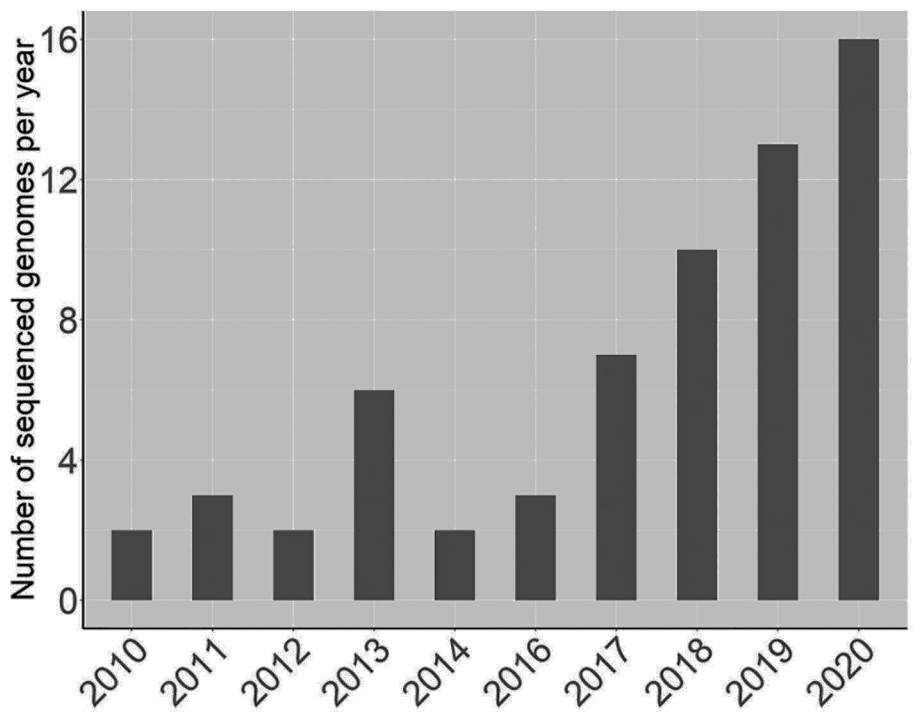

FIGURE 1 | A graph showing the number of newly sequenced Rosaceae genomes per year.

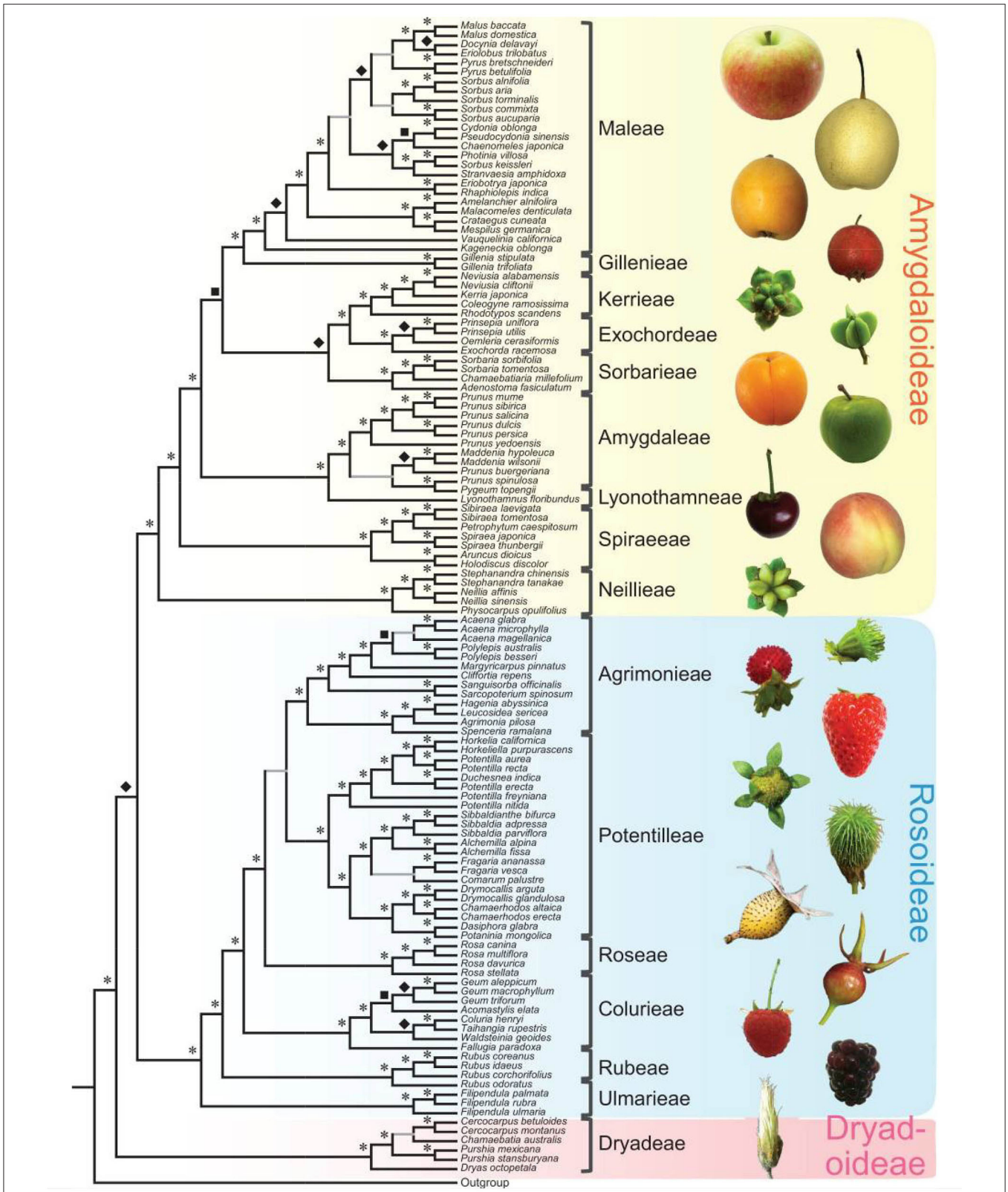

FIGURE 2 | Rosaceae phylogeny and Rosaceae fruit types. At left is the nuclear phylogeny established in Xiang et al. (2017). Asterisks, diamonds, and squares indicate 100, 90, and 80 supports, respectively. Plant photographs on the right show the diversity of Rosaceae fruits. The figure is from Xiang et al. (2017) under the terms of Creative Commons Attribution License (CC BY 4.0).

TABLE 1 | List of selective Rosaceae species and corresponding genome resources.

Species	Ploidy	Common name	Variety	Access genome at	Species website	Reference
Malus domestica	$2n = 2x = 34$	Apple	Golden Delicious doubled haploid (GDDH13)	GDR and NCBI Genome	https://iris.angers.inra.fr/gddh13/	Daccord et al., 2017
Malus domestica	$2n = 2x = 34$	Apple	Hanfu anther-derived homozygous line HFTH1	GDR and NCBI Genome		Zhang et al., 2019
Pyrus bretschneideri	$2n = 2x = 34$	Chinese white pear	.	GDR	http://genedenovoweb.ticp.net:81/pear/	Xue et al., 2018
Pyrus communis	$2n = 2x = 34$	European pear	Bartlett doubled haploid	GDR		Linsmith et al., 2019
Pyrus ussuriensis x *communis*	$2n = 2x = 34$	Harbin x European pear	Zhongai 1	GDR and NCBI Genome		Ou et al., 2019
Prunus armeniaca	$2n = 2x = 16$	Apricot	Chuanzhihong	GDR		Jiang et al., 2019
Prunus armeniaca	$2n = 2x = 16$	Apricot	Rojo Pasion	NCBI Genome		Campoy et al., 2020
Prunus avium	$2n = 2x = 16$	Sweet cherry	Satonishiki	GDR and NCBI Genome	http://cherry.kazusa.or.jp/	Shirasawa et al., 2017
Prunus avium	$2n = 2x = 16$	Sweet cherry	Big Star	NCBI Genome		Pinosio et al., 2020
Prunus avium	$2n = 2x = 16$	Sweet cherry	Tieton	NCBI Genome		Wang et al., 2020a
Prunus avium	$2n = 2x = 16$	Sweet cherry	Tieton	GDR and NCBI Genome		Wang et al., 2020b
Prunus dulcis	$2n = 2x = 16$	Almond	Lauranne	GDR and NCBI Genome		Sánchez-Pérez et al., 2019
Prunus dulcis	$2n = 2x = 16$	Almond	Texas	GDR and NCBI Genome		Alioto et al., 2020
Prunus mume	$2n = 2x = 16$	Japanese apricot	.	NCBI Genome		Zhang et al., 2012
Prunus persica	$2n = 2x = 16$	Peach	Lovell doubled haploid	GDR and NCBI Genome	http://services.appliedgenomics.org/projects/prunus_persica_v2/prunus_persica_v2/intro/index.html	Verde et al., 2017
Prunus salicina	$2n = 2x = 16$	Japanese plum	Sanyueli	GDR and NCBI Genome		Liu C. et al., 2020
Prunus yedoensis var. *nudiflora*	$2n = 2x = 16$	King cherry	.	GDR and NCBI Genome		Baek et al., 2018
Prunus yedoensis	$2n = 2x = 16$	Yoshino cherry	Somei-Yoshino	GDR and NCBI Genome	http://cherry.kazusa.or.jp/	Shirasawa et al., 2019
Fragaria x *ananassa*	$2n = 8x = 56$	Garden strawberry	Reikou	GDR and NCBI Genome	http://strawberry-garden.kazusa.or.jp	Hirakawa et al., 2014
Fragaria x *ananassa*	$2n = 8x = 56$	Garden strawberry	Camarosa	GDR		Edger et al., 2019
Fragaria iinumae	$2n = 2x = 14$	.	.	GDR and NCBI Genome	http://strawberry-garden.kazusa.or.jp	Hirakawa et al., 2014
Fragaria iinumae	$2n = 2x = 14$	.	.	GDR and NCBI Genome		Edger et al., 2020
Fragaria vesca	$2n = 2x = 14$	Woodland strawberry	Hawaii 4	GDR		Edger et al., 2018
Fragaria viridis	$2n = 2x = 14$	.	.	GDR		Feng et al., 2021
Rosa chinensis	$2n = 2x = 14$	Chinese rose	Old Blush homozygous rose line	GDR and NCBI Genome	https://lipm-browsers.toulouse.inra.fr/pub/RchiOBHm-V2/	Raymond et al., 2018
Rosa chinensis	$2n = 2x = 14$	Chinese rose	Old Blush doubled haploid	GDR	https://iris.angers.inra.fr/obh/	Hibrand Saint-Oyant et al., 2018
Rosa multiflora	$2n = 2x = 14$	Multiflora rose	.	GDR and NCBI Genome	http://rosa.kazusa.or.jp	Nakamura et al., 2018
Rubus idaeus	$2n = 2x = 14$	Red raspberry	Joan J.			Wight et al., 2019
Rubus occidentalis	$2n = 2x = 14$	Black raspberry	ORUS 4115-3	GDR		VanBuren et al., 2018

Pome Fruits

Pear and apple share a recent whole-genome duplication event that occurred prior to their divergence and may underlie their pome fruit type (Xiang et al., 2017; Li et al., 2019). Pome fruits are characterized by their hypanthium-derived fruit flesh and agronomic importance world-wide. Multiple species and varieties of apple have been sequenced, including *Malus domestica* Golden Delicious (Daccord et al., 2017), *Malus domestica* Hanfu (Zhang et al., 2019), and *Malus baccata* (Chen et al., 2019) (**Supplementary Table 1**). Similarly, multiple species of pear, such as Chinese white pear *Pyrus bretschneideri* (Wu et al., 2013; Xue et al., 2018), European pear *Pyrus communis* "Bartlett" (Chagné et al., 2014; Linsmith et al., 2019), *Pyrus ussuriensis x communis* (Ou et al., 2019), and a wild Birchleaf pear (*Pyrus betulifolia*-Shanxi Duli, *Pbe*-SD) (Dong et al., 2020), have been sequenced (**Supplementary Table 1**). The ability to generate a double haploid line of "Golden Delicious" (GDDH13) provides an advantage in genome assembly (Daccord et al., 2017). Sequence analysis shows a major burst of different transposable elements (TEs) around 21 million years ago in the precursor of modern apple. The authors propose that the TE bursts may have possibly contributed to the divergence of apple from pear (Daccord et al., 2017). In addition, the higher quality genome allows the exploration of epigenomes and epigenetic effects on agronomic traits, such as fruit size (**Figure 3C**). GDDH13 and GDDH18 are isogenic lines obtained from the same haploid, but they develop different sized fruit. Whole genome bisulfide sequencing identified 22 genes with differentially methylated regions in their promoters at two developmental stages, three of which, SPL13 (MD16G0108400), ACS8 (MD15G0127800), and CYP71A25 (MD14G0147300), possess increased methylation in GDDH18 and could potentially contribute to the smaller fruit size of GDDH18 (Daccord et al., 2017).

Drupe, Stone Fruit, and Sweet Almond

Prunus develops drupe fruit, typically botanic fruit with ovary wall-derived fruit flesh (**Figure 2**). They include many agronomically important species, including peach, apricot, sweet cherry, and plum. They are also called stone fruit because their seeds are enclosed by large and hard (stony) endocarps. Almond (*Prunus dulcis*) is a closely related species with a highly syntenic genome to these *Prunus* species (Dirlewanger et al., 2004), but it offers high-value seeds instead of fleshy fruits. The genome resemblance among the Prunus species explains why they can form inter-specific hybrids. Although wild almonds accumulate a bitter and toxic amygdalin in their seeds, domesticated almonds develop sweet kernels/seeds. The genetic basis of this important domestication trait was recently revealed when the almond genomes were sequenced by two research groups using almond cultivars, Lauranne and Texas, respectively (Sánchez-Pérez et al., 2019; Alioto et al., 2020). The two genomes have similar contig N50-values (Lauranne: 82.26 kb, Texas: 103 kb) and protein-coding genes (Lauranne: 27,817, Texas: 27,969). Subsequent mapping identified a point mutation (Leu to Phe) in the bHLH2 gene that normally controls the expression of two P450 monooxygenase genes *CYP79D16* and *CYP71AN24* required for amygdalin biosynthesis (Sánchez-Pérez et al., 2019). The mutant bHLH2 fails to form a functional dimer, resulting in loss of P450 gene expression and, hence, sweet kernels. Alioto et al. (2020) compare the genomes between *Prunus dulcis* cv. Texas and peach, sweet cherry, and Japanese apricot and observed highly methylated TE insertions surrounding the *CYP71AN24* gene, whose reduced expression was correlated with the sweet kernel trait in the almond cultivar Texas. Therefore, natural mutations and transposable elements contribute to the diversification of *Prunus* species and domestications of almond.

Following the publication of the peach (*Prunus persica*) genome and subsequent improvement (Verde et al., 2013, 2017), the pan-genome of peach (*P. persica*) is a much-welcomed next step (Cao et al., 2020). A pan-genome consists of the entire set of genes and genetic variations within a species, and the portion of the pan-genome common to all cultivars in the species forms the core genome. A pan-genome identifies genetic variations among cultivars, provides valuable resources, and supports evolutionary studies. In this study, 100 *P. persica* accessions were sequenced, giving rise to 27,796 genes in the pan-genome. Furthermore, the genomes of four wild peaches (*Prunus mira*, *Prunus kansuensis*, *Prunus davidiana*, *Prunus ferganensis*) were assembled *de novo*, and the core genome shared by peach and its four wild relatives consists of 15,216 gene families. The analysis reveals dramatic variation in gene content between congeneric species and suggests that *P. mira* is the primitive ancestor of the cultivated peach.

NEW TECHNOLOGIES FOR IMPROVING GENOME ASSEMBLY AND ANNOTATION

The rapid development of sequencing and related technologies, such as PacBio single-molecule real-time (SMRT) sequencing, Oxford Nanopore sequencing, Hi-C, and BioNano optical mapping over the past 10 years have greatly facilitated genome assembly and annotation. PacBio and Nanopore both belong to the third-generation (single-molecule and real-time) sequencing technology. Their long-read DNA-seq helps overcome challenges of genome assembly caused by repetitive regions (Rhoads and Au, 2015; Lu et al., 2016; Jiao and Schneeberger, 2017) and facilitates splicing isoform prediction and genome annotation (Rhoads and Au, 2015). Hi-C and BioNano optical mapping are two scaffolding technologies that help to construct chromosome-level scaffolds from contigs by providing long-range genomic information (Korbel and Lee, 2013; Tang et al., 2015; Jiao and Schneeberger, 2017). Many important crop species' genomes have benefitted from several rounds of genome assembly and annotation whenever a new technology was applied.

For heterozygous diploid species, most genomes were assembled into one pseudo-haploid sequence, ignoring sequence or structural differences between the two parental chromosomes. To generate homozygous lines, traditional methods involve breeding or creating double haploids; however, this can be extremely time-consuming or technically challenging. A recent advancement involves single-cell sequencing of haploid gametes, which enables separation of whole genome sequencing reads into haplotype-specific read sets. Using this method, two

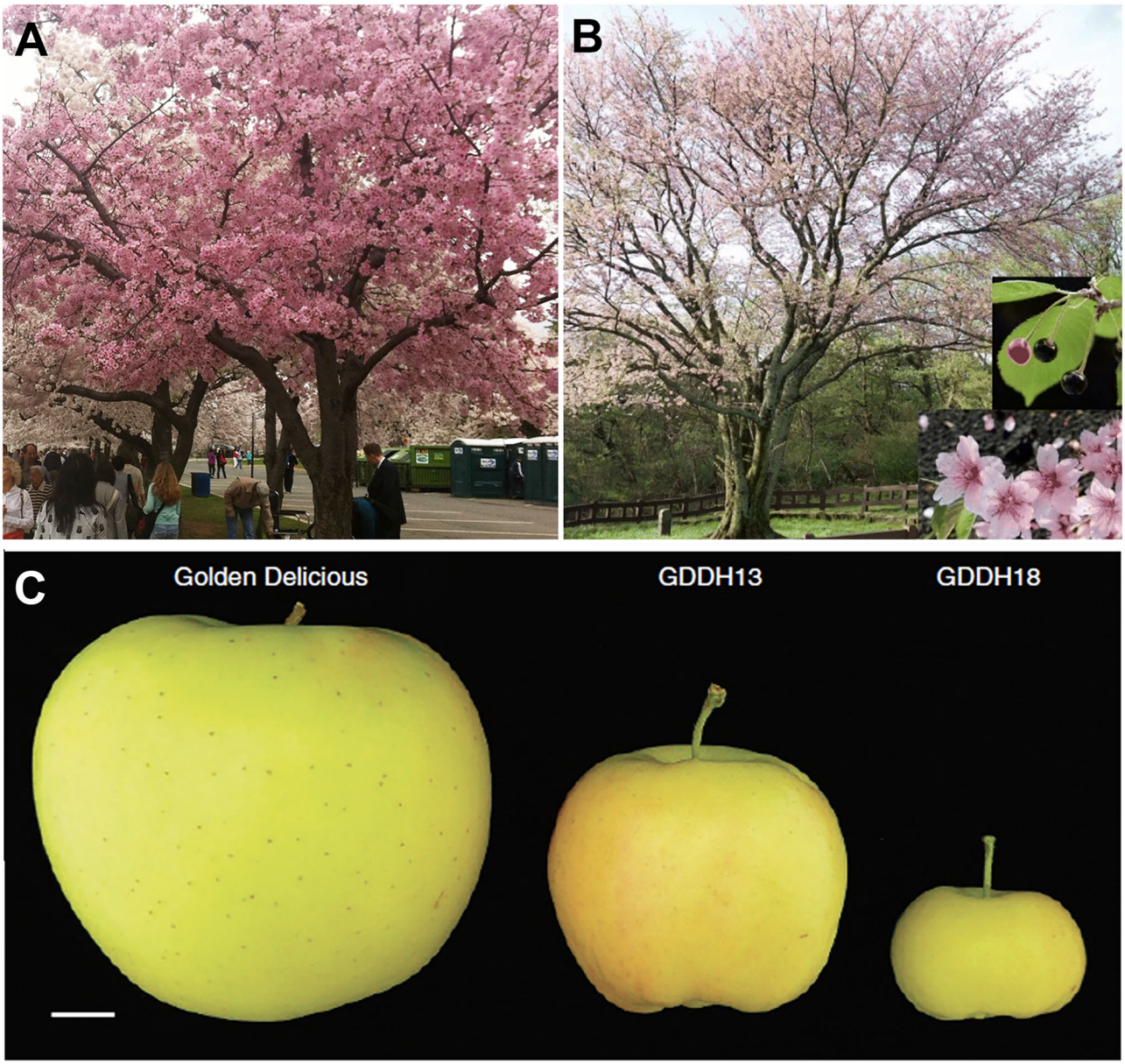

FIGURE 3 | Genomic studies to address questions about genetic relationship in cherry tree and fruit size in apple. **(A)** Yoshino cherry tree (*P. x yedoensis*) in the Washington, D.C., tidal basin. **(B)** A King cherry (*P. yedoensis var. nudiflora* Koehne) has superior flower, fruit, and tree shape. **(C)** A Golden Delicious apple and medium and small size apples from two isogenic lines, GDD13 and GDDH18, derived from the same haploid. The dramatic fruit size difference between GDDH13 and GDDH18 results from epigenetic differences. Photos in **(B)** and **(C)** are from Baek et al. (2018) and Daccord et al. (2017), respectively (both licensed under Creative Commons Attribution License 4.0).

haploid genomes of a diploid apricot tree (*Prunus armeniaca* cultivar "Rojo Pasion") were assembled based on whole genome sequencing of 445 pollen grains (Campoy et al., 2020). This is a much-needed advancement applicable to other Rosaceae species.

Several Updates in Apple Genome Assembly and Annotation

The progressive improvement of apple genome assemblies nicely illustrates the application of newer technologies. The first genome of apple (*Malus domestica* cv. "Golden Delicious") was published in 2010 using traditional Sanger sequencing and 454 next-generation sequencing (Velasco et al., 2010). Six years later, an improved apple genome of "Golden Delicious" was assembled based on a combination of Illumina short reads and PacBio long reads (Li et al., 2016). Accordingly, the contig N50 of the apple genome was 111,619 bp, almost seven times the previous N50 (16,171 bp). In 2017, another *de novo* genome assembly of double haploid "Golden Delicious" (GDDH13) was published (Daccord

et al., 2017). In addition to the Illumina and PacBio data, a BioNano optical mapping was used in scaffolding. As a result, the scaffold N50 was increased to 5,558 kb. In 2019, Illumina, PacBio, BioNano, and Hi-C technologies were integrated to construct a high-quality genome assembly of "Hanfu" (HFTH1) apple, a *Malus domestica* cultivar grown in northern China (Zhang et al., 2019). The scaffold N50 was increased to 6,988 kb. Compared with the HFTH1 genome, the three published "Golden Delicious" genomes shared 11,502 deletions and 6,590 insertions with an average length of 508 bp and 519 bp, respectively (Velasco et al., 2010; Li et al., 2016; Daccord et al., 2017). The average density of shared SNPs with the "Golden Delicious" genomes is 2.15/kb. The HFTH1 genome was utilized to completely fill 488 gaps in the GDDH13 genome; the average length of the filled gaps is 78,864 bp (Zhang et al., 2019). It would be useful if the gap-filled GDDH13 genome could be made publicly available. Because of the genetic variations between "Hanfu" and "Golden Delicious," it is beneficial to use the genome assembly of the cultivar most closely related to the cultivars under one's study as a reference.

In addition to genome assembly, high-quality genome annotations are essential to enhance the utility of the genome. In the first "Golden Delicious" genome published in 2010, the genome annotation was based on the gene prediction programs and ESTs from Genbank (Korf et al., 2001; Birney et al., 2004; Majoros et al., 2004; Solovyev et al., 2006; Velasco et al., 2010; Sayers et al., 2020). In 2014, an improved apple reference transcriptome was constructed using RNA-Seq data generated from "Golden Delicious" fruits at 14 time points during development (Bai et al., 2014). In 2016, the *de novo* "Golden Delicious" genome assembly was supplemented by annotations based on RNA-Seq data from three distinct tissues (leaves, flowers, and stems) as well as *ab initio* and protein homology-based predictions (Li et al., 2016). To annotate the latest "Golden Delicious" GDDH13 genome, mRNA was extracted and sequenced from more tissues, including leaves, roots, fruits, apex, stems, and flowers (Daccord et al., 2017). The GDDH13 genome annotation has the lowest number of protein-coding genes at 42,140 (Daccord et al., 2017) compared with 53,922 (Li et al., 2016) and 63,141 (Velasco et al., 2010). However, GDDH13 possesses the highest BUSCO completeness at 94.9% (Daccord et al., 2017) compared with 51.5% (Li et al., 2016) and 86.7% (Velasco et al., 2010).

Several Updates in Strawberry Genome Assembly and Annotation

As with apples, the diploid woodland strawberry (*Fragaria vesca* ssp. *vesca* "Hawaii4") genome assembly and annotation went through several rounds of updates. The first woodland strawberry genome became available at the end of 2010, and its genome annotation (v1.1) was generated by GeneMark-ES+ (Lomsadze et al., 2005), which integrated *ab initio* gene prediction and EST evidence (Shulaev et al., 2011). In 2015, a new annotation (v1.1.a2) was created that combined different evidence, such as *de novo* and genome-guided transcriptome assembly from RNA-Seq reads, *ab initio* gene models, and plant protein sequences from UniProt (Darwish et al., 2015). More than 2000 new genes were added in the v1.1.a2 annotation. In 2014, dense linkage maps were leveraged to construct an improved woodland strawberry genome assembly (v2.0.a1) (Tennessen et al., 2014). In 2017, based on PacBio long reads and Illumina short reads from *F. vesca* fruit receptacles as well as prior short-read RNA-Seq data, a new annotation (v2.0.a2) was generated (Li et al., 2018). Although the total number of protein-coding genes decreased slightly, 13,168 protein-coding genes were updated in their gene structures, alternatively spliced (AS) isoforms were identified for 7,370 genes, and the BUSCO completeness score was increased to 95.7% from the prior version (88.9%).

At the end of 2017, a high-quality woodland strawberry genome (v4.0.a1) was assembled using PacBio long reads, Illumina short reads, and BioNano optical mapping (Edger et al., 2018). This version uses a different gene-naming system, moving from the geneXXXXX to FvH4XgXXXXX format. Li Y. et al. (2019) include a supplementary table in their publication that correlates the *F. vesca* gene names between the old and new naming systems. In addition, a new annotation (v4.0.a2) was created based on comprehensive short- and long-read RNA-Seq data (Li Y. et al., 2019), adding 5,419 new protein-coding genes, improving the BUSCO completeness score to 98.1% from the prior 91.1%, and adding AS isoforms detected for about 30% of the genes.

In 2013, the first draft octoploid garden strawberry genome (*Fragaria x ananassa* cv. "Reikou") was reported (Hirakawa et al., 2014). Homoeologous sequences of the allo-octoploid strawberry are integrated into a haploid genome named FANhybrid_r1.2 with an N50 of 5.14 kb. Gene prediction was done *ab initio* using Augustus. In the same study, the genomes of several Fragaria species were sequenced and assembled, including *F. orientalis*, *F. iinume*, *F. nipponica*, and *F. bucharica*, and *F. bucharica* (USDA accession CFRA522) was originally misidentified as *Fragaria nubicola* (Tennessen et al., 2014). In 2019, a near-complete chromosome-scale assembly of the *Fragaria x ananassa* cv. "Camarosa" was constructed with a contig N50 of about 79.97 kb, taking advantage of Illumina, 10X Genomics, and PacBio long reads (Edger et al., 2019). This chromosome-scaled genome consists of A, B, C, and D subgenomes, and the genome annotation (v1.0.a1) utilized RNA-Seq data from diverse tissue types (108,087 protein-coding genes) (Edger et al., 2019). In the same year, a garden strawberry reference transcriptome was constructed using PacBio sequencing (Yuan et al., 2019). The PacBio data in this study, together with other publicly available Illumina RNA-Seq data were recently utilized to improve the annotation of the *Fragaria x ananassa* cv. "Camarosa" genome (v1.0.a1) (Liu et al., 2021). Compared with *Fragaria x ananassa* v1.0.a1, the new annotation v1.0.a2 had a slight increase in the number of protein-coding genes (108,447). Importantly, the new annotation (v1.0.a2) for *Fragaria x ananassa* cv. "Camarosa" includes AS isoforms for 11,044 genes and adds 5′ and 3′ UTR information to a large proportion of the protein-coding genes (v1.0.a1: 38.93%, v1.0.a2: 73.61%).

The complete genome sequencing of the *Fragaria x ananassa* cultivar "Camarosa" allowed the identification of diploid

progenitors, which has long been a mystery and recently a topic of intense debate. Based on the tree-searching algorithm (PhyDS), Edger et al. (2019) propose four diploid species (*F. vesca*, *F. iinumae*, *F. viridis*, and *F. nipponica*) as the four progenitors of the octoploid and suggest the hexaploid *F. moschata* as an intermediate species (Edger et al., 2019). However, Liston et al. (2020) reanalyzed the four subgenomes in a phylogenomic context and found support for *F. vesca* and *F. iinumae* but disputed *F. viridis*, *F. nipponica*, and *F. moschata* as progenitors (Liston et al., 2020). In response, a new chromosome-scale genome of *F. iinumae* was subsequently assembled, and a reanalysis using PhyDS supports their original proposal regarding the four diploid species as the progenitors (Edger et al., 2020). A third group recently sequenced and assembled the genomes of three wild diploid species, *F. nilgerrensis*, *F. nubicola*, and *F. viridis* (Feng et al., 2021). Combining these three genomes with the previously sequenced *F. vesca* and *F. iinumae* genomes, the group utilized sppIDer (Langdon et al., 2018) to map short-read sequencing data of *F. x ananassa* to a composite reference genome, and the result supports that *F. vesca* and *F. iinumae*, but not others, are the progenitor species of the cultivated garden strawberry (Feng et al., 2021).

NON-CODING RNA IN ROSACEAE GENOMES

Non-coding RNAs (ncRNAs) are RNAs that do not encode proteins. They are important components of the genomes and play roles in plant development and stress responses (Liu et al., 2017). However, ncRNA prediction is not always included in the annotation of published genomes. Computational tools, such as tRNAscan-SE (Chan and Lowe, 2019) and RNAmmer (Lagesen et al., 2007) are used to predict tRNA and rRNAs, respectively. Infernal (Nawrocki and Eddy, 2013) and Rfam (Kalvari et al., 2018) are often used to identify different types of ncRNAs. Besides the commonly used tools mentioned, additional approaches can be applied to detect ncRNAs, especially small RNAs. To predict miRNAs in the apricot (*Prunus armeniaca* cv. "Chuanzhihong") genome, miRNA sequences derived from miRbase (Kozomara et al., 2019) were mapped against the genome, and the resulting miRNA candidates were further verified by RNAfold analysis (Lorenz et al., 2011; Jiang et al., 2019). In *Rosa chinensis* cv. "Old Blush," an RNA library from pooled tissues was sequenced and analyzed for miRNA identification; tRNA and rRNA-like sequences were removed first, and miRNA precursors were then annotated using an established pipeline (Formey et al., 2014; Raymond et al., 2018). Previously, small RNA libraries derived from diverse tissues were sequenced to detect miRNAs and PhasiRNAs in wild diploid strawberry using established pipelines and criteria (Meyers et al., 2008; Xia et al., 2012, 2015). The same small RNA sequencing data sets were later used to identify small RNAs during the woodland strawberry genome reannotations (v2.0.a2 and v4.0.a2) (Axtell, 2013; Li et al., 2018; Li Y. et al., 2019). In addition to small RNAs, lncRNAs, a class of ncRNAs with length >200 bp, are shown to possess epigenetic regulatory roles in key cellular processes. RNA-Seq data from woodland strawberry flower and fruit tissues were used to identify lncRNAs, leading to 5,884 lncRNAs (Kang and Liu, 2015). In 2017, in updating woodland strawberry genome annotation v2.0.a2, an updated prediction of 4,042 lncRNA was included (Li et al., 2018).

COMPUTATIONAL DATABASES FOR ROSACEAE SPECIES

Computational databases are becoming indispensable tools for research. Below, we discuss databases, highlighting those that are of particular importance to Rosaceae research. Although **Table 1** and **Supplementary Table 1** provide species-specific websites that accompany the genome-sequencing papers, **Table 2** lists highly useful databases with various analysis tools and information.

Rosaceae Genome Databases

Genome Database for Rosaceae (GDR) (www.rosaceae.org) (Jung et al., 2019) is, by far, the best resource hub for Rosaceae research. It hosts the most comprehensive and up-to-date collection of genome assembly and annotation versions for widely studied genera, *Fragaria*, *Malus*, *Prunus*, *Potentilla*, *Pyrus*, *Rosa*, and *Rubus*. For instance, GDR hosts *Fragaria vesca* genome assemblies of v1.0, v1.1 (an improved pseudochromosome assembly of v1.0), v2.0.a1, and v4.0.a1. Moreover, it incorporates corresponding updated annotations v1.1.a2, v2.0.a2, and v4.0.a2. In addition, GDR serves as the database of record for Rosaceae gene names; standardized gene-naming guideline should be followed to ensure uniformity and clarity (Jung et al., 2015). Besides the genes and genomes, GDR provides genetic maps, markers, germplasm, and trait information as well as an impressive set of tools. For example, the search tools of GDR enable users to search for specific gene sequence, maps, and markers; its MegaSearch tool allows downloading different data types in bulk. With the GDRCyc tool, users can search, visualize, and overlay pathway data. With the Synteny Viewer tool, one can select specific Rosaceae species for comparison, visualize syntenic blocks, and obtain information on syntenic genes.

The NCBI Genome (https://www.ncbi.nlm.nih.gov/genome) (Tatusova et al., 1999) on the other hand collects genomes from a broader range of Rosaceae species (**Supplementary Table 1**), including lesser-known species, such as Drummond's mountain avens (*Dryas drummondii*), wood avens (*Geum urbanum*), and bitterbrush (*Purshia tridentate*) (Griesmann et al., 2018; Jordan et al., 2018).

Rosaceae Species-Specific Databases

Many genome sequencing or annotation papers of Rosaceae species are accompanied by species-specific websites that provide tools, including BLAST searches for genes of interest. The URLs for these websites are included in **Table 1** (or **Supplementary Table 1** with a complete list). For instance, the genomes of Yoshino cherry (*Cerasus* x *yedoensis*) and sweet cherry (*Prunus avium*) are both deposited in DBcherry (http://cherry.kazusa.or.jp/) (Shirasawa et al., 2017, 2019). The built-in BLAST enables users to search their sequences of interest against the cherry genomes, and JBrowse is embedded in the

TABLE 2 | List of websites/databases useful for Rosaceae research.

Database name	URL	Species	Information provided	Reference
ROSACEAE DATABASES				
GDR (Genome Database for Rosaceae)	https://www.rosaceae.org	Rosaceae	Genomic	Jung et al., 2019
MDR (Methylation Database for Rosaceae)	http://mdr.xieslab.org	Rosaceae	Methylation	Liu et al., 2019
AppleMDO	http://bioinformatics.cau.edu.cn/AppleMDO	*Malus domestica*	Co-expression	Da et al., 2019
Fragaria vesca co-expression network explorer	http://159.203.72.198:3838/fvesca	*Fragaria vesca*	Co-expression	Shahan et al., 2018
SGR (Strawberry Genome Resources)	http://bioinformatics.towson.edu/strawberry	*Fragaria vesca*	Transcriptome	Darwish et al., 2013
SGD (Strawberry Genome Database)	*http://www.strawberryblast.ml:8080/strawberry/viroblast.php*	*Fragaria x ananassa*	Genomic	Liu et al., 2021
TRANSNAP	http://plantomics.mind.meiji.ac.jp/nashi	*Pyrus pyrifolia*	Transcriptome	Koshimizu et al., 2019
GENERAL PLANT DATABASES				
NCBI Genome	https://www.ncbi.nlm.nih.gov/genome	General	Genomic	Tatusova et al., 1999
PLAZA	https://bioinformatics.psb.ugent.be/plaza	Plant	Genomic	Van Bel et al., 2018
Phytozome	https://phytozome-next.jgi.doe.gov	Plant	Genomic	Goodstein et al., 2012
EnsemblPlants	https://plants.ensembl.org/index.html	Plant	Genomic	Bolser et al., 2017
PMN (Plant Metabolic Network)	https://plantcyc.org	Plant	Functional (Pathway)	Schläpfer et al., 2017
Plant Reactome	https://plantreactome.gramene.org/index.php?lang=en	Plant	Functional (Pathway)	Naithani et al., 2020
PlantTFDB (Transcription Factor Database)	http://planttfdb.gao-lab.org	Plant	Functional (TF Regulation)	Jin et al., 2017
PlantRegMap (Plant Transcriptional Regulatory Map)	http://plantregmap.gao-lab.org	Plant	Functional (TF Regulation)	Tian et al., 2020
Next-Gen Sequence Databases and sRNA Tools	https://mpss.danforthcenter.org	Plant	ncRNA (small RNA)	Nakano et al., 2020
CANTATAdb	http://cantata.amu.edu.pl	Plant	ncRNA (lncRNA)	Szcześniak et al., 2016
RPTEdb (Rosaceae Plant Transposable Element Database)	http://genedenovoweb.ticp.net:81/RPTEdb/index.php	Rosaceae	TE	Ma et al., 2018
PlantRGDB (Plant Retrocopied Gene DataBase)	https://probes.pw.usda.gov/plantrgdb/index.php	Plant	Retrocopied Gene	Wang, 2017

database for visualizing the genomic regions. The genomes of garden strawberry (*Fragaria x ananassa*) and multiflora rose (*Rosa multiflora*) are available in Strawberry GARDEN (http://strawberry-garden.kazusa.or.jp/) and Rosa multiflora DB (http://rosa.kazusa.or.jp/), respectively (Hirakawa et al., 2014; Nakamura et al., 2018). These two websites as well as the database for cherry are all supported by the Kazusa DNA Research Institute.

Several Rosaceae species have developed species-specific databases with multiple analysis tools and resources, which are summarized in **Table 2** and described below. Strawberry Genomic Resources (SGR, http://bioinformatics.towson.edu/strawberry/default.aspx) is a website that integrates different types of woodland strawberry (*Fragaria vesca*) genomic data (Darwish et al., 2013). It allows users to access the transcriptome analysis of the woodland strawberry early fruit development (Kang et al., 2013). Users can acquire differentially expressed genes between distinct tissues and stages by searching the database and use the eFP browser to visualize RNA-Seq data across tissues and stages for genes of interests (Hawkins et al., 2017). An updated *F. vesca* eFP browser is hosted at the ePlant (http://bar.utoronto.ca/). In addition, a recent annotation update of the *Fragaria x ananassa* cv. "Camarosa" genome (v1.0.a2) is accompanied with a separate website, "Strawberry Genome Database" (**Table 2**), that allows users to search for garden strawberry genes (Liu et al., 2021).

A reference transcriptome of Chinese pear (*Pyrus pyrifolia*) was constructed by utilizing PacBio, 454, and Sanger sequencing, and it is stored in the database TRANSNAP (http://plantomics.mind.meiji.ac.jp/nashi/) (Koshimizu et al., 2019). The database also includes gene functional annotation performed by BLASTP (Altschul et al., 1990), KAAS (Moriya et al., 2007), and InterProScan (Jones et al., 2014). Users can examine

gene-expression patterns generated from GEO (https://www.ncbi.nlm.nih.gov/geo/) microarray data.

The *Fragaria vesca* gene co-expression network explorer (http://159.203.72.198:3838/fvesca/) was developed to host the non-consensus and consensus co-expression networks generated using RNA-Seq data from flower and fruit tissues of the woodland strawberry (Shahan et al., 2018). Users are able to search for genes of interest and the transcriptional co-expression clusters to which they belong, obtain network statistics, visualize cluster eigengene expression, examine enriched GO terms in the cluster of interest, and download the cluster graphml structure.

AppleMDO (http://bioinformatics.cau.edu.cn/AppleMDO/) is a multidimensional omics database for apple co-expression networks and chromatin states (Da et al., 2019). The global co-expression network was constructed using transcriptomes from a variety of tissues, stages, and stress treatments. The tissue-preferential network was built based on RNA-Seq data sets of different tissues without stress treatments. A combination of ChIP-seq, DNase-seq, and BS-seq data sets were utilized by ChromHMM (Ernst and Kellis, 2012) to predict the chromatin states. Furthermore, AppleMDO offers tools to perform GO analysis and motif scan.

Methylation Database for Rosaceae (http://mdr.xieslab.org/) is a database presenting methylation analyses of Rosaceae species, including woodland strawberry and Chinese rose (*Rosa chinensis*) (Liu et al., 2019). Using PacBio sequencing data that is publicly available (Edger et al., 2018; Raymond et al., 2018), DNA N6-methyladenine and N4-methylcytosine modifications were identified for woodland strawberry and Chinese rose with the PacBio SMRT analysis software.

The Rosaceae Plant TE Database (RPTEdb, http://genedenovoweb.ticp.net:81/RPTEdb/index.php) provides information on TEs in five Rosaceae species: woodland strawberry, apple, Japanese apricot (*Prunus mume*), Chinese white pear, and peach (Ma et al., 2018). The TEs were detected in three ways, *de novo* identification performed by PILER (Edgar and Myers, 2005) and RepeatModeler (http://www.repeatmasker.org/), signature-based identification achieved by LTR_STRUC (McCarthy and McDonald, 2003) and LTR_FINDER (Xu and Wang, 2007), and similarity-based identification conducted by RepeatMasker (http://www.repeatmasker.org/) using the Repbase database (Jurka et al., 2005; Bao et al., 2015). Users can search and download TEs in each TE family or superfamily and view TE trees constructed using a superfamily of TEs from five Rosaceae species.

Useful Plant Databases for Comparative Genomics, Metabolic Networks, and Others

Although the summary above focuses on Rosaceae databases, many plant databases are also highly useful for Rosaceae research. **Table 2** lists some of the most useful ones, such as Plant Transcription Factor Database (http://planttfdb.gao-lab.org/), Plant Transcriptional Regulatory Map (http://plantregmap.gao-lab.org/), CANTATAdb (http://cantata.amu.edu.pl/) for plant lncRNAs, and Plant Retrocopied Gene DataBase (http://probes.pw.usda.gov/plantrgdb) for plant retrocopied genes (Wang, 2017). Below, we highlight four such databases.

PLAZA (https://bioinformatics.psb.ugent.be/plaza/) (Van Bel et al., 2018) and Phytozome (https://phytozome-next.jgi.doe.gov/) (Goodstein et al., 2012) are databases for plant genome comparisons. Currently, Dicots PLAZA 4.5 has integrated genomic resources from 55 species, including four Rosaceae species, apple (*Malus domestica*), Chinese white pear (*Pyrus bretschneideri*), peach (*Prunus persica*), and woodland strawberry (*Fragaria vesca*). Phytozome v13 has gathered 224 annotated genomes, including three Rosaceae species, woodland strawberry, apple, and peach. The genome assemblies at PLAZA and Phytozome are not always up to date. For instance, older versions of woodland strawberry genome v1.1 and v2.0.a2 are, respectively, hosted at PLAZA and Phytozome at the moment.

Plant Metabolic Network (PMN, https://plantcyc.org/) (Schläpfer et al., 2017) and Plant Reactome (https://plantreactome.gramene.org/index.php?lang=en) (Naithani et al., 2020) are both databases for plant pathways. Plant Metabolic Network is focused on metabolic pathways and hosts the database PlantCyc that contains shared pathways among more than 350 plant species. Additionally, a single-species database was also constructed in PMN, which allows users to access pathways and enzymes for individual species. PpersicaCyc, SweetcherryCyc, MdomesticaCyc, EuropeanpearCyc, Fvesca_VescaCyc, RmultifloraCyc, and RchinensisCyc are developed for Rosaceae family members. Besides the metabolic pathways, Plant Reactome hosts different types of pathways, including gene regulatory pathways, hormone signaling pathways, and others. Users can view and interact with the pathways in the browser and identify chemical compounds and proteins involved in the processes. The database encompasses multiple Rosaceae species, such as peach, woodland strawberry, and apple. Furthermore, the database enables researchers to perform pathway enrichment analysis and species comparison between pathways of rice and those of selected species.

DISCUSSION

As a result of revolutionary improvements in DNA sequencing and analysis software, Rosaceae genome research has seen a dramatic jump in the number of sequenced genomes, transcriptomes, databases, and publications. These genomic data and databases will greatly facilitate the understanding of physiology, growth and development, stress responses, adaptation, and domestication of Rosaceae species, laying the foundation for trait improvement through breeding and genome engineering. This view is also shared by a prior review on the genomes of several commercially important Rosaceae plants (Soundararajan et al., 2019). However, there is still ample room for improvement to fully reap the benefit of the genome sequencing revolution. These include increasing the quality and accuracy of Rosaceae genome assemblies and annotations, in particular, for polyploid and hybrid cultivars; identification and incorporation of AS variants and ncRNA into genome annotations; expansion of pan-genome analyses;

and establishing robust molecular markers. Development of user-friendly databases that integrate, organize, and coordinate different data types and species is also essential to increase the accessibility and impact of the ever-increasing genomic data sets. The genomic revolution will likely propel significant research progress and further increase the agronomic value of Rosaceae fruits, seeds, and ornamentals.

AUTHOR CONTRIBUTIONS

ML and ZL conceived and drafted the manuscript. ML and YX collected information and data. SM provided advice and revised the manuscript. All authors contributed to the article and approved the submitted version.

FUNDING

The research in our labs has been supported by a grant from the National Science Foundation (IOS 1444987) to ZL and SM. ML was supported in part by NSF award DGE-1632976.

SUPPLEMENTARY MATERIAL

The Supplementary Material for this article can be found online at: https://www.frontiersin.org/articles/10.3389/fpls.2021.644881/full#supplementary-material

Supplementary Table 1 | A comprehensive list of Rosaceae genomes and relevant information.

REFERENCES

Alioto, T., Alexiou, K. G., Bardil, A., Barteri, F., Castanera, R., Cruz, F., et al. (2020). Transposons played a major role in the diversification between the closely related almond and peach genomes: results from the almond genome sequence. *Plant J.* 101, 455–472. doi: 10.1111/tpj.14538

Altschul, S. F., Gish, W., Miller, W., Myers, E. W., and Lipman, D. J. (1990). Basic local alignment search tool. *J. Mol. Biol.* 215, 403–410. doi: 10.1016/S0022-2836(05)80360-2

Axtell, M. J. (2013). ShortStack: comprehensive annotation and quantification of small RNA genes. *RNA* 19, 740–751. doi: 10.1261/rna.035279.112

Baek, S., Choi, K., Kim, G.-B., Yu, H.-J., Cho, A., Jang, H., et al. (2018). Draft genome sequence of wild *Prunus yedoensis* reveals massive inter-specific hybridization between sympatric flowering cherries. *Genome Biol.* 19:127. doi: 10.1186/s13059-018-1497-y

Bai, Y., Dougherty, L., and Xu, K. (2014). Towards an improved apple reference transcriptome using RNA-seq. *Mol. Genet. Genomics* 289, 427–438. doi: 10.1007/s00438-014-0819-3

Bao, W., Kojima, K. K., and Kohany, O. (2015). Repbase Update, a database of repetitive elements in eukaryotic genomes. *Mob. DNA* 6:11. doi: 10.1186/s13100-015-0041-9

Birney, E., Clamp, M., and Durbin, R. (2004). GeneWise and Genomewise. *Genome Res.* 14, 988–995. doi: 10.1101/gr.1865504

Bolser, D. M., Staines, D. M., Perry, E., and Kersey, P. J. (2017). "Ensembl plants: integrating tools for visualizing, mining, and analyzing plant genomic data," in *Plant Genomics Databases: Methods and Protocols*, ed A. D. J. van Dijk (New York, NY: Humana Press), 1–31.

Campoy, J. A., Sun, H., Goel, M., Jiao, W.-B. A., Folz-Donahue, K., Kukat, C., et al. (2020). Chromosome-level and haplotype-resolved genome assembly enabled by high-throughput single-cell sequencing of gamete genomes. *bioRxiv* 2020.04.24.060046. doi: 10.1101/2020.04.24.060046

Cao, K., Peng, Z., Zhao, X., Li, Y., Liu, K., Arus, P., et al. (2020). Pan-genome analyses of peach and its wild relatives provide insights into the genetics of disease resistance and species adaptation. *bioRxiv* 2020.07.13.200204. doi: 10.1101/2020.07.13.200204

Chagné, D., Crowhurst, R. N., Pindo, M., Thrimawithana, A., Deng, C., Ireland, H., et al. (2014). The draft genome sequence of European pear (*Pyrus communis* L. 'Bartlett'). *PLOS ONE* 9:e92644. doi: 10.1371/journal.pone.0092644

Chan, P. P., and Lowe, T. M. (2019). "tRNAscan-SE: searching for tRNA genes in genomic sequences," in *Gene Prediction: Methods and Protocols Methods in Molecular Biology*, ed M. Kollmar (New York, NY: Springer), 1–14.

Chen, X., Li, S., Zhang, D., Han, M., Jin, X., Zhao, C., et al. (2019). Sequencing of a wild apple (*Malus baccata*) genome unravels the differences between cultivated and wild apple species regarding disease resistance and cold tolerance. *G3 (Bethesda).* 9, 2051–2060. doi: 10.1534/g3.119.400245

Da, L., Liu, Y., Yang, J., Tian, T., She, J., Ma, X., et al. (2019). AppleMDO: a multi-dimensional omics database for apple co-expression networks and chromatin States. *Front. Plant Sci.* 10:1333. doi: 10.3389/fpls.2019.01333

Daccord, N., Celton, J.-M., Linsmith, G., Becker, C., Choisne, N., Schijlen, E., et al. (2017). High-quality *de novo* assembly of the apple genome and methylome dynamics of early fruit development. *Nat. Genet.* 49, 1099–1106. doi: 10.1038/ng.3886

Darwish, O., Shahan, R., Liu, Z., Slovin, J. P., and Alkharouf, N. W. (2015). Re-annotation of the woodland strawberry (*Fragaria vesca*) genome. *BMC Genomics* 16:29. doi: 10.1186/s12864-015-1221-1

Darwish, O., Slovin, J. P., Kang, C., Hollender, C. A., Geretz, A., Houston, S., et al. (2013). SGR: an online genomic resource for the woodland strawberry. *BMC Plant Biol.* 13:223. doi: 10.1186/1471-2229-13-223

Dirlewanger, E., Graziano, E., Joobeur, T., Garriga-Calderé, F., Cosson, P., Howad, W., et al. (2004). Comparative mapping and marker-assisted selection in Rosaceae fruit crops. *Proc. Natl. Acad. Sci. U.S.A.*101, 9891–9896. doi: 10.1073/pnas.0307937101

Dong, X., Wang, Z., Tian, L., Zhang, Y., Qi, D., Huo, H., et al. (2020). *De novo* assembly of a wild pear (*Pyrus betuleafolia*) genome. *Plant Biotechnol. J.* 18, 581–595. doi: 10.1111/pbi.13226

Edgar, R. C., and Myers, E. W. (2005). PILER: identification and classification of genomic repeats. *Bioinformatics* 21, i152–i158. doi: 10.1093/bioinformatics/bti1003

Edger, P. P., McKain, M. R., Yocca, A. E., Knapp, S. J., Qiao, Q., and Zhang, T. (2020). Reply to: revisiting the origin of octoploid strawberry. *Nat. Genet.* 52, 5–7. doi: 10.1038/s41588-019-0544-2

Edger, P. P., Poorten, T. J., VanBuren, R., Hardigan, M. A., Colle, M., McKain, M. R., et al. (2019). Origin and evolution of the octoploid strawberry genome. *Nat. Genet.* 51, 541–547. doi: 10.1038/s41588-019-0356-4

Edger, P. P., VanBuren, R., Colle, M., Poorten, T. J., Wai, C. M., Niederhuth, C. E., et al. (2018). Single-molecule sequencing and optical mapping yields an improved genome of woodland strawberry (*Fragaria vesca*) with chromosome-scale contiguity. *GigaScience* 7:gix124. doi: 10.1093/gigascience/gix124

Ernst, J., and Kellis, M. (2012). ChromHMM: automating chromatin-state discovery and characterization. *Nat. Methods* 9, 215–216. doi: 10.1038/nmeth.1906

Feng, C., Wang, J., Harris, A. J., Folta, K. M., Zhao, M., and Kang, M. (2021). Tracing the diploid ancestry of the cultivated octoploid strawberry. *Mol. Biol. Evol.* 38, 478–485. doi: 10.1093/molbev/msaa238

Formey, D., Sallet, E., Lelandais-Brière, C., Ben, C., Bustos-Sanmamed, P., Niebel, A., et al. (2014). The small RNA diversity from *Medicago truncatularoots* under biotic interactions evidences the environmental plasticity of the miRNAome. *Genome Biol.* 15:457. doi: 10.1186/s13059-014-0457-4

Goodstein, D. M., Shu, S., Howson, R., Neupane, R., Hayes, R. D., Fazo, J., et al. (2012). Phytozome: a comparative platform for green plant genomics. *Nucleic Acids Res.* 40, D1178–D1186. doi: 10.1093/nar/gkr944

Griesmann, M., Chang, Y., Liu, X., Song, Y., Haberer, G., Crook, M. B., et al. (2018). Phylogenomics reveals multiple losses of nitrogen-fixing root nodule symbiosis. *Science* 361:eaat1743. doi: 10.1126/science.aat1743

Hawkins, C., Caruana, J., Li, J., Zawora, C., Darwish, O., Wu, J., et al. (2017). An eFP browser for visualizing strawberry fruit and flower transcriptomes. *Hortic. Res.* 4: 17029. doi: 10.1038/hortres.2017.29

Hibrand Saint-Oyant, L., Ruttink, T., Hamama, L., Kirov, I., Lakhwani, D., Zhou, N. N., et al. (2018). A high-quality genome sequence of *Rosa chinensis* to elucidate ornamental traits. *Nat. Plants* 4, 473–484. doi: 10.1038/s41477-018-0166-1

Hirakawa, H., Shirasawa, K., Kosugi, S., Tashiro, K., Nakayama, S., Yamada, M., et al. (2014). Dissection of the octoploid strawberry genome by deep sequencing of the genomes of Fragaria species. *DNA Res.* 21, 169–181. doi: 10.1093/dnares/dst049

Jiang, F., Zhang, J., Wang, S., Yang, L., Luo, Y., Gao, S., et al. (2019). The apricot (*Prunus armeniaca* L.) genome elucidates Rosaceae evolution and beta-carotenoid synthesis. *Hortic. Res.* 6:128. doi: 10.1038/s41438-019-0215-6

Jiao, W.-B., and Schneeberger, K. (2017). The impact of third generation genomic technologies on plant genome assembly. *Curr. Opin. Plant Biol.* 36, 64–70. doi: 10.1016/j.pbi.2017.02.002

Jin, J., Tian, F., Yang, D.-C., Meng, Y.-Q., Kong, L., Luo, J., et al. (2017). PlantTFDB 4.0: Toward a central hub for transcription factors and regulatory interactions in plants. *Nucleic Acids Res.* 45, D1040–D1045. doi: 10.1093/nar/gkw982

Jones, P., Binns, D., Chang, H.-Y., Fraser, M., Li, W., McAnulla, C., et al. (2014). InterProScan 5: genome-scale protein function classification. *Bioinformatics* 30, 1236–1240. doi: 10.1093/bioinformatics/btu031

Jordan, C. Y., Lohse, K., Turner, F., Thomson, M., Gharbi, K., and Ennos, R. A. (2018). Maintaining their genetic distance: little evidence for introgression between widely hybridizing species of Geum with contrasting mating systems. *Mol. Ecol.* 27, 1214–1228. doi: 10.1111/mec.14426

Jung, S., Bassett, C., Bielenberg, D. G., Cheng, C. H., Dardick, C., Main, D., et al. (2015). A standard nomenclature for gene designation in the Rosaceae. *Tree Genet. Genomes* 11:108. doi: 10.1007/s11295-015-0931-5

Jung, S., Lee, T., Cheng, C.-H., Buble, K., Zheng, P., Yu, J., et al. (2019). 15 years of GDR: new data and functionality in the genome database for Rosaceae. *Nucleic Acids Res.* 47, D1137–D1145. doi: 10.1093/nar/gky1000

Jurka, J., Kapitonov, V. V., Pavlicek, A., Klonowski, P., Kohany, O., and Walichiewicz, J. (2005). Repbase Update, a database of eukaryotic repetitive elements. *Cytogenet. Genome Res.* 110, 462–467. doi: 10.1159/000084979

Kalvari, I., Argasinska, J., Quinones-Olvera, N., Nawrocki, E. P., Rivas, E., Eddy, S. R., et al. (2018). Rfam 13.0: shifting to a genome-centric resource for non-coding RNA families. *Nucleic Acids Res.* 46, D335–D342. doi: 10.1093/nar/gkx1038

Kang, C., Darwish, O., Geretz, A., Shahan, R., Alkharouf, N., and Liu, Z. (2013). Genome-scale transcriptomic insights into early-stage fruit development in woodland strawberry *Fragaria vesca*. *Plant Cell* 25, 1960–1978. doi: 10.1105/tpc.113.111732

Kang, C., and Liu, Z. (2015). Global identification and analysis of long non-coding RNAs in diploid strawberry *Fragaria vesca* during flower and fruit development. *BMC Genomics* 16:815. doi: 10.1186/s12864-015-2014-2

Korbel, J. O., and Lee, C. (2013). Genome assembly and haplotyping with Hi-C. *Nat. Biotechnol.* 31, 1099–1101. doi: 10.1038/nbt.2764

Korf, I., Flicek, P., Duan, D., and Brent, M. R. (2001). Integrating genomic homology into gene structure prediction. *Bioinformatics* 17, S140–S148. doi: 10.1093/bioinformatics/17.suppl_1.S140

Koshimizu, S., Nakamura, Y., Nishitani, C., Kobayashi, M., Ohyanagi, H., Yamamoto, T., et al. (2019). TRANSNAP: a web database providing comprehensive information on Japanese pear transcriptome. *Sci. Rep.* 9:18922. doi: 10.1038/s41598-019-55287-4

Kozomara, A., Birgaoanu, M., and Griffiths-Jones, S. (2019). miRBase: from microRNA sequences to function. *Nucleic Acids Res.* 47, D155–D162. doi: 10.1093/nar/gky1141

Lagesen, K., Hallin, P., Rødland, E. A., Stærfeldt, H.-H., Rognes, T., and Ussery, D. W. (2007). RNAmmer: consistent and rapid annotation of ribosomal RNA genes. *Nucleic Acids Res.* 35, 3100–3108. doi: 10.1093/nar/gkm160

Langdon, Q. K., Peris, D., Kyle, B., and Hittinger, C. T. (2018). sppIDer: a species identification tool to investigate hybrid genomes with high-throughput sequencing. *Mol. Biol. Evol.* 35, 2835–2849. doi: 10.1093/molbev/msy166

Li, H., Huang, C.-H., and Ma, H. (2019). "Whole-genome duplications in pear and apple," in *The Pear Genome Compendium of Plant Genomes*, ed. S. S. Korban (Cham: Springer International Publishing), 279–299. doi: 10.1007/978-3-030-11048-2_15

Li, X., Kui, L., Zhang, J., Xie, Y., Wang, L., Yan, Y., et al. (2016). Improved hybrid *de novo* genome assembly of domesticated apple (*Malus x domestica*). *GigaScience* 5:35. doi: 10.1186/s13742-016-0139-0

Li, Y., Pi, M., Gao, Q., Liu, Z., and Kang, C. (2019). Updated annotation of the wild strawberry *Fragaria vesca* V4 genome. *Hortic. Res.* 6:61. doi: 10.1038/s41438-019-0174-y

Li, Y., Wei, W., Feng, J., Luo, H., Pi, M., Liu, Z., et al. (2018). Genome re-annotation of the wild strawberry *Fragaria vesca* using extensive Illumina- and SMRT-based RNA-seq datasets. *DNA Res.* 25, 61–70. doi: 10.1093/dnares/dsx038

Linsmith, G., Rombauts, S., Montanari, S., Deng, C. H., Celton, J.-M., Guérif, P., et al. (2019). Pseudo-chromosome–length genome assembly of a double haploid "Bartlett" pear (*Pyrus communis* L.). *GigaScience* 8: giz138. doi: 10.1093/gigascience/giz138

Liston, A., Wei, N., Tennessen, J. A., Li, J., Dong, M., and Ashman, T.-L. (2020). Revisiting the origin of octoploid strawberry. *Nat. Genet.* 52, 2–4. doi: 10.1038/s41588-019-0543-3

Liu, C., Feng, C., Peng, W., Hao, J., Wang, J., Pan, J., et al. (2020). Chromosome-level draft genome of a diploid plum (*Prunus salicina*). *GigaScience* 9:giaa130. doi: 10.1093/gigascience/giaa130

Liu, D., Mewalal, R., Hu, R., Tuskan, G. A., and Yang, X. (2017). New technologies accelerate the exploration of non-coding RNAs in horticultural plants. *Hortic. Res.* 4:17031. doi: 10.1038/hortres.2017.31

Liu, T., Li, M., Liu, Z., Ai, X., and Li, Y. (2021). Reannotation of the cultivated strawberry genome and the establishment of the Strawberry Genome Database *Horticult. Res.* 8:41. doi: 10.1038/s41438-021-00476-4

Liu, Z., Ma, H., Jung, S., Main, D., and Guo, L. (2020). Developmental mechanisms of fleshy fruit diversity in Rosaceae. *Annu. Rev. Plant Biol.* 71, 547–573. doi: 10.1146/annurev-arplant-111119-021700

Liu, Z.-Y., Xing, J.-F., Chen, W., Luan, M.-W., Xie, R., Huang, J., et al. (2019). MDR: an integrative DNA N6-methyladenine and N4-methylcytosine modification database for Rosaceae. *Hortic. Res.* 6:78. doi: 10.1038/s41438-019-0160-4

Lomsadze, A., Ter-Hovhannisyan, V., Chernoff, Y. O., and Borodovsky, M. (2005). Gene identification in novel eukaryotic genomes by self-training algorithm. *Nucleic Acids Res.* 33, 6494–6506. doi: 10.1093/nar/gki937

Lorenz, R., Bernhart, S. H., Höner zu Siederdissen, C., Tafer, H., Flamm, C., Stadler, P. F., et al. (2011). ViennaRNA Package 2.0. *Algorithms Mol. Biol.* 6:26. doi: 10.1186/1748-7188-6-26

Lu, H., Giordano, F., and Ning, Z. (2016). Oxford nanopore MinION sequencing and genome assembly. *Genom. Proteom. Bioinform.* 14, 265–279. doi: 10.1016/j.gpb.2016.05.004

Ma, K., Zhang, Q., Cheng, T., and Wang, J. (2018). Identification of transposons near predicted lncRNA and mRNA pools of *Prunus mume* using an integrative transposable element database constructed from Rosaceae plant genomes. *Mol. Genet. Genomics* 293, 1301–1316. doi: 10.1007/s00438-018-1449-y

Majoros, W. H., Pertea, M., and Salzberg, S. L. (2004). TigrScan and GlimmerHMM: two open source *ab initio* eukaryotic gene-finders. *Bioinformatics* 20, 2878–2879. doi: 10.1093/bioinformatics/bth315

McCarthy, E. M., and McDonald, J. F. (2003). LTR_STRUC: a novel search and identification program for LTR retrotransposons. *Bioinformatics* 19, 362–367. doi: 10.1093/bioinformatics/btf878

Meyers, B. C., Axtell, M. J., Bartel, B., Bartel, D. P., Baulcombe, D., Bowman, J. L., et al. (2008). Criteria for annotation of plant microRNAs. *Plant Cell* 20, 3186–3190. doi: 10.1105/tpc.108.064311

Moriya, Y., Itoh, M., Okuda, S., Yoshizawa, A. C., and Kanehisa, M. (2007). KAAS: an automatic genome annotation and pathway reconstruction server. *Nucleic Acids Res.* 35, W182–W185. doi: 10.1093/nar/gkm321

Naithani, S., Gupta, P., Preece, J., D'Eustachio, P., Elser, J. L., Garg, P., et al. (2020). Plant Reactome: a knowledgebase and resource for comparative pathway analysis. *Nucleic Acids Res.* 48, D1093–D1103. doi: 10.1093/nar/gkz996

Nakamura, N., Hirakawa, H., Sato, S., Otagaki, S., Matsumoto, S., Tabata, S., et al. (2018). Genome structure of *Rosa multiflora*, a wild ancestor of cultivated roses. *DNA Res.* 25, 113–121. doi: 10.1093/dnares/dsx042

Nakano, M., McCormick, K., Demirci, C., Demirci, F., Gurazada, S. G. R., Ramachandruni, D., et al. (2020). Next-generation sequence databases: RNA and genomic informatics resources for plants. *Plant Physiol.* 182, 136–146. doi: 10.1104/pp.19.00957

Nawrocki, E. P., and Eddy, S. R. (2013). Infernal 1.1: 100-fold faster RNA homology searches. *Bioinformatics* 29, 2933–2935. doi: 10.1093/bioinformatics/btt509

Ou, C., Wang, F., Wang, J., Li, S., Zhang, Y., Fang, M., et al. (2019). A *de novo* genome assembly of the dwarfing pear rootstock Zhongai 1. *Sci. Data* 6:281. doi: 10.1038/s41597-019-0291-3

Pinosio, S., Marroni, F., Zuccolo, A., Vitulo, N., Mariette, S., Sonnante, G., et al. (2020). A draft genome of sweet cherry (*Prunus avium* L.) reveals genome-wide and local effects of domestication. *Plant J.* 103, 1420–1432. doi: 10.1111/tpj.14809

Raymond, O., Gouzy, J., Just, J., Badouin, H., Verdenaud, M., Lemainque, A., et al. (2018). The Rosa genome provides new insights into the domestication of modern roses. *Nat. Genet.* 50, 772–777. doi: 10.1038/s41588-018-0110-3

Rhoads, A., and Au, K. F. (2015). PacBio sequencing and its applications. *Genom. Proteom. Bioinform.* 13, 278–289. doi: 10.1016/j.gpb.2015.08.002

Sánchez-Pérez, R., Pavan, S., Mazzeo, R., Moldovan, C., Cigliano, R. A., Cueto, J. D., et al. (2019). Mutation of a bHLH transcription factor allowed almond domestication. *Science* 364, 1095–1098. doi: 10.1126/science.aav8197

Sayers, E. W., Cavanaugh, M., Clark, K., Ostell, J., Pruitt, K. D., and Karsch-Mizrachi, I. (2020). GenBank. *Nucleic Acids Res.* 48, D84–D86. doi: 10.1093/nar/gkaa1023

Schläpfer, P., Zhang, P., Wang, C., Kim, T., Banf, M., Chae, L., et al. (2017). Genome-wide prediction of metabolic enzymes, pathways, and gene clusters in plants. *Plant Physiol.* 173, 2041–2059. doi: 10.1104/pp.16.01942

Shahan, R., Zawora, C., Wight, H., Sittmann, J., Wang, W., Mount, S. M., et al. (2018). Consensus coexpression network analysis identifies key regulators of flower and fruit development in wild strawberry. *Plant Physiol.* 178, 202–216. doi: 10.1104/pp.18.00086

Shirasawa, K., Esumi, T., Hirakawa, H., Tanaka, H., Itai, A., Ghelfi, A., et al. (2019). Phased genome sequence of an interspecific hybrid flowering cherry, 'Somei-Yoshino' (*Cerasus* × *yedoensis*). *DNA Res.* 26, 379–389. doi: 10.1093/dnares/dsz016

Shirasawa, K., Isuzugawa, K., Ikenaga, M., Saito, Y., Yamamoto, T., Hirakawa, H., et al. (2017). The genome sequence of sweet cherry (*Prunus avium*) for use in genomics-assisted breeding. *DNA Res.* 24, 499–508. doi: 10.1093/dnares/dsx020

Shulaev, V., Sargent, D. J., Crowhurst, R. N., Mockler, T. C., Folkerts, O., Delcher, A. L., et al. (2011). The genome of woodland strawberry (*Fragaria vesca*). *Nat. Genet.* 43, 109–116. doi: 10.1038/ng.740

Solovyev, V., Kosarev, P., Seledsov, I., and Vorobyev, D. (2006). Automatic annotation of eukaryotic genes, pseudogenes and promoters. *Genome Biol.* 7:S10. doi: 10.1186/gb-2006-7-s1-s10

Soundararajan, P., Won, S. Y., and Kim, J. S. (2019). Insight on Rosaceae Family with genome sequencing and functional genomics perspective. *BioMed. Res. Int.* 2019:e7519687. doi: 10.1155/2019/7519687

Szcześniak, M. W., Rosikiewicz, W., and Makałowska, I. (2016). CANTATAdb: a collection of plant long non-coding RNAs. *Plant Cell Physiol.* 57:e8. doi: 10.1093/pcp/pcv201

Tang, H., Lyons, E., and Town, C. D. (2015). Optical mapping in plant comparative genomics. *GigaScience* 4:3. doi: 10.1186/s13742-015-0044-y

Tatusova, T. A., Karsch-Mizrachi, I., and Ostell, J. A. (1999). Complete genomes in WWW Entrez: data representation and analysis. *Bioinformatics* 15, 536–543. doi: 10.1093/bioinformatics/15.7.536

Tennessen, J. A., Govindarajulu, R., Ashman, T.-L., and Liston, A. (2014). Evolutionary origins and dynamics of octoploid strawberry subgenomes revealed by dense targeted capture linkage maps. *Genome Biol. Evol.* 6, 3295–3313. doi: 10.1093/gbe/evu261

Tian, F., Yang, D.-C., Meng, Y.-Q., Jin, J., and Gao, G. (2020). PlantRegMap: charting functional regulatory maps in plants. *Nucleic Acids Res.* 48, D1104–D1113. doi: 10.1093/nar/gkz1020

Van Bel, M., Diels, T., Vancaester, E., Kreft, L., Botzki, A., Van de Peer, Y., et al. (2018). PLAZA 4.0: an integrative resource for functional, evolutionary and comparative plant genomics. *Nucleic Acids Res.* 46, D1190–D1196. doi: 10.1093/nar/gkx1002

VanBuren, R., Wai, C. M., Colle, M., Wang, J., Sullivan, S., Bushakra, J. M., et al. (2018). A near complete, chromosome-scale assembly of the black raspberry (*Rubus occidentalis*) genome. *GigaScience* 7:giy094. doi: 10.1093/gigascience/giy094

Velasco, R., Zharkikh, A., Affourtit, J., Dhingra, A., Cestaro, A., Kalyanaraman, A., et al. (2010). The genome of the domesticated apple (*Malus* × *domestica* Borkh.). *Nat. Genet.* 42, 833–839. doi: 10.1038/ng.654

Verde, I., Abbott, A. G., Scalabrin, S., Jung, S., Shu, S., Marroni, F., et al. (2013). The high-quality draft genome of peach (*Prunus persica*) identifies unique patterns of genetic diversity, domestication and genome evolution. *Nat. Genet.* 45, 487–494. doi: 10.1038/ng.2586

Verde, I., Jenkins, J., Dondini, L., Micali, S., Pagliarani, G., Vendramin, E., et al. (2017). The Peach v2.0 release: high-resolution linkage mapping and deep resequencing improve chromosome-scale assembly and contiguity. *BMC Genomics* 18:225. doi: 10.1186/s12864-017-3606-9

Wang, J., Liu, W., Zhu, D., Hong, P., Zhang, S., Xiao, S., et al. (2020a). Chromosome-scale genome assembly of sweet cherry (*Prunus avium* L.) cv. Tieton obtained using long-read and Hi-C sequencing. *Hortic. Res.* 7:122. doi: 10.1038/s41438-020-00343-8

Wang, J., Liu, W., Zhu, D., Zhou, X., Hong, P., Zhao, H., et al. (2020b). A *de novo* assembly of the sweet cherry (*Prunus avium* cv. Tieton) genome using linked-read sequencing technology. *PeerJ* 8, e9114. doi: 10.7717/peerj.9114

Wang, Y. (2017). PlantRGDB: a database of plant retrocopied genes. *Plant Cell Physiol.* 58:e2. doi: 10.1093/pcp/pcw210

Wight, H., Zhou, J., Li, M., Hannenhalli, S., Mount, S. M., and Liu, Z. (2019). Draft genome assembly and annotation of red raspberry *Rubus idaeus*. *bioRxiv* 546135. doi: 10.1101/546135

Wu, J., Wang, Z., Shi, Z., Zhang, S., Ming, R., Zhu, S., et al. (2013). The genome of the pear (*Pyrus bretschneideri* Rehd.). *Genome Res.* 23, 396–408. doi: 10.1101/gr.144311.112

Xia, R., Ye, S., Liu, Z., Meyers, B. C., and Liu, Z. (2015). Novel and recently evolved microRNA clusters regulate expansive F-BOX gene networks through phased small interfering RNAs in wild diploid strawberry. *Plant Physiol.* 169, 594–610. doi: 10.1104/pp.15.00253

Xia, R., Zhu, H., An, Y., Beers, E. P., and Liu, Z. (2012). Apple miRNAs and tasiRNAs with novel regulatory networks. *Genome Biol.* 13:R47. doi: 10.1186/gb-2012-13-6-r47

Xiang, Y., Huang, C.-H., Hu, Y., Wen, J., Li, S., Yi, T., et al. (2017). Evolution of Rosaceae fruit types based on nuclear phylogeny in the context of geological times and genome duplication. *Mol. Biol. Evol.* 34, 262–281. doi: 10.1093/molbev/msw242

Xu, Z., and Wang, H. (2007). LTR_FINDER: an efficient tool for the prediction of full-length LTR retrotransposons. *Nucleic Acids Res.* 35, W265–W268. doi: 10.1093/nar/gkm286

Xue, H., Wang, S., Yao, J.-L., Deng, C. H., Wang, L., Su, Y., et al. (2018). Chromosome level high-density integrated genetic maps improve the *Pyrus bretschneideri* 'DangshanSuli' v1.0 genome. *BMC Genomics* 19:833. doi: 10.1186/s12864-018-5224-6

Yuan, H., Yu, H., Huang, T., Shen, X., Xia, J., Pang, F., et al. (2019). The complexity of the *Fragaria x ananassa* (octoploid) transcriptome by single-molecule long-read sequencing. *Hortic. Res.* 6:46. doi: 10.1038/s41438-019-0126-6

Zhang, L., Hu, J., Han, X., Li, J., Gao, Y., Richards, C. M., et al. (2019). A high-quality apple genome assembly reveals the association of a retrotransposon and red fruit colour. *Nat. Commun.* 10:1494. doi: 10.1038/s41467-019-09518-x

Zhang, Q., Chen, W., Sun, L., Zhao, F., Huang, B., Yang, W., et al. (2012). The genome of *Prunus mume*. *Nat. Commun.* 3:1318. doi: 10.1038/ncomms2290

Conflict of Interest: The authors declare that the research was conducted in the absence of any commercial or financial relationships that could be construed as a potential conflict of interest.

frontiers in Plant Science

ORIGINAL RESEARCH
published: 07 April 2021
doi: 10.3389/fpls.2021.652959

The MADS-Box Transcription Factor *EjAGL65* Controls Loquat Flesh Lignification *via* Direct Transcriptional Inhibition of *EjMYB8*

*Hang Ge[1,2,3], Yan-na Shi[2,3], Meng-xue Zhang[2,3], Xian Li[2,3], Xue-ren Yin[2,3] and Kun-song Chen[2,3]**

[1]Zhejiang Provincial Key Laboratory of Biometrology and Inspection & Quarantine, College of Life Sciences, China Jiliang University, Hangzhou, China, [2]Zhejiang Provincial Key Laboratory of Horticultural Plant Integrative Biology, Zhejiang University, Zijingang Campus, Hangzhou, China, [3]The State Agriculture Ministry Laboratory of Horticultural Plant Growth, Development and Quality Improvement, Zhejiang University, Zijingang Campus, Hangzhou, China

Loquat fruit accumulates lignin in its flesh when undergoing chilling injury during postharvest storage, making it a suitable model for the study of flesh lignification. Transcriptional regulation of lignin biosynthesis is principally controlled by the NAC-MYB transcriptional cascade in model plants. Previous research has demonstrated that EjMYB8 activates lignin biosynthesis through direct interaction with the promoter of *Ej4CL1*. However, the classic NAC-MYB gene regulation network has not been established. Here, the MADS-box gene *EjAGL65* was discovered by screening a cDNA library using the *EjMYB8* promoter as bait in yeast. A phylogenetic analysis and structural comparisons revealed that *EjAGL65* belongs to the Mδ subgroup of the MADS-box family, whose members have not been reported as being involved in the regulation of lignin deposition. *EjAGL65* transcription was downregulated at 0°C compared to 5°C, indicating a negative correlation with the change of lignin content. A dual-luciferase assay indicated that *EjAGL65* is capable of inhibiting the promoter activity of *EjMYB8 in vivo*. These results showed that the Mδ MADS-box gene *EjAGL65* transcriptionally regulates *EjMYB8* during postharvest chilling induced flesh lignification, which differs from the classical regulation model of lignin biosynthesis that has been illustrated for developmental lignin accumulation.

Keywords: loquat, MADS, MYB, chilling injury, lignin biosynthesis, Mδ subgroup

OPEN ACCESS

Edited by:
Jia-Long Yao,
The New Zealand Institute for Plant and Food Research Ltd, New Zealand

Reviewed by:
Yongping Cai,
Anhui Agricultural University, China
Igor Cesarino,
University of São Paulo, Brazil

****Correspondence:***
Kun-song Chen
akun@zju.edu.cn

Specialty section:
This article was submitted to Plant Development and EvoDevo, a section of the journal Frontiers in Plant Science

Received: *26 January 2021*
Accepted: *19 March 2021*
Published: *07 April 2021*

Citation:
Ge H, Shi Y-n, Zhang M-x, Li X, Yin X-r and Chen K-s (2021) The MADS-Box Transcription Factor EjAGL65 Controls Loquat Flesh Lignification via Direct Transcriptional Inhibition of EjMYB8. Front. Plant Sci. 12:652959. doi: 10.3389/fpls.2021.652959

INTRODUCTION

Lignin is a pivotal component of vascular tissues that enabled plants to conquer dry land by reinforcing cell walls. In most cases, a lack of lignin may trigger severe defects in plant development. For example, disruption of lignin biosynthesis results in dwarfism in *Arabidopsis* (Im Kim et al., 2014) and crops, such as rice, suffer lodging due to low lignin deposition in stems (Peng et al., 2014). Although lignin is important for plant growth and development, it may negatively affect the quality of plant products. Many studies have attempted to alleviate the lignification progress in edible plant organs such as fruit (Dangcham et al., 2008; Cao et al., 2010; Suo et al., 2018). Loquat is a fruit common in China that is sensitive to low temperature.

During postharvest storage and transportation, the flesh of loquat fruit readily lignifies if injured by chilling or mechanical force, which limits the distance the fruit can be transported. Lignified flesh becomes less juicy and hard to chew, resulting in the deterioration of fruit quality (Jin et al., 2014; Cao et al., 2018). Due to the negative impact on the postharvest storage of loquat, the molecular mechanism underlying flesh lignification must be determined.

Lignin deposition is a complicated process that includes monolignol synthesis and polymerization. Monolignols are synthesized from phenylalanine *via* the phenylpropanoid pathway in the cytoplasm before they are transported to the apoplast where they undergo oxidation before incorporation into the lignin polymer. The amino group of phenylalanine is first removed by phenylalanine ammonia-lyase (PAL), and *p*-coumaric acid is generated by adding a hydroxyl group to the C_4 position of the aromatic ring by cinnamate 4-hydroxylase (C4H). The *p*-coumaric acid is then catalyzed sequentially by 4-coumarate: coenzyme A (CoA) ligase (4CL), *p*-hydroxycinnamoyl-CoA: quinate shikimate *p*-hydroxycinnamoyltransferase (HCT), *p*-coumarate 3-hydroxylase (C3H), caffeoyl-CoA *O*-methyltransferase (CCoAOMT), cinnamoyl-CoA reductase (CCR), and ferulate 5-hydroxylase (F5H), caffeic acid *O*-methyltransferase (COMT), which results in methyl oxidation in the aromatic ring at the C_3 (coniferaldehyde) site or both the C_3 and C_5 (sinapaldehyde) sites. The *p*-coumaraldehyde can only be converted by 4CL and CCR using *p*-coumaric acid as the substrate. Finally, the products of aldehydes are reduced to alcohols by cinnamyl alcohol dehydrogenase (CAD), generating *p*-coumaryl alcohol, coniferyl alcohol, and sinapyl alcohol (Boerjan et al., 2003; Vanholme et al., 2019). These monomers are oxidized/radicalized by peroxidase (PRX) and laccase (LAC), followed by polymerization *via* oxidative coupling. Several genes encoding key lignin biosynthetic enzymes, such as *Ej4CL1* (Li et al., 2017) and *EjCAD5* (Xu et al., 2019b), have been identified and play a role in loquat flesh lignification; *Ej4CL1* encodes 4CL, which catalyzes *p*-coumaric acid to *p*-coumaroyl-CoA. *EjCAD5* encodes CAD, which converts *p*-coumaraldehyde, coniferaldehyde, and sinapaldehyde to their alcohol forms. Transcript abundance of these genes increases under chilling injury, which is in accordance with the higher lignin content and increased fruit firmness. Nevertheless, it is unknown how these enzymes are precisely regulated.

Flesh lignification is intensely regulated at the transcriptional level. Some evidence has been found indicating the involvement of various transcription factor families in the regulation of lignin biosynthesis. According to previous studies, ectopic expression of MYB (Xu et al., 2014b; Wang et al., 2016), NAC (NAM, ATAF1, ATAF2, and CUC2; Ge et al., 2017), APETALA2/Ethylene Response Factor (AP2/ERF; Zeng et al., 2015; Zhang et al., 2020), Heat Shock Factor (HSF; Zeng et al., 2016), and Homobox from *Arabidopsis thaliana* (HAT; Xu et al., 2019b) family members in loquat flesh resulted in changes in the expression of phenylpropanoid pathway genes. For example, the transcripts of *Ej4CL1* can be induced by EjERF39 and EjHSF1 or repressed by EjAP2-1 and EjbHLH1, resulting in changes in the lignin content (Zeng et al., 2015, 2016; Xu et al., 2019b; Zhang et al., 2020). EjNAC3 and EjHAT1 can modify the expression of *EjCAD*-like and *EjCAD5*, respectively (Ge et al., 2017; Xu et al., 2019b). Although these transcription factors may be regulators of the phenylpropanoid pathway, most cannot physically interact with promoters of target genes on their own, indicating that mediators are required.

Recent publications have shown that MYB family proteins are mediators of most critical regulators of flesh lignification (Kamdee et al., 2014; Zhang et al., 2016). Through binding to the AC elements located in the promoter region, MYB family members provide other transcription factors with physical routes by which they can regulate the transcripts of *Ej4CL1*. For example, by protein interaction with EjMYB1, EjAP2-1 suppresses the EjMYB1-induced expression of *Ej4CL1* (Zeng et al., 2015). Similarly, EjbHLH1 inhibits the transcription of *Ej4CL1* by forming a protein complex with EjMYB2 (Xu et al., 2019a). In addition, the transcripts of *Ej4CL1* that increased due to *EjMYB8* could be further induced by the synergism between EjERF39 and EjMYB8 (Zhang et al., 2020). Thus, lignin biosynthesis can be regulated by protein-protein interactions with MYBs, which is a strategy frequently adopted by transcription factors that cannot directly bind to promoters of genes in the phenylpropanoid pathway.

Despite the numerous studies conducted on manipulating the biological functions of MYB members at the protein-protein level, limited research has been conducted on proteins that transcriptionally regulate MYB genes during flesh lignification. It is widely accepted that NAC domain proteins play a role in the development of the secondary cell wall by affecting transcript abundance of multiple MYB genes (Boerjan et al., 2003; Li et al., 2015; Yang et al., 2017). For instance, *AtMYB58* and *AtMYB63* directly control the monolignol biosynthesis gene *At4CL1*, and *AtMYB58* and *AtMYB63* are both regulated by the secondary cell wall master switch gene AtSND1, which represents a part of the complex NAC-MYB cascade (Zhou et al., 2009). Although several lignification-related NAC family members have been characterized in the loquat lignification process, interactions between NACs and MYBs have not yet been identified. EjNAC3 has been found to directly bind to *EjCAD*-like instead of forming a NAC-MYB cascade (Ge et al., 2017). The findings from studies on loquat support the hypothesis that the regulation of stress induced lignin deposition differs from that of developmental lignin (Cesarino, 2019). Though common regulators are employed, such as MYB and NAC genes, there may be novel regulators involved in regulating stress induced lignification. Therefore, further information is needed on partners that interact with *EjMYBs* to form a transcriptional cascade.

MADS-box genes constitute an important group of transcriptional regulators that have been characterized as regulators of plant morphology (Yu, et al., 2014), flower development (Pelaz et al., 2000), flowering time (Michaels and Amasino, 1999), fruit development, and ripening (Gimenez et al., 2010; Martel et al., 2011). Generally, MADS-box genes are rarely considered as regulators of lignin deposition. Although a thinner pericarp with altered lignin content was observed in tomato fruit with a silenced *TAGL1* MADS-box

gene (Gimenez et al., 2010), the detailed mechanism whereby MADS-box genes regulate components of the secondary cell wall remains unclear.

In the present study, the upstream regulators of a potent activator of lignin, EjMYB8, were investigated, with the aim of discovering the cascade regulation model. Using yeast one-hybrid screening, a MADS-box domain protein EjAGL65 was discovered to physically interact with the promoter region of *EjMYB8*. According to phylogenetic analyses, EjAGL65 was the most similar to AtAGL65, which belongs to the Mδ subgroup of the MADS-box family. Transcript abundance of *EjAGL65* was monitored at 0 and 5°C, two treatments that promote and alleviate lignification, respectively. The expression pattern of *EjAGL65* showed a negative correlation with lignin content and fruit firmness. A dual-luciferase assay confirmed that EjAGL65 inhibited the activity of both *EjMYB8* and the *Ej4CL1* promoter. These results revealed the involvement of MADS-box genes and the novel MADS-MYB transcriptional cascade in fruit flesh lignification.

MATERIALS AND METHODS

Plant Materials and Treatments

Loquat fruits from *Eriobotrya japonica* Lindl. cultivar "LYQ" were collected in Luqiao, Zhejiang Province, China. The fruits and treatments were previously described in Xu et al. (2014b). Generally, the fruits were selected for uniformity and divided into two batches with approximately 150 fruits in each batch. One batch was kept at 5°C, while the other at 0°C, as the control. Fruits were sampled at 0, 1, 2, 4, and 6 days of storage. At each time point, 15 fruits with the pericarp and seeds removed were sampled; therefore, there were three mixed flesh groups containing five fruits each as three biological replicates. The collected flesh samples were immediately frozen in liquid nitrogen and stored at −80°C until use.

Yeast One-Hybrid Screening and Confirmation

Yeast one-hybrid screening was performed using the Matchmaker Gold Yeast One-Hybrid Library Screening System (Clontech, Mountain View, CA, United States). The promoter of *EjMYB8* was isolated using the GenomeWalker universal kit (Clontech) then inserted into the pAbAi vector. Primers used for genome walking and pAbAi construction are listed in **Supplementary Tables S1, S2**, respectively. The recombinant *EjMYB8*-pAbAi vector was linearized and transformed into a Y1HGold yeast strain. After testing for autoactivation, 100 ng/ml Aureobasidin A (AbA) was used for library screening (**Supplementary Figure S1**). The Y1HGold[*EjMYB8*/AbAi] yeast strain was transfected together with the cDNA library, which was previously constructed by Zhang et al. (2016). After 5 days of growth at 30°C, every individual yeast colony was picked for PCR analysis and then sequenced by Huajin Company (Shanghai, China). The obtained cDNA fragments were used for an *in silico* search for annotations using the Basic Local Alignment Search Tool.[1] Five putative transcription factors were selected for further confirmation (listed in **Supplementary Table S3**). Primers designed for full-length CDS isolation and construction of pGADT7 vectors were listed in **Supplementary Tables S4, S5**, respectively. The obtained sequences were uploaded to the NCBI database (GenBank numbers are given in **Supplementary Table S6**).

To confirm true positive interactions, we separately transformed pGADT7 vectors with the genes listed in **Supplementary Table S5** into the Y1HGold [*EjMYB8*/pAbAi] yeast strain. Empty pGADT7 plasmids were transformed as the negative control. Transformed yeast was grown on SD/-Leu medium containing 100 ng/ml of AbA.

Phylogenetic Analysis

Additional nine MADS-box genes were added to the previously reported 107 MADS-box genes by searching the TAIR database.[2] A total of 116 *Arabidopsis* and two Populus MADS-box genes were used in the phylogenetic analysis (**Supplementary Table S7**). The analysis was completed by the ClustalX v1.81. The protein sequence of EjAGL65 was aligned with 116 MADS-box genes using the default settings of gap open and gap extension cost, and the Blosum 30 was selected as the protein weight matrix. A phylogenetic tree was constructed using the neighbor-joining (NJ) method, and the bootstrap value was set to 1,000. Results of the alignments were visualized using Figtree v1.4.4.[3]

RNA Extraction and cDNA Synthesis

The "LYQ" flesh samples collected at each time point were used for total RNA extraction following the method described by Shan et al. (2008). Potential genomic DNA contamination was eliminated using the TURBO DNA-free kit (Ambion, Austin, TX, United States). The quality and quantity of freshly extracted RNA were determined by gel electrophoresis and spectrophotometry, respectively (Implen, Westlake Village, CA, United States). A total of 1 μg DNA-free RNA were used to synthesize first-strand cDNA using the iScript cDNA Synthesis Kit (Bio-Rad, Hercules, CA, United States). A 10-fold dilution of cDNA was made prior to the real-time PCR analysis.

Real-Time PCR Analysis

Real-time PCR was carried out using the CFX96 Real-Time System (Bio-Rad) with SsoFast EvaGreen Supermix (Bio-Rad). The reaction mixture contained 10 μl SYBR PCR supermix, 6 μl diethylpyrocarbonate-treated H_2O, 2 μl diluted cDNA template, and 1 μl of each primer (10 μM). Primers used for real-time PCR were designed using Primer3 (version 4.0.0) and are listed in **Supplementary Table S8**.[4] The primers were tested to ensure their specificity for unique genes (Yin et al., 2010). The real-time PCR program was set as follows: a

[1]https://www.ncbi.nlm.nih.gov/
[2]https://www.arabidopsis.org/
[3]http://tree.bio.ed.ac.uk/software/figtree/
[4]http://bioinfo.ut.ee/primer3/

pre-denaturation step of 95°C for 30 s, followed by for 45 cycles of 95°C for 10 s and 60°C for 10 s. A melting curve analysis was also conducted. Three biological replicates were collected from the data from each time point.

Dual-Luciferase Assay

Dual-luciferase assays were performed as described previously (Min et al., 2014). Full-length *EjAGL65* genes were amplified with the primers listed in **Supplementary Table S9** and integrated into the pGreen II 0029 62-SK vector (SK). The promoter of *EjMYB1*, *EjMYB2*, and *EjMYB8* was individually inserted into the pGreen II 0800-LUC vector (LUC). The LUC vectors containing promoters of lignin biosynthesis genes in *Arabidopsis* were constructed by Xu et al. (2014b).

All of the recombinant SK and LUC vectors were transfected into *Agrobacterium tumefaciens* GV3101 and stored as glycerol stocks. Transfected *Agrobacterium* cultures were grown on LB plates containing 50 μg/ml kanamycin and 25 μg/ml gentamycin for 2 days, then restreaked on new LB plates and grown for 1 day. *Agrobacterium* cultures were suspended in infiltration buffer (10 mM MES, 10 mM $MgCl_2$, 150 mM acetosyringone, pH 5.6) to optimal density (OD_{600} = 0.75), then 1 ml *Agrobacterium* culture containing transcription factors was mixed with 100 μl *Agrobacterium* containing promoters. Finally, the mixtures were injected into tobacco leaves with needleless syringes. Three days after infiltration, the fluorescence intensity of LUC and REN were measured using dual luciferase assay reagents (Promega, Madison, WI, United States). Five replicates were conducted for each transcription factor and promoter combination.

Statistical Analysis

OriginPro 2020 software (Microcal Software Inc., Northampton, MA, United States) was used to perform statistical analyses and to draw figures. Student's *t*-tests were conducted on data from luciferase assays; differences were considered significant at 5%. One-way ANOVA followed by means comparison using a Tukey's test was applied for comparing data from real-time PCR at the 5% confidence level. The average value and SE of three replicates were calculated using Excel 2017 (Microsoft, Seattle, WA, United States).

RESULTS

Screening Potential Targets of *EjMYB8*

Previous research has demonstrated that NAC and MYB genes mediate lignification in loquat flesh (Xu et al., 2014b), but the classic NAC-MYB transcription cascade has not been previously revealed. Here, we chose to identify the upstream regulators of *EjMYB8* because of its significance in cold triggered expression by yeast one-hybrid screening (Wang et al., 2016). The promoter region of *EjMYB8* was integrated into the Y1HGold yeast strain, and we performed a screening under the stress of 100 ng/ml AbA to eliminate the background growth of yeast. Following the amplification of library fragments by yeast colony PCR, a total of 32 colonies were sequenced and annotated (listed in **Supplementary Table S10**). We chose five putative transcription factors for further confirmation. Consequently, a MADS-box domain-containing protein (GenBank No. MF942415) was identified as having a positive interaction with the promoter of *EjMYB8*; the other four proteins had false-positive results (**Figure 1**).

Phylogenetic Analysis of EjAGL65

Previous studies have shown that MADS-box genes are further classified into five subgroups, named MIKC, Mα, Mβ, Mγ, and Mδ, based on four conserved domains in *Arabidopsis* (Parenicová et al., 2003), and each group has a unique biological function. To predict the potential function of the MADS-box domain gene, we conducted a phylogenetic analysis. By comparing the amino acid sequence with MADS-box isoforms in *Arabidopsis*, we found that the *EjMYB8*-associated loquat MADS-box protein clustered with AtAGL65, AtAGL30, and AtAGL94, which are in the Mδ subgroup (**Figure 2**). Therefore, the newly identified MADS-box gene was named *EjAGL65*. AtAGL65, which is the putative ortholog of EjAGL65, forms a heterodimer with AtAGL104

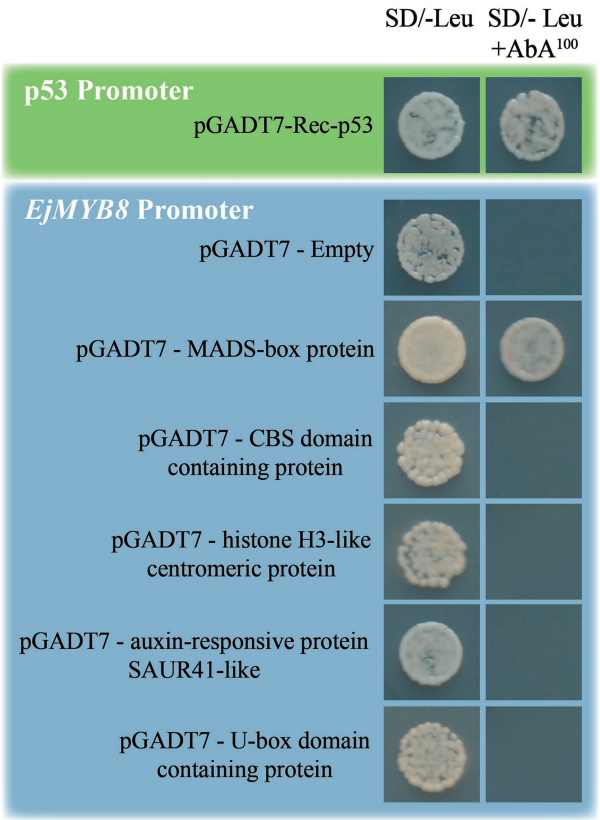

FIGURE 1 | A yeast one-hybrid analysis was used to identify a MADS-box protein, which binds the *EjMYB8* promoter. Sequences of five genes were inserted individually into the pGADT7 vector then transformed into Y1HGold[pro-*EjMYB8*] for an *in vivo* Protein-DNA binding assay based on the results of the yeast one-hybrid library screening. Growth of yeast on SD/-Leu plates with 100 ng/ml Aureobasidin A (AbA) indicates that the interaction is genuinely positive. The promoter of p53 was also transformed into yeast as the positive control. The negative control was an empty pGADT7 vector.

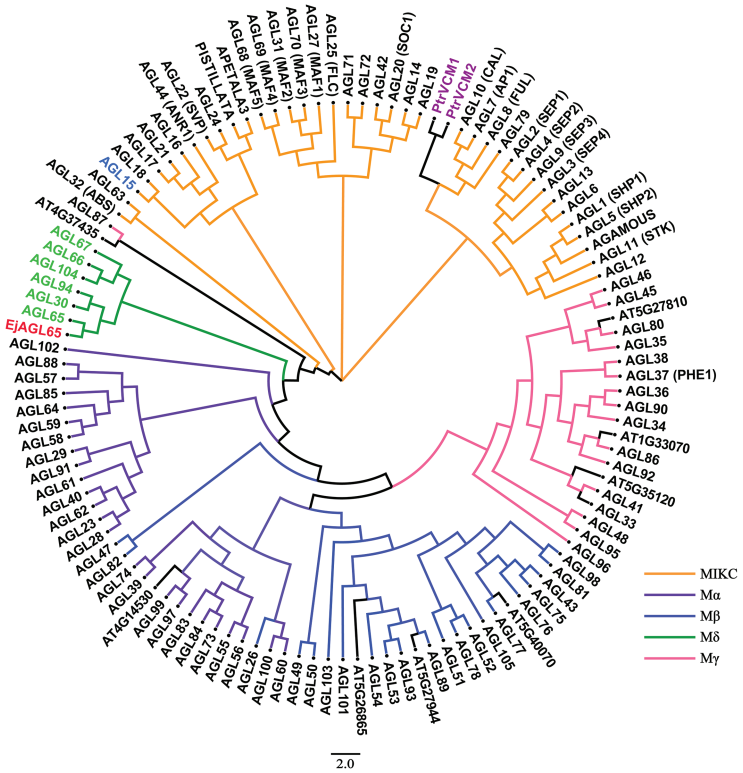

FIGURE 2 | Phylogenetic analysis of EjAGL65 with 116 *Arabidopsis* MADS-box proteins and two Populus MADS-box proteins. The previously defined Mδ group genes are shown in green. EjAGL65 was structurally closest to *Arabidopsis* AGL65 (At1g18750) and is shown in red. AGL15 (At5g13790), which was expressed in the lignified tissue of *Arabidopsis*, is shown in blue. PtrVCM1 and PtrVCM2, which affect vascular cambium proliferation activity, are in purple. The color of clades represents MIKC (orange), Mα (violet), Mβ (blue), Mδ (green), and Mγ (pink) subgroups of *Arabidopsis* MADS-box genes. Genes without annotations are labeled with an ID from the TAIR database.

and regulates pollen activity (Adamczyk and Fernandez, 2009). Besides, the MIKC group gene AtAGL15 regulates the class III peroxidase *PRX17* and the knockout line *prx17* showed reduced lignin content in the stem and siliques. The expression level of *PRX17* is downregulated in a 35S:AGL15 line, indicating the involvement of AtAGL15 in lignin metabolism (Cosio et al., 2017). However, EjAGL65 was not clustered with AtAGL15. These findings indicate that the EjAGL65 may not affect monolignol polymerization. The putative ortholog of EjAGL65 in *Arabidopsis* is not thought to be lignin-related.

Association Between Lignin Accumulation and Expression of *EjAGL65*

The expression of *EjAGL65* was investigated to determine whether it responds to chilling injury, which is critical evidence in support of it regulating chilling-induced lignification. Treatments at 0 and 5°C were routinely applied when characterizing candidate genes that relate to chilling injury of loquat fruits because 0°C induces lignification, while 5°C alleviates it (Cai et al., 2006). As shown in **Figure 3**, the average transcripts of *EjAGL65* decreased at 0°C on the first and second days, though the difference was not significant according to Turkey's test. The transcription of *EjAGL65* did not decrease at 5°C during the first 2 days of treatment, followed by significant increases later. Based on its expression profile, *EjAGL65* was more sensitive to treatment at 0°C than 5°C. Xu et al. (2014b) tested fruit firmness and lignin content using the same batch of materials. The firmness and lignin content increased rapidly at 0 and 5°C during the first 2 days, which was opposite from the observed change of *EjAGL65* transcripts. This information indicates that *EjAGL65* is negatively correlated with changes in fruit firmness and lignin content. In addition, the decrease in *EjAGL65* transcripts stopped after 4 days of storage at 0°C, indicating an unknown mechanism preventing *EjAGL65* transcripts from continuously decreasing. *EjAGL65* is a candidate negative regulator of the cold-induced lignification process in loquat fruit flesh.

Regulation of *EjAGL65* on Promoters of *EjMYB8* and Lignin Biosynthesis-Related Genes

Possible regulatory actions of EjAGL65 were tested with the promoter of *EjMYB8* because of the direct binding confirmed in the yeast one-hybrid assay. The dual-luciferase assay showed that the activity of the *EjMYB8* promoter was significantly repressed after transient overexpression of *EjAGL65*. We also tested the promoter activity of *EjMYB1* and *EjMYB2*, another two EjMYB members related to lignin. However, the transient

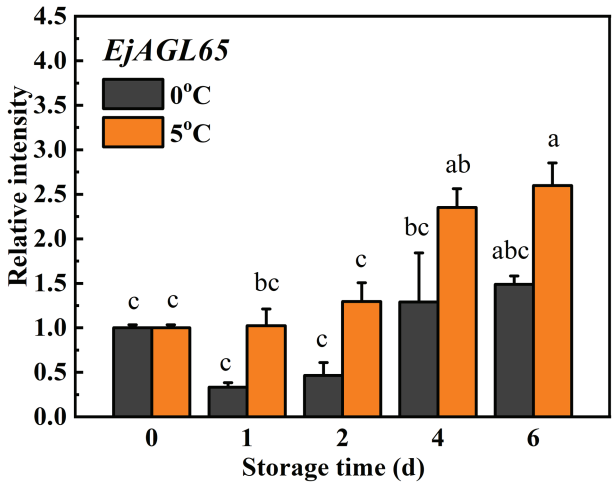

FIGURE 3 | Expression of *EjAGL65* in response to temperature treatments at 0°C (control) and 5°C in "LYQ" loquat. Transcript levels of *EjAGL65* before the temperature treatment were set to 1. Error bars indicate the SE of three biological replicates. One-way ANOVA followed by Tukey's comparison was performed at $p = 0.05$.

overexpression of EjAGL65 did not significantly change the promoter activity of *EjMYB1* and *EjMYB2* (**Figure 4**).

Ej4CL1 is a key gene for loquat fruit lignification and the direct target of EjMYB8. The interaction between EjAGL65 and the promoter of *Ej4CL1* was also tested to further characterize the effect of EjAGL65 on the *Ej4CL1* promoter without EjMYB8. Protein-DNA interaction was analyzed using a yeast one-hybrid assay and dual-luciferase assay. Consequently, the activity of the *Ej4CL1* promoter was slightly but not significantly reduced due to the transient overexpression of EjAGL65 (**Figure 4**). In addition, EjAGL65 cannot bind the promoter of *Ej4CL1 in vivo* as shown by the yeast one-hybrid assay (**Supplementary Figure S2**), suggesting that EjAGL65 alone is not sufficient to affect the activity of the *Ej4CL1* promoter.

In addition, we chose the well-defined lignin biosynthesis-related genes from *Arabidopsis* to discover potential regulatory targets of EjAGL65. Consequently, most of the promoter activity of selected genes could not be regulated by EjAGL65. It is unclear whether the statistically significant activity against *AtC4H* and *AtCCR1* promoters (marked with asterisks in **Figure 5**) is sufficient to alter the biological function. Overall, the target preference of *EjAGL65* suggests it might selectively affect transcription factors, such as MYB family members, rather than structural genes of lignin biosynthesis.

DISCUSSION

Confirmation of a MADS-Box Gene Manipulating Lignin Biosynthesis in Fruit Flesh

In recent years, knowledge on fruit flesh lignification has advanced partially due to experiments on protein-DNA interactions (Xu et al., 2015; Wang et al., 2016) that helped to unravel key aspects of the underlying regulatory network. Previous studies have demonstrated that *EjAP2-1* works in coordination with *EjMYB1* and *EjMYB2* for transcriptional regulation of *Ej4CL1* (Zeng et al., 2015). Zhang et al. (2020) recently found that the EjERF39 and EjMYB8 protein complex activates *Ej4CL1* by protein-DNA interaction with the promoter of *Ej4CL1*. Furthermore, utilization of the loquat transcriptome has allowed for the discovery of more lignification-related transcription factors (Lin et al., 2018; Liu et al., 2019). However, MADS-box genes are not frequently studied. In the presented study, we found the MADS-box domain gene *EjAGL65* using a yeast one-hybrid library screening assay. Data from a luciferase assay suggests that transient overexpression of EjAGL65 represses the transcription of *EjMYB8*, which is considered as a key activator of *Ej4CL1* (Wang et al., 2016), indicating the involvement of EjAGL65 in lignin biosynthesis. Interestingly, there is limited evidence of MADS-box genes being associated with lignin biosynthesis. Instead, MADS-box genes play vital roles in plant morphological development (Yu et al., 2014) and precise control of flowering and fruit development (Michaels and Amasino, 1999). AtAGL65, AtAGL30, and AtAGL94, which were determined to be the closest homologs of EjAGL65, control the maturation of pollen and pollen tube growth (Adamczyk and Fernandez, 2009). Tomato MADS-RIN is a primary ripening regulator that is highly expressed in fruit tissue (Vrebalov et al., 2002). The cell wall components were altered in the *rin* mutant, resulting in firmer texture, but the influence of RIN on lignin deposition was not clear (Li et al., 2018). Although the repression of another tomato MADS-box gene, SlTAGL1, results in lignin accumulation, the regulatory mechanism is unknown. Recently, a link between the MADS-box gene and lignin was established. *AtAGL15*, a MIKC type MADS-box gene, has been found to directly interact with the class III peroxidase PRX17, which causes ectopic lignin distribution in *Arabidopsis* stems if silenced (Cosio et al., 2017). Meanwhile, ectopic expression of *VCM1* and *VCM2*, two Populus MADS-box genes, leads to abnormal secondary growth by the regulation of the auxin transporter PIN5 (Zheng et al., 2020). By comparing amino acid sequences with *Arabidopsis* MADS-box genes, we found that AtAGL15, VCM1, and VCM2 belong to the MIKC group members. However, EjAGL65 lacks the K-box domain and is located in the Mδ subgroup (**Supplementary Figure S3**), indicating different mechanisms of lignin regulation between EjAGL65 and the other reported secondary cell wall related MADS-box genes. The Mδ subgroup consists of only six members in *Arabidopsis* and is crucial for pollen maturation (Verelst et al., 2007). The function of the Mδ genes is conserved in the land plants studied thus far (Kwantes et al., 2012), indicating their importance during plant evolution. The discovery of EjAGL65, which can alter lignin biosynthesis-related transcription factors, might suggest a novel function of the Mδ subgroup that is distinct from pollen development.

Implications for the Regulation Mechanism Underlying the Expression Pattern of *EjAGL65* Transcripts

Several studies have been conducted on the expression of the MADS-box gene transcripts during different developmental

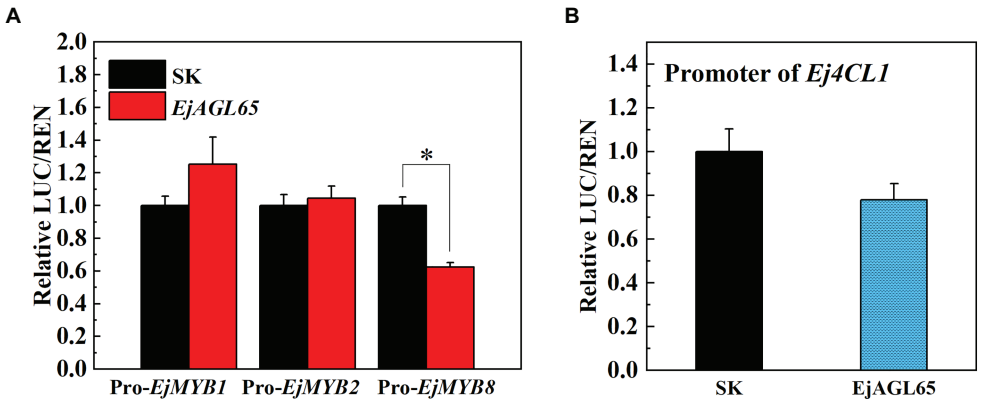

FIGURE 4 | Luciferase assay between EjAGL65 and lignin biosynthesis-related genes. The SK vector contains the coding sequence of EjAGL65; the LUC vectors with the insertion of the *EjMYB1*, *EjMYB2*, *EjMYB8* **(A)**, and *Ej4CL1* **(B)** promoter were pairwise transformed into the *Agrobacterium* strain GV1301 followed by leaf infection. The LUC/REN value represents the activation (above 1) or inhibition (below 1) effect generated by EjAGL65. A combination of the Empty SK vector and LUC vectors with different promoters was used as a calibration (set as 1). Error bars represent five replicates. The asterisk indicates a significant difference according to the Student's *t*-test at a significance level of 0.05 (*$p < 0.05$).

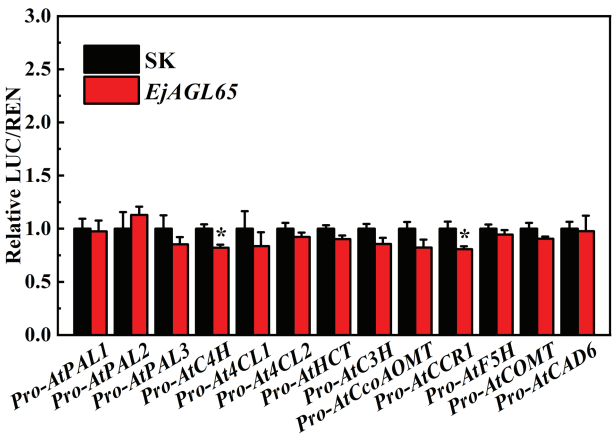

FIGURE 5 | Interactions between *EjAGL65* and *Arabidopsis* genes involved in lignin biosynthesis. A combination of the empty SK vector and LUC vectors with different promoters was used as a calibration (set as 1). Error bars resulted from five replicates. The asterisk indicates that the relative LUC/REN value was significantly different between SK and EjAGL65 based on the Student's *t*-test at a significance level of 0.05.

stages (Qin et al., 2012; Niu et al., 2016). However, in fruit, the dynamic modulations of MADS-box genes in response to environmental stimuli, such as chilling, have rarely been studied. Here, transcript levels of *EjAGL65* were measured during the cold storage of loquat fruits. *EjAGL65* mRNA levels rapidly decreased during the first 48 h, but gradually recovered to their initial level, representing a response to chilling at days 1 and 2. Considering that the lignin content of loquat fruits also correlates with the pattern of *EjAGL65* transcripts, there may be specific mechanisms preventing the *EjAGL65* transcripts from continuing to decrease. Generally, genes responsible for cold perception have various means of preventing overexpression or insufficient expression at the transcriptional or translational level, such as SIZ1 and HOS1 proteins, which antagonistically determine the degradation of the ICE1 protein (Miura et al., 2007). Although, we cannot yet conclude whether *EjAGL65* is located in the cold signal transduction network, revealing such a feedback mechanism for precisely controlling the expression of *EjAGL65* would provide a better understanding of chilling induced flesh lignification.

Lignin-Related *EjMYB8* Is Controlled by a MADS-Box Domain Protein

The relationship between MYB genes and lignin biosynthesis, as well as NAC master switches have been extensively studied in model plants, trees, and grasses. Lignin-related MYB genes are primarily regulated by NAC domain proteins at the transcription level in vascular tissue (Ohtani and Demura, 2019). The NAC-MYB based regulatory network is relatively conserved in the plant kingdom; it even exists in *Physcomitrella patens*, which is a moss that does not accumulate lignin (Xu et al., 2014a). Nevertheless, information about genes other than the NAC family that affect lignin-related MYB genes is still limited. Only the hAT transposase family gene *PtrhAT* was reported as the regulator of *PtrMYB021* (Xie et al., 2018). Several NAC genes have been characterized as activators of the lignification process in loquat flesh. However, no evidence indicates that NAC genes target lignin-related MYB genes, such as *EjMYB1*, whose homologs in *Arabidopsis* (*AtMYB58/63*) are regulated by the NAC-MYB transcription cascade (McCarthy et al., 2009; Zhou et al., 2009). On the contrary, the reported loquat NAC genes were confirmed as neither having a biological effect on MYB genes nor directly binding their promoter (Xu et al., 2015; Ge et al., 2017). These results suggest that the loquat may recruit new players for regulating stress induced lignification in flesh tissue. In this study, we performed a

library-scale screening to determine the upstream regulators of *EjMYB8*. Nevertheless, no NAC genes were found in the library pool after *in vivo* screening in yeast. Interestingly, a MADS-box domain protein, EjAGL65, physically binds to the promoter of *EjMYB8*, forming the MADS-MYB cascade. The results provide additional information about how to unravel a new hub in the complicated regulatory network of fruit flesh lignin biosynthesis.

Multiple Transcription Factors Constitute the Complicated Regulatory Network Based on *Ej4CL1*

Research on transcriptional regulation in the lignification of loquat flesh began with identifying two MYB family genes, *EjMYB1* and *EjMYB2* (Xu et al., 2014b). Subsequently, EjAP2-1 was found to be involved in the regulatory network by showing protein-protein interactions with either *EjMYB1* or *EjMYB2* (Zeng et al., 2015). With the further screening of MYB genes, *EjMYB8* was proposed as an effective activator of lignin biosynthesis (Wang et al., 2016). The activation effect of *EjMYB8* could be further enhanced by forming a protein complex with *EjERF39* (Zhang et al., 2020), but there was limited information about negative regulators of *EjMYB8*. These MYB genes share the same target, located in the promoter region of *Ej4CL1*, a gene that plays an essential role in the biosynthesis of lignin monomers (Li et al., 2017), which complicates the mechanism by which *Ej4CL1* transcripts are adjusted.

The present study showed that the MADS-box gene *EjAGL65* affects loquat flesh lignin accumulation *via* repressing the transcription of the characterized lignin activator *EjMYB8* (**Figure 6**). *EjAGL65* transcripts showed a temperature-dependent pattern similar to its *Arabidopsis* homologs, providing a new hub for characterizing a chilling induced regulation network of flesh lignification. The system contains three MYB genes, two members of the AP2/ERF gene family, and a MADS-box gene, forming three regulatory pathways. Interestingly, only two of the abovementioned genes negatively regulate lignin biosynthesis at a transcription level, while the others either have identical activation effects or function through protein-protein interaction. Identifying additional factors and understanding the synergistic or antagonistic effects among the four pathways of the network will be the main focus of future research.

CONCLUSION

The present study discovered a chilling-repressed MADS-box gene named *EjAGL65*. Results of dual luciferase and yeast one-hybrid assays indicated that *EjAGL65* transcriptionally inhibits the promoter of *EjMYB8*, forming a MADS-MYB transcriptional cascade. The homologs of EjAGL65 were not known to affect the lignin biosynthesis pathway in model plants, revealing a novel route for the regulation of stress induced lignin.

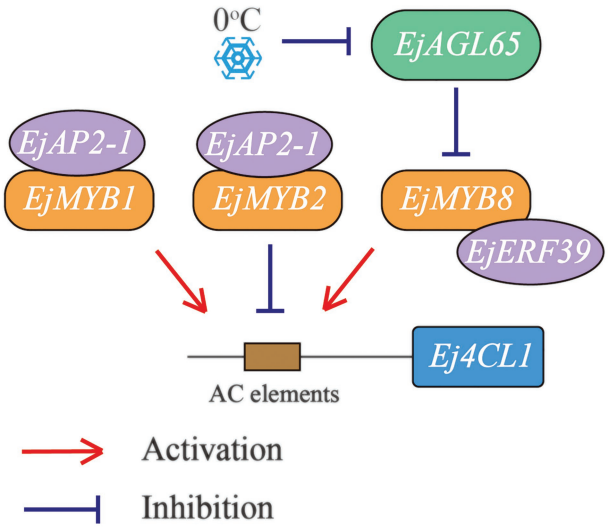

FIGURE 6 | Regulatory routes identified based on *Ej4CL1*. Three MYB genes are physically associated with *Ej4CL1*, acting as mediators for binding with other transcription factors. Both EjMYB1 and EjMYB2 can recruit EjAP2-1 to repress their transcriptional activities. EjMYB8 is controlled at both protein level (by EjERF39) and mRNA level (by EjAGL65). Lines with an arrow or a dashed terminal indicate activation or repression, respectively. Two genes shown in a sequence indicate a confirmed protein-protein interaction with each other.

DATA AVAILABILITY STATEMENT

The datasets presented in this study can be found in online repositories. The names of the repository/repositories and accession number(s) can be found in the article/**Supplementary Material**.

AUTHOR CONTRIBUTIONS

KC conceived the experiments. HG and MZ conducted the study and processed the data. HG and YS wrote the manuscript. KC, XL, and XY revised the manuscript. All authors contributed to the article and approved the submitted version.

FUNDING

This research was supported by the National Natural Science Foundation of China (31630067 and 31901740) and the 111 Project (B17039).

SUPPLEMENTARY MATERIAL

The Supplementary Material for this article can be found online at: https://www.frontiersin.org/articles/10.3389/fpls.2021.652959/full#supplementary-material

REFERENCES

Adamczyk, B. J., and Fernandez, D. E. (2009). MIKC* MADS domain heterodimers are required for pollen maturation and tube growth in *Arabidopsis*. *Plant Physiol.* 149, 1713–1723. doi: 10.1104/pp.109.135806

Boerjan, W., Ralph, J., and Baucher, M. (2003). Lignin biosynthesis. *Annu. Rev. Plant Biol.* 54, 519–546. doi: 10.1146/annurev.arplant.54.031902.134938

Cai, C., Xu, C. J., Shan, L. L., Li, X., Zhou, C. H., Zhang, W. S., et al. (2006). Low temperature conditioning reduces postharvest chilling injury in loquat fruit. *Postharvest Biol. Technol.* 41, 252–259. doi: 10.1016/j.postharvbio.2006.04.015

Cao, S., Shao, J., Shi, L., Xu, L., Shen, Z., Chen, W., et al. (2018). Melatonin increases chilling tolerance in postharvest peach fruit by alleviating oxidative damage. *Sci. Rep.* 8:806. doi: 10.1038/s41598-018-19363-5

Cao, S., Zheng, Y., Wang, K., Rui, H., and Tang, S. (2010). Effect of methyl jasmonate on cell wall modification of loquat fruit in relation to chilling injury after harvest. *Food Chemistry* 118, 641–647. doi: 10.1016/j.foodchem.2009.05.047

Cesarino, I. (2019). Structural features and regulation of lignin deposited upon biotic and abiotic stresses. *Curr. Opin. Biotechnol.* 56, 209–214. doi: 10.1016/j.copbio.2018.12.012

Cosio, C., Ranocha, P., Francoz, E., Burlat, V., Zheng, Y., Perry, S. E., et al. (2017). The class III peroxidase PRX17 is a direct target of the MADS-box transcription factor AGAMOUS-LIKE15 (AGL15) and participates in lignified tissue formation. *New Phytol.* 213, 250–263. doi: 10.1111/nph.14127

Dangcham, S., Bowen, J., Ferguson, I. B., and Ketsa, S. (2008). Effect of temperature and low oxygen on pericarp hardening of mangosteen fruit stored at low temperature. *Postharvest Biol. Technol.* 50, 37–44. doi: 10.1016/j.postharvbio.2008.02.005

Ge, H., Zhang, J., Zhang, Y. J., Li, X., Yin, X. R., Grierson, D., et al. (2017). EjNAC3 transcriptionally regulates chilling-induced lignification of loquat fruit via physical interaction with an atypical CAD-like gene. *J. Exp. Bot.* 68, 5129–5136. doi: 10.1093/jxb/erx330

Gimenez, E., Pineda, B., Capel, J., Anton, M. T., Atares, A., Perez-Martin, F., et al. (2010). Functional analysis of the Arlequin mutant corroborates the essential role of the Arlequin/TAGL1 gene during reproductive development of tomato. *PLoS One* 5:e14427. doi: 10.1371/journal.pone.0014427

Im Kim, J., Ciesielski, P. N., Donohoe, B. S., Chapple, C., and Li, X. (2014). Chemically induced conditional rescue of the reduced epidermal fluorescence8 mutant of *Arabidopsis* reveals rapid restoration of growth and selective turnover of secondary metabolite pools. *Plant Physiol.* 164, 584–595. doi: 10.1104/pp.113.229393

Jin, P., Duan, Y. F., Wang, L., Wang, J., and Zheng, Y. H. (2014). Reducing chilling injury of loquat fruit by combined treatment with hot air and methyl jasmonate. *Food Bioprocess Technol.* 7, 2259–2266. doi: 10.1007/s11947-013-1232-3

Kamdee, C., Imsabai, W., Kirk, R., Allan, A. C., Ferguson, I. B., and Ketsa, S. (2014). Regulation of lignin biosynthesis in fruit pericarp hardening of mangosteen (*Garcinia mangostana* L.) after impact. *Postharvest Biol. Technol.* 97, 68–76. doi: 10.1016/j.postharvbio.2014.06.004

Kwantes, M., Liebsch, D., and Verelst, W. (2012). How MIKC* MADS-box genes originated and evidence for their conserved function throughout the evolution of vascular plant gametophytes. *Mol. Biol. Evol.* 29, 293–302. doi: 10.1093/molbev/msr200

Li, C. F., Wang, X. Q., Ran, L. Y., Tian, Q. Y., Fan, D., and Luo, K. M. (2015). PtoMYB92 is a transcriptional activator of the lignin biosynthetic pathway during secondary cell wall formation in *Populus tomentosa*. *Plant Cell Physiol.* 56, 2436–2446. doi: 10.1093/pcp/pcv157

Li, S., Xu, H., Ju, Z., Cao, D., Zhu, H., Fu, D., et al. (2018). The RIN-MC fusion of MADS-box transcription factors has transcriptional activity and modulates expression of many ripening genes. *Plant Physiol.* 176, 891–909. doi: 10.1104/pp.17.01449

Li, X., Zang, C., Ge, H., Zhang, J., Grierson, D., Yin, X. R., et al. (2017). Involvement of PAL, C4H, and 4CL in chilling injury-induced flesh lignification of loquat fruit. *HortScience* 52, 127–131. doi: 10.21273/HORTSCI11304-16

Lin, S., Wu, T., Lin, H., Zhang, Y., Xu, S., Wang, J., et al. (2018). De novo analysis reveals transcriptomic responses in *Eriobotrya japonica* fruits during postharvest cold storage. *Genes* 9:639. doi: 10.3390/genes9120639

Liu, W. L., Zhang, J., Jiao, C., Yin, X. R., Fei, Z. J., Wu, Q. B., et al. (2019). Transcriptome analysis provides insights into the regulation of metabolic processes during postharvest cold storage of loquat (*Eriobotrya japonica*) fruit. *Hortic. Res.* 6, 1–11. doi: 10.1038/s41438-019-0131-9

Martel, C., Vrebalov, J., Tafelmeyer, P., and Giovannoni, J. J. (2011). The tomato MADS-box transcription factor RIPENING INHIBITOR interacts with promoters involved in numerous ripening processes in a COLORLESS NONRIPENING-dependent manner. *Plant Physiol.* 157, 1568–1579. doi: 10.1104/pp.111.181107

McCarthy, R. L., Zhong, R. Q., and Ye, Z. H. (2009). MYB83 is a direct target of SND1 and acts redundantly with MYB46 in the regulation of secondary cell wall biosynthesis in *Arabidopsis*. *Plant Cell Physiol.* 50, 1950–1964. doi: 10.1093/pcp/pcp139

Michaels, S. D., and Amasino, R. M. (1999). FLOWERING LOCUS C encodes a novel MADS domain protein that acts as a repressor of flowering. *Plant Cell* 11, 949–956. doi: 10.1105/tpc.11.5.949

Min, T., Fang, F., Ge, H., Shi, Y. N., Luo, Z. R., Yao, Y. C., et al. (2014). Two novel anoxia-induced ethylene response factors that interact with promoters of deastringency-related genes from persimmon. *PLoS One* 9:e97043. doi: 10.1371/journal.pone.0097043

Miura, K., Jin, J. B., Lee, J., Yoo, C. Y., Stirm, V., Miura, T., et al. (2007). SIZ1-mediated sumoylation of ICE1 controls CBF3/DREB1A expression and freezing tolerance in *Arabidopsis*. *Plant Cell* 19, 1403–1414. doi: 10.1105/tpc.106.048397

Niu, Q., Li, J., Cai, D., Qian, M., Jia, H., Bai, S., et al. (2016). Dormancy-associated MADS-box genes and microRNAs jointly control dormancy transition in pear (*Pyrus pyrifolia* white pear group) flower bud. *J. Exp. Bot.* 67, 239–257. doi: 10.1093/jxb/erv454

Ohtani, M., and Demura, T. (2019). The quest for transcriptional hubs of lignin biosynthesis: beyond the NAC-MYB-gene regulatory network model. *Curr. Opin. Biotechnol.* 56, 82–87. doi: 10.1016/j.copbio.2018.10.002

Parenicová, L., de Folter, S., Kieffer, M., Horner, D. S., Favalli, C., Busscher, J., et al. (2003). Molecular and phylogenetic analyses of the complete MADS-box transcription factor family in *Arabidopsis*: new openings to the MADS world. *Plant Cell* 15, 1538–1551. doi: 10.1105/tpc.011544

Pelaz, S., Ditta, G. S., Baumann, E., Wisman, E., and Yanofsky, M. F. (2000). B and C floral organ identity functions require SEPALLATA MADS-box genes. *Nature* 405, 200–203. doi: 10.1038/35012103

Peng, D. L., Chen, X. G., Yin, Y. P., Lu, K. L., Yang, W. B., Tang, Y. H., et al. (2014). Lodging resistance of winter wheat (*Triticum aestivum* L.): lignin accumulation and its related enzymes activities due to the application of paclobutrazol or gibberellin acid. *Field Crop Res.* 157, 1–7. doi: 10.1016/j.fcr.2013.11.015

Qin, G., Wang, Y., Cao, B., Wang, W., and Tian, S. (2012). Unraveling the regulatory network of the MADS box transcription factor RIN in fruit ripening. *Plant J.* 70, 243–255. doi: 10.1111/j.1365-313X.2011.04861.x

Shan, L. L., Li, X., Wang, P., Cai, C., Zhang, B., De Sun, C., et al. (2008). Characterization of cDNAs associated with lignification and their expression profiles in loquat fruit with different lignin accumulation. *Planta* 227, 1243–1254. doi: 10.1007/s00425-008-0696-2

Suo, J. T., Li, H., Ban, Q. Y., Han, Y., Meng, K., Jin, M. J., et al. (2018). Characteristics of chilling injury-induced lignification in kiwifruit with different sensitivities to low temperatures. *Postharvest Biol. Technol.* 135, 8–18. doi: 10.1016/j.postharvbio.2017.08.020

Vanholme, R., De Meester, B., Ralph, J., and Boerjan, W. (2019). Lignin biosynthesis and its integration into metabolism. *Curr. Opin. Biotech.* 56, 230–239. doi: 10.1016/j.copbio.2019.02.018

Verelst, W., Twell, D., de Folter, S., Immink, R., Saedler, H., and Munster, T. (2007). MADS-complexes regulate transcriptome dynamics during pollen maturation. *Genome Biol.* 8:R249. doi: 10.1186/gb-2007-8-11-r249

Vrebalov, J., Ruezinsky, D., Padmanabhan, V., White, R., Medrano, D., Drake, R., et al. (2002). A MADS-box gene necessary for fruit ripening at the tomato *Ripening-Inhibitor* (*Rin*) locus. *Science* 296:343. doi: 10.1126/science.1068181

Wang, W. Q., Zhang, J., Ge, H., Li, S. J., Li, X., Yin, X. R., et al. (2016). EjMYB8 transcriptionally regulates flesh lignification in loquat fruit. *PLoS One* 11:e0154399. doi: 10.1371/journal.pone.0154399

Xie, M., Muchero, W., Bryan, A. C., Yee, K., Guo, H. B., Zhang, J., et al. (2018). A 5-enolpyruvylshikimate 3-phosphate synthase functions as a transcriptional repressor in *Populus*. *Plant Cell* 30, 1645–1660. doi: 10.1105/tpc.18.00168

Xu, M., Li, S. J., Liu, X. F., Yin, X. R., Grierson, D., and Chen, K. S. (2019a). Ternary complex EjbHLH1-EjMYB2-EjAP2-1 retards low temperature-induced flesh lignification in loquat fruit. *Plant Physiol. Biochem.* 139, 731–737. doi: 10.1016/j.plaphy.2019.04.032

Xu, B., Ohtani, M., Yamaguchi, M., Toyooka, K., Wakazaki, M., Sato, M., et al. (2014a). Contribution of NAC transcription factors to plant adaptation to land. *Science* 343, 1505–1508. doi: 10.1126/science.1248417

Xu, Q., Wang, W. Q., Zeng, J. K., Zhang, J., Grierson, D., Li, X., et al. (2015). A NAC transcription factor, EjNAC1, affects lignification of loquat fruit by regulating lignin. *Postharvest Biol. Technol.* 102, 25–31. doi: 10.1016/j.postharvbio.2015.02.002

Xu, Q., Yin, X. R., Zeng, J. K., Ge, H., Song, M., Xu, C. J., et al. (2014b). Activator- and repressor-type MYB transcription factors are involved in chilling injury induced flesh lignification in loquat via their interactions with the phenylpropanoid pathway. *J. Exp. Bot.* 65, 4349–4359. doi: 10.1093/jxb/eru208

Xu, M., Zhang, M. X., Shi, Y. N., Liu, X. F., Li, X., Grierson, D., et al. (2019b). EjHAT1 participates in heat alleviation of loquat fruit lignification by suppressing the promoter activity of key lignin monomer synthesis gene EjCAD5. *J. Agric. Food Chem.* 67, 5204–5211. doi: 10.1021/acs.jafc.9b00641

Yang, L., Zhao, X., Ran, L. Y., Li, C. F., Fan, D., and Luo, K. M. (2017). PtoMYB156 is involved in negative regulation of phenylpropanoid metabolism and secondary cell wall biosynthesis during wood formation in poplar. *Sci. Rep.* 7, 1–14. doi: 10.1038/srep41209

Yin, X. R., Allan, A. C., Chen, K. S., and Ferguson, I. B. (2010). Kiwifruit EIL and ERF genes involved in regulating fruit ripening. *Plant Physiol.* 153, 1280–1292. doi: 10.1104/pp.110.157081

Yu, L. H., Miao, Z. Q., Qi, G. F., Wu, J., Cai, X. T., Mao, J. L., et al. (2014). MADS-box transcription factor AGL21 regulates lateral root development and responds to multiple external and physiological signals. *Mol. Plant* 7, 1653–1669. doi: 10.1093/mp/ssu088

Zeng, J. K., Li, X., Xu, Q., Chen, J. Y., Yin, X. R., Ferguson, I. B., et al. (2015). EjAP2-1, an AP2/ERF gene, is a novel regulator of fruit lignification induced by chilling injury, via interaction with EjMYB transcription factors. *Plant Biotechnol. J.* 13, 1325–1334. doi: 10.1111/pbi.12351

Zeng, J. K., Li, X., Zhang, J., Ge, H., Yin, X. R., and Chen, K. S. (2016). Regulation of loquat fruit low temperature response and lignification involves interaction of heat shock factors and genes associated with lignin biosynthesis. *Plant Cell Environ.* 39, 1780–1789. doi: 10.1111/pce.12741

Zhang, J., Ge, H., Zang, C., Li, X., Grierson, D., Chen, K. S., et al. (2016). EjODO1, a MYB transcription factor, regulating lignin biosynthesis in developing loquat (*Eriobotrya japonica*) fruit. *Front. Plant Sci.* 7:1360. doi: 10.3389/fpls.2016.01360

Zhang, J., Yin, X.-R., Li, H., Xu, M., Zhang, M.-X., Li, S.-J., et al. (2020). ETHYLENE RESPONSE FACTOR EjERF39-EjMYB8 complex activates cold-induced lignification of loquat fruit, via the biosynthetic gene Ej4CL1. *J. Exp. Bot.* 71, 3172–3184. doi: 10.1093/jxb/eraa085

Zheng, S., He, J., Lin, Z., Zhu, Y., Sun, J., and Li, L. (2020). Two MADS-box genes regulate vascular cambium activity and secondary growth by modulating auxin homeostasis in *Populus*. *Plant Commun.* 100134. doi: 10.1016/j.xplc.2020.100134 (in press).

Zhou, J., Lee, C., Zhong, R., and Ye, Z. H. (2009). MYB58 and MYB63 are transcriptional activators of the lignin biosynthetic pathway during secondary cell wall formation in *Arabidopsis*. *Plant Cell* 21, 248–266. doi: 10.1105/tpc.108.063321

Conflict of Interest: The authors declare that the research was conducted in the absence of any commercial or financial relationships that could be construed as a potential conflict of interest.

frontiers in Plant Science

ORIGINAL RESEARCH
published: 14 April 2021
doi: 10.3389/fpls.2021.653256

Potential Association of Reactive Oxygen Species With Male Sterility in Peach

*Yaming Cai[1,2,3], Zhishen Ma[4], Collins Otieno Ogutu[1,5], Lei Zhao[1,2,3], Liao Liao[1,3], Beibei Zheng[1,3], Ruoxi Zhang[1,3], Lu Wang[1,3,5] and Yuepeng Han[1,3,5]**

[1] CAS Key Laboratory of Plant Germplasm Enhancement and Specialty Agriculture, Wuhan Botanical Garden, The Innovative Academy of Seed Design, Chinese Academy of Sciences, Wuhan, China, [2] University of Chinese Academy of Sciences, Beijing, China, [3] Center of Economic Botany, Core Botanical Gardens, Chinese Academy of Sciences, Wuhan, China, [4] Shijiazhuang Pomology Institute, Hebei Academy of Agricultural and Forestry Sciences, Shijiazhuang, China, [5] Sino-Africa Joint Research Center, Chinese Academy of Sciences, Wuhan, China

Male sterility is an important agronomic trait for hybrid vigor utilization and hybrid seed production, but its underlying mechanisms remain to be uncovered. Here, we investigated the mechanisms of male sterility in peach using a combined cytology, physiology, and molecular approach. Cytological features of male sterility include deformed microspores and tapetum cells along with absence of pollen grains. Microspores had smaller nucleus at the mononuclear stage and were compressed into belts and subsequently disappeared in the anther cavity, whereas tapetum cells were swollen and vacuolated, with a delayed degradation to flowering time. Male sterile anthers had an ROS burst and lower levels of major antioxidants, which may cause abnormal development of microspores and tapetum, leading to male sterility in peach. In addition, the male sterility appears to be cytoplasmic in peach, which could be due to sequence variation in the mitochondrial genome. Our results are helpful for further investigation of the genetic mechanisms underlying male sterility in peach.

Keywords: ***Prunus persica*, tapetum degradation, pollen development, ROS homeostasis, male sterility**

OPEN ACCESS

Edited by:
Paloma Moncaleán, Neiker Tecnalia, Spain

Reviewed by:
Alejandro Atarés, Polytechnic University of Valencia, Spain
Lorenzo Burgos, Center for Edaphology and Applied Biology of Segura, Spanish National Research Council, Spain

****Correspondence:***
Yuepeng Han
yphan@wbgcas.cn

Specialty section:
This article was submitted to Plant Development and EvoDevo, a section of the journal Frontiers in Plant Science

Received: *14 January 2021*
Accepted: *08 February 2021*
Published: *14 April 2021*

Citation:
Cai Y, Ma Z, Ogutu CO, Zhao L, Liao L, Zheng B, Zhang R, Wang L and Han Y (2021) Potential Association of Reactive Oxygen Species With Male Sterility in Peach. Front. Plant Sci. 12:653256. doi: 10.3389/fpls.2021.653256

INTRODUCTION

A typical flower has four types of floral organs: sepal, petal, stamen, and pistil. The function of the flower is to make seeds for plant propagation. Seed development is initiated by fertilization in which male and female gametes fuse, with the former produced in the anther, a part of stamen, whereas the latter is produced in the ovary, an interior part of the pistil. Hence, the development of male and female gametes is crucial for reproduction of flowering plants. However, some plants lack male gametes, also called pollen grains, despite having complete floral organs. The development of pollen grains is a complex and delicate process. Initially, the pollen mother cell in the pollen sac undergoes meiotic division to produce four daughter cells that are called a tetrad. Later, the tetrad dissociates and develops into mononuclear microspores with the nucleus in the center of the cell. Tapetum cells nourish the microspores, increasing in the size and gradually forming a large central vacuole in the cell. As a result, the nucleus gradually moves from the center to the side. Subsequently, the microspores undergo a mitotic division, producing a larger vegetative cell and a smaller generative cell. Most angiosperms, such as lily, cotton, peach, and orange, have bicellular

pollen grains, containing vegetative and generative cells, when the pollen is mature. However, some plants, such as cereals and rapeseed, have trinuclear pollen grains as their generative cells undergo additional mitotic division to generate two sperm cells before the pollen is released. Pollen grains at the bicellular and tricellular stages are also referred to as male gametophytes. Previous studies have shown that numerous genes are involved in pollen development (Wilson and Zhang, 2009; Zhang et al., 2011; Gómez et al., 2015). Abnormal structure or expression of pollen development–related genes may cause failure of the anther to produce mature pollen grains, resulting in male sterility (McCormick, 2004; Borg et al., 2009; Cai et al., 2015).

To date, numerous genes that are related to male sterility have been discovered in plants (Singh et al., 2010; Lukaszewski, 2017). Particularly, functional disorder of genes related to tapetum development is one of the main causes of pollen abortion. Tapetum is located in the innermost part of anther tissue, and its main function is to provide nutrition for the development of pollen grains. During the late stages of pollen development, the tapetum undergoes cellular degradation, and anthers subsequently crack, causing mature pollen grains to be released (Mariani et al., 1990; Parish and Li, 2010; Zhu et al., 2011; Xie et al., 2014). Therefore, normal tapetum is crucial for the development of pollen grains (Li et al., 2017). For example, mutations of *OsMS1* and *OsTDR* genes that regulate tapetum development can block the degradation of tapetum, leading to male sterility in rice (Li et al., 2006; Yang et al., 2019).

In addition to the dysfunction of genes involved in the regulation of tapetum development, other factors such as the excessive production of reactive oxygen species (ROS) in anthers can also cause male sterility. For example, reducing the expression of *MT-1-4b* gene encoding a type 1 small Cys-rich and metal binding protein increases the level of superoxide anion (O_2^-), which affects tapetum development and thus decreases pollen infertility (Hu et al., 2011). ROS can act as signaling molecules and maintaining their basal levels is essential for plant development (Gechev et al., 2006). Mitochondrion is a main source of ROS production as it is the site of oxidative phosphorylation. Mitochondria structural variation can lead to the ROS burst (Shadel and Horvath, 2015). In addition, the ROS burst can be induced by environmental stress and dysfunction of genes associated with ROS elimination (Gechev et al., 2006; Suzuki et al., 2012; Miller et al., 2010). Plants contain a variety of antioxidants, such as carotenoids, glutathione (GSH), ascorbate, and flavonoids, which serve as ROS scavengers (Mittler et al., 2004). In plants, the production and elimination of ROS are a balanced process, which is called ROS homeostasis. Many studies have shown that loss of ROS homeostasis can lead to male sterility (Hu et al., 2011; Qu et al., 2014; Zhou et al., 2019; Wang et al., 2020; Zhu et al., 2020).

Peach (*Prunus persica*) is a fruit tree widely cultivated in temperate regions of the world, with ornamental and edible properties. Although male sterile frequently occurs in peach, its molecular mechanism is yet to be fully uncovered. In this study, we investigated the mechanism of male sterility in "Jinxiang" ("JX"), a popular yellow flesh peach cultivar in China. Our results indicated that abnormal development of tapetum and microspores are caused by disruption of ROS homeostasis, resulting in male sterility. This finding provides an insight into mechanisms underlying male sterility in peach.

MATERIALS AND METHODS

Plant Materials

Peach varieties used in this study are maintained in the orchard at Shijiazhuang Pomology Institute, Hebei Academy of

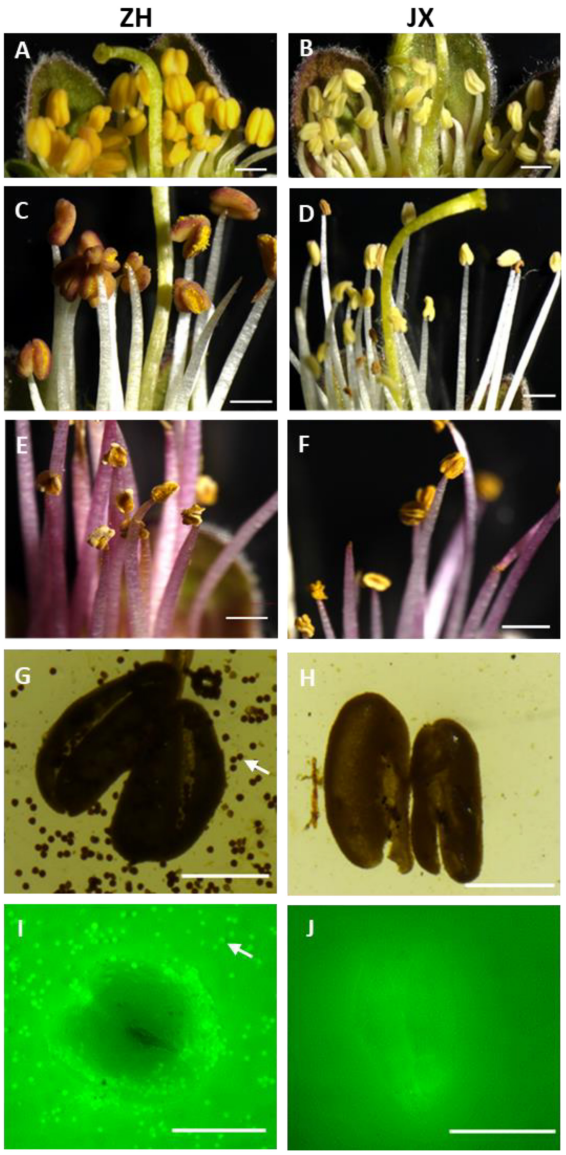

FIGURE 1 | Comparison of anther phenotype between "ZH" and "JX". Panels **(A,B)** show swollen and shrunken anthers in flower buds, respectively. **(C,D)** Anthers at the anthesis. **(E,F)** Anthers 5 days after flowering. **(G,H)** Cracked anthers along with pollen grains stained using I_2/KI. Panels **(I,J)** cracked anthers and pollen grains stained using FDA. The white arrow indicates pollen grains. The white bar represents 1,000 μm in **(A–F)**, and 500 μm in **(G–J)**.

Agriculture and Forestry Sciences, Shijiazhuang, China. Anthers were collected from a male sterile cultivar, JX, and a fertile cultivar, "Zaohong" ("ZH"), as a control. These two cultivars have the same flowering time. Samples were collected at 5-day intervals from March 09, 2019, to April 03, 2019. All samples were divided into six stages based on sampling time, S0, S1, S2, S3, S4, and S5, which were confirmed by paraffin section according to previously reported protocol (Fang et al., 2016). S0–S3 corresponded to 20, 15, 10, and 5 days before anthesis, respectively. S4 corresponded to the anthesis, and S5 represented 5 days after anthesis.

Anatomical Analysis of the Anther Structure

Anthers from the unopened and fully opened flower buds were taken out, put in culture dish, and left to dry. The dried anthers were fixed with glutaraldehyde (pH 6.8) at 4°C for 1.5 h and then washed three times with 0.1 mol/L phosphoric acid buffer (pH 6.8) for 10 min each. Subsequently, the treated samples were dehydrated with 50, 70, 80, and 90% ethanol for 10–15 min each time and finally dehydrated three times with 100% ethanol for 10–15 min each time. Then, the anthers were immersed in 100% ethanol:tert-butanol (vol/vol = 1) for 15 min and transferred to pure tert-butanol for 15 min. The treated samples were dried for 4 h using LABCONCO Freeze Vacuum Dryer (Labconco, MO, United States). Finally, the observation surface of the sample was put in an upward position, fixed with conductive tape, and sprayed with gold powder using Leica EM ACE Ion sputtering coating instrument (Leica, Wetzlar, Germany). Anther morphology was observed using scanning electron microscope (SEM) (Hitachi, Tokyo, Japan). In addition, transmission electron

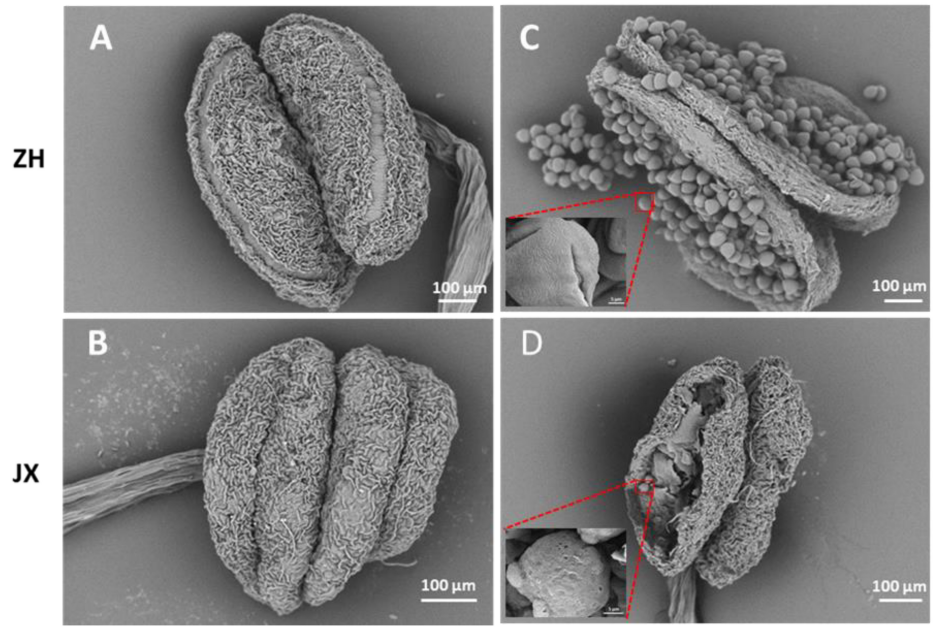

FIGURE 2 | Comparison of anther morphology between "ZH" and "JX" using SEM. **(A,B)** Anthers before dehiscence. **(C,D)** Anthers after dehiscence.

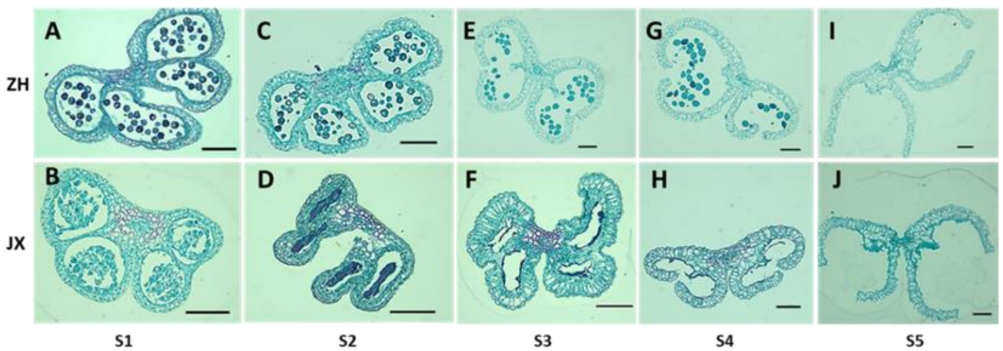

FIGURE 3 | Comparison of transverse section of anthers between "ZH" and "JX" at five development stages as described in Section "Materials and Methods." All bars represent 100 μm. **(A,C,E,G,I)** Transverse section of 'ZH' anthers. **(B,D,F,H,J)** Transverse section of 'JX' anthers.

microscopy (TEM) was performed according to a previous report (Li et al., 2006).

Detection of Pollen Viability

Pollen viability was analyzed by both 1% iodine/potassium iodide (I_2/KI) and fluorescein diacetate (FDA) staining. For the I_2/KI assay, the samples were stained for 5 min and scanned with microscope (Nikon, Tokyo, Japan). For the FDA staining assay, the pollen grains were immersed in a concave slide containing 2 μg/mL FDA solution for 30 min and observed under the fluorescence microscope (Nikon, Tokyo, Japan) after washing out FDA.

Measurement of ROS and Antioxidant Contents in Anthers

The hydrogen peroxide (H_2O_2) content in anthers was measured using H_2O_2 assay kit (Beyotime, Shanghai, China) following the manufacturer's instruction. The O_2^- radical content in anthers at each developmental stage was assayed using nitro-blue tetrazolium (NBT) staining according to a previous report (Xie et al., 2014).

The content of GSH was measured using GSH assay kit (Beyotime, Shanghai, China) according to the manufacturer's instruction. Carotenoid content was measured using plant carotenoid detection kit (Solarbio, Beijing, China) following the manufacturer's instruction. The content of ascorbate peroxidase (APX) and GSH *S*-transferase (GST) was measured by APX and GST detection kit (GeRuiSi, Nanjing, China), respectively, according to the manufacturer's instruction.

RNA-Sequencing Analysis

Three development stages of JX and ZH anthers, S0, S1, and S3, were selected for RNA-sequencing (RNA-seq) analysis. RNA extraction and purity, library construction, and RNA-seq were conducted according our previous report (Wang L. et al., 2013). After removing adapters and low-quality reads, clean reads were mapped to the peach reference genome (International Peach Genome Initiative, 2013). Gene expression levels were estimated based on the value of expected number of fragments per kilobase of transcript sequence per million base pairs sequenced (FPKM). Differentially expressed genes (DEGs) were identified using the following criteria: fold change ≥2.0 and a false discovery rate <0.01.

RNA Extraction and Quantitative Reverse Transcription–Polymerase Chain Reaction Analysis

Total RNA extraction was performed using Plant RNA Extraction Kit (Aidlab Biotech, Beijing, China), and reverse transcription was conducted using Reverse Transcriptase Kit (M-MLV) (Zomanbio, Beijing, China) according to the manufacturer's instructions. Quantitative reverse transcription–polymerase

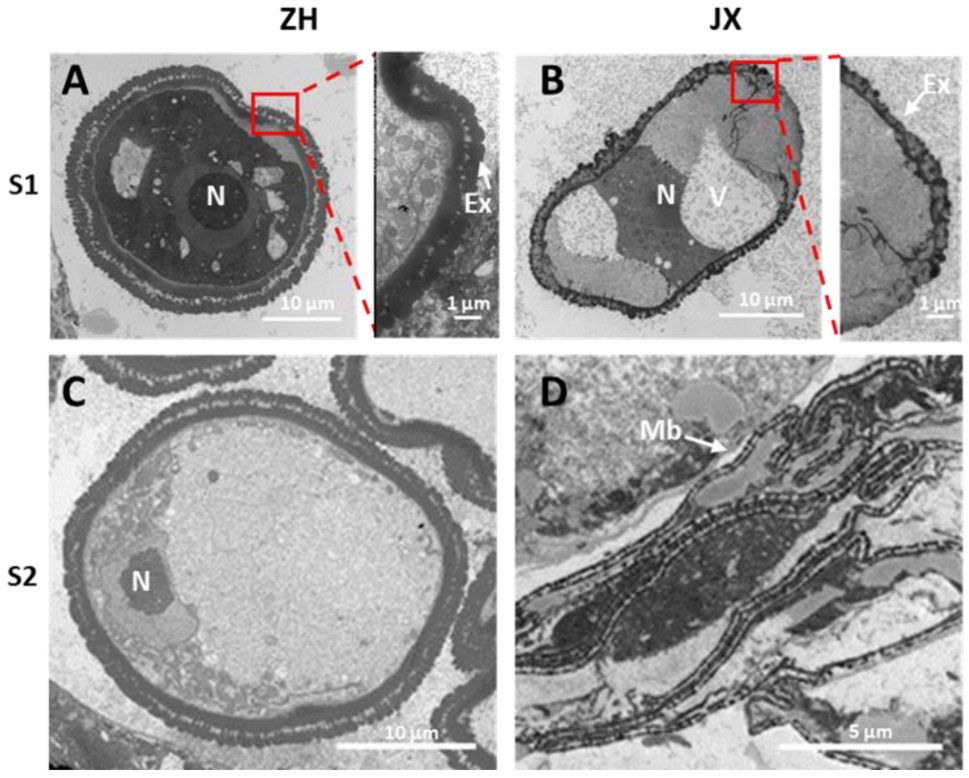

FIGURE 4 | Transmission electron microscopy (TEM) scans of microspore features at two stages in "JX" and "ZH." N, nucleus; Ex, exine; V, vacuole; Mb, microspore bands. **(A,C)** represent microspores of 'ZH' at S1 and S2, respectively. **(B,D)** indicate microspores of 'JX' at S1 and S2, respectively.

chain reaction (qRT-PCR) was performed using TAKARA SYBR® Premix EX Taq TM II (Tli RNaseH Plus), and the amplification program was as follows: one cycle of 30 s at 95°C, followed by 40 cycles of 5 s at 95°C and 34 s at 60°C. Relative expression levels were normalized against the reference gene *GADPH* (Tong et al., 2009). Each treatment contained three biological replicates. Primer sequences for qRT-PCR are listed in **Supplementary Table 1**.

RESULTS

JX Has Abnormal Anther Morphology and Lacks Pollen Grains

Flower buds showed no obvious difference in appearance between the male sterile cv. JX and the fertile cv. ZH before the full blooming stage (**Supplementary Figure 1**), but their inner anthers were different in size and color (**Figures 1A,B**). The anthers of ZH were yellow, swollen, and significantly larger than the shrunken anthers of JX that were pale in color. The anthers of ZH cracked to release pollen grains, and the color changed from yellow to dark orange at the anthesis, whereas the anthers of JX were indehiscent with no obvious change in color (**Figures 1C,D**). Five days after anthesis, the anthers of ZH wilted, whereas dehiscence was observed in some anthers of JX, with filament color both changing to purple (**Figures 1E,F**). Both I_2/KI and FDA staining showed that the anthers of ZH contained viable pollen grains, whereas the anthers of JX had no pollen grains (**Figures 1G–J**).

Scanning electron microscope assay showed that the surface of ZH anthers had opening cracks, whereas abnormal opening cracks were observed in the surface of JX anthers (**Figures 2A,B**). The anthers of ZH released numerous pollen grains during dehiscence, whereas the disrupted anthers of JX had no pollen grains, with few pollen-like spheres (**Figure 2D**) that had no typical wrinkles on their surface as shown in **Figure 2C**.

In summary, the above results suggested that the anthers of JX underwent abnormal development, with delayed dehiscence in some anthers that had no pollen grains.

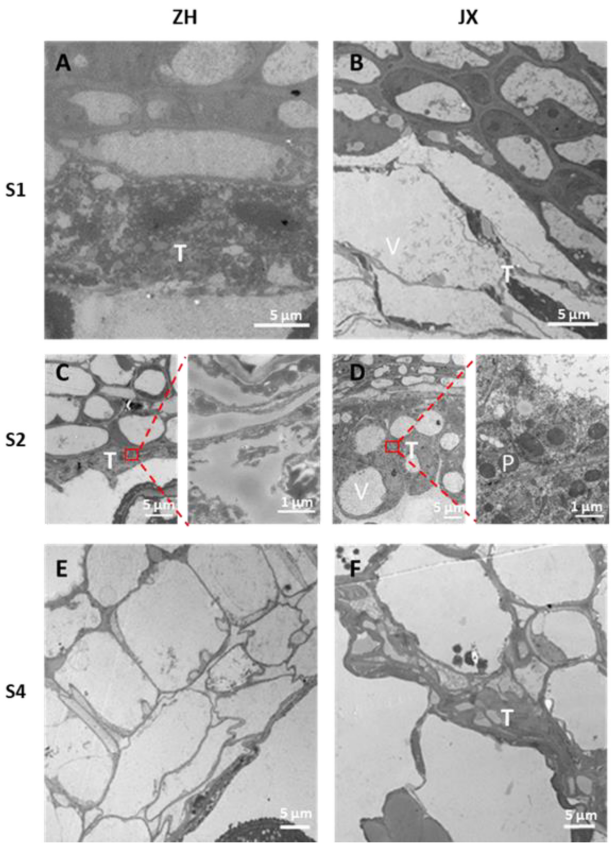

FIGURE 5 | Transmission electron microscopy scans of tapetum morphology in "ZH" and "JX." **(A)** Normal tapetum; **(B)** vacuolized tapetum; **(C)** degraded tapetum; **(D)** swollen tapetum; **(E)** completely degraded tapetum; **(F)** delayed tapetum degradation. T, tapetum; V, vacuole; P, peroxisome.

Microspores of JX Were Compressed Into Bands That Disappeared in Anther Cavity

To investigate the cytological mechanism of pollen abortion in JX, we examined paraffin-embedded anther samples at five stages (S1–S5) using microscope. Microspores were abundant in the anthers of both ZH and JX at S1; however, the anthers JX showed irregular morphology (**Figures 3A,B**). Microspores in each pollen sac were compressed into a single band in JX, whereas no morphological change was detected for microspores of ZH (**Figures 3C,D**). The anthers of ZH cracked normally during the S3 stage, but not for the anthers of JX that had empty pollen sacs, with no pollen grains (**Figures 3E,F**). Interestingly, anther cracking was delayed to the anthesis in JX (**Figure 3H**), in which mature pollen grains were released in ZH (**Figure 3G**). At S5, anthers showed no difference in structure between ZH and JX (**Figures 3I,J**). These results suggested that microspore development was disrupted, leading to pollen abortion in JX.

Ultrastructural Feature of Microspores and Tapetum in ZH and JX

To gain deep insights into abnormal anther development in JX, the ultrastructures of microspores and tapetum were examined using TEM. A single nucleus was present in microspores at S1 and S2 in JX and ZH (**Figure 4**). The microspores of ZH contained large nucleus, whereas the microspores of JX were severely vacuolated, with smaller nucleus (**Figures 4A,B**). Moreover, the exine of microspores in ZH had regular rod-like protrusions, whereas the exine structure of microspores in JX was irregular and incomplete (**Figures 4A,B**). At S2, the nuclear in microspores of ZH was pushed to the side because of vacuole enlargement, whereas microspores of JX were compressed into bands (**Figures 4C,D**).

Tapetum degradation occurred at S1 in ZH, whereas the development of tapetum was abnormal in JX (**Figures 5A,B**). The tapetum cells of JX had loose cytoplasm and heavy vacuolization in contrast to those of ZH at S1. The tapetum was almost completely degraded at S2 in ZH (**Figure 5C**), whereas the

tapetum cells of JX were swollen and contained large vacuoles (**Figure 5D**). At S4, the tapetum of ZH was completely degraded (**Figure 5E**), whereas tapetum degradation was just initiated in JX (**Figure 5F**). Altogether, these results suggested that tapetum development was abnormal and could not be timely degraded to nourish microspores, leading to pollen abortion in JX. In

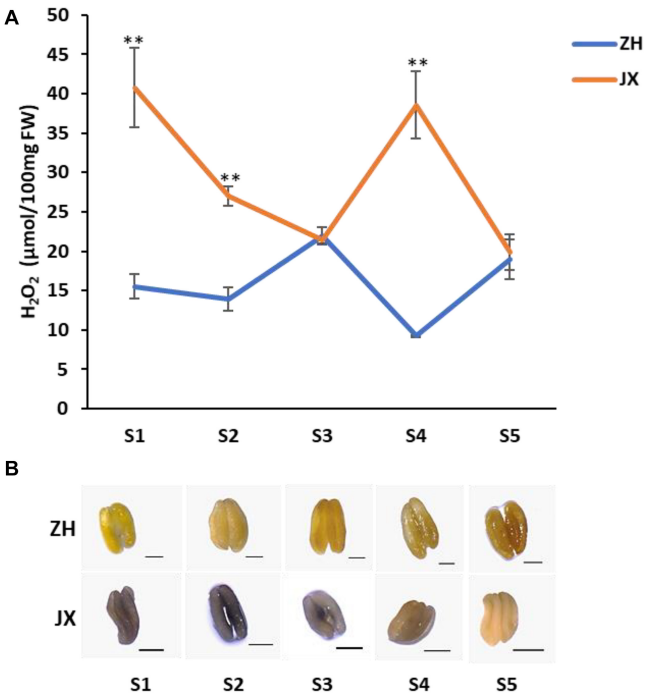

FIGURE 6 | The concentration of ROS in anthers of "ZH" and "JX" throughout their development. **(A)** Accumulation of H_2O_2 in anthers at stages 1–5. Error bars indicate standard deviation (SD) of three biological replicates. Statically significant differences at $P \leq 0.01$ (Student *t*-test) is indicated by **. **(B)** Measurement of O_2^- accumulation in anthers at stages 1–5 using NBT staining. The intensity of blue color indicates high content of O_2^-. All bars represent 500 μm.

TABLE 1 | Summary of RNA-seq data for anthers of two peach cultivars at three stages*.

Library	Total reads	Clean reads	Clean base (bp)	Mapped reads		Unique mapped reads		GC content	% ≥ Q30
				No.	Percentage	No.	Percentage		
B1-S0	55,299,248	27,649,624	8,241,443,970	52,624,756	95.16%	51,189,336	92.57%	46.36%	95.46%
B2-S0	52,472,066	26,236,033	7,835,470,872	49,381,068	94.11%	47,921,503	91.33%	46.38%	94.58%
B3-S0	42,518,758	21,259,379	6,319,171,812	39,177,432	92.14%	38,093,507	89.59%	46.78%	95.09%
B1-S1	49,545,076	24,772,538	7,394,915,150	45,810,911	92.46%	43,410,563	87.62%	46.58%	94.70%
B2-S1	43,014,382	21,507,191	6,426,544,328	39,549,654	91.95%	37,331,283	86.79%	46.63%	95.10%
B3-S1	44,495,164	22,247,582	6,633,928,720	41,781,723	93.90%	39,363,989	88.47%	46.48%	94.57%
B1-S3	51,072,856	25,536,428	7,617,437,418	48,634,923	95.23%	46,403,165	90.86%	46.56%	94.67%
B2-S3	55,679,980	27,839,990	8,304,340,272	53,371,184	95.85%	51,077,734	91.73%	46.32%	94.87%
B3-S3	46,058,244	23,029,122	6,861,185,988	43,908,560	95.33%	42,138,758	91.49%	46.36%	94.99%
C1-S0	39,985,662	19,992,831	5,954,533,580	36,333,712	90.87%	35,370,832	88.46%	46.29%	94.36%
C2-S0	41,941,794	20,970,897	6,239,724,192	38,482,650	91.75%	37,116,815	88.50%	46.54%	94.96%
C3-S0	49,636,558	24,818,279	7,395,890,042	46,277,979	93.23%	44,850,103	90.36%	46.26%	95.02%
C1-S1	40,903,146	20,451,573	6,112,103,674	37,830,395	92.49%	36,339,637	88.84%	46.51%	94.36%
C2-S1	50,895,486	25,447,743	7,586,570,536	46,982,994	92.31%	45,503,392	89.41%	46.31%	95.26%
C3-S1	45,892,436	22,946,218	6,841,578,052	38,945,963	84.86%	37,464,526	81.64%	48.18%	94.58%
C1-S3	42,742,096	21,371,048	6,378,901,298	38,510,897	90.10%	36,854,266	86.22%	46.95%	94.41%
C2-S3	38,611,318	19,305,659	5,767,550,644	34,646,264	89.73%	33,158,174	85.88%	46.82%	94.31%
C3-S3	41,971,228	20,985,614	6,270,251,464	38,802,892	92.45%	37,066,309	88.31%	46.60%	94.65%

**B and C represent "ZH" and "JX", respectively. S0, S1, and S3 indicate three developmental stages of anthers. Each sample contains three biological replicates.*

addition, we observed that tapetal cells at S2 were filled with round, electron dense, and granular organelles, which are typical characteristics of peroxisomes (**Figure 5D**). This suggested the presence of oxidative stress in microspores of JX (Hu et al., 2011).

The ROS Content Was Elevated in the Anthers of JX Compared to Those of ZH

As oxidative stress is associated with excess production of ROS that causes damage to cell structure (Gechev et al., 2006), we measured the contents of H_2O_2 and O_2^-, two main components of ROS (Apel and Hirt, 2004), in anthers of JX and ZH at stages 1–5. The concentration of H_2O_2 was significantly higher in JX than in ZH at S1, S2, and S4 (**Figure 6A**). However, the concentration of H_2O_2 in anthers at S3 and S5 was similar between JX and ZH. Moreover, the NBT staining assay demonstrated that the content of O_2^- at stages 1–4 was higher in JX than in ZH (**Figure 6B**). These results suggested an excessive accumulation of ROS in the anthers of JX.

Comparative Transcriptome Analysis Between the Anthers of JX and ZH

As mentioned previously, abnormal development of microspores was initially detected at S1. Thus, S0 and S1 represent transitional stages that are crucial for comparative transcriptome analysis according to a previous study (Liao et al., 2020). Moreover, microspores gradually degraded and finally disappeared in S3. Based on these findings, three stages, S0, S1, and S3, were selected to conduct comparative transcriptome analysis to further reveal molecular mechanisms of pollen abortion in JX. A total of 18 libraries were sequenced, generating approximately 5.77-Gb raw reads for each library, with an average Q30 value of 94.77% (**Table 1**). The clean reads of each sample were mapped against the peach reference genome[1], with unique mapping rates ranging from 81.64 to 92.57%. Pearson correlation coefficients were greater than 0.9 among three biological replications of each sample (**Supplementary Figure 2**), and 3D principal component analysis (PCA) plot displayed that three biological repeats of each sample clustered together (**Supplementary Figure 3**). This indicated high consistency between biological replicates, which is suitable for conducting comparative transcriptome analysis.

A total of 1,007, 2,612, and 151 DEGs were identified between ZH and JX at S0, S1, and S3, respectively (**Figure 7A**). Gene Ontology (GO) analysis indicated that the all DEGs could be classified into three types: biological process, cellular components, and molecular function (**Supplementary Figure 4**). The top 20 most enriched pathways in Kyoto Encyclopedia of Genes and Genomes (KEGG) analysis are shown in **Figure 7B**. Nine of the 20 enriched pathways are associated with ROS removal processes: (1) galactose metabolism (Hafsa et al., 2019); (2) flavonoid biosynthesis (Agati et al., 2012; Xie et al., 2015; Wei et al., 2019); (3) stilbenoid (Nassiri-Asl and Hosseinzadeh, 2016; Treml et al., 2019), diarylheptanoid (Llano et al., 2019), and gingerol biosynthesis (Dugasani et al., 2010; Si et al., 2018); (4) ascorbate and aldarate metabolism (Zechmann, 2018);

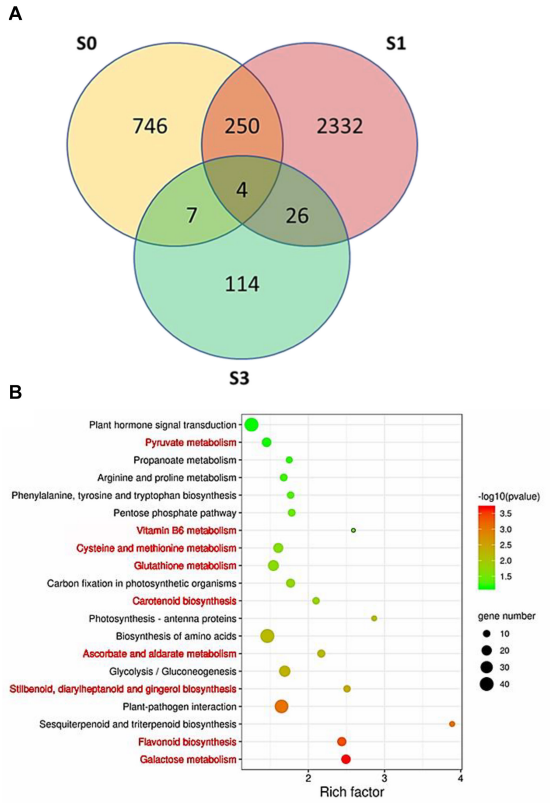

FIGURE 7 | Identification of differentially expressed genes (DEGs) between the anthers of "JX" and "ZH." **(A)** Venn diagram of DEGs at S0, S1, and S3. **(B)** Top 20 most represented categories of KEGG and the gene number predicted to belong to each category. The pathways involved in ROS homeostasis system are highlighted in red color.

(5) carotenoid biosynthesis (Kljak and Grbeša, 2015; Milani et al., 2017; Rojas-Garbanzo et al., 2017); (6) GSH metabolism (Noctor et al., 2012); (7) cysteine (Preczenhak et al., 2019) and methionine metabolism (Bender et al., 2008); (8) vitamin B_6 metabolism (Chandrasekaran and Chun, 2018); and (9) pyruvate metabolism (Ramos-Ibeas et al., 2017; Guarino et al., 2019). The DEGs involved in these ROS-related pathways are listed in **Supplementary Table 2**. These ROS-related DEGs might be responsible for the difference in the ROS content between the anthers of ZH and JX.

The Content of Major Antioxidants in the Anthers Was Lower in JX Than in ZH

To further confirm the association of pollen abortion with the ROS metabolism in JX, we measured the content of four major ROS scavengers in the anthers at S1–S5. Overall, the concentrations of APX and GST were significantly lower in anthers of JX than in those of ZH throughout the development (**Figure 8**). Similarly, the contents of carotenoids and GSH were significantly lower in the anthers of JX than in those of ZH. These results indicated there is a disruption of ROS homeostasis in anthers of JX.

[1]https://www.rosaceae.org/species/prunus_persica/genome_v2.0.a1

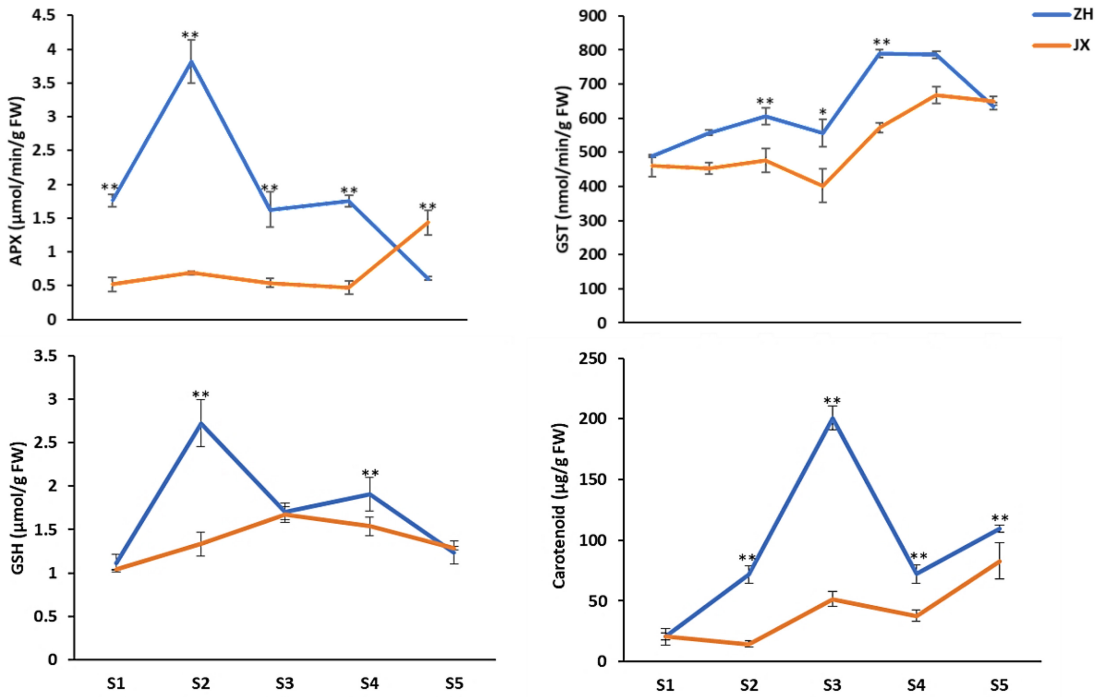

FIGURE 8 | Content of antioxidants in the anthers of "ZH" and "JX" at stages 1–5. Error bars indicate ±SD of three biological replicates. Statically significant differences at $P \leq 0.05$ and $P \leq 0.01$ (Student *t* test) are indicated by * and **, respectively.

Screening the DEGs mentioned previously revealed 12 DEGs involved in the biosynthesis of the four major antioxidants, including five (*Prupe.1G054900*, *Prupe.1G055000*, *Prupe.4G146400*, *Prupe.4G146800*, and *Prupe.4G147400*) encoding GST, one (*Prupe.5G099700*) encoding glutamate–cysteine ligase, two (*Prupe.6G091600* and *Prupe.6G242200*) encoding L-APX proteins, one (*Prupe.2G004500*) encoding zeaxanthin epoxidase, one (*Prupe.3G178500*) encoding phytoene synthase, one (*Prupe.6G072400*) encoding cytochrome P450m, and one (*Prupe.5G105100*) encoding beta-carotene hydroxylase. qRT-PCR showed that these genes had lower levels of expression in the anthers of JX at early stages than in the anthers of ZH (**Figure 9**), which is consistent with the observed lower content of major antioxidants in JX compared with ZH.

DISCUSSION

Pollen Abortion Is Associated With Abnormal Development of Microspores and Tapetum in Peach

To our knowledge, this study reports for the first time the cytological and physiological traits associated with male sterility in peach. Our results show that microspores were severely vacuolated, with deformed and incomplete exine structure, and compressed into belts that disappeared at mononuclear stage in male sterile cv. JX. Moreover, the tapetum cells were swollen, vacuolated, with a delayed degradation to flowering time. Thus, male sterility in JX is characterized by abnormal development of microspores and tapetum at mononuclear stage of pollen development. As mentioned previously, tapetum provides nutrition for the development of pollen grains. Abnormal development of microspores could be partially attributed to the disrupted development of tapetum in peach.

Similar phenotype of male sterility has also been reported in model plants such as rice and *Arabidopsis*, in which pollen abortion is frequently found to be associated with genes that are involved in tapetum development and degradation. For example, mutations of tapetum development-related genes in *Arabidopsis*, such as *MYB103*, *MS1*, *TDF*, *DYT1*, *PRX9*, and *PRX10*, can lead to comparable pollen abortion phenotypes to those observed in this study (Ito et al., 2007; Zhang et al., 2007; Zhu et al., 2008, 2015; Jacobowitz et al., 2019). In rice, functional mutations of *TDR*, *API5*, *DEX1*, *GPAT3*, and *DPW3* cause delayed degradation of tapetum, leading to male sterility with features similar to those in this study (Li et al., 2006, 2011; Yu et al., 2016; Men et al., 2017; Mondol et al., 2020). Therefore, degradation of tapetum in mononuclear stage is crucial for normal development of microspores into mature pollen grains. The delayed degradation of tapetume is likely responsible for male sterility in peach cv. JX.

Disruption of ROS Homeostasis May Hinder Pollen Development, Leading to Male Sterility in Peach

In plants, basal concentration of ROS is important in maintaining normal growth and development. The production

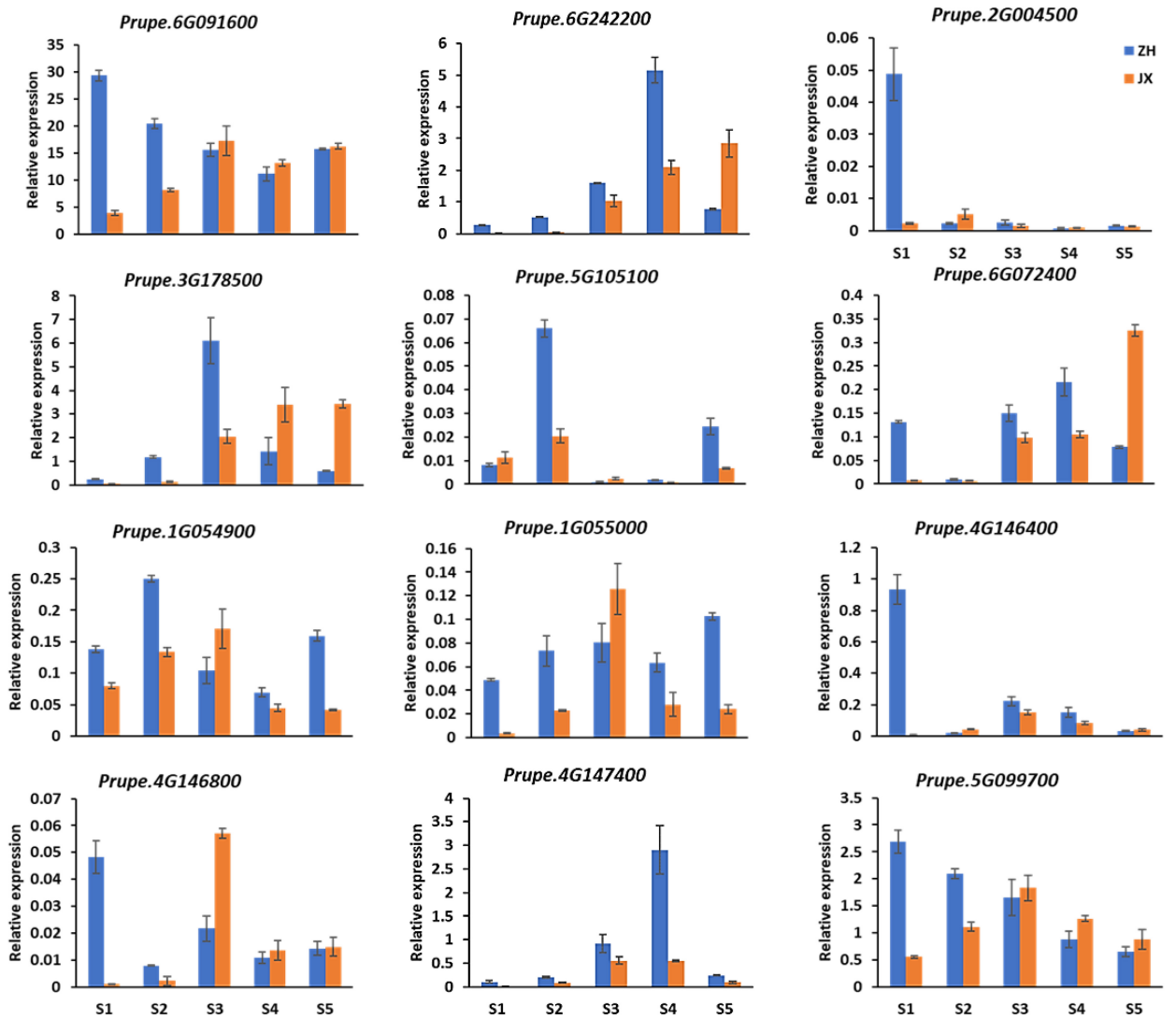

FIGURE 9 | Expression analysis of DEGs by qRT-PCR at S1–S5. Error bars indicate standard deviation from three biological and technical replicates of qRT-PCR.

and elimination of ROS are a complex network involving participation of multiple factors (Gechev et al., 2006; Miller et al., 2010; Suzuki et al., 2012; Shadel and Horvath, 2015). In this study, the anthers of JX were found to accumulate higher levels of H_2O_2 and O_2^- at early stages of development. ROS burst in anther has been found to affect tapetum degradation time (Jiang et al., 2007; Huang et al., 2012; Luo et al., 2013; Wang K. et al., 2013; Yan et al., 2014). ROS burst at the mononuclear stage is likely responsible for the delay of tapetum degradation, leading to abortion of microspores in JX. This finding is consistent with previous reports that disruption of ROS homeostasis contributes to male sterility. For example, the *BZR1* gene is involved in ROS production, and its mutation can delay tapetal cell degeneration, leading to male sterility in tomato (Yan et al., 2020), whereas increased ROS content negatively impacts pollen development in rice (Qu et al., 2014; Zheng et al., 2019; Guo et al., 2020; Zafar et al., 2020).

Plants have a complex enzymatic and non-enzymatic antioxidant system for maintaining the ROS homeostasis (Mittler et al., 2004). In this study, both major enzymatic antioxidants, APX and GST, and major non-enzymatic antioxidants, GSH and carotenoids, were detected in the anthers of ZH and JX. However, the levels of enzymatic antioxidants and non-enzymatic antioxidants were significantly lower in the anthers of JX than in those of ZH. Thus, ROS homeostasis seems to be crucial for pollen development, and its disruption could be associated with male sterility in peach. In addition, a large number of structural genes related to antioxidant production were differentially expressed in the anthers of ZH and JX. It is worthy of further studies to investigate whether antioxidant accumulation is controlled by regulatory genes in peach.

Mitochondrion is a major site of ROS production that is related to oxidative phosphorylation (Gechev et al., 2006; Miller et al., 2010; Suzuki et al., 2012; Shadel and Horvath, 2015).

Dysfunction of mitochondrial genes has been reported to cause excessive production of ROS (Touzet and Meyer, 2014). Insertion of unknown open reading frames into the mitochondrial genome causes excessive accumulation of ROS, leading to male sterility in rice (Luo et al., 2013; Wang K. et al., 2013; Xie et al., 2018). In this study, cytological and physiological characteristics of male sterility in JX were similar to those of cytoplasmic male sterile rice variety, Honglian. In addition, ROS burst was observed in the anther of JX, along with six mitochondrial genes involved in oxidative phosphorylation that were differentially expressed in the anthers of ZH and JX (**Supplementary Table 3**). These findings suggest that male sterility could be cytoplasmic due to sequence variation in the mitochondrial genome in peach, which is consistent with previous finding that ROS burst during pollen development causes Honglian type cytoplasmic male sterility (CMS-HL) in rice (Wang K. et al., 2013). Analysis of structural variation of mitochondrial genome will be a practical way to identify potential candidate genes for male sterility in peach. Notably, a previous study has reported a candidate gene on chromosome 6 (*Prupe.6G024900*) controlling male sterility in peach (Eduardo et al., 2020). However, based on RNA-seq, *Prupe.6G024900* showed no expression in the anther at S0, S1, and S3 of both JX and ZH, suggesting it is unlikely responsible for male sterility in JX. More studies are needed to clarify whether diverse mechanisms are associated with male sterility in peach germplasm.

In summary, our study reveals that disruption of ROS homeostasis may cause abnormal development of microspores and tapetum, leading to cytoplasmic-type male sterility in peach. Our results will be useful for further investigation of mechanisms underlying male sterility in peach.

DATA AVAILABILITY STATEMENT

The original contributions generated for this study are included in the article/**Supplementary Material**, further inquiries can be directed to the corresponding author.

AUTHOR CONTRIBUTIONS

YC conducted most experiments of this study and wrote the manuscript. YC, ZM, and LZ prepared the experimental materials. LL, LW, and BZ participated in the transcriptomic analysis. YH was overall project leader and revised the manuscript. CO and RZ revised the manuscript. All authors read and approved the final manuscript.

FUNDING

This project was supported by funds received from the National Key Research and Development Program (2019YFD1000800), the National Natural Science Foundation of China (31872087), and the China Agriculture Research System (grant no. CARS-30).

SUPPLEMENTARY MATERIAL

The Supplementary Material for this article can be found online at: https://www.frontiersin.org/articles/10.3389/fpls.2021.653256/full#supplementary-material

Supplementary Figure 1 | Appearance of flower buds at different developmental stages in "ZH" and "JX." Bar = 1 cm.

Supplementary Figure 2 | The Pearson correlation between samples. B represents "ZH," and C represents "JX."

Supplementary Figure 3 | The 3D PCA plot between samples. B represents "ZH," and C represents "JX."

Supplementary Figure 4 | GO classifications of DEGs at S0, S1, and S3.

Supplementary Table 1 | The primers used in this article.

Supplementary Table 2 | Differentially expressed genes (DEGs) involved in ROS-related pathways and their description.

Supplementary Table 3 | Mitochondrial DEGs involved in oxidative phosphorylation and their description.

REFERENCES

Agati, G., Azzarello, E., Pollastri, S., and Tattini, M. (2012). Flavonoids as antioxidants in plants: location and functional significance. *Plant Sci.* 196, 67–76. doi: 10.1016/j.plantsci.2012.07.014

Apel, K., and Hirt, H. (2004). Reactive oxygen species: metabolism, oxidative stress, and signal transduction. *Annu. Rev. Plant Biol.* 55, 373–399. doi: 10.1146/annurev.arplant.55.031903.141701

Bender, A., Hajieva, P., and Moosmann, B. (2008). Adaptive antioxidant methionine accumulation in respiratory chain complexes explains the use of a deviant genetic code in mitochondria. *Proc. Natl. Acad. Sci. U.S.A.* 105, 16496–16501. doi: 10.1073/pnas.0802779105

Borg, M., Brownfield, L., and Twell, D. (2009). Male gametophyte development: a molecular perspective. *J. Exp. Bot.* 60, 1465–1478. doi: 10.1093/jxb/ern355

Cai, Q., Guo, L., Shen, Z. R., Wang, D. Y., Zhang, Q., and Sodmergen. (2015). Elevation of pollen mitochondrial DNA copy number by WHIRLY2: altered respiration and pollen tube growth in *Arabidopsis*. *Plant Physiol.* 169, 660–673. doi: 10.1104/pp.15.00437

Chandrasekaran, M., and Chun, S. C. (2018). Vitamin B6 biosynthetic genes expression and antioxidant enzyme properties in tomato against, *Erwinia carotovora* subsp. carotovora. *Int. J. Biol. Macromol.* 116, 31–36. doi: 10.1016/j.ijbiomac.2018.05.024

Dugasani, S., Pichika, M. R., Nadarajah, V. D., Balijepalli, M. K., Tandra, S., and Korlakunta, J. N. (2010). Comparative antioxidant and anti-inflammatory effects of [6]-gingerol, [8]-gingerol, [10]-gingerol and [6]-shogaol. *J. Ethnopharmacol.* 127, 515–520. doi: 10.1016/j.jep.2009.10.004

Eduardo, I., de Tomás, C., Alexiou, K. G., Giovannini, D., Pietrella, M., Carpenedo, S., et al. (2020). Fine mapping of the peach pollen sterility gene (Ps/ps) and detection of markers for marker-assisted selection. *Mol. Breed.* 40:57. doi: 10.1007/s11032-020-01139-3

Fang, X., Fu, H. F., Gong, Z. H., and Chai, W. G. (2016). Involvement of a universal amino acid synthesis impediment in cytoplasmic male sterility in pepper. *Sci. Rep.* 18:23357. doi: 10.1038/srep23357

Gechev, T. S., Van Breusegem, F., Stone, J. M., Denev, I., and Laloi, C. (2006). Reactive oxygen species as signals that modulate plant stress responses and programmed cell death. *Bioessays* 28, 1091–1101. doi: 10.1002/bies.20493

Gómez, J. F., Talle, B., and Wilson, Z. A. (2015). Anther and pollen development: a conserved developmental pathway. *J. Integr. Plant Biol.* 57, 876–891. doi: 10.1111/jipb.12425

Guarino, V. A., Oldham, W. M., Loscalzo, J., and Zhang, Y. Y. (2019). Reaction rate of pyruvate and hydrogen peroxide: assessing antioxidant capacity of pyruvate under biological conditions. *Sci. Rep.* 9:19568. doi: 10.1038/s41598-019-55951-9

Guo, Y., Wu, Q., Xie, Z., Yu, B., Zeng, R., Min, Q., et al. (2020). OsFPFL4 is involved in the root and flower development by affecting auxin levels and ROS accumulation in rice (*Oryza sativa*). *Rice (N. Y.)* 13, 2. doi: 10.1186/s12284-019-0364-0

Hafsa, J., Smach, M. A., Sobeh, M., Majdoub, H., and Yasri, A. (2019). Antioxidant activity improvement of apples juice supplemented with Chitosan-galactose maillard reaction products . *Molecules* 24:4557. doi: 10.3390/molecules24244557

Hu, L., Liang, W., Yin, C., Cui, X., Zong, J., Wang, X., et al. (2011). Rice MADS3 regulates ROS homeostasis during late anther development. *Plant Cell* 23, 515–533. doi: 10.1105/tpc.110.074369

Huang, L., Xiang, J., Liu, J., Rong, T., Wang, J., Lu, Y., et al. (2012). Expression characterization of genes for CMS-C in maize. *Protoplasma* 249, 1119–1127. doi: 10.1007/s00709-011-0358-2

International Peach Genome Initiative (2013). The high-quality draft genome of peach (*P. persica*) identifies unique patterns of genetic diversity, domestication and genome evolution. *Nat. Genet.* 45, 487–494. doi: 10.1038/ng.2586

Ito, T., Nagata, N., Yoshiba, Y., Ohme-Takagi, M., Ma, H., and Shinozaki, K. (2007). *Arabidopsis* male sterility1 encodes a PHD-type transcription factor and regulates pollen and tapetum development. *Plant Cell* 19, 3549–3562. doi: 10.1105/tpc.107.054536

Jacobowitz, J. R., Doyle, W. C., and Weng, J. K. (2019). PRX9 and PRX40 are extensin peroxidases essential for maintaining tapetum and microspore cell wall integrity during *Arabidopsis* anther development. *Plant Cell* 31, 848–861. doi: 10.1105/tpc.18.00907

Jiang, P., Zhang, X., Zhu, Y., Zhu, W., Xie, H., and Wang, X. (2007). Metabolism of reactive oxygen species in cotton cytoplasmic male sterility and its restoration. *Plant Cell Rep.* 26, 1627–1634. doi: 10.1007/s00299-007-0351-6

Kljak, K., and Grbeša, D. (2015). Carotenoid content and antioxidant activity of hexane extracts from selected Croatian corn hybrids. *Food Chem.* 15, 402–408. doi: 10.1016/j.foodchem.2014.07.002

Li, D. D., Xue, J. S., Zhu, J., and Yang, Z. N. (2017). Gene regulatory network for tapetum development in *Arabidopsis thaliana*. *Front. Plant Sci.* 12:1559. doi: 10.3389/fpls.2017.01559

Li, N., Zhang, D. S., Liu, H. S., Yin, C. S., Li, X. X., Liang, W. Q., et al. (2006). The rice tapetum degeneration retardation gene is required for tapetum degradation and anther development. *Plant Cell* 18, 2999–3014. doi: 10.1105/tpc.106.044107

Li, X., Gao, X., Wei, Y., Deng, L., Ouyang, Y., Chen, G., et al. (2011). Rice APOPTOSIS INHIBITOR5 coupled with two DEAD-box adenosine 5′-triphosphate-dependent RNA helicases regulates tapetum degeneration. *Plant Cell* 23, 1416–1434. doi: 10.1105/tpc.110.082636

Liao, H., Fu, X., Zhao, H., Cheng, J., Zhang, R., Yao, X., et al. (2020). The morphology, molecular development and ecological function of pseudonectaries on *Nigella damascena* (Ranunculaceae) petals. *Nat. Commun.* 11:1777. doi: 10.1038/s41467-020-15658-2

Llano, S., Gómez, S., Londoño, J., and Restrepo, A. (2019). Antioxidant activity of curcuminoids. *Phys. Chem. Phys.* 21, 3752–3760. doi: 10.1039/C8CP06708B

Lukaszewski, A. J. (2017). Chromosomes 1BS and 1RS for control of male fertility in wheats and triticales with cytoplasms of *Aegilops kotschyi, Ae. mutica* and *Ae. uniaristata*. *Theor. Appl. Genet.* 130, 2521–2526. doi: 10.1007/s00122-017-2973-6

Luo, D., Xu, H., Liu, Z., Guo, J., Li, H., Chen, L., et al. (2013). A detrimental mitochondrial-nuclear interaction causes cytoplasmic male sterility in rice. *Nat. Genet.* 45, 573–577. doi: 10.1038/ng.2570

Mariani, C., De Beuckeleer, M., Truettner, J., Leemans, J., and Goldberg, R. B. (1990). Induction of male sterility in plants by achimeric ribonuclease gene. *Nature* 347, 737–741. doi: 10.1038/347737a0

McCormick, S. (2004). Control of male gametophyte development. *Plant Cell* 16(Suppl.), S142–S153. doi: 10.1105/tpc.016659

Men, X., Shi, J., Liang, W., Zhang, Q., Lian, G., Quan, S., et al. (2017). Glycerol-3-phosphate acyltransferase 3 (OsGPAT3) is required for anther development and male fertility in rice. *J. Exp. Bot.* 68, 513–526. doi: 10.1093/jxb/erw445

Milani, A., Basirnejad, M., Shahbazi, S., and Bolhassani, A. (2017). Carotenoids: biochemistry, pharmacology and treatment. *Br. J. Pharmacol.* 174, 1290–1324. doi: 10.1111/bph.13625

Miller, G., Suzuki, N., Ciftci-Yilmaz, S., and Mittler, R. (2010). Reactive oxygen species homeostasis and signalling during drought and salinity stresses. *Plant Cell Environ.* 33, 453–467. doi: 10.1111/j.1365-3040.2009.02041.x

Mittler, R., Vanderauwera, S., Gollery, M., and Van Breusegem, F. (2004). Reactive oxygen gene network of plants. *Trends Plant Sci.* 9, 490–498. doi: 10.1016/j.tplants.2004.08.009

Mondol, P. C., Xu, D., Duan, L., Shi, J., Wang, C., Chen, X., et al. (2020). Defective pollen wall 3 (DPW3), a novel alpha integrin-like protein, is required for pollen wall formation in rice. *New Phytol.* 225, 807–822. doi: 10.1111/nph.16161

Nassiri-Asl, M., and Hosseinzadeh, H. (2016). Review of the pharmacological effects of *Vitis vinifera* (Grape) and its bioactive constituents: an update. *Phytother. Res.* 30, 1392–1403. doi: 10.1002/ptr.5644

Noctor, G., Mhamdi, A., Chaouch, S., Han, Y., Neukermans, J., Marquez-Garcia, B., et al. (2012). Glutathione in plants: an integrated overview. *Plant Cell Environ.* 35, 454–484. doi: 10.1111/j.1365-3040.2011.02400.x

Parish, R. W., and Li, S. F. (2010). Death of a tapetum: a programme of developmental altruism. *Plant Sci.* 178, 73–89. doi: 10.1016/j.plantsci.2009.11.001

Preczenhak, A. P., Orsi, B., Lima, G. P. P., Tezotto-Uliana, J. V., Minatel, I. O., and Kluge, R. A. (2019). Cysteine enhances the content of betalains and polyphenols in fresh-cut red beet. *Food Chem.* 15, 600–607. doi: 10.1016/j.foodchem.2019.02.040

Qu, G., Quan, S., Mondol, P., Xu, J., Zhang, D., and Shi, J. (2014). Comparative metabolomic analysis of wild type and mads3 mutant rice anthers. *J. Integr. Plant Biol.* 56, 849–863. doi: 10.1111/jipb.12245

Ramos-Ibeas, P., Barandalla, M., Colleoni, S., and Lazzari, G. (2017). Pyruvate antioxidant roles in human fibroblasts and embryonic stem cells. *Mol. Cell. Biochem.* 429, 137–150. doi: 10.1007/s11010-017-2942-z

Rojas-Garbanzo, C., Gleichenhagen, M., Heller, A., Esquivel, P., Schulze-Kaysers, N., and Schieber, A. (2017).). Carotenoid Profile, antioxidant capacity, and chromoplasts of pink guava (*Psidium guajava* L. Cv. 'Criolla') during Fruit Ripening. *J. Agric. Food Chem.* 65, 3737–3747. doi: 10.1021/acs.jafc.6b04560

Shadel, G. S., and Horvath, T. L. (2015). Mitochondrial ROS signaling in organismal homeostasis. *Cell* 163, 560–569. doi: 10.1016/j.cell.2015.10.001

Si, W., Chen, Y. P., Zhang, J., Chen, Z. Y., and Chung, H. Y. (2018). Antioxidant activities of ginger extract and its constituents toward lipids. *Food Chem.* 15, 1117–1125. doi: 10.1016/j.foodchem.2017.07.055

Singh, S. P., Pandey, T., Srivastava, R., Verma, P. C., Singh, P. K., and Tuli, R. (2010). BECLIN1 from *Arabidopsis thaliana* under the generic control of regulated expression systems, a strategy for developing male sterile plants. *Plant Biotechnol. J.* 8, 1005–1022. doi: 10.1111/j.1467-7652.2010.00527.x

Suzuki, N., Koussevitzky, S., Mittler, R., and Miller, G. (2012). ROS and redox signalling in the response of plants to abiotic stress. *Plant Cell Environ.* 35, 259–270. doi: 10.1111/j.1365-3040.2011.02336.x

Tong, Z., Gao, Z., Wang, F., Zhou, J., and Zhang, Z. (2009). Selection of reliable reference genes for gene expression studies in peach using real-time PCR. *BMC Mol. Biol.* 10:71. doi: 10.1186/1471-2199-10-71

Touzet, P., and Meyer, E. H. (2014). Cytoplasmic male sterility and mitochondrial metabolism in plants. *Mitochondrion* 19(Pt B), 166–171. doi: 10.1016/j.mito.2014.04.009

Treml, J., Leláková, V., Šmejkal, K., Paulíčková, T., Labuda, Š, Granica, S., et al. (2019). Antioxidant activity of selected Stilbenoid derivatives in a cellular model dystem. *Biomolecules* 9:468. doi: 10.3390/biom9090468

Wang, K., Gao, F., Ji, Y., Liu, Y., Dan, Z., Yang, P., et al. (2013). ORFH79 impairs mitochondrial function via interaction with a subunit of electron transport chain complex III in Honglian cytoplasmic male sterile rice. *New Phytol.* 198, 408–418. doi: 10.1111/nph.12180

Wang, L., Zhao, S., Gu, C., Zhou, Y., Zhou, H., Ma, J., et al. (2013). Deep RNA-Seq uncovers the peach transcriptome landscape. *Plant Mol. Biol.* 83, 365–377. doi: 10.1007/s11103-013-0093-5

Wang, R., Shi, C., Wang, X., Li, R., Meng, Y., Cheng, L., et al. (2020). Tomato SlIDA has a critical role in tomato fertilization by modifying reactive oxygen species homeostasis. *Plant J.* 103, 2100–2118. doi: 10.1111/tpj.14886

Wei, L., Yang, M., Huang, L., and Lin Li, J. (2019). Antibacterial and antioxidant flavonoid derivatives from the fruits of *Metaplexis japonica*. *Food Chem.* 15, 308–312. doi: 10.1016/j.foodchem.2019.03.070

Wilson, Z. A., and Zhang, D. B. (2009). From *Arabidopsis* to rice: pathways in pollen development. *J. Exp. Bot.* 60, 1479–1492. doi: 10.1093/jxb/erp095

Xie, H., Peng, X., Qian, M., Cai, Y., Ding, X., Chen, Q., et al. (2018). The chimeric mitochondrial gene orf182 causes non-pollen-type abortion in Dongxiang cytoplasmic male-sterile rice. *Plant J.* 95, 715–726. doi: 10.1111/tpj.13982

Xie, H. T., Wan, Z. Y., Li, S., and Zhang, Y. (2014). Spatiotemporal production of reactive oxygen species by NADPH oxidase is critical for tapetal programmed cell death and pollen development in *Arabidopsis*. *Plant Cell* 26, 2007–2023. doi: 10.1105/tpc.114.125427

Xie, Y., Zheng, Y., Dai, X., Wang, Q., Cao, J., and Xiao, J. (2015). Seasonal dynamics of total flavonoid contents and antioxidant activity of *Dryopteris erythrosora*. *Food Chem.* 186, 113–118. doi: 10.1016/j.foodchem.2014.05.024

Yan, J., Tian, H., Wang, S., Shao, J., Zheng, Y., Zhang, H., et al. (2014). Pollen developmental defects in ZD-CMS rice line explored by cytological, molecular and proteomic approaches. *J. Proteomics* 28, 110–123. doi: 10.1016/j.jprot.2014.05.014

Yan, M. Y., Xie, D. L., Cao, J. J., Xia, X. J., Shi, K., Zhou, Y. H., et al. (2020). Brassinosteroid-mediated reactive oxygen species are essential for tapetum degradation and pollen fertility in tomato. *Plant J.* 102, 931–947. doi: 10.1111/tpj.14672

Yang, Z., Liu, L., Sun, L., Yu, P., Zhang, P., Abbas, A., et al. (2019). OsMS1 functions as a transcriptional activator to regulate programmed tapetum development and pollen exine formation in rice. *Plant Mol. Biol.* 99, 175–191. doi: 10.1007/s11103-018-0811-0

Yu, J., Meng, Z., Liang, W., Behera, S., Kudla, J., Tucker, M. R., et al. (2016). A rice Ca2+ binding protein is required for tapetum function and pollen formation. *Plant Physiol.* 172, 1772–1786. doi: 10.1104/pp.16.01261

Zafar, S. A., Patil, S. B., Uzair, M., Fang, J., Zhao, J., Guo, T., et al. (2020). Degenerated panicle and partial sterility 1 (DPS1) encodes a cystathionine β-synthase domain containing protein required for anther cuticle and panicle development in rice. *New Phytol.* 225, 356–375. doi: 10.1111/nph.16133

Zechmann, B. (2018). Compartment-specific importance of ascorbate during environmental stress in plants. *Antioxid. Redox Signal.* 29, 1488–1501. doi: 10.1089/ars.2017.7232

Zhang, D., Luo, X., and Zhu, L. (2011). Cytological analysis and genetic control of rice anther development. *J. Genet. Genomics* 38, 379–390. doi: 10.1016/j.jgg.2011.08.001

Zhang, Z. B., Zhu, J., Gao, J. F., Wang, C., Li, H., Li, H., et al. (2007). Transcription factor AtMYB103 is required for anther development by regulating tapetum development, callose dissolution and exine formation in *Arabidopsis*. *Plant J.* 52, 528–538. doi: 10.1111/j.1365-313X.2007.03254.x

Zheng, S., Li, J., Ma, L., Wang, H., Zhou, H., Ni, E., et al. (2019). OsAGO2 controls ROS production and the initiation of tapetal PCD by epigenetically regulating OsHXK1 expression in rice anthers. *Proc. Natl. Acad. Sci. U.S.A.* 116, 7549–7558. doi: 10.1073/pnas.1817675116

Zhou, B., Liu, Y., Chen, Z., Liu, D., Wang, Y., Zheng, J., et al. (2019). Comparative transcriptome analysis reveals the cause for accumulation of reactive oxygen species during pollen abortion in cytoplasmic male-sterile kenaf line 722HA. *Int. J. Mol. Sci.* 20:5515. doi: 10.3390/ijms20215515

Zhu, E., You, C., Wang, S., Cui, J., Niu, B., Wang, Y., et al. (2015). The DYT1-interacting proteins bHLH010, bHLH089 and bHLH091 are redundantly required for *Arabidopsis* anther development and transcriptome. *Plant J.* 83, 976–990. doi: 10.1111/tpj.12942

Zhu, J., Chen, H., Li, H., Gao, J. F., Jiang, H., Wang, C., et al. (2008). Defective in tapetal development and function 1 is essential for anther development and tapetal function for microspore maturation in *Arabidopsis*. *Plant J.* 55, 266–277. doi: 10.1111/j.1365-313X.2008.03500.x

Zhu, J., Lou, Y., Xu, X., and Yang, Z. N. (2011). A genetic pathway for tapetum development and function in *Arabidopsis*. *J. Integr. Plant Biol.* 53, 892–900. doi: 10.1111/j.1744-7909.2011.01078.x

Zhu, L., He, S., Liu, Y., Shi, J., and Xu, J. (2020). *Arabidopsis* FAX1 mediated fatty acid export is required for the transcriptional regulation of anther development and pollen wall formation. *Plant Mol. Biol.* 104, 187–201. doi: 10.1007/s11103-020-01036-5

Conflict of Interest: The authors declare that the research was conducted in the absence of any commercial or financial relationships that could be construed as a potential conflict of interest.

frontiers in Plant Science

ORIGINAL RESEARCH
published: 04 May 2021
doi: 10.3389/fpls.2021.639345

Genomic Characterization of the Fruity Aroma Gene, *FaFAD1*, Reveals a Gene Dosage Effect on γ-Decalactone Production in Strawberry (*Fragaria* × *ananassa*)

*Youngjae Oh[1], Christopher R. Barbey[2], Saket Chandra[1], Jinhe Bai[3], Zhen Fan[1], Anne Plotto[3], Jeremy Pillet[2], Kevin M. Folta[2], Vance M. Whitaker[1] and Seonghee Lee[1]**

[1] Department of Horticultural Sciences, Institute of Food and Agricultural Sciences (IFAS) Gulf Coast Research and Education Center, University of Florida, Wimauma, FL, United States, [2] Department of Horticultural Sciences, University of Florida, Gainesville, FL, United States, [3] Horticultural Research Laboratory, Agricultural Research Service (ARS), U.S. Department of Agriculture (USDA), Fort Pierce, FL, United States

Strawberries produce numerous volatile compounds that contribute to the unique flavors of fruits. Among the many volatiles, γ-decalactone (γ-D) has the greatest contribution to the characteristic fruity aroma in strawberry fruit. The presence or absence of γ-D is controlled by a single locus, *FaFAD1*. However, this locus has not yet been systematically characterized in the octoploid strawberry genome. It has also been reported that the volatile content greatly varies among the strawberry varieties possessing *FaFAD1*, suggesting that another genetic factor could be responsible for the different levels of γ-D in fruit. In this study, we explored the genomic structure of *FaFAD1* and determined the allele dosage of *FaFAD1* that regulates variations of γ-D production in cultivated octoploid strawberry. The genome-wide association studies confirmed the major locus *FaFAD1* that regulates the γ-D production in cultivated strawberry. With the hybrid capture-based next-generation sequencing analysis, a major presence–absence variation of *FaFAD1* was discovered among γ-D producers and non-producers. To explore the genomic structure of *FaFAD1* in the octoploid strawberry, three bacterial artificial chromosome (BAC) libraries were developed. A deletion of 8,262 bp was consistently found in the *FaFAD1* region of γ-D non-producing varieties. With the newly developed InDel-based codominant marker genotyping, along with γ-D metabolite profiling data, we revealed the impact of gene dosage effect for the production of γ-D in the octoploid strawberry varieties. Altogether, this study provides systematic information of the prominent role of *FaFAD1* presence and absence polymorphism in producing γ-D and proposes that both alleles of *FaFAD1* are required to produce the highest content of fruity aroma in strawberry fruit.

Keywords: high-resolution melting marker, SNP array, GC-MASS, genome-wide association analysis, octoploid strawberry, fruit flavor

OPEN ACCESS

Edited by:
Zhongchi Liu, University of Maryland, College Park, United States

Reviewed by:
Iraida Amaya, Andalusian Institute for Research and Training in Agriculture, Fisheries, Food and Ecological Production (IFAPA), Spain
Michael Nicolas, Consejo Superior de Investigaciones Científicas (CSIC), Spain
Christophe Rothan, Le nouvel Institut national de recherche sur l'agriculture, l'alimentation et l'environnement en France INRAE, France

***Correspondence:**
Seonghee Lee
seonghee105@ufl.edu

Specialty section:
This article was submitted to Plant Development and EvoDevo, a section of the journal Frontiers in Plant Science

Received: *08 December 2020*
Accepted: *16 March 2021*
Published: *04 May 2021*

Citation:
Oh Y, Barbey CR, Chandra S, Bai J, Fan Z, Plotto A, Pillet J, Folta KM, Whitaker VM and Lee S (2021) Genomic Characterization of the Fruity Aroma Gene, FaFAD1, Reveals a Gene Dosage Effect on γ-Decalactone Production in Strawberry (Fragaria × ananassa). Front. Plant Sci. 12:639345. doi: 10.3389/fpls.2021.639345

INTRODUCTION

Flavor and aroma are important characteristics of fruit quality in the cultivated octoploid strawberry (*Fragaria* × *ananassa*). Over 350 volatile compounds have been characterized in strawberry fruit including alcohols, aldehydes, esters, ketones, lactones, and terpenes (Latrasse, 1991; Urrutia et al., 2017). The major aroma compounds are identified as esters, lactones, furanones, sulfur compounds, and terpenoids (Perez et al., 1992; Zabetakis and Holden, 1997; Dong et al., 2013; Cruz-Rus et al., 2017). Among these flavor and aroma compounds, γ-decalactone (γ-D) has a desirable "fruity," "sweet," or "peach-like" aroma in strawberry fruit (Larsen et al., 1992; Jetti et al., 2007; Ulrich et al., 2007; Jouquand et al., 2008; Olbricht et al., 2008). Presence or absence of γ-D in strawberry fruit is controlled by a single gene, *FaFAD1*, encoding omega-6 fatty acid desaturase. This gene was mapped to the linkage group III (LG3) in the octoploid strawberry (Zorrilla-Fontanesi et al., 2012; Chambers et al., 2014; Sánchez-Sevilla et al., 2014). The abundance of γ-D is closely linked to *FaFAD1* transcript levels, and a PCR-based marker has been developed, which mostly predicts presence/absence of both *FAD1* and γ-D abundance (Cruz-Rus et al., 2017). However, the causal mutation that modulates γ-D abundance remains uncharacterized and prevents the development of a functional marker. While it has been hypothesized that the lack of γ-D is due to a deletion of the *FaFAD1* (Chambers et al., 2014; Sánchez-Sevilla et al., 2014), the precise genomic context of the deletion has not been characterized. Therefore, additional sequencing and comparative analyses are required to characterize the genomic structure of the *FaFAD1* region.

The concentration of γ-D varies widely among different γ-D-producing accessions (Chambers et al., 2014); however, the potential genetic and environmental causes for this variation have not been identified. Gene copy number variation (CNV) and gene dosage effects could be major sources of trait variation, with examples including muscat flavor in grapevine, aluminum tolerance in maize, and flowering time in wheat (Díaz et al., 2012; Maron et al., 2013; Emanuelli et al., 2014). In previous studies, several gene-specific sequence-tagged site (STS) and high-resolution melting (HRM) markers accurately predicted the presence and absence of *FaFAD1* in strawberry cultivars (Sánchez-Sevilla et al., 2014; Noh et al., 2017). However, these dominant markers could not explain any possible gene dosage effects for variation in γ-D content. A functional codominant marker could help characterize gene dosage effects and provide increased efficiency in marker-assisted breeding.

The modern cultivated strawberry (*Fragaria* × *ananassa*) is an allo-octoploid (2n = 8 × = 56), hybridization between a Chilean strawberry (*F. chiloensis*) and a North American native strawberry (*F. virginiana*) (Njunguna et al., 2013). The genome of diploid progenitor species *Fragaria vesca* was sequenced (Shulaev et al., 2011) and has been used as a diploid reference genome for gene-trait association studies in *F.* × *ananassa* and toward DNA marker development. However, the octoploid *F.* × *ananassa* genome is far more complicated than its diploid progenitors. In the last year, the chromosome-scale *F.* × *ananassa* 'Camarosa' reference genome was developed, and *F. vesca* was shown to be the dominant diploid progenitor in terms of gene content, expression abundance, and genetic control for metabolic and disease resistance traits (Edger et al., 2019). Two other diploid progenitors, *F. iinumae* and *F. nipponica*, have been recently fully sequenced[1]. The other new reference genome will serve as a powerful genetic resource to unravel complexity of the octoploid cultivated strawberry genome for gene-trait association studies.

Unlike the diploid genome, polyploid genomes have complex subgenomes that originated from the same/different diploid ancestors (Wendel, 1989, 2000; Levy and Feldman, 2002; Wendel and Cronn, 2003; Aharoni et al., 2004; Edger et al., 2019). Thus, polyploid subgenomes will likely show variation in copy numbers at homoeologous loci. Duplicated homologs are often observed in different subgenomes, which leads to difficulties in the isolation of subgenome-specific sequences or gene variations related to phenotypic trait variations. In particular, when certain genomic information is missing in a reference genome, bacterial artificial chromosome (BAC) libraries carrying large insert genomic DNA can be an effective tool for map-based gene cloning and characterization of target genomic regions in polyploids (Klymiuk et al., 2018; Liu et al., 2018). Because of the complexity of the octoploid strawberry genome, the recent construction of high-quality subgenome-specific reference sequences significantly facilitates identification of quantitative trait loci (QTL) and development of DNA markers tightly linked to agronomical important traits. The current octoploid reference genome (cv. Camarosa) is not phased genome assembly, and thus it does not contain complete genome information of each haplotype. There is another octoploid reference sequence available from Japanese cultivar 'Reikou', which is haplotype-resolved assembly[2], but this draft genome sequence has not been fully characterized. Due to the high levels of genetic variations present in different breeding germplasm, it is not possible to explain all the genetic complexity of the octoploid cultivated strawberry with only two reference genomes. In addition, the two octoploid strawberry reference genomes do not have the *FaFAD1* region, and this hinders dissection of the functional sequence variations linked to γ-D content among cultivated strawberry varieties. Because of these limitations, chromosome specific BAC libraries can be especially valuable in polyploid varieties as they avoid the problem of homoeology (Wang et al., 2007), and they further identify genomic regions of target traits that are absent in the reference genome sequence (Gordon et al., 1999).

This report presents a comprehensive characterization of the genomic context of the *FaFAD1* deletion, along with functional data showing that the gene is both necessary and sufficient for γ-D production. A dosage effect has been observed between the allelic states, allowing the development of co-dominant DNA markers that can be used to assess a genotype's ability to produce this important flavor volatile.

[1] https://www.rosaceae.org/

[2] http://strawberry-garden.kazusa.or.jp/index.html

RESULTS

Physical Mapping of the Major Locus *FaFAD1* That Regulates the Production of γ-D in the Octoploid Strawberry

To characterize the genomic region of *FaFAD1* in the octoploid cultivated strawberry, we conducted multiscale genomic approaches as shown in **Figure 1**. The locus controlling γ-D was previously identified on linkage group LGIII-2 (Sánchez-Sevilla et al., 2014). RNA-sequencing analysis identified a candidate gene, *FATTY ACID DESATURASE GENE 1* (*FaFAD1*), responsible for the presence/absence of γ-D in the octoploid strawberries (Chambers et al., 2014). To determine the physical location of the *FaFAD1* locus in the octoploid strawberry genome, IStraw35 whole genome SNP genotyping was conducted, with a genome-wide association study (GWAS) identifying a single peak for γ-D biosynthesis ($h^2 = 0.536$) on chromosome group 3 (**Figure 2A**). To identify the subgenome harboring *FaFAD1*, 11 significant SNP probes were aligned to the four subgenomes of chromosome group 3 of the 'Camarosa' reference genome (**Table 1**). All of the 11 probes were located from 25.2 to 31.3 M on subgenome 3-2. Single-marker analysis with AX-166512929 that is closely associated with the *FaFAD1* locus suggests that this QTL is responsible for the natural variations of γ-D in the octoploid strawberry accessions (**Figure 2B**). There was also significant variation in γ-D content between homozygous (AA) and heterozygous (AB) accessions (**Figure 2B**).

Agroinfiltration experiments were used to test the requirement of *FAD1* for γ-D production. Developing fruits of a γ-D-producing genotype were treated with *Agrobacterium* cultures containing an RNAi construct targeting *FaFAD1*. Decreased accumulation of *FaFAD1* transcripts was related to a significant reduction in γ-D (**Figure 2C**). These results substantially provide evidence that the *FaFAD1* gene is a key regulator for the production of γ-D in the octoploid strawberry.

A Large Deletion Was the Only Genomic Variation Linked to γ-D Production

The published allele for *FaFAD1* (Sánchez-Sevilla et al., 2014) was not detected in the 'Camarosa' reference genome, which is consistent with this cultivar not producing γ-D. Thus, it is not possible to examine the genomic structure of *FaFAD1* using the current reference genome for the octoploid strawberry. Using hybridization capture-based target enrichment sequencing, we investigated the 100 kb region of *FaFAD1* to examine for the potential genomic variants that could be linked to γ-D content. Hybridization probes for the genomic region of *FaFAD1* were designed using the *F. vesca* genome sequence. A total of 57,308,440 paired-end reads were generated for the target region of 100 kb, and *de novo* assembly was performed on 15 individuals (11 γ-D producers and four γ-D non-producers). A number of SNPs were found in the 100 kb region containing *FaFAD1*, but none correlated with the production of γ-D.

The large deletion of *FaFAD1* occurred only in γ-D non-producers, including the genotypes 'Winter Dawn', 'Mara des Bois', 'Strawberry Festival', and FL 12.74-39 (**Figure 3**). In the *FaFAD1* genomic region, any CNVs associated with the *FaFAD1* gene did not present in all 11 γ-D producers. Because Illumina short reads (150 bp pair end) were used in this analysis, it was not possible to differentiate subgenome-specific sequence variations or determine the exact size of the insertion/deletion.

The Deletion of *FaFAD1* Dictates γ-D Variation in the Octoploid Cultivated Strawberry

In order to exploit the genomic region of *FaFAD1* in γ-D-producing accessions, three BAC libraries developed from the University of Florida strawberry breeding accessions (FL 11.77-96 and 'Florida Brilliance': *FaFAD1*, and FL 14.101-225: *fafad1*) were screened with two gene-based markers, UFGDHRM5 (Noh et al., 2017) and qFaFAD1 (Sánchez-Sevilla et al., 2014) (**Supplementary Tables 1, 3**). Because both 'Camarosa' and 'Reikou' do not contain *FaFAD1*, the genomic structure could not be characterized from the reference sequence.

In the super pool (SP) screening using agarose gel electrophoresis with UFGDHRM5 and qFaFAD1 markers, 2–4 positive clones were identified from each of the BAC libraries, and further initiated to matrix pool (MP) screening for all libraries (**Supplementary Figures 1, 2**). In the result of MP screening, a total of six positive clones from two BAC libraries of γ-D producers, FL 11.77-96 and 'Florida Brilliance', were identified and further processed for sequencing. Illumina short reads from six BAC clones yielded approximately 7.7 million reads (average 149 bp length) and *de novo* assembly was performed (**Supplementary Figure 3** and **Supplementary Table 2**). All of the six BAC clones generated 3–9 contigs with an average length of 135 kb. To determine sequence variations in the genomic region of *FaFAD1* among γ-D producers and γ-D non-producers, the contig sequences from all six BAC clones were aligned to the two octoploid reference sequences (cv. Camarosa and Reikou). A deletion of 8,262 bp, including 2,323 bp for *FaFAD1*, was consistently found in γ-D non-producers 'Camarosa' and 'Reikou' (**Figure 4A** and **Supplementary Figure 4**).

To confirm the difference in the genomic structure of the 8,262 bp indel region between γ-D producers and non-producers, whole genome sequencing reads of two breeding accessions (FL 10-92: γ-D producer, FL 13.55-195: γ-D non-producer) were mapped to the clone, BAC_GD004, from library BB1 ('Florida Brilliance') (**Figure 4B**). Illumina sequence reads were evenly mapped to the 8,262 bp insertion region in the γ-D producer, FL 10-92, while reads associated with *FaFAD1* were missing in the γ-D non-producer, FL 13.55-195. Some short reads were mapped to the flanking region of *FaFAD1* in the non-producer, because these reads are from other homeologous subgenomes of chromosome 3. The reads mapped to the promoter and coding region of *FaFAD1* are from the homologous gene located in chromosome 6. This homologous gene is not functionally associated with the production of γ-D production. Furthermore, to examine if the 8,262 bp presence/absence polymorphism is consistently present in other cultivated strawberry accessions,

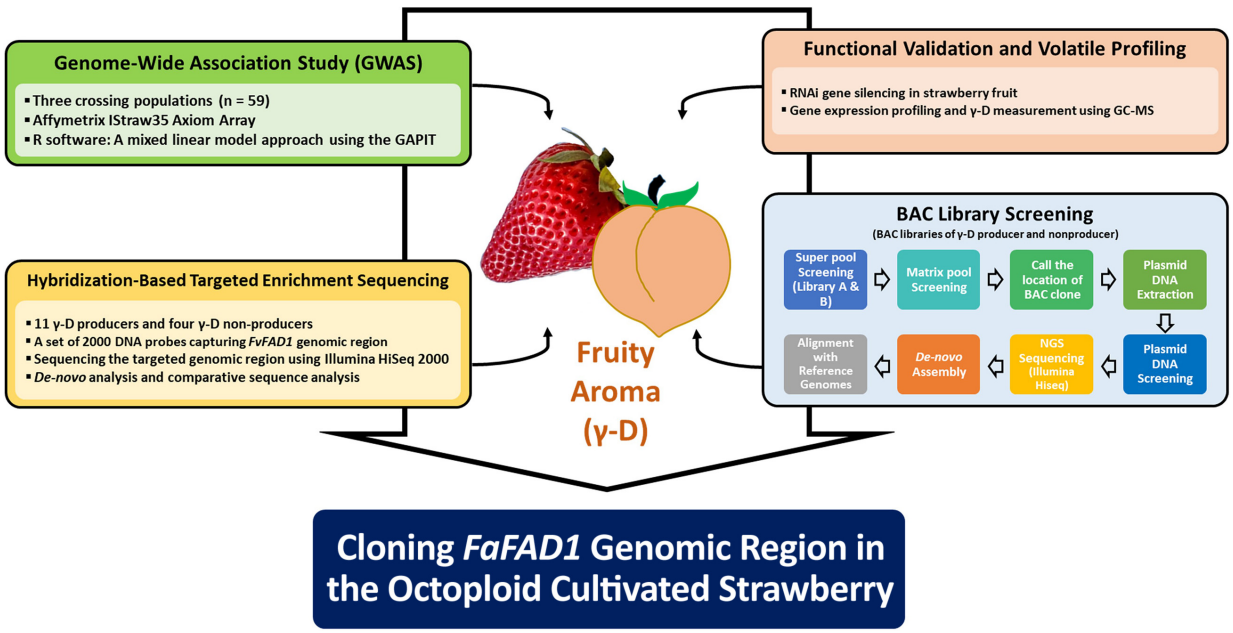

FIGURE 1 | Schematic diagram for the genomic characterization of fruity aroma gene *FaFAD1* in the octoploid cultivated strawberry.

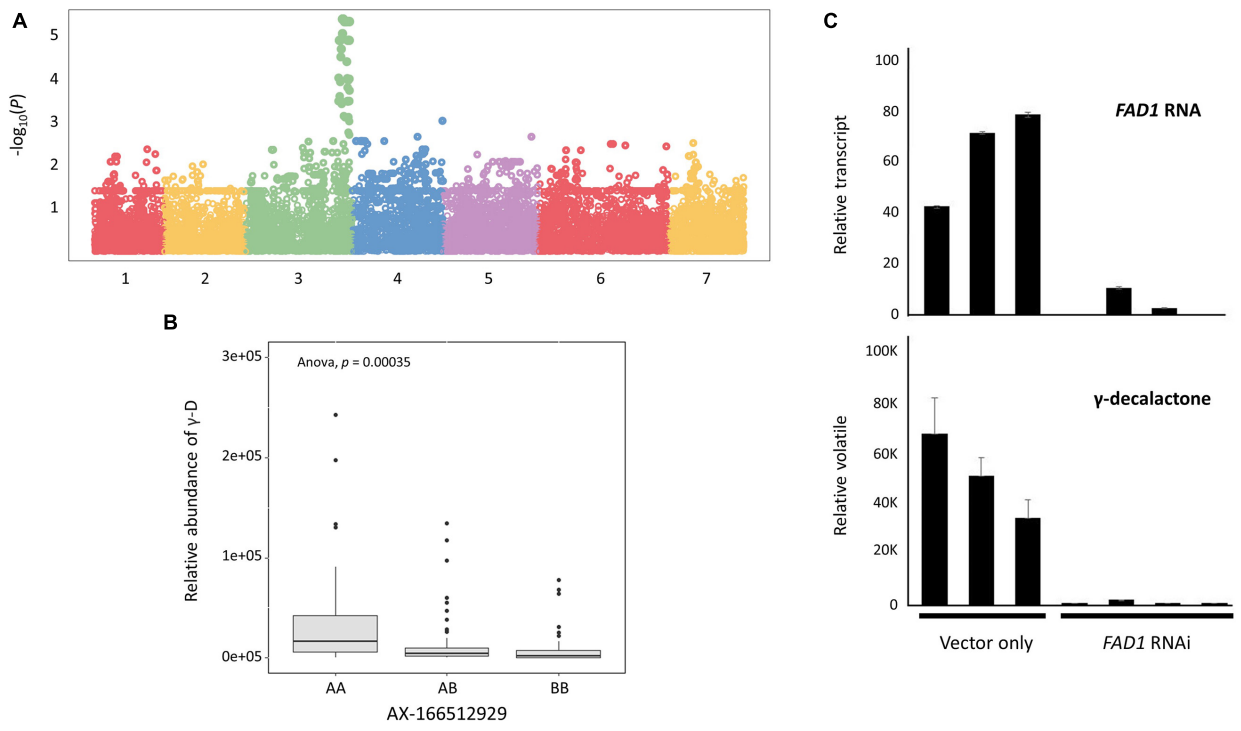

FIGURE 2 | *FaFAD1* is a major locus that regulates for the production of γ-decalactone in the octoploid strawberry. **(A)** Manhattan plot of genome-wide association study for γ-decalactone. **(B)** Comparison of γ-decalactone content between different genotypes of a single marker (AX-166512929). **(C)** RNAi transient assay for *FaFAD1* in strawberry fruit. Bars represent mean, and error bars represent standard deviation for the three biological replicates.

the long-range PCR was conducted with each of five γ-D producers and γ-D non-producers. All five γ-D producers tested had a PCR product of the expected size (9,209 bp), while 947 bp was amplified in other γ-D non-producers due to the absence of 8,262 bp (**Figure 4C**). Taken altogether, our results strongly indicate that the presence/absence variation of *FaFAD1*

TABLE 1 | Physical location of the *FaFAD1* locus in diploid (*F. vesca*) and octoploid (*F.* × *ananassa*) strawberry.

SNP ID[a]	Chr. location (*F. vesca*)	Physical location (*F. vesca*)[b]	SNP marker location in *F.* × *ananassa* cv. Camarosa			
			Chr. 3-1	Chr. 3-2	Chr. 3-3	Chr. 3-4
AX-166512929	Chr. 3	30,211,312	–	29,761,869	–	2,002,493
AX-166504731	Chr. 3	32,524,288	–	30,719,612	–	893,136
AX-166510266	Chr. 3	29,399,062	–	29,191,207	–	3,572,806
AX-166517843	Chr. 3	29,567,447	2,270,475	29,384,352	–	–
AX-166504721	Chr. 3	32,313,444	807,512	30,650,836	–	965,986
AX-166522139	Chr. 3	32,370,296	–	30,668,160	–	–
AX-166512832	Chr. 3	32,424,673	–	30,684,817	–	987,060
AX-89912298	Chr. 3	29,593,040	2,262,160	29,406,849	27,457,717	2,555,020
AX-166519513	Chr. 3	32,812,041	96,868	31,307,920	29,608,552	155,496
AX-89912372	Chr. 3	31,060,850	1,221,378	30,397,639	–	1,385,503
AX-123524646	Chr. 3	24,023,662	6,600,875	25,184,632	23,414,517	6,539,416

[a]*Axiom 35K SNP marker.*
[b]*physical location shown in base pair (bp).*

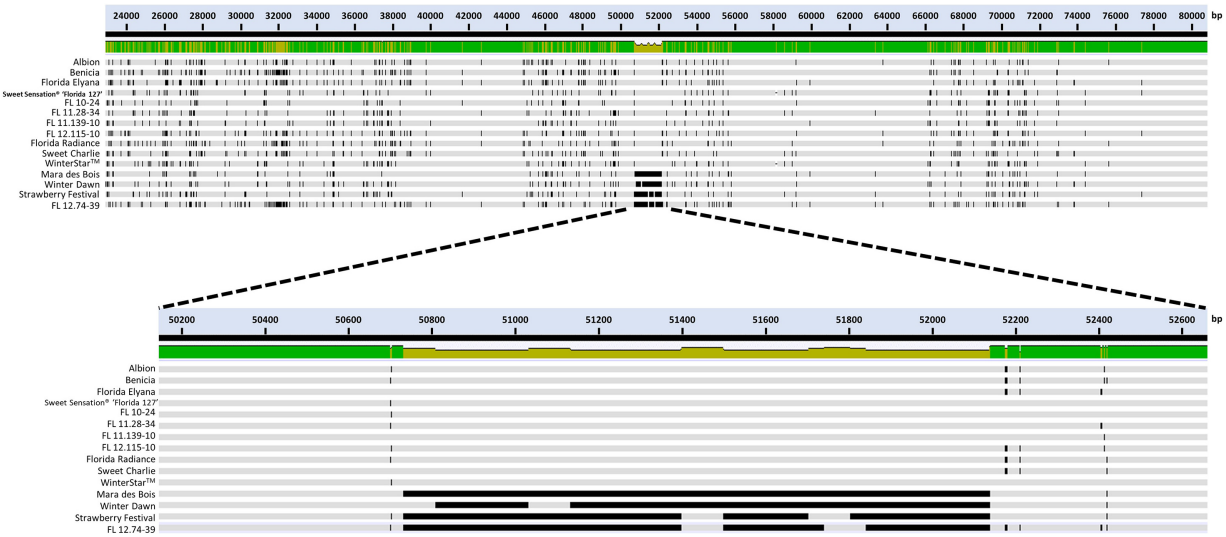

FIGURE 3 | Hybrid-probe captured sequencing for the 100-kb flanking region of *FaFAD1* and comparative analysis among γ-D producers and γ-D non-producers. Illumina short reads (150 bp PE) were assembled to the *FvFAD1* region from the *F. vesca* reference genome (Edger et al., 2018). Each line represents a 100-kb flanking region of *FaFAD1* for 15 genotypes. The dark black lines represent deleted genomic sequences in the *FaFAD1* region.

region is directly related to the production of γ-D in the octoploid strawberry.

Codominant Marker Reveals Gene Dosage Effects on γ-D Production

It has been demonstrated that the content of γ-D varies among producers (Chambers et al., 2014). As shown in **Table 2**, the amount of γ-D in 48 accessions, 38 with *FaFAD1* and 10 accessions without *FaFAD1*, was measured using gas chromatography/mass spectroscopy (GC-MS) (**Table 2**). The content of γ-D is widely diverse among the 38 producers, while γ-D is not detectable in γ-D non-producers. To examine *FaFAD1* gene dosage effects on the variation in γ-D content, codominant high-resolution melting (HRM) and Kompetitive Allele Specific PCR (KASP) markers were developed from the flanking region of *FaFAD1* to amplify a common genomic sequence in both γ-D producers and γ-D non-producers. An 11-bp InDel located at 30,134,000 bp on chromosome 3-2 ('Camarosa') was targeted by HRM and KASP markers and tested on the 48 accessions (**Figure 5**, **Supplementary Figure 4**, and **Supplementary Table 3**). HRM and KASP markers developed from the flanking region of *FaFAD1* were used to amplify a common genomic sequence in both γ-D producers and non-producers to examine the *FaFAD1* gene dosage effects (**Supplementary Figure 4**).

All tested markers including a dominant marker (UFGDHRM5) detected the presence and absence of *FaFAD1* in the accessions (**Figure 5** and **Table 2**). It was of interest to test if variation was associated with dosage imparted from

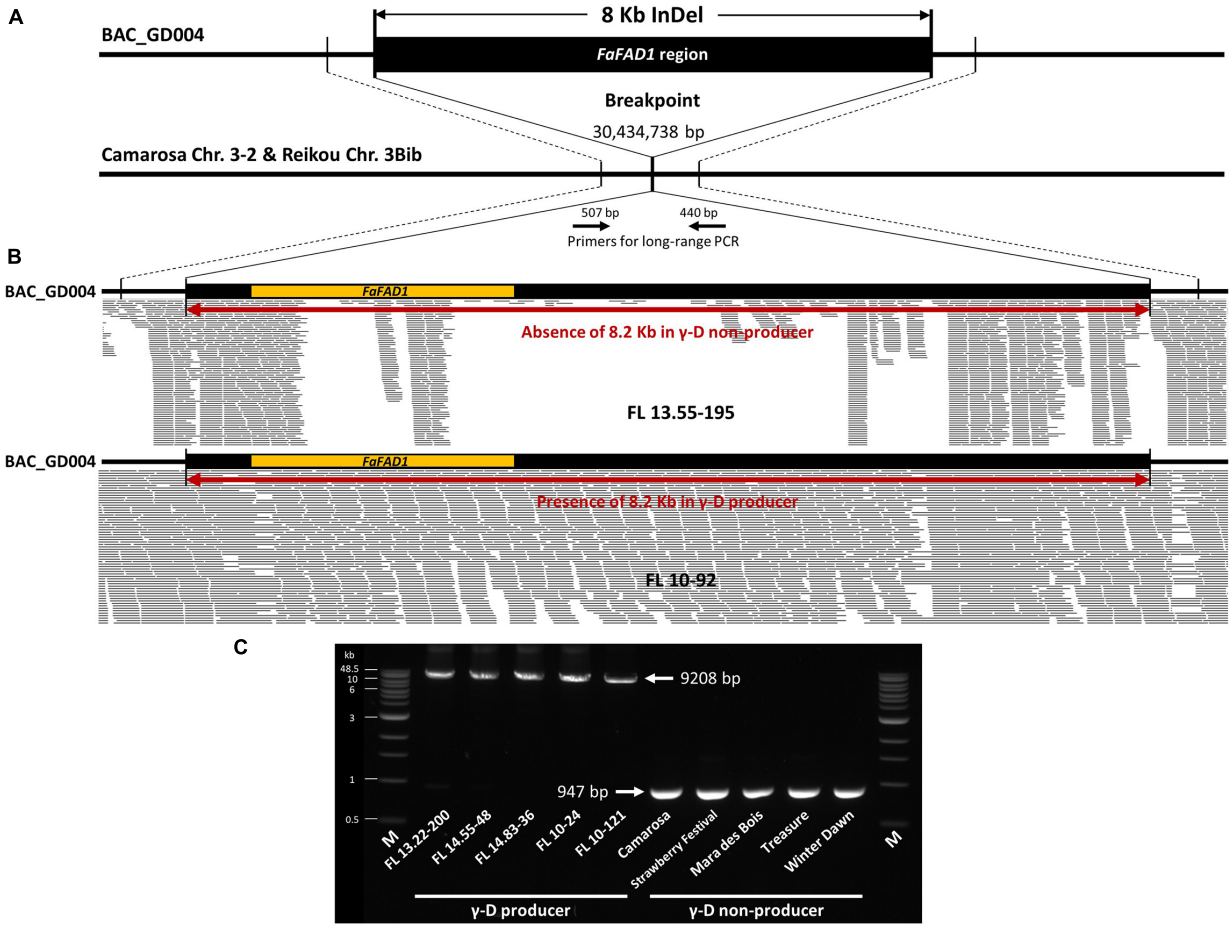

FIGURE 4 | Detecting a deletion of *FaFAD1*. **(A)** Sequence alignment of a BAC clone, BAC_GD004, from library BB1 ('Florida Brilliance': γ-D producer) and corresponding regions of 'Camarosa' chromosome 3-2 and 'Reikou' haplotype 3Bib. An 8,262 bp deletion was detected in 'Camarosa' and 'Reikou', both γ-D non-producers. **(B)** Mapping Illumina sequence reads of γ-D producer (FL 10-92) and γ-D non-producer (FL 13.55-195) to BAC_GD004. **(C)** Long-range PCR results detect an 8,262 bp deletion between five γ-D producers and five γ-D non-producers. All PCR amplicons were similar to the expected size of 9,208 bp for γ-D producers and 947 bp for γ-D non-producers.

the homo- or heterozygous state of the *FaFAD1* gene. The NGD001 and UFGDKASP markers distinguished between heterozygous (Aa) and homozygous (AA) genotypes among γ-D producers (**Figure 5** and **Table 2**). The relative abundance of γ-D was significantly higher in homozygous than heterozygous producers (**Figure 6A**). Steady-state transcript levels for *FaFAD1* between the homozygous (AA) and heterozygous (Aa) γ-D producers were measured via qRT-PCR (**Figure 6B**). We found that transcript levels of the homozygous "AA" genotypes were significantly higher than the heterozygous "Aa" genotypes. The differences in transcript abundance match well with metabolite accumulation, indicating that the allele dosage is the cause for the variations of γ-D content in the octoploid cultivated strawberry.

DISCUSSION

Strawberry fruit has one of the most complex aromas and it has been reported that differences in aroma volatiles can improve strawberry fruit quality (Pelayo-Zaldivar et al., 2005; Dong et al., 2013). Several studies described the importance of key compounds of aroma production and the genetic loci or genes that control fruity aroma in peach (Eduardo et al., 2013; Pirona et al., 2013), apple (Dunemann et al., 2009; Costa et al., 2013), and octoploid strawberry (Aharoni et al., 2004; Zorrilla-Fontanesi et al., 2012). One of the key compounds, γ-decalactone, has a distinctly peach aroma, which increases the perception of sweetness in both peach (Zhang et al., 2010; Zhu and Xiao, 2019) and strawberry fruits (Schwieterman et al., 2014; Ulrich and Olbricht, 2016). While strawberries have a unique combination of sugars, acids, and volatile organic compounds (VOCs), some favorable flavors have been neglected due to the limited resources of strawberry breeding programs (Folta and Klee, 2016; Ulrich and Olbricht, 2016). In recent years, sensory qualities have become popular targets for genetic improvement, including qualities such as sweetness and unique flavors (Latrasse, 1991; Cruz-Rus et al., 2017). *FaFAD1* is a priority for these reasons, as it enhances the fruity flavor and sweetness of

TABLE 2 | Markers genotype data and volatile content of γ-D in 48 accessions using HRM and KASP markers, and gas chromatography/mass spectrometry.

Accession	Female		Male	Source	NGD001	UFGDKASP	Area of Avg. γ-decalactone
FL 18.50-36	Florida Beauty	×	FL 15.89-25	University of Florida	AA	AA	1,906,279,564
FL 18.50-91	Florida beauty	×	FL 15.89-25	University of Florida	AA	AA	1,716,735,350
FL 18.50-96	Florida beauty	×	FL 15.89-25	University of Florida	AA	AA	1,450,960,595
FL 13.22-200	Sweet sensation® "Florida 127"	×	FL 11.28-34	University of Florida	AA	AA	1,337,840,264
FL 18.50-52	Florida beauty	×	FL 15.89-25	University of Florida	AA	AA	1,333,444,656
FL 18.50-124	Florida beauty	×	FL 15.89-25	University of Florida	AA	AA	1,309,594,966
FL 14.55-48	FL 10-121	×	Sweet sensation® "Florida 127"	University of Florida	AA	AA	1,167,611,378
FL 12.115-10	FL 10.133-98	×	FL 11.141-36	University of Florida	Aa	Aa	1,065,855,455
FL 10-24	FL 07-193	×	FL 07-168	University of Florida	AA	AA	1,015,450,185
FL 10-121	FL 07-68	×	FL 08-50	University of Florida	AA	AA	998,243,010
FL 11.31-54	WinterStar™	×	FL 07-193	University of Florida	AA	AA	971,125,697
FL 14.83-36	FL 10-121	×	FL 07-193	University of Florida	AA	AA	951,911,108
Sweet Charlie	FL 80-456	×	Pajaro	University of Florida	Aa	Aa	752,825,948
FL 12.55-220	FL 10-47	×	Sweet sensation® "Florida 127"	University of Florida	AA	AA	643,674,054
WinterStar™	Florida Radiance	×	Earlibrite	University of Florida	Aa	Aa	629,417,671
FL 14.10-17	FL 11.77-96	×	FL 11.31-54	University of Florida	AA	AA	589,598,908
FL 15.56-134	FL 12.5-130	×	FL 10-121	University of Florida	Aa	Aa	588,413,724
FL 15.42-183	FL 10-46	×	FL 11.58-72	University of Florida	Aa	Aa	527,526,224
FL 12.75-77	FL 09-150	×	FL 09-100	University of Florida	Aa	Aa	508,672,061
Florida Brilliance	FL 11.31-14	×	FL 10-153	University of Florida	Aa	Aa	473,334,916
FL 13.27-142	FL 06-89	×	FL 10-47	University of Florida	Aa	Aa	464,913,451
FL 12.26-49	Sweet sensation® "Florida 127"	×	FL 07-134	University of Florida	Aa	Aa	457,110,416
FL 11.71-9	FL 06-38	×	FL 07-193	University of Florida	AA	AA	438,927,503
Florida Beauty	AU 2010-119	×	Florida radiance	University of Florida	Aa	Aa	399,415,427
Sweet Sensation® "Florida 127"	WinterStar™	×	FL 02-58	University of Florida	Aa	Aa	389,982,544
FL 14.37-103	FL 10-24	×	FL 10-89	University of Florida	Aa	Aa	383,769,498
FL 12.93-4	FL 10-24	×	FL 11.107-5	University of Florida	Aa	Aa	364,489,979
FL 11.28-34	Florida radiance	×	FL 07-134	University of Florida	Aa	Aa	333,911,727
Florida Elyana	FL 96-114	×	FL 95-200	University of Florida	Aa	Aa	308,042,692
FL 15.76-45	FL 12.93-4	×	FL 12.55-220	University of Florida	Aa	Aa	305,626,231
FL 13.51-134	Sweet sensation® "Florida 127"	×	FL 10-47	University of Florida	Aa	Aa	285,509,091
Florida Radiance	Winter dawn	×	FL 99-35	University of Florida	Aa	Aa	231,000,642
FL 14.55-203	FL 10-121	×	Sweet sensation® "Florida 127"	University of Florida	Aa	Aa	180,351,763
FL 18.50-120	Florida Beauty	×	FL 15.89-25	University of Florida	Aa	Aa	84,966,825
FL 18.50-20	Florida beauty	×	FL 15.89-25	University of Florida	Aa	Aa	74,313,718
FL 18.50-49	Florida beauty	×	FL 15.89-25	University of Florida	Aa	Aa	71,291,037
FL 18.50-65	Florida beauty	×	FL 15.89-25	University of Florida	Aa	Aa	25,692,788
FL 18.50-42	Florida beauty	×	FL 15.89-25	University of Florida	Aa	Aa	23,038,727
FL 13.22-336	Sweet sensation® "Florida 127"	×	FL 11.28-34	University of Florida	aa	aa	24,924,665
FL 12.74-39	FL 06-89	×	FL 11.63-41	University of Florida	aa	aa	24,864,174
FL 13.19-86	FL 06-134	×	FL 10-51	University of Florida	aa	aa	18,415,501
Fronteras	Unknown	×	Unknown	U. of California Davis	aa	aa	10,899,839
FL 13.55-195	FL 10-47	×	FL 10-153	University of Florida	aa	aa	7,760,551
Camarosa	Douglas	×	Cal. 85.218-605	U. of California Davis	aa	aa	–
Strawberry Festival	Rosa linda	×	OsoGrande	University of Florida	aa	aa	–
Treasure	A3	×	OsoGrande	Florida	aa	aa	–
Winter Dawn	FL 93-103	×	FL 95-316	University of Florida	aa	aa	–
Mara des Bois	Gento × Ostara	×	RedGaunlet × Korona	France	aa	aa	–

AA, homozygote γ-D producer genotype; Aa, heterozygote γ-D producer genotype; aa, homozygote γ-D non-producer genotype;–, unknown.

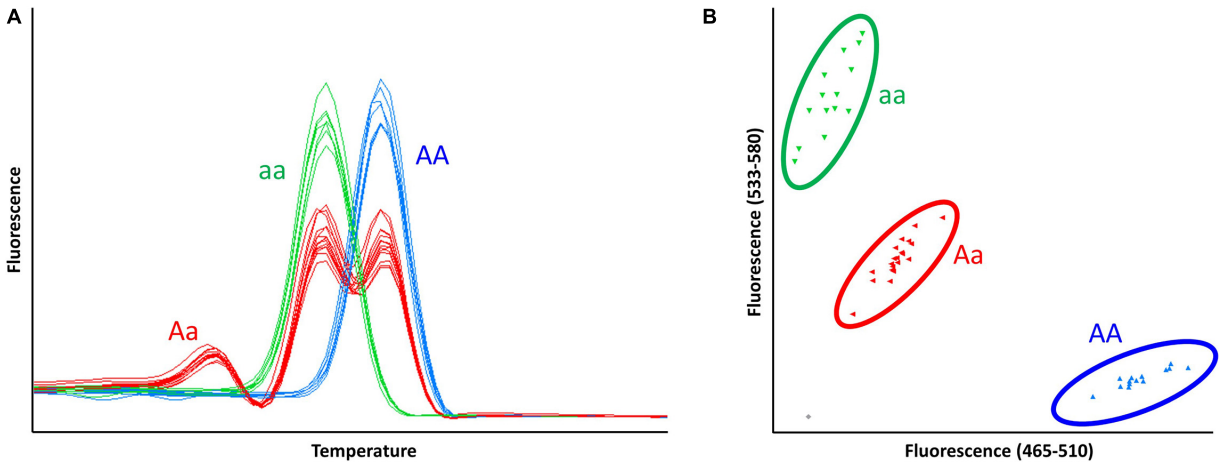

FIGURE 5 | Differentiation of homo- and heterozygous γ-D producers using codominant HRM and KASP markers, NGD001 and UFGDKASP. **(A)** The pattern of HRM melting curve for HRM marker, NGD001, in 48 accessions. **(B)** Endpoint genotyping analysis of KASP marker, UFGDKASP, in 48 accessions. AA: homozygote γ-D producer, Aa: heterozygote γ-D producer, aa: homozygote γ-D non-producer.

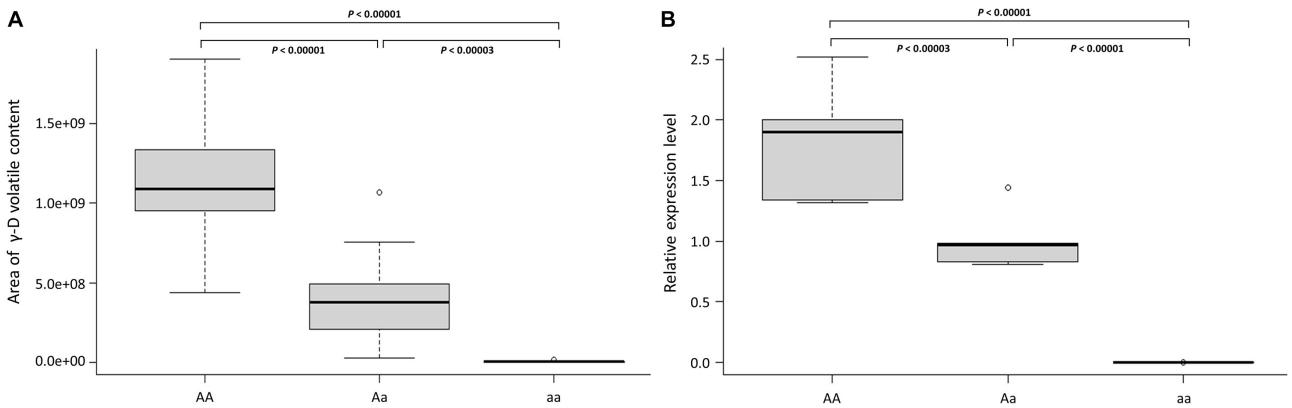

FIGURE 6 | *FaFAD1* transcript dosage regulates γ-D content in the octoploid strawberry. **(A)** Distribution of γ-D volatile abundance per *FaFAD1* genotype. Boxplot showing the area of γ-D volatile content of each genotype for 48 accessions shown in **Table 2**. **(B)** Relative level of *FaFAD1* transcript by *FaFAD1* genotype. The boxplot represents gene expression distribution of each genotype, "AA" (FL 18.50-91, FL 18.50-52, FL 18.50-36, FL 18.50-124, and FL 18.50-96), "Aa" (FL 18.50-120, FL 18.50-49, FL 18.50-20, FL 18.50-42, and FL 18.50-65), and "aa" ('Camarosa', 'Strawberry Festival', 'Mara des Bois', 'Treasure', and 'Winter Dawn'). AA: homozygote γ-D producer, Aa: heterozygote γ-D producer, aa: homozygote γ-D non-producer. The statistical significance of the differences was estimated using *t*-test. Boxplot: the black line in the middle of the boxes is the median, and the bottom and top of the boxes indicate the 25th and 75th percentiles. Whiskers (T-bars) are the minimum and maximum values. The empty dot is outlier. Both experiments **(A,B)** were done with three biological replicates and each replicate has at least three fruits.

strawberries. This report and others have shown that the presence/absence and nature of the causal biosynthetic gene make γ-D an attractive target for marker-assisted breeding for enhanced flavor and aroma.

With the analysis of GWAS, a major locus, *FaFAD1*, controlling the production of γ-D volatile was identified at octoploid chromosome 3-2 (**Table 1**). Although the content of γ-D is controlled by one major locus (a candidate gene *FaFAD1*), the accumulation of γ-D varies widely (Larsen et al., 1992; Jetti et al., 2007; Zorrilla-Fontanesi et al., 2012; Chambers et al., 2014; Sánchez-Sevilla et al., 2014). These reports indicate that the physical presence/absence of the *FaFAD1* gene correlates with γ-D accumulation. In this report, the *FaFAD1* transcript was silenced using *Agroinfiltration* and RNAi in a γ-D-producing cultivar, demonstrating functionally that the gene is both necessary and sufficient for γ-D accumulation and that the volatile is not controlled by another element inside the deleted region.

To sequence the genomic region containing the functional *FaFAD1* allele, probe capture sequencing of the *FaFAD1* flanking region (100 kb) was performed on 11 γ-D producers and four γ-D non-producers. The multiple sequence alignment between the 15 genotypes evidently showed the absence of *FaFAD1* in γ-D non-producers (**Figure 3**). Our findings indicate that a single copy of *FaFAD1* located in chromosome 3 is responsible for production of γ-D.

Among polyploid genomes in general, high sequence similarity between homoeologous chromosomes is often a challenge in differentiating subgenomes (Mandáková et al., 2014). The subgenomes of polyploid plants are generally large and contain extensive repeats, which can greatly impede genome assembly resulting in non-contiguous and incorrect assemblies (Saski et al., 2017). Therefore, it remains challenging to assemble short-read sequences to specific subgenomes (Birchler and Veitia, 2012; Madlung and Wendel, 2013; Mandáková et al., 2014).

To overcome these difficulties, BAC-based physical maps combined with high-density genetic maps were used to improve the accuracy of whole-genome sequence assemblies (Luo et al., 2010; Ariyadasa and Stein, 2012; Sierro et al., 2013). Whole-genome sequencing and BAC libraries are physical and lasting genomic resources that have critical value as tools for positional cloning of genes and associated regulatory sequences (Saski et al., 2017). Here, the causal *FaFAD1* deletion region in the commercial octoploid strawberry was successfully characterized by using the BAC library sequencing approach (**Figure 4**).

In this study, approximately 100-kb *FaFAD1* flanking region of alleles was obtained through the six BAC clones. When comparing these BAC clones to the two reference genomes cv. Camarosa and Japanese cv. Reikou, which are γ-D non-producers, it was confirmed that there is an 8,262 bp deletion in subgenome 3-2 of 'Camarosa' and Ch3Bib of 'Reikou' (**Figure 4A**). Moreover, it was confirmed that γ-D non-producers have the same deletion size of 8,262 bp through long-range PCR using γ-D producers and γ-D non-producers (**Figure 4C**). While these results are confined to University of Florida cultivars, it is likely that the same deletion will be a useful diagnostic tool across strawberry varieties. The two newly developed codominant markers, NGD001 and UFGDKASP, are much improved from the previous dominant marker (Noh et al., 2017) in terms of accuracy and throughput and permit improved parental selection and rapid screening of progeny for homozygous plants likely to be higher γ-D producers. It would be more valuable to further examine the deletion in diverse strawberry accessions from different breeding programs.

Osborn et al. (2003) reported that the allele dosage is expected to relate to different levels of gene expression that affect target traits. Thus, it is highly possible that polyploids could increase the potential variation in their gene expression, which reflects in phenotypic variation. The inclusion of increased variation in dosage-regulated gene expression has become important for genetic studies in polyploid species (Garcia et al., 2013; Hackett et al., 2013; Endelman et al., 2018). To determine allele dosage effects in γ-D producer accessions, the content of γ-D volatile was measured by GC-MS in 48 advanced selections. The genotype results from the two codominant markers were strongly related to γ-D abundance among the 38 γ-D producers (**Table 2**). In addition, the expression level of *FaFAD1* was related to the zygosity of the gene (**Figure 6**). This result indicates that there is a dosage effect on γ-D production.

In summary, the precise location of *FaFAD1* was confirmed in chromosome 3-2 of the octoploid strawberry genome. By utilizing hybridization-based targeted enrichment sequencing and the BAC libraries, a major presence and absence polymorphism (8,262 bp) was substantially found within the *FaFAD1* locus, which is associated with γ-D production in the octoploid strawberry. This *FaFAD1*-containing deletion was present only in γ-D non-producers and directly responsible for lack of fruity aroma flavor. The newly developed codominant markers for *FaFAD1* from this study revealed unique information for the allele dosage effect on the content of γ-D. It provides the new evidence of allele dosage effect on volatile synthesis, suggesting that altering allele number can be a potential tactic for genetic improvement of fruit flavor. Our results provide a directly translatable resource for strawberry breeders and research communities, which will further facilitate the development of new strawberry cultivars with improved flavor.

MATERIALS AND METHODS

Genome-Wide Association Study

For the GWAS of γ-decalactone, we used the three crossing populations ($n = 59$) that were derived from the crosses 'Florida Elyana' × 'Mara de Bois' (population 10.113), 'Mara des Bois' × 'Florida Radiance' (population 13.75), and 'Strawberry Festival' × 'Winter Dawn' (population 13.76) published in Barbey et al. (2020). GWAS for γ-decalactone was conducted via a mixed linear model approach using the GAPIT v2 package (Tang et al., 2016) in R software version 3.3.1. We consider GWAS associations significant at an alpha of 0.05 AFTER correction for FDR. SNP markers from the Affymetrix IStraw35 Axiom Array (Bassil et al., 2015; Verma et al., 2016) were mapped to the diploid *F. vesca* physical map, as available genetic maps in octoploid do not include a majority of the IStraw35 markers used in this study.

Transient Assay

Transient expression in strawberry fruits by agroinfiltration was performed according to Hoffmann et al. (2006). *Agrobacterium tumefaciens* strain EH105 containing the RNAi vector was used to perform transient expression analysis and its effect on γ-D abundance in strawberry fruits. The culture was grown at 28°C overnight, and then the bacterial culture was resuspended in infection buffer (10 mM $MgCl_2$, 100 μM acetosyringone, and 10 mM MES, pH 6.0) and shaken for 4 h at room temperature before infiltration of fruits. After the infection, the fruits were collected for gene expression and measurement of γ-D. For quantitative reverse transcription PCR (qRT-PCR), total RNA from the fruits was isolated as described by Pillet et al. (2017) and 1 μg of total RNA was used to synthesize the cDNA. For the qRT-PCR assay, a transcript corresponding to a conserved hypothetical protein FaCHP1 (Clancy et al., 2013) was used as a constitutive reference. The qRT PCR was run on an Applied Biosystems StepOnePlus Real-Time PCR System using StepOne Software (v2.0) (Applied Biosystems, Foster City, CA, United States). The qRT-PCR data were analyzed using the comparative CT method (ΔΔCT) following the manufacturer's direction. The gene expression of *FaFAD1* was run with three technical replicates and repeated for at least three biological replicates.

Hybridization-Based Targeted Enrichment Sequencing and Data Analysis

Targeted enrichment of *FaFAD1* genomic region was performed by hybrid capture-based next-generation sequencing (NGS) using a synthetic library consisting of a final set of 2,000 Axiom® IStraw35 384HT array probes (Cronn et al., 2012; Verma et al., 2016). The capture oligonucleotides were 150 nt long and were designed to target 100 kb of *FvFAD1* (Fvb3: 31,039,796–31,149,795, *F. vesca* genome v2.0 a2). Probes were designed for covering the entire 100 kb genomic region of *FaFAD1* with 3 × coverage depth. The targeted capture sequencing libraries were constructed using Nextera Rapid Capture Custom Enrichment Kit. The captured sequence was quality controlled using Agilent 2100 Bioanalyzer. All sequencing was accomplished on the Illumina HiSeq 2000 using paired-end 100-bp reads following standard manufacturer protocols. Fifteen accessions were used for this experiment; 11 γ-D producers, 'Albion', 'Benicia', 'Florida Elyana', 'Florida Radiance', 'Sweet Charlie', Sweet Sensation® 'Florida 127', 'Winterstar', (FL 10-24, FL 11.28-34, FL 11.139-10, and FL 12.115-10), and 4 γ-D non-producers, 'Mara des Bois', 'Strawberry Festival', 'Winter Dawn', and FL 12.74-39.

Raw FASTQ files were first checked using the FastQC tool[3]. Raw short reads from each capture library was mapped to a 100-kb region of *FvFAD1* downloaded from Genome Database for Rosaceae (GDR[4]) with CLC Genomics Workbench 11.0[5], using the following parameters: match score 1, mismatch cost 2, cost of insertions and deletions = linear gap cost, insertion cost = 3, deletion cost = 3, length fraction = 0.8, and similarity fraction = 0.9. Consensus sequences were generated from all runs giving a total of 15 accession sequences, which were exported in fasta sequence. The consensus sequences were imported into Geneious 11.0.5[6] and Multiple Sequence Alignment (MSA) was performed using the geneious alignment algorithm.

BAC Library Construction and Screening

Three BAC libraries were prepared from the etiolated leaf tissues of three strawberry accessions, consisting of two γ-D producers (FL 11.77-96 and 'Florida Brilliance') and one γ-D non-producer (FL 14.101-225) (**Supplementary Table 1**). For the tissue etiolation, strawberry plants were covered with black plastic bags and kept in a greenhouse for 2 weeks. The etiolated young white leaf tissues were collected for the DNA extraction. The preparation of high-molecular-weight DNA and library construction was performed at Amplicon Express Inc. (Pullman, Washington). The *Bam*HI or *Hin*dIII digested genomic fragments were cloned into a BAC library vector. The recombinant vector was used to transform DH10B *Escherichia coli* competent cells (Invitrogen, CA, United States). The library was stored in 384-well plates filled with 50 μl freezing LB Lennox medium [36 mM K_2HPO_4, 1.7 mM sodium citrate, 0.4 mM $MgSO_4$, 6.8 mM $(NH_4)_2SO_4$, 4.4% glycerol, and 12.5 lg/ml chloramphenicol]. Plates were incubated for 18 h, replicated, and kept at −80°C for long-term storage. Two libraries *Hin*dIII and *Bam*HI for each accession comprise a total of 32,000 clones, which represent approximately 5 × octoploid strawberry genome coverage. Each library set comprised of 16 super pools (SPs) with individual SPs representing BAC DNA from 10,000 clones for each enzyme. Each SP was divided into 23 MPs each consisting of three plate pools (PPs), eight row pools (RPs), and 12 column pools (CPs). Each library contains approximately 30,000 clones with an average insert size of 150 kb. Three BAC libraries provide about 15 × genome coverage of the octoploid strawberry, respectively.

To identify BAC clones containing *FaFAD1*, two gene-specific markers, UFGDHRM5 (Noh et al., 2017) and qFaFAD1 (Sánchez-Sevilla et al., 2014), were tested for all three libraries (**Supplementary Table 3**). PCR reactions were performed with 16 SPs and 23 MPs with controls, following an online tool from Amplicon Express[7]. All PCR amplifications were performed in 5-μl reactions containing 2 × AccuStart™ II PCR ToughMix® (Quantabio, MA, United States), 1 × LC Green® Plus melting dye (BioFire, UT, United States), 0.5 μM of each HRM primer set, and 0.5 μl of DNA. The reaction conditions were as follows: 95°C for 3 min, 45 cycles at 95°C for 10 sec, 45 cycles at 62°C for 10 sec, and 45 cycles at 72°C for 20 sec.

The plasmid DNA from the BAC clones was isolated using the QIAGEN plasmid midi kit (QIAGEN, Hilden, Germany). For the NGS, each DNA was sequenced by an Illumina high-throughput sequencer with 150-bp paired-end (PE) sequencing strategy. The obtained sequence reads from Illumina were assembled using the *de novo* assembly program from CLC Genomics Workbench, version 11.0[8].

Development and Validation of Functional Codominant Marker

The 48 accessions were used for marker development and validation. DNA extraction was performed using the simplified CTAB method with modifications (Noh et al., 2017). BAC-containing sequences from γ-D-producing accession (FL 11.77-96 and 'Florida Brilliance') were compared to the octoploid reference genome 'Camarosa', which does not produce γ-D. Primers were designed from the polymorphic sequences using IDT's PrimerQuest Software (San Jose, CA, United States). PCR amplifications were performed in a 5-μl reaction containing 2 × AccuStart™ II PCR ToughMix® (Quantabio, MA, United States), 1 × LC Green® Plus melting dye (BioFire, UT, United States), 0.5 μM of each HRM primer sets, and 1 μl of DNA. The PCR and HRM analysis were performed in a LightCycler® 480 system II (Roche Life Science, Germany) using a program consisting of an initial denaturation at 95°C for 5 min; 45 cycles of denaturation at 95°C for 10 sec, annealing at 62°C for 10 sec, and extension at 72°C for 20 sec. After PCR amplification, the samples were heated to 95°C for 1 min and cooled to 40°C

[3]https://www.bioinformatics.babraham.ac.uk/projects/fastqc/

[4]https://www.rosaceae.org/species/fragaria_vesca/genome_v4.0.a1

[5]https://www.qiagenbioinformatics.com/

[6]http://www.geneious.com/

[7]http://puffer.ampliconexpress.com/

[8]www.qiagenbioinformatics.com

for 1 min. Melting curves were obtained by melting over the desired range (60–95°C) at a rate of 50 acquisitions per 1°C. Melting data were analyzed using the Melt Curve Genotyping and Gene Scanning Software (Roche Life Science, Germany). Analysis of HRM variants was based on differences in the shape of the melting curves and in T_m values.

KASP was designed using the 3CR Bioscience website[9], and the genotyping assay was performed using a LightCycler® 480 system II (Roche Life Science, Germany). KASP assays were conducted in 5 μl reactions with 50 ng of DNA template, 2 × PACE™ Genotyping Master Mix (3CR Bioscience, United Kingdom), and PACE™ Assay mix (UFGDKASP-allele-1-FAM, UFGDKASP-allele-2-HEX, and one reverse primer UFGDKASP-common) in a LightCycler® 480 Multiwell 384-well plate. PCR optimization was carried out as follows: initial denaturation at 94°C for 15 min, a touch-down step followed by 10 cycles of 94°C for 20 sec, and 61°C decreasing 0.6°C per cycle to a final annealing/extension temperature of 55°C for 1 min, followed by 33 cycles of 94°C for 20 sec, annealing/extension temperature of 55°C for 1 min, with a final genotyping stage of 37°C for 1 min, a suitable temperature for KASP detection, and finally a plate reading at 37°C for 1 sec. KASP genotyping data were analyzed using Endpoint Genotyping Software (Roche Life Science, Germany).

Long-Range PCR for the *FaFAD1* Region

Tissue samples were collected from five homozygous genotype "AA" accessions (FL 13.22-200, FL 14.55-48, FL 14.83-36, FL 10-24, and FL 10-121) and five "aa" accessions ('Camarosa', 'Florida Festival', 'Mara des Bois', 'Treasure', and 'Winter Dawn'). The DNA was extracted following the simplified CTAB method with modifications (Noh et al., 2017). The primer was designed to have a PCR amplicon size of 9,208 bp in γ-D producers and 947 bp in γ-D non-producers. PCR amplifications were performed in a 10-μl reaction containing Accustart Long Range SuperMix (Quantabio, MA, United States), 0.5 μM of each HRM primer sets, and 2 μl of DNA. PCR was performed in a ProFlex PCR system (Applied Biosystems, United States) using a program consisting of an initial denaturation at 95°C for 3 min followed by 35 cycles of denaturation at 92°C for 30 sec, annealing at 65°C for 10 min, and final extension at 72°C for 10 min. PCR products were separated by agarose gel electrophoresis (1.0%), stained with SYBR® Safe DNA gel stain (Invitrogen, Perth, WA) in TAE-Buffer (TRIS-Acetate-EDTA-buffer, pH 8), and visualized with UVP GelStudio Plus touch imaging system (Analytik Jena, AG Germany).

Volatiles Analysis

The fruit of 48 strawberry accessions was selected in the field of the Gulf Coast Research and Education Center (GCREC) in Wimauma, Florida, during the 2017/2018 season. Harvest dates were December 20, 2017, January 10, 2018, and January 29, 2018. The experiment was done with three biological replicates. Each replicate has at least 6–8 fruits for each genotype. All fruits of the 48 accessions were analyzed for the volatile γ-D using GC-MS in the 2018 season. Fruit processing for volatile analysis was conducted as follows: 4–6 fully ripe, clean, and normal-shaped berries were harvested from each genotype, the calyx from each berry was removed, and approximately 25 g of flesh was collected. Each sample was frozen in liquid nitrogen and stored at −80°C until GC-MS analysis. Each sample was blended with an equal weight of saturated 35% NaCl solution. The volatile 3-hexanone was added as an internal standard to a final concentration of 1 ppm prior to blending. A total of 5 ml aliquots was taken from each sample and dispensed into 20 ml glass vials and sealed with magnetic crimp caps (Gerstel, Baltimore, MD, United States). Samples were frozen at −20°C until analysis by GC-MS.

For GC-MS, a 2 cm tri-phase SPME fiber (50/30 μm DVB/Carboxen/PDMS, Supelco, Bellefonte, PA, United States) was used to collect and concentrate volatiles prior to running on an Agilent 6890 GC coupled with a 5973 N MS detector (Agilent Technologies, Palo Alto, CA, United States). Before analysis, samples were held at 4°C in a Peltier cooling tray attached to a MPS2 autosampler (Gerstel). An authentic γ-D standard (Sigma Aldrich, St. Louis, MO, United States) was run under the same chromatographic conditions as berry samples for verification of volatile identification. The area of each γ-D peak was normalized to the peak area of the internal standard, and normalized peak areas were compared between samples.

Quantitative Real-Time PCR Analysis

For total RNA extraction, five homozygous "AA" genotypes (FL 18.50-91, FL 18.50-52, FL 18.50-36, FL 18.50-124, and FL 18.50-96) and five heterozygote "Aa" genotypes (FL 18.50-120, FL 18.50-49, FL 18-50-20, FL 18.50-42, and FL 18.50-65) were collected from a FL 18.50 advanced selection population. 'Camarosa', 'Strawberry Festival', 'Mara des Bois', 'Treasure', and 'Winter Dawn' with homozygote genotype "aa" were included as the reference genotype of γ-D non-producer. The experiment was performed with three biological replicates, and each replicate contains at least 5–8 fruits. Total RNA was extracted according to the protocol of the Spectrum™ Plant Total RNA Kit (Sigma-Aldrich, St. Louis, MO, United States) and resuspended in a total volume of 50 μl of RNase-free water. cDNA synthesis was performed with the Luna Script RT Super Mix Kit (New England Biolabs. Ipswich, MA). Primer sequence of *FaFAD1*, GD_Rt1, was obtained from NCBI (GeneBank Accession: KF887973.1). Strawberry *GAPDH* gene (GeneBank Accession: AB363963.1), FaGAPDH2, was selected as an endogenous control (**Supplementary Table 3**). qRT-PCRs were carried out with a LightCycler® 480 system II (Roche Life Science, Germany) using Forget-Me-Not™ qPCR Master Mix (Biotium, Corporate Place Hayward, CA, United States). The PCR contents were carried out in a total volume of 5 μl, which contained 1 μl of template cDNA, 0.2 μl of each primer, 2.5 μl of EvaGreen qPCR Master Mix, and 1.1 μl of double-distilled H_2O. The reaction conditions were 95°C for 5 min, followed by 40 cycles of 95°C for 20 sec, 60°C for 20 sec, and 72°C for 20 sec. This was followed by melting curve analysis, which was performed to confirm that each amplicon has a single product. The qRT-PCR experiment was repeated with at least

[9]https://3crbio.com/free-assay-design/

three technical replications for each biological replicate. Relative fold difference was calculated by using the $2^{-\Delta\Delta Ct}$ method (Paolacci et al., 2009).

Data Analysis and Experimental Design

For all comparisons of means among genotypes (AA, Aa, and aa), *t*-test was performed using R software version 3.3.1 (R Core Team, 2017). The procedures and strategies of this study for characterizing the *FaFAD1* region are summarized in **Figure 1**.

DATA AVAILABILITY STATEMENT

The datasets presented in this study can be found in online repositories. The names of the repository/repositories and accession number(s) can be found in the article/**Supplementary Material**. The sequence data of BAC_GD004 is available at this NCBI website (https://www.ncbi.nlm.nih.gov/, accession number MW584663).

AUTHOR CONTRIBUTIONS

YO performed the DNA extractions, bioinformatics study, HRM and KASP marker development, volatile analysis, and data analysis, and drafted the manuscript. CRB performed genome-wide association study, bioinformatics study, and data analysis. SC performed hybridization-based capture sequencing. ZF, JB, and AP participated in volatile analysis. KMF and JP conceived and performed in the transient assay. VMW participated in its design and coordination. SL conceived of the study, data analysis, and drafted the manuscript. All authors have read and approved the final manuscript.

FUNDING

This work was supported by the Florida Strawberry Growers Association, and Specialty Crops Research Initiative grant no. 2017-51181-26833 from the USDA National Institute of Food and Agriculture.

ACKNOWLEDGMENTS

We thank all members of the UF Strawberry Breeding Program and the Strawberry Molecular Genetics and Genomics Program for their technical assistance.

SUPPLEMENTARY MATERIAL

The Supplementary Material for this article can be found online at: https://www.frontiersin.org/articles/10.3389/fpls.2021.639345/full#supplementary-material

Supplementary Figure 1 | Super pool screening of BAC libraries AH3, BB1, and BH3 with two gene based markers, qFaFAD1 and UFGDHRM5. The numbers 1–16 indicate each superpool and "+," "−" indicate positive and negative control. A yellow circle indicates a positive clone. AH3: BAC screening from AH3 SP1-16 using primers qFaFAD1 and UFGDHRM5.

Supplementary Figure 2 | Matrix pool screening of positive clones from each super pools with two gene based markers, qFaFAD1 and UFGDHRM5, and location of positive clone. The number and position of BAC clone is determined by the combination of positive bands in each wells of plate, row, and column.

Supplementary Figure 3 | DNA sequence alignment of six BAC clones. Green bars and blue box show the *FaFAD1* deletion region. Red bars show the *FaFAD1* primer sites of qFaFAD1 and UFGDHRM5.

Supplementary Figure 4 | DNA sequence alignments of 'Camarosa', 'Reikou', and BAC_GD004. The positions of HRM and KASP markers are highlighted with a yellow box and green color, respectively. A blue box indicates the 8,262 bp deletion between γ-D producers and γ-D non-producers. SNPs and InDels were highlighted gray and red colors, respectively.

Supplementary Table 1 | Bacterial Artificial Chromosome (BAC) libraries of three strawberry accessions.

Supplementary Table 2 | *De novo* assembly results of six BAC clones.

Supplementary Table 3 | Marker sequence information used in this study.

REFERENCES

Aharoni, A., Giri, A. P., Verstappen, F. W., Bertea, C. M., Sevenier, R., Sun, Z., et al. (2004). Gain and loss of fruit flavor compounds produced by wild and cultivated strawberry species. *Plant Cell* 16, 3110–3131. doi: 10.1105/tpc.104.023895

Ariyadasa, R., and Stein, N. (2012). Advances in BAC-based physical mapping and map integration strategies in plants. *J. Biomed. Res.* 2012:184854. doi: 10.1155/2012/184854

Barbey, C., Hogshead, M., Schwartz, A. E., Mourad, N., Verma, S., Lee, S., et al. (2020). The genetics of differential gene expression related to fruit traits in strawberry (*Fragaria ×ananassa*). *Front. Genet.* 10:1317. doi: 10.3389/fgene.2019.01317

Bassil, N. V., Davis, T. M., Zhang, H., Ficklin, S., Mittmann, M., Webster, T., et al. (2015). Development and preliminary evaluation of a 90 K Axiom® SNP array for the allo-octoploid cultivated strawberry *Fragaria ×ananassa*. *BMC Genomics* 16:155. doi: 10.1186/s12864-015-1310-1

Birchler, J. A., and Veitia, R. A. (2012). Gene balance hypothesis: connecting issues of dosage sensitivity across biological disciplines. *Proc. Natl. Acad. Sci. U.S.A.* 109, 14746–14753. doi: 10.1073/pnas.1207726109

Chambers, A. H., Pillet, J., Plotto, A., Bai, J., Whitaker, V. M., and Folta, K. M. (2014). Identification of a strawberry flavor gene candidate using an integrated genetic-genomic-analytical chemistry approach. *BMC Genomics* 15:217. doi: 10.1186/1471-2164-15-217

Clancy, M. A., Rosli, H. G., Chamala, S., Brad Barbazuk, W., Civello, P. M., and Folta, K. M. (2013). Validation of reference transcripts in strawberry (*Fragaria* spp.). *Mol. Genet. Genom.* 288, 671–681. doi: 10.1007/s00438-013-0780-6

Costa, F., Cappellin, L., Zini, E., Patocchi, A., Kellerhals, M., Komjanc, M., et al. (2013). QTL validation and stability for volatile organic compounds (VOCs) in apple. *Plant Sci.* 211, 1–7. doi: 10.1016/j.plantsci.2013.05.018

Cronn, R., Knaus, B. J., Liston, A., Maughan, P. J., Parks, M., Syring, J. V., et al. (2012). Targeted enrichment strategies for next-generation plant biology. *Am. J. Bot.* 99, 291–311. doi: 10.3732/ajb.1100356

Cruz-Rus, E., Sesmero, R., Ángel-Pérez, J. A., Sánchez-Sevilla, J. F., Ulrich, D., and Amaya, I. (2017). Validation of a PCR test to predict the presence of flavor volatiles mesifurane and γ-decalactone in fruits of cultivated strawberry (*Fragaria × ananassa*). *Mol. Breed.* 37:131.

Díaz, A., Zikhali, M., Turner, A. S., Isaac, P., and Laurie, D. A. (2012). Copy number variation affecting the Photoperiod-B1 and Vernalization-A1 genes is

associated with altered flowering time in wheat (*Triticum aestivum*). *PLoS One* 7:e33234. doi: 10.1371/journal.pone.0033234

Dong, J., Zhang, Y., Tang, X., Jin, W., and Han, Z. (2013). Differences in volatile ester composition between *Fragaria* × *ananassa* and *F. vesca* and implications for strawberry aroma patterns. *Sci. Hortic.* 150, 47–53. doi: 10.1016/j.scienta.2012.11.001

Dunemann, F., Ulrich, D., Boudichevskaia, A., Grafe, C., and Weber, W. (2009). QTL mapping of aroma compounds analysed by headspace solid-phase microextraction gas chromatography in the apple progeny 'Discovery'×'Prima'. *Mol. Breed.* 23, 501–521. doi: 10.1007/s11032-008-9252-9

Edger, P. P., Poorten, T. J., Vanburen, R., Hardigan, M. A., Colle, M., Mckain, M. R., et al. (2019). Origin and evolution of the octoploid strawberry genome. *Nat. Genet.* 51, 541–547.

Edger, P. P., VanBuren, R., Colle, M., Poorten, T. J., Wai, C. M., Niederhuth, C. E., et al. (2018). Single-molecule sequencing and optical mapping yields an improved genome of woodland strawberry (*Fragaria vesca*) with chromosome-scale contiguity. *Gigascience* 7:gix124.

Eduardo, I., Chietera, G., Pirona, R., Pacheco, I., Troggio, M., Banchi, E., et al. (2013). Genetic dissection of aroma volatile compounds from the essential oil of peach fruit: QTL analysis and identification of candidate genes using dense SNP maps. *Tree Genet. Genomes* 9, 189–204. doi: 10.1007/s11295-012-0546-z

Emanuelli, F., Sordo, M., Lorenzi, S., Battilana, J., and Grando, M. S. (2014). Development of user-friendly functional molecular markers for VvDXS gene conferring muscat flavor in grapevine. *Mol. Breed.* 33, 235–241. doi: 10.1007/s11032-013-9929-6

Endelman, J. B., Carley, C. A. S., Bethke, P. C., Coombs, J. J., Clough, M. E., Da Silva, W. L., et al. (2018). Genetic variance partitioning and genome-wide prediction with allele dosage information in autotetraploid potato. *Genetics* 209, 77–87. doi: 10.1534/genetics.118.300685

Folta, K. M., and Klee, H. J. (2016). Sensory sacrifices when we mass-produce mass produce. *Hortic. Res.* 3, 1–6.

Garcia, A. A., Mollinari, M., Marconi, T. G., Serang, O. R., Silva, R. R., Vieira, M. L., et al. (2013). SNP genotyping allows an in-depth characterisation of the genome of sugarcane and other complex autopolyploids. *Sci. Rep.* 3:3399.

Gordon, S. V., Brosch, R., Billault, A., Garnier, T., Eiglmeier, K., and Cole, S. T. (1999). Identification of variable regions in the genomes of tubercle bacilli using bacterial artificial chromosome arrays. *Mol. Microbiol.* 32, 643–655. doi: 10.1046/j.1365-2958.1999.01383.x

Hackett, C. A., Mclean, K., and Bryan, G. J. (2013). Linkage analysis and QTL mapping using SNP dosage data in a tetraploid potato mapping population. *PLoS One* 8:e63939. doi: 10.1371/journal.pone.0063939

Hoffmann, T., Kalinowski, G., and Schwab, W. (2006). RNAi-induced silencing of gene expression in strawberry fruit (*Fragaria* ×*ananassa*) by agroinfiltration: a rapid assay for gene function analysis. *Plant J.* 48, 818–826. doi: 10.1111/j.1365-313x.2006.02913.x

Jetti, R., Yang, E., Kurnianta, A., Finn, C., and Qian, M. (2007). Quantification of selected aroma-active compounds in strawberries by headspace solid-phase microextraction gas chromatography and correlation with sensory descriptive analysis. *J. Food Sci.* 72, 487–496.

Jouquand, C., Chandler, C., Plotto, A., and Goodner, K. (2008). A sensory and chemical analysis of fresh strawberries over harvest dates and seasons reveals factors that affect eating quality. *J. Am. Soc. Hortic. Sci.* 133, 859–867. doi: 10.21273/jashs.133.6.859

Klymiuk, V., Yaniv, E., Huang, L., Raats, D., Fatiukha, A., Chen, S., et al. (2018). Cloning of the wheat Yr15 resistance gene sheds light on the plant tandem kinase-pseudokinase family. *Nat. Commun.* 9, 1–12.

Larsen, M., Poll, L., and Olsen, C. E. (1992). Evaluation of the aroma composition of some strawberry (*Fragaria ananassa* Duch) cultivars by use of odour threshold values. *Z. Lebensm. Unters. Forsch.* 195, 536–539. doi: 10.1007/bf01204558

Latrasse, A. (1991). "Fruits III," in *Volatile Compounds in Fruits and Beverages*, ed. H. Maarse (New York, NY: Dekker), 333–387.

Levy, A. A., and Feldman, M. (2002). The impact of polyploidy on grass genome evolution. *Plant Physiol.* 130, 1587–1593. doi: 10.1104/pp.015727

Liu, Y., Zhang, B., Wen, X., Zhang, S., Wei, Y., Lu, Q., et al. (2018). Construction and characterization of a bacterial artificial chromosome library for *Gossypium mustelinum*. *PLoS One* 13:e0196847. doi: 10.1371/journal.pone.0196847

Luo, M.-C., Ma, Y., You, F. M., Anderson, O. D., Kopecký, D., Šimková, H., et al. (2010). Feasibility of physical map construction from fingerprinted bacterial artificial chromosome libraries of polyploid plant species. *BMC Genomics* 11:122. doi: 10.1186/1471-2164-11-122

Madlung, A., and Wendel, J. (2013). Genetic and epigenetic aspects of polyploid evolution in plants. *Cytogenet. Genome Res.* 140, 270–285. doi: 10.1159/000351430

Mandáková, T., Marhold, K., and Lysak, M. A. (2014). The widespread crucifer species C ardamine flexuosa is an allotetraploid with a conserved subgenomic structure. *New Phytol.* 201, 982–992. doi: 10.1111/nph.12567

Maron, L. G., Guimarães, C. T., Kirst, M., Albert, P. S., Birchler, J. A., Bradbury, P. J., et al. (2013). Aluminum tolerance in maize is associated with higher MATE1 gene copy number. *Proc. Natl. Acad. Sci. U.S.A.* 110, 5241–5246. doi: 10.1073/pnas.1220766110

Njunguna, W., Liston, A., Cronn, R., Ashman, T. L., and Bassil, N. (2013). Insights into phylogeny, sex function and age of *Fragaria* based on whole chloroplast genome sequencing. *Mol. Phylogenet. Evol.* 66, 17–29. doi: 10.1016/j.ympev.2012.08.026

Noh, Y.-H., Lee, S., Whitaker, V. M., Cearley, K. R., and Cha, J.-S. (2017). A high-throughput marker-assisted selection system combining rapid DNA extraction high-resolution melting and simple sequence repeat analysis: Strawberry as a model for fruit crops. *J. Berry Res.* 7, 23–31. doi: 10.3233/jbr-160145

Olbricht, K., Grafe, C., Weiss, K., and Ulrich, D. (2008). Inheritance of aroma compounds in a model population of *Fragaria* × *ananassa* Duch. *Plant Breed.* 127, 87–93.

Osborn, T. C., Pires, J. C., Birchler, J. A., Auger, D. L., Chen, Z. J., Lee, H. S., et al. (2003). Understanding mechanisms of novel gene expression in polyploids. *Trends Genet.* 19, 141–147. doi: 10.1016/s0168-9525(03)00015-5

Paolacci, A. R., Tanzarella, O. A., Porceddu, E., and Ciaffi, M. (2009). Identification and validation of reference genes for quantitative RT-PCR normalization in wheat. *BMC Mol. Biol.* 10:11. doi: 10.1186/1471-2199-10-11

Pelayo-Zaldivar, C., Ebeler, S. E., and Kader, A. A. (2005). Cultivar and harvest date effects on flavor and other quality attributes of California strawberries. *J. food Qual.* 28, 78–97. doi: 10.1111/j.1745-4557.2005.00005.x

Perez, A. G., Rios, J. J., Sanz, C., and Olias, J. M. (1992). Aroma components and free amino acids in strawberry variety Chandler during ripening. *J. Agric. Food Chem.* 40, 2232–2235. doi: 10.1021/jf00023a036

Pillet, J., Chambers, A. H., Barbey, C., Bao, Z., Plotto, A., Bai, J., et al. (2017). Identification of a methyltransferase catalyzing the final step of methyl anthranilate synthesis in cultivated strawberry. *BMC Plant Biol.* 17:147. doi: 10.1186/s12870-017-1088-1

Pirona, R., Vecchietti, A., Lazzari, B., Caprera, A., Malinverni, R., Consolandi, C., et al. (2013). Expression profiling of genes involved in the formation of aroma in two peach genotypes. *Plant Biol.* 15, 443–451. doi: 10.1111/j.1438-8677.2012.00666.x

R Core Team (2017). *R: A Language and Environment for Statistical Computing*. Vienna: R foundation for statistical computing.

Sánchez-Sevilla, J. F., Cruz-Rus, E., Valpuesta, V., Botella, M. A., and Amaya, I. (2014). Deciphering gamma-decalactone biosynthesis in strawberry fruit using a combination of genetic mapping, RNA-Seq and eQTL analyses. *BMC Genomics* 15:218. doi: 10.1186/1471-2164-15-218

Saski, C. A., Scheffler, B. E., Hulse-Kemp, A. M., Liu, B., Song, Q., Ando, A., et al. (2017). Sub genome anchored physical frameworks of the allotetraploid Upland cotton (*Gossypium hirsutum* L.) genome, and an approach toward reference-grade assemblies of polyploids. *Sci. Rep.* 7, 1–14.

Schwieterman, M. L., Colquhoun, T. A., Jaworski, E. A., Bartoshuk, L. M., Gilbert, J. L., Tieman, D. M., et al. (2014). Strawberry flavor: diverse chemical compositions, a seasonal influence, and effects on sensory perception. *PLoS One* 9:e88446. doi: 10.1371/journal.pone.0088446

Shulaev, V., Sargent, D. J., Crowhurst, R. N., Mockler, T. C., Folkerts, O., Delcher, A. L., et al. (2011). The genome of woodland strawberry (*Fragaria vesca*). *Nat. Genet.* 43:109.

Sierro, N., Battey, J. N., Ouadi, S., Bovet, L., Goepfert, S., Bakaher, N., et al. (2013). Reference genomes and transcriptomes of *Nicotiana sylvestris* and *Nicotiana tomentosiformis*. *Genome Biol.* 14:R60.

Tang, Y., Liu, X., Wang, J., Li, M., Wang, Q., Tian, F., et al. (2016). GAPIT version 2: an enhanced integrated tool for genomic association and prediction. *Plant Genome* 9:120.

Ulrich, D., Komes, D., Olbricht, K., and Hoberg, E. (2007). Diversity of aroma patterns in wild and cultivated *Fragaria* accessions. *Genet. Resour. Crop Evol.* 54:1185. doi: 10.1007/s10722-006-9009-4

Ulrich, D., and Olbricht, K. (2016). A search for the ideal flavor of strawberry-Comparison of consumer acceptance and metabolite patterns in *Fragaria*× *ananassa* Duch. *J. Appl. Bot. Food Qual.* 89:6450.

Urrutia, M., Rambla, J. L., Alexiou, K. G., Granell, A., and Monfort, A. (2017). Genetic analysis of the wild strawberry (*Fragaria vesca*) volatile composition. *Plant Physiol. Biochem.* 121, 99–117. doi: 10.1016/j.plaphy.2017.10.015

Verma, S., Bassil, N., Van De Weg, E., Harrison, R., Monfort, A., Hidalgo, J., et al. (2016). Development and evaluation of the Axiom® IStraw35 384HT array for the allo-octoploid cultivated strawberry *Fragaria*× *ananassa*. *Proc. VIII Int. Strawberry Symp.* 1156, 75–82. doi: 10.17660/actahortic.2017.1156.10

Wang, K., Guo, W., and Zhang, T. (2007). Detection and mapping of homologous and homoeologous segments in homoeologous groups of allotetraploid cotton by BAC-FISH. *BMC Genomics* 8:178. doi: 10.1186/1471-2164-8-178

Wendel, J. F. (1989). New World tetraploid cottons contain Old World cytoplasm. *Proc. Natl. Acad. Sci. U.S.A.* 86, 4132–4136. doi: 10.1073/pnas.86.11.4132

Wendel, J. F. (2000). "Genome evolution in polyploids," in *Plant Molecular Evolution*, eds B. S. Gaut and J.J. Doyle (Dordrecht: Springer), 225–249. doi: 10.1007/978-94-011-4221-2_12

Wendel, J. F., and Cronn, R. C. (2003). Polyploidy and the evolutionary history of cotton. *Adv. Agron.* 78:139. doi: 10.1016/s0065-2113(02)78004-8

Zabetakis, I., and Holden, M. A. (1997). Strawberry flavour: analysis and biosynthesis. *J. Sci. Food Agric.* 74, 421–434. doi: 10.1002/(sici)1097-0010(199708)74:4<421::aid-jsfa817>3.0.co;2-6

Zhang, B., Shen, J.-Y., Wei, W.-W., Xi, W.-P., Xu, C.-J., Ferguson, I., et al. (2010). Expression of genes associated with aroma formation derived from the fatty acid pathway during peach fruit ripening. *J. Agric. Food Chem.* 58, 6157–6165. doi: 10.1021/jf100172e

Zhu, J., and Xiao, Z. (2019). Characterization of the key aroma compounds in peach by gas chromatography–olfactometry, quantitative measurements and sensory analysis. *Eur. Food Res. Technol.* 245, 129–141. doi: 10.1007/s00217-018-3145-x

Zorrilla-Fontanesi, Y., Rambla, J.-L., Cabeza, A., Medina, J. J., Sánchez-Sevilla, J. F., Valpuesta, V., et al. (2012). Genetic analysis of strawberry fruit aroma and identification of O-methyltransferase FaOMT as the locus controlling natural variation in mesifurane content. *Plant Physiol.* 159, 851–870. doi: 10.1104/pp.111.188318

Conflict of Interest: The authors declare that the research was conducted in the absence of any commercial or financial relationships that could be construed as a potential conflict of interest.

The reviewer IA declared a past co-authorship with several of the authors YO, VMW to the handling editor.

frontiers in Plant Science

ORIGINAL RESEARCH
published: 27 August 2021
doi: 10.3389/fpls.2021.688481

Autophagy Is Required for Strawberry Fruit Ripening

José F. Sánchez-Sevilla[1], *Miguel A. Botella*[2], *Victoriano Valpuesta*[2] *and Victoria Sanchez-Vera*[2]*

[1] Unidad Asociada al CSIC de I+D+i Biotecnología y Mejora en Fresa, Instituto Andaluz de Investigación y Formación Agraria y Pesquera (IFAPA), Centro IFAPA Málaga, Junta de Andalucía, Málaga, Spain, [2] Departamento de Biología Molecular y Bioquímica, Instituto de Hortofruticultura Subtropical y Mediterránea (IHSM), Universidad de Málaga-Consejo Superior de Investigaciones Científicas, Málaga, Spain

Autophagy is a catabolic and recycling pathway that maintains cellular homeostasis under normal growth and stress conditions. Two major types of autophagy, microautophagy and macroautophagy, have been described in plants. During macroautophagy, cellular content is engulfed by a double-membrane vesicle called autophagosome. This vesicle fuses its outer membrane with the tonoplast and releases the content into the vacuole for degradation. During certain developmental processes, autophagy is enhanced by induction of several autophagy-related genes (*ATG* genes). Autophagy in crop development has been studied in relation to leaf senescence, seed and reproductive development, and vascular formation. However, its role in fruit ripening has only been partially addressed. Strawberry is an important berry crop, representative of non-climacteric fruit. We have analyzed the occurrence of autophagy in developing and ripening fruits of the cultivated strawberry. Our data show that most *ATG* genes are conserved in the genome of the cultivated strawberry *Fragaria x ananassa* and they are differentially expressed along the ripening of the fruit receptacle. ATG8-lipidation analysis proves the presence of two autophagic waves during ripening. In addition, we have confirmed the presence of autophagy at the cellular level by the identification of autophagy-related structures at different stages of the strawberry ripening. Finally, we show that blocking autophagy either biochemically or genetically dramatically affects strawberry growth and ripening. Our data support that autophagy is an active and essential process with different implications during strawberry fruit ripening.

Keywords: autophagy, fruit ripening, strawberry, plant development, senescence, vascular tissue

OPEN ACCESS

Edited by:
Jia-Long Yao,
The New Zealand Institute for Plant and Food Research Ltd, New Zealand

Reviewed by:
Luis Morales-Quintana,
Autonomous University of Chile, Chile
Raili Ruonala,
University of Helsinki, Finland
Juan Muñoz-Blanco,
University of Cordoba, Spain

***Correspondence:**
Victoria Sanchez-Vera
victoriasv@uma.es

Specialty section:
This article was submitted to Plant Development and EvoDevo, a section of the journal Frontiers in Plant Science

Received: *30 March 2021*
Accepted: *14 June 2021*
Published: *27 August 2021*

Citation:
Sánchez-Sevilla JF, Botella MA, Valpuesta V and Sanchez-Vera V (2021) Autophagy Is Required for Strawberry Fruit Ripening. Front. Plant Sci. 12:688481. doi: 10.3389/fpls.2021.688481

INTRODUCTION

Autophagy is a general mechanism in eukaryotes that maintains the cell homeostasis through the degradation of intracellular targeted organelles, proteins, and major compounds (Marshall and Vierstra, 2018). Several autophagic routes have been described in animals, fungi, and plants, with the best known initially referred to as macroautophagy (hereafter named as autophagy) (Galluzzi et al., 2017). In this pathway, a double membrane structure is initiated that grows until its complete closure, engulfing cytoplasmic material and giving rise to a structure called autophagosome. The autophagosome fuses its outer membrane with the tonoplast, releasing its content into the vacuole where it gets degraded by vacuolar proteases and hydrolases (Wen and Klionsky, 2016). Under

favorable conditions, low levels of autophagy flux serve as a housekeeping function by clearing obsolete cytoplasmic content, whereas, during periods of stress or starvation, autophagy flux is enhanced to promote cell survival by recycling damaged proteins and organelles and thereby reallocating energy and building blocks for biosynthetic processes (Rabinowitz and White, 2010). Autophagy is driven by a set of core autophagy-related proteins (ATG) first described in yeast and conserved in almost all eukaryotes (Tsukada and Ohsumi, 1993; Meijer et al., 2007). They participate in all the stages of the pathway, from cargo recognition and autophagosome formation to docking to the vacuole and release of the content (Marshall and Vierstra, 2018).

In plants, it has been shown that autophagy plays a crucial role not only in resistance to stress but also in development, thanks mostly to studies performed in *Arabidopsis* (Su et al., 2020). Lines lacking functional ATG proteins show an overall reduction in plant fitness, including reduced growth and fecundity, accelerated senescence, as well as high susceptibility to biotic and abiotic stresses (Li and Vierstra, 2012). Autophagy has been associated with the metabolic adjustment taking place during the plant developmental transitions (Michaeli et al., 2016). The maintenance of adequate supplies of nutrients needed for all developmental processes requires the release of nutrients from stores and the recycling of macromolecules, in addition to nutrition acquisition and synthesis. Autophagy is one recycling route that might provide essential nutrients for its reuse by the plant cell (Marshall and Vierstra, 2018).

In the last years, given the relevance of autophagy for plant fitness, the study of this catabolic process in crops has gathered more interest. To date, autophagy in crops has been studied in the context of several developmental processes, such as leaf senescence, seed and reproductive development, and vascular formation (Tang and Bassham, 2018). A highly relevant developmental process that is absent in *Arabidopsis* but is extremely important for agriculture is the ripening of fleshy fruits. Ripening of fleshy fruits comprises changes in color, size, hardness, and production of metabolites that generate fruity smells and sweetness (Giovannoni, 2001). Although, a plethora of molecular players have been described to be related to this developmental process using tomato as model (Osorio et al., 2013), very little is known about autophagy in the context of fruit ripening. Transcriptomic analyses on grape berry skin revealed that a set of *ATG* genes (*ATG18g, ATG9, ATG11,* and *ATG2*) showed a higher expression concomitant with ripening, supporting a role for autophagy in fruit senescence (Ghan et al., 2017). A recent study, analyzing autophagy related genes and proteins (*ATG8, ATG4, ATG5, ATG9,* and *NBR1*), and confirming the presence of autophagic-like structures, suggested that autophagy occurs during ripening in pepper (López-Vidal et al., 2020). However, the importance of autophagy during fruit ripening has not been elucidated yet.

Strawberry is a non-climacteric achenetum-type of fruit that develops into a fleshy receptacle, in which the dry achenes are embedded (Liu et al., 2020). The receptacle of the ripe fruits is a major contributor to the mass of the fruit and the main determinant of the quality parameters. During the development of the fruit receptacle the cellular changes are well-defined, from cell division to cell expansion (Havis, 1943), as well as the metabolic changes (Fait et al., 2008) and gene expression (Sánchez-Sevilla et al., 2017). In the present work, we have studied whether autophagy could play a role in the strawberry fruit ripening process. We have analyzed the changes in expression of autophagy-related genes during ripening of the cultivated strawberry *Fragaria x ananassa*, as well as the ATG8 protein content and its lipidation, as a required step for the formation of the autophagosomes. Here, we report that most of the *ATG genes*, as well as the regulatory *ATAF1* and the autophagy marker *NBR1*, show a significant level of expression in the receptacle, and this expression changes along the ripening process. The amount of lipidated ATG8 peaked at the white and ripe stages of development, supporting the existence of two autophagic waves along strawberry ripening. At the cellular level, we have identified the presence of autophagy-related structures at different stages of the receptacle ripening, including autophagosomes. Finally, we show that blocking autophagy in fruits, either biochemically or genetically, dramatically affects the ripening process. Taking all this data together, we propose that autophagy is a key process in strawberry ripening with clear implications in vascular development and senescence of the fruit.

MATERIALS AND METHODS

Plant Material and Growth Conditions

Plants of the short-day variety *Fragaria x ananassa* Duch (cv. "Camarosa") and the neutral day *Fragaria x ananassa* cv. "San Andreas" were grown under greenhouse conditions (IHSM, Málaga, Spain). In the case of *F x ananassa* cv "San Andreas" a supplement of light was applied from 8:00 to 20:00 and from October to February when sunlight intensity was below 5,000 lux.

For developmental assays, fruits were harvested at six different developmental stages corresponding to green (G), white (W), turning (T), red (R), ripe (Rp), and over-ripe (Or). We determined each stage based on the following hallmarks: (i) green: small green receptacle with green achenes, (ii) white: white receptacle with yellow achenes, (iii) turning: semi-red receptacle, (iv) red: red receptacle, (v) ripe: hard and dark red receptacle, and (vi) over-ripe: soft and dark red receptacle. Examples of the stages can be found in **Figure 5A** and **Supplementary Figure 2A**. Each sample corresponded to a pool of 4–5 fruits that were harvested and flash-frozen in liquid nitrogen. Achenes and receptacle develop coordinately but suffer different developmental programs as can be deduced by their different appearance and metabolic composition (Fait et al., 2008). In order to be sure that our molecular analysis corresponded to receptacle exclusively, we removed achenes from frozen fruits with the help of a scalpel.

Identification of Strawberry Autophagy-Related Genes, Read Mapping, Expression Analysis, and Sequence Alignments

In order to identify the orthologs of autophagy-related genes in *F. x ananassa*, first a BLAST of the *Arabidopsis ATG* genes on

the well-annotated genome of the diploid *Fragaria vesca* was performed (https://www.rosaceae.org/species/fragaria/fragaria_vesca). Retrieved sequences were confirmed by analyzing their protein domains with pHMMER and comparing it with the Arabidopsis orthologs (https://www.ebi.ac.uk/Tools/hmmer/search/phmmer). The e-value cutoff used in the gene search was 0.001, however the genes confirmed with HMMR as putative orthologs showed an e-value below 1e-40 in all cases.

Correspondences between *Arabidopsis*, *F. vesca* (v4.0.a1) (Edger et al., 2018), and *F. ananassa* (v1.0.a2) *ATG* genes were established with BLAST.

Next, we investigated the expression of these genes using the transcriptome data previously generated by our group that include fruits of *F. x ananassa cv.* "Camarosa" at different ripening stages (green, white, turning, and red) (Sánchez-Sevilla et al., 2017). Reads mapping and differential gene expression analysis were performed according to the Tuxedo protocol workflow for RNA-seq differential expression analysis (Hisat2/Cufflinks/CummRbund) using the default parameters (Trapnell et al., 2012). As reference genome we used the *Fragaria x ananassa* "Camarosa" Genome Assembly v1.0 (Edger et al., 2019) and as reference annotation *Fragaria x ananassa "Camarosa" Genome v1.0.a2 (Re-annotation of v1.0.a1)* (Liu et al., 2021) available at GDR (https://www.rosaceae.org/species/fragaria/fragaria_x_ananassa). Statistical analysis of RNAseq data was performed with the false discovery rate (FDR) method after Benjamini-Hochberg correction for multiple-testing. For *ATG8*, 36 gene sequences were retrieved after BLAST against *F x ananassa* genome, however due to poor assembly of the genomic sequence in the case of one of them (FxaC_27g11741) we decided not to include it in the subsequent analysis.

All bioinformatics processes were developed at the Supercomputing and Bioinnovation Center of the University of Malaga (https://www.scbi.uma.es/site/). Reads are stored at the European Nucleotide Archive (https://www.ebi.ac.uk/ena) with the study reference PRJEB12420. Nucleotide and amino acid sequences were aligned, clustered, and analyzed with MAFFT online service (Katoh et al., 2018). Alignment data can be found in **Supplementary Material** (Data Sheet 1). The phylogenetic tree was inferred by the Neighbor-Joining method with a bootstrap analysis. A total of 1,000 replicates were used to estimate the reliability of internal nodes. The evolutionary distances were computed using the Maximum Composite Likelihood method. Evolutionary analyses were conducted in MEGA X (Stecher et al., 2020) and tree was displayed using FigTree (http://tree.bio.ed.ac.uk/software/figtree/).

Transmission Electron Microscopy

F x ananassa cv. "Camarosa" fruits were cross sectioned and 2 mm thick pie sections containing the epidermis, cortex, and pith were dissected with a scalpel. Samples were fixed in 2,5% glutaraldehyde (Acros organics, Thermo Fisher Scientific) and 50 mM sodium cacodylate buffer (pH 7,4) under vacuum for 2 × 15 min at 4°C and left in fixative o/n. Fixed samples were washed with buffer three times for 10 min and then post- fixed in buffered 1% OsO4 (Electron Microscopy Sciences, 19150) for 60 min. After washing them in water, samples were incubated with 2% uranyl acetate (aqueous) (Electron Microscopy Sciences, 22400) for 2 h and then washed with water. After samples were dehydrated through an ethanol series (Panreac, 141086.1214; 50, 70, and 95% each step 30 min; 100% for 30 min and 100% for 30 min) and incubated in a solution of London Resin White (Electron Microscopy Sciences, 14381-UC) and ethanol (1:1) overnight. Samples were incubated in pure London Resin White for 5 h and London Resin White overnight; polymerization was performed at 65°C for 24 h. Ultrathin sections (50–70 nm) were obtained with an ultramicrotome Leica EM UC7/FC7. Sections were examined with a JEM-1400 (Jeol, Málaga, Spain) transmission electron microscopy.

Western Blotting

Protein extractions were performed from de-achenized receptacles grounded in liquid nitrogen. In all cases, 600µl of extraction buffer [Tris-HCl 50 mM pH 7,5, Nonidet N-40, P9599 protease inhibitors (Sigma) and PMSF 1 mM] was mixed with 300 mg of tissue powder and incubated for 10 min on ice with eventual vortex. Samples were sonicated for 10 min on an ice-cold water bath and filtered through one-layer miracloth. Proteins were quantified by Bradford assay with Bio-Rad protein assay (Bio-Rad, 5000001) and 10 µg of protein were loaded into SDS-PAGE gels. For ATG8 and NBR1 detection, 15 or 8% acrylamide/bis-acrylamide resolving gels were used, respectively. Proteins were transfered onto polyvinylidene difluoride membranes (Merck-Millipore). AntiATG8 raised against *Chlamydomonas reinhardtii* (Agrisera, AS14 2769) and antiNBR1 raised against *Arabidopsis thaliana* NBR1 (Agrisera, AS14 2805) were used at 1:2,000 dilution. Secondary antibody was used at 1:5,000 dilution. Blots were developed using ECL substrate (Thermo Fisher Scientific). The developing reaction was detected using a Chemidoc XRS+ (Bio-Rad). Band quantification was performed with Image Lab software (Bio-rad).

Quantitative Real-Time PCR

Pooled de-achened receptacles of the different developmental stages or individual de-achened receptacles, in the case of the silencing experiment, were grounded in liquid nitrogen and RNA was extracted using a rapid CTAB method previously described (Gambino et al., 2008). RNA concentration was measured with a Nanodrop instrument (Thermo Fisher Scientific, USA) and samples were treated with DNAse TURBO (Thermo Fisher Scientific, AM2238) according to the manufacturer's protocol. 1 µg RNA was used for cDNA synthesis using iScript cDNA synthesis kit (Bio-Rad, 1708890) and 1/10 of each reverse transcription reaction was used for quantitative real-time PCR (qRT-PCR) analysis. SsoFast Evagreen supermix (Bio-Rad, USA, 1725200) was used for qRT-PCR. Reactions were run in a CFX Real Time PCR detection system (Bio-Rad) with the following protocol: 95°C, 10 min, 40 cycles of 95°C, 15 s and 60°, 1 min, 95°C, 1 min. qRT-PCR efficiency was determined by LinReg PCR program. Normalization was performed against *FaActin* and *FaDBP* genes (Galli et al., 2015) and ΔΔCT was used to quantify fold change difference expression among samples. All primers used in this experiment were designed with Primer3

software (primer3.ut.ee, Untergasser et al., 2012) and are listed in **Supplementary Table 1-S1**.

Plasmid Construct, Transient Silencing, and 3-Methyladenine Infiltration Experiments

Infiltration experiments on strawberry receptacles were performed in *F. x ananassa* cv "San Andreas." For transient silencing of *FxaATG5* or *FxaATG7*, RNAi constructs were developed using the gateway-based vector pHELLSGATE12 (Helliwell and Waterhouse, 2005). Forward and reverse specific primers were designed and attb1 and attb2 sites, respectively were added to them (**Supplementary Table 1-S1**). Sequences were PCR amplified using *F. x ananasa* cv. "San Andreas" cDNA as template. The resulting fragments (307 bp for *FxaATG5* and 358 bp for *FxaATG7*) were recombined in independent pDONR-Zeo. The corresponding pENTRY vectors were finally recombined with pHELLSGATE12. The design of this vector allows the recombination of the sequence of interest both in sense and antisense. AGL0 strain of *Agrobacterium tumefaciens* was transformed with the different constructs (pHELLSGATE12, PHELLSGATE12-FxaATG5i, and pHELLSGATE12-FxaATG7i) and grown at 28°C until OD_{600} reached 0,7. Cells were centrifuged at 3,000*g* for 10 min, resuspended in infiltration buffer (10 mM $MgCl_2$, 10 mM MES, pH 5.6, and 200 mM acetosyringone), and incubated for at least 1 h at room temperature. Approximately 500 µl of *Agrobacterium* suspension was evenly infiltrated into green stage fruits (14 days after anthesis approximately) with the help of a 1 ml syringe. 14 fruits were injected with each construct. Fruits remained attached to the plant and were harvested, and flash-frozen in liquid nitrogen 9 days after infiltration. Achenes were removed from frozen fruits with the help of a scalpel. For 3-methyladenine (3-MA) treatment, infiltration assays were performed as described for silencing experiments. Green stage fruits were evenly injected either with mock (milli-Q water) or 5 mM solution of 3-MA (Merck, M9281) dissolved in milli-Q water. Fruits were harvested and photographs were taken 9 days after infiltration. 10 fruits were injected with either mock or 3-MA. Fruit size comparison was performed measuring fruit area in photographs using ImageJ.

RESULTS

Autophagy Related Genes Are Differentially Expressed During Strawberry Fruit Ripening

The cultivated strawberry *F. x ananassa* is an allo-octoploid (2n = 8x = 56) originated by hybridization of two octoploid species in the 18th century (Duchesne, 1766). A recent study has established that the ancestral parental diploid species of *F. x ananassa* were *Fragaria iinumae*, *Fragaria niponica*, *Fragaria viridis,* and *Fragaria vesca*, this last one being the subgenome that has increased its dominance over the other three along evolution (Edger et al., 2019). For this work, we first searched in the genome of *F. vesca* for putative orthologs of the *Arabidopsis* autophagy-related genes. As expected, we found orthologs of all key *ATG* genes, the selective autophagy gene *NBR1,* and the Phosphatidyl inositol 3 kinase type III VPS34 (**Supplementary Table 1-S2**). It is interesting to note that the number of genes belonging to each family in the diploid *F. vesca* was very similar to *Arabidopsis thaliana*, including those described as single copy genes.

Next, we identified in the recently sequenced and re-annotated genome of the octoploid *F. x ananassa* (Edger et al., 2019; Liu et al., 2021) the homoeologs for the autophagy-related genes found in *F. vesca*. Previously, our group generated a set of transcriptomic data during the fruit ripening of *F. x ananassa* after mapping the reads of a RNAseq experiment in the sequenced reference genome *F. vesca* (Sánchez-Sevilla et al., 2017). In the present work, we have mapped those reads to the last annotation of *F. x ananassa* genome and we have analyzed the expression of key autophagy genes belonging to the different functional groups of this pathway in the receptacle. Different autophagy genes participate at the different stages of the process. These stages are: (i) induction (ATG1, ATG13, ATG11, and ATG101), (ii) vesicle nucleation (ATG6 and VPS34), (iii) membrane delivery (ATG9, ATG2, and ATG18), and (iv) autophagosome expansion and closure (ATG4, ATG5, ATG7, ATG8, ATG10, and ATG12) (Marshall and Vierstra, 2018). We have found that all these autophagy genes are expressed during strawberry fruit receptacle ripening (**Supplementary Table 2**).

ATG5 and ATG7 are two proteins that are essential for the lipidation of ATG8, a process required for autophagosome expansion (Marshall and Vierstra, 2018). It has been reported that mutants of these genes show impaired autophagosomes formation and autophagy blocking in different plant species, mammals, and yeast (Phillips et al., 2008; Minina et al., 2013; Sanchez-Vera et al., 2017; Klionsky et al., 2021). We have identified three *ATG5* and four *ATG7* genes in *F. x ananassa*. In the ripening fruits, the three *ATG5* and two of the *ATG7* genes are expressed (above 0,5 FPKM), with minor differences, between the different developmental stages (**Figures 1A,B**).

VPS34 is a phosphatidyl inositol 3-kinase (PI3K) that belongs to the PI3K complex. This complex participates at early stages of the autophagy process with an essential role in vesicle nucleation (Zhuang et al., 2018). We have found four *VPS34* genes expressed during ripening in *F. x ananassa* showing significant expression increase in white and turning compared to green and red (**Figure 1C**).

NBR1 is a protein that acts as a cargo receptor and that gets degraded during autophagy. It has been proposed to play a conserved role in selective autophagy in plants (Svenning et al., 2011; Ji et al., 2020). We found that the four putative homoeologs of this gene were expressed, and their expression levels steadily increased from green to red fruits (**Figure 1D**).

Also in plants, two regulators of the autophagy process have been proposed: the transcription factor ATAF1 (Garapati et al., 2015) and the SnRK1 kinase complex (Soto-Burgos and Bassham, 2017). The expression of the *KIN10* genes, encoding the catalytic subunit of the complex, and the *ATAF1* genes in the ripening receptacle of the strawberry fruit are shown in **Figures 1E,F**. While the *KIN10* expression peaked at the white

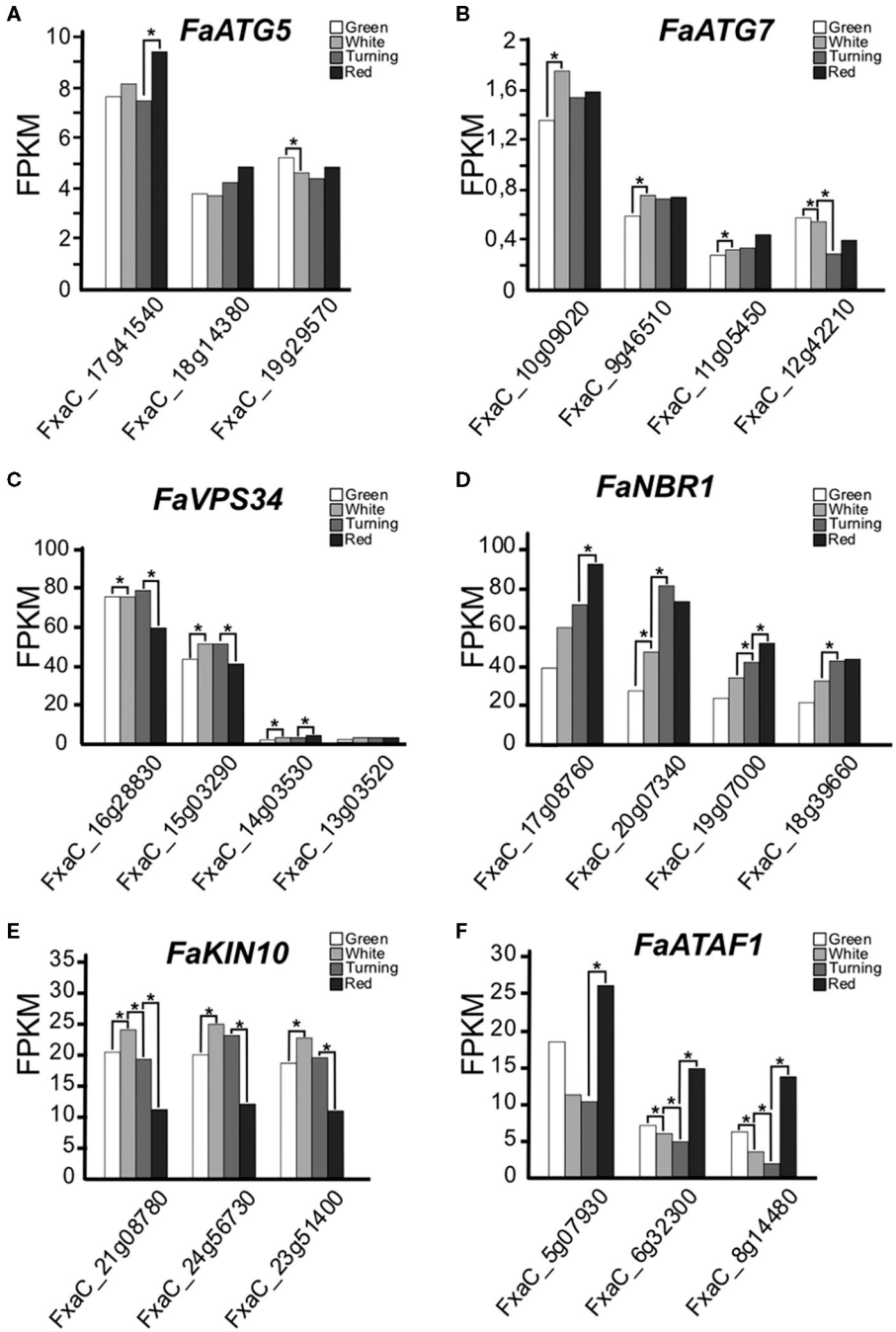

FIGURE 1 | (A–F) Expression of autophagy-related genes along ripening in *F. x ananassa* cv. Camarosa. Data for this analysis were extracted from the RNAseq generated by Sánchez-Sevilla et al. (2017). RNA was extracted from de-achene receptacles at the stages green, white, turning, and red. Statistical significance was determined between one stage and the next; it is indicated with an asterisk. Statistical analysis was performed with the false discovery rate (FDR) method after Benjamini-Hochberg correction for multiple-testing. Complete statistical analysis can be found in **Supplementary Table 2**.

stage, the expression of *ATAF1* displayed higher values at green and red stages.

ATG8 proteins play a key role in the autophagosome expansion that occurs during autophagy (Martens and Fracchiolla, 2020). Upon autophagy activation, ATG8 undergoes a lipidation process mediated by a ubiquitin-like system in which ATG5 and ATG7 participate (Marshall and Vierstra, 2018). This lipidation consists of the binding of a phosphatidylethanolamine (PE) molecule to a Glycine at the ATG8 C-terminus end. For this to happen, first ATG8 has to be cleaved by ATG4 in

order to get this Glycine exposed (Yoshimoto et al., 2004). Once ATG8 proteins are lipidated, they can be anchored to the autophagosome membrane. We found nine *ATG8* genes in the genome of *F. vesca* and 36 homoeologs in *F. x ananassa*. To establish the relation between each *F. vesca* gene with its correspondent homoeologs, we performed an alignment of the nucleotide sequences with the *F. vesca* and *F. x ananassa ATG8* genes that produced the dendrogram displayed in **Figure 2A**. The clustering pattern indicates the correspondences between the genes of both species. Some of the *ATG8* homoeologs identified in the *F. x ananassa* genome did not show expression in any of the tissues analyzed (receptacle, achenes, leaves, and roots) (indicated with asterisks in **Figure 2A**) and two of them were expressed <1 FPKM during receptacle ripening, so they were not included in the expression analysis. The expression of the *ATG8* genes at four stages of receptacle ripening (green, white, turning, and red) is shown in **Figure 2B**. There is a high variability in the expression both in absolute values and stage-dependent values. Three main expression patterns were found, one with increasing expression from green to red stages (*ATG8a*, *ATG8g*), another decreasing from green to red (*ATG8f*), and a third with highest values at green and red stages (*ATG8b, ATG8c, ATG8h*).

ATG8 proteins are also essential for autophagosome-cargo recognition. ATG8 present two hydrophobic pockets that determine the interaction with proteins containing the so called ATG8-interaction motifs (or AIM) (Noda et al., 2010). These AIM-containing proteins are located at the surface of organelles, protein complexes, and other structures working as docking platforms for ATG8 and around which the autophagosome grows and engulfs them (Marshall and Vierstra, 2018). When analyzing the FaATG8 aminoacidic sequences, we found that the residues located at the key positions of the two hydrophobic pockets shows a high level of conservation (**Supplementary Figure 1**, black and red arrows) (Kellner et al., 2017). Furthermore, apart from two of them, all shared the C-terminal Glycine required for the lipidation (**Figure 2C**), however the downstream sequence showed high variability both in terms of amino acid number (0, 2, 3, and 5) and nature.

Processing of ATG8 previous to its lipidation is done by the protease ATG4. In the diploid *F. vesca*, as reported in *Arabidopsis*, we identified two *ATG4* genes, while in *F. ananassa* eight ATG4 genes were identified included in two possibly homoeologs groups, *ATG4a* and *ATG4b*. Their expression is shown in **Figure 2D**. The analyses of the joint expression of all putative homoeologs of *ATG4a* and *ATG4b* (**Figure 2E**) show that from green to white stage *ATG4b* has a prevalent expression and goes down from white to red, whereas *ATG4a* expression increases from white to turning and gets reduced toward red.

Autophagic Structures Are Present at Different Stages of Strawberry Receptacle Ripening

The transcriptomic data indicate that genes involved in autophagy are expressed during fruit ripening. To investigate the presence of autophagic process at the cellular level, we performed an ultrastructure analysis of the receptacle along fruit ripening using transmission electron microscopy (TEM). It has been described that autophagy is involved in the process of tracheary element formation (Kwon et al., 2010), so we analyzed cells at the vascular tissue from green receptacle. The strawberry receptacle develops vascular bundles that connect the achenes with the pith (Aharoni et al., 2002). As expected, a significantly high amount of autophagy-related structures could be found in immature xylem cells (**Figure 3B1**). These cells are easily distinguishable in TEM images thanks to the characteristic patterned cell wall deposition that they present. Many single membrane vesicles (of around 0,5 to 1 micrometers) previously described as autolysosome-like structures (Takatsuka et al., 2004; Sanchez-Vera et al., 2017), presenting electron - dense amorphous content in some cases or structures resembling autophagic bodies in other cases, were found in those cells and in the surrounding cells, probably xylem parenchymatic cells (**Figures 3A1,A2,B1,B2,C1** white and black arrowheads, respectively). Autophagosomes were also visible in both cell types (**Figures 3B2,C2**, empty white arrowheads).

Cells present at the cortex and pith of *F x ananassa* receptacle are composed by a big central vacuole and a thin layer of cytoplasm pressed to the cell wall. When we analyzed cortical cells located at the subepidermal space of the receptacle of *F. x ananassa* cv. "Camarosa" at stages green, white, and red both autophagosomes (**Figure 4A**, inlet) and autolysosome-like structures with degrading content and autophagic bodies were found (**Figures 4A–C**; white and black arrowheads, respectively). This made them the most abundant the autolysosome-like structures. It is interesting to note that even though autophagy is considered a relatively fast process in plants, difficult in some cases to monitor by TEM without the help of inhibitors, we have been able to identify those structures directly in non-treated cells.

Strawberry Fruits Show Two Waves of Increased Autophagy Flux During Ripening

Although the differential expression of autophagy-related genes and the presence of autophagy structures at the cellular level supports that autophagy could be active during ripening, this observation does not demonstrate by itself the existence of an increased autophagy flux. Therefore, we analyzed the levels of ATG8 lipidation and NBR1 that have been described as markers of autophagy flux (Klionsky et al., 2021). As previously indicated, lipidation of ATG8 is essential for autophagosome formation. When ATG8 lipidation is abolished, as happens in certain *ATG* gene mutants, autophagosome formation is prevented and autophagy flux is blocked (Chung et al., 2010). Thus, the level of ATG8 lipidation has been used as a measure of autophagy activity (Bao et al., 2017). Therefore, we examined by immunoblot analysis the levels of ATG8 protein and its lipidated form (ATG8-PE) using an antibody raised against *Chlamydomonas rheinardtii* ATG8 that recognizes all ATG8 isoforms (Pérez-Pérez et al., 2010). For this analysis we decided to include two more developmental stages corresponding with the late

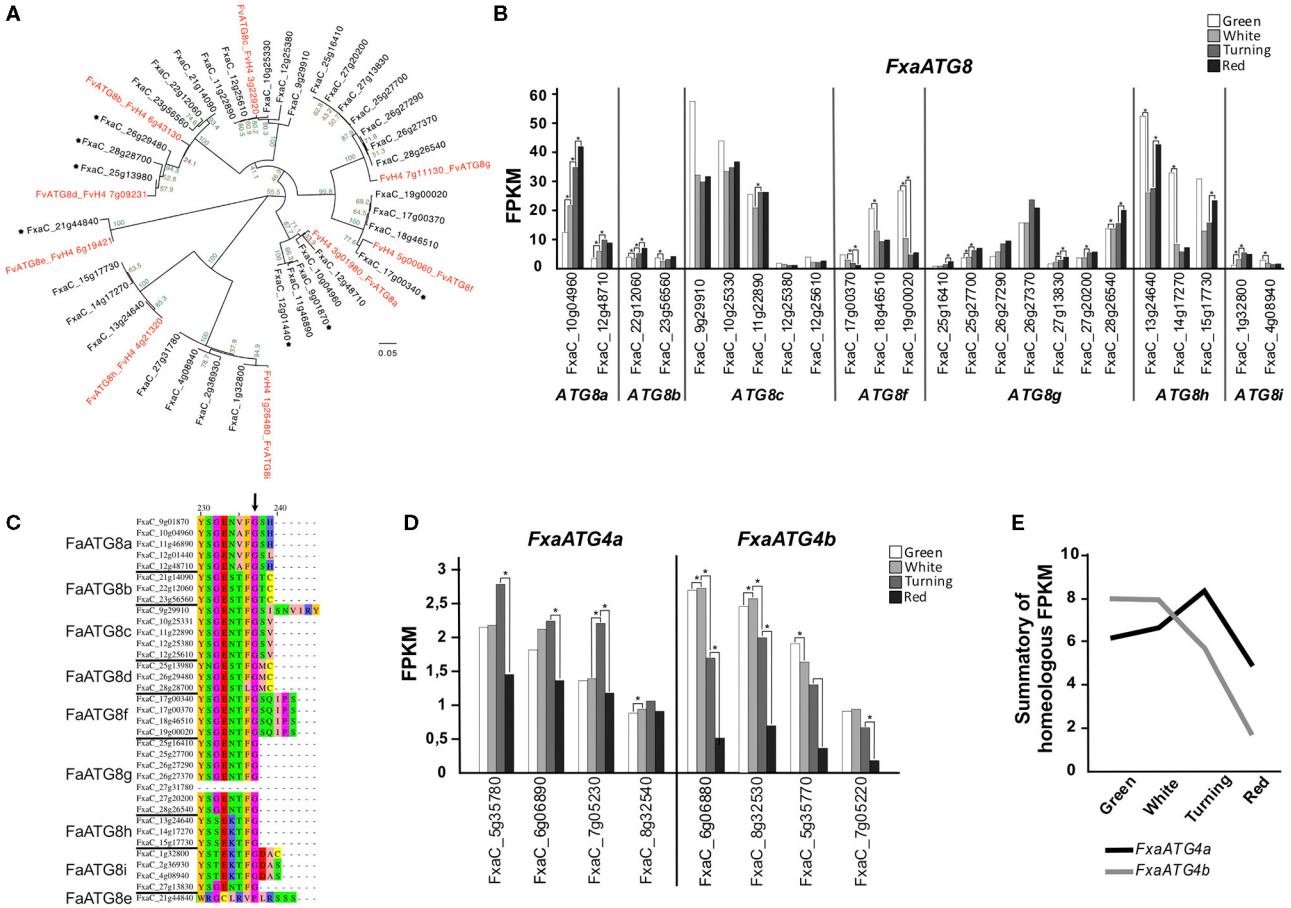

FIGURE 2 | Analysis of FaATG8 and FaATG4. **(A)** Phylogenetic tree of *F. vesca* and *F. x ananassa ATG8* genes. Nucleotide sequences were aligned by MAFFT and the tree was generated by the neighbor-joining method and displayed using FigTree. Asterisks mark genes with <0,5 FPKM expression values in all tissue tested (achenes, receptacle, leaves, and roots). **(B)** Representation of Fa*ATG8* genes expressed at least 1 FPKM in any stage of the process of receptacle ripening. **(C)** Alignment of C′-terminus end of the different *FaATG8* homoeologs. Arrow indicates the conserved Glycine essential for lipidation. **(D)** Representation of *FaATG4* expression during strawberry ripening. **(E)** Expression trend of *FaATG4a* and *FaATG4b* homoeologs during ripening. Data shown in **(B–E)** were extracted from the RNAseq dataset generated by Sánchez-Sevilla et al. (2017). Statistical significance between one stage and the following stage it is indicated with an asterisk. Statistical analysis was performed with the false discovery rate (FDR) method after Benjamini-Hochberg correction for multiple-testing. Complete statistical analysis can be found in **Supplementary Table 2**. Alignment that generated phylogenetic tree (2A) can be found in **Supplementary Data Sheet 1**.

maturation process and to use the variety "San Andreas" that is a day neutral cultivar. "San Andreas" comes from the same breeding program of cv. "Camarosa" but presented slightly lower content of anthocyanins and phenolics at the ripe stage, as well as lower fruit firmness, under specific growth conditions (Lalk et al., 2020), and has the advantage of producing fruits throughout the year. Thus, we analyzed the receptacle of "San Andreas" strawberry fruits at six developmental stages: green, white, turning, red, ripe, and over-ripe (pre-senescent) fruits (**Figure 5A**). The relative level of total ATG8 protein, which is the sum of non-lipidated ATG8 and lipidated ATG8, showed a first maxima at the white stage and a second maxima at the end of the ripening period (**Figure 5B**). Interestingly, the ratio ATG8PE/ATG8 shows an important increase at the white stage and a more dramatic one at the ripe stage (1,75-fold change of the ratio between white and ripe). These results clearly show that there is an autophagy induction at both stages supported both by an increase in the ATG8 protein amount and by its lipidation level, being the second induction of higher intensity. As expected, cv "Camarosa" shows a very similar pattern of ATG8 expression and lipidation at those stages (**Supplementary Figure 2B**).

NBR1 is an autophagy substrate, therefore when autophagy is active NBR1 gets degraded, so its protein levels gets reduced even though its mRNA expression remains high. Regarding the levels of NBR1, we found that the protein levels at the over-ripe stage was lower than at the ripe stage (**Figure 5C**). To elucidate whether this was an effect of the degradation through autophagy of NBR1 or a diminishing of the mRNA expression, we performed qRT-PCR of *NBR1* in the receptacle at the different stages (**Figure 5D**). Our data show that *NBR1* mRNA levels are not reduced at the over-ripe stage, so our results support that the depletion of NBR1

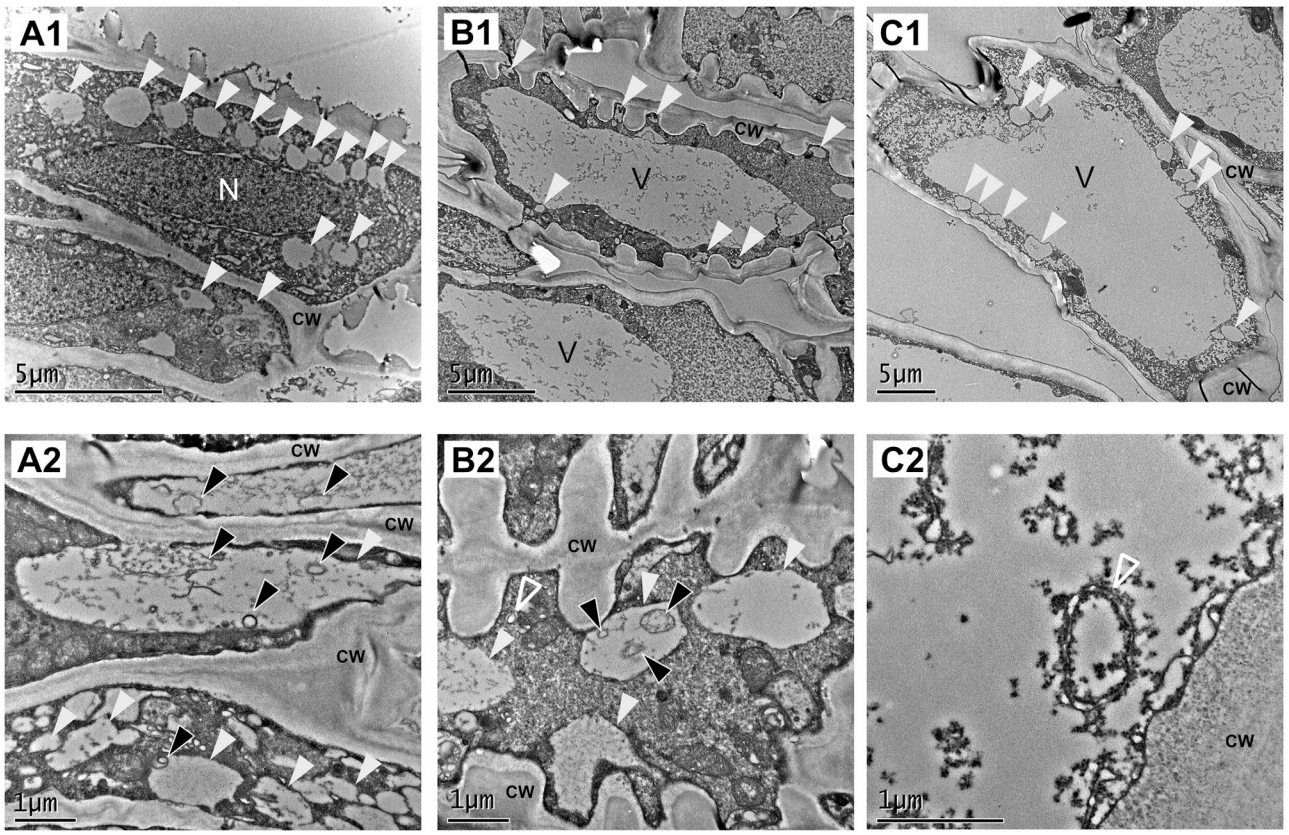

FIGURE 3 | Vascular tissue is a place of active autophagy. TEM micrographs from representative cells of the green receptacle vascular tissue. **(A–C)** Different cell types found in vascular tissue. **(A,C)** Parenchymatic cells of the vascular tissue. **(B)** Immature xylem cells. **(1)** Overview of the cells and **(2)** close up of the same type of cells showing autophagy-related structures. White arrowheads: single membrane compartments with degraded content, black arrowheads: autophagic bodies, empty white arrowheads: autophagosomes. CW, cell wall; n, nucleus; v, Vacuole.

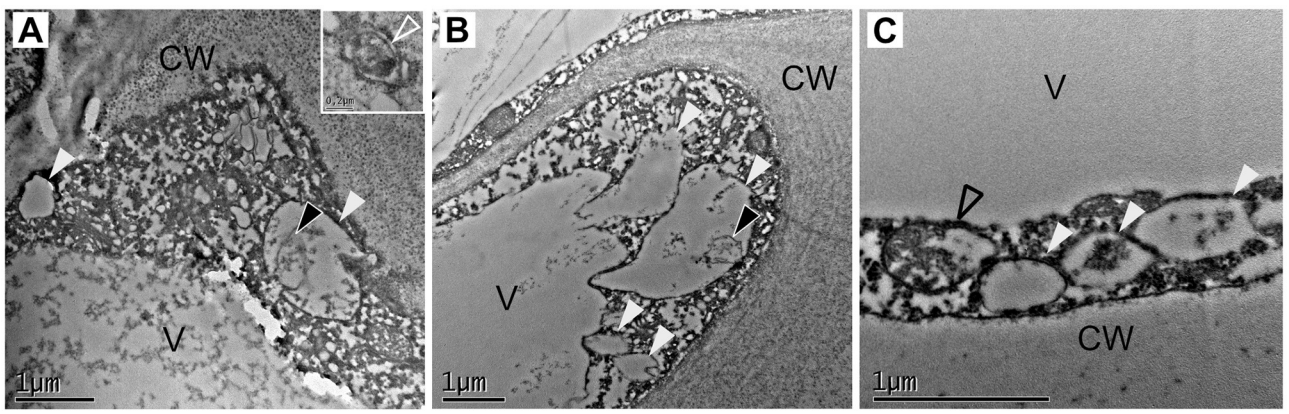

FIGURE 4 | Identification of autophagy-related structures in *F x ananassa* receptacle along ripening. TEM micrographs from receptacle cortical cells showing autophagy-related structures. **(A)** Green receptacle cell, **(B)** white receptacle cell, and **(C)** red receptacle cell. White arrowheads: single membrane compartments with degraded content, black arrowheads: autophagic bodies, empty black arrowhead: disassembling mitochondria. CW, cell wall; V, Vacuole.

protein levels at the over-ripe stage is probably due to its degradation by autophagy, consistent with the levels of ATG8 lipidation. It is interesting to note that we see a correlation between lipidation levels of ATG8 at the white stage and depletion of NBR1 protein but not mRNA also in "Camarosa" (**Supplementary Figures 2B,C**).

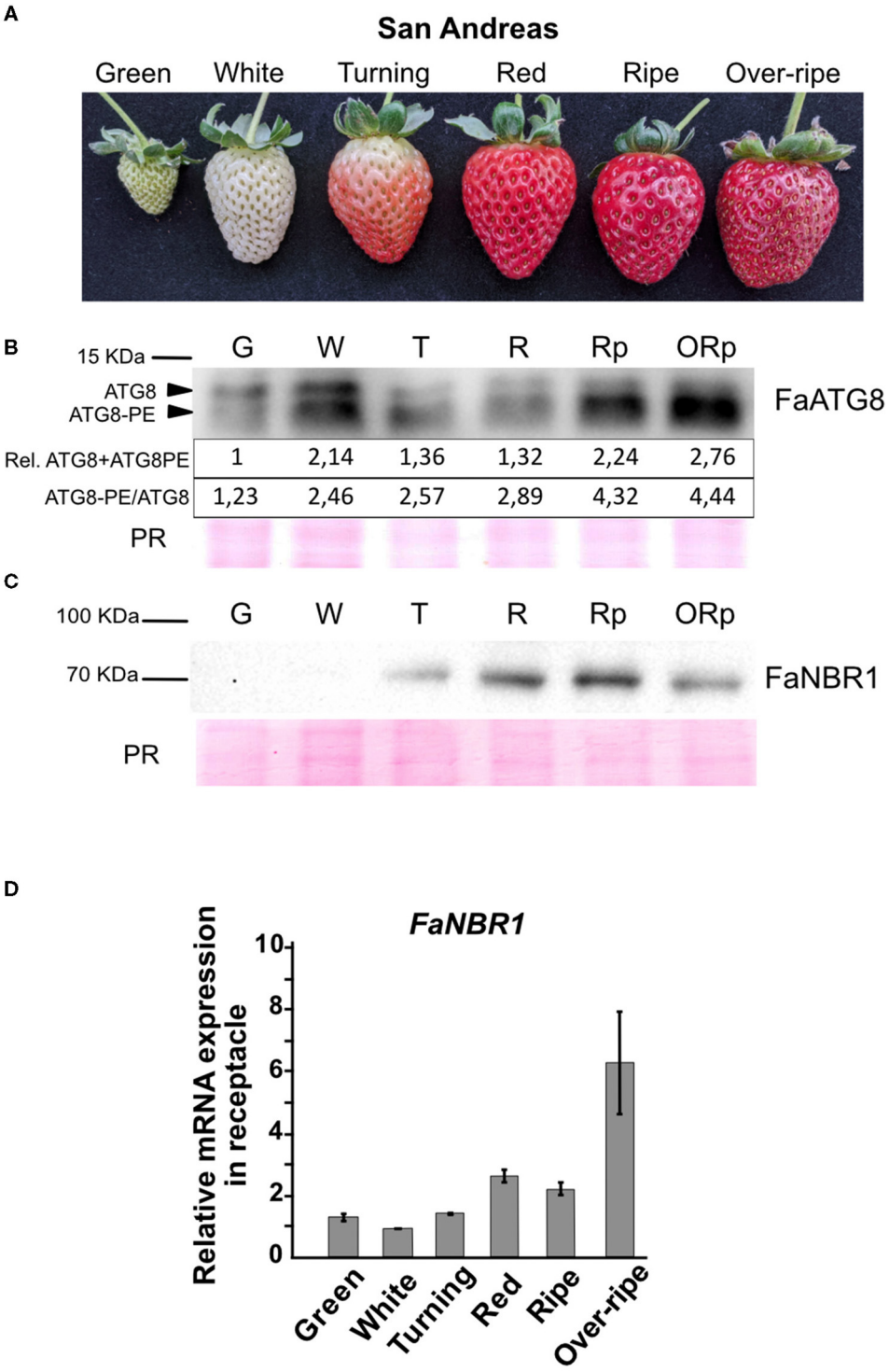

FIGURE 5 | Identification of two waves of autophagy flux along strawberry ripening. **(A)** Stages of strawberry ripening (cv. "San Andreas") analyzed for autophagy flux. **(B)** Immunoblot of ATG8 showing non-lipidated (ATG8) and lipidated form (ATG8-PE) along ripening. Quantifications of band intensities are shown in arbitrary units. Rel. ATG8+ATG8PE shows relative quantification of the summatory of ATG8 and ATG8PE signal. ATG8PE/ATG8 shows the ratio of both protein forms. **(C)** Immunoblot of NBR1 along ripening. **(D)** qRT-PCR analysis of *FaNBR1* in *F. x ananassa* cv "San Andreas" along ripening. Error bars represent standard deviation. PR, Ponceau red.

Taken all together, our data support the presence of two marked waves of autophagy flux induction during strawberry ripening supported by the ratio of ATG8-PE/ATG8 and the level of both protein forms, peaking at white and ripe stages.

Autophagy Inhibition Affects the Fruit Development and Delays the Ripening

A number of autophagy inhibitors have been reported (Marshall and Vierstra, 2018). Among them, the 3-Methyladenine (3-MA) has been broadly used to block autophagy in different species including plants (Klionsky et al., 2021). 3-MA inhibits the Phosphatidylinositol-3-kinase activity of the PI3K complex (Takatsuka et al., 2004), more precisely through inhibition of VPS34, a protein highly expressed throughout ripening (**Figure 1C**) that participates in the vesicle nucleation stage of the autophagy pathway. Treatment of "San Andreas" fruits at the green stage with a 5 mM solution of 3-MA caused a dramatic delay in the ripening progress (**Figure 6A**) compared with the mock treated fruits. The delay in ripening was evident by the lack of red color, probably due to the lack of anthocyanin accumulation, and by the reduced size of the fruit. Although the variability in fruit size in the water infiltrated fruits was high, we observed a significant reduction in the size range that 3-MA treated fruits reached 9 days after infiltration (**Figure 6B**).

It is possible that besides its effect over autophagy, inhibition of VPS34 by 3-MA could be having an additional effect over other cellular processes different from autophagy, such as the endocytic pathway where VPS34 also participates (Bhati et al., 2021). Therefore, we performed transient silencing in green fruits of two of the genes essential for the ATG8 lipidation process, *ATG5* and *ATG7,* using RNAi. The phenotypic analysis of the infiltrated fruits showed a significant delay of the fruit ripening in the silenced fruits compared with the controls (**Figure 6C**). Next, we were interested in determining whether this silencing could have a correlation with a diminishing in the lipidation of ATG8. Thus, we measured the ATG8 levels by immunoblot as described before and quantified the lipidation to non-lipidation ratio. As expected, the ratio of ATG8-PE/ATG8 also decreased in the transiently silenced fruits confirming that the reduction of ATG5 or ATG7 activity was having an effect over ATG8 lipidation process (**Figure 6C**).

Overall, our transcriptomic data, cytological analyses, and biochemical and genetic studies supports that autophagy has a relevant role in the ripening of the strawberry fruit, happening in two waves and with direct implications in, at least, the vascular development and the senescence of the fruit.

DISCUSSION

Our study shows that strawberry receptacle is a place of constant autophagy activity with two points of autophagy flux induction. Analysis of *ATG* genes and ATG8 protein expression in the receptacle of strawberry fruits from green to red stage shows a basal level of transcripts at every stage, with enhanced expression of some of them at specific stages. On the other hand, autophagy related structures can be observed in the cortical cells in different stages of the ripening process. This supports a dual role of autophagy during strawberry fruit ripening, as a housekeeping process to maintain the cellular nutrient homeostasis and as a specific recycling mechanism to cope with developmental conditions that requires the generation of new cellular compounds or environmental situations that challenge the energy balance in the cell (McLoughlin et al., 2020).

A process that accompanies strawberry fruit growth from the early stages is the formation of the vascular network that connects the achenes to the different cell types of the receptacle and the central pith. Qualitative markers of vascular development were found at all the developmental stages of strawberry ripening (Aharoni et al., 2002). In other plant organs, the activation of autophagy in the differentiation of the xylem before the lignification of the cells has been reported (Kwon et al., 2010; Wojciechowska et al., 2019). Here we show the presence of autolysosome-like structures and autophagosomes in cells of the vascular tissue of the receptacle, so it would be expected that occurrence of autophagy in the fruits is taking place associated with the vascular development, that is parallel to the growth in size of the fruit. This would also explain the relatively steady expression of some of the *ATG* genes found in the growing receptacle, from green to red stage.

The occurrence of an elevated number of ATG8 isoforms in plants opens the question of their contribution to the diversification of selective autophagy pathways (Kellner et al., 2017). It has been proposed that possible functional diversification can be supported by their association with a number of ATG8-interacting proteins which act as cargo receptors (Marshall and Vierstra, 2018). Sequence analysis of the *ATG8* genes in the *F. x ananassa* genome shows high conservation of residues in the two hydrophobic pockets that interact with proteins containing the AIM domain (Kellner et al., 2017). There are some differences in the amino acid positions around the binding pockets in the ATG8 proteins, but only the structural analysis of the ATG8 isoforms and the possible interactors could establish the relevance of the sequence variability on their functional diversity. However, the occurrence of co-expression patterns between the ATG8 isoforms and the possible interacting proteins would be a step to explain the functional diversity of ATG8. In this sense, we have found that the known NBR1 interactor (Svenning et al., 2011) presents the highest expression level at late stages of fruit ripening, coincident with the peak of expression of several of the ATG8 isoforms. Previously, it has been reported that the NBR1-dependent selective autophagy in plants occurs under different stress and non-stress conditions (Zhou et al., 2013; Chi et al., 2020; Jung et al., 2020), being common to the different conditions observed during the occurrence of oxidative stress. An early analysis of the transcriptional changes in the ripening strawberry fruit associated the ripening process to a response to oxidative stress (Aharoni et al., 2002), which would be in agreement with the possible interaction of some isoforms of the ATG8 family and NBR1 in the autophagy occurring in the ripening receptacle of the strawberry fruit. In *Arabidopsis*, NBR1 showed different levels of interaction with the members of the ATG8 family of proteins (Svenning et al., 2011).

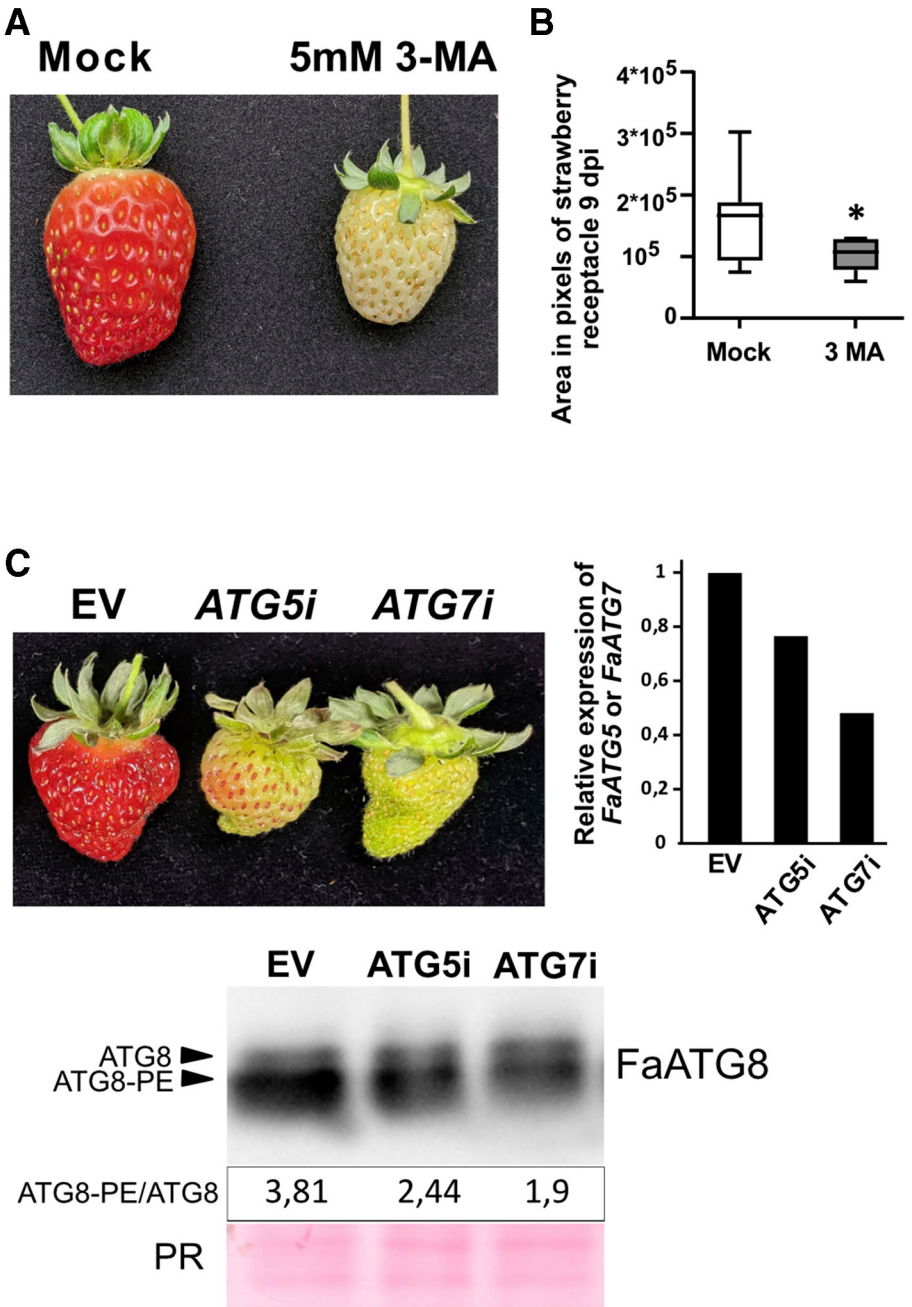

FIGURE 6 | Effect of autophagy blocking over strawberry ripening. **(A)** Representative image showing the effect over ripening of 3-MA in *F x ananassa* cv "San Andreas". **(B)** Fruit area in 3-MA treated fruits compared to mock treated samples. Variance difference between mock treated lines and 3-MA treated lines were analyzed using an F-test and * denote significantly different with a $P < 0{,}005$. **(C)** Up-left, representative image showing the effect over ripening of *FaATG5* or *FaATG7* silencing. Up-right, qRT-PCR analysis of *ATG5* or *ATG7* expression in infiltrated receptacles. Down, immunoblot analysis of ATG8 levels in control and silenced fruits and quantification of ratio between lipidated (ATG8-PE) and non-lipidated form (ATG8). The **(C)** panel is representative of three independent experiments. EV, Empty vector; PR, Ponceau Red.

The set of putative homoeologs of *ATG8c*, *ATG8f, and ATG8h* genes present an expression induction in green. This suggests a specific involvement in the autophagic processes occurring at this early stage. Among them, in *ATG8c* and *ATG8f,* the increase of expression happens only in green but not in other stages of the ripening process. Intriguingly, all members of the ATG8f and one of the ATG8c show a longer amino acid sequence at the C-terminus after the site of proteolysis by ATG4. In the diploid *F. vesca*, as in *Arabidopsis* (Seo et al., 2016), two *ATG4* and nine *ATG8* genes are identified. In *Arabidopsis*, *in vitro* studies of the activity of the two ATG4 against different ATG8 showed a difference in the activity and the substrate

specificity of the two proteases (Woo et al., 2014). Moreover, broad studies on the specificity between ATG4 and ATG8 in a more diverse range of species support that the processing activity is determined by the ATG8 sequence rather than the ATG4 (Seo et al., 2016). Interestingly, the joint expression of all the *F. x ananassa* ATG4 genes corresponding to the two *F. vesca* genes show equivalent values of expression, but with ATG4a having the highest expression at the turning stage and ATG4b at the green/white stages. Whether the C-terminal sequences of the strawberry ATG8s determine the selectivity for its processing by ATG4 would be of interest to know, since it would provide valuable information about the functional diversity of the ATG8 genes in strawberry.

Our analysis of the ATG8 lipidation, which is a critical step in the autophagy progress, points to two time points during ripening of highest ATG8 content and lipidation: during the white stage and at the end of ripening in a pre-senescent stage. Growth of strawberry fruit, as in other fleshy fruits, is supported by fruit metabolism that must be energetically adjusted during the transition from green to ripe stage (Carrari and Fernie, 2006; Fait et al., 2008; Jing and Malladi, 2020; Martín-Pizarro et al., 2021). In this process, there is a critical step when the limited photosynthetic capacity of the green fruit is completely lost after the loss of chlorophyll. Autophagy has been associated with the metabolic adjustment taking place during the plant developmental transitions (Michaeli et al., 2016). The increase of ATG8 lipidation found in the receptacle at the white stage can be explained by the need to maintain the nutrients supply required to continue the fruit growth. The growth conditions of the fruit under the loss of chlorophyll could be similar to the nutrient deprivation found in other plant tissues, where the autophagic response contributes to the energy adjustment (McLoughlin et al., 2020). The SnRK1 complex is a kinase that functions as an energy sensor (Broeckx et al., 2016) and acts as an autophagy activator (Marshall and Vierstra, 2018). It is significant that the expression of KIN10, a component of the SnRK1 complex, increases from green to white stage in the three homoeologs. It would be of interest to know whether KIN10 also plays a regulatory role of autophagy in the receptacle of the strawberry fruit, that increases the autophagic flux at the white stage as a response to low energy conditions, as reported in *Arabidopsis* (Soto-Burgos and Bassham, 2017). In climacteric fruits the reduction of photosynthetic capacity during ripening is coupled with the burst of aerobic metabolism, whose energy balance is more favorable. To our knowledge, the only publications showing increasing expression of autophagy genes with ripening has been made in non-climacteric fruits such as pepper, grapevine, and the present one made in strawberry (Ghan et al., 2017; López-Vidal et al., 2020). This brings the questions of whether autophagy is a relevant process during ripening of climacteric fruits.

Several autophagy inhibitors have been described in plants although most of them have effects over other non-autophagy processes (Marshall and Vierstra, 2018). 3-Methyladenine is a compound that inhibits VPS34 of the PI3K complex that participates in autophagy initiation but also in the endocytic pathway (Bhati et al., 2021). The effect over ripening of 3-MA treatment is very similar to the effect of *ATG5* or *ATG7* silencing, this is a delay in the progress of the process in both cases, showing clearly that autophagy has an important role in the ripening of strawberry. Regarding the possible implications of the endocytic pathway during strawberry ripening a more detailed study, treating fruits with specific endocytic pathway inhibitors such a Brefeldin A, could shed light into this question.

Aging and senescence are physiological stages where autophagy also plays a main role in plants (Wang and Schippers, 2019). The final stage of fruit ripening is followed by senescence. This is a phase of development that it is dependent on cell viability and the expression of specific genes (Thomas, 2013). This process is a way to recycle resources from aging organs to developing structures. We have found that the abundance of ATG8-PE greatly increases with fruit ripening, reaching a highest value in over-ripe fruits. In addition, the increased expression of cargo receptor *NBR1* with ripening and over-ripening and the decreased content of the NBR1 protein in the over-ripe fruits is further proof of the induction of autophagy at these developmental stages. Our results support that autophagy continues after fruit ripening as a recycling strategy prior to the onset of senescence. Analysis in *Arabidopsis* of autophagy function, by the induction of ATG genes expression or silencing in mutant lines under aging and senescence, concluded the existence of a dual role for autophagy, that prevents senescing while aging, but controls the salvage pathway when senescence occurs. The possible role of autophagy to prevent senescence in strawberry fruits could be critical for conservation of the fruit integrity after harvest since post-harvest behavior of the fruits mimics a senescent process (Pott et al., 2020).

Our results in strawberry point to a house-keeping autophagy activity along fruit growth inherent to growth processes as vascular development, as well as two periods of enhanced autophagy in response to nutrients shortage and senescence. To our knowledge, this is the first work showing clear evidence of the role of autophagy in the process of fleshy fruit ripening. The knowledge of the components and the extension of autophagy in the growth and development of fleshy fruits might be of great relevance in a sink organ that is predominantly heterotrophic.

DATA AVAILABILITY STATEMENT

Publicly available datasets were analyzed in this study. This data can be found here: https://www.ebi.ac.uk/ena/browser/view/PRJEB12420.

AUTHOR CONTRIBUTIONS

VS-V and VV conceived the study. VS-V, MB, and VV planned and reviewed the experiments. JS-S identified the *F. x ananassa* genes and re-mapped and quantified the RNAseq data. VS-V executed the experiments, analyzed the data, and wrote the paper. All authors reviewed and approved the final manuscript.

FUNDING

This work was supported by a Marie Sklodowska-Curie Individual Fellowship granted to VS-V (FrATGaria-GA-844365),

by the Ministerio de Economía y Competitividad, co-financed by the European Regional Development Fund (grant BIO2017-82609-R) to MB and by the Plan Propio of the University of Malaga.

ACKNOWLEDGMENTS

The authors want to thank Dr. Emilio Gutiérrez Beltrán (University of Seville) for technical advice and for kindly providing antiATG8 and antiNBR1 antibodies.

SUPPLEMENTARY MATERIAL

The Supplementary Material for this article can be found online at: https://www.frontiersin.org/articles/10.3389/fpls.2021.688481/full#supplementary-material

Supplementary Figure 1 | Alignment of FaATG8 aminoacidic sequences. Black and red arrows mark the residues that form the W and L pockets as shown for ATG8 from Brassicales, Solanaceae, and Poaceae (Kellner et al., 2017). Black asterisk marks the conserved Glycine to which PE is bond after ATG8 lipidation.

Supplementary Figure 2 | Analysis of autophagy flux in *F. x ananassa* cv. "Camarosa," **(A)** Stages of strawberry ripening in *F. x ananassa* cv. "Camarosa" analyzed for autophagy flux. **(B)** Immunoblot of ATG8 showing non-lipidated (ATG8) and lipidated form (ATG8-PE) and immunoblot of NBR1 along ripening. **(C)** Summatory of all NBR1 homoeologs RNAseq data.

Supplementary Data Sheet 1 | Alignment of the *FaATG8* nucleotides sequences that generated phylogenetic tree shown in **Figure 2A**.

Supplementary Table 1 | (S1) List of primers used in this work. **(S2)** Autophagy related genes found in *F. vesca* genome.

Supplementary Table 2 | Expression levels in FPKM of all autophagy-related genes analyzed in this work along ripening in *F. x ananassa* receptacle and achenes.

REFERENCES

Aharoni, A., Keizer, L. C. P., Van den Broeck, H. C., Blanco-Portales, R., Muñoz-Blanco, J., Bois, G., et al. (2002). Novel insight into vascular, stress, and auxin-dependent and -independent gene expression programs in strawberry, a non-climacteric fruit. *Plant Physiol.* 129, 1019–1031. doi: 10.1104/pp.003558

Bao, Y., Mugume, Y., and Bassham, D. C. (2017). Biochemical methods to monitor autophagic responses in plants. *Methods Enzymol.* 588, 497–513. doi: 10.1016/bs.mie.2016.09.090

Bhati, K. K., Luong, A. M., and Batoko, H. (2021). VPS34 complexes in plants: untangled enough? *Trends Plant Sci.* 26, 303–305. doi: 10.1016/j.tplants.2021.02.001

Broeckx, T., Hulsmans, S., and Rolland, F. (2016). The plant energy sensor: evolutionary conservation and divergence of SnRK1 structure, regulation, and function. *J. Exp. Bot.* 67, 6215–6252. doi: 10.1093/jxb/erw416

Carrari, F., and Fernie, A. R. (2006). Metabolic regulation underlying tomato fruit development. *J. Exp. Bot.* 57, 1883–1897. doi: 10.1093/jxb/erj020

Chi, C., Li, X., Fang, P., Xia, X., Shi, K., Zhou, Y., et al. (2020). Brassinosteroids act as a positive regulator of NBR1-dependent selective autophagy in response to chilling stress in tomato. *J. Exp. Bot.* 71, 1092–1106. doi: 10.1093/jxb/erz466

Chung, T., Phillips, A. R., and Vierstra, R. D. (2010). ATG8 lipidation and ATG8-mediated autophagy in Arabidopsis require ATG12 expressed from the differentially controlled ATG12A and ATG12B loci. *Plant J.* 62, 483–493. doi: 10.1111/j.1365-313X.2010.04166.x

Duchesne, A. N. (1766). Histoire naturelle des fraisiers contenant les vues d'économie réunies à la botanique, et suivie de remarques particulières sur plusieurs points qui ont rapport à l'histoire naturelle générale, par M. Duchesne fils. chez Didot le jeune. Available online at: https://books.google.es/books?id=vSbcsW4KFjcC (accessed March 25, 2021).

Edger, P. P., Poorten, T. J., Vanburen, R., Hardigan, M. A., Colle, M., Mckain, M. R., et al. (2019). Origin and evolution of the octoploid strawberry genome. *Nat. Genet.* 51, 541–547. doi: 10.1038/s41588-019-0356-4

Edger, P. P., VanBuren, R., Colle, M., Poorten, T. J., Wai, C. M., Niederhuth, C. E., et al. (2018). Single-molecule sequencing and optical mapping yields an improved genome of woodland strawberry (Fragaria vesca) with chromosome-scale contiguity. *Gigascience* 7, 1–7. doi: 10.1093/gigascience/gix124

Fait, A., Hanhineva, K., Beleggia, R., Dai, N., Rogachev, I., and Nikiforova, V. J. (2008). Reconfiguration of the achene and receptacle metabolic networks during strawberry fruit development. *Plant Physiol.* 148, 730–750. doi: 10.1104/pp.108.120691

Galli, V., Moura, J., Cristina, E., Messias, S., Labonde, J., Pereira, S., et al. (2015). Validation of reference genes for accurate normalization of gene expression for real time-quantitative PCR in strawberry fruits using different cultivars and osmotic stresses. *Gene* 554, 205–214. doi: 10.1016/j.gene.2014.10.049

Galluzzi, L., Baehrecke, E. H., Ballabio, A., Boya, P., Bravo-San Pedro, J. M., Cecconi, F., et al. (2017). Molecular definitions of autophagy and related processes. *EMBO J.* 36, 1811–1836. doi: 10.15252/embj.201796697

Gambino, G., Perrone, I., and Gribaudo, I. (2008). A rapid and effective method for RNA extraction from different tissues of grapevine and other woody plants. *Phytochem. Anal.* 19, 520–525. doi: 10.1002/pca.1078

Garapati, P., Feil, R., Lunn, J. E., Van Dijck, P., Balazadeh, S., and Mueller-Roeber, B. (2015). Transcription factor arabidopsis activating factor1 integrates carbon starvation responses with trehalosemetabolism. *Plant Physiol.* 169, 379–390. doi: 10.1104/pp.15.00917

Ghan, R., Petereit, J., Tillett, R. L., Schlauch, K. A., Toubiana, D., Fait, A., et al. (2017). The common transcriptional subnetworks of the grape berry skin in the late stages of ripening. *BMC Plant Biol.* 17, 1–21. doi: 10.1186/s12870-017-1043-1

Giovannoni, J. (2001). Molecular biology of fruit maturation and ripening. *Annu. Rev. Plant Physiol. Plant Mol. Biol.* 52, 725–749. doi: 10.1146/annurev.arplant.52.1.725

Havis, A. L. (1943). A developmental analysis of the strawberry fruit. *Am. J. Bot.* 30, 311–314. doi: 10.1002/j.1537-2197.1943.tb14763.x

Helliwell, C. A., and Waterhouse, P. M. (2005). Constructs and methods for hairpin RNA-mediated gene silencing in plants. *Meth. Enzymol.* 392, 24–35. doi: 10.1016/S0076-6879(04)92002-2

Ji, C., Zhou, J., Guo, R., Lin, Y., Kung, C. H., Hu, S., et al. (2020). AtNBR1 is a selective autophagic receptor for AtExo70E2 in arabidopsis. *Plant Physiol.* 184, 777–791. doi: 10.1104/pp.20.00470

Jing, S., and Malladi, A. (2020). Higher growth of the apple (Malus × domestica Borkh.) fruit cortex is supported by resource intensive metabolism during early development. *BMC Plant Biol.* 20, 1–19. doi: 10.1186/s12870-020-2280-2

Jung, H., Lee, H. N., Marshall, R. S., Lomax, A. W., Yoon, M. J., Kim, J., et al. (2020). Arabidopsis cargo receptor NBR1 mediates selective autophagy of defective proteins. *J. Exp. Bot.* 71, 73–89. doi: 10.1093/jxb/erz404

Katoh, K., Rozewicki, J., and Yamada, K. D. (2018). MAFFT online service: multiple sequence alignment, interactive sequence choice and visualization. *Brief. Bioinformatics* 20, 1160–1166. doi: 10.1093/bib/bbx108

Kellner, R., De la Concepcion, J. C., Maqbool, A., Kamoun, S., and Dagdas, Y. F. (2017). ATG8 expansion: a driver of selective autophagy diversification? *Trends Plant Sci.* 22, 204–214. doi: 10.1016/j.tplants.2016.11.015

Klionsky, D. J., Abdel-Aziz, A. K., Abdelfatah, S., Abdellatif, M., Abdoli, A., Abel, S., et al. (2021). Guidelines for the use and interpretation of assays for monitoring autophagy. *Autophagy* 8, 445–544. doi: 10.1080/15548627.2020.1797280

Kwon, S. I, Cho, H. J., Jung, J. H., Yoshimoto, K., Shirasu, K., and Park, O. K. (2010). The Rab GTPase RabG3b functions in autophagy and contributes to tracheary element differentiation in Arabidopsis. *Plant J.* 2, 151–164. doi: 10.1111/j.1365-313X.2010.04315.x

Lalk, G. T., Bi, G., Zhang, Q., Harkess, R. L., and Li, T. (2020). High-tunnel production of strawberries using black and red plastic mulches. *Horticulturae* 6, 1–16. doi: 10.3390/horticulturae6040073

Li, F., and Vierstra, R. D. (2012). Autophagy : a multifaceted intracellular system for bulk and selective recycling. *Trends Plant Sci.* 17, 526–537. doi: 10.1016/j.tplants.2012.05.006

Liu, T., Li, M., and Liu, Z. (2021). Reannotation of the cultivated strawberry genome and establishment of a strawberry genome database. *Hortic. Res.* 8, 1–9. doi: 10.1038/s41438-021-00476-4

Liu, Z., Ma, H., Jung, S., Main, D., and Guo, L. (2020). Developmental mechanisms of fleshy fruit diversity in Rosaceae. *Annu. Rev. Plant Biol.* 71, 547–573. doi: 10.1146/annurev-arplant-111119-021700

López-Vidal, O., Olmedilla, A., Sandalio, L. M., Sevilla, F., and Jiménez, A. (2020). Is autophagy involved in pepper fruit ripening? *Cells* 9:106. doi: 10.3390/cells9010106

Marshall, R. S., and Vierstra, R. D. (2018). Autophagy : the master of bulk and selective recycling. *Annu. Rev. Plant Biol.* 69, 173–208. doi: 10.1146/annurev-arplant-042817-040606

Martens, S., and Fracchiolla, D. (2020). Activation and targeting of ATG8 protein lipidation. *Cell Discov.* 6, 1–11. doi: 10.1038/s41421-020-0155-1

Martín-Pizarro, C., Vallarino, J. G., Osorio, S., Meco, V., Urrutia, M., Pillet, J., et al. (2021). The NAC transcription factor FaRIF controls fruit ripening in strawberry. *Plant Cell* 33, 1574–1593. doi: 10.1093/plcell/koab070

McLoughlin, F., Marshall, R. S., Ding, X., Chatt, E. C., Kirkpatrick, L. D., Augustine, R. C., et al. (2020). Autophagy plays prominent roles in amino acid, nucleotide, and carbohydrate metabolism during fixed-carbon starvation in maize. *Plant Cell* 32, 2699–2724. doi: 10.1105/tpc.20.00226

Meijer, W. H., van der Klei, I. J., Veenhuis, M., and Kiel, J. A. K. W. (2007). ATG genes involved in non-selective autophagy are conserved from yeast to man, but the selective Cvt and pexophagy pathways also require organism-specific genes. *Autophagy* 3, 106–116. doi: 10.4161/auto.3595

Michaeli, S., Galili, G., Genschik, P., Fernie, A. R., and Avin-wittenberg, T. (2016). Autophagy in plants – what' s new on the menu? *Trends Plant Sci.* 21, 134–144. doi: 10.1016/j.tplants.2015.10.008

Minina, E. A., Filonova, L. H., Fukada, K., Savenkov, E. I., Gogvadze, V., Clapham, D., et al. (2013). Autophagy and metacaspase determine the mode of cell death in plants. *J. Cell Biol.* 203, 917–927. doi: 10.1083/jcb.201307082

Noda, N. N., Ohsumi, Y., and Inagaki, F. (2010). Atg8-family interacting motif crucial for selective autophagy. *FEBS Lett.* 584, 1379–1385. doi: 10.1016/j.febslet.2010.01.018

Osorio, S., Scossa, F., and Fernie, A. R. (2013). Molecular regulation of fruit ripening. *Front. Plant Sci.* 4, 1–8. doi: 10.3389/fpls.2013.00198

Pérez-Pérez, M. E., Florencio, F. J., and Crespo, J. (2010). Inhibition of target of rapamycin signaling and stress activate autophagy in *Chlamydomonas reinhardtii*. Plant Physiol. 152, 1874–1888. doi: 10.1104/pp.109.152520

Phillips, A. R., Suttangkakul, A., and Vierstra, R. D. (2008). The ATG12-conjugating enzyme ATG10 is essential for autophagic vesicle formation in *Arabidopsis thaliana*. *Genetics* 1353, 1339–1353. doi: 10.1534/genetics.107.086199

Pott, D. M., Vallarino, J. G., and Osorio, S. (2020). Metabolite changes during postharvest storage: effects on fruit quality traits. *Metabolites* 10, 1–24. doi: 10.3390/metabo10050187

Rabinowitz, J. D., and White, E. (2010). Autophagy and metabolism. *Science* 330, 1344–1348. doi: 10.1126/science.1193497

Sánchez-Sevilla, J. F., Vallarino, J. G., Osorio, S., Bombarely, A., Merchante, C., Botella, M. A., et al. (2017). Gene expression atlas of fruit ripening and transcriptome assembly from RNA-seq data in octoploid strawberry (Fragaria × ananassa). *Sci. Rep.* 7, 1–13. doi: 10.1038/s41598-017-14239-6

Sanchez-Vera, V., Kenchappa, C. S., Landberg, K., Bressendorff, S., Schwarzbach, S., Martin, T., et al. (2017). Autophagy is required for gamete differentiation in the moss Physcomitrella patens. *Autophagy* 13, 1939–1951. doi: 10.1080/15548627.2017.1366406

Seo, E., Woo, J., Park, E., Bertolani, S. J., Siegel, J. B., Choi, D., et al. (2016). Comparative analyses of ubiquitin-like ATG8 and cysteine protease ATG4 autophagy genes in the plant lineage and cross-kingdom processing of ATG8 by ATG4. *Autophagy* 12, 2054–2068. doi: 10.1080/15548627.2016.1217373

Soto-Burgos, J., and Bassham, D. C. (2017). SnRK1 activates autophagy via the TOR signaling pathway in Arabidopsis thaliana. *PLoS ONE* 12:e0182591. doi: 10.1371/journal.pone.0182591

Stecher, G., Tamura, K., and Kumar, S. (2020). Molecular evolutionary genetics analysis (MEGA) for macOS. *Mol. Biol. Evol.* 37, 1237–1239. doi: 10.1093/molbev/msz312

Su, T., Li, X., Yang, M., Shao, Q., Zhao, Y., and Ma, C. (2020). Autophagy : an intracellular degradation pathway regulating plant survival and stress response. *Front. Plant Sci.* 11, 1–16. doi: 10.3389/fpls.2020.00164

Svenning, S., Lamark, T., Krause, K., and Johansen, T. (2011). Plant NBR1 is a selective autophagy substrate and a functional hybrid of the mammalian autophagic adapters NBR1 and p62 / SQSTM1. *Autophagy* 7, 993–1010. doi: 10.4161/auto.7.9.16389

Takatsuka, C., Inoue, Y., Matsuoka, K., and Moriyasu, Y. (2004). 3-Methyladenine inhibits autophagy in tobacco culture cells under sucrose starvation conditions. *Plant Cell Physiol.* 45, 265–274. doi: 10.1093/pcp/pch031

Tang, J., and Bassham, D. C. (2018). Autophagy in crop plants: what's new beyond Arabidopsis? *Open Biol.* 8, 1–13. doi: 10.1098/rsob.180162

Thomas, H. (2013). Senescence, ageing and death of the whole plant. *New Phytol.* 197, 696–711. doi: 10.1111/nph.12047

Trapnell, C., Roberts, A., Goff, L., Pertea, G., Kim, D., Kelley, D. R., et al. (2012). Differential gene and transcript expression analysis of RNA-seq experiments with TopHat and Cufflinks. *Nat. Protoc.* 7, 562–578. doi: 10.1038/nprot.2012.016

Tsukada, M., and Ohsumi, Y. (1993). Isolation and characterization of autophagy-defective mutants of Saccharomyces cerevisiae. *FEBS* 333, 169–174. doi: 10.1016/0014-5793(93)80398-E

Untergasser, A., Cutcutache, I., Koressaar, T., Ye, J., Faircloth, B. C., Remm, M., et al. (2012). Primer3-new capabilities and interfaces. *Nucleic Acids Res.* 40, 1–12. doi: 10.1093/nar/gks596

Wang, H., and Schippers, J. H. M. (2019). The role and regulation of autophagy and the proteasome during aging and senescence in plants. *Genes (Basel).* 10:40267. doi: 10.3390/genes10040267

Wen, X., and Klionsky, D. J. (2016). An overview of macroautophagy in yeast. *J. Mol. Biol.* 428, 1681–1699. doi: 10.1016/j.jmb.2016.02.021

Wojciechowska, N., Smugarzewska, I., Marzec-Schmidt, K., Zarzyńska-Nowak, A., and Bagniewska-Zadworna, A. (2019). Occurrence of autophagy during pioneer root and stem development in Populus trichocarpa. *Planta* 250, 1789–1801. doi: 10.1007/s00425-019-03265-5

Woo, J., Park, E., and Dinesh-Kumar, S. P. (2014). Differential processing of Arabidopsis ubiquitin-like Atg8 autophagy proteins by Atg4 cysteine proteases. *Proc. Natl. Acad. Sci. U. S. A.* 111, 863–868. doi: 10.1073/pnas.1318207111

Yoshimoto, K., Hanaoka, H., Sato, S., Kato, T., Tabata, S., and Noda, T. (2004). Processing of ATG8s, ubiquitin-like proteins, and their deconjugation by ATG4s are essential for plant autophagy. *Plant Cell* 16, 2967–2983. doi: 10.1105/tpc.104.025395

Zhou, J., Wang, J., Cheng, Y., Chi, Y., Fan, B., Yu, J., et al. (2013). NBR1-mediated selective autophagy targets insoluble ubiquitinated protein aggregates in plant stress responses. *PLoS Genet.* 9:e1003196. doi: 10.1371/journal.pgen.1003196

Zhuang, X., Chung, K. P., Luo, M., and Jiang, L. (2018). Autophagosome biogenesis and the endoplasmic reticulum: a plant perspective. *Trends Plant Sci.* 23, 677–692. doi: 10.1016/j.tplants.2018.05.002

Conflict of Interest: The authors declare that the research was conducted in the absence of any commercial or financial relationships that could be construed as a potential conflict of interest.

Publisher's Note: All claims expressed in this article are solely those of the authors and do not necessarily represent those of their affiliated organizations, or those of the publisher, the editors and the reviewers. Any product that may be evaluated in this article, or claim that may be made by its manufacturer, is not guaranteed or endorsed by the publisher.

frontiers in Plant Science

REVIEW
published: 05 January 2022
doi: 10.3389/fpls.2021.644424

The Roles of Floral Organ Genes in Regulating Rosaceae Fruit Development

*Jia-Long Yao[1], Chunying Kang[2], Chao Gu[3] and Andrew Peter Gleave[1]**

[1]The New Zealand Institute for Plant and Food Research Limited, Auckland, New Zealand, [2]College of Horticulture and Forestry, Huazhong Agricultural University, Wuhan, China, [3]State Key Laboratory of Crop Genetics and Germplasm Enhancement, Nanjing Agricultural University, Nanjing, China

The function of floral organ identity genes, *APETALA1/2/3*, *PISTILLATA, AGAMOUS*, and *SEPALLATA1/2/3*, in flower development is highly conserved across angiosperms. Emerging evidence shows that these genes also play important roles in the development of the fruit that originates from floral organs following pollination and fertilization. However, their roles in fruit development may vary significantly between species depending on the floral organ types contributing to the fruit tissues. Fruits of the Rosaceae family develop from different floral organ types depending on the species, for example, peach fruit flesh develops from carpellary tissues, whereas apple and strawberry fruit flesh develop from extra-carpellary tissues, the hypanthium and receptacle, respectively. In this review, we summarize recent advances in understanding floral organ gene function in Rosaceae fruit development and analyze the similarities and diversities within this family as well as between Rosaceae and the model plant species Arabidopsis and tomato. We conclude by suggesting future research opportunities using genomics resources to rapidly dissect gene function in this family of perennial plants.

Keywords: AP2, MADS-box, miR172, fruit development, apple, peach, strawberry

OPEN ACCESS

Edited by:
Barbara Ambrose, New York Botanical Garden, United States

Reviewed by:
Vicente Balanzà, Polytechnic University of Valencia, Spain
Stefan de Folter, Center for Research and Advanced Studies (CINVESTAV), Mexico

****Correspondence:***
Andrew Peter Gleave
andrew.gleave@plantandfood.co.nz

Specialty section:
This article was submitted to Plant Development and EvoDevo, a section of the journal Frontiers in Plant Science

Received: *21 December 2020*
Accepted: *22 November 2021*
Published: *05 January 2022*

Citation:
Yao J-L, Kang C, Gu C and Gleave AP (2022) The Roles of Floral Organ Genes in Regulating Rosaceae Fruit Development. Front. Plant Sci. 12:644424. doi: 10.3389/fpls.2021.644424

INTRODUCTION

Floral organs are classified into four types, sepals, petals, stamens, and carpels. Their development is regulated by four different classes of floral organ identity genes according to the proposed ABCE model (Coen and Meyerowitz, 1991; Weigel and Meyerowitz, 1994; Krizek and Fletcher, 2005). In summary, for *Arabidopsis* sepal formation is specified by the class A genes *APETALA1* (*AP1*) and *AP2*, petal formation is specified by the class A genes and two class B genes [*APETALA3* (*AP3*) and *PISTILLATA* (*PI*)]; stamen formation requires *AP3* and *PI* together with the class C gene *AGAMOUS* (*AG*); and carpel formation is controlled by the *AG* alone (Weigel and Meyerowitz, 1994). Proper development of all four whorls of floral organs also requires the class E *SEPALLATA* (*SEP*) genes. The consequence of mutating all four *SEPALLATA* genes (*sep1, sep2, sep3, and sep4*) simultaneously is a plant that produces flowers consisting of reiterating whorls of leaf-like organs (Krizek and Fletcher, 2005). All class A, B, C, and E genes encode MADS-box transcription factors, except for *AP2*, which encodes a transcription factor belonging to the super-family of AP2/ERF proteins (Okamuro et al., 1997). However, classification of a gene as being a member of the ABCE model is based on its function

and not sequence similarity to other members of the ABCE model.

The diversity of fruit types seen between various flowering plant species is primarily a consequence of different carpellary and/or extra-carpellary floral tissues contributing to fruit formation (Spjut, 1994). Botanical fruit, also known as true fruit, is derived from carpellary tissues, whereas accessory fruit, also known as pseudo fruit, has fruit flesh derived from extra-carpellary tissues (Liu et al., 2020). With fruit being derived from floral organs, the genes that regulate the growth of floral organs also play important roles in the control of fruit development. This was clearly demonstrated by the functions of the Arabidopsis *FRUITFULL* (*FUL*), an *AP1* homolog (Gu et al., 1998), tomato *TM29*, a *SEPALLATA* homolog (Ampomah-Dwamena et al., 2002), and poppy *AP1/FUL* homologs (Pabón-Mora et al., 2012).

Rosaceae species produce flowers with five sepals and petals, and a varied number of stamens and carpels. Their carpels show variations in shape, degrees of fusion, and relative position to other floral organs. These variations are the key contributing factors of fruit type diversity in Rosaceae (Liu et al., 2020). For example, peach develops a superior ovary as the single carpel is positioned above all other floral organs and goes on to develop a drupe. In contrast, apple has five fused carpels that are below the attachment point of all other floral organs, develops an inferior ovary that fuses with the surrounding hypanthium tissues formed from the bases of sepals, petals, and stamens and develops a pome (Liu et al., 2020).

In addition to floral structure variations, differential enlargement of specific floral tissues also contributes to fruit type diversity in Rosaceae. Strawberry and raspberry, for example, have a similar floral structure that consists of numerous carpels growing on a receptacle. Strawberry is an achenetum because its carpels are not enlarged after fertilization and become dry achenes, but the receptacle is enlarged and grows into the fleshy pseudo fruit. In contrast, raspberry is a drupetum because its carpels are enlarged after fertilization to form fleshy drupelets but the receptacle is not enlarged or fleshy (Liu et al., 2020).

Together with flower and fruit morphological differences, duplicated floral organ genes have the opportunity to play diversified roles in fruit development. In Rosaceae, whole-genome duplication (WGD) events have resulted in gene copies and their potential to have dosage effects, redundancy of function, or for copies to have undergone functional changes, such as neo-functionalization (one gene copy taking on a totally new function) or sub-functionalization (each gene copy retaining a subset of the original ancestral functions; Conant et al., 2014; Xiang et al., 2017). In the following sections, we summarize recent advances in understanding floral organ gene duplication, expression profiles, and function in relation to Rosaceae fruit development. We also analyze the similarities and diversities within this family predominantly using apple, peach, and strawberry as examples representing the diversity of fruit types in the family. The similarities and diversities between Rosaceae and other plants, in particular Arabidopsis and tomato, are also analyzed.

GENE DUPLICATION AND FRUIT EXPRESSION PATTERN DIVERSITY OF FLORAL ORGAN GENES INDICATE THEIR DIVERSIFIED FUNCTIONS IN REGULATING FRUIT DEVELOPMENT

Prior to the assembly of reference genome sequences, sequence-based approaches using homology to the *Arabidopsis* genes were used to clone and identify floral organ MADS-box genes from Rosaceae species. In apple, several studies identified a total of two *AP1*-related genes, *MdMADS5* (*MdAP1*; Yao et al., 1999; Kotoda et al., 2002) and *MdMADS2* (Sung et al., 1999), one *PI* homolog, *MdPI* (Yao et al., 2001), two *AP3* homologs, *MdMADS13* (Van Der Linden et al., 2002) and *MdTM6* (Kitahara et al., 2004), three *AG*-related genes, *MdMADS10* (Yao et al., 1999), *MdMADS14*, and *MdMADS15* (Van Der Linden et al., 2002), and five *SEP*-related genes, *MdMADS4* (Sung et al., 2000), *MdMADS6*, *7*, *8*, and *9* (Yao et al., 1999). After the first apple reference genome was assembled (Velasco et al., 2010), three additional *SEP*-related genes were identified, *MdMADS18*, *104*, and *118* (Ireland et al., 2013). All these genes, except for *MdPI*, have been annotated in the second apple reference genome generated using a haploid plant derived from the cultivar "Golden Delicious" (Daccord et al., 2017).

In this review, floral MADS-box genes are identified from the reference genome of peach (Verde et al., 2013), strawberry (Edger et al., 2017), and apple (Daccord et al., 2017). Their gene IDs are listed in **Table 1** together with their class, based on gene lineage, and the relevant references. Their relationship is shown in a protein sequence-based phenology tree in **Figure 1A**. One or more genes from peach, strawberry, and apple are identified as homologs of each of the Arabidopsis floral MADS-box genes. In apple, 12 floral MADS-box genes are present as homolog pairs, most likely due to a recent apple-specific whole-genome duplication (Velasco et al., 2010).

Expression patterns of *SEP-like* genes in apple fruit have been described previously, such as the *AtSEP1/2*-like *MADS1/MADS8*, and *MADS9* showing high expression at two to seven days after pollination, the *PhFBP9/23*-like *MADS3/MADS7* and *MADS6* showing high expression at four to eight weeks after pollination, and the *AtSEP4*-like *MADS4* showing strong expression in young fruits (Sung and An, 1997; Yao et al., 1999; Sung et al., 2000). In addition, Yao et al. (1999) demonstrated the expression of class *AP1*- and *AG*-related genes in the fruit flesh of apple. Detection of their expression in fruit indicates that *AP1*-, *AG*-, and *SEP*-related *MADS*-box genes have a potential role in apple fruit development.

Transcriptome analyses of whole fruit tissues without seeds collected from five developmental stages revealed that two *FUL* homologs (*PpMADS6* and XM_007209438), an *AG* homolog (*PpAG*), and three *SEP* homologs (*PpMADS2, PpSEP1*, and *PpSEP3*) are expressed in peach fruit. The same analyses showed that an *AG* homolog (*FveAG*), a *SHP* homolog (FvH6g37880), and three *SEP* homologs (*FveSEP1/3/4*) are expressed in strawberry (*Fragaria* x *ananassa*) fruit (Pei et al., 2020; **Figure 1B**). In addition, two *AP3*-related genes (XM007202440

TABLE 1 | Floral MADS-box and AP2 genes in peach, strawberry, and apple.

Species	Gene ID	Class	Gene name	References
		Floral MADS-box		
Peach	Pp_XM_020564301.1	FUL	*PpMADS6*	Xu et al., 2014
	Pp_XM_007209438.2	FUL		
	Pp_XM_020559852.1	AP1		
	Pp_XM_007223759.2	AP1	*PpAP1*	Zhang et al., 2008
	Pp_XM_007202441.2	AP3		
	Pp_XM_007202440.2	AP3		
	Pp_XM_020560155.1	AP3	*PpMADS11*	
	Pp_XM_020561783.1	AG	*PpAG*	Tani et al., 2009
	Pp_XM_020560664.1	STK	*PpAGL11*	
	Pp_XM_020559281.1	SHP	*PpSHP*	
	Pp_XM_007211863.2	AG	*PpAG*	
	Pp__007220032.2	SEP		
	Pp_XM_007209443.2	SEP	*PpMADS2*	Xu et al., 2008
	Pp_XM_007215814.2	SEP	*PpSEP1*	
	Pp_XM_007221786.2	SEP		
	Pp_XM_007223746.2	SEP	*PpSEP3*	Xu et al., 2008
	Pp_XM_020557124.1	SEP	*PpAGL6*	
Strawberry	FvH4_4g29600	AP1	*FveAP1*	Hollender et al., 2014
	FvH4_1g12260	AP3	*FveAP3*	
	FvH4_2g27860	PI	*FvePIa*	
	FvH4_2g27870	PI	*FvePIb*	
	FvH4_3g06720	AG	*FveAG*	
	FvH4_5g13500	FUL		
	FvH4_5g32540	STK		
	FvH4_6g37880	SHP		
	FvH4_4g23530	SEP	*FveSEP3*	Hollender et al., 2014
	FvH4_4g29610	SEP	*FveSEP-LIKE1*	
	FvH4_5g13510	SEP	*FveSEP4*	
	FvH4_6g46420	SEP	*FveSEP1*	
Apple	MD06G1204400	FUL		
	MD13G1059200	AP1	*MdAP1-like*	Van Der Linden et al., 2002
	MD14G1215700	FUL		
	MD17G1065500	AP1		
	MD09G1074100	AP1		
	MD16G1058500	AP1	*MdMADS5*	Yao et al., 1999; Kotoda et al., 2002
	MD02G1136500	AP3	*MdMADS13*	Van Der Linden et al., 2002
	MD15G1250200	AP3	*MdTM6*	Kitahara et al., 2004
	MD08G1021300	AP3		
	MDP0000286643	PI	*MdPI*	Yao et al., 2001, 2018
	MD05G1293700	AG	*MdAMDS22*	Klocko et al., 2016
	MD08G1216500	STK	*MdMADS10*	Yao et al., 1999
	MD09G1155200	SHP	*MdMADS14*	Van Der Linden et al., 2002
	MD10G1271000	AG	*MdMADS15*	Klocko et al., 2016
	MD15G1403600	STK		
	MD01G1192400	SEP		
	MD06G1204100	SEP		
	MD06G1204300	SEP	*MdMADS6*	Yao et al., 1999; Ireland et al., 2013
	MD09G1073900	SEP		
	MD13G1059300	SEP	*MdMADS4*	Sung et al., 2000
	MD13G1121500	SEP	*MdMADS18*	Ireland et al., 2013
	MD14G1215600	SEP	*MdMADS7*	Yao et al., 1999; Ireland et al., 2013
	MD16G1058600	SEP		
	MD17G1065400	SEP	*MdMADS8*	Yao et al., 1999; Ireland et al., 2013
	MD02G1197600	SEP		

(Continued)

TABLE 1 | Continued

Species	Gene ID	Class	Gene name	References
		Floral AP2		
Peach	XM_007205081.2	AP2	*PpTOE1a*	Gattolin et al., 2018
	XM_007220804.2	AP2	*PpTOE2*	
	XM_007207942.2	AP2	*PpAP2*	
	XM_020566630.1	AP2		
	XM_020565001.1	AP2	*PpTOE1b*	
Strawberry	FvH4_1g16350	AP2		Hollender et al., 2014
	FvH4_7g20380	AP2		
	FvH4_3g33940	AP2		
	FvH4_6g15180	AP2		
Apple	MD01G1113400	AP2		Yao et al., 2015
	MD02G117600	AP2		
	MD03G1107900	AP2		
	MD04G1105200	AP2		
	MD07G1180900	AP2		
	MD11G1121200	AP2		
	MD12G1125900	AP2		
	MD15G1286400	AP2		

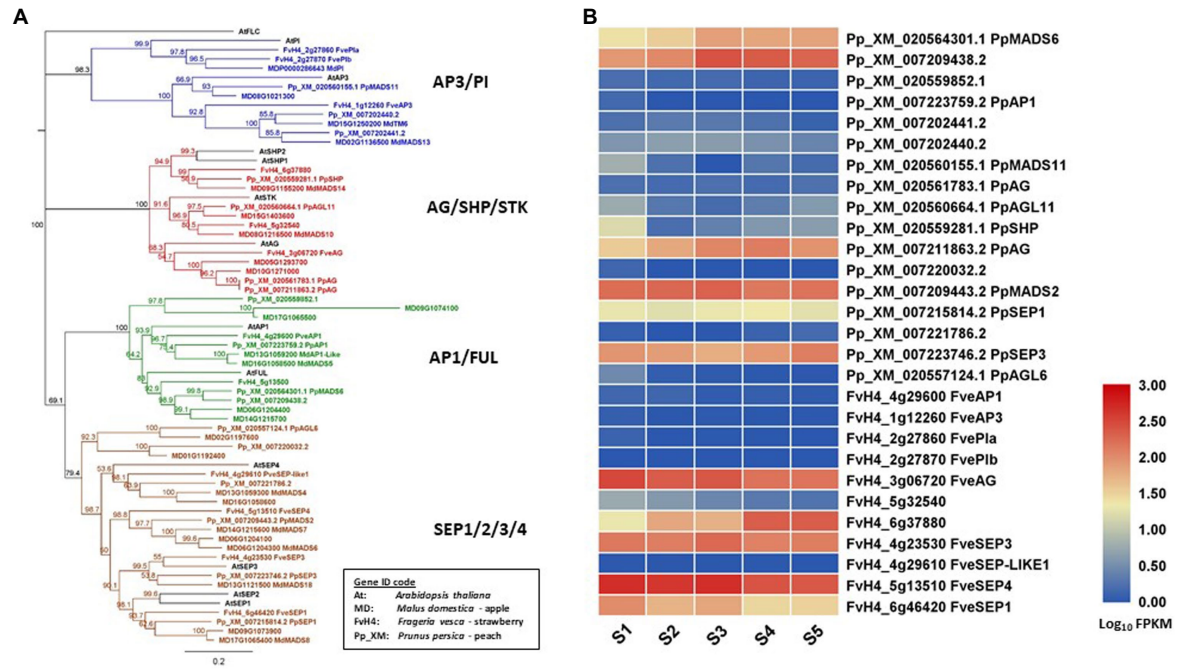

FIGURE 1 | Phylogeny tree of floral MADS-box proteins and their gene expression in developing fruit tissues. **(A)** a Neighbor-Joining consensus tree was constructed using Geneious software (v10.0.9) with 1,000 bootstrap replicates after protein sequences were aligned using Geneious Alignment software (v10.0.9). MADS-box protein sequences downloaded from the reference genome of apple (Daccord et al., 2017), peach (Verde et al., 2013), strawberry (Edger et al., 2017), and Arabidopsis. The Arabidopsis protein IDs are AT1G69120.1 (AtAP1), AT5G60910.1 (AtFUL), AT5G20240.1(AtPI), AT3G54340.1 (AtAP3), AT4G18960.1 (AtAG), AT3G58780.1 (AtSHP1), AT2G42830.1 (AtSHP2), AT4G09960.1 (AtSTK), AT5G15800.1 (AtSEP1), AT3G02310.1 (AtSEP2), AT1G24260.1 (AtSEP3), AT2G03710.1 (AtSEP4), and AT5G10140.1 (AtFLC). **(B)** a heatmap shows the expression patterns of floral MADS-box genes in fruit tissues of peach and strawberry at five developmental stages (S1-S5) based on previously published RNA-seq data (Pei et al., 2020). Rosaceae Gene IDs are coded as: MD for apple (*Malus domestica*), Pp_XM for peach (based on Prunus_persica_NCBIv2) and FvH4 for strawberry (based on *Fragaria vesca* H4). S1 to S5: 21, 42, 56, 84, and 105 days after full bloom for peach, and 11, 27, 31, 43, and 47 DAFB for strawberry.

and *PpMADS11*) are also expressed in peach fruit during development although their expression levels are relatively low (**Figure 1B**). The expression of *AP3*-related genes in peach fruit is interesting because this expression is not detected in apple or strawberry fruit. In contrast, expression of *AP1/FUL* homologs is at a high level in apple and peach but not detected

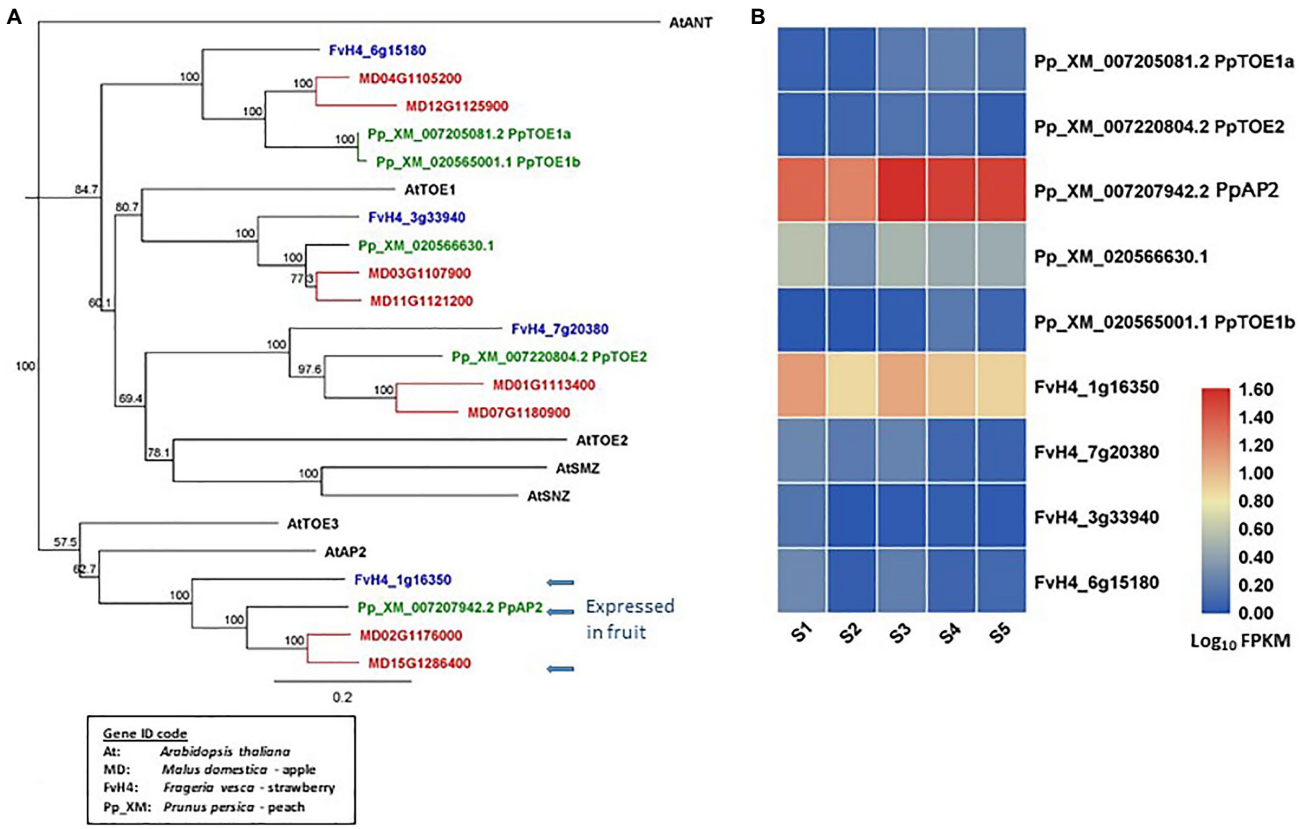

FIGURE 2 | Phylogeny tree of AP2-like proteins and their gene expression in developing fruit tissues. **(A)** a Neighbor-Joining consensus tree was constructed using Geneious software (v10.0.9) with 1,000 bootstrap replicates after protein sequences were aligned using Geneious Alignment software (v10.0.9). AP2-like protein sequences downloaded from the reference genome of apple, peach, strawberry, and Arabidopsis. The Arabidopsis protein IDs are AT4G36920.1 (AtAP2), AT2G28550.3 (AtTOE1), AT5G60120.2 (AtTOE1), AT5G67180.1 (AtTOE3), AT3G54990.1 (AtSMZ), AT2G39250.1 (AtSNZ), and AT4G37750.1 (AtANT). **(B)** a heatmap shows the expression patterns of *AP2-like* genes in fruit tissues of peach and strawberry at five developmental stages (S1-S5) based on previously published RNA-seq data (Pei et al., 2020). Rosaceae Gene IDs are coded as: MDs for apple (*Malus domestica*), Pp_XM for peach (based on Prunus_persica_NCBIv2), and FvH4 for strawberry (based on *Fragaria vesca* H4). S1 to S5: 21, 42, 56, 84, and 105 days after full bloom for peach, and 11, 27, 31, 43, and 47 DAFB for strawberry. The arrows indicate *AP2* genes predominantly expressed in fruits.

in strawberry. It would be worthwhile determining the functions of the*AP1/FUL* and *AP3/PI* homologs in regulating fruit development of Rosaceae.

AP2 homologous genes have been identified from the reference genomes of apple (Daccord et al., 2017), peach (Verde et al., 2013), and strawberry (Edger et al., 2017; **Figure 2A**). In apple, there are eight *euAP2* (Kim et al., 2006) homologs that contain a miR172 target site in the coding sequences and encode proteins containing two AP2 domains (Yao et al., 2015). In peach and strawberry, five and four such AP2 homologs have been identified, respectively. The AP2 homologs of these species are classified into four distinct clades. Each clade contains two apple and one strawberry homolog. One clade contains two peach homologs and of other three clades each contains one peach homolog (**Figure 2A**). The specific duplication of AP2 homologs in apple provides new potential of dosage effect or functional changes. Among the eu*AP2* homologs, one in each species (MD15G1286400, FvH_1g16350, and Pp_XM_007207942) is expressed predominantly in the developing fruit tissues (Yao et al., 2015; Pei et al., 2020; **Figures 2A,B**). These three homologs are in the same clade as Arabidopsis AP2 (AtAP2) in the phylogenetic tree (**Figure 2A**). Further insights into the roles of these floral MADS-box and eu*AP2-like* genes in fruit development may be obtained by analyzing their expression patterns using transcriptome data sets generated in Rosaceae species (Kang et al., 2013; Hawkins et al., 2017; Hu et al., 2018; Pei et al., 2019; Shahan et al., 2019; Tan et al., 2019; Ying et al., 2019; Shang et al., 2020).

From the above analyses of gene sequences and expression patterns, it is clear that these three species in the Rosaceae family contain similar genes in the floral MADS-box and AP2 clades, but the gene number varies among the three species (**Figure 2A**). Expression of these genes generally shows a degree of similarity across the three species described, although specific temporal and spatial expression patterns are present (**Figure 2B**; Kang et al., 2013; Hawkins et al., 2017; Hu et al., 2018; Pei et al., 2019; Shahan et al., 2019; Tan et al., 2019; Ying et al., 2019; Shang et al., 2020). Evidence to date would indicate that there are conserved and diversified functions for these

genes in different species, although the research to understanding these functions is very much in its infancy.

MIR172 AND AP2 HAVE DIVERSIFIED ROLES IN REGULATING FRUIT DEVELOPMENT

In plants, microRNA172 (miR172) is highly conserved and targets a subfamily of *AP2-like* genes to repress their expression, by initiating degradation and/or inhibiting translation of the target mRNA (Aukerman and Sakai, 2003; Chen, 2004; Zhu et al., 2009; Zhu and Helliwell, 2011). As members of the euAP2 subfamily have different spatial and temporal patterns of expression (Okamuro et al., 1997; Tang et al., 2007; Yao et al., 2015) and interact with different proteins (Teotia and Tang, 2015), the *MIR172* gene family has the potential to affect a number of aspects of plant development.

In annual plant species, early flowering is a phenotypic change commonly observed for over-expression of miR172 (Aukerman and Sakai, 2003; Chen, 2004; Mlotshwa et al., 2006; Zhu and Helliwell, 2011; Teotia and Tang, 2015), and in some instances abnormalities of the floral organs have been observed (Mlotshwa et al., 2006; Zhu et al., 2009). As AP2 governs floral organ size (Jofuku et al., 2005) and floral organ development (Yant et al., 2010), then miR172 has the potential to influence growth of fruit.

In *Arabidopsis*, miR172 positively regulates *Arabidopsis* silique growth (Ripoll et al., 2015). The silique is derived from carpel tissues and its growth is negatively regulated by AP2 (Ripoll et al., 2011). The expression of AP2 is repressed in the silique valve by miR172 (Ripoll et al., 2015). Therefore, suppression of the function of miR172, through the use of microRNA mimicry technology, results in a reduction in silique size. Similarly, a reduction in the size of the silique occurs in transgenic plants expressing a modified *AP2* gene without a functional miR172-target sequence (Ripoll et al., 2015).

Apple fruit flesh, is derived largely from the hypanthium, hypothesized to consist of the fused bases of the stamens, petals, and sepals (Pratt, 1988) and fruit core is derived from the carpellary tissues. Further molecular studies have indicated that sepal bases make the greatest contribution to apple flesh formation (Yao et al., 2001). Negative regulation of apple fruit growth by miR172 was demonstrated in transgenic plants over-expressing miR172 and also observed in natural variants of apple. Over-expression of miR172 in apple converted segments of sepals to petal-like tissues, indicating that AP2-like transcription factors are required for sepal development and furthermore the miR172 over-expression reduced fruit weight more than 60-fold (**Figure 3**; Yao et al., 2015). A transposable element (TE) insertional allele of the apple *MIR172p* gene is associated with reduction of *MIR172* expression and co-located with one of four fruit size QTLs (Yao et al., 2015). In the progeny of a controlled cross, the TE insertional allele is associated with large fruit and underlies the evolution of fruit size from the small wild crabapples to large cultivated apples. Although the correlation between fruit size and the level of AP2 expression during fruit development could be interpreted as a direct effect of AP2 on fruit growth, one cannot discount that this is an indirect effect because AP2 represses the function of class C genes (e.g., *AG*) in the first whorl, according to the ABCE model (Wollmann et al., 2010). Therefore, miRNA-mediated reduction of AP2, resulting in elevated expression of class C genes in the first whorl during flower development, could lead to a conversion of sepals to carpel-like structures. As sepals contribute to the apple fruit flesh we postulate that

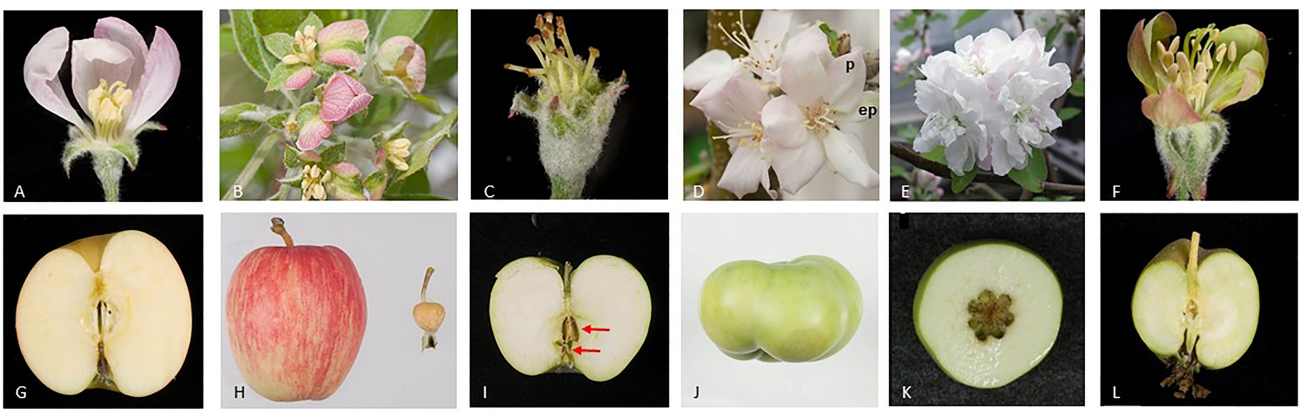

FIGURE 3 | Apple flower and fruit phenotypes after alteration of the expression of floral organ genes. The images show open flowers **(A–F)** and mature fruit **(G–L)** of wild-type **(A,G)** and transgenic apple plants **(B–F, H–L)**. miR172 is known to inhibit the expression of the *AP2*- and *AP2-like* genes. miR172 over-expression converts sepal segments to petal-like tissues **(B)** outer petals are removed to show sepal-petal conversion and dramatically reduces fruit size **(H)**, wild-type fruit on left and transgenic fruit on right (Yao et al., 2015). Repressing expression of the *MdPI* gene converts petals to sepals, and stamens to carpels **(C)**, and results in parthenocarpic (seedless) fruit with two whorls of carpels marked using two red arrows **(I)**. However, over-expressing *MdPI* converts sepals to petals (p, petal; ep, ectopic petal) **(D)** and suppresses fruit tissue growth resulting in altered fruit shape **(J)** (Yao et al., 2001, 2018). Repressing expression of two *AG* homologs, *MdMADS15/22*, converts stamens to petals **(E)** and increases carpel number and therefore fruit locule number **(K)** (Klocko et al., 2016). Repressing expression of two *SEP* homologs, *MdMADS8/9*, partially converts petals to greenish sepal-like organs **(F)** and suppresses fruit flesh growth **(L)** (Ireland et al., 2013).

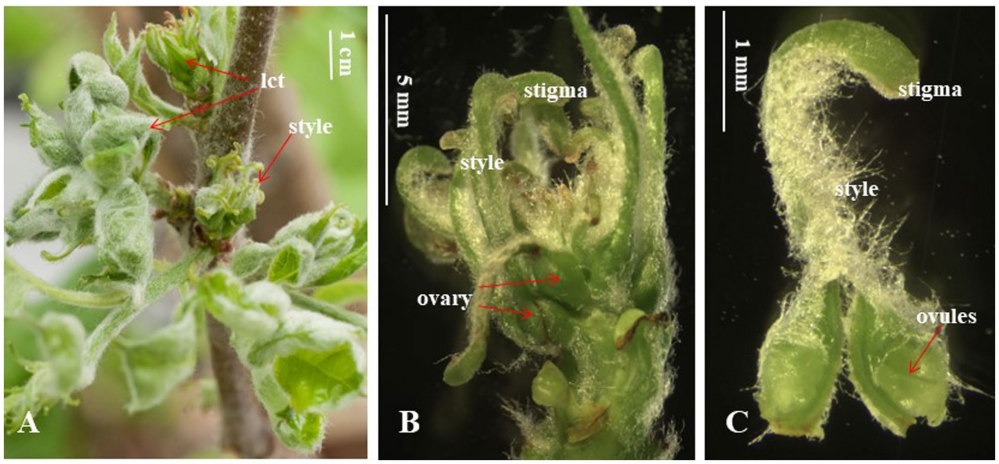

FIGURE 4 | Flowers of apple transgenic plants over-expressing miR172. **(A)** Floral inflorescences show abnormal flowers consisting of leaf-like carpel tissues (lct), style, and stigma, but no sepals, petals, or stamens. **(B)** A florescence of **(A)** with leaf-like carpels removed reveals separate carpels consisting of ovary, style, and stigma. **(C)** A single carpel removed from the inflorescence in **(B)** reveals two ovules after cutting the ovary open (This figure is re-produced from Yao et al., 2015).

this conversion of floral organs could account for the reduction in fruit size. However, a sepal to carpel conversion in apple over-expressing miR172 was not reported (Yao et al., 2015).

In tomato, over-expression of miR172 produced flowers consisting entirely of ovary tissues that develop into parthenocarpic fruit, with a fruit-in-fruit phenotype observed in some extreme cases (Yao et al., 2016). As in apple, the size of the tomato fruit was reduced significantly compared with wild-type control fruit, although the tomato fruit size reduction (4-5-fold) was not as dramatic as that observed in apple. Growth of tomato fruit flesh tissue is dependent largely on division and expansion of cells occurring post-fertilization through the stimulation by hormones released from the seeds. Although over-expression of miR172 may promote fruit development in the absence of fertilization, the parthenocarpic fruit is smaller than wild-type fruit. This "smaller than wild-type" size of plants over-expressing miR172 indicates that the direct or indirect influence of the miR172 transgene on promoting tomato fruit growth in these parthenocarpic fruit does not fully compensate for the growth stimulation of seed-derived hormones in wild-type fruit.

The reports described above have shown miR172/AP2 playing different roles in the regulation of the development of different fruit types represented by apple, Arabidopsis, and tomato. This suggests that miR172/AP2 has the potential for a diversified function in regulating the development of different fruits of the Rosaceae family, although to date, their function has not been reported in any Rosaceae species other than apple. It is interesting to note that the extreme phenotype of apple transgenic plants over-expressing miR172 displays abnormal flowers without sepals, petals, or stamens, but with separate carpels rather than the fused the carpels of normal apples, and no hypanthium surrounding the ovary (**Figure 4**; Yao et al., 2015). If these flowers were to develop into fruit, the fruit would resemble peach rather than apple, indicating miR172/AP2 could be involved in the diversification of fruit types in Rosaceae.

PI/AP3 HOMOLOGS NEGATIVELY REGULATE FRUIT GROWTH

The Arabidopsis *PI* and *AP3* are single-copy class B genes, expressed specifically in petals and stamens during their development (Goto and Meyerowitz, 1994; Jack et al., 1992). In *PI* or *AP3* loss of function mutants, the flower phenotype is double the number of carpels, two whorls of sepals, and the absence of stamens or petals (Goto and Meyerowitz, 1994; Jack et al., 1992). Three apple varieties, Rae Ime, Spencer Seedless, and Wellington Bloomless, produce abnormal flowers that resemble Arabidopsis *pi* and *ap3* mutants. Interestingly, the flowers of these three apple varieties develop parthenocarpic fruit, and their single-copy *MdPI* gene is not expressed owing to the presence of a long-terminal-repeat TE (Yao et al., 2001). Consistently, a similar flower phenotype and parthenocarpic fruit development are achieved with *MdPI* cosuppression in apple transgenic plants (Yao et al., 2018). The parthenocarpic trait of apple in *MdPI* loss of function mutants and cosuppression transgenic plants may be explained by the conversion of petals to sepals that are the key floral organs contributing to apple flesh tissue growth (Yao et al., 2001). An additional or alternative explanation for this parthenocarpic trait is that the loss of stamens, as a consequence of suppression of the class B *MdPI*, results in male sterility. Male sterility has been associated with parthenocarpic fruit production in multiple plant species, including tomato (Ingrosso et al., 2011; Medina et al., 2013; Takei et al., 2019), citrus (Vardi et al., 2008), and grape (Royo et al., 2016). In contrast, ectopic *MdPI* expression coverts sepals to petals and inhibits apple fruit growth toward the base of the fruit resulting in short and flat fruit (**Figure 3**). Histological analyses showed that suppression of cell expansion was likely to be the key reason for the reduced tissue growth, although the possibility of inhibition of cell division could not be ruled out

(Yao et al., 2018). These two studies clearly indicated *MdPI* plays an inhibitory role on fruit growth.

The inhibitory role of the class B genes in fruit growth is also supported by studies in other plant species. For example, ectopic expression of *VvPI*, caused by an insertion of a miniature inverted-repeat TE, inhibits the growth of fruit flesh tissue and results in small, fleshless berries in grape (*Vitis vinifera*; Fernandez et al., 2013). In tomato, *DEFICIENS* (an *AP3* homolog) expression is temporarily upregulated before and throughout anthesis in the wild-type but not in the *parthenocarpic fruit* (*pat*) mutant (Mazzucato et al., 2008), and silencing of *TM6* (an *AP3* homolog) expression using RNA interference produced parthenocarpic fruit (De Martino et al., 2006). These results suggest that the *AP3* and *PI* homologs in other fruit crops also may suppress ovary and fruit development.

In Arabidopsis, PI and AP3 function together through forming protein heterodimers in petals and stamens (Goto and Meyerowitz, 1994). As apple and grape have several copies of *AP3* paralogues, some have acquired new expression patterns, like the sepal and fruit tissue expression observed in apple (Van Der Linden et al., 2002; Kitahara et al., 2004) and grape (Poupin et al., 2007). Ectopic expression of *VvPI* in grape or *MdPI* in apple inhibits fruit flesh tissue growth (Fernandez et al., 2013; Yao et al., 2018). A possible explanation for this phenotype in apple and grape is that the ectopic expression of PI and the new expression patterns of AP3 homologues results in the concomitant presence of AP3 and PI in fruit flesh tissue allowing the formation of functional AP3/PI heterodimers which repress fruit flesh tissue growth.

In cultivated strawberry (*Fragaria* x *ananassa*), two *AP3* homologues (*FaAP3* and *FaTM6*) exhibited an expression pattern equivalent to that of *AP3* in Arabidopsis. CRISPR/Cas9-mediated genome editing of strawberry to knockout *FaTM6* inhibited anther development although normal fruit development occurred after pollination with wild-type pollen (Martin-Pizarro et al., 2019), indicating *FaTM6* plays an important role in strawberry anther development. Comparison of the phenotypes between *MdPI* mutants of apple and *FaTM6* knockout of strawberry indicates the function of AP3/PI homologs is conserved in regulating floral organ development, but different in promoting fruit growth.

AG/*SHP*-RELATED GENES REGULATE APPLE AND PEACH FRUIT DEVELOPMENT

Apple has one *SHATTERPROOF* (*SHP*), two *AG*, and two *SEEDSTICK* (*STK*) homologs (**Table 1**; **Figure 1A**). When two *AG* homologs (*MdMADS15* and MdMADS22) are knocked out together the transgenic plants produce flowers with an increased number of petals, but these flowers still have stamens and carpels and can be pollinated to produce normal sized fruit with increased number of locules (**Figure 3**; Klocko et al., 2016). However, the simultaneous knockout of three genes, *MdMADS15/22*and *MdMADS14* (a *SHP* homolog), results in the flowers of these transgenic plants having increased numbers of petals and no stamens or carpels. This phenotype resembles the floral phenotype of Arabidopsis *agamous* mutants. The absence of the carpel in these apple mutant flowers means that they cannot be pollinated; however, they can be induced to produce pseudo fruit without any seed or fruit core by treatments with a combination of plant growth regulators including auxin, cytokinin, and gibberellin (Schaffer et al., 2017; Ireland et al., 2021). This is the first study to show pseudo fruit development without the development of carpel tissue. It is not fruit development in the true sense but extra-carpellary tissue continuing its development when carpels are not formed.

In peach, expression of *PrpPLENA*, a homolog of *SHP*, increases during fruit ripening. Ectopic expression of *PrpPLENA* in tomato plants results in the conversion of sepals into carpel-like structures that, like real fruits, become fleshy and ripen. These transgenic tomatoes also show accelerated ripening (Tadiello et al., 2009). This phenotype is the same as that of tomato over-expressing a *SHP* homolog *TAGL1* (Vrebalov et al., 2009), indicating that *PrpPLENA* is likely the functional homologue of tomato's *TAGL1*. Another class C-related gene of peach, *PrpSHP*, is expressed from the full anthesis until the fruit harvest stages. *PrpSHP* expression levels differ between those peach cultivars sensitive to split-pit and those resistant to split-pit (Tani et al., 2007). These findings suggest that temporal regulation of *PrpSHP* expression may influence the split-pit process of peach, which is a process similar to the silique dehiscence in Arabidopsis regulated by *SHP1* and *SHP2* (Liljegren et al., 2000).

The *AG/SHP* homologs of apple and peach have similar functions in regulating the growth of carpellary tissues during fruit development. The difference is that the carpellary tissues contribute to the growth of the whole fruit in peach, but only to the fruit core of apple. As demonstrated in the MADS15/15/22 knockout transgenic plants coreless apple pseudo fruit can be induced to develop from the extra-carpellary hypanthium when the function of all *AG/SHP* homologs is lost. In contrast, complete loss of function of *AG/SHP* homologs in peach would likely result in no fruit being produced, although such experiments have yet to be reported.

SEP-RELATED GENES REGULATING FRUIT FLESH GROWTH AND RIPENING

The class E *SEP* genes show partial redundancy in *Arabidopsis* with single *SEP* mutants showing only subtle phenotypes, in contrast to the triple *sep1/2/3* mutant which displays indeterminate flowers and whorls of sepals (Pelaz et al., 2000) and the quadruple *sep1/2/3/4* mutant which has whorls of leaf-like organs but no flower-like structures (Ditta et al., 2004). The role of *AtSEP* genes as floral meristem identity genes has been highlighted by their over-expression. Plants with a *SEP4* transgene under the control of the CaMV35S promoter exhibit replacement of the inflorescence meristem with fused terminal flowers (Ditta et al., 2004), while plants with a *SEP3* transgene

expressed from the CaMV35S promoter are early flowering with solitary flowers subtended by curled cauline leaves (Pelaz et al., 2001).

The functions of *SEP* homologs in regulating fruit development have been shown in tomato. Suppression of expression of either the *AtSEP1/2*-like gene *TM29* or *AtSEP3*-like gene *TM5* promotes parthenocarpic fruit development in transgenic tomato (Pnueli et al., 1994; Ampomah-Dwamena et al., 2002). This suggests that *SEP* genes repress tomato fruit development. Vrebalov et al. (2002) demonstrated that the *AtSEP4*-like *LeMADS-RIN* (*RIN*) gene is a "master regulator" of fruit ripening in tomato. *RIN* is proposed to act upstream of, and independently to, ethylene-mediated regulation of ripening. *Rin* mutant plants show inhibition of all ripening-related traits, including autocatalytic ethylene production, carotenoid accumulation, softening, and volatile production. The *rin* mutant fails to ripen even under ethylene treatment (Vrebalov et al., 2002). Furthermore, RIN can bind and activate the promoter of ethylene responsive genes, such as *LeACS2* (Ito et al., 2008) and in the *rin* mutant, the expression of *LeACS2* is suppressed (Barry et al., 2000).

In strawberry (*Fragaria* x *ananassa* Duch.) downregulation of *FaMADS9* (an *AtSEP1/2*-like gene) results in increased green coloration of petals toward a sepaloid form (Seymour et al., 2011), similar to the sepaloid petals seen in *Arabidopsis sep3* single mutants (Pelaz et al., 2001). Seymour et al. (2011) also showed that although fruit development appears normal when *FaMADS9* is downregulated, ripening is delayed with respect to the accumulation of anthocyanin, degreening of achenes, and fruit softening, akin to the *SEP4*-like *rin* mutant of tomato. Furthermore, complete suppression of *FaMADS9* leads to severe inhibition of fruit development such that the receptacle develops only to an immature stage (Seymour et al., 2011). Another study showed that over-expression of *FaMADS1α*, also belonging to the *SEP1/2* clade, reduced the expression of anthocyanin-related genes and delayed fruit ripening (Lu et al., 2018). Point mutations of *FveSEP3* (FvH4_4g23530) generated by EMS treatment and CRISPR/Cas9-mediated gene editing convert petals, stamens, and carpels to sepaloid organs, promote parthenocarpic fruit growth, and delay fruit ripening in woodland strawberry (Pi et al., 2021).

In apple (*Malus* x *domestica*), suppression of *MdMADS8/9*, a member of the *SEP1/2* clade, partially converts petals to sepals and reduces fruit flesh growth, resulting in small fruit (**Figure 3**). At fruit maturity, the *MADS8/9*-suppressed apples produce no ethylene and fail to ripen, showing no starch degradation or ethylene-modulated ripening traits (Ireland et al., 2013). Unlike the tomato *rin* mutant, the *MADS8/9*-suppressed apples ripen when supplied exogenous ethylene, suggesting that in this case the *SEP*-like genes are not acting as a master regulator controlling the competency of the fruit to ripen, but instead control the developmental regulation of distinct facets of apple fruit ripening, including the initiation of ethylene production.

Over-expression of the peach (*Prunus persica*) *PrpMADS5*, an *AtSEP3*-like gene, in *Arabidopsis* results in an early flowering phenotype and over-expression of the peach *PrpMADS7, an AtSEP1/2*-like gene causes extremely early flowering, with bolting after the cotyledon stage (Xu et al., 2008). The *PrpSEP1* gene is closely related to apple *MdMADS8 and MdMADS9* and is expressed in peach flesh. Its expression pattern during the storage of melting flesh peach is consistent with that of ethylene- and ripening-related genes. Suppression of *PrpSEP1* expression by virus-induced gene silencing (VIGS) delays fruit ripening and softening in melting flesh peach. PrpSEP1 can interact with the promoter of a ripening-related gene encoding a cell wall softening enzyme polygalacturonase (PG; Li et al., 2017).

From the studies discussed above, it is clear that *SEP* homologs play similar function in regulating fruit ripening among apple, peach, and strawberry. When the expression level of *SEP* homologs is reduced, fruit ripening is delayed in all three species. However, *SEP* homologs show opposite functions in regulating fruit flesh growth between apple and strawberry, i.e., promoting flesh tissue growth in apple (Ireland et al., 2013) but inhibiting flesh tissue growth function in strawberry (Pi et al., 2021). This difference may be related the difference of floral organs contributing to development of fruit flesh between apple and strawberry. Apple fruit flesh develops from a hypanthium containing the bases of sepals, petals, and stamens, whereas strawberry flesh develops from a receptacle known as a stem tip. However, further research is required to understand the mechanisms of this differential regulation.

CONCLUSION AND FUTURE PROSPECTS

The studies on apple floral MADS-box genes started in the mid-1990s. Recent advancements of reference genome assembly for multiple Rosaceae species have facilitated the genome-wide

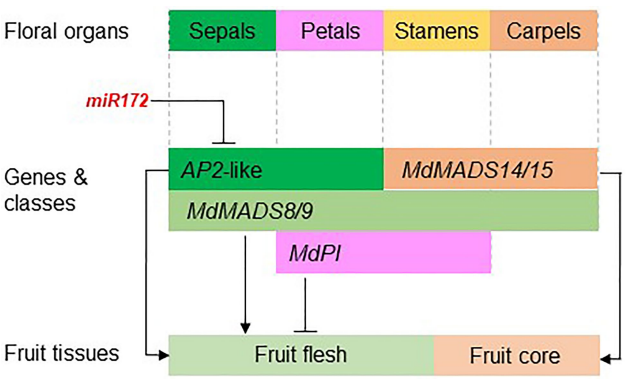

FIGURE 5 | The apple floral organ genes regulate fruit development. The diagram shows the apple floral organ genes that have been functionally studied in apple transgenic plants. miR172 inhibits the expression of *AP2-like* genes that promote apple fruit flesh growth (Yao et al., 2015). Ectopic expression of *MdPI* inhibits fruit flesh growth (Yao et al., 2018) while knockout of *MdPI* promotes parthenocarpic fruit development (Yao et al., 2001). The *AG/SHP* homologs *MADS14/15* are required for fruit core growth and coreless fruit can be produced by knocking out *MADS14/15* (Schaffer et al., 2017; Ireland et al., 2021). The class E genes *MdMADS8/9* are required for fruit flesh growth and fruit ripening (Ireland et al., 2013).

identification of floral MADS-box and *AP2* genes, and their expression patterns in developing fruit tissue have been analyzed using transcriptome data. These genome and transcriptome resources have allowed identification of promising candidate genes for analyzing their function in the regulation of fruit development and quality. So far, functional analyses of these genes have been predominantly in apple and strawberry because these two species are relatively easy to transform, and strawberry has a relatively short generation time. The function of a few genes, such as *MdPI* and miR172, has also been shown using natural mutants. The functional analyses of floral organ genes in regulating apple fruit development are summarized in **Figure 5**.

Future studies should be directed to functionally analyzing the roles of floral organ genes in a wider range of Rosaceae species for a greater understanding of the molecular mechanisms regulating fruit type diversity and fruit development in the family. Gene editing, using CRISPR-Cas9 or similar, offers the opportunity to disrupt the function of specific gene family members to elucidate their precise role, the degree of redundancy within the gene family and any neo- and sub-functionalization that has evolved. However, as most Rosaceae plants are woody perennials, the challenges of elucidating a gene's role in the regulation of fruit development and fruit quality are the relatively long time to the plants first flowering and fruiting and their recalcitrance to transformation. These challenges may be overcome by using transgenes to promote early flowering, as has been achieved using the *Betula pendula* (silver birch) *BpMADS4* gene to accelerate apple flowering (Weigl et al., 2015), and transgenes to enhance the efficiency of plant transformation and regeneration, as has been achieved using the *Baby boom* gene to improve maize and apple transformation (Lowe et al., 2016; Chen et al., 2021). In addition, recent accumulation of genome sequence data from a large number of cultivars and germplasm accessions of some of the Rosaceae family, along with transcriptomics data, is proving useful for the identification of alleles associated with key fruit development traits. With the ongoing expansion of genomics data, more refined spatio-temporal transcriptomics, new gene editing, and transformation technologies and their application across a wider range of Rosaceae family members, we would expect that significantly faster progress will be made in the next decade to understand how floral *MADS-box* and *AP2* genes regulate fruit development and fruit quality in Rosaceae, a family that produces such a wide array of fruit types.

AUTHOR CONTRIBUTIONS

All authors contributed to the design of the review and approved the manuscript. J-LY completed the first draft. J-LY, CK, and AG revised the manuscript.

REFERENCES

Ampomah-Dwamena, C., Morris, B. A., Sutherland, P., Veit, B., and Yao, J. L. (2002). Down-regulation of TM29, a tomato SEPALLATA homolog, causes parthenocarpic fruit development and floral reversion. *Plant Physiol.* 130, 605–617. doi: 10.1104/pp.005223

Aukerman, M. J., and Sakai, H. (2003). Regulation of flowering time and floral organ identity by a microRNA and its APETALA2-like target genes. *Plant Cell* 15, 2730–2741. doi: 10.1105/tpc.016238

Barry, C. S., Llop-Tous, M. I., and Grierson, D. (2000). The regulation of 1-aminocyclopropane-1-carboxylic acid synthase gene expression during the transition from system-1 to system-2 ethylene synthesis in tomato. *Plant Physiol.* 123, 979–986. doi: 10.1104/pp.123.3.979

Chen, X. M. (2004). A microRNA as a translational repressor of APETALA2 in Arabidopsis flower development. *Science* 303, 2022–2025. doi: 10.1126/science.1088060

Chen, J., Tomes, S., Gleave, A., Hall, W., Luo, Z., Xu, J., et al. (2021). Significant improvement of apple (Malus domestica Borkh.) transgenic plant production by pre-transformation with a Baby Boom transcription factor *Horticulture Research*. doi: 10.1093/hr/uhab014 (in press).

Coen, E. S., and Meyerowitz, E. M. (1991). The war of the whorls: genetic interactions controlling flower development. *Nature* 353, 31–37. doi: 10.1038/353031a0

Conant, G. C., Birchler, J. A., and Pires, J. C. (2014). Dosage, duplication, and diploidization: clarifying the interplay of multiple models for duplicate gene evolution over time. *Curr. Opin. Plant Biol.* 19, 91–98. doi: 10.1016/j.pbi.2014.05.008

Daccord, N., Celton, J. M., Linsmith, G., Becker, C., Choisne, N., Schijlen, E., et al. (2017). High-quality de novo assembly of the apple genome and methylome dynamics of early fruit development. *Nat. Genet.* 49, 1099–1106. doi: 10.1038/ng.3886

De Martino, G., Pan, I., Emmanuel, E., Levy, A., and Irish, V. F. (2006). Functional analyses of two tomato APETALA3 genes demonstrate diversification in their roles in regulating floral development. *Plant Cell* 18, 1833–1845. doi: 10.1105/tpc.106.042978

Ditta, G., Pinyopich, A., Robles, P., Pelaz, S., and Yanofsky, M. F. (2004). The *SEP4* gene of *Arabidopsis thaliana* functions in floral organ and meristem identity. *Curr. Biol.* 14, 1935–1940. doi: 10.1016/j.cub.2004.10.028

Edger, P. P., Vanburen, R., Colle, M., Poorten, T. J., Wai, C. M., Niederhuth, C. E., et al. (2017). Single-molecule sequencing and optical mapping yields an improved genome of woodland strawberry (Fragaria vesca) with chromosome-scale contiguity. *Gigascience* 7, 1–7. doi: 10.1093/gigascience/gix124

Fernandez, L., Chaib, J., Martinez-Zapater, J. M., Thomas, M. R., and Torregrosa, L. (2013). Mis-expression of a PISTILLATA-like MADS box gene prevents fruit development in grapevine. *Plant J.* 73, 918–928. doi: 10.1111/tpj.12083

Gattolin, S., Cirilli, M., Pacheco, I., Ciacciulli, A., Da Silva Linge, C., Mauroux, J. B., et al. (2018). Deletion of the miR172 target site in a TOE-type gene is a strong candidate variant for dominant double-flower trait in Rosaceae. *Plant J.* 96, 358–371. doi: 10.1111/tpj.14036

Goto, K., and Meyerowitz, E. M. (1994). Function and regulation of the Arabidopsis floral homeotic gene pistillata. *Genes Dev.* 8, 1548–1560. doi: 10.1101/gad.8.13.1548

Gu, Q., Ferrandiz, C., Yanofsky, M. F., and Martienssen, R. (1998). The FRUITFULL MADS-box gene mediates cell differentiation during Arabidopsis fruit development. *Development* 125, 1509–1517. doi: 10.1242/dev.125.8.1509

Hawkins, C., Caruana, J., Li, J. M., Zawora, C., Darwish, O., Wu, J., et al. (2017). An eFP browser for visualizing strawberry fruit and flower transcriptomes. *Horticulture Res.* 4:17029. doi: 10.1038/hortres.2017.29

Hollender, C. A., Kang, C., Darwish, O., Geretz, A., Matthews, B. F., Slovin, J., et al. (2014). Floral transcriptomes in woodland strawberry uncover developing receptacle and anther gene networks. *Plant Physiol.* 165, 1062–1075. doi: 10.1104/pp.114.237529

Hu, P. P., Li, G., Zhao, X., Zhao, F. L., Li, L. J., and Zhou, H. C. (2018). Transcriptome profiling by RNA-Seq reveals differentially expressed genes related to fruit development and ripening characteristics in strawberries (*Fragaria* x *ananassa*). *Peerj* 6:e4976. doi: 10.7717/peerj.4976

Ingrosso, I., Bonsegna, S., De Domenico, S., Laddomada, B., Blando, F., Santino, A., et al. (2011). Over-expression of a grape stilbene synthase gene in tomato induces parthenocarpy and causes abnormal pollen development. *Plant Physiol. Biochem.* 49, 1092–1099. doi: 10.1016/j.plaphy.2011.07.012

Ireland, H. S., Tomes, S., Hallett, I. C., Karunairetnam, S., David, K. M., Yao, J.-L., et al. (2021). Coreless apples generated by the suppression of carpel genes and hormone-induced fruit set. *Fruit Res.* 1, 1–9. doi: 10.48130/FruRes-2021-0002

Ireland, H. S., Yao, J.-L., Tomes, S., Sutherland, P. W., Nieuwenhuizen, N., Gunaseelan, K., et al. (2013). Apple SEPALLATA1/2-like genes control fruit flesh development and ripening. *Plant J.* 73, 1044–1056. doi: 10.1111/tpj.12094

Ito, Y., Kitagawa, M., Ihashi, N., Yabe, K., Kimbara, J., Yasuda, J., et al. (2008). DNA-binding specificity, transcriptional activation potential, and the *rin* mutation effect for the tomato fruit-ripening regulator *RIN*. *Plant J.* 55, 212–223. doi: 10.1111/j.1365-313X.2008.03491.x

Jack, T., Brockman, L. L., and Meyerowitz, E. M. (1992). The homeotic gene APETALA3 of Arabidopsis thaliana encodes a MADS box and is expressed in petals and stamens. *Cell* 68, 683–697. doi: 10.1016/0092-8674(92)90144-2

Jofuku, K. D., Omidyar, P. K., Gee, Z., and Okamuro, J. K. (2005). Control of seed mass and seed yield by the floral homeotic gene APETALA2. *Proc. Natl. Acad. Sci. U. S. A.* 102, 3117–3122. doi: 10.1073/pnas.0409893102

Kang, C. Y., Darwish, O., Geretz, A., Shahan, R., Alkharouf, N., and Liu, Z. C. (2013). Genome-scale transcriptomic insights into early-stage fruit development in woodland strawberry Fragaria vesca. *Plant Cell* 25, 1960–1978. doi: 10.1105/tpc.113.111732

Kim, S., Soltis, P. S., Wall, K., and Soltis, D. E. (2006). Phylogeny and domain evolution in the APETALA2-like gene family. *Mol. Biol. Evol.* 23, 107–120. doi: 10.1093/molbev/msj014

Kitahara, K., Ohtsubo, T., Soejima, J., and Matsumoto, S. (2004). Cloning and characterization of apple class MADS-box genes including a novel AP3 homologue MdTM6. *J. Japanese Soci. Horticultural Sci.* 73, 208–215. doi: 10.2503/jjshs.73.208

Klocko, A. L., Borejsza-Wysocka, E., Brunner, A. M., Shevchenko, O., Aldwinckle, H., and Strauss, S. H. (2016). Transgenic suppression of AGAMOUS genes in apple reduces fertility and increases floral attractiveness. *PLoS One* 11:e0159421. doi: 10.1371/journal.pone.0159421

Kotoda, N., Wada, M., Kusaba, S., Kano-Murakami, Y., Masuda, T., and Soejima, J. (2002). Overexpression of MdMADS5, an APETALA1-like gene of apple, causes early flowering in transgenic Arabidopsis. *Plant Sci.* 162, 679–687. doi: 10.1016/S0168-9452(02)00024-9

Krizek, B. A., and Fletcher, J. C. (2005). Molecular mechanisms of flower development: An armchair guide. *Nat. Rev. Genet.* 6, 688–698. doi: 10.1038/nrg1675

Li, J. J., Fang, L., Qian, M., Han, M. Y., Liu, H. K., Zhang, D., et al. (2017). Characteristics and regulatory pathway of the PrupeSEP1 SEPALLATA gene during ripening and softening in peach fruits. *Plant Sci.* 257, 63–73. doi: 10.1016/j.plantsci.2017.01.004

Liljegren, S. J., Ditta, G. S., Eshed, H. Y., Savidge, B., Bowman, J. L., and Yanofsky, M. F. (2000). SHATTERPROOF MADS-box genes control seed dispersal in Arabidopsis. *Nature* 404, 766–770. doi: 10.1038/35008089

Liu, Z., Ma, H., Jung, S., Main, D., and Guo, L. (2020). Developmental mechanisms of fleshy fruit diversity in Rosaceae. *Annu. Rev. Plant Biol.* 71, 547–573. doi: 10.1146/annurev-arplant-111119-021700

Lowe, K., Wu, E., Wang, N., Hoerster, G., Hastings, C., Cho, M. J., et al. (2016). Morphogenic regulators baby boom and Wuschel improve monocot transformation. *Plant Cell* 28, 1998–2015. doi: 10.1105/tpc.16.00124

Lu, W. J., Chen, J. X., Ren, X. C., Yuan, J. J., Han, X. Y., Mao, L. C., et al. (2018). One novel strawberry MADS-box transcription factor FaIVIADS1 alpha acts as a negative regulator in fruit ripening. *Sci. Hortic.* 227, 124–131. doi: 10.1016/j.scienta.2017.09.042

Martin-Pizarro, C., Trivino, J. C., and Pose, D. (2019). Functional analysis of the TM6 MADS-box gene in the octoploid strawberry by CRISPR/Cas9-directed mutagenesis. *J. Exp. Bot.* 70, 885–895. doi: 10.1093/jxb/ery400

Mazzucato, A., Olimpieri, I., Siligato, F., Picarella, M. E., and Soressi, G. P. (2008). Characterization of genes controlling stamen identity and development in a parthenocarpic tomato mutant indicates a role for the DEFICIENS ortholog in the control of fruit set. *Physiol. Plant.* 132, 526–537. doi: 10.1111/j.1399-3054.2007.01035.x

Medina, M., Roque, E., Pineda, B., Cañas, L., Rodriguez-Concepción, M., Beltrán, J. P., et al. (2013). Early anther ablation triggers parthenocarpic fruit development in tomato. *Plant Biotechnol. J.* 11, 770–779. doi: 10.1111/pbi.12069

Mlotshwa, S., Yang, Z., Kim, Y., and Chen, X. (2006). Floral patterning defects induced by Arabidopsis APETALA2 and microRNA172 expression in Nicotiana benthamiana. *Plant Mol. Biol.* 61, 781–793. doi: 10.1007/s11103-006-0049-0

Okamuro, J. K., Caster, B., Villarroel, R., Vanmontagu, M., and Jofuku, K. D. (1997). The AP2 domain of APETALA2 defines a large new family of DNA binding proteins in Arabidopsis. *Proc. Natl. Acad. Sci. U. S. A.* 94, 7076–7081. doi: 10.1073/pnas.94.13.7076

Pabón-Mora, N., Ambrose, B. A., and Litt, A. (2012). Poppy APETALA1/FRUITFULL orthologs control flowering time, branching, perianth identity, and fruit development. *Plant Physiol.* 158, 1685–1704. doi: 10.1104/pp.111.192104

Pei, M. S., Cao, S. H., Wu, L., Wang, G. M., Xie, Z. H., Gu, C., et al. (2020). Comparative transcriptome analyses of fruit development among pears, peaches, and strawberries provide new insights into single sigmoid patterns. *BMC Plant Biol.* 20:108. doi: 10.1186/s12870-020-2317-6

Pei, M. S., Gu, C., and Zhang, S. L. (2019). Genome-wide identification and expression analysis of genes associated with peach (Prunus persica) fruit ripening. *Sci. Hortic.* 246, 317–327. doi: 10.1016/j.scienta.2018.10.065

Pelaz, S., Ditta, G. S., Baumann, E., Wisman, E., and Yanofsky, M. F. (2000). B and C floral organ identity functions require *SEPALLATA* MADS-box genes. *Nature* 405, 200–203. doi: 10.1038/35012103

Pelaz, S., Gustafson-Brown, C., Kohalmi, S. E., Crosby, W. L., and Yanofsky, M. F. (2001). *APETALA1* and *SEPALLATA3* interact to promote flower development. *Plant J.* 26, 385–394. doi: 10.1046/j.1365-313X.2001.2641042.x

Pi, M., Hu, S., Cheng, L., Zhong, R., Cai, Z., Liu, Z., et al. (2021). The MADS-box gene FveSEP3 plays essential roles in flower organogenesis and fruit development in woodland strawberry. *Horticulture. Demogr. Res.* 8, 1–5. doi: 10.1038/s41438-021-00673-1

Pnueli, L., Hareven, D., Broday, L., Hurwitz, C., and Lifschitz, E. (1994). The *TM5* MADS box gene mediates organ differentiation in the three inner whorls of tomato flowers. *Plant Cell* 6, 175–186. doi: 10.2307/3869637

Poupin, M. J., Federici, F., Medina, C., Matus, J. T., Timmermann, T., and Arce-Johnson, P. (2007). Isolation of the three grape sub-lineages of B-class MADS-box TM6, PISTALLATA and APETALA3 genes which are differentially expressed during flower and fruit development. *Gene* 404, 10–24. doi: 10.1016/j.gene.2007.08.005

Pratt, C. (1988). Apple flower and fruit: morphology and anatomy. *Hortic. Rev.* 10, 273–308. doi: 10.1002/9781118060834.ch8

Ripoll, J. J., Bailey, L. J., Mai, Q.-A., Wu, S. L., Hon, C. T., Chapman, E. J., et al. (2015). microRNA regulation of fruit growth. *Nature Plants* 1:15036. doi: 10.1038/nplants.2015.36

Ripoll, J. J., Roeder, A. H., Ditta, G. S., and Yanofsky, M. F. (2011). A novel role for the floral homeotic gene APETALA2 during Arabidopsis fruit development. *Development* 138, 5167–5176. doi: 10.1242/dev.073031

Royo, C., Carbonell-Bejerano, P., Torres-Pérez, R., Nebish, A., Martínez, Ó., Rey, M., et al. (2016). Developmental, transcriptome, and genetic alterations associated with parthenocarpy in the grapevine seedless somatic variant Corinto bianco. *J. Exp. Bot.* 67, 259–273. doi: 10.1093/jxb/erv452

Schaffer, R. J., Ireland, H. S., and Yao, J.-L. (2017). Methods and Materials for Producing Coreless Fruit. *US Patent App*. 15/329,229.

Seymour, G. B., Ryder, C. D., Cevik, V., Hammond, J. P., Popovich, A., King, G. J., et al. (2011). A *SEPALLATA* gene is involved in the development and ripening of strawberry (*Fragaria x ananassa* Duch.) fruit, a non-climacteric tissue. *J. Exp. Bot.* 62, 1179–1188. doi: 10.1093/jxb/erq360

Shahan, R., Li, D. D., and Liu, Z. C. (2019). Identification of genes preferentially expressed in wild strawberry receptacle fruit and demonstration of their promoter activities. *Horticulture Res.* 6:50. doi: 10.1038/s41438-019-0134-6

Shang, X. L., Zhang, J. P., Ma, Y. H., and Wang, L. R. (2020). Preliminary identification of candidate genes associated with the peach fruit sorbitol content based on comparative transcriptome analysis. *Sci. Hortic.* 263:109151. doi: 10.1016/j.scienta.2019.109151

Spjut, R.W. (1994). *A Systematic Treatment of Fruit Types*. Bronx, New York: New York Botanical Garden.

Sung, S. K., and An, G. H. (1997). Molecular cloning and characterization of a MADS-box cDNA clone of the Fuji apple. *Plant Cell Physiol.* 38, 484–489. doi: 10.1093/oxfordjournals.pcp.a029193

Sung, S. K., Yu, G. H., and An, G. H. (1999). Characterization of MdMADS2, a member of the SQUAMOSA subfamily of genes, in apple. *Plant Physiol.* 120, 969–978. doi: 10.1104/pp.120.4.969

Sung, S. K., Yu, G. H., Nam, J., Jeong, D. H., and An, G. (2000). Developmentally regulated expression of two MADS-box genes, MdMADS3 and MdMADS4, in the morphogenesis of flower buds and fruits in apple. *Planta* 210, 519–528. doi: 10.1007/s004250050040

Tadiello, A., Pavanello, A., Zanin, D., Caporali, E., Colombo, L., Rotino, G. L., et al. (2009). A PLENA-like gene of peach is involved in carpel formation and subsequent transformation into a fleshy fruit. *J. Exp. Bot.* 60, 651–661. doi: 10.1093/jxb/ern313

Takei, H., Shinozaki, Y., Yano, R., Kashojiya, S., Hernould, M., Chevalier, C., et al. (2019). Loss-of-function of a tomato receptor-Like kinase impairs male fertility and induces Parthenocarpic fruit set. *Front. Plant Sci.* 10:403. doi: 10.3389/fpls.2019.00403

Tan, B., Lian, X. D., Cheng, J., Zeng, W. F., Zheng, X. B., Wang, W., et al. (2019). Genome-wide identification and transcriptome profiling reveal that E3 ubiquitin ligase genes relevant to ethylene, auxin and abscisic acid are differentially expressed in the fruits of melting flesh and stony hard peach varieties. *BMC Genomics* 20:892. doi: 10.1186/s12864-019-6258-0

Tang, M., Li, G., and Chen, M. (2007). The phylogeny and expression pattern of APETALA2-like genes in rice. *J. Gene. Genom.* 34, 930–938. doi: 10.1016/S1673-8527(07)60104-0

Tani, E., Polidoros, A. N., Flemetakis, E., Stedel, C., Kalloniati, C., Demetriou, K., et al. (2009). Characterization and expression analysis of AGAMOUS-like, SEEDSTICK-like, and SEPALLATA-like MADS-box genes in peach (Prunus persica) fruit. *Plant Physiol. Biochem.* 47, 690–700. doi: 10.1016/j.plaphy.2009.03.013

Tani, E., Polidoros, A. N., and Tsaftaris, A. S. (2007). Characterization and expression analysis of FRUITFULL- and SHATTERPROOF-like genes from peach (Prunus persica) and their role in split-pit formation. *Tree Physiol.* 27, 649–659. doi: 10.1093/treephys/27.5.649

Teotia, S., and Tang, G. (2015). To bloom or not to bloom: role of MicroRNAs in plant flowering. *Mol. Plant* 8, 359–377. doi: 10.1016/j.molp.2014.12.018

Van Der Linden, C. G., Vosman, B., and Smulders, M. J. M. (2002). Cloning and characterization of four apple MADS box genes isolated from vegetative tissue. *J. Exp. Bot.* 53, 1025–1036. doi: 10.1093/jexbot/53.371.1025

Vardi, A., Levin, I., and Carmi, N. (2008). Induction of seedlessness in citrus: from classical techniques to emerging biotechnological approaches. *J. Am. Soc. Hortic. Sci.* 133, 117–126. doi: 10.21273/JASHS.133.1.117

Velasco, R., Zharkikh, A., Affourtit, J., Dhingra, A., Cestaro, A., Kalyanaraman, A., et al. (2010). The genome of the domesticated apple (*Malus* x *domestica Borkh.*). *Nat. Genet.* 42, 833–839. doi: 10.1038/ng.654

Verde, I., Abbott, A. G., Scalabrin, S., Jung, S., Shu, S. Q., Marroni, F., et al. (2013). The high-quality draft genome of peach (Prunus persica) identifies unique patterns of genetic diversity, domestication and genome evolution. *Nat. Genet.* 45, U487–U447. doi: 10.1038/ng.2586

Vrebalov, J., Pan, I. L., Arroyo, A. J. M., Mcquinn, R., Chung, M., Poole, M., et al. (2009). Fleshy fruit expansion and ripening are regulated by the tomato SHATTERPROOF gene TAGL1. *Plant Cell* 21, 3041–3062. doi: 10.1105/tpc.109.066936

Vrebalov, J., Ruezinsky, D., Padmanabhan, V., White, R., Medrano, D., Drake, R., et al. (2002). A MADS-box gene necessary for fruit ripening at the tomato *ripening-inhibitor* (*rin*) locus. *Science* 296, 343–346. doi: 10.1126/science.1068181

Weigel, D., and Meyerowitz, E. M. (1994). The ABCs of floral homeotic genes. *Cell* 78, 203–209. doi: 10.1016/0092-8674(94)90291-7

Weigl, K., Wenzel, S., Flachowsky, H., Peil, A., and Hanke, M. V. (2015). Integration of BpMADS4 on various linkage groups improves the utilization of the rapid cycle breeding system in apple. *Plant Biotechnol. J.* 13, 246–258. doi: 10.1111/pbi.12267

Wollmann, H., Mica, E., Todesco, M., Long, J. A., and Weigel, D. (2010). On reconciling the interactions between APETALA2, miR172 and AGAMOUS with the ABC model of flower development. *Development* 137, 3633–3642. doi: 10.1242/dev.036673

Xiang, Y. Z., Huang, C. H., Hu, Y., Wen, J., Li, S. S., Yi, T. S., et al. (2017). Evolution of Rosaceae fruit types based on nuclear phylogeny in the context of geological times and genome duplication. *Mol. Biol. Evol.* 34:msw242. doi: 10.1093/molbev/msw242

Xu, Z. D., Zhang, Q. X., Sun, L. D., Du, D. L., Cheng, T. R., Pan, H. T., et al. (2014). Genome-wide identification, characterisation and expression analysis of the MADS-box gene family in Prunus mume. *Mol. Gen. Genomics.* 289, 903–920. doi: 10.1007/s00438-014-0863-z

Xu, Y., Zhang, L., Xie, H., Zhang, Y.-Q., Oliveira, M. M., and Ma, R.-C. (2008). Expression analysis and genetic mapping of three SEPALLATA-like genes from peach (Prunus persica (L.) Batsch). *Tree Genet. Genomes* 4, 693–703. doi: 10.1007/s11295-008-0143-3

Yant, L., Mathieu, J., Dinh, T. T., Ott, F., Lanz, C., Wollmann, H., et al. (2010). Orchestration of the floral transition and floral development in Arabidopsis by the bifunctional transcription factor APETALA2. *Plant Cell* 22, 2156–2170. doi: 10.1105/tpc.110.075606

Yao, J.-L., Dong, Y.-H., Kvarnheden, A., and Morris, B. (1999). Seven MADS-box genes in apple are expressed in different parts of the fruit. *J. Am. Soc. Hortic. Sci.* 124, 8–13. doi: 10.21273/JASHS.124.1.8

Yao, J.-L., Dong, Y.-H., and Morris, B. A. (2001). Parthenocarpic apple fruit production conferred by transposon insertion mutations in a MADS-box transcription factor. *Proc. Natl. Acad. Sci.* 98, 1306–1311. doi: 10.1073/pnas.98.3.1306

Yao, J. L., Tomes, S., Xu, J., and Gleave, A. P. (2016). How microRNA172 affects fruit growth in different species is dependent on fruit type. *Plant Signal. Behav.* 11:e1156833. doi: 10.1080/15592324.2016.1156833

Yao, J.-L., Xu, J., Cornille, A., Tomes, S., Karunairetnam, S., Luo, Z., et al. (2015). A microRNA allele that emerged prior to apple domestication may underlie fruit size evolution. *Plant J.* 84, 417–427. doi: 10.1111/tpj.13021

Yao, J. L., Xu, J., Tomes, S., Cui, W., Luo, Z. W., Deng, C., et al. (2018). Ectopic expression of the PISTILLATA homologous MdPI inhibits fruit tissue growth and changes fruit shape in apple. *Plant Direct* 2:e00051. doi: 10.1002/pld3.51

Ying, H., Shi, J., Zhang, S. S., Pingcuo, G. S., Wang, S., Zhao, F., et al. (2019). Transcriptomic and metabolomic profiling provide novel insights into fruit development and flesh coloration in Prunus mira Koehne, a special wild peach species. *BMC Plant Biol.* 19:463. doi: 10.1186/s12870-019-2074-6

Zhang, L., Xu, Y., and Ma, R. (2008). Molecular cloning, identification, and chromosomal localization of two MADS box genes in peach (Prunus persica). *J. Gene. genom.* 35, 365–372. doi: 10.1016/S1673-8527(08)60053-3

Zhu, Q.-H., and Helliwell, C. A. (2011). Regulation of flowering time and floral patterning by miR172. *J. Exp. Bot.* 62, 487–495. doi: 10.1093/jxb/erq295

Zhu, Q.-H., Upadhyaya, N. M., Gubler, F., and Helliwell, C. A. (2009). Over-expression of miR172 causes loss of spikelet determinacy and floral organ abnormalities in rice (*Oryza sativa*). *BMC Plant Biol.* 9:149. doi: 10.1186/1471-2229-9-149

Conflict of Interest: Authors AG and J-LY were employed by company The New Zealand Institute for Plant and Food Research Limited.

The remaining authors declare that the research was conducted in the absence of any commercial or financial relationships that could be construed as a potential conflict of interest.

Publisher's Note: All claims expressed in this article are solely those of the authors and do not necessarily represent those of their affiliated organizations, or those of the publisher, the editors and the reviewers. Any product that may be evaluated in this article, or claim that may be made by its manufacturer, is not guaranteed or endorsed by the publisher.

Advantages of publishing in Frontiers

OPEN ACCESS
Articles are free to read for greatest visibility and readership

FAST PUBLICATION
Around 90 days from submission to decision

HIGH QUALITY PEER-REVIEW
Rigorous, collaborative, and constructive peer-review

TRANSPARENT PEER-REVIEW
Editors and reviewers acknowledged by name on published articles

Frontiers
Avenue du Tribunal-Fédéral 34
1005 Lausanne | Switzerland

Visit us: www.frontiersin.org
Contact us: frontiersin.org/about/contact

REPRODUCIBILITY OF RESEARCH
Support open data and methods to enhance research reproducibility

DIGITAL PUBLISHING
Articles designed for optimal readership across devices

FOLLOW US
@frontiersin

IMPACT METRICS
Advanced article metrics track visibility across digital media

EXTENSIVE PROMOTION
Marketing and promotion of impactful research

LOOP RESEARCH NETWORK
Our network increases your article's readership